The Perturbed Universe: Dynamics, Statistics and Phenomenology

Geraint Pratten

Cardiff - 2014

The Perturbed Universe: Dynamics, Statistics and Phenomenology

Geraint Pratten

Thesis Submitted for the Degree of Doctor of Philosophy
at the School of Physics and Astronomy
Cardiff University

Submitted by
Geraint Pratten

Cardiff, July 2014

External Examiner: Sabino Matarrese
Internal Examiner: Stephen Fairhurst
Supervisor: Bangalore Sathyaprakash
Date of Viva: 01/08/2014

Declaration of Authorship

- DECLARATION:
  This work has not previously been accepted in substance for any degree and is not concurrently submitted in candidature for any degree.

  Signed: ..... (candidate) Date: .....

- STATEMENT 1:
  This thesis is being submitted in partial fulfillment of the requirements for the degree of Doctor of Philosophy (PhD).

  Signed: ..... (candidate) Date: .....

- STATEMENT 2:
  This thesis is the result of my own independent work/investigation, except where otherwise stated. Other sources are acknowledged by explicit references.

  Signed: ..... (candidate) Date: .....

- STATEMENT 3
  I hereby give consent for my thesis, if accepted, to be available for photocopying and for inter-library loan, and for the title and summary to be made available to outside organisations.

  Signed: ..... (candidate) Date: .....

- STATEMENT 4: PREVIOUSLY APPROVED BAR ON ACCESS
  I hereby give consent for my thesis, if accepted, to be available for photocopying and for inter-library loans **after expiry of a bar on access previously approved by the Academic Standards & Quality Committee.**

  Signed: ..... (candidate) Date: .....

Declaration of Work

The research presented in this thesis was performed in the School of Physics and Astronomy at Cardiff University between October 2010 and July 2014. This thesis is the result of my own work, except as stated below and where explicit reference has been made to the results of others. I am also grateful to the University of Cape Town, where a portion of this work was completed.

The content of this thesis is based on the following published or in preparation papers:

- G. Pratten and D. Munshi, "Non-Gaussianity in Large Scale Structure and Minkowski Functionals,", MNRAS **423** (2012) 3209, arXiv:1108.1985.
- G. Pratten and D. Munshi, "BAOs and Non-linearities: 3D Spherical Analysis," MNRAS **436** (2013) 3792, arXiv:1301.3673.
- G. Pratten and D. Munshi, "Reconstructing the Thermal Sunyaev-Zel'dovich Effect in 3D," MNRAS **442** 1 arXiv:1404.2782.
- G. Pratten, "Comment on 'Covariant perturbations of Schwarzschild black holes'," CQG **31** (2014) 038001.
- G. Pratten and C. Clarkson, "Covariant Perturbations of LTB Spacetimes," *In Preparation*, (2014).
- G. Pratten, "Covariant Perturbations of Vacuum LRS-II Spacetimes," *In Preparation*, (2014).
- G. Pratten, "Covariant Perturbations of f(R) Black Holes: The Weyl Terms," *In Preparation*, (2014).

The work in Chapter 4 is based on [434] for which I performed a lot of the analytical and numerical calculations. The text was written collaboratively with Dipak Munshi. The work in Chapter 5 is based on [435], with analytical results derived collaboratively with Dipak Munshi and numerical results derived by myself. The work in Chapter 6 is based on [436], for which the analytical results were derived collaboratively with Dipak Munshi and numerical results were derived by myself. The work in Chapter 8 is based on [437; 438; 439; 440]. All analytical results were derived by myself with the help of Maple and Mathematica worksheets. The results in Chapter 9 are based on [438], a project undertaken in collaboration with Chris Clarkson. The analytical results were derived by myself with the aid of Maple and Mathematica worksheets. The Maple worksheets for Chapter 9 build on worksheets provided to me by Anne Marie Nzioki and Sean February, to which I am very grateful.

Thesis Summary

This thesis is broadly concerned with the dynamics, statistics and phenomenology of the perturbed Universe. By studying the perturbations to cosmological spacetimes, and the subsequent growth of large scale structure, we find that we can link both fundamentally and astrophysically interesting physics to cosmological observables. We use a healthy mix of statistical, analytical and numerical techniques throughout this thesis.

In Chapter 2 we introduce and summarise the statistics of random fields, as these are fundamental objects used to model cosmological observables. We introduce the spherical Fourier-Bessel expansion as a tool to perform genuine 3-dimensional studies of cosmological random fields. In Chapter 3 we introduce the theory of inflation and discuss the basic machinery that allows us to calculate the statistical properties of the quantum mechanical flucatuations that seed large scale structure. What we see is that different fundamental physics in the early Universe leads to different statistical properties that we may test. The second half of Chapter 3 introduces the large scale structure of the Universe that describes the clustering of galaxies on cosmological scales. We discuss the growth and evolution of structure under gravitational collapse and the core observables that are predicted, such as the power spectrum, variance and skewness.

Chapter 4 introduces the Minkowski functionals. These are a set of topological statistics that probe the morphological properties of random fields. In particular they may be used to quantify deviations from Gaussianity in the large scale structure of galaxies. The deviations from Gaussianity can be generated by two primary mechanisms: 1) The gravitational collapse of perturbations is a non-linear process. Even if we have Gaussian initial conditions, gravitational collapse will induce non-Gaussianity. 2) Different theories for the early Universe will imprint different non-Gaussian features in the primordial perturbations that seed large scale structure, i.e. we have non-Gaussian initial conditions. We can connect the amplitude and momentum dependence of the non-Gaussianity to different fundamental interactions. We introduce a topological statistic based on the Minkowski functionals that retains the momentum dependence giving us greater distinguishing power between different contributions to non-Gaussianity.

In Chapter 5 we introduce the Baryon Acoustic Oscillations (BAOs) as described in the spherical Fourier-Bessel formalism. The BAOs are a solid prediction in cosmology and should help us to constrain cosmological parameters. We implement a full 3-dimensional study and study how redshift space distortions, induced by the motion of galaxies, and non-linearities, induced by gravitational collapse, impact the characteristics of these BAOs.

Chapter 6 extends the spherical Fourier-Bessel theme by introducing the thermal Sunyaev-Zel'dovich (tSZ) effect and cosmological weak lensing (WL). It is thought that weak lensing will provide an unbiased probe of the dark Universe and that the tSZ effect will probe the thermal history of the Universe. Unfortunately, the tSZ effect loses redshift information as it is a line of sight projection. We study the cross-correlation of the tSZ effect with WL in order to reconstruct the tSZ effect in a full 3-dimensional study in an attmept to recover the lost distance information. We use the halo model, spectroscopic redshift surveys and suvery effects to understand how detailed modelling effects the tSZ-WL cross correlation.

Chapter 7 marks a real change in theme and introduces the subject of relativistic cosmology. In particular we introduce the 1+3, 1+1+2 and 2+2 formalisms as tools to study cosmological perturbations. We provide rather self-contained introductions and provide some minor corrections to the literature in the 1+1+2 formalism as well as introducing new results.

In Chapter 8 we apply the 1+1+2 and 2+2 approaches to the Schwarzschild spacetime. Here we outline the full system of equations in both approaches and how they are related, setting up a correspondence between the two. Our aim is to construct closed, covariant, gauge-invariant and frame-invariant wave equations that govern the gravitational perturbations of the Schwarzschild spacetime. We correct a result in the literature and derive two new equations. The first governs axial gravitational perturbations and is related to the magnetic Weyl scalar. The second is valid for both polar and axial perturbations and is given by a combination of the magnetic and electric Weyl 2-tensors. We discuss their relation to the literature at large.

Finally, in Chapter 9 we apply the 1+1+2 and 2+2 approaches the LTB spacetime. This inhomogeneous but spherically symmetric spacetime is the first stepping stone into genuinely inhomogeneous cosmological spacetimes. We seek a closed, covariant master equation for the gravitational perturbations of the LTB spacetime. We present an equation governing axial gravitational perturbations and a preliminary equation, valid for both the polar and axial sectors, that is constructed from the electric and magnetic Weyl 2-tensors but is coupled to the energy-momentum content of the LTB spacetime. We discuss how auxilliary equations may be introduced in order to close the master equation for polar and axial perturbations. This last result leads to the identification of $\mathcal{H}$ as a master variable for axial perturbations of all vacuum LRS-II spacetimes and the LTB spacetime. It is thought that these results can be extended to non-vacuum LRS-II spacetimes. Likewise, the master variable constructed from Weyl variables constitutes a master variable for all vacuum LRS-II spacetimes and it is thought that this will extend to the non-vacuum case.

Acronyms

ADM	Arnowitt-Deser-Misner
BAO	Baryon Acoustic Oscillations
BH	Black Hole
CMB	Cosmic Microwave Background
dS	de Sitter
EFE	Einstein Field Equations
FLRW	Friedman-Lemâitre-Robertson-Walker
GIC	Gauge Invariant and Covariant
GMG	Gundlach and Martin-Garcia
GRF	Gaussian Random Field
GS	Gerlach and Sengupta
GW	Gravitational Wave
kSZ	Kinetic Sunyaev-Zel'dovich
KVF	Killing Vector Field
LTB	Lemâitre-Tolman-Bondi
LPT	Lagrangian Perturbation Theory
LRS	Locally Rotationally Symmetric
LRS-II	Locally Rotationally Symmetric Class-II
LSS	Large Scale Structure
MF	Minkowski Functional
NG	Non-Gaussianity
N-PCF	N Point Correlation Function
PCL	Pseudo $\mathcal{C}_\ell$
PS	Press-Schechter
QFT	Quantum Field Theory
QML	Quadratic Maximum Likelihood
QNM	Quasi-Normal Mode
RSD	Redshift Space Distortions
RW	Regge-Wheeler
sFB	Spherical Fourier-Bessel
SKA	Square Kilometer Array
S/N	Signal-to-Noise
SPT	Standard Perturbation Theory
ST	Sheth-Tormen
SZ	Sunyaev-Zel'dovich
tSZ	Thermal Sunyaev-Zel'dovich
WL	Weak Lensing
ΛCDM	Λ Cold Dark Matter

Acknowledgements

The research presented in this thesis can be broadly broken down into two main themes, statistical cosmology and relativistic cosmology. The work presented here is the result of a large number of wonderful discussions with many colleagues and friends. These discussions are not taken for granted and for that I thank you!

First, I would like to thank Dipak Munshi for the three papers we were able to produce together, without this collaboration there would be no thesis! I would also like to thank Peter Coles for the useful discussions and insights on such a wide range of topics. Many thanks must go to Sathya, whose insight, knowledge and mentorship have been very much appreciated, and to Stephen Fairhurst, for his incredible breadth and depth of knowledge and life experiences, as well as to Patrick Sutton and Mark Hannam. I would also like to take the time to thank all the amazing staff in the office whose help and support has been much appreciated throughout my PhD.

Next, I would like to thank all the individuals who have contributed to the second half of the thesis on relativistic cosmology. First and foremost I have to thank Chris Clarkson for the long, useful discussions on the horrors of covariant perturbations in LTB spacetimes. The insight and knowledge I have gained through these exchanges has been irreplaceable. Thank you! I also have to give a huge thanks to the researchers in UCT (especially to Sean February, Anne Marie Nzioki and Alvaro de la Cruz Dombriz) for the scientific exchanges and for such wonderful hospitality, it made my stay in Cape Town unforgettable!

I want to say thank you to both my office mates and all the others in Cardiff who made the department a great place to work. In particular - Ian Harrison, Jo Short, Tom Adams, Duncan Macleod, Ian Harry, Frank Ohme, Laura Nuttall and Andrew Williamson. I have a huge amount of respect for you all and greatly appreciate the downtime we had in Cardiff.

Finally, I must thank my family and friends for the good times and continuous unwavering support. To my Mum and Dad, I cannot begin to thank you enough for all the sacrifices and hard work that you have invested in me over the years. It's a debt I could never hope to repay! To my brothers, Gareth and Andrew, thank you so much for being there and for always being up for a discussion!

Ich möchte mich bei Evi und Gerhard Ramsl für ihre Liebe und Unterstützung bedanken. Ich kann mich nur für ihre Freundlichkeit bedanken. Ein herzliches Dankeschön gilt auch meinen anderen Freunden und Bekannten in Österreich.

Lastly, I have to find a way to thank my partner Patricia Schmidt. This is perhaps one of the toughest acknowledgments to write as I cannot begin to put into words the gratitude I feel for your love and support over these past few years. Without you, I am sure there would be no thesis, you have always been a source of inspiration for me. Thank you so much!

Table of Contents

List of Figures

Chapter 1

The Standard Model of Cosmology

1.1 Introduction

The current standard model of cosmology is based on a Universe that underwent a period of accelerated expansion in the early Universe with the current energy-matter content consisting of baryonic matter (b), radiation (e.g. photons, three generations of sterile neutrino, etc) , cold dark matter (CDM) and dark energy (Λ). This model is refered to as the ΛCDM model and the underlying framework is provided by General Relativity, assuming the Einstein-Hilbert action, and the minimal standard model of particle physics. The ΛCDM model is in good agreement with observational data ranging from the cosmic microwave background (CMB), large scale structure surveys, supernovae observations, gamma ray burst observations and others.

As experiments become ever more precise and new experiments are devised to probe previously unexplored regimes (e.g. gravitational wave observations, CMB polarisation, 21cm cosmology) then it becomes increasingly important to explore and understand the fundamental framework of the standard model of cosmology in a self-consistent manner. General relativity is best described as an effective field theory that is incompatible with quantum theory motivating an entire industry in quantum theories for gravity. Currently Einstein gravity is believed to become an invalid description for gravity above a fundamental energy scale, the Planck scale, $E \gtrsim M_{\rm planck}$. In this regime the standard models of gravity and particle physics break down and it is believed that new physics (e.g. new degrees of freedom or significant changes to the fundamental laws of physics) could become important. Under the ΛCDM model the early Universe initially starts in a high dense state (i.e. big bang models) with an initial, unavoidable, singularity if we assume isotropy and homogeneity in our cosmological model. The presence of this unavoidable high density state implies that our current theories of fundamental physics have limited applicability to the very early Universe. It is very possible that a quantum theory of gravity in the very early Universe could become important at early times and even provide a natural explanation for an inflationary mechanism.

1.2 General Relativity for Cosmology

General Relativity (GR) is a classical theory for gravitation and is a generalisation of special relativity, which itself is based on the notion spacetime as a unifying feature. In GR we treat gravity as a geometric theory intrinsically linked to the curvature of spacetime and that gravitational interactions are just manifestations of the curvature of spacetime itself. In fact, one of the key foundations of GR is that both matter and energy will produce curvature. The link between the way in which energy and matter curve spacetime and the way in which curvature induces gravitational interactions on the energy and matter is specified by the Einstein Field Equations (EFEs), which form a system of second order, non-linear partial differential equations.

GR is primarly based on understanding the geometry of spacetime. The branch of mathematics on which GR is founded is known as *Riemannian Geometry*. In the classical theory of GR, neither the spacetime, nor its topology, are given *a priori*. Instead, we must construct models by specifying a background spacetime that sets the arena for our analysis. This is often done by careful studies, such as the identification of symmetries in the system that may be imposed on the spacetime. An example of this line of reasoning is the study of spherically symmetric solutions within GR in order to model stellar objects or black holes. The natural language to use in GR is that of *Differential Geometry* and as such we will provide a very brief, concise introduction to the core topics. More detailed introductions and explanations may be found in [89; 172; 244; 459; 492; 493; 582].

Definition 1.1. A *spacetime* is defined by the pair $(\mathcal{M}, g)$, where $\mathcal{M}$ is a Lorentzian manifold[1] and g is a pseudo-Riemannian metric on $\mathcal{M}$. Together, this pair forms the fundamental object in GR.

Definition 1.2. The set of all vectors at a point $p \in \mathcal{M}$ form a vector space called the *tangent space* $T_p\mathcal{M}$ and the collection of all tangent spaces on $\mathcal{M}$ is the tangent bundle $T\mathcal{M}$. Similarly, the set of dual vectors, also called *one-forms*, at a point $p \in \mathcal{M}$ forms the *cotangent space* $T^*\mathcal{M}$ where the collection of all cotangent spaces on $\mathcal{M}$ forms the cotangent bundle $T^*\mathcal{M}$.

Definition 1.3. The *metric tensor* is a vital object in the description of curved spacetimes and is conventionally denoted by g_{ab}. Formally, the metric is defined as a symmetric, non-degenerate[2] bilinear form g_p on $T_p\mathcal{M}$ for all $p \in \mathcal{M}$. As the metric is non-degenerate, we can define an inverse metric g^{ab} via

$$g_{ab}g^{bc} = \delta^c_a, \tag{1.1}$$

where g^{ab} inherits the symmetry of g_{ab}. As such, the metric also provides a 1-1 correspondence between vectors and dual vectors, $v_a = g_{ab}v^b$ and $v^a = g^{ab}v_b$. The metric tensor is involved in many important aspects of GR including [89]: 1) causal structure of spacetime; 2) calculating physical distances and proper time along curves; 3) replacing the Newtonian gravitational field ϕ; 4) generalising the notions of a dot product to curved spacetimes. The notion of the metric being a bilinear form simply means that we define a rule that maps two vectors to the real numbers, this is just a statement regarding the generalisation of the inner product to a curved spacetime

$$g(\mathbf{v}, \mathbf{u}) = g(\mathbf{u}, \mathbf{v}) = \mathbf{v} \cdot \mathbf{u}. \tag{1.2}$$

[1] Note that by Lorentzian we just means that metric has a signature of $(-, +, \ldots, +)$.
[2] *Non-degenerate* simply means that $g(\mathbf{v}, \mathbf{u}) = 0$ for all $\mathbf{u}$ iff $\mathbf{v} = 0$

Now, perhaps most importantly, the metric can be used to define a line element ds^2 which can be used to calculate the length of a path in a spacetime. In a given basis, coordinate or general, the metric specifies the line element as follows

$$g(dx, dx) = ds^2 = g_{ab}dx^a dx^b. \tag{1.3}$$

The metric contains all the information needed in order to describe the curvature of the manifold. A general metric is said to be *orthonormal* if

$$g(e_a, e_b) = \eta_{ab} \qquad \eta_{ab} = \text{diag}(-1, 1, 1, 1) \tag{1.4}$$

and in the absence of gravitational fields, the metric simply reduces to that of flat spacetime, the Minkowski metric η_{ab}

$$ds^2_{\text{Minkowski}} = \eta_{ab}dx^a dx^b \qquad \eta_{ab} = \text{diag}(-1, 1, 1, 1). \tag{1.5}$$

Given a vector basis $\{e_a\}$, the components of the metric tensor are specified by

$$g_{ab} = g(e_a, e_b) = e_a \cdot e_b, \tag{1.6}$$

demonstrating how the metric encodes the geometric notions of orthogonality and norm of a vector. The metric assigns a norm or magnitude $|v|^2 = g_{ab}v^a b^b$ to each vector $\mathbf{v} \in T_p\mathcal{M}$. If $g_{ab}v^a u^b = 0$ then v^a and u^a are said to be *orthogonal*.

Definition 1.4. In a curved spacetime we face an additional problem, namely that parallelism breaks down. This arises as, under general coordinate changes, we may have non-trivial basis vectors meaning that as we consider the change in a tensor field moving around a manifold we must take into account both the changes to the tensor components themselves as well as the fact that the basis in which these components are calculated could be changing from point to point. The core problem at work is that there is no natural way to compare vectors at two different points of a manifold unless we introduce additional structure. The structure that we introduce is called the *covariant derivative*. The metric g_{ab} allows us to uniquely identify a unique derivative operator ∇_a that is defined to be metric compatible, i.e. $\nabla_a g_{bc} = 0$. This is called the Levi-Civita connection. Using this definition, the covariant derivative of a vector v^a and a dual vector ω_a are defined as follows

$$\nabla_a v^b = \partial_a v^b + \Gamma^b_{ak} v^k \tag{1.7}$$

$$\nabla_a \omega_b = \partial_a \omega_b - \Gamma^k_{ab} \omega_k \tag{1.8}$$

where the objects Γ^a_{bc} are the Christoffel symbols and are defined by

$$\Gamma^a_{bc} = \frac{1}{2} g^{ad} \left(\partial_c g_{bd} + \partial_b g_{cd} - \partial_d g_{bc} \right). \tag{1.9}$$

The structure of these equations simply correspond to the partial derivative term plus some additional correction where the partial derivative term arises from the change of the vector field from

x^a to $x^a + dx^a$ and the correction term accounts for the change in the basis vectors. If we have a curve $\gamma : I \to \mathcal{M}$ with tangent vector v^a, then the curve will be geodesic iff

$$v^a \nabla_a v^b = f v^b. \tag{1.10}$$

If $f = 0$ then the curve is said to be affinely parameterised. Similarly, a vector field u^a along the curve is said to be parallel transported along the curve γ if

$$v^a \nabla_a u^b = 0. \tag{1.11}$$

An affinely parameterised geodesic is just one for which the tangent vector is parallely transported along itself. The concept of parallel transport is interesting as it provides a framework for understanding how we can move a tensor along a path whilst keeping it constant. In curved spacetimes, parallel transport of a vector from point to point is path dependent.

1.2.0.1 Curvature

The notion of curvature arises by considering the *commutator* of covariant derivatives acting on a vector v^a

$$\nabla_a \nabla_b v^c - \nabla_b \nabla_a v^c = R^c{}_{dab} v^d, \tag{1.12}$$

where $R^c{}_{dab}$ is the Riemann curvature tensor. In local coordinates x^μ the Riemann tensor can be written as

$$R^\mu{}_{\nu\lambda\rho} = \partial_\lambda \Gamma^\mu_{\nu\rho} - \partial_\rho \Gamma^\mu_{\nu\lambda} + \Gamma^\mu_{\lambda\sigma}\Gamma^\sigma_{\nu\rho} - \Gamma^\nu_{\rho\sigma}\Gamma^\sigma_{\nu\lambda}. \tag{1.13}$$

Taking traces of this tensor we can construct the Ricci tensor $R_{ab} = R^c{}_{acb}$ and the Ricci scalar $R = R^a{}_a$.

1.2.0.2 Einstein's Field Equations

The Einstein-Hilbert action for General Relativity is based on the following action:

$$S = \int d^4x \sqrt{-g} \left[\frac{M_{\rm pl}^2}{2} (R - \Lambda) + \mathcal{L}_m \right] \tag{1.14}$$

where we have introduced the reduced Planck mass $M_{\rm pl}^2 = (8\pi G)^{1/2}$. Here $R = R^a_a$ is the Ricci scalar and Λ dark energy. The field equations are defined as functional derivatives with respect to the metric g_{ab}. Einstein gravity is often interpreted as a geometrical theory for gravity with the Einstein field equations describing both how matter moves within a spacetime but also how the presence of matter generates curvature within the spacetime. The Einstein field equations (EFE) are given by:

$$G_{ab} \equiv R_{ab} - \frac{1}{2} g_{ab} R = T_{ab} - \Lambda g_{ab}. \tag{1.15}$$

For convenience, we set the reduced Planck mass, $M_{\rm pl}^2 = (8\pi G)^{-1/2}$, to unity. In the EFE, G_{ab} is known as the Einstein tensor, $R_{ab} = R^c{}_{acb}$ was the previously defined Ricci tensor, T_{ab} is the energy-momentum tensor and Λ is the cosmological constant. The EFE are central to the study of General Relativity describing how gravitational interactions arise as a manifestation of the curvature of spacetime.

1.3 The Friedmann-Walker Universe

The Friedmann-Lemaitre-Robertson-Walker (FLRW) cosmological model is a maximally symmetric, non-static, non-vacuum, spatially homogeneous and isotropic solution to Einstein's field equations described by the following metric [187; 188; 318; 319; 462; 583]:

$$ds^2 = -dt^2 + a^2(t)\left[dr^2 + f_K^2(r)\left(d\theta^2 + \sin^2\theta d\phi^2\right)\right], \tag{1.16}$$

where $f_K(r)$ is a function that depends on the curvature of our three-dimensional spatial hypersurfaces

$$f_K(r) = \begin{cases} K^{-1/2}\,\sin(\sqrt{K}r) & K > 0 \\ r & K = 0 \\ (-K)^{-1/2}\,\sinh(\sqrt{-K}r) & K < 0. \end{cases} \tag{1.17}$$

The function K is the mean spatial curvature of the spatial hypersurfaces. The metric Eq. (1.16) admits a perfect fluid source given by

$$T_{ab} = (\mu + p)\,u_a u_b + p g_{ab}, \tag{1.18}$$

where μ and p are the energy density and pressure of the Universe[3]. Calculating the Einstein tensor for this metric and substituting the energy-momentum tensor into these expressions recovers a system of equations that determines the evolution of the energy density and the scale factor:

$$H^2 = \frac{8\pi G}{3}\mu - \frac{K}{a^2}, \tag{1.19}$$

$$\frac{\ddot{a}}{a} = -\frac{4\pi G}{3}(\mu + 3p) \tag{1.20}$$

$$\dot{\mu} = -3H(\mu + p). \tag{1.21}$$

The first of these equations is the Hamiltonian constraint (the G_{00} term), more commonly known as the *Friedmann equation*. The second of the equations is the *Raychaudhuri equation* governing the acceleration of the scale factor. The last equation is the conservation equation and tells us about the time evolution of the energy density.

[3]Note that the energy density is sometimes labelled by ρ instead of μ, e.g. [566]. We will typically use μ to uphold the conventions of [166].

1.4 Dimensionless Parameters

It is conventional to re-write the Friedmann equations in a dimensionless form by introducing reduced quantities. These are the well known energy density parameters

$$\Omega_{(i)} = \frac{\kappa \mu_{(i)}}{3H^2}, \tag{1.22}$$

where $\mu_{(i)}$ denotes the energy density for a given species of particle. Some of the standard contributions that we will use are

$$\Omega = \frac{\kappa \mu}{3H^2}, \quad \Omega_\Lambda = \frac{\Lambda}{3H^2}, \quad \Omega_K = -\frac{K}{H^2 a^2}, \tag{1.23}$$

where Ω_m denotes non-relativistic matter, Ω_Λ denotes dark energy contributions and Ω_K denotes curvature contributions. By inspection, Friedmann's equation can take the form of a constraint

$$\sum_X \Omega_X + \Omega_\Lambda + \Omega_K = 1. \tag{1.24}$$

In terms of these parameters the function K can be defined by

$$K = H_0^2(\Omega_{m0} + \Omega_{\Lambda_0} - 1) = -H_0^2 \Omega_K. \tag{1.25}$$

We can re-write 1.21 in terms of an equation of state parameter $w = p/\mu$ as follows

$$\frac{d \ln \mu}{d \ln a} = -3(1 + w). \tag{1.26}$$

The solutions to this equation are of the form $\mu \propto a^{-3(1+w)}$. As soon as we fix the equation of state, we can study the redshift evolution of the density parameter for the given form of matter.

$$\Omega_{(i)} = \Omega_{(i),0} \left(\frac{a}{a_0}\right)^{-3(1+w_{X_0})} \left(\frac{H_0}{H}\right)^2 \tag{1.27}$$

Standard Density Parameters in Cosmology

Type of Matter	Equation of State	Density Parameter	Redshift Evolution
Generic	$w = w_X$	Ω_X	$\propto a^{-3(1+w)}$
Relativistic Matter	$w = 1/3$	Ω_r	$\propto a^{-4}$
Non-Relativistic Matter	$w = 0$	Ω_m	$\propto a^{-3}$
Curvature	$w = -1/3$	Ω_K	$\propto a^{-2}$
Cosmological Constant	$w = -1$	Ω_Λ	$\propto a^0$

Using these density parameters we can also introduce a relation for the Hubble parameter

$$E^2(a) = \left(\frac{H(a)}{H_0}\right)^2 = \sum_X \Omega_{X,0} \left(\frac{a}{a_0}\right)^{-3(1+w_X)} + \Omega_{K,0} \left(\frac{a}{a_0}\right)^{-2} + \Omega_{\Lambda,0}. \tag{1.28}$$

Similarly, these parameters can be used to characterise the curvature of the spatial surfaces in an FLRW spacetime.

Curvature in FLRW

$\Omega + \Omega_\Lambda$	Curvature of Spatial Surfaces	K	Ω_K
> 1	Closed	> 0	< 0
$= 1$	Flat	$= 0$	$= 0$
< 1	Open	< 0	> 0

1.5 Distances in Standard Cosmology

There are various possible definitions for distance that we may use in cosmology. In practice, this will often depend on the physical situation at hand and the observational data that we are working with. If we have redshift data available, we can define a comoving radial distance of an object at the given redshift. Alternatively, we may choose to use the comoving transverse size of an object leading to a comoving angular diameter distance. In this section we introduce some key formula for distances and redshift that will be used throughout the thesis.

Definition 1.5. The *comoving radial distance* r, characterises the distance between two points measured along a path between an observer at $r = 0$ out to an object at redshift z by integrating along the radial null geodesic. The form of the metric introduced earlier 1.16 along the Hubble relation given in 1.28 leads to

$$r(z) = \lambda_H \int_0^z \frac{dz'}{E(z')}, \tag{1.29}$$

where, in our convention, a_0 is simply unity. The factor λ_H is the *Hubble distance* and has a numerical value on order $9.26 \times 10^{26}\, h^{-1}\,\mathrm{m}$. Also note that χ is another common variable used to denote the comoving radial distance (e.g. as in [154]) and r to denote a radial coordinate defined by $r_{\mathrm{radial}} = f_K(\chi)$. This should not provide any confusion in this thesis and is simply a matter of convention.

Definition 1.6. The *comoving angular diameter* relates the the comoving transverse size of an object to the solid angle under which it is observed. The definition is given by

$$dS^{\mathrm{com}}_{\mathrm{source}} = R^2_{\mathrm{ang}}(r)\, d\Omega^2_{\mathrm{obs}}. \tag{1.30}$$

The surface area of a comoving sphere centered around $r = 0$ out to a comoving radius r has a surface $S^{(\mathrm{com})} = 4\pi f_K^2(r)$ leading to

$$R_{\mathrm{ang}}(z) = f_K[r(z)]. \tag{1.31}$$

Definition 1.7. The *angular diamter distance* is a generalisation of parallax and is defined as the ratio of the transverse physical size of an object to the solid angle under which it is observed for a geodesic bundle converging at the observer. The angular diamter distance D_A is therefore defined

by

$$D_A(z) = \frac{f_K[r(z)]}{(1+z)}. \tag{1.32}$$

Definition 1.8. Finally, the *luminosity distance* is defined by relating the luminosity of a given source at a comoving radial distance r from the observer to the observed flux. As a result we find

$$D_L(z) = (1+z)\, f_K[r(z)]. \tag{1.33}$$

Chapter 2

Cosmological Random Fields

2.1 Introduction

Cosmology aims to understand the formation, dynamics and phenomenology of structure on large scales. Unfortunately, the language we must use in order to describe cosmological structure is that of statistics. The reasons for this are three-fold. First, the typical sizes we deal with when talking about cosmological structure make it impossible to follow the evolution of all systems. Secondly, when we take into account the timescales over which evolution occurs, it is impossible to follow the dynamical evolution of a single system. Instead we make observations down our past light cone meaning that we observe objects at different times in their evolution. We do not observe across a single spatial hypersurface. Lastly, we do not have direct observational access to the primordial fluctuations that seed cosmological structure. This means that we have no definite initial conditions for deterministic evolution and our resulting model will be statistical in nature, not deterministic.

When we put all these various caveats together, it quickly becomes apparent that the observable Universe should really be modeled as a stochastic realisation of a statistical ensemble. In the vanilla models for inflationary cosmology, the primordial perturbations are seeded as quantum fluctuations of a hypothetical quantum field that drives a period of exponential expansion. These vacuum fluctuations will be highly Gaussian and adiabatic. The fact that the primordial density perturbations are seeded in such a quantum mechanical manner implicitly imply that the stochastic nature of our Universe was set from the very earliest periods. Strictly speaking, the initial conditions for large scale structure are non-Gaussian as nonlinear evolution of the density perturbations leading up to the formation of the CMB will induce non-Gaussianities, even if the initial quantum fluctuations are perfectly Gaussian [450]. This means that the description and statistical understanding of Gaussian random fields and perturbations about Gaussian random fields will be of prime importance.

In the rest of this chapter we introduce a number of concepts that will be vital to later chapters and are vital to a working understanding of modern cosmology. In particular we will introduce the spherical harmonic decomposition, the spherical Fourier-Bessel formalism and various other quantities that are pre-requisite to an understanding of the applications in Chapter 5 and

Chapter 6. A more detailed introduction to some of the concepts used in the description of cosmological random fields can be found in Appendix F.1.1. For now we provide a basic introduction to cosmological random fields.

2.2 Random Fields

2.2.1 Introduction

As outlined above, cosmological random fields form the fundamental objects in the analysis of cosmological phenomena. The statistical and stochastic nature of these fields, however, means that we do not aim to predict the precise locations of galaxies, for example, but rather the average separations of galaxies on a given scale. Much of these notions should be familiar from quantum mechanical arguments in which we do not predict the precise position or momentum of individual particles but rather the statistical distribution of the position and momenta across an ensemble of particles. The perturbations that arise in the early Universe are of a quantum mechanical nature and are therefore treated as stochastic random fields.

2.2.2 3D Random Fields

A perturbation evaluated at some time t can be described as a *random variable* $f(\mathbf{x})$ corresponding to the assignment of a real value to an element $\mathbf{x} \in \mathbb{R}$ according to a probability density function $P[f(\mathbf{x})]$, i.e. each point $f(\mathbf{x})$ is a real number. Here, $P[f(\mathbf{x})]$ is a functional that gives the probability of yielding some field configuration. A *random field* is formed from a set of N random variables $f(\mathbf{x}_i)$ for which $\mathbf{x}_i \in \mathbb{R}^n$ according to some joint probability distribution. The set of functions is referred to as an *ensemble* and each individual function is a *realisation* of the ensemble.

Correlators of the fields are the expectation values of products of the field at different spatial points and, in general, times. The two-point correlator is defined by

$$\xi(\mathbf{x},\mathbf{y}) = \langle f(\mathbf{x}) f(\mathbf{y})\rangle = \int \mathcal{D}f\, P[f]\, f(\mathbf{x})\, f(\mathbf{y}), \tag{2.1}$$

where the integral is defined as path integral over the field configurations. Alternatively, we can choose to work in the Fourier domain instead of the spatial domain. Adopting the symmetric Fourier convention, we have

$$f(\mathbf{x}) = \int \frac{d^3\mathbf{k}}{(2\pi)^{3/2}}\, f(\mathbf{k})\, e^{-i\,\mathbf{k}\cdot\mathbf{x}} \tag{2.2}$$

$$f(\mathbf{k}) = \int \frac{d^3\mathbf{x}}{(2\pi)^{3/2}}\, f(\mathbf{x})\, e^{+i\,\mathbf{k}\cdot\mathbf{x}}. \tag{2.3}$$

For real fields, we also have the hermiticity constraint $f(\mathbf{k}) = f^*(-\mathbf{k})$. Using these definitions we can introduce the Fourier domain two point correlation function

$$\langle f(\mathbf{k})\, f^*(\mathbf{k}')\rangle = P_f(k)\, \delta_D(k-k') \tag{2.4}$$

$$= \frac{2\pi^2}{k^3}\mathcal{P}_f(k)\, \delta_D(k-k'), \tag{2.5}$$

where $\mathcal{P}_f(k)$ is the dimensionless power spectrum, given that $f(\mathbf{x})$ is dimensionless. The spatial two-point correlation function can therefore be expressed in terms of the Fourier space two point correlator as follows

$$\xi(\mathbf{x},\mathbf{y}) = \langle f(\mathbf{x}) f(\mathbf{y})\rangle = \int \frac{d^3\mathbf{k}}{(2\pi)^{3/2}} \int \frac{d^3\mathbf{k}'}{(2\pi)^{3/2}} \langle f(\mathbf{k}) f^*(\mathbf{k}')\rangle \, e^{i\,\mathbf{k}\cdot\mathbf{x}}\, e^{-i\,\mathbf{k}'\cdot\mathbf{y}} \tag{2.6}$$

$$= \frac{1}{4\pi} \int \frac{dk}{k}\, \mathcal{P}_f(k) \int d\Omega_k\, e^{i\mathbf{k}\cdot(\mathbf{x}-\mathbf{y})}, \tag{2.7}$$

where we have simply substituted for the definition of the two point correlator, as per Eq. (2.5), and integrated over the delta function. We can proceed further by performing an angular integration over a variable μ defined by $\mathbf{k}\cdot(\mathbf{x}-\mathbf{y}) = \mu k\,|\mathbf{x}-\mathbf{y}|$. The angular integration reduces to the following expression

$$2\pi \int_{-1}^{+1} d\mu\, e^{ik\mu|\mathbf{x}-\mathbf{y}|} = 4\pi\, j_0(k|\mathbf{x}-\mathbf{y}|), \tag{2.8}$$

where $j_0(x) = \sin(x)/x$. Finally, the two-point correlation function is given by

$$\xi(\mathbf{x},\mathbf{y}) = \int \frac{dk}{k}\, \mathcal{P}_f(k)\, j_0(k|\mathbf{x}-\mathbf{y}|), \tag{2.9}$$

and the variance by

$$\sigma^2 = \xi(0) = \int \frac{dk}{k}\, \mathcal{P}_f(k). \tag{2.10}$$

In addition to the two point correlation function, we may define higher order correlators in a logical way. For example, the *bispectrum* or three point correlation function is defined by

$$\langle f(\mathbf{k}_1) f(\mathbf{k}_2) f(\mathbf{k}_3)\rangle = (2\pi)^3\, B(\mathbf{k}_1,\mathbf{k}_2,\mathbf{k}_3)\, \delta_D(\mathbf{k}_1+\mathbf{k}_2+\mathbf{k}_3) \tag{2.11}$$

and the *trispectrum* or four point correlation function is defined by

$$\langle f(\mathbf{k}_1) f(\mathbf{k}_2) f(\mathbf{k}_3) f(\mathbf{k}_4)\rangle = (2\pi)^3\, T(\mathbf{k}_1,\mathbf{k}_2,\mathbf{k}_3,\mathbf{k}_4)\, \delta_D(\mathbf{k}_1+\mathbf{k}_2+\mathbf{k}_3+\mathbf{k}_4). \tag{2.12}$$

A random field will be defined by the infinite hierarchy of such polyspectra but in reality we tend to focus on the lowest order polyspectra as a probe of the random field.

2.2.3 Gaussian Random Fields

One of the most important classes of random fields that occur in cosmology and statistics is that of the Gaussian random field (GRF). This is a very special field that is completely characterised by it's power spectrum or, equivalently, by it's two point correlation function. The multivariate joint probability distribution function for the Gaussian random field has the form

$$P\,[f_1,\ldots,f_N]\, df_1,\ldots,df_N = \frac{1}{\sqrt{(2\pi)^N \det\sigma}} \exp\left[-\frac{1}{2}\sum_{ab} f_a \sigma^{-1}_{ab} f_b\right] df_1,\ldots,df_N, \tag{2.13}$$

where σ_{ab} is the covariance matrix constructed from $\langle f_a f_b \rangle$. An important result of the Gaussian random field is that all odd correlators vanish, as $\langle f \rangle = 0$ can always be enforced, and all even correlators factorise into products of the two point correlation function. This is why the power spectrum completely characterises a Gaussian random field. Subsequently, the bispectrum is the lowest order correlator for which a non-zero measurement would signify some departure from Gaussianity. This is also why statistical predictions for the shape and amplitude of the bispectrum from theoretical models has received a lot of attention.

2.2.4 Smoothed Random Fields

In making the transition from the mathematical framework describing the statistical properties of random fields to real world observations, we must take into account the finite resolution available to us. Typically this means that we are not interested in observations of a random field below some smoothing scale R. In cosmology, it is very common to deal with a random field smoothed by a window function $W_R(\mathbf{x})$ rather than the underlying field itself

$$\tilde{f}(\mathbf{x}) = \int d^3\mathbf{x}' \, W_R(\mathbf{x}' - \mathbf{x}) f(\mathbf{x}). \tag{2.14}$$

A prototypical smoothing function is the Gaussian filter

$$W_R(x) = \exp\left(-\frac{x^2}{2}\right) \; ; \quad x = kR, \tag{2.15}$$

though we may choose normalise the window function such that $\int d^3x W_R(x) = 1$.

2.3 Spherical Harmonics

The spherical harmonics have a special place in cosmology. These functions are defined as the eigenfunctions of the Laplacian on S^2 and can therefore be used as a complete set of basis functions on the sphere. This means that any cosmological observable on the sky can be decomposed into a 2-dimensional projection onto the sky via these harmonics. This is exactly the situation encountered in studies of the CMB and tomographic analysis of large scale structure. In this section we gather some core definitions and relationships that will be crucial to the analysis presented later and, whilst being part of the standard literature in cosmology, should serve as a self-contained reference to the material in this thesis.

2.3.1 Definition

The spherical harmonics $Y(\theta, \varphi)$ can be defined in terms of Legendre polynomials $P_{\ell m}$ as follows

$$Y(\theta, \varphi) = (-1)^m \sqrt{\frac{(2\ell + 1)(\ell - m)!}{4\pi(\ell + m)!}} \, P_{\ell m}(\cos\theta) \, e^{im\varphi}, \tag{2.16}$$

where the Legendre polynomials are defined by

$$P_{\ell m}(x) = \frac{\left(1-x^2\right)^{m/2}}{2^\ell \ell!} \frac{d^{\ell+m}}{dx^{\ell+m}} \left[x^2-1\right]^\ell. \tag{2.17}$$

The are the position space representation of the eigenstates of the momentum operators $\hat{L}^2 = -\nabla^2$ and $\hat{L}_z = -i\partial_\varphi$:

$$\nabla^2 Y_{\ell m} = -\ell\,(\ell+1)\; Y_{\ell m} \tag{2.18}$$

$$\partial_\varphi Y_{\ell m} = im\, Y_{\ell m}, \tag{2.19}$$

such that $\ell \geq 0$ and $|m| \leq \ell$. The spherical harmonics form a complete orthonormal set of complex valued basis functions on the sphere. These harmonics are something of the spherical analogue to the Cartesian Fourier expansion. In the flat sky limit, the eigenfunctions to the Laplacian $\nabla^2\psi = 0$ are plane wave solutions of the form $\propto e^{i\mathbf{k}\cdot\mathbf{x}}$.

2.3.2 Orthogonality and Completeness

In the usual convention adopted in cosmology, the spherical harmonics form a set of orthonormal basis functions

$$\int Y_{\ell m}(\Omega)\, Y^*_{\ell' m'}(\Omega') d\,\Omega = \delta^{\mathrm{K}}_{\ell\ell'}\, \delta^{\mathrm{K}}_{mm'} \tag{2.20}$$

leading to a closure relation

$$\sum_{\ell m} Y_{\ell m}(\Omega)\, Y_{\ell m}(\Omega') = \delta_{2D}(\Omega - \Omega'). \tag{2.21}$$

2.3.3 Functions on the Sphere

We are now in a position where we can expand a random field on the 2-sphere S^2. The eigenfunctions to the Laplacian on S^2 are the spherical harmonics $Y_{\ell m}$. The coordinates on the sphere are given by $\hat{\Omega} = (\theta, \phi)$.

Definition 2.1. The *spherical harmonic expansion* of a square integrable function is given by

$$f(\hat{\Omega}) = \sum_{\ell m} f_{\ell m}\, Y_{\ell m}(\hat{\Omega}) \tag{2.22}$$

with an inverse transformation given by

$$f_{\ell m} = \int d\hat{\Omega}\, f(\hat{\Omega})\, Y^*_{\ell m}(\hat{\Omega}). \tag{2.23}$$

Definition 2.2. The *2D angular power spectrum* is defined by the 2-point correlation function

$$\langle f_{\ell m} f^*_{\ell' m'} \rangle = \delta_{\ell\ell'}\, \delta_{mm'}\, \mathcal{C}_\ell. \tag{2.24}$$

Definition 2.3. Similarly, the *angular bispectrum* is defined by the 3-point correlation function

$$\langle f_{\ell_1 m_1}\, f_{\ell_2 m_m}\, f_{\ell_3 m_3}\rangle = \begin{pmatrix} j_1 & j_2 & j_3 \\ m_1 & m_2 & m_3 \end{pmatrix} B_{\ell_1 \ell_2 \ell_3}, \tag{2.25}$$

where the term in brackets is the Wigner-$3j$ symbol discussed shortly in Section 2.5.

2.4 Spherical Fourier-Bessel Expansion

In this section we introduce an extension to the Cartesian Fourier and spherical harmonic analysis presented previously. In cosmology, spherical coordinates are often a very natural choice as they can be, by an appropriate choice of basis, be used to place an observer at the origin of the analysis. Many upcoming cosmological surveys, such as wide-field BAO and LSS surveys, will provide both large and deep coverage of the sky demanding a simultaneous treatment of both the extended radial coverage as well as the spherical sky geometry. For such surveys, the spherical Fourier-Bessel (sFB) formalism provides a natural decomposition. This formalism will be introduced and used extensively in Chapter 5 and Chapter 6. We leave more detailed comments and analysis of the formalism to these chapters. Here, we just wish to provide a schematic and functional overview of the sFB formalism and some of the key results.

The Laplacian in 3D spherical coordinates $\mathbf{r} = \{r, \theta, \varphi\}$ may be decomposed into an angular and a radial component as follows

$$\nabla^2 = \nabla_r^2 + \frac{1}{r^2}\nabla_\Omega^2, \tag{2.26}$$

where r is the comoving radial distance and Ω correspond to the 2D angular coordinates $\{\theta, \varphi\}$. The radial part of the Laplacian is given by

$$\nabla_r^2 = \frac{1}{r^2}\frac{\partial}{\partial r}\left[r^2 \frac{\partial}{\partial r}\right] \tag{2.27}$$

and the angular part is given by

$$\nabla_\Omega^2 = \frac{1}{\sin\theta}\frac{\partial}{\partial\theta}\left[\sin\theta \frac{\partial}{\partial\theta}\right] + \frac{1}{\sin\theta}\frac{\partial^2}{\partial\varphi^2} \tag{2.28}$$

The spherical Fourier-Bessel (sFB) formalism works by assuming that the 3D function in question may be decomposed into a product of an angular and a radial function. We consider an arbitrary 3D homogeneous and isotropic random field $\Psi(\mathbf{r})$ and decompose the function into its radial and angular terms

$$\Psi(\hat{\Omega}, r) = R(r)\,\Phi(\Omega). \tag{2.29}$$

The Helmholtz equation in spherical coordinates may therefore be written as

$$\nabla^2\Psi = -k^2\Psi \tag{2.30}$$

$$\nabla_r^2 \Psi + \frac{1}{r^2} \nabla_\Omega^2 \Psi = -k^2 \Psi. \tag{2.31}$$

The solution to the angular sector is simply the standard spherical harmonic

$$\Phi(\Omega) = Y_{\ell m}(\Omega), \tag{2.32}$$

where the Laplacian acting on the spherical harmonic obeys the relation

$$\nabla_\Omega^2 Y_{\ell m}(\Omega) = -\ell\,(\ell+1)\, Y_{\ell m}(\Omega). \tag{2.33}$$

The radial function is determined by the following equation

$$\frac{1}{r^2} \frac{\partial}{\partial r} \left[r^2 \frac{\partial}{\partial r} \right] R + \left[k^2 - \frac{\ell\,(\ell+1)}{r^2} \right] R = 0, \tag{2.34}$$

which has a non-singular solution of the form

$$R(r) = j_\ell(r), \tag{2.35}$$

where $j_\ell(r)$ is the standard spherical Bessel function of order ℓ. This may be related the normal Bessel functions by $j_\ell(r) = \sqrt{\pi/(2r)}\, J_{\ell+\frac{1}{2}}(r)$ but for our purposes the spherical Bessel functions will be most convenient. The eigenfunctions to the 3D Laplacian in spherical coordinates are therefore products of spherical harmonics and spherical Bessel functions, $Y_{\ell m}(\Omega)\, j_\ell(r)$, with an eigenvalue of $-k^2$. Putting this together, we can construct normalised basis functions for the sFB transformations

$$Z_{k\ell m}(\Omega, r) = \sqrt{\frac{2}{\pi}}\, k\, j_\ell(kr)\, Y_{\ell m}(\Omega). \tag{2.36}$$

It should be noted that, in general, the radial eigenfunctions are ultra-spherical Bessel functions but when the spatial curvature of the Universe is small, they can be well approximated by spherical Bessel functions. This is the approach we adopt. The sFB decomposition of a 3D homogeneous and isotropic random field is given by

Definition 2.4. The *spherical Fourier-Bessel decomposition* of a random field Ψ is defined by

$$\Psi(\Omega, r) = \int dk \sum_{\{\ell m\}} \Psi_{\ell m}(k)\, Z_{k\ell m}(\Omega, r) \tag{2.37}$$

with an inverse relation

$$\Psi_{\ell m}(k) = \int d^3\mathbf{r}\, \Psi(\mathbf{r})\, Z^*_{k\ell m}(\Omega, r). \tag{2.38}$$

In our notation, $\{\ell, m\}$ are the normal quantum numbers and k is the wavenumber or momenta. This formalism can be extended to finite surveys where the wavenumbers become discrete case but we defer that discussion to Section 5.6.3.

2.4.1 Homogeneous and Isotropic 3D Random Field

We now consider a 3D statistically homogeneous and isotropic random field $\Psi(\mathbf{r}; r)$ defined at a time instant r. When appearing after the semi-colon, the r dependence is simply an expression of the time-dependence of the function. Remember, the transform of a field at a distance r corresponds to the transform of the homogeneous field everywhere on a single hypersurface defined at a time equal to the time the observed light left the source. The coefficients of our expansion depend on the look back time of the observation and hence on the distance itself. This is simply a statement equivalent to the fact that cosmological observations are down our past light cone and not on the spacelike hypersurface defined at a time t. We use the comoving distance r as a measure of the cosmological time t. The power spectrum of the 3D homogeneous and isotropic field at a time r is defined by

$$\langle \Psi_{\ell m}(k; r)\, \Psi^*_{\ell' m'}(k'; r)\rangle = \mathcal{C}_\ell^{\Psi\Psi}(k; r)\, \delta_D(k - k')\, \delta_{\ell\ell'}\, \delta_{mm'}. \tag{2.39}$$

In the homogeneous case, the power spectrum is independent of ℓ and collapses to $\mathcal{C}_\ell(k; r) = P(k; r)$, where $P(k; r)$ is the standard Cartesian Fourier power spectrum. The 3D Fourier expansion of the field $\Psi(\mathbf{r}; r)$ is given by

$$\langle \Psi(\mathbf{k}; r)\Psi^*(\mathbf{k}'; r)\rangle = (2\pi)^3 P(k; r)\delta_D^3(\mathbf{k} - \mathbf{k}'). \tag{2.40}$$

Given that the 3D Fourier expansion is denoted by

$$\Psi(\mathbf{r}; r) = \frac{1}{(2\pi)^3} \int d^3\mathbf{k}\, \Psi(\mathbf{k}; r)\, e^{i\mathbf{k}\cdot\mathbf{r}} \tag{2.41}$$

and that we have the Rayleigh expansion of the exponential

$$e^{i\mathbf{k}\cdot\mathbf{r}} = 4\pi \sum_{\{\ell m\}} i^\ell\, j_\ell(kr)\, Y_{\ell m}(\Omega_k)\, Y_{\ell m}(\Omega), \tag{2.42}$$

we can construct a relation between the Fourier coefficients and the sFB coefficients by inserting the Rayleigh expansion into the Fourier expansion. Using that $d^3k = k^2 d\Omega_k\, dk$, we find that

$$\Psi_{\ell m}(k; r) = \frac{1}{\sqrt{8\pi^3}}\, k\, i^\ell \int d\Omega_k\, \Psi(\mathbf{k}; r)\, Y_{\ell m}(\Omega_k). \tag{2.43}$$

As well as calculating the power spectrum of the field at a given time, we can also evaluate the coefficients of the fields at two different times r and r' to effectively calculate a cross-power spectrum of two different homogeneous fields $\Psi(\mathbf{r}; r)$ and $\Psi(\mathbf{r}'; r')$. Assuming that homogeneity and isotropy still hold the cross-spectra reduces to

$$\langle \Psi_{\ell m}(k; r)\Psi^*_{\ell' m'}(k'; r')\rangle = \mathcal{C}_\ell(k; r, r')\, \delta_D(k - k')\, \delta_{\ell\ell'}\, \delta_{mm'}. \tag{2.44}$$

The homogeneity of the field means that the Fourier identity still holds and $\mathcal{C}_\ell(k; r, r') = P(k; r, r')$. For many of the cosmological fields that we consider, the correlations of the field are reasonably localised in the sense that correlations become negligible for sufficiently large separations and the

only significant contributions arise from small scales. Typically $|\mathbf{r} - \mathbf{r}'| \lesssim 150\text{Mpc}$. Over such a scale, the cosmological times are approximately equal and we can make the approximation that $\mathbf{r} \sim \mathbf{r}'$ and hence that the power spectrum is calculated on the same spatial hypersurface [90]. The general form for the power spectrum adopted is

$$P(k; r, r') \simeq \sqrt{P(k; r)\, P(k; r')}. \tag{2.45}$$

Following [90], we adopt the geometric mean of the power spectra rather than choosing one power spectra or the other. This allows us to split the integral into two internal integrals which reduces the computation time of the problem at hand.

2.4.2 Inhomogeneous 3D Random Field

In the case where the random field is inhomogeneous in 3D space but the 2D projection retains the homogeneous and isotropic characteristics, then the sFB power spectrum does not collapse down to the Cartesian Fourier power spectrum. This scenario can occur when the random field at question, for instance, depends on a line of sight integral from the source to us. This is the case for weak lensing which is often considered a 2D radial projection of the underlying 3D gravitational potential. In reality, it is given by the 2D projection at each source at a distance of r of the gravitational potential along the line of sight. This means that it maintains the 2D homogeneity and isotropy but it does not have such a property in the radial direction. The density field, however, is a genuine 3D homogeneous and isotropic random field. Now, the power spectrum at two different distances for an inhomogeneous field is given by

$$\langle \Psi_{\ell m}(k; r) \Psi^*_{\ell' m'}(k'; r') \rangle = \mathcal{C}_\ell(k, k')\, \delta_{\ell\ell'}\, \delta_{mm'}. \tag{2.46}$$

In such a scenario, the power spectrum does not reduce down to its Fourier counterpart.

2.4.3 Cross-Correlating 3D Random Fields

We can study the cross-correlation of two different random fields in the sFB formalism by using the same approach as previously but for two fields Ψ and Φ. The cross-spectra is given by

$$\langle \Psi_{\ell m}(k; r) \Phi^*_{\ell' m'}(k'; r') \rangle = \mathcal{C}_\ell^{\Psi\Phi}(k, k')\, \delta_{\ell\ell'}\, \delta_{mm'}. \tag{2.47}$$

Such cross-correlations are becoming increasingly important in modern cosmology due to the astrophysical and cosmological information probed by different observables. This will be the case in Chapter 6.

2.4.4 Projected 2D Random Field

We can extend this formalism to studies that include a 2D projected field $\psi(\hat{\Omega})$ that samples some underlying 3D field $\Psi(\mathbf{r})$ according to some arbitrary weight function $w_\psi(r)$

$$\psi(\hat{\Omega}) = \int dr\, w_\psi(r)\, \Psi(\mathbf{r}). \tag{2.48}$$

In order to derive the underlying harmonics we first perform a 2D decomposition of the field and then perform a spectral decomposition of the underlying 3D fields in the sFB formalism.

$$\begin{aligned}
\psi_{\ell m} &= \int d\Omega\, Y^*_{\ell m}(\hat{\Omega})\, y(\hat{\Omega}) && (2.49)\\
&= \int d\Omega\, Y^*_{\ell m}(\Omega) \left[\int_0^\infty dr\, w_\psi(r)\, \Psi(\mathbf{r})\right] && (2.50)\\
&= \int d\Omega\, Y^*_{\ell m}(\Omega) \left[\int_0^\infty dr w_\psi(r) \sqrt{\frac{2}{\pi}} \int k dk \sum_{\{\ell' m'\}} Y_{\ell' m'}(\Omega) \Psi_{\ell' m'}(k;r)\, j_{\ell'}(kr)\right] && (2.51)\\
&= \int d\Omega \left[\sum_{\{\ell m\}} Y^*_{\ell m}(\Omega)\, Y_{\ell' m'}(\Omega)\right] \int_0^\infty dr\, w_\psi(r) \sqrt{\frac{2}{\pi}} \int k dk\, \Psi_{\ell' m'}(k;r) j_{\ell'}(kr) && (2.52)\\
&= \int_0^\infty dr\, w_\psi(r) \sqrt{\frac{2}{\pi}} \int k\, dk\, j_\ell(kr)\, \Psi_{\ell m}(k;r). && (2.53)
\end{aligned}$$

To make last the step to 2.53, we used the spherical harmonic orthogonality relation as per equation 2.20. The sFB harmonics associated with a projected 2D field sampling an underlying 3D field according to the window function $w_\psi(r)$ is therefore

$$\psi_{\ell m} = \sqrt{\frac{2}{\pi}} \int_0^\infty dr\, w_\psi(r) \int dk\, k\, j_\ell(kr)\, \Psi_{\ell m}(k;r). \tag{2.54}$$

From this representation we can construct the power spectra and related cross-correlation spectra of a 2D projected field with other 2D projected fields of 3D fields. The cross-correlation of a 2D projected field $\psi_{\ell m}$ with another 2D projected field $\varphi_{\ell m}$ yields the following angular spectra

$$\langle \psi_{\ell m} \varphi^*_{\ell' m'} \rangle = \mathcal{C}_\ell^{\psi\varphi} \delta_{\ell\ell'} \delta_{mm'}. \tag{2.55}$$

Similarly, the cross-correlation of a 2D projected field $\psi_{\ell m}$ with a 3D field $\phi_{\ell m}$ yields

$$\langle \phi_{\ell m}(k) \psi^*_{\ell' m'} \rangle = \mathcal{C}_\ell^{\phi m}(k) \delta_{\ell\ell'} \delta_{mm'}. \tag{2.56}$$

2.4.5 Spin-s 3D Random Field

Up to this point we have only dealt with scalar fields, which are spin-0 quantities. The spherical Fourier-Bessel formalism may be extended to fields of arbitrary spin-s, generalising our results. Specific spin-weighted fields that will be of interest later in the thesis are the shear and flexion fields found in 3D weak lensing. The spectral decomposition of such fields necessitates the in-

troduction of a set of 3D basis functions that are constructed from products of the spin-weighted spherical harmonics ${}_sY_{\ell m}(\hat{\Omega})$ on the sphere and the radial spherical Bessel functions $j_\ell(kr)$. As we will see, an expansion in the spin-weighted basis can also be related to a scalar function through the use of spin-lowering and spin-raising operators. As before, the spherical coordinates provide a natural choice for the eigendecomposition of spin-weighted functions, providing a clear separation in terms of radial and spherical harmonic modes. Extending the definition of the spin-0 eigenfunctions $Z_{k\ell m}(r)$, we introduce the spin-s eigenfunctions

$$ {}_sZ_{k\ell m}(\mathbf{r}) = \sqrt{\frac{2}{\pi}}\, k\, j_\ell(kr)\, {}_sY_{\ell m}(\hat{\Omega}). \tag{2.57} $$

We briefly want to say a few words on the spin-weighted spherical harmonics in order to set the notation and provide some useful relations. The spin weighted spherical harmonics are defined in terms of the Wigner D-matrices

$$ {}_sY_{\ell m}(\hat{\Omega}) = \sqrt{\frac{2\ell+1}{4\pi}}\, D^{\ell}_{-s,m}\left(\theta,\phi,0\right). \tag{2.58} $$

The Wigner D-matrices were originally introduced in quantum mechanics as an eigenfunction of the Hamiltonian for spherical and symmetric rigid rotors. The matrix is intrinsically connected to the irreducible representation of the $SU(2)$ and $SO(3)$ groups.

Definition 2.5. The *Wigner D-matrices* are defined by

$$ D^{j}_{mm'}\left(\alpha,\beta,\gamma\right) = \exp(-im'\alpha)\, d^{j}_{m'm} \exp(-im\gamma), \tag{2.59} $$

where $\{\alpha,\beta,\gamma\}$ are *Euler angles* and *Wigner's small d-matrix* is defined by the following expression

$$ d^{j}_{m'm} = \left[(j+m)!\,(j-m)!\,(j+m)!\,(j-m)!\right]^{1/2} \sum_s \frac{(-1)^{m'-m+s}}{(j+m-s)!s!\,(m'-m+s)!\,(j-m'-s)!} \tag{2.60} $$

$$ \times \left[\cos\left(\frac{\beta}{2}\right)\right]^{2j+m-m'-2s} \left[\sin\left(\frac{\beta}{2}\right)\right]^{m'+2s-m}. $$

These formula make assumptions about the order and structure of rotations around the Euler angles. The Euler angles are simply a way of representing the orientation of a reference frame with respect to a known, fixed original frame. In our convention we assume the zyz rotation operation. This simply means that the Euler angles correspond to a rotation around the z axis by α, a rotation around the y' axis by β and a final rotation about the z'' axis by γ. The Wigner D matrices form a complete set of orthonormal functions of the Euler angles $\{\alpha,\beta,\gamma\}$

$$ \int_0^{2\pi} d\alpha \int_0^{\pi} \sin\beta\, d\beta \int_0^{2\pi} d\gamma\, D^{j}_{mk}(\alpha,\beta,\gamma)\, D^{j'}_{m'k'}(\alpha,\beta,\gamma) = \frac{8\pi^2}{2j+1}\delta_{jj'}\delta_{mm'}\delta_{kk'}. \tag{2.61} $$

Having defined the spin weighted spherical harmonics and the appropriate functions, we generalise the orthogonality relationship of the spin-0 spherical harmonics to spherical harmonics of

spin-s

$$\int d\hat{\Omega}\ \left[{}_sY_{\ell m}(\hat{\Omega})\right]\ \left[{}_{s'}Y_{\ell' m'}(\hat{\Omega})\right]\ \left[{}_{s''}Y_{\ell'' m''}(\hat{\Omega})\right] = \sqrt{\frac{(2\ell+1)(2\ell'+1)(2\ell''+1)}{4\pi}} \begin{pmatrix} \ell & \ell' & \ell'' \\ m & m' & m'' \end{pmatrix} \times \begin{pmatrix} \ell & \ell' & \ell'' \\ -s & -s' & -s'' \end{pmatrix}. \tag{2.62}$$

where the terms in brackets are the Wigner-3j symbols that will be discussed in Section 2.5. The completeness relations for the spin weighted spherical harmonics can be shown to obey

$$\sum_{\ell m} \left[{}_sY_{\ell m}(\hat{\Omega})\right]\ \left[{}_sY_{\ell m}(\hat{\Omega}')\right] = \delta_D\left(\hat{\Omega}-\hat{\Omega}'\right), \tag{2.63}$$

and the complex conjugate of a spin-s harmonics is given by

$${}_sY^*_{\ell m} = (-1)^m\ {}_{-s}Y_{\ell -m}(\hat{\Omega}). \tag{2.64}$$

With all this machinery in place, the spin weighted spherical Fourier-Bessel decomposition can be written as

$${}_s\psi(\mathbf{r}) = \int_0^\infty dk \sum_{\{\ell m\}} \left[{}_s\psi_{\ell m}\right]\ \left[{}_sZ_{k\ell m}(\mathbf{r})\right] \tag{2.65}$$

$${}_s\psi_{\ell m}(k) = \int d^3\mathbf{r}\ \left[{}_s\psi(\mathbf{r})\right]\ \left[{}_sZ^*_{k\ell m}(\mathbf{r})\right]. \tag{2.66}$$

We now wish to introduce one final concept that will be vital in linking a field of spin-s to a field of spin-s', namely the spin-raising and spin-lowering operators. The spin raising operator, or edth, $\eth$ is a geometric operator that can be defined as a totally projected covariant derivative with respect to a null-tetrad defined on the 2-surface (see Section C.0.1 for a more detailed treatment). The operator $\eth$ acts as a spin raising operator on the quantum number s and its complex conjugate $\bar{\eth}$ acts as a spin lowering operator

$$\eth\ \left[{}_sY_{\ell m}\right] = \left[(\ell-s)\ (\ell+s+1)\right]^{1/2}\ \left[{}_{s+1}Y_{\ell m}\right] \tag{2.67}$$

$$\bar{\eth}\ \left[{}_sY_{\ell m}\right] = -\left[(\ell+s)\ (\ell-s+1)\right]^{1/2}\ \left[{}_{s-1}Y_{\ell m}\right] \tag{2.68}$$

The spin weighted spherical harmonics are eigenfunctions of the operator $\eth\,\bar{\eth}$

$$\bar{\eth}\,\eth\ \left[{}_sY_{\ell m}\right] = -\left(\ell-s\right)\left(\ell+s+1\right)\ \left[{}_sY_{\ell m}\right] \tag{2.69}$$

$$\eth\,\bar{\eth}\ \left[{}_sY_{\ell m}\right] = -\left(\ell+s\right)\left(\ell-s+1\right)\ \left[{}_sY_{\ell m}\right]. \tag{2.70}$$

Using these relations, we can map the scalar spherical harmonics onto the spin-2 spherical harmonics as follows

$$\eth\,\eth\,Y_{\ell m} = \sqrt{\frac{(\ell+2)!}{(\ell-2)!}}\left[{}_2Y_{\ell m}\right] \qquad \bar{\eth}\,\bar{\eth}\,Y_{\ell m} = \sqrt{\frac{(\ell+2)!}{(\ell-2)!}}\left[{}_{-2}Y_{\ell m}\right] \tag{2.71}$$

These functions will be particularly useful when decomposing a complex valued spin-2 field into two scalar real functions that can be shown to correspond to the even and odd parity components of the spin-2 field.

2.5 Wigner $3j$ Symbols

The Wigner matrices are some of the stranger objects that are typically encountered in statistical cosmology. In essence, these matrices are just rescalings of the Clebsch-Gordan coefficients, placing all multipoles on an equal footing. The matrix essentially describes the quantum mechanical coupling of two angular momentum eigenstates into a third eigenstate.

Definition 2.6. The *Wigner* $3j$ *symbol* can be defined by its relation to the Clebsch-Gordan coefficient $\langle \ell_1, \ell_2, m_1, m_2 | \ell_3, m_3 \rangle$

$$\begin{pmatrix} \ell_1 & \ell_2 & \ell_3 \\ m_1 & m_2 & m_3 \end{pmatrix} = (-1)^{-\ell_1+\ell_2+m_3} \left[2\ell_3+1\right]^{-1/2} \langle \ell_1, \ell_2, m_1, m_2 | \ell_3, m_3 \rangle. \tag{2.72}$$

This symbol obeys a number of useful symmetry properties:

$$\begin{pmatrix} \ell_1 & \ell_2 & \ell_3 \\ m_1 & m_2 & m_3 \end{pmatrix} = (-1)^{\ell_1+\ell_2+\ell_3} \begin{pmatrix} \ell_1 & \ell_3 & \ell_2 \\ m_1 & m_3 & m_2 \end{pmatrix} \tag{2.73}$$

$$= (-1)^{\ell_1+\ell_2+\ell_3} \begin{pmatrix} \ell_2 & \ell_1 & \ell_3 \\ m_2 & m_1 & m_3 \end{pmatrix} \tag{2.74}$$

$$= (-1)^{\ell_1+\ell_2+\ell_3} \begin{pmatrix} \ell_1 & \ell_2 & \ell_3 \\ -m_1 & -m_2 & -m_3 \end{pmatrix}. \tag{2.75}$$

Some of the main identities associated to this matrix that we will abuse are given by the orthogonality of the $3j$ symbols

$$\sum_{\ell_3 m_3} (2\ell_3+1) \begin{pmatrix} \ell_1 & \ell_2 & \ell_3 \\ m_1 & m_2 & m_3 \end{pmatrix} \begin{pmatrix} \ell_1 & \ell_2 & \ell \\ m_1' & m_2' & m \end{pmatrix} = \delta^K_{m_1 m_1'} \delta^K_{m_2 m_2'} \tag{2.76}$$

$$\sum_{m_1 m_2} (2\ell_3+1) \begin{pmatrix} \ell_1 & \ell_2 & \ell_3 \\ m_1 & m_2 & m_3 \end{pmatrix} \begin{pmatrix} \ell_1 & \ell_2 & \ell_3' \\ m_1 & m_2 & m_3' \end{pmatrix} = \delta^K_{m m'} \delta^K_{\ell \ell'}. \tag{2.77}$$

Finally, we introduce the Gaunt integral which is defined as the overlap of three spherical harmonics of spin weight s.

Definition 2.7. The *Gaunt integral* is defined to be

$$\int d\hat{\Omega} \left[{}_{s_1}Y_{\ell_1 m_1}(\hat{\Omega})\right] \left[{}_{s_2}Y_{\ell_2 m_2}(\hat{\Omega})\right] \left[{}_{s_3}Y_{\ell_3 m_3}(\hat{\Omega})\right] = I_{\ell_1 \ell_2 \ell_3} \begin{pmatrix} \ell_1 & \ell_2 & \ell_3 \\ s_1 & s_2 & s_3 \end{pmatrix} \begin{pmatrix} \ell_1 & \ell_2 & \ell_3 \\ m_1 & m_2 & m_3 \end{pmatrix} \tag{2.78}$$

$$I_{\ell_1 \ell_2 \ell_3} = \sqrt{\frac{(2\ell_1+1)(2\ell_2+1)(2\ell_3+1)}{4\pi}}. \tag{2.79}$$

This is exactly the orthogonality condition that we encountered for the spin weighted spherical harmonics 2.62. For the scalar spherical harmonics, $s = 0$ and the expression simplifies somewhat.

2.6 Spherical Bessel Functions

The spherical Bessel functions have some useful properties that we wish to introduce here. These will be used repeatedly in our subsequent analysis. First of all is the recurrence relation that allows us to generate spherical Bessel functions of a higher ℓ

$$\frac{d}{dx}\left[x^{\ell+1} j_\ell(x)\right] = x^{\ell+1}\, j_{\ell+1}(x) \qquad j_{\ell-1}(x) + j_{\ell+1}(x) = \frac{(2\ell+1)}{x}\, j_\ell(x); \tag{2.80}$$

$$\frac{d}{dx}\left[x^{-\ell} j_\ell(x)\right] = x^{-\ell}\, j_{\ell+1}(x) \qquad \ell\, j_{\ell-1}(x) - (\ell+1)\, j_{\ell+1}(x) = (2\ell+1)\, \frac{d}{dx} j_\ell(x). \tag{2.81}$$

We can also define the first derivative of the spherical Bessel functions as

$$j'_\ell(r) = \frac{1}{2\ell+1}\Big[\ell j_{\ell-1}(r) - (\ell+1) j_{\ell+1}(r)\Big], \tag{2.82}$$

and the second-order derivative by applying 2.82 to itself

$$j''_\ell(r) = \Big[\frac{(2\ell^2+2\ell-1)}{(2\ell+3)(2\ell+1)} j_\ell(r) - \frac{\ell(\ell-1)}{(2\ell-1)(2\ell+1)} j_{\ell-2}(r) - \frac{(\ell+1)(\ell+2)}{(2\ell+1)(2\ell+3)} j_{\ell+2}(r)\Big]. \tag{2.83}$$

2.7 Limber Approximation and its Extension

The Limber approximation, along with its Fourier space counterpart, is a very useful and widely used tool in cosmology [323]. Often we will want to investigate particular limits for our 2-point correlators and the Limber approximation provides what is known as a *small angle approximation*. Here, we assume that we are dealing with small angular separations and that certain functions vary relatively slowly. This method is more exact in the high-ℓ limit and typically breaks down for small multipoles. In practice the Limber approximation often amounts to replacing our Bessel functions with an appropriately weighted delta function, at least to leading order. An immediate outcome is that we reduce the dimensionality of our integrals by using the delta function to collapse an integral. This can often prove useful when dealing with large multi-dimensional integrals in the calculation of covariance matrices [297].

Definition 2.8. The extended *Limber approximation* is implemented through the following approximate relation

$$\int k^2\, F(k)\, j_\ell(k r_a)\, j_\ell(k r_b) dk \approx \left[\frac{\pi}{2\nu}\right] F\left(\frac{\ell}{r_a}\right) \frac{\delta_{1\mathrm{D}}(r_a - r_b)}{r_a^2}; \qquad \nu = \ell + 1/2. \tag{2.84}$$

For high ℓ the spherical Bessel functions can be replaced by a Dirac delta function δ_{1D}:

$$\lim_{\ell\to\infty} j_\ell(x) = \sqrt{\frac{\pi}{2\nu}} \delta_{1\mathrm{D}}\left(\nu - x\right). \tag{2.85}$$

At small ℓ this approximation breaks down. We could improve our Limber approximation by incorporating higher order corrections [329]

$$\int dx F(x) J_\nu(x) = \left[F(x) - \frac{1}{2}\frac{x^2}{\nu^2} F''(x) - \frac{1}{6}\frac{x^3}{\nu^2} F'''(x) \right]_{x=\nu} + \mathcal{O}(\nu^{-4}), \tag{2.86}$$

where spherical Bessel functions $j_\ell(x)$ are related to the ordinary Bessel function $J_\nu(x)$ via

$$j_\ell(x) = \sqrt{\frac{\pi}{2x}}\, J_\nu(x). \tag{2.87}$$

In practice, we will typically only use the leading order result in the Limber approximation or we will perform a full numerical calculation. An examples of the improvement in accuracy when going to higher orders in the Limber approximation may be found in [56]. Though for $\ell \gtrsim 10$ the differences between the various approximations and numerical schemes is on the percent level.

Chapter 3

Inflationary Cosmology and Large Scale Structure

3.1 Inflationary Cosmology

3.1.1 Introduction

Any cosmological model that aims to describe the origin and dynamics of structure on large scales must satisfy a growing number of constraints. It is well known that the Universe appears to be highly homogeneous and isotropic on the largest scales. However, the presence of large scale structure (e.g. clustering of galaxies) means that we must provide a mechanism that is capable of generating the primordial density perturbations that seed this structure. The current favoured mechanism is inflation, as we shall outline shortly. First, we will recall some of the key constraints and problems that inflationary cosmology was invoked to solve.

- **Flatness Problem:** In the flatness problem, we note that Ω_K is extraordinarily close to zero at the current time but it also represents an unstable point in the matter and radiation dominated era. This means that if Ω_K is so close to zero now, it must have been even more so in the past. This constitutes an extreme fine tuning problem in the early Universe, i.e. $|\Omega_K(t_f)| \leq 10^{-60}$.

- **Horizon Problem:** Observations of the CMB, and its near perfect blackbody spectra, suggest that distant regions of the Universe were in causal contact in the far past. If we rewind the expansion, assuming standard FLRW expansion with the cosmological parameters from today, then we see that two regions that are causally disconnected today will remain causally disconnected. This is clearly an issue.

- **Relic Particle Abundances:** This is a statement to the effect that particles produced in some approximate GUT regime are not observed today and we would need to explain the abnormally low abundances in a rather natural way.

- **Coherence of Perturbations:** This is a more subtle point but is often one of the key constraints that kills many theories for the early Universe. In particular we require shape and structure in the power spectra for the CMB and LSS. Many theories for the early Universe can generate perturbations of the right amplitude and scale but, as there is no mechanism that enforces coherence, result in a whitened power spectrum.
- **Superhorizon Fluctuations:** This constraint tells us that we need a mechanism that is capable of generating perturbations on scales larger than the particle horizon.
- **Gaussianity, Scale Invariance and Adiabaticity of Perturbations:** Observations of the CMB tell us that the primordial perturbations seeding large scale structure must have been highly Gaussian, near scale invariant and highly adiabatic. A theory for the early Universe must clearly satisfy these constraints.

The theory of inflation [383; 325; 532; 245; 231; 326] was introduced as a rather natural mechanism that solves the horizon and flatness problems but also introduces a mechanism that allows for coherent perturbations in the early Universe. These perturbations arise from the quantum mechanical fluctuations of a hypothetical quantum field that drives a period of quasi-de Sitter inflation. Inflation solves the flatness problem by providing a mechanism, i.e. the exponential expansion, that drives the Universe towards $\Omega_K = 0$ sufficiently fast to compensate for the subsequent drift at the end of inflation. This alleviates the problem of fine tuning as Ω_K is pushed incredibly close to 0 for rather generic initial conditions. For exponential expansion, we see that the comoving Hubble radius will decrease with time and this means that two points that were in causal contact at some Planckian size patch can be dragged outside the horizon by the exponential expansion to cosmological scales. In effect, two points at cosmological distances apart today could have been in causal contact in the early Universe. A similar argument will apply for relic particle abundances, by introducing a period of rapid exponential expansion in the early Universe these relic particles would be rapidly diluted and hence unobservable today. Superhorizon perturbations are also natural in inflation as perturbations generated on quantum scales can be dragged to cosmological scales by the expansion. One of the real powers of inflationary cosmology, however, is that it allows us to generate a coherent power spectrum. The argument goes as follows: modes generated on quantum scales get dragged outside the horizon during the expansion where they subsequently freeze out. This means that the modes do not undergo dynamical evolution, their wavelengths have become sufficiently long that causal physics can alter them. After inflation, the Hubble radius grows and modes slowly re-enter the horizon. Once the modes enter the horizon they become dynamical and start to oscillate, the wavelengths are now below the horizon scale and causal physics can once again affect them. The important point here is that once the modes freeze out, the amplitude is fixed. All modes enter the horizon with some constant amplitude and are hence coherent. This gives the characteristic shape and structure to the power spectrum of primordial perturbations but also sets an important bench mark. For coherent phases, the most basic requirement is that at some point in the distant past the modes of interest had to be within the horizon. Currently, only inflation offers such a self-consistent explanation for all these features. Finally, the observed Gaussianity of the CMB places strict limits on the interactions of the quantum field(s) in the early Universe. In particular, for highly Gaussian perturbations we require that higher order interactions are relatively suppressed. It is a major goal of modern cosmology

to detect and study such non-Gaussianities as their imprint in the CMB and LSS can tell us a huge amount about fundamental interactions in the early Universe as each interaction induces a particular shape and structure to the n-point correlators.

The modern vanilla model for inflation is based on a set of rather reasonable and generic initial conditions. First of all we assume that the whole calculation can be done within the semiclassical framework. By this we simply refer to the fact that we have a classical homogeneous and isotropic background spacetime governed by the EFEs on top of which we quantise our field theory. For the simplest models we just adopt a single scalar field ϕ that is assumed to be minimally coupled to gravity, canonically normalised and equipped with a simple quadratic mass potential. The initial conditions for the system are set by assuming the Bunch-Davies prescription in which we assume that there exist no excited states at an initial time t_0 and that as we approach small scales, modes will be deep within the horizon and curvature effects may be neglected. In such a limit we asymptotically recover the conventional Minkowski vacuum. Finally, in order to violate the strong energy prediction and generate exponential expansion, we assume that the field initially starts off in some excited state such that the potential energy dominates over the kinetic energy. These last two points raise interesting and important questions regarding the fine-tuning of initial conditions required for inflation. We will discuss that in a little more detail later. First, we want to sketch out the various assumptions in a some mathematical detail to fix our notation:

- Einstein Gravity

$$G_{\mu\nu} = 8\pi G\, T_{\mu\nu} \tag{3.1}$$

- Homogeneous and Isotropic Background Solution

$$ds^2 = -dt^2 + e^{2\rho(t)} dx_i dx_i \qquad \dot{\rho} = H \tag{3.2}$$

- Free Scalar Field ϕ Driving Inflation

$$S = \frac{1}{2}\int d^4x\sqrt{g}\left[M_{\rm pl}^2 R - (\nabla\phi)^2 - 2V(\phi)\right] \tag{3.3}$$

- Canonical Kinetic Terms

$$\mathcal{L} = \mathcal{L}(X,V) \qquad X = -\frac{1}{2}g^{\mu\nu}\partial_\mu\phi\,\partial_\nu\phi \quad \Big\} \rightarrow \mathcal{L} = X - V(\phi) \tag{3.4}$$

- Bunch-Davies Vacuum (Initial Conditions)

$$\phi_k(t_0) \sim A_k e^{-ik\eta} \tag{3.5}$$

- Perturbations Around Background

$$\phi(t,x) = \bar{\phi}(t) + \delta\phi(t,x) \qquad g_{\mu\nu}(t,x) = \bar{g}_{\mu\nu}(t) + \delta g_{\mu\nu}(t,x) \tag{3.6}$$

- Slow Roll Dynamics

$$V(\phi) \gg \dot{\phi}^2. \tag{3.7}$$

- Potential, such as

$$V(\phi) = \frac{1}{2}m^2\phi^2 \tag{3.8}$$

Now that we've introduced the notation and set the scene we can start to build up the machinery that is required in order to calculate non-Gaussianities during inflation. What we will see is that the hierarchy of n-point correlation functions are sensitive to the underlying field theory assumed to drive inflation and its interactions. In essence, the dynamics and interactions of the field imprint themselves on the correlation functions by inducing amplitude and momentum dependence. This is important as it states that by studying the n-point correlation functions of the cosmic microwave background or large scale structure, both of which can be related to the primordial density perturbations, we can probe the dynamics of the very early Universe. In the next section we will introduce the In-In formalism as a tool for calculating n-point correlation functions. This is the modern approach championed by [345] in his classic paper.

3.1.2 In-In Formalism

There are by now many references in the literature available that give good overviews of the In-In formalism in cosmology. Some of the key papers on which the foundations of this chapter are based can be found in [345; 589; 100; 306; 123]. We make no attempt at providing a detailed or technical discussion but simply aim to give a schematic overview of how non-Gaussianities may be calculated given a field theory for inflation in the more modern notation of [345].

For the In-In or Keldysh-Schwinger formalism, we are no longer interested in calculating transition probabilities but are interested in calculating an expectation value of some arbitrary operator Q constructed from the product of field perturbations $\delta\phi_a$ and $\delta\pi_a$. In a non-static spacetime, such as a de-Sitter spacetime, the initial vacuum $|0_-\rangle$ is generically different from the final vacuum $|0_+\rangle$. This is due to time varying strong gravitational fields that effectively induce a gravitational Schwinger effect, i.e. gravitational particle production [495; 225; 226; 227; 352]. The matrix elements $\langle 0_+|Q(t)|0_-\rangle$ are, in general, complex and will not correspond to observables of physical interest.

This is in stark contrast to the In-Out formulation of QFT which is conventionally formulated as a boundary value problem. Here, the boundary values are defined by two asymptotically well-defined states, i.e. particles. In scattering processes, for example, we start out with some initial state, evolve the operators from $t = -\infty$ to $t = \infty$ and then evaluate the overlap of the the initial state with some final state.

In the In-In approach, we re-cast the problem in terms of an initial value formulation where the aim is to calculate a correlation function at some arbitrary time t given some initial Cauchy data at t_0. The initial data in this instance is just a prescription for the initial vacuum state. In inflationary cosmology, the initial vacuum Ω is usually given by following the Bunch-Davies prescription, for which the vacuum state is defined by the asymptotic limit $\eta \to -\infty$ such that

the momenta of interest are deep within the horizon and curvature effects may be neglected. We also make the implicit assumption that no degrees of freedom are excited on these scales, we are effectively stating that there is zero particle content and that no Planckian degrees of freedom may be excited. The appropriate vacuum state in this limit is just the Minkowski vacuum $|0\rangle$.

In the Heisenberg picture the expectation value of our operator is given by:

$$\langle Q \rangle = \langle \Omega | Q(t) | \Omega \rangle, \tag{3.9}$$

where we conventionally wish to evaluate this expectation value at the end of the inflationary period t. In order to construct a quantum field theory for inflation we are required to specify a Hamiltonian of the system:

$$H[\phi(t), \pi(t)] = \int d^3x \mathcal{H}[\phi_a(\mathbf{x}, t), \pi_a(\mathbf{x}, t)]. \tag{3.10}$$

The canonical coordinates $\phi_a(\mathbf{x}, t)$ and $\pi_a(\mathbf{x}, t)$ obey the canonical commutation relations:

$$[\phi_a(\mathbf{x}, t), \pi_b(\mathbf{y}, t)] = i\delta_{ab}\delta^3(\mathbf{x} - \mathbf{y}), \tag{3.11}$$

$$[\phi_a(\mathbf{x}, t), \phi_b(\mathbf{y}, t)] = [\pi_a(\mathbf{x}, t), \pi_b(\mathbf{y}, t)] = 0. \tag{3.12}$$

The time dependency of the canonical coordinates is generated by the total Hamiltonian through Heisenberg's equations of motion:

$$\dot{\phi_a}(\mathbf{x}, t) = i \left[H[\phi_a(t), \pi_a(t)], \phi_a(\mathbf{x}, t) \right], \tag{3.13}$$

$$\dot{\pi_a}(\mathbf{x}, t) = i \left[H[\phi_a(t), \pi_a(t)], \pi_a(\mathbf{x}, t) \right]. \tag{3.14}$$

In order to proceed we split the field into a classical time-dependent homogeneous background solution and a small perturbation:

$$\phi_a(\mathbf{x}, t) = \bar{\phi}_a(t) + \delta\phi_a(\mathbf{x}, t) \tag{3.15}$$

$$\pi_a(\mathbf{x}, t) = \bar{\pi}_a(t) + \delta\pi_a(\mathbf{x}, t). \tag{3.16}$$

The Hamiltonian H generates the time-dependence of the fields but it is the terms of H of quadratic order and higher in the perturbations that generate the time dependence of the fluctuations. The total Hamiltonian can therefore be split into the zeroth and first order terms $\bar{H}$ alongside the time-dependent Hamiltonian $\tilde{H}$: $H = \bar{H} + \tilde{H}$. The time-dependence of the fluctuations is given by:

$$\delta\dot{\phi}_a(\mathbf{x}, t) = i \left[\tilde{H}[\phi(t), \pi(t); t], \delta\phi_a(\mathbf{x}, t) \right], \tag{3.17}$$

$$\delta\dot{\pi}_a(\mathbf{x}, t) = i \left[\tilde{H}[\phi(t), \pi(t); t], \delta\pi_a(\mathbf{x}, t) \right]. \tag{3.18}$$

The operator formalism outlined by [589] expresses the fluctuations at time t in terms of the unitary time evolution of the fluctuations at some initial time t_0:

$$\delta\phi_a(t) = U^{-1}(t, t_0)\delta\phi_a(t_0)U(t, t_0), \tag{3.19}$$

$$\delta\pi_a(t) = U^{-1}(t,t_0)\delta\pi_a(t_0)U(t,t_0), \tag{3.20}$$

where the unitary time evolution operator is defined by an initial condition $U(t_0,t_0)=1$ and the differential equation:

$$\frac{d}{dt}U(t,t_0) = -i\tilde{H}[\delta\phi(t),\delta\pi(t);t]U(t,t_0). \tag{3.21}$$

In order to calculate $U(t,t_0)$ we switch to the interaction picture and decompose the higher order Hamiltonian $\tilde{H}$ into a quadratic kinematical term and an interaction term:

$$\tilde{H}[\delta\phi(t),\delta\pi(t);t] = H_0[\delta\phi(t),\delta\pi(t);t] + H_I[\delta\phi(t),\delta\pi(t);t], \tag{3.22}$$

such that we aim to express U as a series expansion of the interaction terms. The time-dependency of the perturbations is governed by the quadratic term H_0 with the interaction picture operators being free fields. It can be shown that the unitary time evolution operator is given by [589]:

$$U(t,t_0) = U_0(t,t_0)F(t,t_0), \tag{3.23}$$

where

$$F(t,t_0) = T\exp\left(-i\int_{t_0}^{t} H_I(t)dt\right). \tag{3.24}$$

Combining Eq. (3.24) and Eq. (3.19) we can express the expectation value of an operator by:

$$\langle Q\rangle = \langle\Omega|F^{-1}(t,t_0)Q^I(t)F(t,t_0)|\Omega\rangle, \tag{3.25}$$

$$= \langle\Omega|\left[\bar{T}\exp\left(i\int_{t_0}^{t} H_I(t)dt\right)\right]Q^I(t)\left[T\exp\left(-i\int_{t_0}^{t} H_I(t)dt\right)\right]|\Omega\rangle. \tag{3.26}$$

In the above prescription we are free to write the vacuum of our interacting theory in terms of the vacuum for the free theory $|0\rangle$ as we do not generate non-trivial vacuum fluctuations through interactions. This arises as $F^{-1}F=1$ and we essentially find that in the In-In approach the vacuum fluctuation diagrams automatically cancel. For inflationary cosmology this formalism is useful as it allows us to calculate the n-point correlators for an arbitrary model, as an example the three-point correlator would be:

$$\langle\mathcal{R}_{k_1}\mathcal{R}_{k_2}\mathcal{R}_{k_3}\rangle(\eta) = \tag{3.27}$$

$$\langle 0|\left[\bar{T}\exp\left(-i\int_{-\infty(1-i\epsilon)}^{\eta} H_I(\eta')d\eta'\right)\right]\mathcal{R}_{k_1}(\eta)\mathcal{R}_{k_2}(\eta)\mathcal{R}_{k_3}(\eta)\left[T\exp\left(-i\int_{-\infty(1+i\epsilon)}^{\eta} H_I(\eta'')d\eta''\right)\right]|0\rangle. \tag{3.28}$$

3.1.3 Maldacena's Calculation

3.1.3.1 ADM Approach

Maldacena's calculation [345] uses the In-In formalism to compute the leading order corrections to the scalar and tensor perturbations in the minimal single field inflationary model that we introduced earlier. The action for this inflationary model is perturbatively expanded about the spatially homogeneous background FLRW solution. The leading order term is quadratic in the fluctuations

representing the Gaussian contribution from the free field. The non-Gaussianities that arise in the three-point function are generated due to the non-linear nature of the Einstein field equations as well as non-linearities in the inflaton potential. As with all areas of physics, choice of notation and convention is a particular problem in the literature. Maldacena [345] happens to adopt rather obscure notation in comparison the much of the literature in cosmology. We will introduce this notation and make the connection to the Mukhanov-Sasaki notation [383; 471; 472].

The action for the vanilla model described above is that for a free scalar field minimally coupled to gravity with some arbitrary potential $V(\phi)$

$$S = \frac{1}{2}\int \sqrt{g}\left[R - (\nabla\phi)^2 - 2V(\phi)\right]. \tag{3.29}$$

Note that we have set the reduced Planck mass to unity $M_{pl}^{-2} = 8\pi G_N = 1$. The homogeneous background de Sitter spacetime has a metric that can be recast in the following form [345]

$$ds^2 = -dt^2 + e^{2\rho(t)}dx_i dx_i = e^{2\rho}(-d\eta^2 + dx_i dx_i). \tag{3.30}$$

Solving the EFE and equations of motion for the scalar field provides us with a set of equations that govern the background spacetime

$$3\dot{\rho}^2 = \frac{1}{2}\dot{\phi}^2 + V(\phi), \tag{3.31}$$

$$\ddot{\rho} = 0\frac{1}{2}\dot{\phi}^2, \tag{3.32}$$

$$0 = \ddot{\phi} + 3\dot{\rho}\dot{\phi} + V_{,\phi}(\phi). \tag{3.33}$$

As mentioned, Maldacena adopts a somewhat unconventional notation but the relation to the more normal Hubble parameter and scale factor in cosmology is as follows $\dot{\rho} = H = \dot{a}/a$. Following the normal procedure in inflationary cosmology, we consider quantum fluctuations about the background solution

$$g_{ab}(t) \to g_{ab}(t) + \delta g_{ab}(t, \mathbf{x}), \tag{3.34}$$

$$\phi(t) \to \phi(t) + \delta\phi(t, \mathbf{x}). \tag{3.35}$$

An initial problem in describing these quantum fluctuations lies in removing unphysical degrees of freedom from our calculations. The fluctuations above can be described by five scalar fields of which four arise from the metric: $\delta g_{00}, \delta g_{jj}, \delta g_{oi} \sim \partial_i B, \delta g_{ij} \sim \partial_i\partial_j H$ and the fifth from the scalar fluctuation $\delta\phi$. Not all of these scalar fields have physical significance and we can remove two of the scalars by considering the gauge invariances on our action from reparametrisations of the form $x^i \to x^i + \partial^i\epsilon$, (see [345; 123] for more explicit details). A further two modes are removed due to constraints on the action leaving only a single physical field.

In order to proceed, it will be important to separate out the dynamical and gauge degrees of freedom. A useful way to do this is to adopt the ADM formalism [21] in which we re-write our metric in terms of the Lagrange multipliers $N(t, \mathbf{x})$ and $N^i(t, \mathbf{x})$ along with the dynamical variables

h_{ij} and ϕ. In the relativity community, the variables $N(t,\mathbf{x})$ and $N^i(t,\mathbf{x})$ are known as the *lapse* and *shift* respectively.

The ADM approach is based on a foliation of spacetime with a set of preferred spatial 3-surfaces. We implicitly assume that the spacetime $(\mathcal{M}, g_{ab})$ is globally hyperbolic, where a spacetime is said to be globally hyperbolic if it admits a Cauchy surface Σ [220]. In turn, a Cauchy surface is simply a spacelike hypersurface in the manifold $\mathcal{M}$ such that each timelike curve without end intersects Σ once and only once. The topological structure of the manifold is therefore $\mathbb{R}\times\Sigma$. This means that spacetime is simply foliated by hypersurfaces Σ_t for $t\in\mathbb{R}$ such that

$$\mathcal{M} = \bigcup_{t\in\mathbb{R}} \Sigma_t, \tag{3.36}$$

where the hypersurfaces Σ_t are defined at a given coordinate time t forming the leaves in our foliation. We therefore identify Σ_t with $\{t\}\times\Sigma$ noting that the leaves are implicitly assumed to be defined such that they do not intersect. This formulation of General Relativity is particularly suited for studying the initial value formulation where Σ_0 is the initial hypersurface on which the constraint equations are solved.

The spacetime metric g_{ab} will induce a spatial metric h_{ij} on each leaf Σ_t which corresponds to the orthogonal projection of the space of all spacetime vectors at each point $p\in\Sigma$. The projection tensor h_{ij} onto Σ can be defined by

$$h_{ij} = g_{ij} + n_i n_j, \tag{3.37}$$

where n^i the unit normal vector to the hypersurface Σ_t. Physically, the lapse represents the rate of flow of proper time with respect to coordinate time t, $N=-t^\mu n_\mu$ and the shift represents displacements tangential to the hypersurface Σ_t, $N^i = h^i_j t^j$. Under this prescription, the metric may be written as:

$$ds^2 = -N^2dt^2 + h_{ij}\left(dx^i + N^i dt\right)\left(dx^j + N^j dt\right) \tag{3.38}$$

with metric components:

$$g_{00} = h_{ij}N^iN^j - N^2; \qquad g^{00} = N^{-2}, \tag{3.39}$$

$$g_{0j} = h_{ij}N^i; \qquad g^{0j} = -N^{-2}N^j, \tag{3.40}$$

$$g_{ij} = h_{ij}; \qquad g^{ij} = -N^{-2}\left[N^2h^{ij} - N^iN^j\right] \tag{3.41}$$

The action Eq. (3.29) can therefore be rewritten as [345; 123]

$$S = \frac{1}{2}\int d^4x\,\sqrt{h}\left[N\hat{R} - 2NV + N^{-1}\left(E_{ij}E^{ij} - E^2\right) + N^{-1}\left(\dot{\phi} - N^i\partial_i\phi\right)^2 - Nh^{ij}\partial_i\phi\partial_j\phi\right], \tag{3.42}$$

where we have introduced a normalised extrinsic curvature $K_{ij} = N^{-1}E_{ij}$ defined by the Lie derivative of the spatial metric:

$$K_{ij} = \frac{1}{2}\mathcal{L}_n h_{ij}, \tag{3.43}$$

$$E_{ij} = \frac{1}{2}\left(\dot{h}_{ij} - D_iN_j - D_jN_i\right), \tag{3.44}$$

$$E = E^j_j. \tag{3.45}$$

The variable $\hat{R}$ corresponds to the 3-dimensional Ricci curvature scalar for a hypersurface Σ_t and D_i are the covariant derivatives induced by the spatial 3-metric h_{ij}. See Section 7.4 for a further treatment in the 1+3 formalism.

In order to perform actual calculations we will need to adopt a particular gauge. Following [345], we adopt the uniform inflaton gauge in which all degrees of freedom are absorbed by the metric tensor such that γ_{ij} parameterises the gravitational degrees of freedom [345]:

$$\delta\phi = 0; \qquad h_{ij} = e^{2\rho(t)}\left[(1+2\zeta(t,\mathbf{x}))\delta_{ij} + \gamma_{ij}\right]; \qquad \partial_i\gamma_{ij}; \qquad \gamma_{jj} = 0, \tag{3.46}$$

with the last two constraints ensuring that the perturbations are transverse and traceless.

The action for the dynamical degrees of freedom can be found by solving the equations of motion for the lapse and shift. These equations are derived, from a field theoretic perspective, by the functional derivative of the action with respect to the Lagrange multipliers. The resulting equations of motion are the momentum constraint and the Hamiltonian constraint

$$0 = D_i\left[N^{-1}\left(E^i_j - \delta^i_j E\right)\right], \tag{3.47}$$

$$0 = \hat{R} - 2V - N^{-2}\left(E_{ij}E^{ij} - E^2\right) - N^{-2}\dot{\phi}^2. \tag{3.48}$$

It can be shown that we only need to expand the action to the necessary order in the fluctuations for the n-point correlator that we wish to calculate [345]. For example, when calculating the 2-point correlator we only need to work to quadratic order in the fluctuations. However, to work with the 3-point correlator we need to expand the solutions to cubic order in the fluctuations. The lapse and shift can be defined in terms of a general parameterisation of the scalar fluctuations n the metric

$$N = 1 + 2\Phi(t,\mathbf{x}), \qquad N^i = \delta^{ij}\partial_j B(t,\mathbf{x}). \tag{3.49}$$

For convenience we also re-write the metric h_{ij} as

$$h_{ij} = e^{2\rho(t)+2\zeta(t,\mathbf{x})}\delta_{ij}. \tag{3.50}$$

The momentum constraint equation can be shown to reduce to

$$-3\dot{\rho}\left[2\dot{\rho}\Phi - \dot{\zeta}\right] - \partial_k\partial^k\left[\dot{\rho}B + e^{-2\rho}\zeta\right] + \dot{\phi}^2\Phi = 0, \tag{3.51}$$

and the Hamiltonian constraint reduces to

$$2\partial_i\left[2\dot{\rho}\Phi - \dot{\zeta}\right] = 0. \tag{3.52}$$

These constraint equations can be used to remove a scalar degree of freedom as we can fix Φ by setting

$$\Phi = \frac{1}{2}\frac{\dot{\zeta}}{\dot{\rho}}, \tag{3.53}$$

and implicitly choosing the constant of integration to be zero such that, when fluctuations are

turned off, we recover the original background metric. Substituting this into the momentum constraint removes another degree of freedom as it fixes the scalar field B with the following equation

$$B = -\frac{e^{-2\rho}}{\dot{\rho}}\zeta + \partial^{-2}\left(\frac{1}{2}\frac{\dot{\phi}^2}{\dot{\rho}^2}\dot{\zeta}\right). \tag{3.54}$$

These results are plugged back into the ADM action Eq. (3.42) and expanded to the appropriate order.

3.1.3.2 2-Point Correlator

As a consequence of the previous section, the only remaining scalar field of physical significance is ζ. We now expand Eq. (3.29) to quadratic order and derive the 2-point correlator. Using Friedmann's equation (i.e. the G_{00} term of EFE) we can relate the inflaton potential to the background equations as follows

$$V = 3\dot{\rho}^2 - \frac{1}{2}\dot{\phi}^2. \tag{3.55}$$

After inserting this into the action and performing an integration by parts, in which we neglect a total derivative, we obtain [345]

$$S = \frac{1}{2}\int dt\, d^3x \frac{\dot{\phi}^2}{\dot{\rho}^2}\left[e^{3\rho}\dot{\zeta}^2 - e^{\rho}\left(\partial\zeta\right)^2\right] \tag{3.56}$$

$$= \frac{1}{2}\int dt\, d^3x \frac{\dot{\phi}^2}{H^2}\left[a^3\dot{\zeta}^2 - a\left(\partial\zeta\right)^2\right] \tag{3.57}$$

This final action is for a free scalar field which can be interpreted in terms of a collection of harmonic oscillators and we perform the conventional mode expansion found in QFT

$$\zeta(t,x) = \int \frac{d^3k}{(2\pi)^3}\zeta_k(t)e^{ikx}, \tag{3.58}$$

where each oscillator has a time-dependent mass arising due to the fact that we are working in an expanding spacetime. The classical equations of motion are given by the functional derivative

$$\frac{\delta\mathcal{L}}{\delta\zeta} = -\frac{d}{dt}\left(a^3\frac{\dot{\phi}^2}{H^2}\dot{\zeta}_k\right) - \frac{\dot{\phi}^2}{H^2}ak^2\zeta_k = 0, \tag{3.59}$$

which generates two independent classical solutions. Using these solutions we can perform the usual creation-annihilation operator expansion

$$\zeta_k(t) = \zeta_k^{cl}(t)a_k^\dagger + \zeta_k^{cl*}(t)a_{-k}. \tag{3.60}$$

where the creation and annihilation operators obey the following commutation relation

$$\left[a_I(k_1), a_I^\dagger(k_2)\right] = (2\pi)^3\delta(k_1 - k_2). \tag{3.61}$$

We can introduce the conformal time, $dt = ad\eta$, which allows us to rewrite the action by the following

$$S = \frac{1}{2}\int [ad\eta]\, d^3x \frac{\dot{\phi}^2}{H^2}\, a \left[(\zeta')^2 - (\partial\zeta)^2\right]. \tag{3.62}$$

We can connect this to the literature at large in the inflation by noting that we can define a Mukhanov-Sasaki variable $v = z\zeta$ such that $z = 2a^2\epsilon$. This variable reduces to the conventional Mukhanov-Sasaki action [383]

$$S_{\rm MS} = \frac{1}{2}\int d\tau\, d^3x \left[v'^2 - (\partial v)^2 - \frac{z''}{z}v^2\right]. \tag{3.63}$$

The equation of motion is given by

$$v_k'' + \left(k^2 - \frac{2}{\eta^2}\right) v_k = 0, \tag{3.64}$$

leading to an exact solution for the mode functions v_k of the form

$$v_k(\eta) = \alpha \frac{e^{-ik\eta}}{\sqrt{2k}}\left(1 - \frac{i}{k\eta}\right) + \beta\frac{e^{ik\eta}}{\sqrt{2k}}\left(1 + \frac{i}{k\eta}\right). \tag{3.65}$$

The Bunch-Davies prescription tells us that at very early times, $\eta \to -\infty$, we want to isolate the positive frequency modes leading to initial conditions of $\beta = 0$ and $\alpha = 1$. The Bunch-Davies mode functions are therefore given by

$$v_k(\eta) = \frac{e^{-ik\eta}}{\sqrt{2k}}\left(1 - \frac{i}{k\eta}\right) \tag{3.66}$$

The mode functions presented here are promoted to operators via

$$\hat{v}_k = v_k(\eta)\hat{a}_k + v^*_{-k}(\eta)\hat{a}^\dagger_{-k}, \tag{3.67}$$

where

$$\left[\hat{a}_k, \hat{a}^\dagger_{k'}\right] = (2\pi)^3\delta(k - k') \leftrightarrow W[v_k, v_k] = 1. \tag{3.68}$$

We can use these results to calculate the 2-point correlation function for the field ζ

$$\langle 0|\zeta_k(t)\zeta_{k'}(t)|0\rangle \sim (2\pi)^3\delta^3(k + k')\frac{\dot{\rho}_*^4}{2k^3M_{pl}^2\dot{\phi}_*^2} \sim (2\pi)^3\delta(k + k')P_s(k), \tag{3.69}$$

with the star denoting that we evaluate the quantity at horizon crossing, $k = aH1$. Letting $\dot{\rho}^2/\dot{\phi}^2 = 1/2\epsilon$, the dimensionless scalar power spectrum is given by

$$\frac{k^3}{2\pi^2}P_s(k) = \Delta_s^2(k) \sim \frac{1}{\epsilon}\frac{1}{8\pi^2}\frac{H^2}{M_{pl}^2}\bigg|_{k=aH}, \tag{3.70}$$

noting that $P_\zeta = z^{-2}P_v$.

3.1.3.3 Gravitational Wave 2-Point Correlator

The action quadratic in the tensor perturbation γ can be written as [345]

$$S = \frac{1}{8}\int \left[e^{3\rho}\dot{\gamma}_{ij}\dot{\gamma}_{ij} - e^{\rho}\partial_l\gamma_{ij}\partial_l\gamma_{ij}\right]. \tag{3.71}$$

The tensor perturbations are expanded as a series of plane wave solutions with a given helicity

$$\gamma_{ij} = \int \frac{d^3k}{(2\pi)^3}\sum_{s=\pm}\epsilon^s_{ij}(k)\gamma^s_k(t)e^{ikx}, \tag{3.72}$$

such that $\epsilon_{jj} = 0 = k^j\epsilon_{ij}$ and $\epsilon^s_{ij}(k) = \epsilon^{s'}_{ij}(k) = 2\delta_{ss'}$. The 2-point correlator reduces to

$$\langle\gamma^s_k\gamma^{s'}_{k'}\rangle = (2\pi)^3\delta^3(k+k')\frac{1}{2k^3}\frac{4\dot{\rho}^2_*}{M^2_{pl}}\delta_{ss'}. \tag{3.73}$$

As such, the dimensionless tensor power spectrum is therefore given by

$$\frac{k^3}{2\pi^2}P_t(k) = \Delta^2_t(k) = \frac{2}{\pi^2}\frac{H^2}{M^2_{pl}}\bigg|_{k=aH}. \tag{3.74}$$

3.1.3.4 3-Point Correlator

The cubic order action can be shown to be

$$S_3 = \int \frac{\dot{\phi}^4}{\dot{\rho}^4}e^{5\rho}\dot{\rho}\dot{\zeta}^2_c\partial^{-2}\dot{\zeta}_c + \dots \tag{3.75}$$

Using the In-In formalism we seek to calculate the 3-point correlation function of operators $\mathcal{O}(t)$ constructed from products of the field and its derivatives

$$\langle\mathcal{O}(t)\rangle = \langle U^{-1}_{int}(t,t_0)\mathcal{O}(t_0)U_{int}(t,t_0)\rangle. \tag{3.76}$$

It has been shown that this can be re-written in the following equivalent form [345]

$$\langle\mathcal{O}(t)\rangle = -i\int^t_{t_0}dt'\langle[\mathcal{O}(t), H_I(t')]\rangle. \tag{3.77}$$

For an operator of the form $\mathcal{O}(t) = \zeta^3(t)$, the general structure of the 3-point correlator was shown to be given by [345]

$$\langle\zeta_{k_1}\zeta_{k_2}\zeta_{k_3}\rangle = (2\pi)^3\delta^3(\sum k_i)\frac{\dot{\rho}^4_*}{\dot{\phi}^4_*}\frac{H^4_*}{M^4_{pl}}\frac{1}{\Pi_i(2k^3_i)}\mathcal{A}_* \tag{3.78}$$

with $\mathcal{A}_*$ encoding the momentum dependence of our function. Naturally, for operators of a different structure, for example $\mathcal{O}(t) = \dot{\zeta}^2\zeta$, the momentum and amplitude dependence of the 3-point correlator will be different. The key and crucial point here is that by analysing the shape and structure of the bispectrum we can distinguish between different physical contributions. Similarly,

by changing the underlying field theory we introduce different dynamics and different interactions that will introduce different momenta dependence into the bispectrum. We briefly survey some of the key ways in which you can relax the assumptions that go into the vanilla model of inflationary cosmology in Section 3.2.

3.1.3.5 Tensor-to-Scalar Ratio

The tensor to scalar ratio is a dimensionless number that characterises the relative amplitude of the tensor perturbations to the scalar perturbations. This number has seen something of a resurgence with preliminary reports from BICEP2 suggesting a possible B-mode polarisation at scales associated with primordial gravitational waves [3]. This quantity is, as the name suggests, simply defined by the ratio between the tensor and scalar power spectra

$$r = \frac{P_t(k)}{P_s(k)}. \tag{3.79}$$

3.2 Non-Gaussianity

The result presented in [345] corresponds to a vanilla model for inflation adopting minimal physics beyond the standard model. By considering all possible generalisations to this model, such as the presence of additional fields or deviations from Einstein General Relativity, we are able to probe the observational consequences of non-standard physics on the statistical properties of the CMB and LSS. We could also work to higher orders in the perturbative expansion and investigate the statistical properties of higher order correlators such as the *trispectrum*. In this section we will briefly outline some of the key mechanisms that give rise to non-Gaussianity to provide more concrete motivation for Chapter 4.

- **Modified Gravity**: By allowing deviations from Einstein gravity (see [111] for a recent overview of current research trends in modified gravity) it is possible to generate non-Gaussianities due to the inherent non-linearities in the field equations. Einstein gravity predicts $f_{\rm NL} \sim 1$ [450; 345] and it is plausible that deviations from standard General Relativity could generate more prominent non-Gaussianities but also give rise to a different structure in the bispectrum and other higher order correlators. Examples of studies of this nature include investigations into Gauss-Bonnet models (e.g. [330; 574]) and $f(R)$ models [141] among many others.

- **Higher Order Contributions**: These calculations can broadly be split into two categories: higher order correlation functions and additional contributions beyond tree level calculations. Examples of trispectrum calculations include [509; 25; 26; 378; 42] and examples of leading order contributions from, for example, loops include [527; 528; 509; 510; 147; 460; 516].

- **Non-Canonical Models**: The vanilla inflationary model assumes canonically normalised kinetic terms. By relaxing this assumption on our Lagrangian it is possible to construct models that give rise to non-trivial levels of non-Gaussianity. An example of such a model is $\mathcal{L} = p(X, \phi)$ where $X = -\frac{1}{2}(\partial\phi)^2$ is the canonical kinetic term [186]. The framework

for this sort of analysis is more general than assuming a canonically normalised kinetic term and many studies adopt a non-canonical picture when deriving results such that in the limit $p \to X$ we recover the canonical results. Examples of these types of calculations can be found in [505; 186; 80]

- **Multi-Field Models**: By including additional quantum fields in inflationary scenarios it is possible to introduce interaction terms or other non-linearities that generate non-Gaussianity. There are a vast number of models of this nature so we pick out only a handful of relevant references: [506; 7; 25; 43; 516].

- **String Motivated Cosmology**: It is thought, given the energy scales approached during inflation, that inflationary cosmology, and its subsequent observables, could be sensitive to quantum gravitational effects. In particular, much progress has been made in embedding inflation in string theory with many attempts relying on compactification schemes in type IIB string theories with a focus on creating (meta-)stable de Sitter vacua that can undergo a period of sustained stable inflation (e.g. [288; 46; 597]). An alternative approach, in the string scenario, is to make use of braneworlds, with the Dirac-Born-Infeld (DBI) models receiving much attention (e.g. [14; 308; 48; 26; 378]). Given the success of the AdS/CFT correspondence [344], there have been attempts to model inflation from a holographic point of view, e.g. [537; 345; 508; 146; 241]. The dS/CFT correspondence states that quantum gravity in a 4- dimensional de Sitter spacetime is dual to a 3-dimensional Euclidean CFT where the timelike coordinate in dS becomes the scale parameter of the CFT.

- **Non Bunch-Davies Vacuum**: Inflation can potentially be sensitive to the initial conditions of our model. The approach we adopted was given by the Bunch-Davies prescription. This assumed that no Planckian degrees of freedom could be active and that there was zero particle content in the Universe. This is highly likely to be an over simplification and the extent to which our semiclassical approach is valid is not known. Some have argued that as we approach small scales, and hence high energies, it is possible that physics beyond the standard model can excite additional degrees of freedom or introduce physics beyond our current theories and hence generate deviations to the initial conditions for inflation (e.g. [15; 155; 156; 137; 122; 138; 479; 140; 224]). We are constrained by observations in conjunction with the current paradigm for inflation to be reasonably close to the Bunch-Davies vacuum. A good, though purely phenomenological, example is that of the α-vacua, which correspond to the excitation of a narrow range of momenta. The appropriate prescription for generating such an initial state is to take the Bunch-Davies vacuum and apply a squeezing operator to create a new squeezed state parameterised by α. Typical calculations of the bispectrum for these models are demonstrated in [372; 600]. Deviations from Bunch-Davies typically encounter problems arising from more formal considerations of QFT in curved spacetimes or introduce deviations from Gaussianity that are not observed [75].

- **Non de Sitter Geometry**: Inflation is often taken to occur in a (quasi-)de Sitter background. However, it is possible to allow variations in the underlying isometries of our spacetime to model inflation occurring in various other cosmological backgrounds. Notable examples would include the anisotropic solutions such as the Bianchi models or inhomogeneous solu-

tions such as the LTB and Szekeres models. Alternatively, models in which anisotropy is sourced by primordial vector fields have been considered with the appropriate calculations found in (e.g. [41; 148]).

- **Features in Inflaton Potential**: This encapsulates a number of models that introduce features into the inflaton potential through various mechanisms. Some good examples of such models include those based on the axion monodromy model (e.g. [37; 38; 240; 185; 365]), supergravity based models (e.g. [269]) and more generalised studies of features in the power spectrum (e.g. [8]).

Large Scale Structure: Simulations

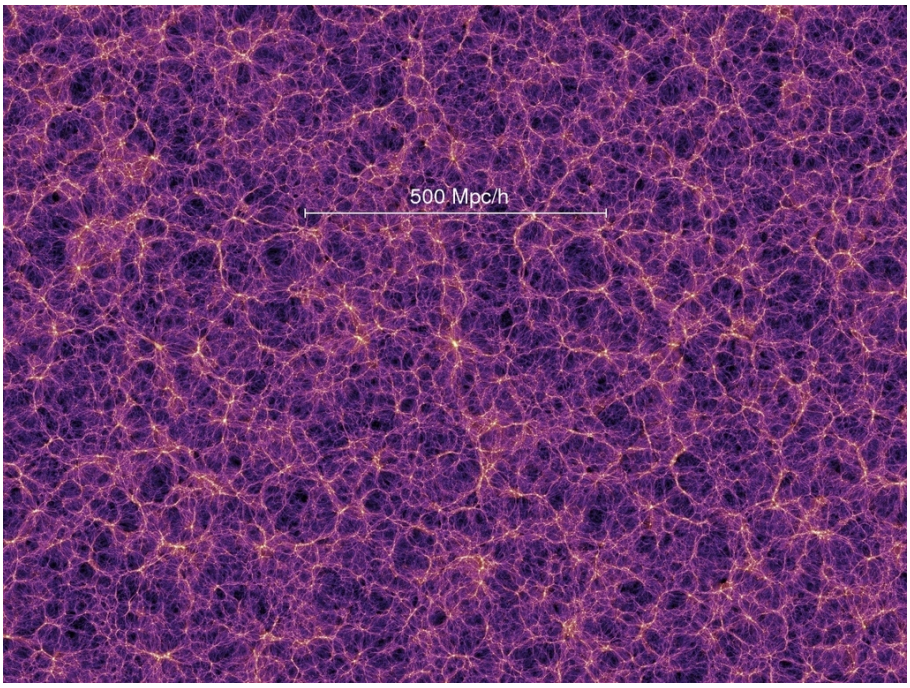

Figure 3.1: A public release image of the large scale structure of dark matter halos from the Millenium simulation[1].

Large Scale Structure: Observations

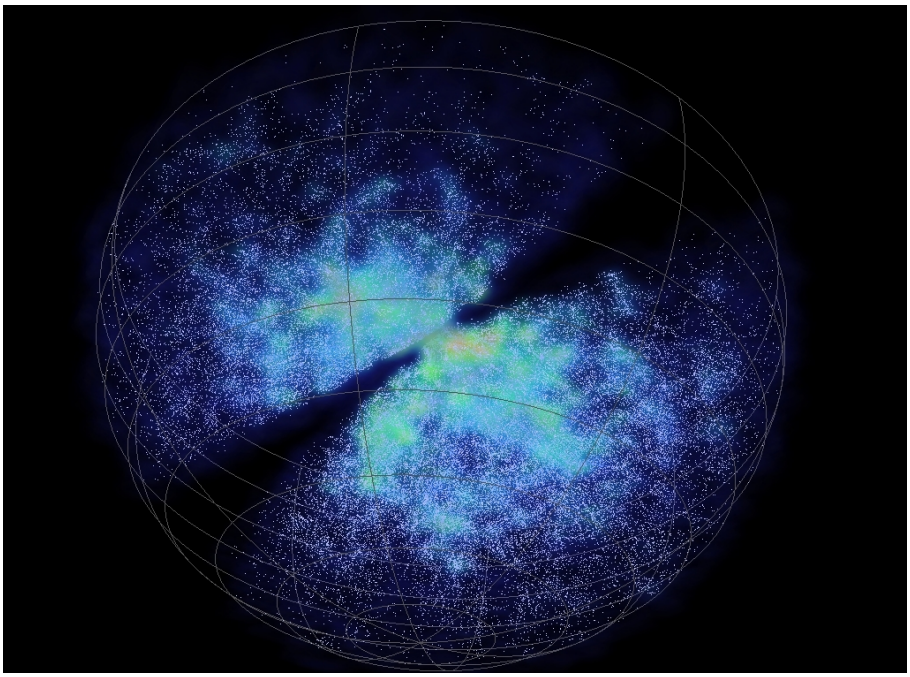

Figure 3.2: A public release image of the large scale structure of galaxies from the 6dF Galaxy Survey. Visualisations by C.Fluke, Swinburne University of Technology [2].

3.3 Large Scale Structure

3.3.1 Newtonian Structure Formation

3.3.1.1 Introduction

In this section we briefly outline the key equations that come into play when describing the growth of structure in the Newtonian approximation. Here we implicitly assume that the matter content is unrelativistic and we are considering scales far smaller than the Hubble scale. In this approach, we first outline the formation of large scale structure from the gravitational collapse of the density fluctuations of a pressureless fluid, cold dark matter, before moving to an expanding spatially homogeneous and isotropic spacetime. We will assume that the geometry of spacetime is very close to FLRW and is spatially flat. This approach to structure formation is suitable at late times during the matter dominated era and full relativistic treatments are possible but necessarily require additional structure that we do not wish to discuss here. Parts of this treatment follow the derivation and notation in [432].

3.3.1.2 Static Euclidean Case

In the static Euclidean case, the hydrodynamical equations of motion coupled to gravity describe the evolution of 6 parameters $\mathbf{X} = \{X_i\} = \{\rho, \mathbf{v}, P, \Phi\}$

$$\partial_t \rho + \nabla \cdot (\rho \mathbf{v}) = 0 \tag{3.80}$$

$$\partial_t \mathbf{v} + (\mathbf{v} \cdot \nabla)\, \mathbf{v} = -\frac{1}{\rho} \nabla P - \nabla \Phi \tag{3.81}$$

$$\Delta \Phi = 4\pi G \rho, \tag{3.82}$$

where we have introduced the energy density $\rho = \rho(t, \mathbf{x})$, the pressure $P = P(t, \mathbf{x})$, the velocity of the fluid $\mathbf{v} = \mathbf{v}(t, \mathbf{x})$ and the gravitational potential $\Phi = \Phi(t, \mathbf{x})$. We have neglected the entropy S, which would contribute an entropy conservation equation, as this is a reasonable approximation to dark matter, the dominant matter component in large scale structure formation. In addition, the system of equations is not closed and we need an additional constraint, the equation of state $P = P(\rho, S)$, to complete the equations. These equations will be valid in the non-relativistic regime such that $|\mathbf{v}| \ll c$ and $P \ll \rho c^2$.

Schematically, our approach will be to introduce a perturbative expansion around the background quantities up to arbitrary order

$$X_i = \bar{X}_i + \epsilon\, \delta X_i + \frac{1}{2} \epsilon^2\, \delta^2 X_i + \mathcal{O}(\epsilon^3). \tag{3.83}$$

The system of equation is then solved perturbatively. The background field equations, i.e. zeroth order, are given by

$$\partial_t \bar{\rho} + 3H\bar{\rho} = 0 \tag{3.84}$$

$$\partial_t \bar{\mathbf{v}} + (\bar{\mathbf{v}} \cdot \nabla)\, \bar{\mathbf{v}} = -\nabla \bar{\Phi} \tag{3.85}$$

$$\Delta \bar{\Phi} = 4\pi G \bar{\rho}, \tag{3.86}$$

where we have used the Hubble relation

$$\bar{\mathbf{v}} = H(t)\,\mathbf{r} \qquad \nabla \cdot \mathbf{v} = 3H \tag{3.87}$$

Initially neglecting gravity, we can write down the system of linear order equations by eliminating the background

$$\partial_t\,\delta\rho + \bar{\rho}\,\nabla\cdot\delta\mathbf{v} + \nabla\cdot(\delta\rho\,\mathbf{v}) = 0 \tag{3.88}$$

$$\partial_t\delta\mathbf{v} + (\delta\mathbf{v}\cdot\nabla)\,\bar{\mathbf{v}} + (\bar{\mathbf{v}}\cdot\nabla)\,\delta\mathbf{v} = -\frac{1}{\bar{\rho}}\left(c_s^2\delta\rho\right) - \nabla\delta\Phi \tag{3.89}$$

$$\Delta\,\delta\Phi = 4\pi G\,\delta\rho. \tag{3.90}$$

Here we have introduced the sound speed c_s which is defined with respect to the adiabatic compressibility coefficient

$$\chi_a = \frac{1}{\rho}\left(\frac{\partial P}{\partial\rho}\right)_a, \tag{3.91}$$

where a is either the temperature (T) or the entropy (S). The sound speed is defined to be

$$c_s^2 = \rho\,\chi_S. \tag{3.92}$$

Initially neglecting gravity, we can write down a wave equation at linear order that relates the density and pressure perturbations

$$\partial_t^2\delta\rho - \Delta\delta P = 0. \tag{3.93}$$

If we introduce the adiabatic compressibility coefficient, this reduces to

$$\chi_a = \frac{1}{\rho}\left(\frac{\partial P}{\partial\rho}\right)_a, \tag{3.94}$$

where a is either the temperature (T) or the entropy (S), then we can rewrite the wave equation as

$$\delta_t^2\delta\rho - c_s^2\Delta\delta\rho = 0 \tag{3.95}$$

The solutions to this equation will be waves of a constant amplitude propagating with a sound speed c_s with no flow of heat and therefore constant entropy. Folding gravity into the mix we find that the wave equation gets modified, picking up an additional source term

$$\partial_t^2\delta\,\rho - c_s^2\Delta\delta\rho = 4\pi G\bar{\rho}\,\delta\rho. \tag{3.96}$$

We proceed by decomposing this equation into a series of plane wave solutions such that $\delta\rho \propto \exp[i(\omega t - \mathbf{k}\cdot\mathbf{x})]$. This allows us to quickly and conveniently switch to the Fourier domain by noting that $\partial_t \to i\omega$ and $\Delta \to -k^2 = -(2\pi/\lambda)^2$. Each wavenumber will now satisfy a dispersion

relation given by

$$\omega^2 = \frac{4\pi c_s^2}{\lambda_J^2}\left(\frac{\lambda_J^2}{\lambda^2} - 1\right), \tag{3.97}$$

where we have introduced the Jeans length

$$\lambda_J = c_s\sqrt{\frac{\pi}{G\bar{\rho}}}. \tag{3.98}$$

Modes that are smaller than the Jeans length oscillate and the conventional sound waves are recovered. If the modes are larger than the Jeans length then the perturbations are unstable and grow exponentially. This means that long wavelength perturbations $\lambda > \lambda_J$ are dominated by gravitational effects whereas short wavelengths $\lambda < \lambda_J$ gravitational effects are negligible and we recover sound waves. Heuristically, for $\lambda > \lambda_J$, pressure is no longer able to support gravity and large inhomogeneities may develop. We can associate a mass to the Jeans length in the conventional way

$$M_J = \frac{4\pi}{4}\left(\frac{\lambda_J}{3}\right)^3 \tag{3.99}$$

3.3.1.3 Expanding Space

We now want to fold in the effects of an expanding spacetime and see what happens to our naive description of the growth of large scale structure. First, we introduce comoving coordinates $\mathbf{x}$ defined by

$$\mathbf{r}(t) = a(t)\,\mathbf{x} \tag{3.100}$$

where $a(t)$ was just the scale factor of the spacetime. The velocity field is then given by the time derivative of the physical coordinate $\mathbf{r}$

$$\mathbf{v}(t) = \dot{\mathbf{r}} = H\mathbf{r} + \mathbf{u}. \tag{3.101}$$

Here $\mathbf{u} = a\dot{\mathbf{x}}$ is just the proper velocity. We can now re-write the hydrodynamical equations of motion by re-writing the spatial derivatives $\nabla_{\mathbf{r}}$ in terms of the comoving coordinates $\nabla_{\mathbf{x}}/a$ and the time derivatives $\partial_t\rho(t,\mathbf{r})$ as $\partial_t\rho(t,\mathbf{x}) - H\,\mathbf{x}\cdot\nabla_{\mathbf{x}}\rho(t,\mathbf{x})$. The equations of motion become

$$\dot{\rho}(t,\mathbf{x}) + 3H\rho(t,\mathbf{x}) + \frac{1}{a}\nabla_{\mathbf{x}}\left[\rho(t,\mathbf{x})\,\mathbf{u}(t,\mathbf{x})\right] = 0 \tag{3.102}$$

$$\dot{\mathbf{u}}(t,\mathbf{x}) + H\,\mathbf{u}(t,\mathbf{x}) + \frac{1}{a}\left(\mathbf{u}\cdot\nabla_{\mathbf{x}}\right)\mathbf{u}(t,\mathbf{x}) = -\frac{1}{a}\nabla_{\mathbf{x}}\,\Phi(t,\mathbf{x}) - \frac{1}{a\rho}\,\nabla_{\mathbf{x}}P(t,\mathbf{x}). \tag{3.103}$$

where $\nabla_{\mathbf{x}}\cdot\mathbf{x} = 3$. We can now introduce the density contrast δ, one of the most important variables in modern cosmology

$$\delta(t,\mathbf{x}) = \frac{\rho(t,\mathbf{x}) - \bar{\rho}(t)}{\bar{\rho}(t)}; \qquad \rho(t,\mathbf{x}) = \bar{\rho}(t)\left[1 + \delta(t,\mathbf{x})\right]. \tag{3.104}$$

The first equation above then reduces to

$$\dot{\delta} + \frac{1}{a}\nabla\left[(1+\delta)\,\mathbf{u}\right] = 0 \tag{3.105}$$

where we will set $\nabla_{\mathbf{x}}$ to ∇ unless explicitly stated otherwise. The equation of motion becomes

$$\ddot{\delta} + 2H\dot{\delta} = \frac{1}{\rho a^2}\,\Delta P + \frac{1}{a^2}\nabla\cdot\left[(1+\delta)\,\nabla\Phi\right] + \frac{1}{a^2}\partial_i\partial_j\left[(1+\delta)u^i u^j\right] \tag{3.106}$$

The gravitational potential is determined from the Poisson equation

$$\Delta\Phi = 4\pi G\,\bar{\rho}\,a^2(t)\,\delta, \tag{3.107}$$

which has a solution of the form

$$\Phi(t,\mathbf{x}) = -G\,\bar{\rho}a^2\int d^3\mathbf{x}'\,\frac{\delta(t,\mathbf{x}')}{|\mathbf{x}-\mathbf{x}'|}. \tag{3.108}$$

3.3.1.4 Linearised Solutions and the Growth of Structure

We can now limit our analysis to systems for which the fluid is only weakly perturbed from the background configuration. The perturbative expansion can be written as

$$\delta = \delta^{(1)} + \delta^{(2)} + \ldots, \tag{3.109}$$

but we only consider solutions for which $\delta \ll 1$ and we neglect terms of order $\mathcal{O}(\epsilon^2)$ and higher. Linearising our equation of motion Eq. (3.106) we find

$$\ddot{\delta} + 2H\dot{\delta} = \frac{c_s^2}{a^2}\,\Delta\,\delta + 4\pi G\,\bar{\rho}\,\delta. \tag{3.110}$$

This equation is a second order differential equation and we therefore seek solutions of the form

$$\delta(t,\mathbf{x}) = D_+(t)\,\epsilon_+(\mathbf{x}) + D_-(t)\epsilon_-(\mathbf{x}), \tag{3.111}$$

where $\epsilon(\mathbf{x})$ is the initial density field and D_+ and D_- are growing and decaying modes respectively. These modes are solutions of the equation

$$\ddot{D} + 2H(t)\,\dot{D} - \frac{3}{2}H^2(t)\Omega_m(t)D = 0 \tag{3.112}$$

where the mean matter density is denoted by

$$4\pi G\rho_m(t) = \frac{3}{2}H^2\Omega_m(t). \tag{3.113}$$

The solutions can be shown to be given by

$$D_+(a) = \frac{5}{2}\frac{H(a)}{H_0}\,\Omega_{m0}\int_0^a \frac{da'}{\left[a'E(a')\right]^3} \tag{3.114}$$

$$D_-(a) = H(a), \tag{3.115}$$

where

$$E^2(z) = \left[\frac{H(z)}{H_0}\right]^2 = \Omega_\Lambda + \Omega_K(1+z) + \Omega_m(1+z)^3. \tag{3.116}$$

as in Eq. (1.28). In a flat dust dominated Universe this simply reduces to $D_+ = a$. In Eq. (3.114) we can see that the growth of structure is driven by the matter density, which sources the gravitational potential which in turn determines the rate of structure formation, but the Hubble parameter prevents structures from undergoing gravitational collapse. This can be seen, for example, in Eq. (3.110) by the appearance of a Hubble dependent friction term.

3.3.2 Matter Power Spectrum

3.3.2.1 Transfer Function

We can perform a somewhat simplified study of the shape of the linear matter power spectrum by analytically modelling a transfer function characterising the evolution of the density fluctuations during the radiation era and describing the interactions between photons and baryons [174; 175]

$$T(k,z) = \frac{\delta(k,z)}{\delta(k,z_i)}\,\frac{D_+(z_i)}{D_+(z)}, \tag{3.117}$$

where, naturally, the transfer function depends on the cosmological parameters and content of the Universe. This function is defined to have the limit

$$\lim_{k\to 0} T(k) = 1 \tag{3.118}$$

as super-horizon modes will not be affected by radiation domination as they only re-enter the horizon during the matter era. The aim of this approach is to relate the dark matter power spectrum to the initial power spectrum of density fluctuations

$$P_\delta(k,z) \Longleftrightarrow P_\zeta(k,z), \tag{3.119}$$

hence we need to connect the linear density contrast δ to Bardeen's curvature perturbation Φ. This is achieved by invoking Poisson's equation

$$k^2\Phi_k\, k\, T(k) = 4\pi G\rho_m(z)\,\frac{\delta_{m,k}(z)}{(1+z)^2} = \frac{3}{2}\Omega_m\, H_0^2\,\delta_{m,k}(z)\,(1+z) \tag{3.120}$$

where $T(k)$ is the linear transfer function that describes the evolution of density fluctuations in the radiation era and hence the interactions between photons and baryons. At early times, non-linear evolution may be neglected and ignored on the scales we are interested in. The result is that we can write the linear density perturbation in terms of the primordial potential

$$\delta_{\mathrm{lin,k}}(z) = \frac{M(k)}{(1+z)}\Phi_k \tag{3.121}$$

$$M(k) = \frac{2}{3}\frac{k^2 T(k)}{\Omega_m H_0^2}. \tag{3.122}$$

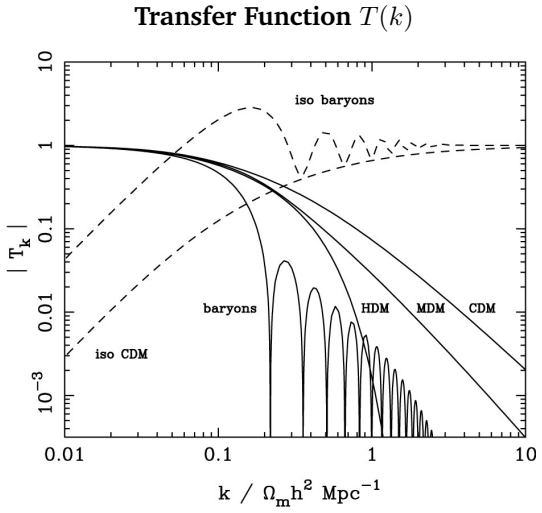

Figure 3.3: Here we show transfer functions $T(k)$ for various different scenarios. For different species of matter, the scales at which features become dynamically important differ. For instance, in CDM models the small scale features at high k are clearly suppressed in comparison to larger scales. For baryons, this transition scale is larger due to the erasure of small scale structure by the heating induced by tight coupling between photons and baryons. From [425].

The time evolution of the primordial potential is therefore given by

$$P_\Phi(k, a_0) = T^2(k, a_0) P_\Phi(k, a_i) \tag{3.123}$$

and, because $P_\delta(k, a_i) = k^4 P_\Phi(k, a_i)$, we have the time evolution of the matter power spectrum

$$P_\delta(k, a_0) = P_\delta(k, a_i)\, T^2(k, a_0) \left[\frac{D_+(a_0)}{D_+(a_i)}\right]^2 . \tag{3.124}$$

The approximate shape of the transfer function can be deduced from reasonable physical assumptions. Modes that become sub-Hubble during the radiation dominated era $k \gg k_{\rm eq}$ remain almost constant, if we ignore logarithmic growth contributions, from $\eta \sim 1/k$ to $\eta \sim 1/k_{\rm eq}$. As $k > k_{\rm eq}$, we expect the transfer function to behave as $T \propto (k_{\rm eq}/k)^2$ due to this lack of growth. For modes that undergo growth $k \ll k_{\rm eq}$ we have $T(k, a_0) \sim 1$. This approximate transfer function encapsulates some of the key ideas but is far from accurate due to the step in the function and the rather grotesque simplifications. More accurate formula exist for modelling the transfer function [36; 174; 175]. The classic transfer function of [36] is given by (see Fig. 3.3)

$$T(q) = \frac{\ln(1 + 2.34q)}{2.34q} \left[1 + 3.89q + (16.1)^2 + (5.46q)^3 + (6.71q)^4\right]^{-1/4} , \tag{3.125}$$

where $q = k/(\Gamma {\rm Mpc}^{-1})$ and $\Gamma = \Omega_{m0} h^2$. This transfer function is valid for cold dark matter models with adiabatic initial conditions. Extensions to isocurvature conditions have been given

$$T(q) = (5.6q)^2 \left\{1 + \left[15q + (0.9q)^{3/2} + (5.6q)^2\right]^{1.24}\right\}^{-1/1.24} . \tag{3.126}$$

We will not need this form but will use the adiabatic result in Chapter 4. This builds on the

work of many authors but notable contributions can be found in [36; 68; 69; 157]. In Fig. 3.4 we show a number of cosmological measurements for the 3-dimensional Fourier power spectrum compared to the linear matter power spectrum extrapolated to $z = 0$ assuming the best fit ΛCDM parameters.

Finally, we note that the most accurate approach would be to solve the full relativistic Boltzmann equation. We will often use publicly available numerical packages, such as CAMB [320], to accurately calculate the matter power spectrum for a set of cosmological parameters.

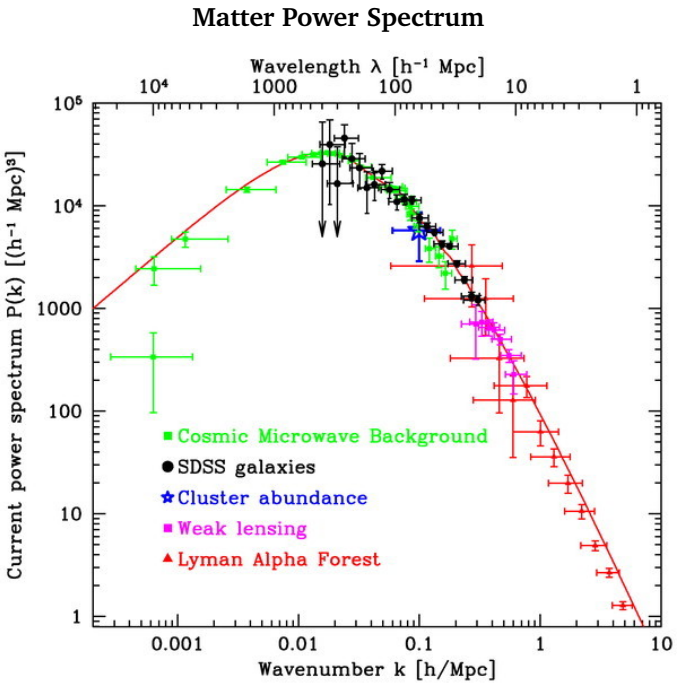

Figure 3.4: The matter power spectrum compared to observations that range from linear scales, such as the CMB, to non-linear scales such as those probed by weak lensing. The various measurements are labeled on the figure and the solid line is the matter power spectrum extrapolated to $z = 0$ assuming the best fit parameters in the ΛCDM model. From [555].

3.3.3 Variance of Large Scale Structure

The variance of the matter power spectrum is given by

$$\sigma_0^2 = \langle \delta^2 \rangle \tag{3.127}$$

where we can also introduce analogous quantities that are related to derivatives of the density field

$$\sigma_1^2 = -\langle \delta \, \nabla^2 \delta \rangle, \tag{3.128}$$

$$\sigma_2^2 = \langle \nabla^2 \delta \, \nabla^2 \delta \rangle. \tag{3.129}$$

These quantities will be used extensively in our discussion on Minkowski functionals where we introduce a series expansion about a Gaussian background using the variance parameters σ_j to track the order of the expansion. For large scale structure, the variance parameters of the unsmoothed field density fluctuations are calculated by integrating over the matter power spectrum

$$\sigma_j^2 = \int \frac{k^2 dk}{2\pi^2}\, k^{2j} P(k), \tag{3.130}$$

and the variance parameters of the smoothed density fluctuations, with smoothing function $W(kR)$ of smoothing length R, will be calculated by

$$\sigma_j^2 = \int \frac{k^2 dk}{2\pi^2}\, k^{2j} P(k) W^2(kR). \tag{3.131}$$

Finally, we introduce one last quantity, $\sigma_{8h^{-1}\mathrm{Mpc}}$, which is *not* the same as σ_8 in the notation above. The quantity $\sigma_{8h^{-1}\mathrm{Mpc}}$ is a crucial parameter in cosmology which does have a large influence over the growth of fluctuations in the early Universe. The normalisation of the initial power spectrum is specified such that the variance of the density fluctuations in a sphere of radius $R_8 = 8h^{-1}\mathrm{Mpc}$ is on order unity

$$\sigma^2_{8h^{-1}\mathrm{Mpc}} = \left\langle \frac{3}{4\pi R_8^3} \int \delta(\mathbf{x})\, d^3\mathbf{x} \right\rangle \sim 1. \tag{3.132}$$

In essence, this length scale R_8 tells us the fundamental scale below which non-linearities cannot be neglected as the density contrast becomes too large for linear theory to be a good approximation. Remember, the linear approach works very well for $\delta \ll 1$. In order to account for non-linear evolution of the density field, it is conventional to perform a perturbative expansion

$$\delta = \delta^{(1)} + \delta^{(2)} + \dots \tag{3.133}$$

with each term $\delta^{(n)}$ being of order ϵ^n in the initial density field.

3.3.4 Skewness

The skewness of large scale structure has long been used as a testing ground for deviations from Gaussianity [285; 286]. The skewness is simply related to the variance weighted third-order moment of the density field [432], which is defined by

$$\langle \delta^3 \rangle = \left\langle (\delta^{(1)})^3 \right\rangle + \left\langle (\delta^{(1)})^2 \delta^{(2)} \right\rangle + \mathcal{O}(\epsilon^5). \tag{3.134}$$

The skewness itself is defined by the following expression

$$S_3(0) = \frac{\langle \delta^3 \rangle}{\langle \delta^2 \rangle^2} \sim \frac{34}{7} - (n+3), \tag{3.135}$$

where the last relation holds if we neglect the presence of a window function $W(kR)$.

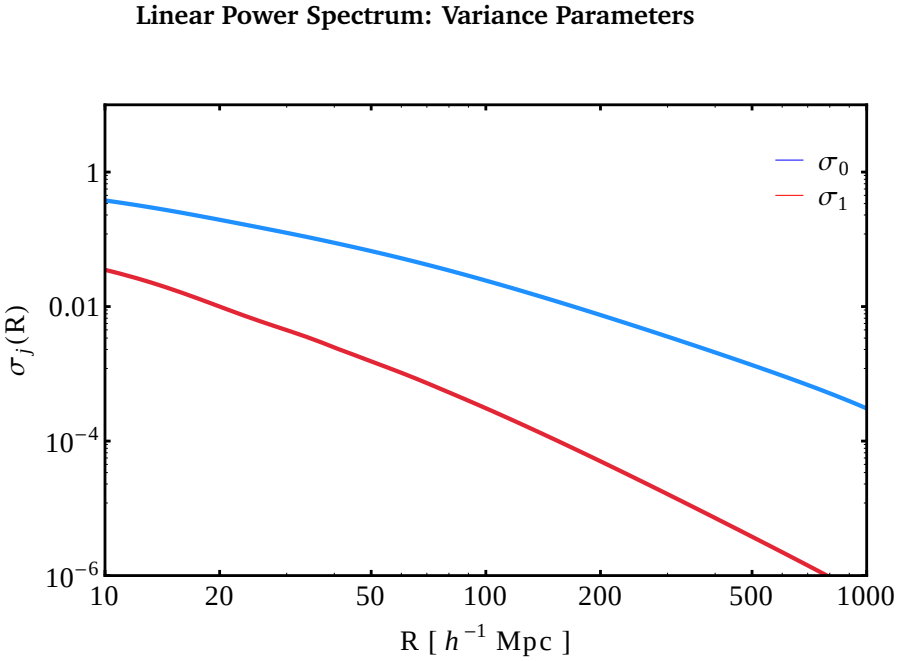

Figure 3.5: Here we plot the two variance parameters for a linear matter power spectrum $P_{\rm Lin}(k)$ smoothed by a Gaussian window of smoothing length R where the parameters are defined by Eq. (3.131).

Chapter 4

Minkowski Functionals and Large Scale Structure

4.1 Introduction

As we saw in the previous Chapter, the canonical model for inflation is a single free scalar field obeying the Hamilton-Jacobi slow-roll constraints in a semiclassical background governed by Einstein gravity with initial conditions set by assuming that the vacuum state asymptotically approaches the Bunch-Davies vacuum. The appeal of invoking such an inflationary model is that it provides a rather natural mechanism for solving the causality and flatness problems whilst allowing for the generation of primordial density perturbations through quantum mechanical fluctuations [383; 325; 532; 245; 231; 326]. The scalar field model draws motivation from concepts in particle physics and in many ways represents a vanilla model for inflation in the sense that we have made rather minimal assumptions about the presence of physics beyond the standard model in the early Universe. It should be emphasized, however, that whilst the scalar field models draw on ideas from particle physics there is, as of yet, no known candidate particle that could source the hypothetical quantum field driving inflation as we saw in Section 3.2. The energy scales typically associated with inflationary cosmology are currently far beyond that accessible to terrestrial experiments and we must necessarily extrapolate current theories to these energy scales prompting questions over the validity of the effective field theories in describing inflationary models and possible quantum gravity (i.e. UV) inspired corrections (e.g. [155; 137; 288; 46]).

The CMB probes the early Universe in a linear regime acting, currently, as one of the most direct probes of the dynamics of the early Universe. One of the largest problems with current and future CMB surveys (e.g. polarization) is the relatively small signal-to-noise ratios. Planck is expected to exhaust the information content of the temperature anisotropies but will not provide strong statistical constraints on the polarization with a number of dedicated polarization missions in the development stage (e.g. CMBPol [44], COrE [74]). Given that we only have access to one realization of the Universe, it is important to use as many cosmological data sets as possible to analyse the statistical properties of primordial density perturbations (e.g. [500; 576; 144; 322; 389]).

A number of recent papers have suggested that the statistics of dark halos may provide as stringent constraints on primordial non-Gaussianity as CMB observations (e.g. [87; 136; 355]). When observing large scale structure we encounter more severe non-linearities, for which there a plethora of mechanisms for generating significant non-Gaussianity. The first and most prominent is the non-linear evolution of structure through gravitational instability. A second source of non-linearity is the bias relation between the galaxy and matter distributions that arises when considering large scale structure surveys. The final, and in our case most interesting, source of non-Gaussianity is primordial in origin. In this Chapter we consider the role of large scale structure (LSS) surveys in providing a probe of early Universe cosmology and further develop the skew-spectra as a tool to distinguish between various contributions to the observed bispectrum of LSS.

The set of statistics that we will be the central focus of this chapter are a set of topological statistics known as the Minkowski functionals, which can be used to characterise the morphological properties of cosmological random fields. These functionals have been extensively developed as a statistical tool in a cosmological setting for both 2-dimensional (projected) and 3-dimensional (redshift) surveys and are analytically known for Gaussian and weakly non-Gaussian random fields, making them suitable for studies of non-Gaussianity. Examples of such studies include CMB data [113; 422; 118; 484; 414; 303; 178; 145; 261; 401], weak lensing [358; 477; 549; 396], large scale structure [212; 113; 213; 373; 114; 382; 215; 370; 461; 465; 86; 483; 466; 474; 485; 486; 293; 423; 262; 260; 257; 259], 21cm [203], Sunyaev-Zel'dovich (SZ) maps [395] and N-body simulations [486; 293; 258]. Note that this is an incomplete list of references and we have selected a sample of representative papers from the literature.

The Minkowski functionals, being intrinsically defined in the spatial domain, provide a probe of all orders of correlation functions in contrast to the more conventional polyspectra or Fourier-space methods (e.g. power spectrum, bispectrum and trispectrum). In the weakly-non-Gaussian limit it was shown [260] that the Minkowski functionals reduce to a weighted probe of the bispectrum given in terms of a set of skewness parameters. This makes the Minkowski functionals complementary to Fourier based methods as it offers an alternative probe of the data in the presence of contaminants such as survey masks, inhomogeneous noise, foregrounds, etc [260].

The next decade should see the next generation of large scale structure surveys beginning to produce cosmological data sets in unprecedented detail with the most notable of these surveys including: WiggleZ [1] [63], Euclid [2] [310], WFIRST [3] [222], Boss [4], BigBoss [5] [480] and Subaru PFS [6]. These future surveys can be combined with the latest CMB measurements to effectively trace the growth of structure formation from the surface of last scattering ($z \approx 1100$) through to the local Universe ($z \sim \mathcal{O}(1)$). The availability of such data sets promises to provide tight constraints on cosmological parameters [586; 556], angular diameter distance derived from BAO measurements [430], Hubble expansion rate, growth rate of structure formation [431], Gaussianity of initial conditions and the nature of late time cosmic acceleration [10]. With more comprehensive data sets, a deeper understanding of systematics (e.g. [263]) and improved understanding of both primordial and late time contributions to non-linearity of the growth of structure (e.g. [54; 100])

[1] http://wigglez.swin.edu.au/site/
[2] http://euclid.gsfc.nasa.gov/
[3] http://wfirst.gsfc.nasa.gov/
[4] http://cosmology.lbl.gov/BOSS/
[5] http://bigboss.lbl.gov/
[6] http://sumire.ipmu.jp/en/

it becoming possible to do comprehensive studies utilising higher order statistics. In particular, we are slowly reaching a point where it will be possible to break degeneracies between various contributions to observed non-linearity (primordial, gravitational instability, bias, systematics, etc) and constrain theories for the early and late Universe.

The work presented in this Chapter is based on [434] and the outline for this Chapter is as follows: In Section 4.2 we introduce the foundations of integral geometry and differential topology that will be needed in order to understand the geometrical interpretations of the Minkowski functionals. This section can be considered as somewhat optional and the main statistical results and analysis is presented in Sections 4.3.5 and 4.4 and We proceed to introduce the Minkowski functionals via Crofton's Intersection formula in Section 4.2.4.1 and via the Koenderink invariants in Section 4.2.4.2. We subsequently discuss analytical results for the Minkowski Functionals in a Gaussian random field in Section 4.3.4 before detailing the extension to weakly non-Gaussian fields using the perturbative approach in Section 4.3.5.

The particular cosmology that we will adopt for numerical studies in this Chapter is defined by the following parameters: $\Omega_\Lambda = 0.741, h = 0.72, \Omega_b = 0.044, \Omega_{\rm CDM} = 0.215, \Omega_{\rm M} = \Omega_b + \Omega_{\rm CDM}, n_s = 0.964, w_0 = -1, w_a = 0, \sigma_8 = 0.803, \Omega_\nu = 0$.

4.2 The Minkowski Functionals

4.2.1 Introduction

As we mentioned in the introduction, the Minkowski functionals were originally introduced in cosmology as a means to study the morphological and topological properties of large scale structure and, more recently, cosmological random fields. The Minkowski functionals were originally introduced by Minkowski in 1903 [375] as a means to associate a probability measure with a transformation group, with the Minkowski functionals being distinguished by a strict motion invariance, to solve long standing problems in stochastic geometry. It was the further work of Austrian mathematician Blaschke that resulted in the systematic study of what is now known as integral geometry [64]. It was this work that introduced the Quermaß integrals or the *scalar Minkowski functionals*. This initiated a whole field of study with many important insights into geometric probability and stochastic geometry being introduced as a result [234; 469].

In this section we will concisely introduce some fundamental concepts and basic notions in the fields of integral geometry and differential topology. These two branches of mathematics provide us with two distinct routes that lead to technically different definitions of the topological characteristics but, for applications to cosmology, remain numerically equivalent or approximately so [115]. Differential topology defines the topological characteristics based on the spatial derivatives of the contour surfaces and provides a very elegant framework from which we can derive analytical results. The primary downside is that the resulting numerical calculations often become somewhat cumbersome. Integral geometry, however, provides a numerically convenient framework in which we can calculate the topological properties of a random field but is analytically cumbersome and analytical results do not arise as elegantly as in differential topology.

4.2.2 Differential Topology

We first outline some key results in differential topology that will be of use in understanding the Minkowski Functionals, many of these results are quoted without proof and the reader is referred to the literature for a detailed overview [1]. In reality, much of the mathematical literature is overloaded with additional structure that is not needed in cosmological applications and we will often drop such rigour in favour of physical intuition. In this brief introduction we will be strongly guided by the presentation in [115].

Given a random field $\Psi(\mathbf{x})$ defined on a d-dimensional support $\mathcal{V} \subseteq \mathbb{R}^d$, the excursion set Q is the set of all points for a given threshold ν for which $Q = \{\mathbf{x}|\Psi(\mathbf{x}) > \nu\sigma\}$, where $\sigma = \{\Psi\}^{1/2}$ is the standard deviation. The bounding surface of the excursion set is given by ∂Q, this is the focus of differential topology and not the excursion set. If we consider a 2-dimensional manifold $\mathcal{M}$ with one-dimensional boundary $\partial\mathcal{M}$, which is piecewise smooth[7]. The Gauss-Bonnet theorem states that the Euler characteristic of the manifold is defined by

$$2\pi\chi_E(\mathcal{M}) = \int_{\mathcal{M}} K\, dA + \int_{\partial\mathcal{M}} k_g\, ds + \sum_{i=1}^{n}(\pi - \alpha_i), \tag{4.1}$$

where K is the Gaussian curvature of $\mathcal{M}$, k_g is the geodesic curvature of the curve $\partial\mathcal{M}$, ds is a length element, dA is an area element and α_i are the set of n interior angles of the vertices of the boundary $\partial\mathcal{M}$. In this thesis we will not consider any applications where vertices in the boundary will occur and we will drop this term from our discussion. The Gauss-Bonnet theorem as it stands is relevant to both 2- and 3-dimensional excursion sets. In the 2-dimensional case, defined on a flat surface, the Gaussian curvature K vanishes and the Euler characteristic is simply given by a contour integral along the boundary

$$2\pi\chi_E = \int_{\partial\mathcal{M}} k_g ds, \tag{4.2}$$

which may be interpreted as the number of isolated regions minus the number of holes in the isolated regions. In the 3-dimensional case, such that we have an excursion set bounded by a 2-dimensional surface with no boundary[8], the Euler characteristic reduces to an integral of the Gaussian curvature of the surface over all compact pieces of the excursion set [115]

$$2\pi\chi_E = \int_{\mathcal{M}} K\, dA. \tag{4.3}$$

This quantity is the one that we will be interested in, as our focus will be on 3-dimensional random fields. The literature tends to be rather split as to which quantity is of interest: the Euler characteristic χ_E or the genus g. The genus is approximately the number of handles that a compact two-dimensional surface possesses. A sphere will have a genus of zero whereas a torus will have a genus of 1. Similarly, a coffee cup will have a genus of 1 and is topologically equivalent to the torus as it may be smoothly deformed into a torus but we may not smoothly remove the handle.

[7] This simply means that we allow vertices to appear where differentiability of the boundary breaks down.
[8] E.g. a sphere or torus would ensure that k_g vanishes.

The two topological invariants are related by the following equation

$$\chi_E = 2(1-g). \tag{4.4}$$

The genus is a topological quantity that is defined for 3-dimensional sets with closed 2-dimensional surfaces. If we were to include a boundary term then this relation is modified to $\chi_E = 2(1-g)-b$. The quantity g has no direct analogue in the 2-dimensional situation but the Euler characteristic may be well-defined in both dimensions. The genus defined in this way is somewhat problematic as it does not obey additivity. An example of this behaviour was detailed in [115] and we reproduce their argument here. Given two disjoint spheres, each sphere on its own will have a genus of zero so, intuitively, one would imagine that the total genus is zero. However, the integrated curvature over the surface of each sphere must be 4π such that the total for the set including both spheres is 8π. The Gauss-Bonnet theorem then tells us that the Euler characteristic for each sphere is $\chi_E = 2$. The total set then has an Euler characteristic of $\chi_E = 4$ and thus the genus is given by $g = -1$. The cosmology community has taken to defining an additive topological quantity that is also termed the *genus*

$$g_s = -\frac{\chi_E}{2}. \tag{4.5}$$

Reproducing our discussion above for the quantity g_s we see that for each sphere $g_s = -1$ and for the total set $g_s = -2$, as we would expect in the additive case. For simply connected surfaces, such as the scenario we just described, $g_s < 0$ and for multiply connected surfaces $g_s \geq 0$.

4.2.3 Integral Geometry

4.2.3.1 The Convex Set

A landmark result in integral geometry is Hadwiger's theorem [234] demonstrating the uniqueness and completeness of the Minkowski functionals under rather general assumptions

Definition 4.1. Hadwiger's theorem states that the morphological properties of a d dimensional convex set, or any finite union of convex sets, that satisfies motion invariance, additivity and continuity will completely described by a set of $d+1$ functionals known as the Minkowski functionals [234; 235].

By *morphological*, we simply mean the properties of a random field that are invariant under translations, rotations and obey additivity. We will provide a more mathematical definition of these properties in Section 4.2.3.2. A collection of points $\mathcal{K}$ in a d-dimensional Euclidean space $\mathbf{R}^d$ is a convex set if for every pair of points in $\mathcal{K}$ we can join them with a line segment that is contained in $\mathcal{K}$. If the interior of this set is not empty then we say that we have a convex body. If the set is also bounded and closed, we say that the set is *compact*. The class of all convex sets that are bounded and closed is denoted by $\mathbb{K}$. The *outer parallel set* $\mathcal{K}_r$ of distance r to the convex set $\mathcal{K}$ is the union of all closed balls of radius r centered at the point k

$$\mathcal{K}_r = \bigcup_{k\in\mathcal{K}} b(k,r). \tag{4.6}$$

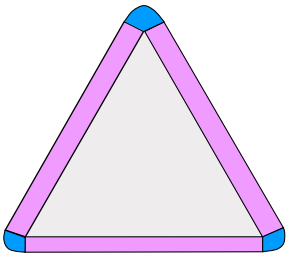

Figure 4.1: To find the area of the parallel set $\mathcal{K}_r$ that encloses the original triangle $\mathcal{K}$ (in grey) we can use the Steiner formula. In 2-dimensions this reduces to a sum over three components: the area of the original triangle (in grey), the area of the corners (in blue) and the perimeter (in purple). Each of these contributions is related to one the Minkowski functionals in 2-dimensions W_i for $i \in \{0, 1, 2\}$.

From this definition, we can invoke what is known as the Steiner formula to relate the volume of $\mathcal{K}_r$ to the Minkowski functionals W_i as follows [234; 591; 374]

$$\mathcal{V}(\mathcal{K}_r) = \sum_{i=0}^{d} \binom{d}{i} W_i(\mathcal{K}) r^i \tag{4.7}$$

where $\mathcal{V}$ denotes the n-dimensional volume. In low-dimensions the Minkowski functionals take on simple geometrical interpretations. We can build up a lot of intuition by first considering 2-dimensions before generalising to the 3-dimensional case. In 2-dimensions we find that [591]

$$W_0(\mathcal{K}) = \mathcal{A}(\mathcal{K}) \tag{4.8}$$

$$W_1(\mathcal{K}) = \frac{1}{2}\mathcal{L}(\mathcal{K}) \tag{4.9}$$

$$W_2(\mathcal{K}) = \pi, \tag{4.10}$$

where $\mathcal{A}$ is the 2-dimensional area, $\mathcal{L}$ is the boundary length or perimeter in 2-dimensions and W_2 is just π as the Euler characteristic of a disk is just unity (Fig. 4.1). The area of the parallel set $\mathcal{V}(\mathcal{K}_r)$ can then be written as

$$\mathcal{V}(\mathcal{K}_r) = \mathcal{A}(\mathcal{K}) + r\mathcal{L}(\mathcal{K}) + \pi r^2. \tag{4.11}$$

This has a neat geometric interpretation attached to it. Consider a convex set constructed from a regular triangle Fig. 4.1. In order to find the area of the parallel set that engulfs our triangle we need to sum three different components

1. The area of the original triangle (grey shaded in Fig. 4.1): $\mathcal{A}(\mathcal{K})$.
2. The area of the rectangles in that join the corners (purple shaded in Fig. 4.1): $r\mathcal{L}(\mathcal{K})$.
3. The area of the three corner sections, whose union forms a circle with Euler characteristic of unity, $\chi_E(\mathcal{K}) = 1$, and a radius r (blue shaded in Fig. 4.1): πr^2.

This concept is visually shown in Fig. 4.1. With this intuition in place, we can now move one dimension higher and consider the 3-dimensional case. The Minkowski Functionals W_i are now

defined by

$$W_0(\mathcal{K}) = \mathcal{V}(\mathcal{K}) \tag{4.12}$$

$$W_1(\mathcal{K}) = \frac{1}{3}\mathcal{S}(\mathcal{K}) \tag{4.13}$$

$$W_2(\mathcal{K}) = \frac{2\pi}{3}\mathcal{B}(\mathcal{K}) \tag{4.14}$$

$$W_3(\mathcal{K}) = \frac{4\pi}{3} \tag{4.15}$$

where $\mathcal{V}$ is the 3-dimensional volume of the convex set $\mathcal{K}$, $\mathcal{S}$ is the surface area of $\mathcal{K}$, $\mathcal{B}$ is the mean width of $\mathcal{K}$, also related to the integrated mean curvature, and W_3 is related to the volume of a sphere. This means that the volume of the 3-dimensional volume $\mathcal{V}(\mathcal{K}_r)$ is given by

$$\mathcal{V}(\mathcal{K}_r) = W_0(\mathcal{K}) + 3rW_1(\mathcal{K}) + 3r^2W_2(\mathcal{K}) + r^3W_2(\mathcal{K}) \tag{4.16}$$

$$= \mathcal{V}(\mathcal{K}) + r\mathcal{S}(\mathcal{K}) + 2\pi r^2\mathcal{B}(\mathcal{K}) + \frac{4\pi r^3}{3}. \tag{4.17}$$

Again, we can attach a geometric picture to this formula. Let our 3-dimensional volume $\mathcal{K}$ be that of a regular cube. In order to find the volume of the 3-dimensional tube engulfing the original cube we need 4 different components:

1. The volume of the original cube: $\mathcal{V}(\mathcal{K})$.
2. The volume of the section of the tube that connects the corners to one another, i.e. the surface area of the cube: $r\mathcal{S}(\mathcal{K})$.
3. The mean width $\mathcal{B}(\mathcal{K})$.
4. The volume of the corners, whose union forms a sphere of radius r: $\frac{4}{3}\pi r^3$.

The mean width is related to integrated mean curvature as follows

$$\mathcal{B}(\mathcal{K}) = \int_{\partial\mathcal{K}} \frac{H}{2\pi} ds, \tag{4.18}$$

where the mean curvature is given by $2H = (\kappa_1 + \kappa_2)$.

So, what does this all mean? Hadwiger's theorem is just telling us that given simple geometrical objects, currently just a convex set $\mathcal{K}$, we can evaluate the change in the geometrical properties of the object as long as the object is smoothly deformed such that its topology does not change. This was one of the bedrocks and foundational principles in providing a complete morphological characterisation of convex sets in Euclidean space. However, the machinery we have defined above is only valid for the convex set and this clearly reflects some underlying constraints on the shape of our object. We need to extend this definition to relax the constraints and consider objects of generic shape. To do this we need to introduce some additional machinery into our framework.

4.2.3.2 The Convex Ring

In Section 4.2.3.1 we developed some intuition into how the Minkowski functionals are tied to geometrical concepts by using Steiner's formula 4.7 to study the Minkowski functionals applied

to convex sets. We now need to extend the principles above to objects with no constraints on the shape. This is clearly not possible with just a convex set and we will need to slightly modify the machinery to expand our definitions to the finite union of all convex sets, known as the *convex ring*. The *convex ring* is class of all subsets T of $\mathbb{R}^d$ that may be expressed as a union of compact convex sets:

$$T = \bigcup_{i=1}^{r} \mathcal{K}_i \quad ; \quad \mathcal{K}_i \in \mathcal{K} \tag{4.19}$$

A more intuitive view, perhaps, is that we can treat a pixel as a convex set and element of $\mathbb{K}$ and hence an image or cosmological data set will just be an instance of the convex ring $\mathcal{R}$. So whilst the concepts introduced can seem rather abstract, their physical relations are surprisingly simple. In this section we will provide a more mathematical definition for motion invariance, additivity and continuity and sketch out their physical implications. We will then proceed to construct a functional that obeys these properties for a convex set and outline how this generalises to the convex ring.

As before, we now introduce a continuous map $\varphi : \mathcal{K} \to \mathbf{R}$ such that the map obeys the following properties [1; 591; 374] [591; 374]

1. *Motion Invariance*: Given the group $\mathcal{G}$ of all translations and rotations in $\mathbf{R}^d$, a function is motion invariant if it obeys

$$\varphi(g\mathcal{K}) = \varphi(\mathcal{K}); \quad \forall \mathcal{K} \in \mathbb{K}, g \in G_d. \tag{4.20}$$

2. *Additivity*: A functional is additive, on the convex set $\mathcal{K}$, if it obeys

$$\varphi(\mathcal{K}_1 \bigcup \mathcal{K}_2) + \varphi(\mathcal{K}_1 \bigcap \mathcal{K}_2) = \varphi(\mathcal{K}_1) + \varphi(\mathcal{K}_2). \tag{4.21}$$

   Note that this criterion is not just a technicality, the union of two convex sets will not necessarily be itself convex, even if the intersection is.

3. *Continuity*: The functional φ is continuous if

$$\lim_{r\to\infty} \varphi(\mathcal{K}_r) = \varphi(\mathcal{K}), \tag{4.22}$$

   whenever $\{\mathcal{K}_r\}$ is a sequence of compact sets such that $\lim_{r\to\infty} \mathcal{K}_r = \mathcal{K}$ in the Hausdorff metric.

These are not just enforced for fun, not only do they have important implications for the definition of the Minkowski functionals but they also have important implications for data sets in cosmology. For instance, motion invariance simply ensures that the measurement φ does not depend on our choice of coordinate system. Additivity is important for constructing global properties of the random field from local ones and is one of the backbones of Hadwiger's theorem. Finally, continuity is just an overbearing technical criterion that is automatically satisfied when working with digitised or pixalised images and is just a way of saying that we can smoothly shrink the parallel $\mathcal{K}_r$ back towards the original set $\mathcal{K}$ in a continuous way. These criteria seem rather general and it would

be natural to think that we are left with a vast choice of functionals. To our surprise, however, Hadwiger's theorem states that there are only $d+1$ independent functionals for a d-dimensional space. Put differently, the continuous functional $\varphi(\mathcal{K})$ can be expressed as a linear combination of the Minkowski functionals [591]

$$\varphi(\mathcal{K}) = \sum_{i=0}^{d} \alpha_i W_i(\mathcal{K}), \quad \alpha_i \in \mathbb{R}. \tag{4.23}$$

This means that the $d+1$ Minkowski functionals provide a complete set of morphological measures on the set of convex bodies $\mathcal{K}$. An important point that was rather glossed over in the discussion above is that the additivity criterion was defined for convex sets. What we really require in cosmology is a set of morphological estimators defined on the convex ring $\mathcal{R}$. As before, we can define an additive functional $\tilde{\varphi}$ such that

$$\tilde{\varphi}\left(T_1 \bigcup T_2\right) + \tilde{\varphi}\left(T_1 \bigcap T_2\right) = \tilde{\varphi}\left(T_1\right) + \tilde{\varphi}\left(T_2\right) \; ; \; T_1, T_2 \in \mathcal{R}. \tag{4.24}$$

We have denoted the functional on the convex ring as $\tilde{\varphi}$ just to make the transition a little more transparent. One of the most important jumps made when extending from a convex set $\mathbb{K}$ to the convex ring $\mathcal{R}$ is the introduction of the Euler characteristic such that (see [374] for a nice introduction)

$$\chi_E(\mathcal{K}) = \begin{cases} 1 & \mathcal{K} \neq \emptyset \\ 0 & \mathcal{K} = \emptyset \end{cases} \tag{4.25}$$

for all $\mathcal{K} \in \mathbb{K}$. For an empty disc or circle is just $\chi_E = 0$ whereas for a non-empty disk $\chi_E = 1$. Remember, in 2-dimensions the Euler characteristic is roughly the number of isolated regions minus the number of holes. The Euler characteristic is additive, motion invariant and continuous on $\mathcal{R}$. Hence, for our element T of the convex ring $\mathcal{R}$ we see that [1; 115; 374]

$$\chi_E(T) = \chi_E\left(\bigcup_{i=1}^{r} \mathcal{K}_i\right). \tag{4.26}$$

This can be used to define the entire set of Minkowski functionals for all elements of the convex ring $T \in \mathbb{R}$ such that $W_i^{(d)}(T) = \omega_i \chi(T)$, this procedure is defined by Crofton's intersection formula as in Section 4.2.4.1. These $d+1$ Minkowski functionals will provide a complete system of additive functionals on the set of objects that are construction from the finite union of convex bodies [374]. Note that we have purposefully left the mathematical details to the literature as it does not add any extra intuition at this point. In summary, we have just demonstrated that the Hadwiger characterisation theorem can be generalised to the convex ring and thereby defined the Minkowski functionals over the convex ring.

We will often find it more convenient to renormalise the Minkowski functionals in terms volumes of unit balls in d-dimensions such that [481; 591; 374]

$$M_i(\mathcal{K}) = \frac{\omega_{d-i}}{\omega_d \omega_i} W_i(\mathcal{K}), \tag{4.27}$$

where

$$\omega_d = \frac{\pi^{d/2}}{\Gamma(1+d/2)}. \tag{4.28}$$

In the notation given here, the 3-dimensional Minkowski functionals reduce to

$$M_0(\mathcal{K}) = \mathcal{V}(\mathcal{K}) \tag{4.29}$$

$$M_1(\mathcal{K}) = \frac{1}{8}\mathcal{S}(\mathcal{K}) \tag{4.30}$$

$$M_2(\mathcal{K}) = \frac{1}{\pi}\mathcal{B}(\mathcal{K}) \tag{4.31}$$

$$M_3(\mathcal{K}) = \frac{3}{4\pi}\chi_E(\mathcal{K}). \tag{4.32}$$

4.2.4 Practical Calculations

In terms of practical applications and practical calculations using the Minkowski functionals, we need a formalism that we can apply to Gaussian and weakly non-Gaussian random fields. Two of the main approaches to calculating the Minkowski functionals in this instance are through Crofton's intersection formula and via curvature weighted integrals. Crofton's intersection formula is particularly apt for numerical calculations and we only mention it in passing. The main approach adopted in this thesis is via the curvature weighted integrals. An additional extension to the local curvature method was given by Koenderink [298] in which 2-dimensional images were analysed with respect to geometric invariants formed from the first and second derivatives of the random field. The calculations have been done in 2- and 3-dimensions [482; 483] and have been particularly successful in applications to the CMB (e.g. [414; 260]).

4.2.4.1 Crofton's Intersection Formula

Crofton's intersection formula is one of the classic results in integral geometry and enables us to relate the Minkowski functionals from different dimensions [135]. Here, we consider a body K in d dimensions along with an arbitrary k dimensional hyperplane E and seek to calculate the Euler characteristic χ of the intersection $K \bigcap E$ in k dimensions. By integrating this quantity over the space of all possible hyperplanes $\mathcal{E}_k^{(d)}$, we arrive at the kth Minkowski functional of the body k in d dimensions. Crofton's formula reduces to

$$v_k^{(d)}(K) = \frac{\omega_d}{\omega_{d-k}\omega_k} \int_{\mathcal{E}_k^{(d)}} d\mu_k(E)\, \chi^{(k)}\left(K \bigcap E\right). \tag{4.33}$$

Note that the measure $d\mu_k$ is normalised such that

$$\int_{\mathcal{E}_k^{(d)}} d\mu_k(E) = 1. \tag{4.34}$$

The power of this approach is that if we let K represent the excursion set of some homogeneous and isotropic random field sampled for L points in a cubic lattice of spacing a, then it is possible to just sum over the set $\mathcal{L}_k^{(d)}$ of all dual lattice hyperplanes [483]. The integral can then be replaced

by a summation over the hyperplanes

$$v_k^{(d)}(K) = \frac{\omega_d}{\omega_{d-k}\omega_k} \sum_{E \in \mathcal{L}_k^{(d)}} \frac{1}{a^k L} \frac{k!(d-k)!}{d!} \chi^{(k)} \left(K \bigcap E \right). \tag{4.35}$$

We do not discuss this approach further and instead refer the reader to [483] for further details. We do note however that this approach is particularly optimised for numerical calculations due to the cubic lattice structure implemented.

4.2.4.2 Koenderink Invariants

We can now consider the differential topology approach to evaluate the Minkowski functionals in terms of a spatial average of Koenderink invariants. This approach will be the most useful in the application of the Minkowski functionals presented later on in this Chapter. We closely follow the presentation of [484]. Consider a random field $\Psi(\mathbf{x})$ defined on a d dimensional support $\mathcal{V} \subseteq \mathbb{R}^d$. The excursion set Q can be calculated for a given threshold ν by taking all points in the random field above the threshold: $Q = \{\mathbf{x} | \Psi(\mathbf{x}) > \nu\sigma\}$, where $\sigma = \{\Psi^2\}^{1/2}$ is the standard deviation. We now wish to calculate the Minkowski functionals per unit volume $V_k^{(d)}(\nu)$. The zeroth Minkowski functional corresponds to a volume functional and can simply be defined via a volume integration over the excursion set Q. This can be written in terms of a Heaviside step function Θ as

$$V_0(\nu) = \frac{1}{|\mathcal{V}|} \int_{\mathcal{V}} d^d x \, \Theta \left(\nu - \Psi(\mathbf{x}) \right). \tag{4.36}$$

Assuming that the excursion set has a smooth boundary ∂Q, the remaining Minkowski functionals will be given by surface integrals [488]

$$V_i(\nu) = \frac{1}{|\mathcal{V}|} \frac{1}{\omega_{i-1} \binom{d}{i}} \int_{\partial Q} ds \, \mathfrak{S}_i \left(\kappa_1 \dots \kappa_{d-1} \right). \tag{4.37}$$

where ds is the surface element defined on Q, κ_i are the principal curvatures of the $d-1$ boundary and $\mathfrak{S}_i$ is the ith elementary symmetric function defined by (e.g. [484])

$$\prod_{i=1}^{d-1} (x + \kappa_i) = \sum_{j=1}^{d} x^{d-j} \, \mathfrak{S}_j \left(\kappa_1 \dots \kappa_{d-1} \right) \tag{4.38}$$

from which we obtain $\mathfrak{S}_1 = 1$, $\mathfrak{S}_2 = \kappa_1 + \dots + \kappa_{d-1}$ all the way to $\mathfrak{S}_d = \kappa_1 \dots \kappa_{d-1}$. The Koenderink approach evaluates the local curvatures in terms of geometric invariants that are formed from the first and second derivatives, such as the square of the gradient. In three dimensions we observe that as the isodensity contour forms a surface there will be two principal curvatures

$$\kappa_1 + \kappa_2 = \frac{\epsilon_{ijm} \, \epsilon_{klm} \, \Psi_{,i} \, \Psi_{,jk} \, \Psi_{,l}}{(\Psi_{,n} \, \Psi_{,n})^{3/2}} \tag{4.39}$$

$$\kappa_1 \kappa_2 = \frac{1}{2} \frac{\epsilon_{ijk} \, \epsilon_{lmn} \, \Psi_{,i} \, \Psi_{,l} \, \Psi_{,jm} \, \Psi_{,kn}}{(\Psi_{,p} \Psi_{,p})^2}, \tag{4.40}$$

where repeated lower indices implies summation. In 3-dimensions, the volume weighted Minkowski functionals $V_k^{(d)}(\nu)$ can be explicitly expressed in terms of curvature (κ_1, κ_2) weighted integrals

$$V_0(\nu) = \frac{1}{|\mathcal{V}|}\int_{\mathcal{V}} d^3x\,\Theta\left(\nu\sigma - \Psi(\mathbf{x})\right) \tag{4.41}$$

$$V_1(\nu) = \frac{1}{6}\frac{1}{|\mathcal{V}|}\int_{\partial Q} ds \tag{4.42}$$

$$V_2(\nu) = \frac{1}{6\pi}\frac{1}{|\mathcal{V}|}\int_{\partial Q} ds\,\left[\kappa_1(\mathbf{x}) + \kappa_2(\mathbf{x})\right] \tag{4.43}$$

$$V_3(\nu) = \frac{1}{4\pi}\frac{1}{|\mathcal{V}|}\int_{\partial Q} ds\,\kappa_1(\mathbf{x})\,\kappa_2(\mathbf{x}). \tag{4.44}$$

The term in 4.43 is related to the integral mean curvature $H(T)$ such that $H(T) = 2\pi\mathcal{B}(T)$ as per 4.2. Similarly, the term in 4.44 is related to the integral of the Gaussian curvature K such that $K(T) = 2\pi\chi_E(\partial T)$ and $\chi_E(\partial T) = 2(1-g)$ as per 4.3. Note that $\chi(\partial T) = \chi(T)\left[1-(-1)^n\right]$ where n is the dimension of the body T such that $(n \leq d)$.

Though we will not discuss this here, there are subtle effects with respect to the boundary effects that can become important in cosmological applications [179; 1; 115]. The details of these corrections and how the integral geometric predictions can differ from the differential topology predictions is outlined very aptly in [115]. We also refer the reader to [115] for a very good discussion of the differential topology and integral geometry approaches discussed here and their applications to cosmology. The estimator arising in differential topology coincides with that from integral geometry if there are no intersections of the set with the boundary or if the random field is periodic.

4.2.5 Geometric Summary

We now briefly summarise the geometrical interpretations of the Minkowski functionals in 1-, 2- and 3-dimensions.

The Minkowski Functionals: Geometric Meaning

d	1	2	3
V_0	Length	Area	Volume
V_1	χ_E	Perimeter	Surface Area
V_2	-	χ_E	Integrated Mean Curvature
V_3	-	-	χ_E

The Euler characteristic has additional geometric meaning that we quickly outline here, though we have discussed this characteristic in detail above. In one dimension, the Euler characteristic of a compact, non-empty interval is unity and for an empty interval is zero. In two dimensions χ_E equals the number of isolated regions minus the number of holes. In three dimensions the Euler characteristic is given by the number of isolated regions minus the number of tunnels plus the number of cavities. Alternatively, the Euler characteristic in 3-dimensions is the number of handles a compact 2-dimensional surface possesses.

4.2.6 Isoperimetric Inequalities

Before we continue to the Gaussian and weakly non-Gaussian random fields, we first want to mention the isoperimetric inequalities, of which the *Shapefinders* of [466] are widely used in cosmology. We do not directly use these quantities in this thesis but the work presented could happily be extended to reconstruct the shapefinders. This is likely to be more important when we take into account, for instance, redshift space distortions which are prone to introducing elongations into large scale structure surveys to to a Doppler shift sourced by the peculiar velocity of galaxies in clusters [275]. Here, the shapefinders may be useful in quantifying the structure induced by these distortions.

It can be shown via mixed volumes that in 3-dimensions the Minkowski functionals obey the Alexandrov-Fenchel inequality. This leads to the following independent but non-trivial isoperimetric inequalities

$$[V_1]^2 \geq \frac{\pi}{4} V_0 \, V_2 \tag{4.45}$$

$$[V_2]^2 \geq \frac{8}{3\pi} V_1 \, V_3. \tag{4.46}$$

This allows us to introduce a set of isoperimetric ratios as follows

$$x = \frac{\pi}{4} \frac{V_0 V_2}{V_1^2} \tag{4.47}$$

$$y = \frac{8}{3\pi} \frac{V_1 V_3}{V_2^2}. \tag{4.48}$$

These can be used to map a convex body to a point (x, y) known as a Blaschke diagram [233]. Alternatively, we can take the approach of [466] and introduce a set of ratios of Minkowski functionals known as shapefinders. We introduce three quantities with a dimension of length such that

$$\text{Thickness } T = \frac{V_0}{2V_1} \tag{4.49}$$

$$\text{Width } W = \frac{2}{\pi} \frac{V_1}{V_2} \tag{4.50}$$

$$\text{Length } L = \frac{3}{4} \frac{V_2}{V_3}. \tag{4.51}$$

These can be used to re-express the isoperimetric inequalities such that $L \geq W \geq T$ for any convex body. In addition, these variables describe the spatial dimensions of the object in question. For example, pancake like cosmological structure would have one dimension much larger than the other two, $L \gg W \simeq T$. The shapefinders are now defined by the following ratios

$$\text{Planarity } \mathcal{P} = \frac{W - T}{W + T} \tag{4.52}$$

$$\text{Filamentarity } \mathcal{F} = \frac{L - W}{L + W}. \tag{4.53}$$

Whilst it would be possible to apply these objects to study the *global* geometrical and topological properties of random fields, their real power is in studying *local* properties of individual objects,

such as clusters of galaxies, where we are particularly interested in characterising the dimensions of that object which may be more sensitive to different scenarios of structure formation with regards to superclusters and voids. The work we present later is primarily related to the Minkowski functionals but could, in principal, be used to construct shapefinder like relations for our random field.

4.3 Weakly Non-Gaussian Random Fields

4.3.1 Introduction

Now that we have introduced the Minkowski functionals and given a rather broad introduction to their properties, we can take a step back and introduce a formalism that will allow us to actually evaluate the Minkowski functionals for Gaussian and weakly non-Gaussian random fields. In particular, we will introduce a perturbative expansion around a Gaussian field and use the partition function formalism to generate the lowest order normalised cumulants that characterise deviations from Gaussianity. This section adopts the approach presented in [360] and much of this formalism forms the foundations of the concomitant analysis presented in this chapter. This section does not aim to generate a detailed re-derivation of the results in [360] but is aimed at providing an understanding of where the terms used in the next section arise.

4.3.2 Smoothed Random Fields

Consider an n-dimensional random field $\tilde{f}(\mathbf{x})$ which may be used to represent any cosmological random field constructed from observable quantities, such as a density field of arbitrary dimension. Typically, the coordinates used will either be 2- or 3-dimensional. In applications to large scale structure we will predominantly be interested in 3-dimensional random fields. We construct a smoothed random field $f(\mathbf{x})$ from our original random field $\tilde{f}(\mathbf{y})$ by convoluting the random field with a window function of smoothing length R

$$f(\mathbf{x}) = \int d^n y \, W_R(|\mathbf{x}-\mathbf{y}|) \, \tilde{f}(\mathbf{y}). \tag{4.54}$$

Typically we will consider smoothing by a Gaussian window which, as we will see later, allows us to derive some useful analytical results

$$W_R(k) = \exp\left(-\frac{1}{2}\frac{k^2}{R^2}\right) \tag{4.55}$$

The random field is also assumed to have zero mean $\langle f \rangle = 0$ with finite variance $\langle f^2 \rangle = \sigma_0^2$. It is convenient to introduce a further normalisation of the random field such that it has unit variance

$$g = \frac{f}{\sigma_0}; \qquad \langle g^2 \rangle = 1. \tag{4.56}$$

Following [360], we introduce a set of variables A_μ that enumerate the series of spatial derivatives of the random field. For our 3-dimensional random field, this set will schematically look like

$$A_\mu = \left(g, \partial_1 g, \partial_2 g, \partial_3 g, \partial_1^2 g, \partial_2^2 g, \partial_3^2, \partial_1\partial_2 g, \partial_1\partial_3 g, \partial_2\partial_3 g, \dots\right), \tag{4.57}$$

where $\mu = 0, 1, 2, 3, (11), (22), (33), (12), (13), (23), \dots$. The set of variables A_μ form a multivariate random field which is encapsulated in an N-dimensional vector $\mathbf{A}$. The dimension N enumerates the total number of derivatives that appear in the statistic of interest. The statistical properties of the multivariate random field are described by the PDF, $P(\mathbf{A})$. We can introduce the partition function $Z(\mathbf{J})$ as a Fourier transform of the PDF

$$Z(\mathbf{J}) = \int_{-\infty}^{\infty} d^N A P(\mathbf{A}) \, \exp(i\mathbf{J}\cdot\mathbf{A}). \tag{4.58}$$

The cumulant expansion theorem tells us that the cumulant generating function is $\ln Z$. This allows us to produce the set of cumulants $M^n_{\mu_1\dots\mu_n} = \langle A_{\mu_1}\dots A_{\mu_n}\rangle_c$

$$\ln Z(\mathbf{J}) = \sum_{n=1}^{\infty} \frac{i^n}{n!} \sum_{\mu_1=1}^{N} \dots \sum_{\mu_n=1}^{N} M^{(n)}_{\mu_1\dots\mu_n} J_{\mu_1}\dots J_{\mu_n}. \tag{4.59}$$

Given that the random field is zero mean the first few cumulants of interest can be written explicitly as

$$M^{(1)}_{\mu} = 0, \tag{4.60}$$
$$M^{(2)}_{\mu_1\mu_2} = \langle A_{\mu_1} A_{\mu_2}\rangle, \tag{4.61}$$
$$M^{(3)}_{\mu_1\mu_2\mu_3} = \langle A_{\mu_1} A_{\mu_2} A_{\mu_3}\rangle. \tag{4.62}$$

Using 4.59 we can reconstruct the partition function by exponentiation

$$Z(\mathbf{J}) = \exp\left(\sum_{n=1}^{\infty} \frac{i^n}{n!} \sum_{\mu_1=1}^{N} \dots \sum_{\mu_n=1}^{N} M^{(n)}_{\mu_1\dots\mu_n} J_{\mu_1}\dots J_{\mu_n}\right) \tag{4.63}$$

However, if we consider the first two terms in the series we see that the $n = 1$ term vanishes due to 4.60 and the $n = 2$ term reduces to a correlation matrix contribution that encapsulates the contributions from the Gaussian part of the partition function

$$\exp\left(-\frac{1}{2}\sum_{\mu_1=1}^{N}\sum_{\mu_2=1}^{N} M^{(2)}_{\mu_1\mu_2} J_{\mu_1} J_{\mu_2}\right) = \exp\left(-\frac{1}{2}\mathbf{J}^T\,\mathbf{M}\,\mathbf{J}\right). \tag{4.64}$$

The partition function therefore simplifies to the following form in terms of this correlation matrix $\mathbf{M}$

$$Z(\mathbf{J}) = \exp\left(-\frac{1}{2}\mathbf{J}^T\mathbf{M}\mathbf{J}\right)\exp\left(\sum_{n=3}^{\infty}\frac{i^n}{n!}\sum_{\mu_1\dots\mu_2} M^{(n)}_{\mu_1\dots\mu_n} J_{\mu_1}\dots J_{\mu_n}\right). \tag{4.65}$$

The first exponential represents the Gaussian contribution and the second exponential the weakly non-Gaussian corrections to the partition function. Using this form for the partition function, we

can reconstruct the PDF via the inverse Fourier transform

$$P(\mathbf{A}) = \frac{1}{(2\pi)^N} \int_{-\infty}^{\infty} d^N J \, Z(\mathbf{J}) \, \exp(-i\mathbf{J}\cdot\mathbf{A}) \tag{4.66}$$

Again, separating our the $n = 2$ term it can be shown, by setting $J_\mu \to i\partial/\partial A_\mu$, that the PDF reduces to [360]

$$P(\mathbf{A}) = \exp\left(\sum_{n=3}^{\infty} \frac{(-1)^n}{n!} \sum_{\mu_1\ldots\mu_n} M^{(n)}_{\mu_1\ldots\mu_n} \frac{\partial^n}{\partial A_{\mu_1}\ldots\partial A_{\mu_n}}\right) P_G(\mathbf{A}), \tag{4.67}$$

where the multivariate Gaussian PDF $P_G(\mathbf{A})$ is given by

$$P_G(\mathbf{A}) = \frac{1}{(2\pi)^{N/2}\sqrt{|\mathbf{M}|}} \exp\left(-\frac{1}{2}\mathbf{A}^T\mathbf{M}^{-1}\mathbf{A}\right). \tag{4.68}$$

We can now define any statistical quantity of a smoothed cosmological random field as an expectation value $\langle F\rangle$ for a given function $F(\mathbf{A})$

$$\langle F\rangle = \int_{-\infty}^{\infty} d^N A \, P(\mathbf{A}) F(\mathbf{A}) \tag{4.69}$$

$$= \left\langle \exp\left(\sum_{n=3}^{\infty} \frac{(-1)^n}{n!} \sum_{\mu_1\ldots\mu_n} M^{(n)}_{\mu_1\ldots\mu_n} \frac{\partial^n}{\partial A_{\mu_1}\ldots\partial A_{\mu_n}}\right) F(\mathbf{A})\right\rangle_G, \tag{4.70}$$

where we have introduced a Gaussian averaging procedure

$$\langle\ldots\rangle_G = \int_{-\infty}^{\infty} d^N A \, P_G(\mathbf{A}) \, [\ldots]. \tag{4.71}$$

In this formalism the series expansion contains an infinite number of terms corresponding to weakly non-Gaussian corrections. For practical calculations, we will often find it useful to enforce a cut-off in terms of the variance at some arbitrary order. For weakly non-linear evolution, cosmological random fields approximately scale as $M^{(n)} \sim \mathcal{O}(\sigma_0^{n-2})$ and we can expand the distribution function to arbitrary order in σ_0. The normalised cumulants can therefore be defined up to $\mathcal{O}(\sigma_0)$ as

$$\tilde{M}^{(n)}_{\mu_1\ldots\mu_n} = \frac{M^{(n)}_{\mu_1\ldots\mu_n}}{\sigma_0^{n-2}}. \tag{4.72}$$

It should be noted that the conventional statistical cumulants are normalised differently to that presented here. For instance, the conventional skewness is defined by $S^{(0)}_{stat} = M^{(3)}_{000} = \langle f^3\rangle/\sigma_0^3$ but the literature on gravitational instability and large scale structure typically adopts, for convenience and physical relevance, the convention that $S^{(0)}_{grav} = M^{(3)}_{000}/\sigma_0$. The expectation value 4.70 can then be solved perturbatively to $\mathcal{O}(\sigma_0)$ [360]

$$\langle F\rangle = \langle F\rangle_G + \frac{1}{3!}\sum \tilde{M}^{(3)}_{\mu_1\mu_2\mu_3} \langle F_{,\mu_1\mu_2\mu_3}\rangle_G \, \sigma_0 + \mathcal{O}(\sigma_0^2) \tag{4.73}$$

where we have introduced the notation $F_{,\mu_1\mu_2\ldots\mu_n} \equiv \partial^n F/\partial A_{\mu_1}\partial A_{\mu_2}\ldots\partial A_{\mu_n}$. The expansion in 4.73 therefore depends on knowledge of the factors $\langle F_{,\mu_1\mu_2\ldots}\rangle_G$ as well the normalised cumu-

lants $\tilde{M}^{(n)}_{\mu_1\ldots\mu_n}$. As we will mostly be interested in the bispectrum, we will explicitly write out the contributions to $M^{(3)}_{ijk}$. First, we define the following useful identities [360]

$$S^{(0)} = \frac{\langle f^3\rangle}{\sigma_0^4} \tag{4.74}$$

$$S^{(1)} = -\frac{3}{4}\frac{\langle f^2\left(\nabla^2 f\right)\rangle}{\sigma_0^2\sigma_1^2} \tag{4.75}$$

$$S^{(2)} = -\frac{3d}{2(d-1)}\frac{\langle(\nabla f\cdot\nabla f)\left(\nabla^2 f\right)\rangle}{\sigma_1^4}. \tag{4.76}$$

These are called the skewness parameters $S^{(a)}$ and will be encountered extensively in the rest of this Chapter. The first term $S^{(0)}$ corresponds to the normalised skewness and the other terms represent derivatives of the skewness. The third order correlations have been explicitly written out in [360] with some of the most interesting quantities being

$$\tilde{M}^{(3)}_{000} = S^{(0)} \tag{4.77}$$

$$\tilde{M}^{(3)}_{00(ii)}) = -\frac{4}{9}\frac{\sigma_1^2}{\sigma_0^2}S^{(1)} \tag{4.78}$$

$$\tilde{M}^{(3)}_{0ii} = \frac{2}{9}\frac{\sigma_1^2}{\sigma_0^2}S^{(1)} \tag{4.79}$$

$$\tilde{M}^{(3)}_{ii(jj)} = -\frac{2}{27}\frac{\sigma_1^4}{\sigma_0^4}S^{(2)} \tag{4.80}$$

$$\tilde{M}^{(3)}_{ij(ij)} = \frac{1}{27}\frac{\sigma_1^4}{\sigma_0^4}S^{(2)}. \tag{4.81}$$

Finally, the term $\langle F_{,\mu_1\mu_2\mu_3}\rangle$ is calculated explicitly for the function F. In the case of the Minkowski functionals, these have been explicitly calculated in [360].

4.3.3 Minkowski Functionals: The F Terms

Schematically, the functional form for these terms has some intuitive origins. Following our discussion in Section 4.2, we know that the lowest order Minkowski functional V_0 is related to the volume functional, V_1 is related to a surface area, V_2 is related to an integrated mean curvature and V_3 is related to the 3-dimensional genus or the Euler characteristic. These quantities were shown to be equivalent to a set of level crossing statistics $N_i(\nu)$ and the 2- and 3-dimensional genus G_i[360], this follows from Crofton's intersection formula [135] defined in 4.33. It is this step that is most important in connecting the formalism employed in [360] to the Minkowski functional discussion of Section 4.2. The relations are as follows [360]

$$V_0(\nu) = N_0(\nu) \tag{4.82}$$

$$V_1(\nu) = \frac{\omega_3}{2\omega_2\omega_1}N_1(\nu) \tag{4.83}$$

$$V_2(\nu) = \frac{\omega_3}{\omega_1\omega_2}G_2(\nu) \tag{4.84}$$

$$V_3(\nu) = -\frac{\omega_3}{\omega_0\omega_3}G_3(\nu), \tag{4.85}$$

In the formalism of [360], these quantities can be calculated by taking a Gaussian average of the appropriate kernel F. The kernels are schematically given by

$$N_0(\nu) \mapsto F = \langle \theta(\nu - g) \rangle \tag{4.86}$$

$$N_1(\nu) \mapsto F = \langle \delta(g - \nu) |\partial_1 g| \rangle \tag{4.87}$$

$$G_2(\nu) \mapsto F = -\frac{1}{2} \langle \delta(g - \nu)\, \delta(\partial_1 g)\, |\partial_2 g|\, \partial_{11} g \rangle \tag{4.88}$$

$$G_3(\nu) \mapsto F = -\frac{1}{2} \left\langle \delta(g - \nu)\, \delta(\partial_1 g)\, \delta(\partial_2 g)\, |\partial_3 g|\, \left(\partial_{11} g\, \partial_{22} g - \partial^2_{12} g\right) \right\rangle . \tag{4.89}$$

For V_0, the kernel N_0 is just an object that isolates the parts of the excursion set that are above the threshold, i.e. the volume of the 3-dimensional excursion set [360]. The term in N_1 is only non-zero for the parts of the excursion set that are equal to the threshold for which we evaluate the absolute value of the partial derivative, this just translates into a measure of the mean area of the contour surface in 3-dimensions [464; 359]. The next order Minkowski functional, V_2 is related to the 2-dimensional genus G_2 or mean curvature of the excursion set [1; 113; 373; 214; 360]. The final statistic V_3 is equivalent to the full 3-dimensional genus G_3 or the Euler characteristic χ which, as we discussed earlier, are just related by a numerical factor of $-1/2$ [356; 212; 359; 360]. The Gaussian averaging of these quantities has already been calculated and has been the focus of much attention in the literature culminating in [360].

4.3.4 Gaussian Random Fields: Tomita's Formula

All the Minkowski functionals for a Gaussian random field are analytically known [564]. We consider a random field $\Psi(\mathbf{x})$ in d dimensions. The key result of [564] and others was to show that the functions defined in 4.86-4.89 can be analytically calculated for the Gaussian averaging procedure defined by 4.70. For the Gaussian limit, where the only contribution is from the first term in 4.73, the results simply rather nicely [564; 360]

$$N_0(\nu) = \frac{1}{2}\text{erfc}\left(\frac{\nu}{\sqrt{2}}\right) \tag{4.90}$$

$$N_1(\nu) = \frac{1}{\pi}\left(\frac{\sigma_1}{\sqrt{3}\sigma_0}\right) \exp\left(-\frac{\nu^2}{2}\right) H_0(\nu) \tag{4.91}$$

$$G_2(\nu) = \frac{1}{(2\pi)^{3/2}}\left(\frac{\sigma_1}{\sqrt{3}\sigma_0}\right)^2 \exp\left(-\frac{\nu^2}{2}\right) H_1(\nu) \tag{4.92}$$

$$G_3(\nu) = \frac{1}{(2\pi)^2}\left(\frac{\sigma_1}{\sqrt{3}\sigma_0}\right)^3 \exp\left(-\frac{\nu^2}{2}\right) H_2(\nu). \tag{4.93}$$

Introducing the following notation

$$H_{-1}(\nu) = \exp\left[\frac{\nu^2}{2}\right] \int_\nu^\infty d\nu \, \exp\left[-\frac{\nu^2}{2}\right] = \sqrt{\frac{\pi}{2}} \exp\left[\frac{\nu^2}{2}\right] \text{erfc}\left[\frac{\nu}{\sqrt{2}}\right], \tag{4.94}$$

and using 4.82-4.85, we see that we can re-write the Minkowski functionals in the following compact form for d-dimensions

$$V_k^{(d)}(\nu) = \frac{1}{(2\pi)^{(k+1)/2}} \frac{\omega_d}{\omega_{d-k}\omega_k} \left(\frac{\sigma_1}{\sqrt{d}\sigma_0}\right)^k \exp\left[-\frac{\nu^2}{2}\right] H_{k-1}(\nu). \tag{4.95}$$

The Hermite polynomials of order n are explicitly defined by the following expression

$$H_n(\nu) = \left(-\frac{d}{d\nu}\right)^n \frac{1}{\sqrt{2\pi}} \exp\left(-\frac{1}{2}\nu^2\right), \tag{4.96}$$

with the first few Hermite polynomials being given by

$$\begin{aligned} H_{-1}(\nu) &= \sqrt{\frac{2}{\pi}} \exp\left[\frac{\nu^2}{2}\right] \text{erfc}\left[\frac{\nu}{\sqrt{2}}\right] && (4.97)\\ H_0(\nu) &= 1 & H_1(\nu) &= \nu \\ H_2(\nu) &= \nu^2 - 1 & H_3(\nu) &= \nu^3 - 3\nu \qquad H_4(\nu) = \nu^4 - 6\nu^2 + 3. \end{aligned}$$

Setting $d = 3$ we obtain the complete set of Minkowski functionals in 3-dimensions for a Gaussian random field

$$V_0(\nu) = \frac{1}{2}\text{erfc}\left[\frac{\nu}{\sqrt{2}}\right] \tag{4.98}$$

$$V_1(\nu) = \frac{2}{3}\frac{1}{(2\pi)} \exp\left[-\frac{\nu^2}{2}\right] \left[\frac{\sigma_1}{\sqrt{3}\sigma_0}\right] \tag{4.99}$$

$$V_2(\nu) = \frac{2}{3}\frac{\nu}{(2\pi)^{3/2}} \exp\left[-\frac{\nu^2}{2}\right] \left[\frac{\sigma_1}{\sqrt{3}\sigma_0}\right]^2 \tag{4.100}$$

$$V_3(\nu) = \frac{\nu^2 - 1}{(2\pi)^2} \exp\left[-\frac{\nu^2}{2}\right] \left[\frac{\sigma_1}{\sqrt{3}\sigma_0}\right]^3, \tag{4.101}$$

where $\nu = u/\sigma_0$. The Minkowski functionals for a Gaussian random field are plotted in Fig. 4.2 for a threshold range $\nu = \{-3, \ldots, 3\}$. This is a reproduction of Figure 4 from [260] with the variance parameters calculated from the linear matter power spectrum and a Gaussian smoothing window with a smoothing length of $R = 100h^{-1}\text{Mpc}$.

4.3.5 Weakly Non-Gaussian Random Fields

We now proceed to perform the exact same analysis as we did earlier but this time we allow for higher order corrections to 4.73 using the $\tilde{M}_{\mu_1\mu_2\mu_3}$ matrices defined earlier. Luckily for us, the Gaussian integration for these 4 statistics has already been done [360] and we will simply quote the results for 3-dimensions here

$$V_0(\nu) = \frac{1}{2}\text{erfc}\left(\frac{\nu}{\sqrt{2}}\right) + \frac{1}{\sqrt{2\pi}} \exp\left(-\frac{\nu}{\sqrt{2}}\right) \left\{\left[\frac{S^{(0)}}{6} H_2(\nu)\right] \sigma_0^2 + \mathcal{O}(\sigma_0^2)\right\} \tag{4.102}$$

$$N_1(\nu) = \frac{1}{\pi}\left(\frac{\sigma_1}{\sqrt{3}\sigma_0}\right) \exp\left(-\frac{\nu^2}{2}\right) \left\{H_0(\nu) + \left[\frac{S^{(0)}}{6} H_3(\nu) + \frac{S^{(1)}}{3} H_1(\nu)\right] \sigma_0 + \mathcal{O}(\sigma_0^2)\right\} \tag{4.103}$$

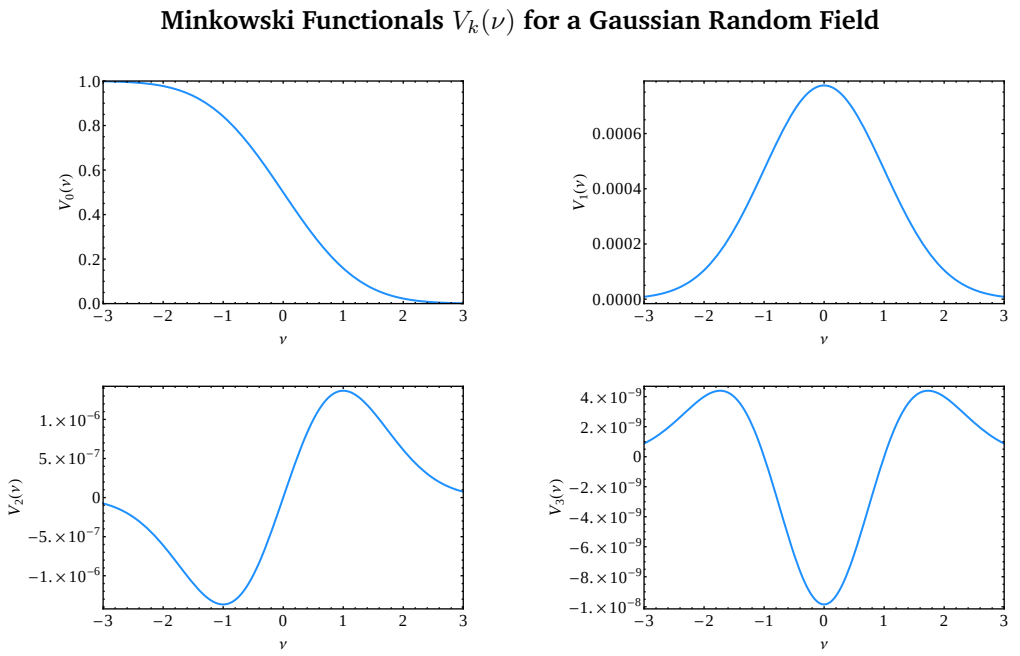

Figure 4.2: Minkowski Functionals for a Gaussian random field where the excursion set is defined for a threshold $\nu = \{-3, 3\}$. The variance parameters σ_0 and σ_1 have been calculated via the linear matter power spectrum and Gaussian window function at a smoothing radius of $R = 100h^{-1}\mathrm{Mpc}$, as outlined in [260].

$$G_2(\nu) = \frac{1}{(2\pi)^{3/2}} \left(\frac{\sigma_1}{\sqrt{3}\sigma_0}\right)^2 \exp\left(-\frac{\nu^2}{2}\right) \left\{ H_1(\nu) + \left[\frac{S^{(0)}}{6} H_4(\nu) + 2\frac{S^{(1)}}{3} H_2(\nu) + \frac{S^{(2)}}{3}\right]\sigma_0 + \mathcal{O}(\sigma_0^2) \right\} \tag{4.104}$$

$$G_3(\nu) = -\frac{1}{(2\pi)^2} \left(\frac{\sigma_1}{\sqrt{3}\sigma_0}\right)^3 \exp\left(-\frac{\nu^2}{2}\right) \left\{ H_2(\nu) + \left[\frac{S^{(0)}}{6} H_5(\nu) + S^{(1)} H_3(\nu) + S^{(2)} H_1(\nu)\right]\sigma_0 + \mathcal{O}(\sigma_0^2) \right\}. \tag{4.105}$$

By inspection, and by the analysis in the Gaussian case 4.95, we can start to see a general structure that unifies the various Minkowski functionals. For instance, we have a pre-factor exponential term, a variance parameter term that is weighted by the Minkowski functional number k as well as a set of Hermite polynomials that are also weighted with respect to k. Following the notation of [360; 260], the formula for a MF in a weakly non-Gaussian field can be given as a sum of term Gaussian term plus the non-Gaussian corrections as function of the threshold ν with an overall amplitude A_k

$$V_k(\nu) = A_k v_k(\nu) \tag{4.106}$$

The amplitude of the Minkowski Functionals are weighted by the spatial dimension, the variance of the random field σ_0 and the variance of the derivative field σ_1

$$A_k = \frac{1}{(2\pi)^{(k+1)/2}} \left(\frac{\omega_2}{\omega_{2-k}\omega_k}\right) \left(\frac{\sigma_1}{\sqrt{2}\sigma_0}\right)^k \tag{4.107}$$

where $\omega_k = \pi^{k/2}/\Gamma(k/2+1)$ was defined to be the volume of a k-dimensional unit ball. The structure of the amplitude normalised Minkowski Functionals $v_k(\nu)$ can be given as a sum of the Gaussian term $v_k^{(0)}(\nu)$ plus a perturbative expansion $v_k^{(n)}(\nu)$ with respect to the variance σ_0

$$v_k(\nu) = v_k^{(0)}(\nu) + v_k^{(1)}(\nu)\sigma_0 + v_k^{(2)}(\nu)\sigma_0^2 + v_k^{(3)}(\nu)\sigma_0^3 + \dots \tag{4.108}$$

In this thesis we are purely interested in the leading order corrections which correspond to the skewness parameters. We could, in principle, extend our analysis to higher order corrections which probe higher order cumulants. For instance, the term $v_k^{(2)}(\nu)\sigma_0^2$ will correspond to non-Gaussian corrections that effectively probe the trispectrum or 4-point correlation function. The Gaussian term is given by

$$v_k^{(G)} = e^{-\nu^2/2} H_{k-1}(\nu), \tag{4.109}$$

and the non-Gaussian term at order σ_0 is given by

$$v_k^{(NG)} = e^{-\nu^2/2}\left\{\left[\frac{1}{6}S_{(0)}H_{k+2}(\nu) + \frac{k}{3}S_{(1)}H_k(\nu) + \frac{k(k-1)}{6}S_{(2)}H_{k-2}(\nu)\right]\sigma_0 + \mathcal{O}(\sigma_0^2)\right\}, \tag{4.110}$$

where $H_k(\nu)$ denotes the k-th Hermite polynomial and $S_{(k)}$ are the skewness parameters. Remember, the skewness parameters were defined by products of the field or its derivatives [360]

$$S_0 = \frac{\langle\Psi^3\rangle}{\sigma_0^4}; \qquad S_1 = \frac{\langle\Psi^2\nabla^2\Psi\rangle}{\sigma_0^2\sigma_1^2}; \qquad S_2 = \frac{2\langle|\nabla\Psi|^2\nabla^2\Psi\rangle}{\sigma_1^4}; \quad \sigma_j^2 = \int \frac{k^2dk}{2\pi^2}k^{2j}P_\Psi(k). \tag{4.111}$$

The key points to this discussion are as follows

1. We have detailed analytical formula for the perturbative expansion for weakly non-Gaussian random fields up to arbitrary order in the variance.

2. From this, we can construct analytical expressions for the Minkowski functionals via the formalism of [564; 360] and many others.

3. The Minkowski functionals can be studied by exploring the skewness parameters or, as we shall see, their skew-spectra generalisations. Once we have the full range of skewness parameters we can reconstruct the Minkowski functionals via 4.106. This is shown in Fig. 4.4 for a bispectrum corresponding to gravitational instability at a smoothing length of $R = 200h^{-1}\mathrm{Mpc}$. We will define the bispectrum and the necessary physics shortly (see 4.125) but for now just appreciate that the non-Gaussian corrections of interest induce very small changes to the Minkowski functionals themselves.

4. The skewness parameters can be re-expressed as momenta weighted integrals of the bispectrum.

As we will be specialising this approach to large scale structure, we note that the Fourier coefficients will be defined in terms of the density contrast of galaxies $\delta(\mathbf{x}, z)$

$$\delta(\mathbf{x}, z) = \frac{1}{(2\pi)^3}\int d^3\mathbf{k}\,\tilde{\delta}(\mathbf{k})\,e^{i\mathbf{k}\cdot\mathbf{x}}. \tag{4.112}$$

Minkowski Functionals $V_k(\nu)$ for a Weakly Non-Gaussian Random Field

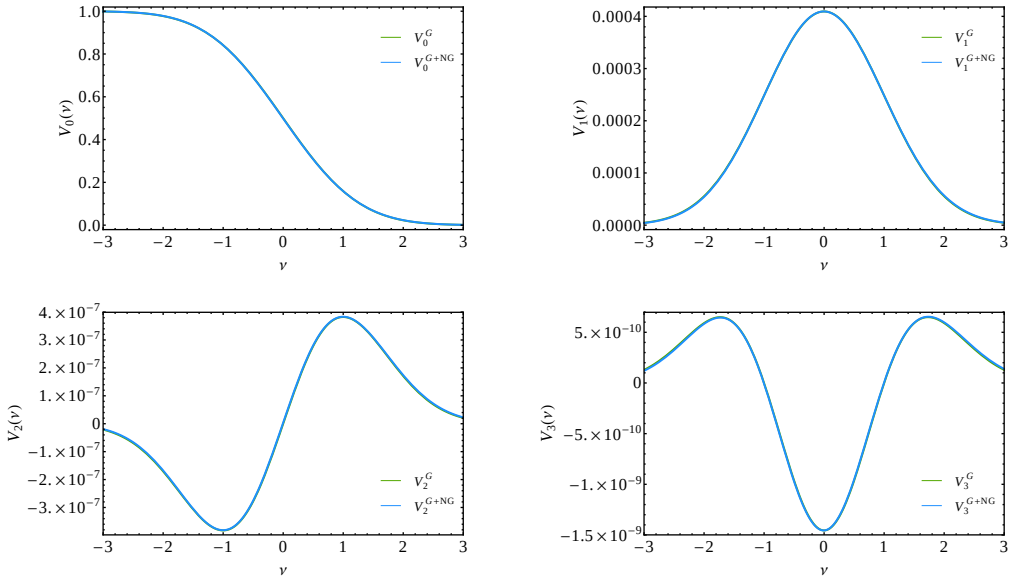

Figure 4.3: Minkowski Functionals for weakly non-Gaussian random field with a bispectrum corresponding to that of gravitational instability at a smoothing length of $R = 200h^{-1}\mathrm{Mpc}$. We will define the bispectrum and the necessary physics shortly (see 4.125) but for now just appreciate that the non-Gaussian corrections of interest induce very small changes to the Minkowski functionals themselves.

Difference in the Minkowski functionals $V_k(\nu)$ for a Weakly Non-Gaussian Random Field

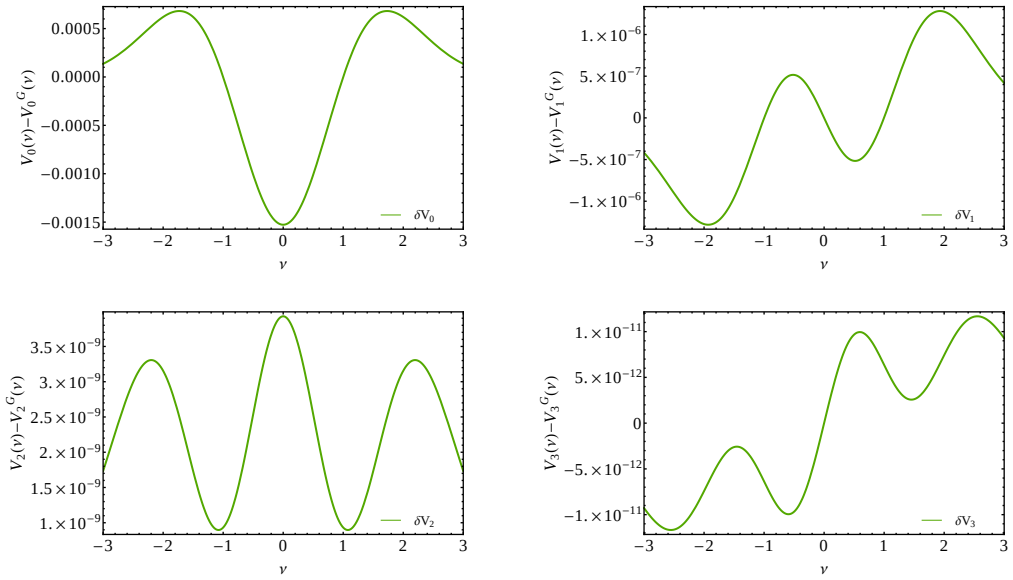

Figure 4.4: Here we plot the difference between the Gaussian and weakly non-Gaussian Minkowski functionals for a bispectrum corresponding to that of gravitational instability at a smoothing scale of $R = 200h^{-1}\mathrm{Mpc}$. We will define the bispectrum and the necessary physics shortly but for now just appreciate that the non-Gaussian corrections of interest induce very small changes to the Minkowski functionals themselves.

Now that we have this formalism in place, we seek to extend the definitions even further by generalising the skewness parameters to their skew-spectra counterparts.

4.4 Generalised Skew-Spectra

Previous work has resulted in the development of optimal 3-point estimators for simple models of the bispectrum, most notably for the phenomenological local configuration parameterised by $f_{\rm NL}^{\rm loc}$. Most of these optimal approaches compresses the data into a single estimate based on $f_{\rm NL}$ and consequentially we lose sensitivity in distinguishing between various contributions to the observed non-Gaussianity.

The skew-spectra are a proposed method utilising cubic statistics constructed from the cross-correlation of two differing fields. These fields are constructed as a product of the maps and their derivatives. The three different skewness parameters that we generate will reduce to a weighted probe of the bispectrum. Following the method developed in [388; 390] we can define a power spectrum associated with each of these skewness parameters and hence we can associate a power spectrum to each of the Minkowski functionals. The power spectrum associated with a given MF will, by construction, have the same correspondence with the various skew-spectra $S_l^{(j)}$ as the Minkowski functionals have with the one-point cumulants $S^{(j)}$ [390].

The advantage to the associated power spectra is that we retain more of an ability to distinguish between various models for non-Gaussianity rather than collapsing all information into a single estimator (e.g. estimators for $f_{\rm NL}$). This is due to the generic momenta dependence of higher order correlators such as the bispectrum. A previous paper [393] derived analytic results for topological statistics based on the use of skew-spectra [388] allowing us to relate the analytic skewness parameters to the topological properties of large scale structure. Each of the generalised skewness parameters or generalised cumulant correlators can be constructed from triplets of field variables that relate to either the original density contrast or to variables constructed from derivatives of the fields:

$$S_0(\mathbf{x}_1,\mathbf{x}_2) = \frac{\langle \delta^2(\mathbf{x}_1)\delta(\mathbf{x}_2)\rangle_c}{\sigma_0^4} \tag{4.113}$$

$$S_1(\mathbf{x}_1,\mathbf{x}_2) = \frac{\langle \delta^2(\mathbf{x}_1)\nabla^2\delta(\mathbf{x}_2)\rangle_c}{\sigma_0^2\sigma_1^2} \tag{4.114}$$

$$S_2(\mathbf{x}_1,\mathbf{x}_2) = \frac{\langle \nabla\delta(\mathbf{x}_1)\cdot\nabla\delta(\mathbf{x}_1)\nabla^2\delta(\mathbf{x}_2)\rangle_c}{\sigma_1^4}. \tag{4.115}$$

The Bispectrum $B(k_1,k_2,k_3)$ is defined in the Fourier domain as a three-point correlation function of the Fourier coefficients:

$$\langle \delta(z)(\mathbf{k}_1)\delta(z)(\mathbf{k}_2)\delta(z)(\mathbf{k}_3)\rangle_c = (2\pi)^3\delta_D(\mathbf{k}_1+\mathbf{k}_2+\mathbf{k}_3)B_g(k_1,k_2,k_3,z). \tag{4.116}$$

The skewness parameters are calculated by integrating over the bispectrum using the appropriate weights:

$$S_0(k_2,z) = \frac{1}{\sigma_0^4}\frac{1}{4\pi^2}\int_0^\infty \frac{k_1^2 dk_1}{4\pi^2}\int_{-1}^{1} d\mu\, B_\delta(k_1,k_2,|\mathbf{k}_1+\mathbf{k}_2|,z)W(k_1R)W(|\mathbf{k}_1+\mathbf{k}_2|R), \tag{4.117}$$

$$S_1(k_2,z)=\frac{3}{4\sigma_0^2\sigma_1^2}\frac{1}{4\pi^2}\int_0^\infty\frac{k_1^2dk_1}{4\pi^2}\int_{-1}^1 d\mu\,|\mathbf{k}_1+\mathbf{k}_2|^2B_\delta(k_1,k_2,|\mathbf{k}_1+\mathbf{k}_2|,z)W(k_1R)W(|\mathbf{k}_1+\mathbf{k}_2|R), \tag{4.118}$$

$$S_2(k_2,z)=\frac{9}{4\sigma_1^4}\frac{1}{4\pi^2}\int_0^\infty\frac{k_1^2dk_1}{4\pi^2}\int_{-1}^1 d\mu\,(\mathbf{k}_1\cdot\mathbf{k}_2)|\mathbf{k}_1+\mathbf{k}_2|^2B_\delta(k_1,k_2,|\mathbf{k}_1+\mathbf{k}_2|,z)W(k_1R)W(|\mathbf{k}_1+\mathbf{k}_2|R), \tag{4.119}$$

$$S_i=\int_0^\infty k^2dk\;\mathcal{S}_i(k)W(kR);\quad i=\in\{0,1,2\}. \tag{4.120}$$

with $W(kR)$ an arbitrary window function of smoothing radius R. Although the window may be generic the two most commonly adopted forms are the top-hat and Gaussian window functions. We will assume a Gaussian window function, for results on the top-hat window function we refer the reader to the literature [52]. We adopt the following notation: $|\mathbf{k}_1+\mathbf{k}_2|=(k_1^2+k_2^2+2k_1k_2\mu)^{1/2}$ and the angular terms are given by $\mu=(\mathbf{k}_1\cdot\mathbf{k}_2)/(k_1k_2)$. In our convention the one-point skewness parameters can be recovered by integrating over the second momenta k_2

$$S_{(i)}(z)=\int_0^\infty k_2^2dk_2\;S_{(i)}(k,z). \tag{4.121}$$

These were the parameters investigated in [260] and are shown in Fig. 4.9. The skew-spectra shown here are related to the skewness parameters but avoid the compression of information encapsulated in the integral over k_2. In the approach presented above we are able to define a power spectrum associated to the Minkowski functionals by considering the leading order corrections, $\mathcal{O}(\sigma_0)$, to the Gaussian Minkowski functionals generalised to our skewness parameters:

$$v_m^{(NG)}(\nu,k,z)\propto\left\{\frac{1}{6}S_0(k,z)H_{m+2}(\nu)+\frac{m}{3}S_1(k,z)H_m(\nu)+\frac{m(m-1)}{6}H_{m-2}(\nu)S_2(k,z)\right\}. \tag{4.122}$$

Essentially, we have associated to each Minkowski Functional a power spectrum defined in terms of the three skew-spectra. The advantage to this approach is that we can study the contributions to the Minkowski functionals as a function of the Fourier mode k. This is useful as a generic model for non-Gaussianity carries momenta dependence giving us greater distinguishing power than the conventional approach which compresses information from all modes into a single statistic. This compression represents a loss of distinguishing power. The skew-spectra presented above are relatively independent of our choice of background cosmology but will be dependent on the model for non-Gaussianity due to the aforementioned momenta dependence.

We now specialise this formalism to different physically motivated configurations for the bispectrum corresponding to non-Gaussianity induced by gravitational collapse as well as different configurations for non-Gaussianity sourced in the early Universe by non-vanilla theories for inflationary cosmology Chapter 3.

4.5 Non-Gaussianity: Primordial and Gravity Induced

In the weakly non-linear regime ($\delta \leq 1$) the description of gravitational clustering can be described by Eulerian Perturbation Theory (see e.g. [54]). As the density contrast at a given scale becomes highly non-linear ($\delta \geq 1$) the perturbative treatment breaks down and we observe an increase in the growth of clustering. Perturbative studies of gravitational clustering have previously garnered a lot of attention. Starting with [427], there have been a significant number of attempts to reproduce the observed clustering of a self-gravitating fluid in a cosmological setting, most of which adopt a brute force approach using N-body simulations [54]. In the perturbative approach, solutions are generated by performing a series expansion with higher order corrections being introduced to the Fourier expansion of the linear density contrast under the assumption that the density contrast is less than unity for the series to be convergent:

$$\delta(\mathbf{k}) = \delta^{(1)}(\mathbf{k}) + \delta^{(2)}(\mathbf{k}) + \delta^{(3)}(\mathbf{k}) + \ldots; \tag{4.123}$$

$$\delta^{(2)}(k) = \int \frac{d^3k_1}{2\pi} \int \frac{d^3k_2}{2\pi} \delta_D(\mathbf{k_1} + \mathbf{k_2} - \mathbf{k}) F_2(k_1, k_2)\, \delta^{(1)}(\mathbf{k}_1)\, \delta^{(1)}(\mathbf{k}_2). \tag{4.124}$$

The linearized solution for the density field is $\delta^{(1)}(\mathbf{k})$ with the higher order terms describing corrections to the linear term. Using a fluid approach, known to be valid at large scales, before shell crossing, one can write the second order corrections to the linearized density field by introducing a coupling kernel, $F_2(\mathbf{k_1}, \mathbf{k_2})$. Newtonian gravity coupled with the Euler and Continuity equations can be used to solve a system of non-linear coupled integral-differential equations, in order to generate the kernels $F_2(k_1, k_2)$ and $F_3(k_1, k_2, k_3)$, by solving perturbatively order by order. The expression for the matter bispectrum can be written in terms of an effective fitting formula that allows us to interpolate between the quasilinear and highly nonlinear regimes:

$$B_{\rm lin}(\mathbf{k}_1, \mathbf{k_2}, \mathbf{k}_3) = 2F_2(\mathbf{k_1}, \mathbf{k_2}) P_{\rm lin}(\mathbf{k}_1) P_{\rm lin}(\mathbf{k_2}) + \text{cyc.perm.}; \tag{4.125}$$

$$F_2(\mathbf{k_1}, \mathbf{k_2}) = \frac{5}{7} a(n_e, k_1) a(n_e, k_2) + \left(\frac{\mathbf{k}_1 \cdot \mathbf{k}_2}{2k_2^2} + \frac{\mathbf{k}_1 \cdot \mathbf{k}_2}{2k_1^2} \right) b(n_e, k_1) b(n_e, k_2) + \frac{2}{7} \left(\frac{\mathbf{k}_1 \cdot \mathbf{k}_2}{k_1 k_2} \right)^2 c(n_e, k_1) c(n_e, k_2). \tag{4.126}$$

The coefficients $a(n_e, k), b(n_e, k)$ and $c(n_e, k)$ are defined as follows:

$$a(n_e, k) = \frac{1 + \sigma_8^{-0.2}(z) \sqrt{(q/4)^{n_e+3.5}}}{1 + (q/4)^{n_e+3.5}}; \tag{4.127}$$

$$b(n_e, k) = \frac{1 + 0.4(n_e + 3) q^{n_e+3}}{1 + q^{n_{eff}+3}}; \tag{4.128}$$

$$c(n_e, k) = \frac{(2q)^{n_e+3}}{1 + (2q)^{n_e+3.5}} \left\{ 1 + \left(\frac{4.5}{1.5 + (n_e + 3)^4} \right) \right\}. \tag{4.129}$$

Here n_e is the effective spectral slope associated with the linear power spectra $n_e = d \ln P_{\rm lin}/d \ln k$, q is the ratio of a given length scale to the non-linear length scale $q = k/k_{nl}$, where

$$\frac{k^3}{2\pi^2} D^2(z) P_{\rm lin}(k_{nl}) = 1 \tag{4.130}$$

and

$$Q_3(n_e) = \frac{(4 - 2^{n_e})}{(1 + 2^{n_e})}. \tag{4.131}$$

Where we have introduced $\sigma_8(z) = D(z)\sigma_8$, this parameter measures the amplitude of the linear power spectrum on the scale of $8h^{-1}\mathrm{Mpc}$. At scales where $q \ll 1$, and the relevant length scales are well within the quasilinear regime, then $a = b = c = 1$ and we recover the tree-level perturbative results. In the regime where $q \gg 1$, and the length scales under consideration are well within the nonlinear scales, we recover $a = \sigma_r^{-0.2}(z)\sqrt{0.7Q_3(n_e)}$ with $b = c = 0$. In this limit the bispectrum becomes independent of configuration and we recover a hierarchical form for the bispectrum. The possibility, however, of weak violations of the hierarchical ansatz in the highly nonlinear regime is still not clear and can only be determined by higher resolution N-body simulations when they become available. Similar fitting functions for a dark energy dominated Universe calibrated against simulations are also available and, at least in the quasilinear regime, most of the differences arise due to the linear growth factor [332].

The analytical modeling of the matter bispectrum presented here is equivalent to the so called halo model predictions (see, for example, [395] for discussions of the perturbative treatment in the context of Minkowski functionals).

4.5.1 Primordial Non-Gaussianity: Bispectrum

In this section we will introduce and discuss three templates for the bispectrum that have received much attention in the literature. These configurations encapsulate much of the physics with many theories tending towards one of these templates in an appropriate limit. Studies of the bispectrum are simplified by the closure relationship stating that the momenta in Fourier space must close to form a triangle and hence $\mathbf{k}_1 + \mathbf{k}_2 + \mathbf{k}_3 = 0$. A specific triangle can be completely determined by the length of its sides such that, if we enforce isotropy, we can completely describe the bispectrum with three momenta $\{\mathbf{k}_1, \mathbf{k}_2, \mathbf{k}_3\}$. The three limiting cases that we will consider are the *local* model or *squeezed* configuration for which $k_3 \ll k_1, k_2$, the equilateral configuration $k_1 \approx k_2 \approx k_3$ and the folded configuration $k_1 \approx k_2 + k_3$. Each of these can be motivated by various physical effects but at the very worst they can be considered as prototypical templates that allow us to study the phenomenology of non-Gaussianity in cosmological observables.

4.5.1.1 Primordial Non-Gaussianity: Local Model

Much of the interest in primordial non-Gaussianity has focused on a phenomenological *local* f_{NL} parametrization in terms of the perturbative non-linear coupling in the primordial curvature perturbation [467; 196; 575; 300]:

$$\Phi(x) = \Phi_L(x) + f_{NL}(\Phi_L^2(x) - \langle\Phi_L^2(x)\rangle) + g_{\mathrm{NL}}\Phi_L^3(x) + h_{\mathrm{NL}}\left(\Phi_L^4(x) - 3\langle\Phi_L^2(x)\rangle\right) + \ldots, \tag{4.132}$$

where $\Phi_L(x)$ denotes the linear Gaussian term of the Bardeen curvature and the amplitudes of the various non-Gaussian contributions are parameterised by the set of variables $\{f_{\mathrm{NL}}, g_{\mathrm{NL}}, h_{\mathrm{NL}}, \ldots\}$. In this parameterisation, the leading order non-Gaussian contributions are described by the bispectrum or, in configuration space, the three-point correlator. A large number of studies involving

primordial non-Gaussianity are based around the bispectrum as it will contain complete information (in a statistical sense) regarding f_{NL} [30]. The bispectrum has been extensively studied [302; 131; 132; 371; 84; 530], with most of these measurements providing convolved estimates of the bispectrum. In Fourier space, the local-type bispectrum corresponding to 4.132 is maximised for $k_3 \ll k_1, k_2$ and has the following form for the primordial potential Φ perturbations

$$B_\delta^{loc}(k_1, k_2, k_{12}) = 2 f_{\rm NL}^{loc} \left[P_\Phi(k_1) P_\Phi(k_2) + \text{cyc.} \right]. \tag{4.133}$$

Standard inflationary models predict a primordial power spectrum that obeys a power law of the form: $P^\Phi(k) \propto k^{n-4}$, where n is the spectral index. We can explicitly relate the linear density contrast to Bardeen's curvature perturbations in the matter dominated era through Poisson's equation [260]:

$$k^2 \tilde{\Phi}_k T(k) = 4\pi G_N \rho_m(z) \frac{\delta(\mathbf{k}, z)}{(1+z)^2} = \frac{3}{2} \Omega_M H_0^2 \delta(\mathbf{k}, z)(1+z). \tag{4.134}$$

In the above, T(k) is the transfer function describing the evolution of the density contrast. We adopt the BBKS approximation given in [36]. We also point the reader to [174; 175] for further discussions on transfer functions for large scale structure and the physical assumptions that go into the construction of a transfer function. At early times, where non-linear evolution may be neglected, the linear density contrast can be written in terms of an effective transfer kernel:

$$\delta(\mathbf{k}, z) = \frac{M(k)\Phi_k}{(1+z)} = D(z) M(k) \Phi_k; \quad M(k) = \frac{2}{3} \frac{k^2 T(k)}{\Omega_M H_0^2}. \tag{4.135}$$

Here, $D(z)$ is the linear growth factor normalised such that $D(z) \to 1/(1+z)$. This allows us to express the linear power spectrum in terms of the transfer kernel $M(k)$ and the primordial power spectrum $P_\phi(k)$:

$$P_\delta(k, z) = \frac{M^2(k)}{(1+z)^2} P_\phi(k). \tag{4.136}$$

We can relate the bispectrum for the primordial density perturbations to the bispectrum for the primordial potential perturbations by:

$$B_\delta^{prim}(k_1, k_2, k_{12}, z) = D^3(z) M(k_1) M(k_2) M(k_{12}) B_\Phi^{prim}(k_1, k_2, k_{12}, z). \tag{4.137}$$

Therefore, in the linear regime (i.e. valid at large length scales), the primordial bispectrum for the local model B^{prim} will evolve according to the following expression:

$$B_\delta^{loc}(\mathbf{k}_1 \mathbf{k}_1, \mathbf{k}_3; z) = 2 f_{NL}^{loc} D^3(z) \left[\frac{M(k_3)}{M(k_1) M(k_2)} P_\delta(k_1) P_\delta(k_2) + \text{cyc.} \right]. \tag{4.138}$$

The local model is well motivated physically as it encompasses superhorizon effects during inflation in which a large scale mode k_3 that exits the horizon exerts some non-linear influence on the evolution of small scale modes k_1 and k_2. Remember, in Fourier space, large scale modes correspond to small momenta (IR limit) and small scale effects correspond to high momenta (UV-limit). Typically this contribution will be relatively suppressed throughout inflation but non-standard inflationary models, in particular multi-field models, are though to induce much larger amplitudes for this type of non-Gaussianity.

4.5.1.2 Primordial Non-Gaussianity: Equilateral Model

The equilateral configuration is maximised when all three momenta are approximately equal $k_1 \approx k_2 \approx k_3$. In this configurations, the primordial potential bispectrum can be expressed as [132; 47]:

$$B_{\Phi}^{equi} = 6 f_{\rm NL}^{equi} \left[-(P_{\Phi}(k_1)P_{\Phi}(k_2) + \text{cyc.}) - 2(\mathrm{P_{\Phi}(k_1)P_{\Phi}(k_2)P_{\Phi}(k_3)})^{2/3} + (\mathrm{P_{\Phi}(k_1)P_{\Phi}^2(k_2)P_{\Phi}^3(k_3)} + \text{cyc.})^{1/3} \right]. \tag{4.139}$$

The primordial density bispectrum will therefore evolve according to:

$$B_{\delta}^{equi}(\mathbf{k}_1\mathbf{k}_1, \mathbf{k}_3; z) = 6 f_{NL}^{equi} D^3(z) \Bigg[- \left(\frac{M(k_3)}{M(k_1)M(k_2}) P_{\delta}(k_1)P_{\delta}(k_2) + \text{cyc.perm.} \right)$$
$$- 2\left(M(k_1)M(k_2)M(k_3)\right)^{1/3} \{P_{\delta}(k_1)P_{\delta}(k_2)P_{\delta}(k_3)\}^{2/3} + \tag{4.140}$$
$$\left(\left[\frac{M(k_1)}{M^2(k_2)M^3(k_3)} \right]^{1/3} \{P_{\delta}(k_1)P_{\delta}(k_2)^2 P_{\delta}(k_3)^3\}^{1/3} + \text{cyc.perm.} \right) \Bigg]. \tag{4.141}$$

Unlike the local model, the functional form for the equilateral model does not hold any relationship to fundamental physics but should be interpreted as something akin to a fitting function that describes a number of models for which the exact analytical expressions are more complicated.

4.5.1.3 Primordial Non-Gaussianity: Folded Model

The folded configuration is maximised when two of the sides of the triangle are approximately equal such that $k_2 \approx k_3 \approx k_1/2$. The folded bispectrum is approximated by the following functional form [99; 372]:

$$B_{\phi}^{fold} = 6 f_{\rm NL}^{fold} \left[(P_{\Phi}(k_1)P_{\Phi}(k_2) + \text{cyc.}) + 3(\mathrm{P_{\Phi}(k_1)P_{\Phi}(k_2)P_{\Phi}(k_3)})^{2/3} - (\mathrm{P_{\Phi}(k_1)P_{\Phi}^2(k_2)P_{\Phi}^3(k_3)} + \text{cyc.})^{1/3} \right]. \tag{4.142}$$

Following the outlined procedure we can re-write this in terms of the density perturbations

$$B_{\delta}^{fold}(k_1, k_2, k_3, z) = \frac{6 f_{\rm NL}^{fold}}{D(z)} \Bigg[\left(\frac{M(k_3)}{M(k_1)M(k_2)} P_{\delta}(k_1, z)P_{\delta}(k_2, z) + cyc. \right)$$
$$+ 3(M(k_1)M(k_2)M(k_3))^{-1/3} \{P_{\delta}(k_1, z)P_{\delta}(k_2, z)P_{\delta}(k_3, z)\}^{2/3}$$
$$- \left(\frac{M^{1/3}(k_1)}{M^{1/3}(k_2)M(k_3)} \{P_{\delta}(k_1, z)P_{\delta}(k_2, z)^2 P_{\delta}(k_3, z)^3\}^{1/3} + cyc. \right) \Bigg]. \tag{4.143}$$

The evolution of the primordial bispectrum is different compared to the one generated by gravitational evolution. The primordial bispectrum demonstrate momenta dependence and as a result the shape of the bispectrum configuration differs between the various primordial models as well as that for gravitational instability. At large angular scales, which will be probed by future weak lensing surveys, the gravitational instability may not yet have erased the memory of primordial non-Gaussianity, which can provide complementary information to results obtained from CMB surveys such as Planck [433].

4.6 Three-dimensional Density Fields

4.6.1 Gravitationally Induced Bispectrum

The first scenario that we will investigate is a three-dimensional smoothed field with galaxy density contrast δ_g. The matter bispectrum is given by 4.125 which, when substituted into the skewness parameters 4.113 in the limit $q \ll 1$, gives:

$$S_0(k_2,z) = \frac{1}{\sigma_0^4}\frac{1}{(2\pi^2)}\int_0^\infty \frac{k_1^2 dk_1}{(2\pi^2)}\int_{-1}^{+1} d\mu W(k_1R)W(k_3R) \times \left[\frac{15}{7}+\frac{3}{2}\mu\left(\frac{k_1}{k_2}+\frac{k_2}{k_1}\right)+\frac{6}{7}\mu^2\right]P_\delta(k_1)P_\delta(k_2) \tag{4.144}$$

$$S_1(k_2,z) = \frac{3}{4\sigma_0^2\sigma_1^2}\frac{1}{(2\pi^2)}\int_0^\infty \frac{k_1^2 dk_1}{(2\pi^2)}\int_{-1}^{+1} d\mu W(k_1R)W(k_3R) \times \left(k_2^1+k_2^2+\mu k_1k_2\right)\left[\frac{10}{7}+\mu\left(\frac{k_1}{k_2}+\frac{k_2}{k_1}\right)+\frac{4}{7}\mu^2\right]P_\delta(k_1)P_\delta(k_2) \tag{4.145}$$

$$S_2(k_2,z) = \frac{9}{4\sigma_1^4}\frac{1}{(2\pi^2)}\int_0^\infty \frac{k_1^2 dk_1}{(2\pi^2)}\int_{-1}^{+1} d\mu W(k_1R)W(k_3R) \times \left[k_1^2k_2^2(1-\mu^2)\right]\left[\frac{10}{7}+\mu\left(\frac{k_1}{k_2}+\frac{k_2}{k_1}\right)+\frac{4}{7}\mu^2\right]P_\delta(k_1)P_\delta(k_2), \tag{4.146}$$

in agreement with [360; 260]. We now specialise our analysis to a Gaussian window function $W(x) = \exp(-x^2/2)$ as this allows us to make the following simplifications [360]:

$$\frac{W\left(\sqrt{l_1^2+l_2^2+2l_1l_2\mu}\right)}{W(l_1)W(l_2)} = \exp(-l_1l_2\mu); \quad l = kR, \tag{4.147}$$

with R the smoothing scale and k the Fourier mode.

The angular integration over μ can now be analytically performed by relating the terms in the above skewness parameter to terms corresponding to the m^{th} Legendre polynomial. This allows us to use the following relation between integrals over the Legendre polynomials and the modified Bessel functions $I_\mu(z)$ [328; 360]:

$$\int_{-1}^{1} d\mu\, P_m(\mu)e^{-\mu z} = (-1)^m\sqrt{\frac{2\pi}{z}}I_{m+1/2}(z). \tag{4.148}$$

The relevant Legendre polynomials are:

$$P_0(\mu)=1; \qquad P_1(\mu)=\mu; \qquad P_2(\mu)=\frac{1}{2}(3\mu^2-1); \qquad P_3(\mu)=\frac{1}{2}(5\mu^3-3\mu); \qquad P_4(\mu)=\frac{1}{8}(35\mu^4-30\mu^2+3). \tag{4.149}$$

Using these results we can systematically perform the angular integration over μ in 4.144-4.146

$$S_0(k_2,z) = \frac{1}{\sigma_0^4}\frac{1}{(2\pi^2)}\int_0^\infty \frac{l_1^2 dl_1}{(2\pi^2)R^3}W^2(l_1)W(l_2)P_\delta\left(\frac{l_1}{R}\right)P_\delta\left(\frac{l_2}{R}\right)\sqrt{\frac{2\pi}{l_1l_2}} \times \left[\frac{17}{7}I_{1/2}(l_1l_2)-\frac{3}{2}\left(\frac{l_1}{l_2}+\frac{l_2}{l_1}\right)I_{3/2}(l_1l_2)+\frac{4}{7}I_{5/2}(l_1l_2)\right] \tag{4.150}$$

$$S_1(k_2,z) = \frac{1}{\sigma_0^2\sigma_1^2}\frac{1}{(2\pi^2)}\int_0^\infty \frac{l_1^2 dl_1}{(2\pi^2)R^5}W^2(l_1)W(l_2)P_\delta\left(\frac{l_1}{R}\right)P_\delta\left(\frac{l_2}{R}\right)\sqrt{2\pi l_1 l_2}$$
$$\times\left[\frac{41}{28}\left(\frac{l_1}{l_2}+\frac{l_2}{l_1}\right)I_{1/2}(l_1l_2) - \left(\frac{99}{35}+\frac{3}{4}\left[\frac{l_1^2}{l_2^2}+\frac{l_2^2}{l_1^2}\right]\right)I_{3/2}(l_1l_2)\right. \quad (4.151)$$
$$\left.+\frac{11}{14}\left(\frac{l_1}{l_2}+\frac{l_2}{l_1}\right)I_{5/2}(l_1l_2) - \frac{6}{35}I_{7/2}(l_1l_2)\right], \quad (4.152)$$
$$S_2(k_2,z) = \frac{1}{\sigma_0^4}\frac{1}{(2\pi^2)}\int_0^\infty \frac{l_1^2 dl_1}{(2\pi^2)R^7}W^2(l_1)W(l_2)P_\delta\left(\frac{l_1}{R}\right)P_\delta\left(\frac{l_2}{R}\right)\sqrt{2\pi}(l_1l_2)^{3/2}$$
$$\times\left[\frac{81}{35}I_{1/2}(l_1l_2) - \frac{9}{10}\left(\frac{l_1}{l_2}+\frac{l_2}{l_1}\right)I_{3/2}(l_1l_2) - \frac{99}{49}I_{5/2}(l_1l_2)\right. \quad (4.153)$$
$$\left.+\frac{9}{10}\left(\frac{l_1}{l_2}+\frac{l_2}{l_1}\right)I_{7/2}(l_1l_2) - \frac{72}{245}I_{9/2}(l_1l_2)\right]. \quad (4.154)$$

where we have used the relationship $l = kR$ as introduced in 4.147. Following the notation for the skewness parameters used in [360], we can simplify the above equations with following variable:

$$S_m^{\alpha\beta}(l_2,R) = \frac{\sqrt{2\pi}}{\sigma_0^4}\frac{1}{2\pi^2}\left(\frac{\sigma_0}{\sigma_1 R}\right)^{\alpha+\beta-2}\int\frac{l_1^2 dl_1}{2\pi^2R^3}P_\delta\left(\frac{l_1}{R}\right)P_\delta\left(\frac{l_2}{R}\right)e^{-l_1^2}e^{-l_2^2/2}l_1^{\alpha-3/2}l_2^{\beta-3/2}I_{m+1/2}(l_1\,l_2). \quad (4.155)$$

In this notation the skew-spectra parameters become:

$$S_0 = \frac{17}{7}S_0^{11} - 3S_1^{(02)} + \frac{4}{7}S_2^{11}, \quad (4.156)$$
$$S_1 = \frac{41}{14}S_0^{(13)} - \frac{3}{2}S_1^{(04)} - \frac{99}{35}S_1^{22} + \frac{11}{7}S_2^{(13)} - \frac{6}{35}S_3^{22}, \quad (4.157)$$
$$S_2 = \frac{81}{35}S_0^{33} - \frac{9}{5}S_1^{(15)} - \frac{99}{49}S_2^{33} + \frac{9}{5}S_3^{(15)} - \frac{72}{245}S_4^{33}. \quad (4.158)$$

where we have adopted the following convention: $S_m^{(\alpha\beta)} = \frac{1}{2}(S_m^{\alpha\beta} + S_m^{\beta\alpha})$. The results shown here demonstrate the analytic dependence of the gravitationally induced bispectra on a weighted integral over the modes in terms of Bessel functions. These equations are analogous to those presented in [360] but generalised to the skew-spectra formalism. The skew-spectra have been numerically calculated for three different smoothing scales $R[h^{-1}\mathrm{Mpc}] \in \{10, 15, 20\}$ and are shown in Figure 4.5. The non-Gaussianity generated from gravitational instability gives rise to a positively skewed perturbation unlike a generic inflationary model which could predict negatively skewed perturbations (e.g. [260]). It can also be seen that as the smoothing scale increases the amplitude increase but the scale at which we observe a cut-off increases (i.e. a cut-off occurs at smaller momenta). In the full skewness the gravitationally induced contributions are independent of smoothing scale [260]. Additionally, due to the dependence of the gravitationally induced skew-spectra on the matter power spectrum and the variance of the field, we find that the generalised skew parameters are independent of redshift under the adopted normalisation.

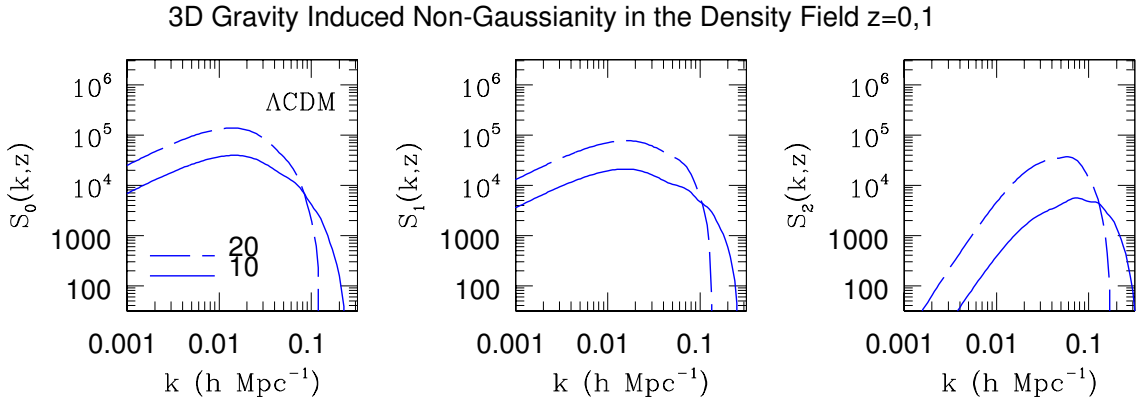

Figure 4.5: The three *gravity induced* skew-spectra $S_0(k,z)$ (left panel), $S_1(k,z)$ (middle panel) and $S_2(k,z)$ (right panel) are depicted 3D cosmological density field. The spectra have been calculated for two different Gaussian smoothing scales $R = 10, 20h^{-1}\mathrm{Mpc}$ for $z = 0$. The skew-spectra for the redshifts $z = 0$ and $z = 1$ are identical in the quasilinear regime due to the specific normalisation adopted. A ΛCDM background cosmology was assumed. The results are plotted for redshift $z = 0$. The skew-spectra are normalized in such a way that they are virtually independent of redshift. The expressions for $S_0(k,z)$, $S_1(k,z)$ and $S_2(k,z)$ are given in Eq.(4.150), Eq.(4.152) and Eq.(4.154).

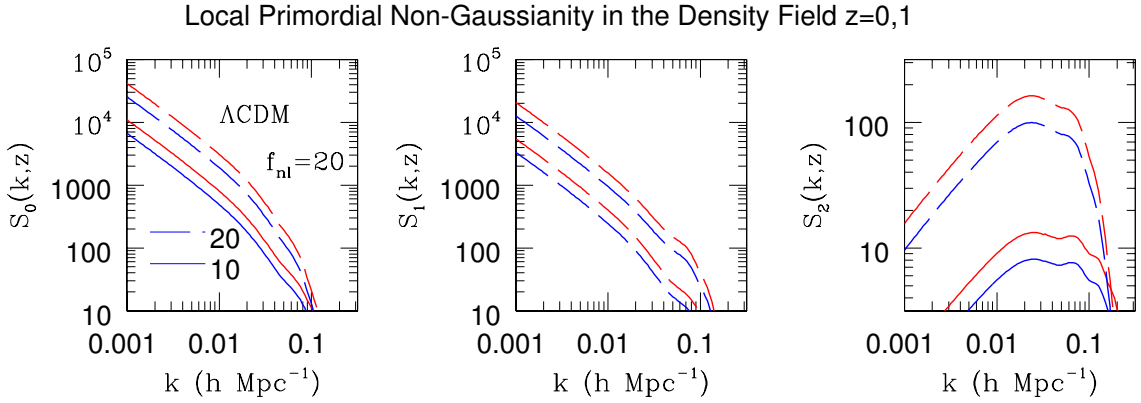

Figure 4.6: The skew-spectra for primordial non-Gaussianity in a 3D cosmological density field is displayed for *local* type primordial non-Gaussianity. The spectra have been calculated for two different smoothing scales $R = 10, 20\mathrm{h}^{-1}\mathrm{Mpc}$ with the left panel showing $S_0(k,z)$, the central panel $S_1(k,z)$ and the right panel $S_2(k,z)$. For each smoothing scale the upper curves correspond to a higher redshift of $z = 1$ and the lower curves to $z = 0$. The local type primordial non-Gaussianity is considered which is defined in Eq.(4.133). We have taken a ΛCDM cosmology with $f_{NL} = 20$.

4.6.2 Primordial Bispectrum

Using the above formalism we can calculate the skew-spectra for the primordial bispectrum in the local, equilateral and folded models. This is done by substituting the appropriate primordial bispectrum [4.133,4.141,4.143] into the expressions for the skew-spectra [4.117,4.118,4.119] and evaluating. Due to the dependence of the primordial bispectra on the angular terms and the transfer function there does not appear to be a trivial analytical solution to these models and it is more elucidating to proceed by numerically integrating the resulting expressions allowing us to obtain the shape and amplitude of the spectra as a function of momenta. The resulting

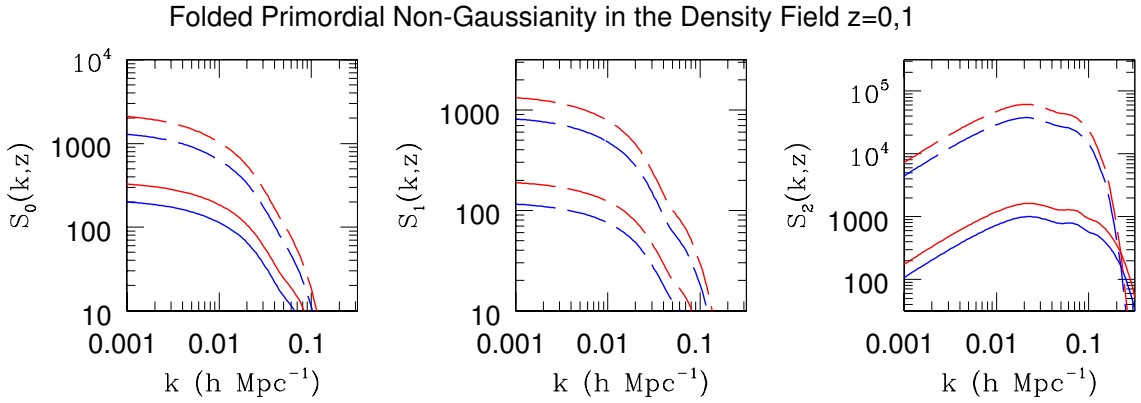

Figure 4.7: Same as previous figure but for primordial non-Gaussianity of *folded* type Eq.(4.143).

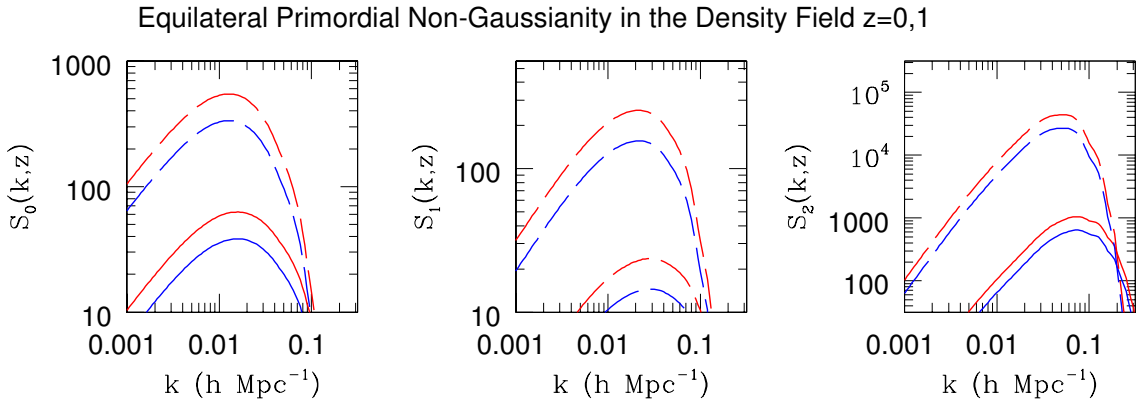

Figure 4.8: Same as previous figure but for primordial non-Gaussianity of *equilateral* type 4.141

skew-spectra are shown in Fig. 4.6, Fig. 4.7 and Fig. 4.8. Unlike gravitational instability the primordial models have redshift dependence and exhibit similar behaviour to the gravitationally induced models for varying smoothing scales. In the full skewness the primordial models grow in amplitude as we increase the smoothing scale [260].

4.6.3 Skewness

As we noted in 4.121, we can recover the one point skewness terms by performing the integration over the second momenta k_2 and collapsing all the statistical information into a one-point estimator for a given smoothing radius R and redshift z. This was the approach taken in [260] and is a good sanity check that we are calculating the same quantities. It was noted in [260] that non-Gaussianity from non-linear gravitational clustering always gives positively skewed density fluctuations and hence $S^{(a)}_{\rm grav} > 0$. However, primordial non-Gaussianity can have either positive or negative $f_{\rm NL}$ in the local model yielding either positively or negatively skewed density fluctuations. This would make it easier to distinguish from $S^{(a)}_{\rm grav}$. In addition, [260] points out that as we increase the smoothing scale R, the non-Gaussianity induced by non-linear clustering $S^{(a)}_{\rm grav}\sigma_0$ becomes weaker, while primordial non-Gaussianity $S^{(a)}_{\rm prim}\sigma_0$ is approximately constant. At local

redshifts $z \approx 0$, the primordial contribution exceeds non-linear gravitational effects for very large scales on order $R > 200h^{-1}\mathrm{Mpc}$ for $f_{\mathrm{NL}} = 100$. Moving to higher redshifts, the relative contribution from non-linear collapse is weaker and primordial contributions can be dominant for $R > 120h^{-1}\mathrm{Mpc}$ for $f_{\mathrm{NL}} = 100$. The analogous plots in the skew-spectra approach would be Fig. 4.5 for gravitational instability and Fig. 4.6-Fig. 4.8 for primordial non-Gaussianity. For the local model, we see that at $k < 0.005h\mathrm{Mpc}^{-1}$ for $f_{\mathrm{NL}} = 20$ the local contributions start to exceed gravitationally induced contributions. I the folded model, the $S^{(0)}$ and $S^{(1)}$ terms are relatively suppressed whereas $S^{(2)}$ could possibly dominate over the gravitational instability contributions for $k < 0.1h\mathrm{Mpc}^{-1}$. In Fig. 4.9 we reproduce Figure 3 from [260] to demonstrate the concepts discussed here.

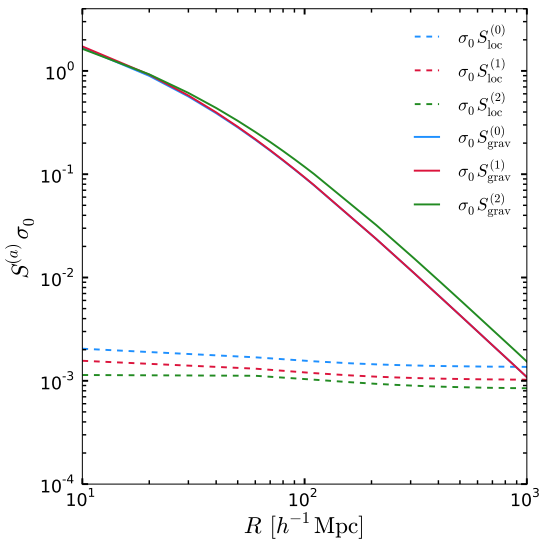

Figure 4.9: This is a reproduction of Figure 3 from [260] showing the skewness parameters $S^{(a)}(z)$ multiplied by the variance σ_0 for both gravitational instability and local primordial non-Gaussianity for $f_{\rm NL} = 10$ at a redshift of $z = 0$. As can be seen, the weighted local primordial spectra demonstrate little dependence on the smoothing scale R. The gravitationally induced contributions to the skewness parameters show a weakening with smoothing scale. At large R it can be seen that the primordial contributions are on order those of gravitational instability.

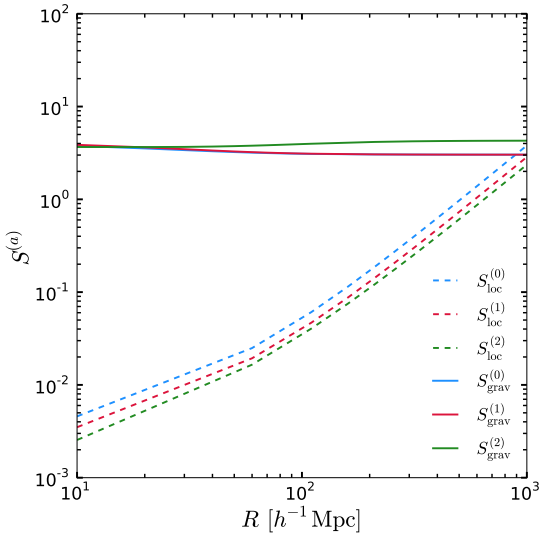

Figure 4.10: This is a reproduction of Figure 3 from [260] showing the skewness parameters $S^{(a)}(z)$ for both gravitational instability and local primordial non-Gaussianity for $f_{\rm NL} = 10$ at a redshift of $z = 0$.

4.6.4 Minkowski Functional Reconstruction

Using the procedure outlined in 4.122 we can associate a power spectrum to the Minkowski functionals by substituting $S_i(k,z)$ into 4.106 instead of the one-point skewness parameters $S_i(z)$. This allows us to plot the Minkowski functionals on the full (k,ν) space for a given smoothing length R, redshift z and, where applicable, an amplitude for non-Gaussianity $f_{\rm NL}$.

In Fig. 4.11-Fig. 4.14 we plot the gravitationally induced bispectrum at a smoothing length of $R = 10h^{-1}\mathrm{Mpc}$. Contrast this to the local primordial model in Fig. 4.15-Fig. 4.18, the folded model Fig. 4.19-Fig. 4.22 and the equilateral model Fig. 4.23-Fig. 4.23. The primordial non-Gaussianity models have been evaluated for an amplitude of non-Gaussianity $f_{\rm NL} = 20$. As can be seen, the amplitude of the primordial contributions is certainly one of the toughest challenges in modern cosmology. To accurately detect and characterise these primordial contributions will require the heroic challenge of highly accurate and detailed understandings of foregrounds, systematics and instrumentation noise. This is true for both CMB and large scale structure surveys. However, should we find ourselves in such a position we see that the various models for the primordial contributions are momenta dependent. The shape of the bispectrum, and hence the shape of the skew-spectra and the Minkowski functional reconstructions, can therefore be distinguished. The functional dependence of the various models for non-Gaussianity shows significant variation allowing for a clearer test for the hypothesis that non-Gaussianity is primordial in origin. This in contrast to the one-point statistics for non-Gaussianity. A similar procedure could be performed for the velocity and 2D projected cosmological random fields.

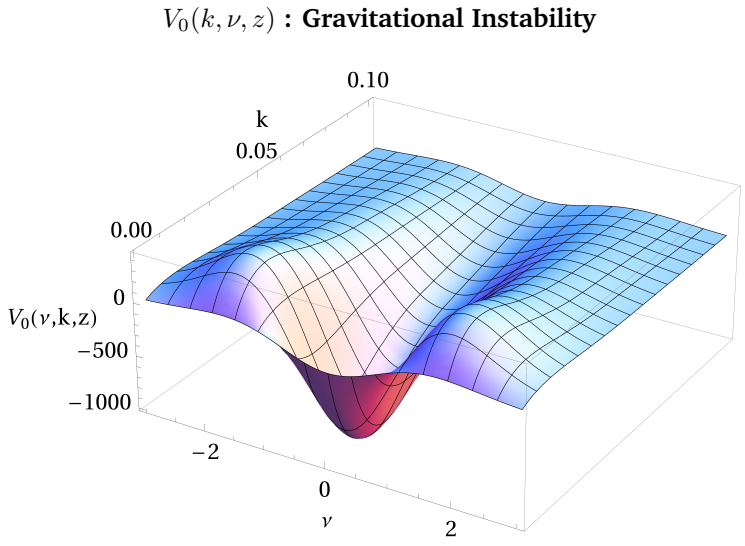

Figure 4.11: Here we plot the power spectrum associated to the Minkowski functionals $V_i(k,\nu,z)$ on the full (k,ν) space for a smoothing length $R = 10h^{-1}\mathrm{Mpc}$ and a redshift $z = 0$. We use the gravitational instability bispectrum.

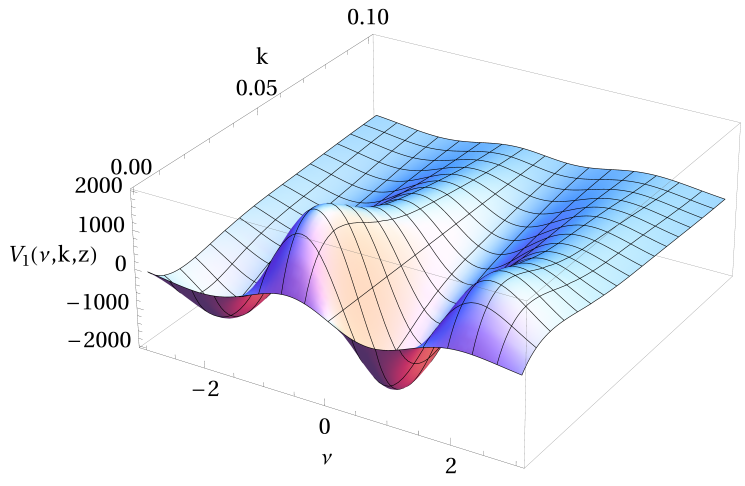

Figure 4.12: Same as previous figure.

$V_2(k,\nu,z)$ **: Gravitational Instability**

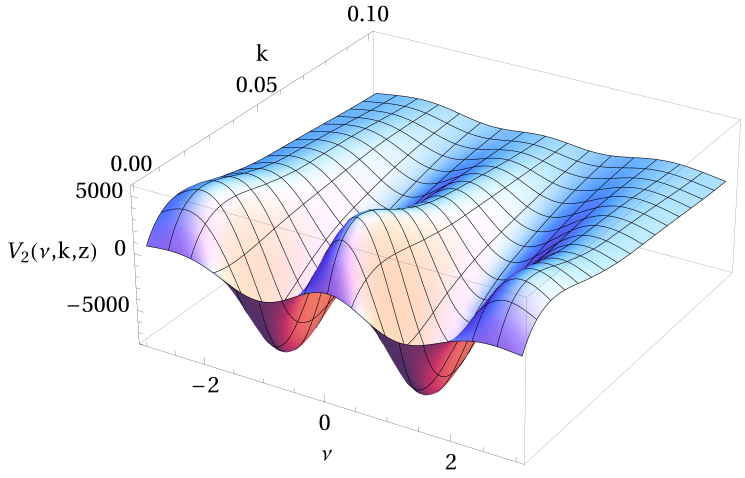

Figure 4.13: Same as previous figure.

$V_3(k,\nu,z)$ **: Gravitational Instability**

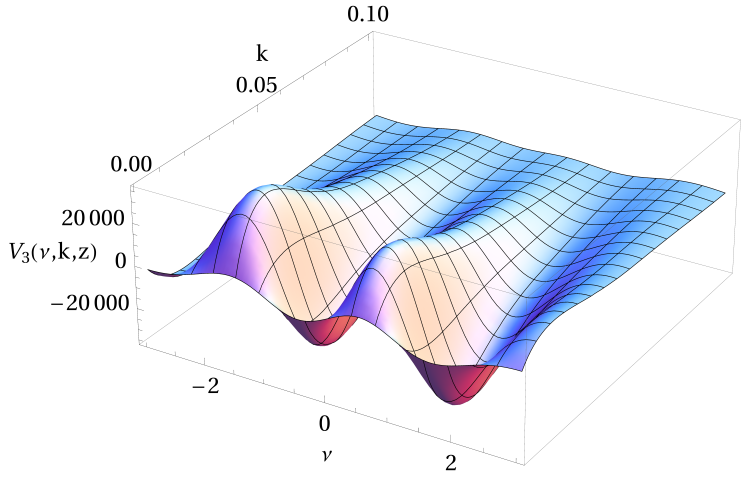

Figure 4.14: Same as previous figure.

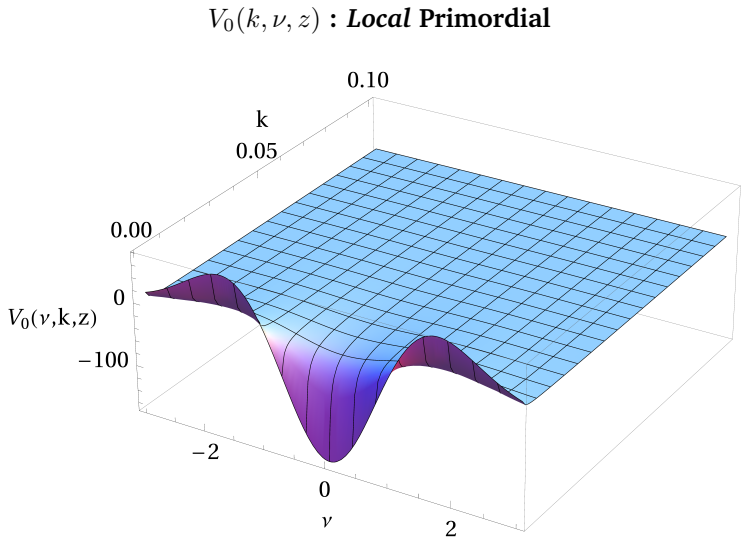

Figure 4.15: Here we plot the power spectrum associated to the Minkowski functionals on the full (k, ν) space for a given smoothing length $R = 10h^{-1}\mathrm{Mpc}$, redshift $z = 0$ and an amplitude for non-Gaussianity $f_{\mathrm{NL}} = 20$. These have been reconstructed by using the skew-spectra $S_i(k, z)$ instead of the one-point skewness parameters in 4.106. For this plot we adopt the *local* primordial bispectrum.

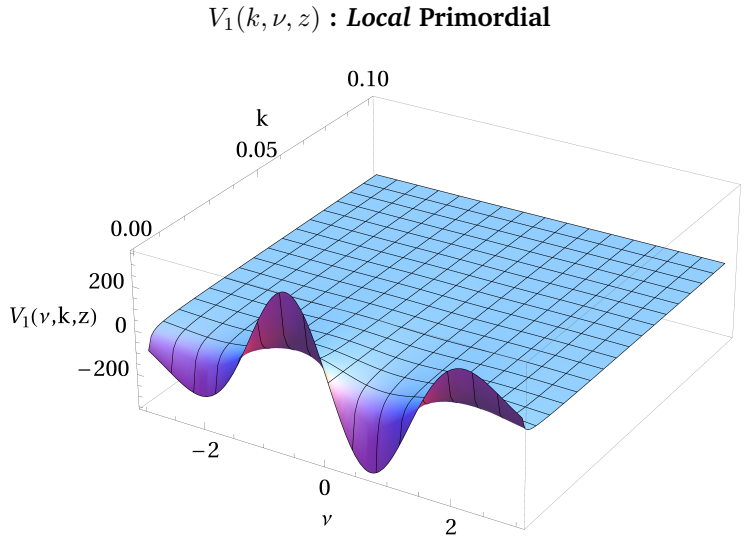

Figure 4.16: Same as previous figure.

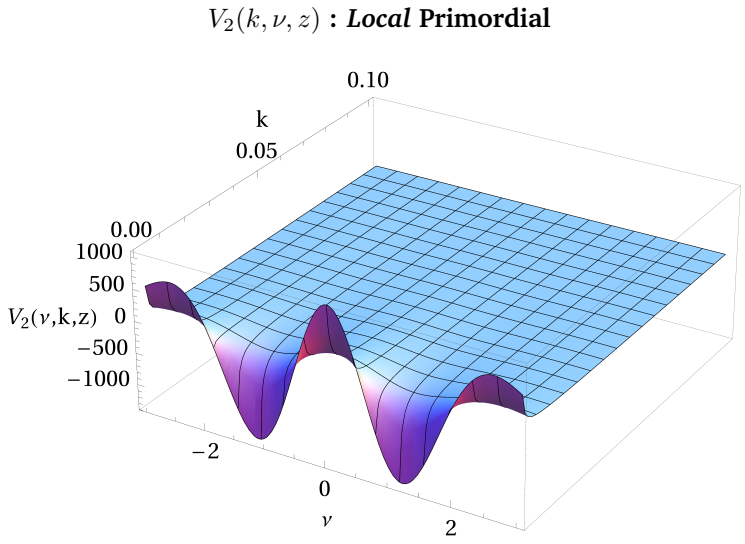

Figure 4.17: Same as previous figure.

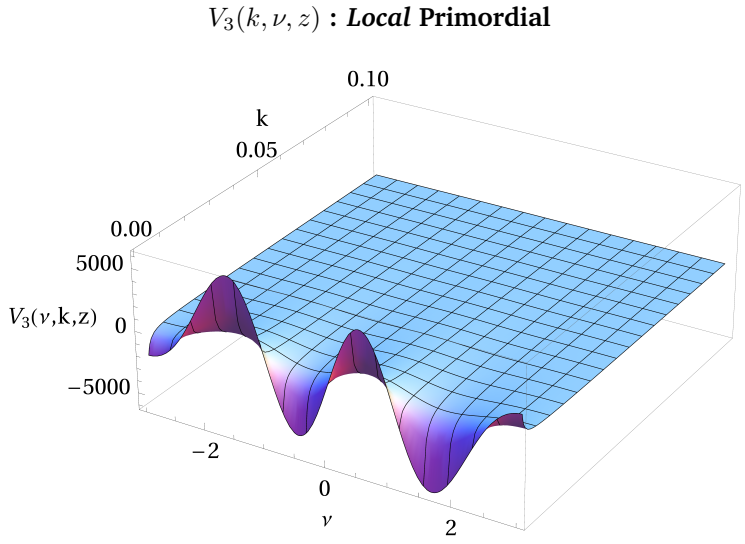

Figure 4.18: Same as previous figure.

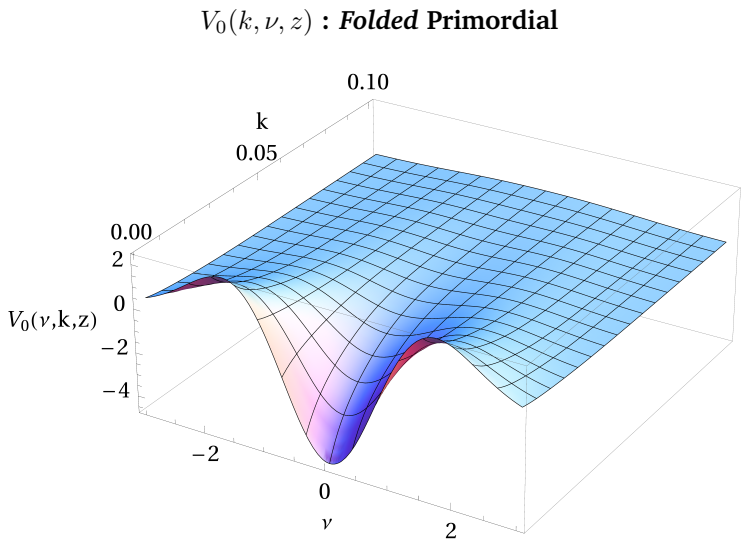

Figure 4.19: Here we plot the power spectrum associated to the Minkowski functionals on the full (k,ν) space for a given smoothing length $R = 10h^{-1}\mathrm{Mpc}$, redshift $z = 0$ and an amplitude for non-Gaussianity $f_{\mathrm{NL}} = 20$. These have been reconstructed by using the skew-spectra $S_i(k,z)$ instead of the one-point skewness parameters in 4.106. For this plot we adopt the *folded* primordial bispectrum.

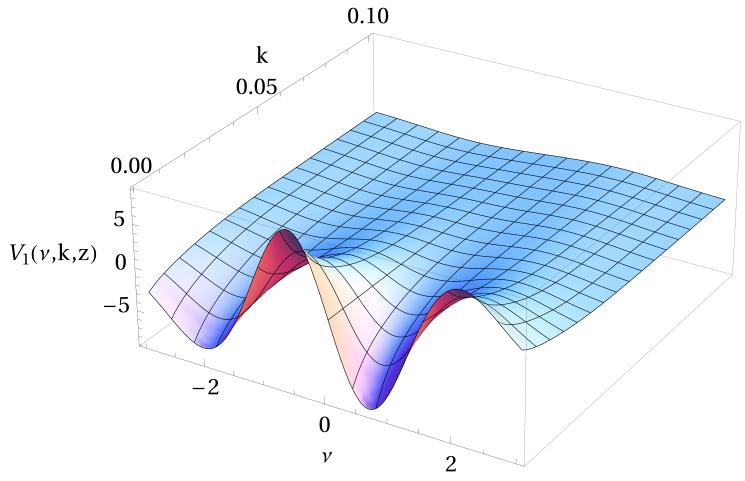

Figure 4.20: Same as previous figure.

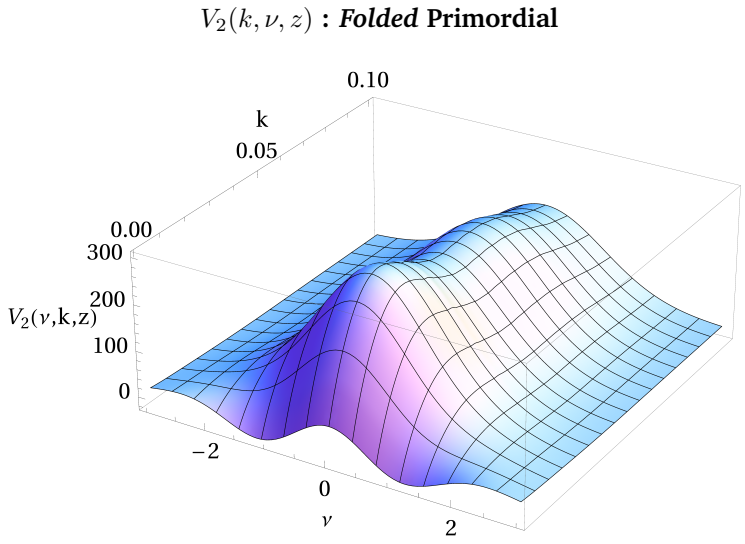

Figure 4.21: Same as previous figure.

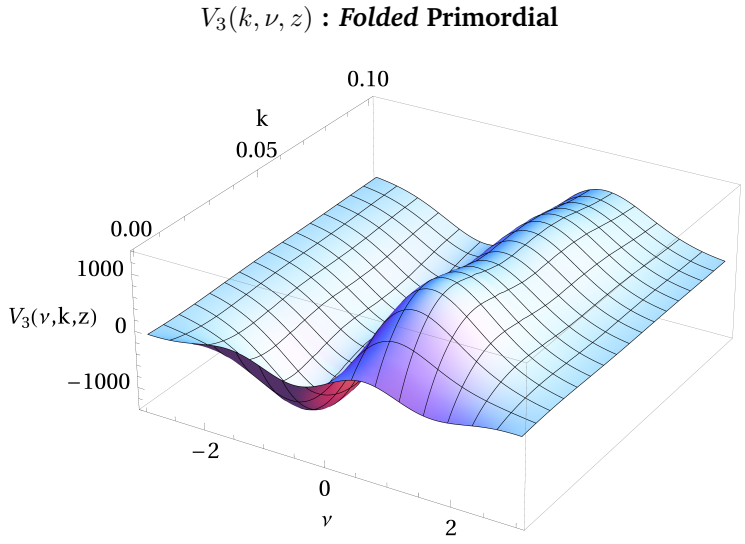

Figure 4.22: Same as previous figure.

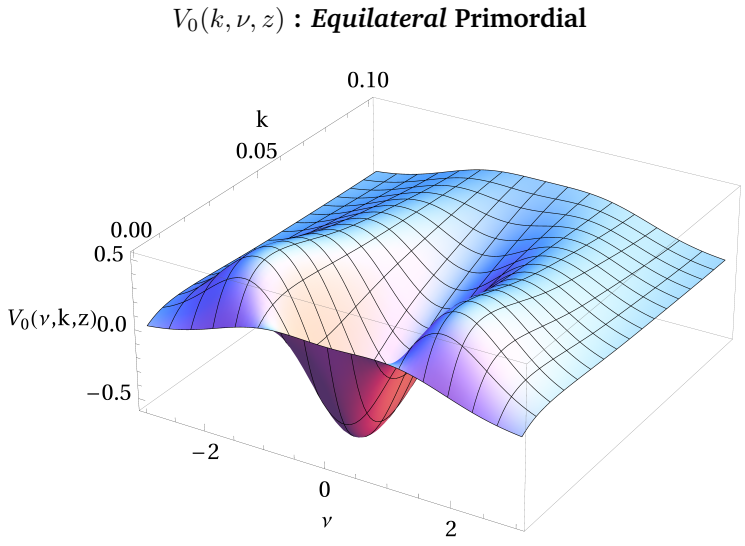

Figure 4.23: Here we plot the power spectrum associated to the Minkowski functionals on the full (k,ν) space for a given smoothing length $R = 10h^{-1}\mathrm{Mpc}$, redshift $z = 0$ and an amplitude for non-Gaussianity $f_{\mathrm{NL}} = 20$. These have been reconstructed by using the skew-spectra $S_i(k,z)$ instead of the one-point skewness parameters in 4.106. For this plot we adopt the *equilateral* primordial bispectrum.

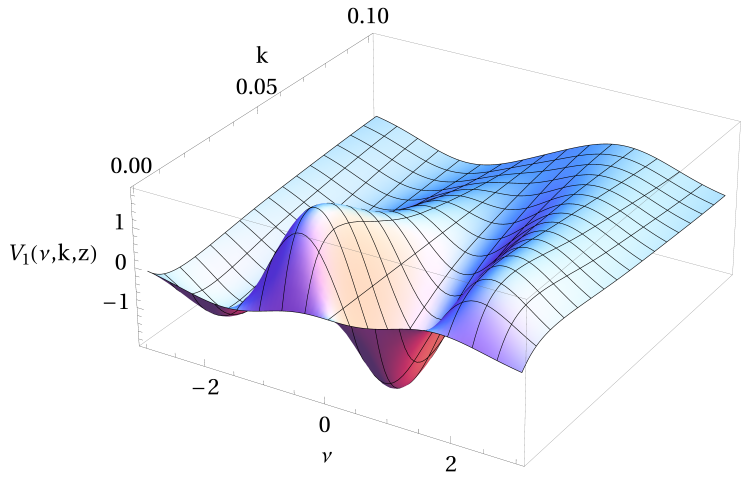

Figure 4.24: Same as previous figure.

$V_2(k,\nu,z)$ **:** ***Equilateral*** **Primordial**

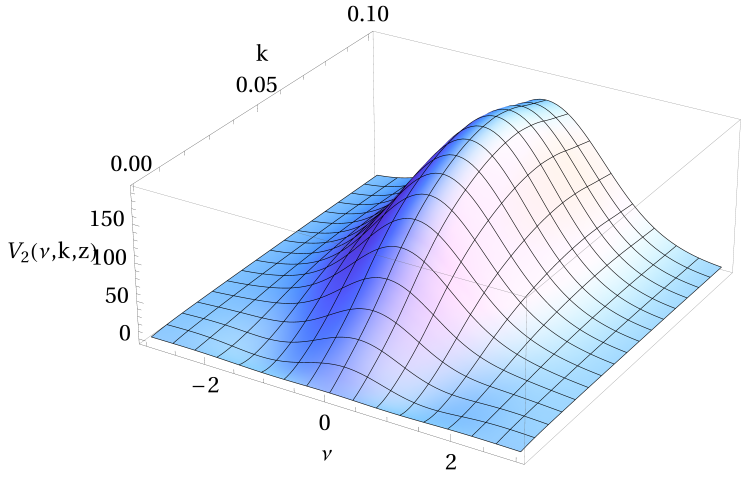

Figure 4.25: Same as previous figure.

$V_3(k,\nu,z)$ **:** ***Equilateral*** **Primordial**

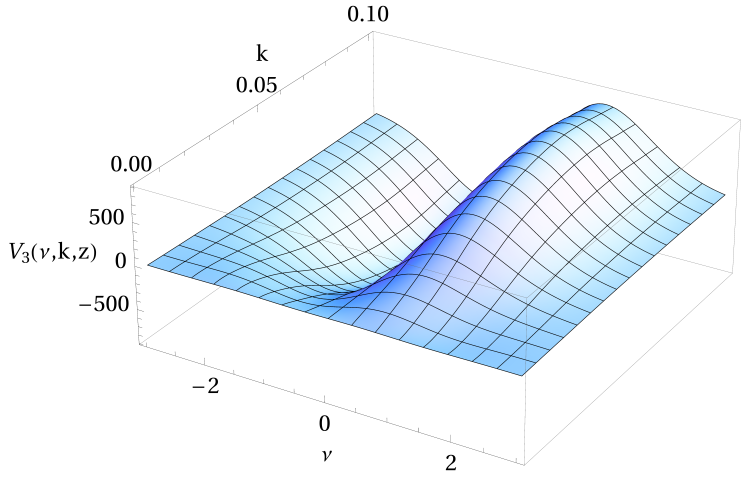

Figure 4.26: Same as previous figure.

4.7 Three-dimensional Velocity Field

The linear density perturbations δ_g was introduced in 4.133 as being related to Bardeen's curvature potential in the matter dominated era Φ. In the Newtonian limit the Universe can be treated as a pressure-less fluid and the continuity equation allows us to relate the linear density perturbations to an associated peculiar velocity $\mathbf{v}(\mathbf{k}, z)$:

$$\dot{\delta_g}(\mathbf{k}) + \nabla \cdot \mathbf{v}(\mathbf{k}) = 0. \tag{4.159}$$

In the basic inflationary paradigm and observationally the linear primordial density perturbations are highly Gaussian. Through the continuity equation we expect that deviations from Gaussianity will impact the observed peculiar velocity field. Following [360] we introduce a dimensionless scalar field normalised by the Hubble variable H:

$$\Theta(\mathbf{x}) = \mathrm{H}^{-1}\nabla \cdot \mathbf{v}(\mathbf{x}). \tag{4.160}$$

Due to the expansion of the Universe, the velocity field is described purely by the diverge (i.e. rotation-free) term with the rotational components being described by decaying solutions in perturbation theory (see, for example, [360; 54]). Using second order perturbation theory the power spectrum and bispectrum can be analytically calculated ([52; 53; 360]):

$$P_\Theta(k) = g_\theta^2 P_\delta(k) + \mathcal{O}(\sigma_0^4); \tag{4.161}$$

$$B_\Theta(k_1, k_2, k_3) = -g_\theta^3 \left[\frac{6}{7} + \mu\left(\frac{k_1}{k_2} + \frac{k_2}{k_1}\right) + \frac{8}{7}\mu^2\right] P_\delta(k_1)P_\delta(k_2) + cyc.perm. + \mathcal{O}(\sigma_0^6). \tag{4.162}$$

The factor g_θ is the logarithmic derivative of the growth factor $D(z)$ with respect to the scale factor a:

$$g_\theta = \frac{d\ln D}{d\ln a} = \Omega_M^{4/7} + \frac{\Lambda}{70}\left(1 + \frac{\Omega_M}{2}\right). \tag{4.163}$$

4.7.1 Gravitationally Induced Bispectrum

Using the modified power spectrum and bispectrum 4.162 we can calculate the skewness parameters for the peculiar velocity field:

$$\begin{aligned} S_0(l_2, z) &= \frac{-1}{g_\theta \sigma_0^4}\frac{1}{2\pi^2}\int \frac{l_1^2 dl_1}{2\pi^2 R^3} W^2(l_1)W(l_2)P_\delta\left(\frac{l_1}{R}\right)P_\delta\left(\frac{l_2}{R}\right)\sqrt{\frac{2\pi}{l_1 l_2}} \\ &\quad \times\left[\frac{13}{7}I_{1/2}(l_1 l_2) - \frac{3}{2}\left(\frac{l_2}{l_1} + \frac{l_1}{l_2}\right)I_{3/2}(l_1 l_2) + \frac{8}{7}I_{5/2}(l_1 l_2)\right], \end{aligned} \tag{4.164}$$

$$\begin{aligned} S_1(l_2, z) &= \frac{-1}{g_\theta \sigma_0^2 \sigma_1^2}\frac{1}{2\pi^2}\int \frac{l_1^2 dl_1}{2\pi^2 R^5} W^2(l_1)W(l_2)P_\delta\left(\frac{l_1}{R}\right)P_\delta\left(\frac{l_2}{R}\right)\sqrt{2\pi l_1 l_2} \\ &\quad \times\left[\frac{33}{28}\left(\frac{l_1}{l_2} + \frac{l_2}{l_1}\right)I_{1/2}(l_1 l_2) - \left[\frac{3}{4}\left(\frac{l_1^2}{l_2^2} + \frac{l_2^2}{l_1^2}\right) + \frac{93}{35}\right]I_{3/2}(l_1 l_2)\right. \\ &\quad \left. + \frac{15}{14}\left(\frac{l_1}{l_2} + \frac{l_2}{l_1}\right)I_{5/2}(l_1 l_2) - \frac{12}{35}I_{7/2}(l_1 l_2)\right], \end{aligned} \tag{4.165}$$

$$S_2(l_2,z) = \frac{-1}{g_\theta \sigma_1^4}\frac{1}{2\pi^2}\int \frac{l_1^2 dl_1}{2\pi^2 R^7} W^2(l_1)W(l_2)P_\delta\left(\frac{l_1}{R}\right)P_\delta\left(\frac{l_1}{R}\right)\sqrt{2\pi}(l_1 l_2)^{3/2}$$

$$\times\left[\frac{57}{35}I_{1/2}(l_1l_2) - \frac{9}{10}\left(\frac{l_1^3}{l_2}+\frac{l_2^3}{l_1}\right)I_{3/2}(l_1l_2) - \frac{51}{49}I_{5/2}(l_1l_2)\right.$$
$$\left.+\frac{9}{10}\left(\frac{l_1^3}{l_2}+\frac{l_2^3}{l_1}\right)I_{7/2}(l_1l_2) - \frac{144}{245}I_{9/2}(l_1l_2)\right]. \quad (4.166)$$

Using the parameterisation presented for the 3-dimensional cosmological density fields we can simplify the above expressions:

$$S_0(k_2,R) = \frac{1}{g_\theta}\left(-\frac{13}{7}S_0^{11} + \frac{3}{2}S_1^{(02)} - \frac{8}{7}S_2^{11}\right), \quad (4.167)$$
$$S_1(k_2,R) = \frac{1}{g_\theta}\left(-\frac{33}{14}S_0^{(13)} + \frac{3}{2}S_1^{(04)} - \frac{93}{35}S_1^{22} - \frac{15}{7}S_2^{(13)} + \frac{12}{35}S_3^{22}\right), \quad (4.168)$$
$$S_2(k_2,R) = \frac{1}{g_\theta}\left(-\frac{57}{35}S_0^{33} + \frac{9}{5}S_1^{(15)} + \frac{51}{49}S_2^{33} - \frac{9}{5}S_3^{(15)} + \frac{144}{245}S_4^{33}\right). \quad (4.169)$$

These are, again, analogous to the appropriate expressions in [360]. The skew-spectra for the three different smoothing scales are shown in Fig. 4.27.

4.7.2 Primordial Bispectrum

The 3D cosmological velocity field can be used to probe primordial contributions. We calculate the skew-spectra for the local model (Fig. 4.28), the equilateral model (Fig. 4.30) and the folded model (Fig. 4.29). All models have been calculated for redshifts $z = 0, 1$ and for smoothing scales $R = 10, 20\,h^{-1}\mathrm{Mpc}$.

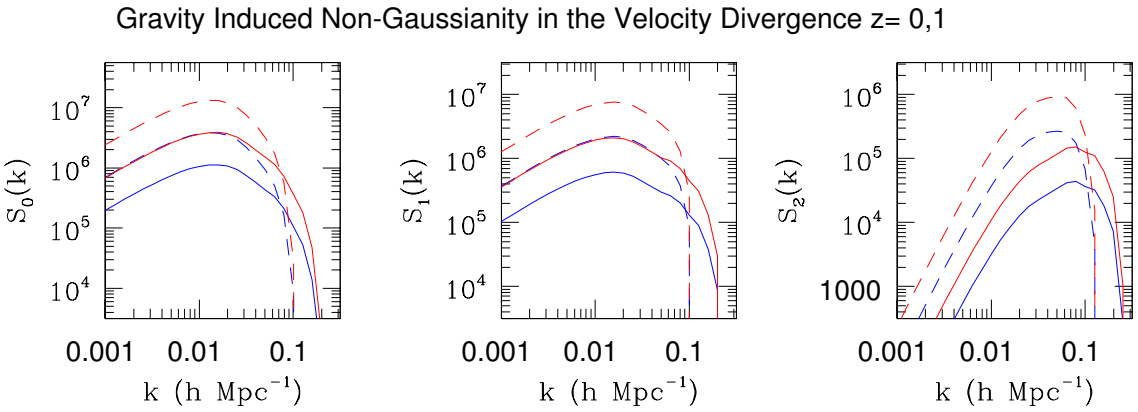

Figure 4.27: The skew-spectra for *gravitational instability* in a 3D cosmological velocity field Θ. The spectra have been calculated for two different smoothing scales $R = 10, 20\mathrm{h}^{-1}\mathrm{Mpc}$ with the left panel showing $S_0(k,z)$, the central panel $S_1(k,z)$ and the right panel $S_2(k,z)$. The results for two different redshift slices are shown. For each smoothing scale the upper curves correspond to a higher redshift of $z = 1$ and the lower curves correspond to $z = 0$. The skew spectra are defined in 4.164, 4.165 and 4.166 respectively. The velocity divergence Θ is defined in 4.160. The bispectrum for Θ is given in 4.162. The redshift dependence for velocity divergence bispectrum depends on g_θ defined in 4.163.

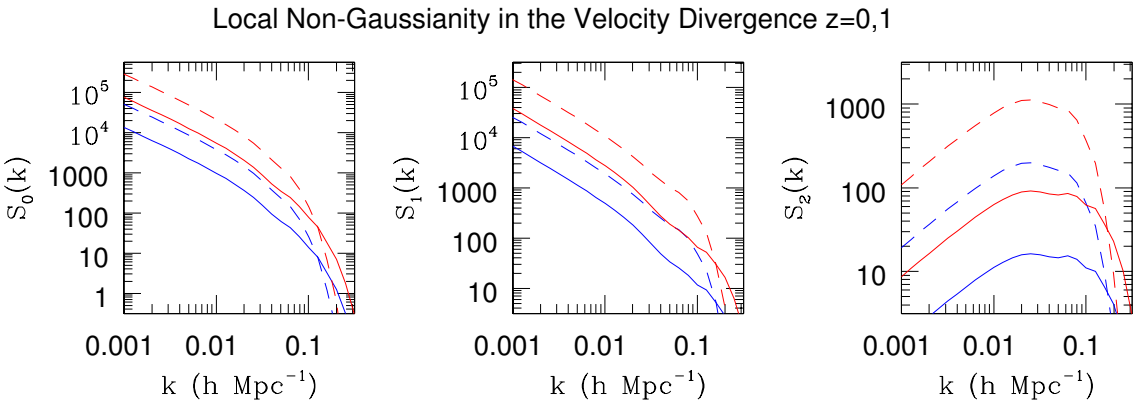

Figure 4.28: Same as previous figure but for non-Gaussianity induced due to primordial non-Gaussianity of *local* type with $f_{NL} = 20$.

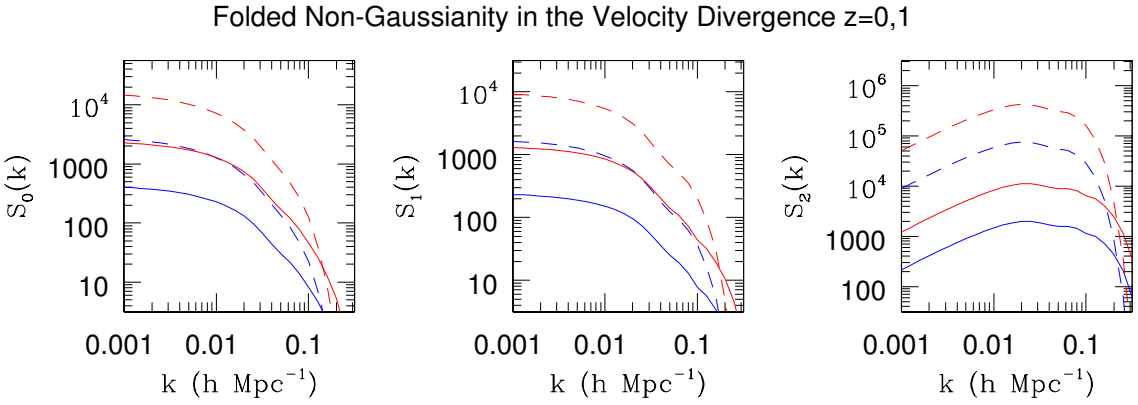

Figure 4.29: Same as previous figure but for non-Gaussianity induced due to primordial non-Gaussianity of *folded* type with $f_{NL} = 20$.

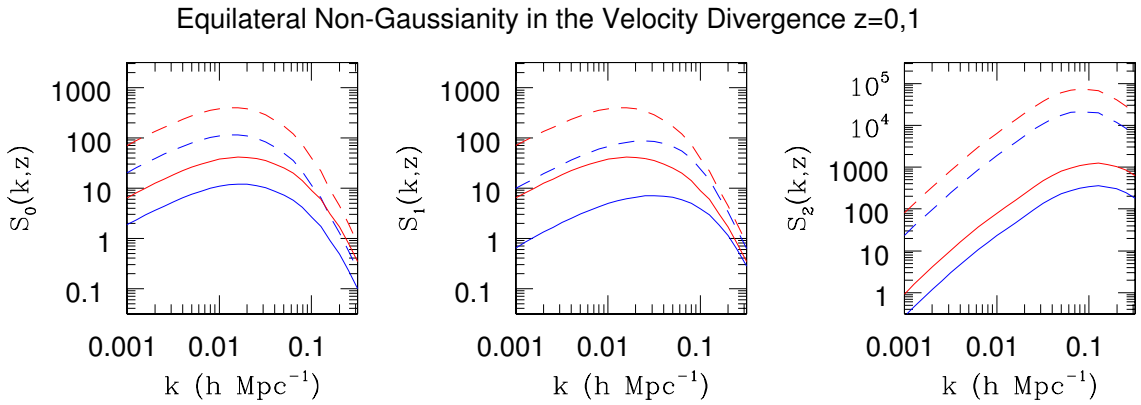

Figure 4.30: Same as previous figure but for non-Gaussianity induced due to primordial non-Gaussianity of *equilateral* type with $f_{NL} = 20$.

4.8 Two-Dimensional Projected Density Fields

Often cosmological data sets can be cast in the form of a projection over the sky. This requires us to introduce a correspondence between three-dimensional density fields and the observed two-dimensional projection. The formalism adopted here follows [360]. When working with a two-dimensional projected field one of the key observables are angular distances for objects placed at a given comoving distance r. Under the assumption of statistical homogeneity and isotropy the Universe can be approximated by the FLRW cosmological models. The line element for an FLRW cosmology can be expressed as:

$$ds^2 = -c^2dt^2 + a^2(t)\left[dr^2 + d_A(r)^2(\sin^2\theta d\theta^2 + d\phi^2)\right]. \tag{4.170}$$

where we $d_A(r)$ is the angular diameter distance to radial comoving distance r. The scale factor is denoted by $a(t)$. We have $d_A(r) = \sinh(\mathrm{K}^{-1/2}r), r, \sin(\mathrm{K}^{-1/2}r)$ for a Universe of negative, zero and positive curvature respectively. The curvature is given by $\mathrm{K} = (\Omega_M - 1)\mathrm{H}_0^2$. The three dimensional density field is then projected onto a two-sphere through the use of a selection function $n(\mathbf{r})$ and the angular diameter distance $d_A(r)$ to relate the projected density contrast field $\Psi(\hat{\Omega})$ to the underlying three-dimensional density field δ_g. Under the flat sky approximation this reduces to

$$\Psi(\hat{\Omega}) = \int dr\ d_A^2(r)\ \delta_g\left(\mathbf{r}, r\right) n(r). \tag{4.171}$$

We can use a similar approach to move beyond one point statistics and consider the projected polyspectra. The two lowest order spectra of interest to us are the projected power spectrum P_{2D} and the projected bispectrum B_{2D}

$$P_\Psi(\ell) = \int dr\ d_A^2(r)\ n^2(r) P_\delta\left[\frac{\ell}{d_A(r)}; r\right]; \tag{4.172}$$

$$B_\Psi(\ell_1, \ell_2, \ell_3) = \int dr d_A^2(r)\ n^3(r) B_\delta\left[\frac{\ell_1}{d_A(r)}; \frac{\ell_2}{d_A(r)}; \frac{\ell_3}{d_A(r)}; r\right]. \tag{4.173}$$

The three-dimensional power spectra $P_\delta(k; r)$ has already been specified and the bispectrum $B_\delta(k_i; r)$ will be evaluated for the appropriate model. In a manner analogous to the three-dimensional density fields, we construct the variance and skewness parameters in order to allow us to investigate the contributions from various sources of non-Gaussianity to the projected bispectrum. The main difference in this approach is that we will be required to introduce the necessary formalism to cope with projection effects. The necessary machinery is discussed in [360] though we have introduced the appropriate modifications to generalise the results to the proposed skew-spectra approach. The variance parameters of a projected field smoothed by an arbitrary window function, $W(\ell\theta_b)$, at a given smoothing scale, θ_b, is given by

$$\sigma_j^2\left(\theta_b\right) = \int \frac{\ell d\ell}{2\pi} \ell^{2j} P(\ell) W^2(\ell\theta_b) = \frac{1}{\theta_b^{2j+1}} \int dr d_A^2(r) n^2(r) D^2(r) \Sigma_j^2\left[d_A(r)\theta_b\right]. \tag{4.174}$$

We have introduced a variance function Σ_j to relate the three-dimensional field to our projected field

$$\Sigma_j^2(R) = R^{2j+2} \int \frac{kdk}{2\pi} k^{2j} P_\delta^{lin}(k) W^2(kR). \tag{4.175}$$

The skew-spectra parameters can then be found by introducing the appropriate functions of the projected field and projected derivative fields Eq.(4.113)

$$S_{2D}^j(\theta_b) = \frac{1}{\sigma_0^4 \theta_b^4} \left(\frac{\sigma_0}{\sigma_1 \theta_b}\right)^{2j} \int dr d_A^2(r) n^3(r) D^4(r) \Sigma_0^{4-2j} \left[d_A(r)\theta_b\right] \Sigma_1^{2j} \left[d_{\rm A}(r)\theta_b\right] \mathcal{C}^{(j)} \left[d_A(r)\theta_b\right], \tag{4.176}$$

where skew-spectra parameters are given by

$$\mathcal{C}_0(l_2, R) = \frac{6}{\Sigma_0^4} \int \frac{l_1 dl_1}{2\pi} \int \frac{d\mu}{2\pi\sqrt{1-\mu^2}} B_\delta(l_1, l_2, l_3, z) W(l_1\theta_b) W(|\mathbf{l}_1 + \mathbf{l}_2|\theta_b), \tag{4.177}$$

$$\mathcal{C}_1(l_2, R) = \frac{3}{\Sigma_0^2 \Sigma_1^2} \int \frac{l_1 dl_1}{2\pi} \int \frac{d\mu}{2\pi\sqrt{1-\mu^2}} |\mathbf{l}_1 + \mathbf{l}_2|^2 B_\delta(l_1, l_2, l_3, z) W(l_1\theta_b) W(|\mathbf{l}_1 + \mathbf{l}_2|\theta_b), \tag{4.178}$$

$$\mathcal{C}_2(l_2, R) = \frac{12}{\Sigma_1^4} \int \frac{l_1 dl_1}{2\pi} \int \frac{d\mu}{2\pi\sqrt{1-\mu^2}} (\mathbf{l}_1 \cdot \mathbf{l}_2) |\mathbf{l}_1 + \mathbf{l}_2|^2 B_\delta(l_1, l_2, l_3, z) W(l_1\theta_b) W(|\mathbf{l}_1 + \mathbf{l}_2|\theta_b). \tag{4.179}$$

For the 2-dimensional spectra the angular integration is performed by using the integral representation of the modified Bessel functions $I_m(l_1 l_2)$ along with the recursion relations $I'_m = (I_{m-1} + I_{m+1})/2$. The integral representation of the modified Bessel functions is given by:

$$\frac{1}{\pi} \int_{-1}^{1} \frac{d\mu}{\sqrt{1-\mu^2}} \mu^m e^{-l_1 l_2 \mu} = \left(-\frac{d}{d(l_1 l_2)}\right)^m I_0(l_1 l_2); \qquad I_0(l_1 l_2) = \frac{1}{\pi} \int_{-1}^{1} \frac{d\mu}{\sqrt{1-\mu^2}} e^{-l_1 l_2 \mu}. \tag{4.180}$$

Proceeding analogously to the 3-dimensional case, the 2-dimensional skew-spectra reduce to a weighted integral over the the modes $k = l/R$:

$$C_0(l_2, R) = \frac{1}{\Sigma_0^4} \int \frac{l_1 dl_1}{2\pi} P\left(\frac{l_1}{R}\right) P\left(\frac{l_2}{R}\right) W^2(l_1) W(l_2) \left[\frac{23}{7} I_0(l_1 l_2) - 3\left(\frac{l_1}{l_2} + \frac{l_2}{l_1}\right) I_1(l_1 l_2) + \frac{6}{7} I_2(l_1 l_2)\right], \tag{4.181}$$

$$C_1(l_2, R) = \frac{1}{\Sigma_0^2 \Sigma_1^2} \int \frac{l_1 dl_1}{2\pi} P\left(\frac{l_1}{R}\right) P\left(\frac{l_2}{R}\right) W^2(l_1) W(l_2) \times \left[\frac{93}{28}(l_1^2 + l_2^2) I_0(l_1 l_2) - \frac{3}{2}\left(\frac{l_1^3}{l_2} + \frac{l_2^3}{l_1} + \frac{27}{7} l_1 l_2\right) I_1(l_1 l_2) + \frac{33}{28}(l_1^2 + l_2^2) I_2(l_1 l_2) - \frac{3}{14} l_1 l_2 I_3(l_1 l_2)\right], \tag{4.182}$$

$$C_2(l_2, R) = \frac{1}{\Sigma_1^4} \int \frac{l_1 dl_1}{2\pi} P\left(\frac{l_1}{R}\right) P\left(\frac{l_2}{R}\right) W^2(l_1) W(l_2) \times \left[\frac{33}{7} l_1^2 l_2^2 I_0(l_1 l_2) - \frac{3}{2}(l_1^3 l_2 + l_2^3 l_1) I_1(l_1 l_2) - \frac{30}{7} l_1^2 l_2^2 I_2(l_1 l_2) - \frac{3}{2}(l_1^3 l_2 + l_2^3 l_1) I_3(l_1 l_2) + l_1^2 l_2^2 I_4(l_1 l_2)\right]. \tag{4.183}$$

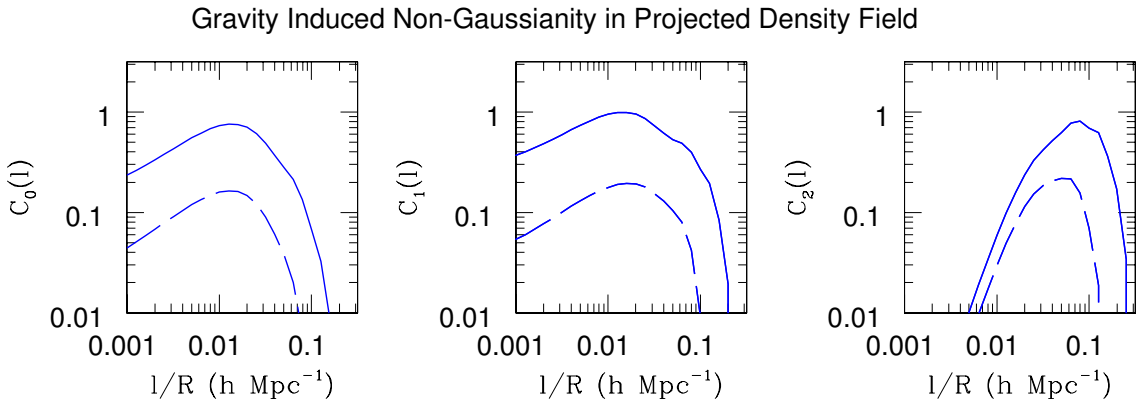

Figure 4.31: The skew-spectra induced by gravitational instability for projected (2D) cosmological density field. The spectra have been calculated for two different smoothing angular scales $R = 10, 20h\mathrm{Mpc}^{-1}$ with the left panel showing $C_0(l)$, the central panel $C_1(l)$ and the right panel $C_2(l)$. The solid line corresponds to $R = 10h\mathrm{Mpc}^{-1}$ and the dashed line corresponds to $R = 20h\mathrm{Mpc}^{-1}$. The projected skew-spectra are defined in 4.177, 4.178 and 4.179.

We adopt a parameterisation in terms of the variable $C_m^{\alpha\beta}$:

$$C_m^{\alpha\beta}(l_2, R) = \frac{1}{\Sigma_0^4}\left(\frac{\Sigma_0}{\Sigma_1}\right)^{\alpha+\beta-2} \int \frac{l_1 dl_1}{2\pi} P\left(\frac{l_1}{R}\right) P\left(\frac{l_2}{R}\right) W^2(l_1) W(l_2) I_m(l_1 l_2) l_1^{\alpha-1} l_2^{\beta-1}. \quad (4.184)$$

The skew-spectra can then be written as:

$$C_0(l_2, R) = \frac{23}{7} C_0^{11} - 6C_1^{(02)} + \frac{6}{7} C_2^{11}, \quad (4.185)$$

$$C_1(l_2, R) = \frac{93}{14} C_0^{(31)} - 3C_1^{(40)} - \frac{81}{14} C_1^{22} + \frac{33}{14} C_2^{((31)} - \frac{3}{14} C_3^{22}, \quad (4.186)$$

$$C_2(l_2, R) = \frac{33}{7} C_0^{33} - 3C_1^{(42)} - \frac{30}{7} C_2^{33} - 3C_3^{42} + C_4^{33}. \quad (4.187)$$

The resulting skew-spectra for gravitational instability are shown in Fig. 4.31 for smoothing scales $R = 10, 20\, h\mathrm{Mpc}^{-1}$.

The 2D projected surveys can be used with the primordial bispectra by simply replacing the bispectrum kernel in [4.177,4.178,4.179] with the corresponding primordial model. The results are shown in Fig. 4.32,Fig. 4.34 and Fig. 4.33.

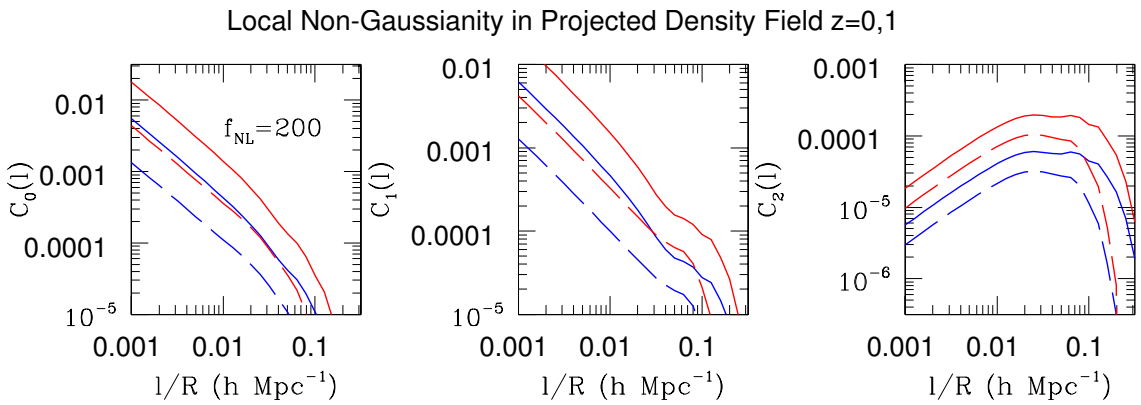

Figure 4.32: Same as previous figure but for *local* type primordial non-Gaussianity for $f_{NL} = 200$.

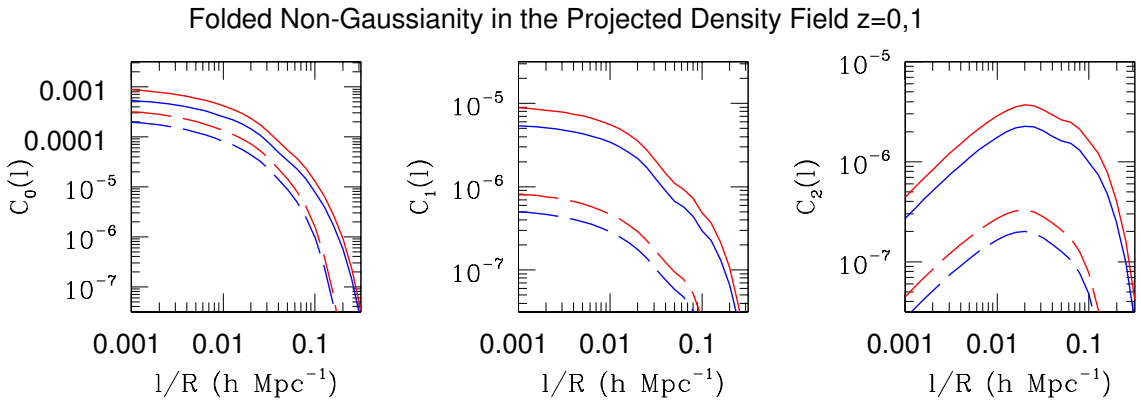

Figure 4.33: Same as previous figure but for *folded* type primordial non-Gaussianity.

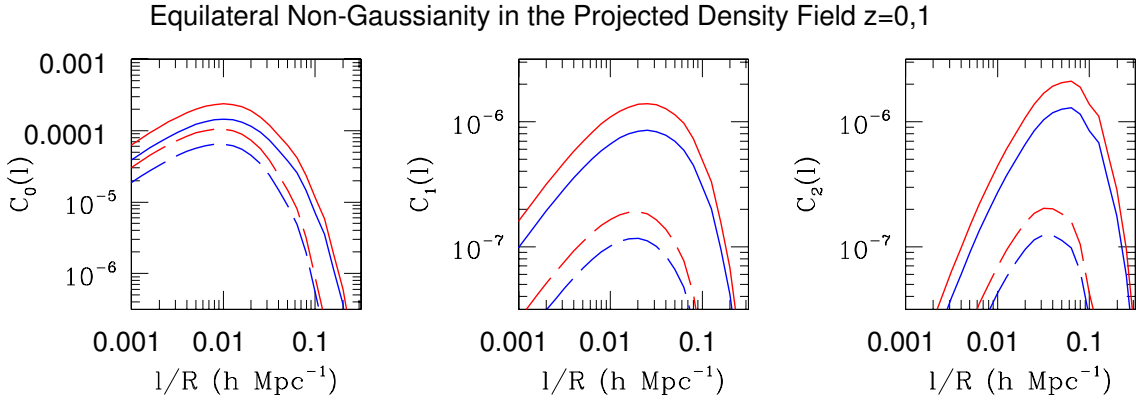

Figure 4.34: Same as previous figure but for *equilateral* type primordial non-Gaussianity.

4.9 Real World Effects

In this section we briefly outline some key observational and systematic effects that lead to corrections and modifications to measured quantities (e.g. power spectrum). This Chapter does not attempt to deal with real world effects, but a more general treatment incorporating real world effects would be a useful and vital increment to the work presented here.

4.9.1 Redshift Space Distortions

Real world observations and surveys consist of constructing a map detailing the frequency and intensity of radiation across the sky or a patch of the sky. Cosmological distances are constructed under the assumption that the frequency of a particular emitter (e.g. CO emission) is known allowing us to estimate the redshift to the source. Under the assumption that we inhabit a spatially homogeneous, isotropic, irrotational and expanding spacetime then the redshift may be converted to a coordinate distance in a fairly straightforward manner. Redshift distance estimates consist of a number of contributions of which the two most physically relevant, for cosmological observations, are the metric expansion of spacetime (as the dominant factor) and the Doppler shifts arising from local peculiar velocities of a source along the line of sight.

The non-linear nature of the mapping from real space to redshift space means that a Gaussian random field will have non-Gaussian corrections when observed in redshift space. In addition to these non-Gaussian corrections there will be modifications to the observed power spectrum. Such systematics will become increasingly important with the precision of the surveys mentioned in Section 4.1. There exists analytic results for the linear results ([289; 237; 238; 357]) and recent studies have begun to investigate the full non-linear redshift-space power spectra (e.g. [521]). The linear result first provided in [289] introduces the following modification to the 2-point function

$$P_{g,s}(k) = b^2(1 + b^{-1} f \mu_k^2)^2 P_\delta(k), \tag{4.188}$$

where b is a linear bias factor, f the derivative of the linear growth factor and $\mu_k = \hat{\mathbf{n}} \cdot \hat{\mathbf{k}}$.

4.9.2 Galaxy Bias

The formation of galaxies and collapsed objects is highly dependent on the total local matter density. An important point to note is that large scale structure surveys only probe the luminous baryonic matter and we find that there are nonlinearities in the biased relationship between the observable baryonic matter distribution (i.e. galaxies) and the underlying total matter distribution (i.e. baryonic plus cold dark matter). This nonlinearity can give rise to an effective non-Gaussianity that must be taken into account when performing statistical tests of large scale structure. Following [190] we can assume that galaxy formation is a local deterministic process and perturbatively expand the galaxy density contrast δ_g in terms of the underlying matter density contrast δ_m

$$\delta_g(z) = b_0(z) + b_1(z)\delta_m(z) + \frac{b_2(z)}{2}\delta_m^2(z) + \mathcal{O}(\delta_m^3), \tag{4.189}$$

where $b_0(z)$ is set by the constraint $\langle \delta_g(z) \rangle = 0$. The two remaining parameters $b_1(z)$ and $b_2(z)$ are the galaxy bias parameters. The 2-point and 3-point correlators of the galaxy distribution are

therefore weighted functions of the 2-point and 3-point correlators of the matter distribution

$$P_g(k,z) = b_1^2(z)P_m(k,z), \tag{4.190}$$

$$B_g(k_1,k_2,k_3,z) = b_1^3(z)B_m(k_1,k_2,k_3,z) + b_1^2(z)b_2(z)\left[P_m(k_1,z)P_m(k_2,z) + \text{cyc.}\right]. \tag{4.191}$$

In the above $B_m(k_1,k_2,k_3,z)$ is the bispectrum for the matter distribution. In this thesis we have neglected the bispectral contributions from galaxy biasing and have focused primarily on primordial non-Gaussianities and gravitationally induced contributions. For a detailed discussion of biasing effects see [190; 498; 367; 368; 116; 511; 281; 282] for a selection of relevant papers.

4.9.3 Survey Effects

In addition to redshift space distortions and biasing effects we also have to consider additional observational effects such as survey geometry, survey volume and corrections to the radial selection function arising from magnitude limited surveys. Other effects include the survey specifications (e.g. range of redshifts probed), instrumental noise and additional complex non-linearities that can manifest at high k altering the power spectrum. Examples of these complex non-linearities include both instrumental transfer function effects in Fourier space and survey specific sample biasing. A specific model for the instrument transfer function must be assumed to investigate effects at high k for a given survey. Such a modification is arbitrary and survey dependent. Skew spectra, being high order statistics, will be affected more by sample (cosmic) variance. The resulting bias and scatter of these estimators will have to be dealt with more precautions than their ordinary power spectrum counterparts. Such issues will be dealt with in a separate publication. We shall provide a quick discussion of magnitude limited surveys, radial selection function and volume of the survey following the discussion presented in [257].

In an apparent-magnitude limited survey the number density of observed galaxies will decrease with redshift. This means that for the galaxies to be appropriately resolved, and hence a reliable density field reconstructed, we need an appropriate smoothing length $R > R_g$ such that R_g is the mean separation of galaxies at our specified redshift. This means that we have a maximum redshift $z_{\max} = z_{\max}(R_g)$ such that R_g will be the mean separation of the magnitude limited galaxy sample at our maximum redshift $z_{\max}$ [580]. The number of independent resolution elements in each survey volume will be given by [257] $N_{\text{Res}} = V_{\text{surv}}(< Z_{\max})/(2\pi)^{3/2}R_g^3$. This Chapter does not attempt to take real-world systematics into account and a detailed treatment of real-world systematics and error estimates would be an important next step in the study of Minkowski functionals using the skew-spectra formalism.

4.10 Future Work?

In brief we outline a few points that can be made with regards to future studies. The first natural extension to the work presented here is to incorporate higher order terms in the series expansion for the Minkowski functionals [363] for 3-dimensional studies such as the one applied here to large scale structure. Although the CMB constraints on the kurtosis, and hence trispectrum, are weaker than those of the bispectrum, the overall amplitude of the trispectrum can make it difficult

to study in detail. It is hoped, however, that upcoming large scale structure surveys will give access to a greater number of Fourier modes and perhaps a greater S/N ratio. Studies of the trispectrum and the Suyama-Yamaguchi inequality have been the focus of recent studies in the literature [221] and it would be interesting to see what the Minkowski functionals and the skew-spectra formalism can say about these parameters.

It is also possible to apply the skew-spectra method to the study of Minkowski functionals for other cosmological random fields, such as the 21cm background (e.g [203]), in order to probe cosmologically and astrophysically interesting physics. This includes studies of the effects of reionisation on the 21cm background as well as more exotic possibilities such as cosmic strings [369].

More importantly, it will be necessary to extend the preliminary analysis of the skew-spectra presented here to consider what information can be recovered and probed from upcoming large scale structure surveys. Important questions that can be asked using the approach presented here include the level to which we can realistically expect to discriminate between the various contributions to the bispectrum and the concomitant amplitude. A standard technique used to answer such questions is the Fisher information matrix formalism, which allows us to estimate the projected errors of various parameters p_i from measurement errors on the MFs. The Fisher information matrix F_{ij} is written in terms of the inverse of the covariance matrix Σ^{-1} as follows

$$F_{ij} = \sum_{\alpha\beta} \frac{\partial V_\alpha}{\partial p_i} \left[\Sigma^{-1}\right]_{\alpha\beta} \frac{\partial V_\beta}{\partial p_j}, \tag{4.192}$$

where we note that the MFs will be correlated at different threshold values ν and across various smoothing scales R. The covariance matrix will therefore of the form

$$\Sigma_{\alpha\beta}\left(\nu,\nu'\right) = \left\langle V_\alpha(\nu)\, V_\beta(\nu')\right\rangle \neq \delta_{\alpha\beta}\ \left(\nu-\nu'\right). \tag{4.193}$$

The connection to the projected errors is given by the Cramér-Rao bound, expressing the lower bound that we could theoretically achieve, for the variance of the estimators $\Delta p_i \geq \sqrt{\left[F^{-1}\right]_{ii}}$. This provides a limit to the accuracy with which we can estimate the parameter p_i. These equations, as presented, are suitable for the full Minkowski functional and not our skew-spectra counterparts. The extension to the skew-spectra formalism would re-introduce the momentum dependence into the equations.

Lastly, it is possible to move beyond the scalar Minkowski functionals to the even more complete set of tensorial Minkowski functionals [49; 50; 491]. These objects provide a geometric characterisation of the spatial structure of a random field with information that goes beyond that of the scalar Minkowski functionals. Minkowski tensors are tensorial shape indices that should allow for the characterisation of the anisotropy of a random field being the simplest generalisation of the concepts of volume, surface and integral curvatures to tensor valued objects [491]. These could possibly have applications to both the CMB, upcoming all sky polarisation maps, weak lensing as well as the corresponding large scale structure surveys.

4.11 Conclusion

New surveys proposed over the next decade or two offer the possibility of probing large scale structure in an unprecedented manner. It is hoped that larger, more comprehensive cosmological data sets along with a more sophisticated understanding of the underlying systematics will allow us to investigate the role of non-Gaussian initial conditions along with the physics underlying gravitational instability in an FLRW Universe. This makes the statistics of galaxy clustering an interesting playground for model testing and discrimination.

In this Chapter we have adopted the conventional approach to describing gravitational clustering through a hierarchy of higher order correlation functions. There exist numerous statistical methods to characterise the higher order correlators ranging from polyspectra defined in Fourier space to the spatially defined Minkowski Functionals adopted in this Chapter. The Minkowski functionals are a topological statistic that characterise the morphological properties of a random field. In particular it has been shown that the morphological properties of a Gaussian random field are analytically known with non-Gaussian corrections giving rise to changes in the morphological properties of a random field. The Minkowski functionals are therefore sensitive to non-Gaussianity allowing us to construct a statistical estimator based on analytically known results for a Gaussian random field. Using the formalism presented by [360] and [260] it has been shown that the Minkowski functionals, to leading order, depend on a set of skewness parameters S_0, S_1, S_2 that encapsulate the non-Gaussian corrections to the random field. In particular, for a weakly non-Gaussian random field, the skewness parameters, a set of one-point estimators, reduce to a weighted probe of the bispectrum. The currently adopted approach has been to collapse all the information into the one-point estimators but at a loss of the ability to effectively discriminate between different types of non-Gaussianity. The shape of the bispectrum has been strongly emphasized as an extremely important tool in discriminating between various models for an inflationary scenario as well as secondary non-Gaussianity such as gravitationally induced nonlinearity. Motivated by this we have presented a generalisation of these one-point estimators to a set of skew-spectra S_l^0, S_l^1, S_l^2 that avoid collapsing all the information into a single estimator. It has been argued that by investigating the shape of the skew-spectra and it's relation to the bispectrum $B_{l_1 l_2 l_3}$ we can discriminate more effectively between the various bispectral configurations and ideally separate out the primordial and secondary contributions.

These generalised skew-spectra are two-point statistics spatially but the dependence on the bispectrum is related to the fact that they are third (leading terms) order statistics in terms of non-Gaussianity. A cumulant correlator of order $p+q$ is constructed from the cross-correlation of the spatial fields (or the derivative fields) $\langle \Psi^p(\mathbf{x}) \Psi^q(\mathbf{x}) \rangle$. This cumulant correlator will probe the polyspectra of order $p+q$ [388].

This Chapter has only considered the generalised skewness parameters up to $\mathcal{O}(\sigma_0)$ with the resulting spectra corresponding to a weighted probe of bispectrum. The formalism is developed in terms of a perturbative expansion about a Gaussian random field and we necessarily truncate the results to the desired order. We could consider higher order corrections with the results of $\mathcal{O}(\sigma_0^2)$ for which the resulting spectra would provide a weighted probe of the trispectrum (see e.g. [363; 398]). The next-to-leading order results are appropriately named kurt-spectra due to their relation to the more conventionally used kurtosis parameters. Although we have not considered

the next-to-leading order non-Gaussian corrections, the unprecedented level of detail in upcoming surveys makes investigations of next-to-leading order statistics a promising future direction.

The skew-spectra have been constructed from various products of the spatial and derivative fields (e.g. $\nabla\Psi, \nabla^2\Psi, \nabla\Psi \cdot \nabla\Psi$, etc). The skew-spectra can be related to the spatially defined cumulant correlators and the skewness parameters can be constructed from the corresponding skew-spectra. Given the momenta-dependence of the skew-spectra it was shown that they carry greater discriminating power against the various bispectra configurations which can be compared to observational or numerical results. Something that has not yet been considered is the role of noisy data, systematics or survey masks. A discussion of error on the estimators and their scatter will be presented elsewhere. The presence of such noise will lead to scatter in our estimators necessitating a greater understanding of the systematics in upcoming LSS surveys (see e.g. [263]).

The systematic study of the skew-spectra presented in this Chapter focused on three different cosmological data sets: 3D density, 3D velocity and 2D projected. For each of these models we numerically investigated the shape of the bispectrum for three primordial models (local, equilateral and folded) along with the analytical gravitationally induced bispectrum. The primordial bispectra were shown to be dependent on the underlying matter power spectrum, transfer function with an overall amplitude set by the background cosmology and smoothing scale. The 2D skew-spectra were calculated for the innermost kernel in the integral with the integral over the background geometry neglected. The shape and amplitude of the underlying spectra is still of interest however.

The approach to probing non-Gaussianity presented in this Chapter is just one of many areas of similar work. It is accepted that the CMB should provide one of the cleanest probes of the early Universe with the density perturbations being adequately modeled by linear perturbation theory. The non-linear nature of gravitational instability means that the primary source of non-Gaussianity in LSS or weak-lensing surveys is most likely non-primordial. Nevertheless, LSS surveys are currently thought to be able to place comparable constraints on primordial non-Gaussianity to that of the CMB. Likewise, recent developments on the analytical modeling of weak lensing has lead to the hope that upcoming weak lensing surveys could provide an unbiased probe of the underlying matter distribution yielding a cleaner probe of the statistics of gravitational clustering than conventional LSS surveys (e.g. [398]). Another possibility that could offer the cleanest probe of primordial non-Gaussianity is that of a non- Gaussian stochastic background of gravitational waves. The prospects for direct detection are not currently optimistic due to the weakness of the 3-point term in the graviton interactions [6] though it is hoped that indirect detection through, for example, CMB polarisation could be a possibility.

An assumption that was made throughout this Chapter was the use of a Gaussian window function. This is a popular, though arbitrary, choice and we could equally have performed the analysis using alternative window functions. Another popular window function used in the literature is the top-hat window function [54]. The formalism presented allows the results to be generalised to arbitrary functions but this is not thought to change the overall conclusions of this Chapter.

In all models the gravitational instability bispectrum was an order of magnitude or two greater than that of the primordial bispectra. At very small wavenumbers the local primordial bispectra was starting to become comparable to the gravitational instability skewness. The results quoted are for $f_{\rm NL} \sim 20$ which may be somewhat optimistic with the true amplitude for non-Gaussianity

lying closer to unity and as a result this would further reduce the skew-spectra amplitudes by an order of magnitude. Interestingly it seems that the shapes of the primordial bispectra are distinguishable even if the gravitational instability non-Gaussianity is the dominant contribution for all surveys discussed. The results do not take into account systematics or noise so no constraints on the signal-to-noise ratio may be discussed but a more detailed account will be presented elsewhere. The shape of the gravitational instability skew-spectra could be useful in quantifying predictions from perturbative treatments of gravitational instability, N-body simulations or semi-analytic approximations and it is worthwhile considering the prospects for disentangling any primordial contributions from gravitational instability.

We have studied the skew-spectra for the 3D galaxy distribution as well as 2D projected surveys. For the 3D surveys we ignored the effects of redshift space distortion. Redshift space effects are important as these correspond more directly to the observables in conventional large scale structure surveys. Examples of the role of redshift space distortion can be found in [289; 238; 521; 417; 478]. A more general treatment taking into account redshift space effects will be presented elsewhere.

4.12 Summary of Key Points and Key Results

- In this section we began by detailing various approaches to the Minkowski functionals and presented a self-contained treatment as to how the underlying mathematical structures may be related to weakly non-Gaussian random fields by perturbation theory. The underlying perturbative approach is based on an Edgeworth expansion and the key results follow that of [360].

- Having previously emphasies the importance of non-Gaussianity in both characterising a random field and disentangling the underlying physics, we introduced the skew-spectra formalism [388] as a two-point statistic, defined in the spatial domain, that act as a weighted probe of the bispectrum. The cumulant correlators of order $p+q$ are constructed by cross-correlating a spatial field and its derivatives, $\langle \Psi^p(\mathbf{x})\Psi^q(\mathbf{x})\rangle$. This correlator probes polyspectra of order $p+q$.

- We argued that this approach should be more sensitive to different contributions to the underlying bispectrum as it avoids compressing all information into a one-point statistic probing non-Gaussianity. Rather, we retain both the momentum and amplitude dependence. This is important as different underlying field theoretic models for inflation, for example, have different momentum and amplitude dependence. The conventional one-point statistics only probe the amplitude of non-Gaussian corrections, integrating out the momentum dependence. The skew-spectra have greater distinguishing power, due to momentum dependence, but at a lower signal-to-noise ratio. This will be less of an issue in upcoming large scale structure surveys.

- We provided explicit expressions for the skewness parameters $S_i(k_2, z)$ as weighted integrals over the bispectrum $B(k_1, k_2, k_3, z)$.

- We then proceeded to calculate the skewness parameters for a serious of popular template configurations for the bispectrum.
- For a template corresponding to the gravitationally induced bispectrum, we derived analytical results for the skewness parameters $S_i(k_2, z)$ and numerical results for the skewness parameters and the power spectrum associated to the Minkowski functionals $V_i(k_2, \nu, z)$.
- For three primordial non-Gaussianity templates, corresponding to the local, equilateral and folded templates, we numerically calculated the skewness parameters and a power spectrum associated to the Minkowski functionals.
- An important result is that the amplitude and momentum dependence of $S_i(k_2, z)$ and $V_i(k_2, \nu, z)$ differs from template to template. A good future exercise would be to construct a pipeline for performing model selection based on the skew-spectra obtained from either numerical simulations or observations. To what degree can we distinguish the various models and to what level can we constrain primordial non-Gaussianity in realistic survey configurations? The results in this Chapter act as a solid proof of concept for such a study.
- This analysis was regurgitated for 3-dimensional velocity fields and for 2-dimensional projected surveys. The observed peculiar velocity field can be related to the underlying linear density perturbations via the continuity equation. The equations for the 2-dimensional case are suitable for cosmological data sets that have been projected over the entire sky. Again, we derive analytical results for the gravitationally induced bispectra and numerical results for both primordial and gravitationally induced bispectra.
- Finally, we detailed some real world effects that are of interest in future studies as well as outlining a parameter error study using the Fisher information matrix formalism.

Chapter 5

Baryon Acoustic Oscillations

5.1 Introduction

Observations of the cosmic microwave background (CMB) and large-scale structure (LSS) will carry complementary cosmological information. While all-sky CMB observations, such as NASA'a WMAP[1] or ESA's Planck[2] experiments, primarily probe the distribution of matter and radiation at redshift $z = 1300$, large scale surveys such as ESA's Euclid[3] or the Square Kilometer Array (SKA)[4] will provide a window at lower redshifts on order $z \approx 0 - 2$. The study of large scale structure appears to be a promising candidate in the study of the influence and role of the dark sectors in the standard model of cosmology. One particular phenomena of interest are the Baryon Acoustic Oscillations (BAOs) that manifest themselves in the matter power spectrum of galaxy clusters on cosmological scales of order $100h^{-1}$Mpc. These oscillations in the matter power spectrum are generated just before recombination through the interplay between a coupled photon-baryon fluid and gravitationally interacting dark matter [543; 426; 174; 175; 176; 503; 504].

The scale of the peaks and oscillatory features of the BAOs promises to be an important cosmological tool that acts as a standard ruler from which we can investigate and constrain dark energy parameters (see [176; 16; 149; 587] for a small selection or representative literature), neutrino masses [219], modified theories of gravitation [9; 312] and deviations from the standard model of cosmology [194; 195; 180]). Significant attention has been devoted to the BAOs and they were first detected with SDSS [5] data [176; 5] and in subsequent surveys [119; 430].

The BAOs have been studied using standard Fourier space decompositions [503; 504; 431], real space analysis [176; 526; 598; 287], in 2D spherical harmonics defined on thin spherical shells [149], but also in the sFB expansion [452]. It is important to note that different frameworks will make use of different information and will therefore have different constraining power for different cosmological parameters emphasising the complementarity of mixed studies [451]. Previous studies, having predominantly focused on projected 2D surveys, have discarded radial

[1] http://map.gsfc.nasa.gov/
[2] http://sci.esa.int/planck
[3] http://sci.esa.int/euclid
[4] http://www.skatelescope.org/
[5] http://www.sdss.org/

information by projecting galaxy positions into tomographic redshift bins however, such a loss of information could be avoided by adopting a full 3D description (e.g. [27]).

Upcoming large scale structure surveys will provide cover for both large and deep areas of the sky and this will necessitate a formalism that can provide a simultaneous treatment of both the spherical sky geometry as well as an extended radial coverage. A natural basis for such a survey is provided by the sFB decomposition, (see [251; 184; 428; 90; 177; 2; 316; 519; 452; 309; 27] for an incomplete selection of literature on the subject). In this prescription we expand a 3D tracer field, such as the galaxy density contrast, using the radial (k) and tangential (i.e. along the surface of a sphere) (ℓ) dependence.

The galaxy matter power spectrum is conventionally modelled using cosmological perturbation theory (PT). The linear order results will be valid at large scales where non-linear growth of structure under gravitational instability can be neglected. At smaller scales it is no longer possible to neglect the non-linear growth of structure and we need to incorporate higher-order corrections to the matter power spectrum. There are a number of different approaches currently in the literature to tackle this problem and we will present a more detailed description later on. Non-linear galaxy clustering bias arises from a non-linear mapping between the underlying matter density field and observed collapsed objects (e.g. galaxies or dark matter haloes) and galaxy bias is, in essence, an isocurvature perturbation. Current literature has investigated more detailed prescriptions for galaxy bias such as the effects of primordial non-Gaussianity, scale dependence or non-local bias. Another form of non-linearity arises from RSD generated through the internal motion of galaxies within haloes. This effect is known as the Finger-of-God effect [275] and is distinct from the linear RSD considered in this paper [289]. It is also possible to investigate the role of non-Gaussian initial conditions, such as those generated in various inflationary models, and how this propagates non-linear corrections through to the growth of structure. The signatures of non-Gaussianity in these models will be distinctly different (e.g. a modified bispectrum) to the signatures of non-Gaussianity in models that have Gaussian initial conditions and are allowed to undergo gravitational collapse.

Throughout this paper we will follow the construction outlined in [452] and generalise the method to study the role of redshift space distortions (RSD) and the non-linear (NL) evolution of density perturbations. Previous investigations have used standard perturbation theory (SPT), galaxy bias models and Lagrangian perturbation theory (LPT) to characterise the role of various non-linear corrections to the BAO signal using the 3D Fourier power spectrum $P(k)$ [279; 407; 280; 412; 413]. These nonlinear corrections can be reassessed within the sFB framework to aid our understanding of how real world effects can impact the radialisation of information.

Recent work [27] utilising the sFB formalism has focused on how to recover the full 3D clustering information including RSD from 2D tomography using the angular auto and cross spectra of different redshift bins. Traditionally, RSD measurements have been made through spectroscopic redshift surveys such as the 2dF Galaxy Redshift Survey [119] and the Sloan Digital Sky Survey [601] with photometric surveys often being neglected because of the loss of RSD through photometric redshift errors. Upcoming surveys, spectroscopic and photometric, such as the Dark Energy Survey (DES)[6], Euclid, SKA, Physics of the Accelerating Universe Survey (PAU)[7] [51], Large Syn-

[6] www.darkenergysurvey.org
[7] www.pausurvey.org

optic Survey Telescope (LSST)[8] or the Panoramic Survey Telescope and Rapid Response System (PanStarrs)[9] offer the possibility of investigating the BAO and RSD through angular or projected clustering measurements [51; 409; 134; 198; 311; 463].

As RSD and distortions arising from an incorrect assumption for the underlying geometry are similar [12] the analyses of RSD using 3D data has to be used in conjunction with geometrical constraints [468]. As approaches based purely on angular correlation functions do not depend on the background cosmological model, the angular clustering measures will be considerably simpler. The sFB is something of a mid-point between these two approaches and will, in general, be sensitive to the choice of fiducial concordance cosmology. This paper is organised as follows. In Section 5.4 we discuss the sFB expansion. In Section 5.5 we outline the effect of linear RSD and Section 5.6 is devoted to issues related to realistic surveys. In Section 5.7 we consider perturbative corrections to linear real-space results and consider the structure of the sFB spectra. Results are discussed at the end of the appropriate sections and the conclusions are given in Section 6.10. Discussions about finite size of the survey and discrete sFB transforms are detailed in the appendices.

Throughout we will adopt the WMAP 7 cosmological parameters [305]: $h = 0.7, \Omega_b h^2 = 0.0226, \Omega_c h^2 = 0.112, \Omega_\Lambda = 0.725, \sigma_8 = 0.816$.

5.2 Baryon Acoustic Oscillations

Before last scattering, the early Universe consisted of a hot, dense, tightly coupled photon-baryon plasma. The temperature of the Universe at this point is sufficiently high that the photons ionise any hydrogen atoms that form resulting in a plasma of free electrons, protons and photons. The photons propagating in this medium are tightly coupled as they will not travel far before interacting with the plasma via Thomson scattering off the free electrons. The presence of perturbations implies that there are regions of the plasma that are overdense, leading to the gravitational collapse of the plasma. This collapse is, in turn, resisted by radiation pressure. Contrastingly, underdensities will correspond to potential hills where the opposite processes are taking place. It is the competing forces of gravitational collapse and radiation pressure that induce an oscillatory behaviour in the fluid. The acoustic waves generated by the compression and rarefaction of the plasma propagate with a characteristic speed of $c_s^2 = (1 + R)^{-1}$ where $R = 3\rho_b/\rho_\gamma$.

However, as the Universe expands the temperature of the plasma decreases. Eventually the photon energy drops below the ionisation energy and the free electrons combine with the free protons, this is known as *recombination*. As the free electron density rapidly drops, the photons become *decoupled* and the mean free path length rapidly increases, tending towards the Hubble scale. The photons *free-stream* then propagate through the Universe and are observed as the cosmic microwave background (CMB). At decoupling, the radiation pressure on the baryons disappears and the baryon acoustic wave is frozen. The photons have free streamed out of the gravitational potentials but the baryonic matter undergoes gravitational collapse. This leads to an enhanced baryon overdensity at a distance equal to that of the distance travelled by a sound wave at decoupling. This forms the baryon acoustic oscillations (BAOs) that we see in the CMB and galaxy correlation function. The gravitational effect of this baryon overdensity will be imprinted

[8] www.lsst.org
[9] pan-starrs.ifa.hawaii.edu

on the cold dark matter (CDM) perturbations as these are coupled gravitationally (see Fig. 5.1 for an extended commentary). We see this imprint in the galaxy distribution Fourier space power spectrum. Naturally, this contribution to the power spectrum evolves with redshift making it a particularly effective probe of the background geometry and cosmological evolution [176; 197].

This plasma was oscillating due to the presence of primordial density perturbations, areas of overdensity induce gravitational collapse of the plasma but, as the fluid collapses, the plasma heats up and radiation pressure drives the fluid out. This results in a spherical sound wave that travels through the plasma with a characteristic speed of $c_s^2 = (1+R)^{-1}$, where $R = 3\rho_b/\rho_\gamma$. At recombination, the photon-baryon fluid decouples as the photons can no longer ionise the atoms that form and hence they are not tightly coupled.

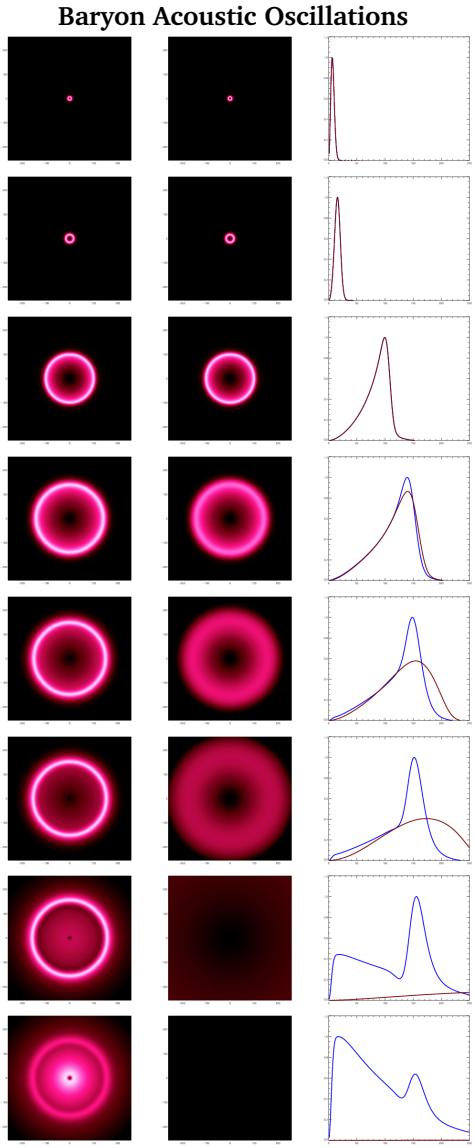

Figure 5.1: This series of plots shows the formation of the BAO peak and attempts to build an understanding of the physical processes at work. The left panel shows the baryon density, the middle panel the radiation density and the right panel shows the mass profile for baryons (blue) and radiation (red). In the early Universe, the primordial plasma is a tightly coupled mix of energetic photons, ionised hydrogen and a gravitationally interacting dark matter. Consider a single perturbation and a uniform plasma with a mass overdensity at the origin (Panel 1). The pressure drives the coupled gas-photon fluid outward, the radius of the shell increases at relativistic speeds (Panels 2 and 3). This expansion continues and the photons cool due to the expansion. Eventually we hit a point where the photons are no longer energetic enough to ionise the plasma and the protons combine with the electrons forming neutral hydrogen. This occurs at a time of $\sim 10^5$ years. The photons free- stream away as the optical depth approached that of the Hubble radius but the baryons, with no pressure to drive them outwards, remain in place (Panels 4 and 5). The radiation becomes increasingly uniform but the baryons remain in an overdense shell with a characteristic size on order $100\mathrm{Mpc}$ (Panel 6). The gravitational potential, centred at the origin due to the gravitationally interacting dark matter, begins to draw material back to the centre (Panel 7). The perturbations continue to grow as the baryons and dark matter virialise. The result is that we end up with a density profile that is sharply peaked around the origin but with an imprint of the shell of matter at a scale of $100\mathrm{Mpc}$ on the profile (Panel 8). The radius of this shell is approximately that of the sound horizon. Figures taken from Martin White's website.

5.3 Characterisation

The purpose of this Section is to compare and contrast different approaches to the characterisation of BAOs, namely

1. Full Fourier space power spectrum $P(k)$.
2. Smoothed Fourier space power spectrum $P(k)/P_S(k)$, i.e. a *wiggle free* approach.
3. Spherical harmonic angular power spectrum C_ℓ.
4. Spherical Fourier-Bessel power spectrum $C_\ell(k)$.

Each of these approaches offers different advantages and disadvantages and in reality a joint analysis using multiple methods and external cosmological observables will provide the strongest constraints and characterisation of the BAOs [451]. The application of these methods to real cosmological observables is also dependent on the particular survey in question.

5.3.1 Fourier Space Power Spectrum $P(k)$

The full Fourier space power spectrum is the standard starting point in many cosmological analyses. This approach takes information from a large range of Fourier modes meaning that, in principle, it should be able to constrain cosmological parameters with high levels of precision and accuracy [451]. This means that the method will be a strong probe of the geometry and growth of large scale structure. However, because of the large number of Fourier modes available it is also suspected that this method will be highly sensitive systematic errors and non-linearities. For instance, the linear bias $b(z)$ will affect both the amplitude of the power spectrum as well as the amplitude of redshift space distortions via the distortion parameter β which is defined with respect to the linear growth factor. If this linear bias is also scale dependent then this could distort the power spectrum over a range of scales such that there are high sensitivities to systematics [451]. There is also some concern that this method is not optimal or easy to implement for wide-field survey geometries due to the spherical sky-geometry. On smaller scales, the power spectrum will be more sensitive to non-linear redshift space distortions and the non-linear growth of structure [501].

The observables in a typical spectroscopic survey are a galaxy redshift z and the angular position on the sky (θ, ϕ). In order to calculate the Cartesian 3-dimensional power spectrum, we need a way to relate the momenta $\mathbf{k}$ to the redshift. This transformation is typically done by assuming some cosmological dependent radial distance to give a scale to the measurement. This means that a Cartesian 3-dimensional analysis will be sensitive to the detailed modelling of the background cosmological model. We will leave a more detailed discussion of redshift space distortions in the Fourier power spectrum for later.

5.3.2 Smoothed Fourier Space Power Spectrum $P(k)/P_S(k)$

The BAO *wiggles only* method aims to avoid potential systematics in the full $P(k)$ method by smoothing out the global shape of the power spectrum. Doing so, we can focus our analysis on

specific scales related to the BAOs. A potential pitfall in this approach is that the global shape of the power spectrum can be defined in numerous ways. As an example, we could simply apply an interpolation scheme to an observed power spectrum and remove the BAO bumps [62; 504]. Alternatively, we could construct a baryon-free power spectrum using the transfer functions from [175] which contains information regarding the shape and normalisation of the power spectrum but does not contain the wiggles generated by baryonic physics. An advantage to this approach is that we have a weaker dependence on bias and non-linearities but we necessarily restrict ourselves to a more limited range of scales. In terms of characterising the BAOs this may not be too detrimental as the BAOs are present on scales of order $100 - 150h^{-1}\mathrm{Mpc}$.

5.3.3 Spherical Harmonic Angular Power Spectrum C_ℓ

For 3-dimensional data it is often more convenient to consider a spherical harmonic decomposition, separating the data into radial and transverse modes that are independent. The conventional spherical harmonic approach projects the data onto 2-dimensional slices discarding information by projecting out the redshift dependence. We can attempt to partly recover some of the information by using tomographic reconstruction, a first step towards the full 3-dimensional analysis. Tomographic methods amount to crudely binning the data into redshift slices and calculating the angular power spectrum, and its cross correlations, for all redshift bins. In essence, we are just discretising the redshift dependence. The angular power spectrum for two redshift bins i and j is given by [421]

$$\mathcal{C}_\ell^{i,j} = \frac{2}{\pi} \int dk\, k^2\, P_{\mathrm{lin}}(k)\, W_\ell^i(k)\, W_\ell^j(k) \tag{5.1}$$

$$W_\ell^i = \int dr\, D(r)\, \phi_i(r)\, j_\ell(kr). \tag{5.2}$$

This spherical harmonic approach has a strong dependence on the bias and non-linearities that are fed into our description for large scale structure. The primary advantages of this method are that redshift space distortions will have an exact description, unlike the small angle approximation in the Fourier analysis, and that the transformation from the survey observables for a galaxy (θ, ϕ, z) to the spherical harmonic coordinates (ℓ, z) is independent of the model for the background cosmology. We will briefly discuss redshift space distortions later on.

5.3.4 Spherical Fourier-Bessel Power Spectrum $C_\ell(k)$

It should be clear by now that different approaches to the characterisation of the BAOs uses different information. The wiggles only method used information from both the radial and tangential modes but discards information regarding the broad band shape of the power spectrum, the redshift space distortions and the amplitude of the BAOs. The spherical harmonic analysis, however, does not use the radial scale of the BAOs. Something of a hybrid method can be introduced by using the spherical Fourier-Bessel formalism. In this instance we retain much of the power of the spherical harmonic decomposition but the formalism is genuinely 3-dimensional as the redshift information from objects in a survey is necessarily taken into account [452]. In addition, this method should be rather practical for upcoming surveys that have both wide-field and ex-

tended radial coverage. In this approach we can use an exact prescription for the redshift space distortions and how these affect the characterisation of BAOs [435]. This method also becomes increasingly difficult for surveys with many galaxies but by performing a two step transformation using a spherical Fourier-Bessel transform followed by a fast spherical harmonic transform (e.g. Healpix) then computational costs can be brought under control [316].

5.4 3D Spherical Analysis

5.4.1 Theory

As we discussed in Section 2.4, the spherical Fourier-Bessel expansion is something of a natural hybrid between the more conventional Fourier and spherical harmonic decompositions. Spherical coordinates are a natural choice for the analysis of cosmological data as they can, by an appropriate choice of basis, be used to place an observer at the origin of the analysis. Upcoming wide-field BAO surveys will provide both large and deep coverage of the sky and we therefore require a simultaneous treatment of the extended radial coverage and spherical sky geometry. For this problem, the sFB expansion is a natural basis for the analysis of random fields in such a survey.

We introduce a homogeneous 3D random field $\Psi(\hat{\Omega}, r)$ with $\hat{\Omega}$ defining a position on the surface of a sphere and r denoting the comoving radial distance. The eigenfunctions of the Laplacian operators are constructed from products of the spherical Bessel functions of the first kind $j_\ell(kr)$ and spherical harmonics $Y_{\ell m}(\hat{\Omega})$ with eigenvalues of $-k^2$ for a 2-sphere. Assuming a flat background Universe, the sFB decomposition of our random field [60; 183; 184; 251; 90; 435] is given by:

$$\Psi(\hat{\Omega}, r) = \sqrt{\frac{2}{\pi}} \int dk \sum_{\{\ell m\}} \Psi_{\ell m}(k)\, k\, j_\ell(kr) Y_{\ell m}(\hat{\Omega}), \tag{5.3}$$

and the corresponding inverse relation given by:

$$\Psi_{\ell m}(k) = \sqrt{\frac{2}{\pi}} \int d^3\mathbf{r}\, \Psi(\mathbf{r})\, k\, j_\ell(kr) Y^*_{\ell m}(\hat{\Omega}). \tag{5.4}$$

In our notation, $\{\ell m\}$ are quantum numbers and k represents the wavenumber.[10]

Note that the 3D harmonic coefficients, $\Psi_{\ell m}(k)$ are a function of the radial wavenumber k. This decomposition can be viewed as the spherical polar analogy to the conventional Cartesian Fourier decomposition defined by:

$$\Psi(\mathbf{r}) = \frac{1}{(2\pi)^{3/2}} \int d^3k\, \Psi(k)\, \mathrm{e}^{\mathrm{i}\mathbf{k}\cdot\mathbf{r}}, \tag{5.5}$$

$$\Psi(\mathbf{k}) = \frac{1}{(2\pi)^{3/2}} \int d^3x\, \Psi(\mathbf{r})\, \mathrm{e}^{-\mathrm{i}\mathbf{k}\cdot\mathbf{r}}. \tag{5.6}$$

The Fourier power spectrum, $P_{\Psi\Psi}$, is defined as the 2-point correlation function of the Fourier

[10] We follow the same conventions as [316; 452; 90] but have made the substitutions $f(\mathbf{r}) \to \Psi(\mathbf{r})$ and $W_\ell(k_1, k_2) \to I^{(0)}_\ell(k_1, k_2)$.

coefficients $\Psi(k)$:

$$\langle \Psi(\mathbf{k})\Psi^*(\mathbf{k}')\rangle = (2\pi)^3 P_{\Psi\Psi}(k)\delta^3\left(\mathbf{k}-\mathbf{k}'\right). \tag{5.7}$$

Similarly we can define a 3D sFB power spectrum, $C_\ell(k)$, of our random field by calculating the 2-point correlation function of the 3D harmonic coefficients:

$$\langle \Psi_{\ell m}(k)\Psi^*_{\ell' m'}(k')\rangle = \mathcal{C}_\ell(k)\delta^{1\mathrm{D}}(k-k')\delta^{\mathrm{K}}_{\ell\ell'}\delta^{\mathrm{K}}_{mm'}. \tag{5.8}$$

It is possible to relate the Fourier coefficients $\Psi(\mathbf{k})$ with their sFB analogue $\Psi_{\ell m}(k)$ through the following expression

$$\Psi_{\ell m}(k) = \frac{i^\ell k}{(2\pi)^{3/2}}\int d\Omega_k \Psi(\mathbf{k})Y_{\ell m}(\hat{\Omega}_k) \tag{5.9}$$

where the angular position of the wave vector $\mathbf{k}$ in Fourier space is denoted by the unit vector $\hat{\Omega}(\theta_k,\phi_k)$. The Rayleigh-expansion of a plane wave is particularly useful in connecting the spherical harmonic description with the 3D Cartesian expression. The second expression we present here is derived by differentiating the first and will be used in the derivation of RSD:

$$\mathrm{e}^{i\mathbf{k}\cdot\mathbf{r}} = 4\pi\sum_{\ell m} i^\ell\, j_\ell(kr)Y_{\ell m}(\hat{\Omega}_k)Y_{\ell m}(\hat{\Omega}); \tag{5.10}$$

$$i(\hat{\Omega}_k\cdot\hat{\Omega})\mathrm{e}^{i\mathbf{k}\cdot\mathbf{r}} = 4\pi\sum_{\ell m} i^\ell\, j'_\ell(kr)Y_{\ell m}(\hat{\Omega}_k)Y_{\ell m}(\hat{\Omega}). \tag{5.11}$$

In general the radial eigenfunctions are ultra-spherical Bessel functions but they can be approximated by spherical Bessel functions when the curvature of the Universe is small (e.g. [604]). Throughout this paper we will use $j'_\ell(x)$ and $j''_\ell(x)$ to denote the first and second derivatives of $j_\ell(x)$ with respect to its argument x. The expressions for the first and second derivatives are given in Eq. (2.82) and Eq. (2.83). Imposing a finite boundary condition on the radial direction will result in a discrete sampling of the k-modes. This will be discussed in more detail later.

5.4.2 Finite Surveys

In order to consider realistic cosmological random fields, such as the galaxy density contrast, we need to take into account the partial observation effects arising from finite survey volumes. Concise discussions of this point are given in [452; 27] and as such we will not devote much time to this point referring the reader to the given references.

The selection function simply denotes the probability of including a galaxy within a given survey. An observed random field $\Psi^{\mathrm{obs}}(\mathbf{r})$ can be related to an underlying 3D random field through a survey-dependent radial selection function $\phi(r)$ that modulates the underlying field:

$$\Psi^{\mathrm{obs}}(\mathbf{r}) = \phi(r)\Psi(\mathbf{r}). \tag{5.12}$$

It is possible to introduce an analogous tangential selection function but we will, as per [452], neglect this possibility assuming that we have full sky coverage. The resulting sFB power spectrum is given by

$$\mathcal{C}_\ell^{(00),\text{obs}}(k_1,k_2) = \left(\frac{2}{\pi}\right)^2 \int k'^2 dk'\, I_\ell^{(0)}(k_1,k') I_\ell^{(0)}(k_2,k') P_{\delta\delta}(k') \tag{5.13}$$

where the modified window function is given by:

$$I_\ell^{(0)}(k,k') = \int dr\, r^2 \phi(r)\, k\, j_\ell(kr)\, j_\ell(k'r). \tag{5.14}$$

The sFB power spectrum tends to rapidly decay as we move away from the diagonal $k = k'$ and it will often be much more useful to focus purely on the diagonal contribution $C_\ell^{(00)}(k,k)$.

5.5 Redshift Space Distortions

The measured distribution of galaxies is not without limits though as various systematic and survey dependent errors become more important. In practice, the observed galaxy redshift distributions are distorted due to the peculiar velocity of each galaxy. The anisotropies generated by the peculiar velocities are known as *redshift space distortions*. Although this distortion of the measured redshifts will necessarily complicate the cosmological interpretation of the spectroscopic galaxy surveys, RSD are currently one of the most optimistic probes for the measurement of the growth rate of structure formation and, as a result, an interesting probe of models for dark energy and modified theories of gravity.

The effect of RSD on the matter power spectrum can be split into two effects, the Kaiser effect and the FoG effect. The Kaiser effect corresponds to the coherent distortion of the peculiar velocity along the line of sight with an amplitude controlled by the growth-rate parameter, leading to an enhancement of the power spectrum amplitude at small k [289]. The FoG effect arises due to the random distribution of peculiar velocities leading to an incoherent contribution in which dephasing occurs and the clustering amplitude is suppressed [275]. It is thought that the suppression of the amplitude is particularly important around the size of halo forming regions, i.e. at large k [551].

For an isotropic structure in linear theory, the Kaiser effect means that an observer will measure more power in the radial direction than in the transverse modes. The amplitude of this distortion is modulated by the distortion parameter

$$\beta = \frac{f(\Omega_0)}{b(z)} = \frac{1}{b(z)} \frac{d\ln D(a)}{d\ln a} \approx \frac{\Omega_m^\gamma(a)}{b(z)} \tag{5.15}$$

where:

$$\Omega_m(a) = \frac{\Omega_{m,0}}{a^3} \frac{H_0^2}{H^2(a)} \tag{5.16}$$

such that a is the scale factor, $H(a)$ is the Hubble parameter, H_0 is the Hubble parameter at present time and $D(z)$ the linear growth factor for which $f(z) \equiv d\ln D/d\ln a$. In this parametrisation, γ is directly related to our theory of gravitation such that General Relativity predicts $\gamma \simeq 0.55$ and Ω_m is the usual mass density parameter [586; 327]. This means that RSD can be used to probe the growth of structure, the galaxy clustering bias function $b(z)$ as well as probing dark energy and

modified theories of gravity [232]. Measuring the growth rate from RSD is a non-trivial procedure and a detailed understanding of systematic errors is crucial in order to disentangle different theories of gravity or dark energy [142]. Euclid aims to constrain the growth rate parameter to the percent level but incomplete modelling of RSD introduces systematics on order $10 - 15\%$ [551; 417; 59; 142]. This makes the study of RSD in the sFB formalism all the more timely. In this next section we will outline some of the basic ingredients that are used in modelling RSD in Fourier space before constructing the analogous results in the sFB formalism.

5.5.1 RSD in Fourier Space

Before presenting the RSD in the sFB formalism we briefly review some of the key results from modelling RSD in Fourier space and the appropriate limitations that are adopted in the model.

The effect of a peculiar velocity $\mathbf{v}$ is to distort the apparent comoving position $\mathbf{s}$ of a galaxy from its true comoving position $\mathbf{r}$:

$$\begin{aligned}\mathbf{s} &= \mathbf{r} + \frac{v_{\parallel}(\mathbf{r})\hat{n}}{aH(a)} \\ &= \mathbf{r} + f\phi(\mathbf{r})\hat{n}\end{aligned} \tag{5.17}$$

where f is the linear growth rate, $\hat{n}$ is a vector lying parallel to an observer's line of sight and $v_{\parallel}$ is the component of the velocity parallel to the line of sight. The resulting redshift space density field $\delta_s(\mathbf{s})$ is obtained by imposing mass conservation, $[1 + \delta_s(\mathbf{s})]\, d^3\mathbf{s} = [1 + \delta_r)\mathbf{r})]\, d^3\mathbf{r}$, which results in the following:

$$[1 + \delta_s(\mathbf{s})] = [1 + \delta_r(\mathbf{r})] \left| \frac{d^3\mathbf{s}}{d^3\mathbf{r}} \right|^{-1}. \tag{5.18}$$

To simplify the analysis we can adopt the distant observer approximation in which we neglect the curvature of the sky and the Jacobian reduces to a term relating only to the line of sight

$$\frac{\partial s}{\partial r} = 1 + f\phi' \tag{5.19}$$

where a prime denotes differentiation with respect to the line of sight, i.e. parallel to $\hat{n}$:

$$\phi'(\mathbf{r}) = \partial_{\parallel} \left[\frac{v_{\parallel}}{faH(a)} \right]. \tag{5.20}$$

The redshift space density contrast can be re-written as:

$$\delta_s(\mathbf{s}) = \frac{(\delta(\mathbf{r}) - f\phi'(\mathbf{r}))}{(1 + f\phi'\mathbf{r})}. \tag{5.21}$$

Assuming an irrotational velocity field with a velocity divergence field $\theta(\mathbf{r}) = \nabla \cdot \mathbf{v}(\mathbf{r})$ we obtain the following useful relationship, $\phi(\mathbf{r}) = -(\nabla^{-1}\theta(\mathbf{r}))'$. In Fourier space these equations simplify as $\phi'(k) = -\mu^2\theta(k)$, where we have made use of the fact that $(\nabla^{-1})'' = (k_{\parallel}/k)^2 = \mu^2$. In our notation $k_{\parallel}$ denotes the modes parallel to the line of sight and $k_{\perp}$ denotes modes perpendicular to the line of sight where $k^2 = k_{\parallel}^2 + k_{\perp}^2$. The redshift space density field can be written as (e.g.

[497])

$$\begin{aligned}\delta_s(k,\mu) &= \int \frac{d^3\mathbf{s}}{(2\pi)^3} e^{-i\mathbf{k}\cdot\mathbf{s}} \delta_s(\mathbf{s}) \\ &= \int \frac{d^3\mathbf{r}}{(2\pi)^3} e^{-i\mathbf{k}\cdot\mathbf{r}} e^{-ikf\mu} \left[\delta(\mathbf{r}) + f\mu^2\theta(\mathbf{r})\right] \end{aligned} \tag{5.22}$$

and the corresponding power spectrum as:

$$\begin{aligned}P_s(k,\mu) = \int \frac{d^3\mathbf{r}}{(2\pi)^3} e^{-\mathbf{k}\cdot\mathbf{r}} \Big\langle & e^{-ikf\mu(\phi(\mathbf{r})-\phi(\mathbf{r}'))} \\ & \times \left[\delta(\mathbf{r}) + f\mu^2\theta(\mathbf{r})\right] \left[\delta(\mathbf{r}') + f\mu^2\theta(\mathbf{r}')\right] \Big\rangle. \end{aligned} \tag{5.23}$$

This prescription for the Fourier power spectrum has been constructed in the plane-parallel or distant observer approximation. The terms in the square brackets is the conventional Kaiser effect as described earlier. The exponential prefactor corresponds to the small-scale velocity dispersion and relates to the Fingers-of-God effect described earlier. A simplified phenomenological power spectrum was derived by [501] by assuming that the exponential prefactor may be separated from the ensemble average

$$P_s(k,\mu) = e^{-(fk\mu\sigma_v)^2} \left[P_{\delta\delta}(k) + 2f\mu^2 P_{\delta\theta}(k) + f^2\mu^4 P_{\theta\theta}(k)\right], \tag{5.24}$$

where σ_v is a velocity dispersion defined in [501]. In the linear regime we have $P_{\delta\delta} = P_{\delta\theta} = P_{\theta\theta}$ and the velocity dispersion prefactor tends towards zero. In such a limit we simply recover the linear result of [289]:

$$P_s(k,\mu) = \left[1 + 2f\mu^2 + f^2\mu^4\right] P_{\delta\delta}(k). \tag{5.25}$$

Such a limit corresponds to making a number of approximations. For example, we require that the velocity gradient is sufficient small, the density and velocity perturbations must be accurately described by the linear continuity equations, the real-space density perturbations are well described by the linear results, i.e. $\delta(\mathbf{r}) \ll 1$, such that higher-order contributions are suppressed and we also require that the small-scale velocity dispersion tends towards zero and may be neglected. Such approximations appear to hold on the largest scales and a lot of distortion features are well modelled by this approximation. It is however known that this theory breaks down as we approach the quasi-linear and non-linear regimes. The result of [501] makes certain approximations about the separability of the exponential prefactor which neglects possible coupling terms between the velocity and density fields. A lot of effort has been invested in constructing non-linear models for RSD and upcoming surveys should prove to be a fruitful testing ground for many of these models [266; 497; 501; 133; 361; 362; 550; 551; 364; 418; 478; 142]. We construct the RSD in the sFB formalism by working to the linear Kaiser approximation and exploring the phenomenology of this extension.

5.5.2 RSD in Spherical Harmonic Space

In the spherical harmonic approach, RSDs have a relatively simple, exact prescription [184; 421; 28] but as we project onto a 2-dimensional surface, radial information is lost. As mentioned previously, we can attempt to tomographically reconstruct the radial information by binning data into redshift slices and calculating the angular spectrum in each bin (auto-correlation) and between bins (cross-correlation). The angular power spectrum including the linear Kaiser effect for two redshift bins i and j with radial survey selection functions $\phi_i(r)$ and $\phi_j(r)$ is given by

$$\mathcal{C}_\ell^{i,j} = \frac{2}{\pi}\int dk\, k^2\, P_{\rm lin}(k, z=0)\left[W_\ell^i(k) + \beta W_\ell^{i,\rm RSD}(k)\right]\left[W_\ell^j + \beta W_\ell^{j,\rm RSD}(k)\right], \tag{5.26}$$

where $W_\ell^i(k)$ is the unredshifted real-space window function and $W_\ell^{i,\rm RSD}(k)$ includes the linear RSD correction. These window functions are defined by

$$W_\ell^i(k) = \int dr\, D(r)\, b(r)\, \phi_i(r)\, j_\ell(kr) \tag{5.27}$$

$$W^{i,\rm RSD}(k) = \int dr\, D(r)\, f(r)\, \phi_i(r) \times \left[\frac{(2\ell^2+2\ell-1}{(2\ell+3)(2\ell-1)} j_\ell(kr) - \frac{\ell(\ell-1)}{(2\ell-1)(2\ell+1)} j_{\ell-2}(kr) - \frac{(\ell+1)(\ell+2)}{(2\ell+1)(2\ell+3)} j_{\ell+2}(kr)\right], \tag{5.28}$$

we have included the linear bias $b(r)$, linear growth factor $D(r)$ and the growth rate $f(r) \equiv \partial \ln D / \partial \ln a$. We do not wish to discuss this approach further and instead refer the reader to the literature [421; 28; 405]. The comparisons between the full 3-dimensional sFB approach and the tomographic spherical harmonic approach should be relatively transparent.

5.5.3 RSD in sFB Space

In the Fourier approach, the distortion equation presented in Eq. (5.25) is only universally valid when we assume that the survey subtends a sufficiently small angle such that radial distortions may be approximated by a line of sight distortion. In larger wide field surveys it is possible we may be able to split the survey into small, independent volumes but even then we implicitly assume that the wavelengths probed subtend a sufficiently small angle. In the Fourier approach, we would really like to analyse short wavelengths such that the small angle approximation would hold. However, shorter wavelengths are necessarily more non-linear, making the analysis increasingly difficult. Surveys need to be of a sufficient depth such that you probe wavenumbers that are both linear and subtend a small angle [112; 251]. In addition, the choice of a Fourier decomposition means that RSDs will be purely radial but this induces a mixing of the Fourier modes [605; 251].

As previously mentioned, the effect a peculiar velocity, or a departure from the Hubble flow, $v(\mathbf{r})$ at $\mathbf{r}$ is to introduce a distortion to the galaxy positions in the redshift space $\mathbf{s}$:

$$\mathbf{s}(\mathbf{r}) = \mathbf{r} + \mathbf{v}(\mathbf{r}) \cdot \hat{\Omega}. \tag{5.29}$$

We denote the harmonics of a field $\Psi(\mathbf{r})$ when convolved with a selection function, $\phi(s)$, by

$\tilde{\Psi}_{lm}(k)$. These harmonics take into account the RSD:

$$\tilde{\Psi}_{\ell m}(k) = \sqrt{\frac{2}{\pi}} \int s^2 ds \int d\hat{\Omega}\, \phi(s) \Psi(\mathbf{r})\, k\, j_\ell(ks) Y^*_{\ell m}(\hat{\Omega}). \tag{5.30}$$

The Fourier transform of the linearised Euler equation can be used to relate the Fourier transform of the density contrast, $\delta(\mathbf{k})$, to that of the peculiar velocity field $v(\mathbf{r})$:

$$\mathbf{v}(\mathbf{k}) = -i\beta \mathbf{k} \frac{\delta(\mathbf{k})}{k^2} \tag{5.31}$$

where b is the linear bias parameter. Following the procedure outlined in [251], we can establish a series expansion in β such that the lowest order coefficients $\Psi^{(0)}_{\ell m}(k)$ are obtained by neglecting the RSD:

$$\tilde{\Psi}_{\ell m}(k) = \tilde{\Psi}^{(0)}_{\ell m}(k) + \tilde{\Psi}^{(1)}_{\ell m}(k) + \ldots; \tag{5.32}$$

$$\tilde{\Psi}^{(0)}_{\ell m}(k) = \sqrt{\frac{2}{\pi}} \int_0^\infty k' dk'\, \Psi_{\ell m}(k') I^{(0)}_\ell(k', k); \tag{5.33}$$

$$\tilde{\Psi}^{(1)}_{\ell m}(k) = \sqrt{\frac{2}{\pi}} \int_0^\infty k' dk'\, \Psi_{\ell m}(k') I^{(1)}_\ell(k', k). \tag{5.34}$$

The kernels $I^{(0)}_\ell(k', k)$ and $I^{(0)}_l(k', k)$ define the convolution and are dependent on the choice of selection function. Note that $I^{(0)}_\ell(k', k)$ is simply the window function we encountered previously in Eq. (5.14). The kernels can be shown to be:

$$I^{(0)}_\ell(k, k') = \int dr\, r^2 \phi(r)\, k\, j_\ell(kr)\, j_\ell(k'r) \tag{5.35}$$

$$I^{(1)}_\ell(k, k') = \frac{\beta}{k'} \int dr\, r^2\, k\, \frac{d}{dr} \left(\phi(r) j_\ell(kr)\right)\, j'_\ell(k'r). \tag{5.36}$$

The lowest order corrections due to RSD are therefore encapsulated in $\Psi^{(1)}_{lm}(k)$. We can define a set of power spectra by using these harmonic coefficients:

$$\langle \Psi^\alpha_{\ell m}(k) \Psi^{\beta *}_{\ell' m'}(k') \rangle = \mathcal{C}^{(\alpha\beta)}_\ell(k, k') \delta_{1D}(k - k') \delta_{\ell\ell'} \delta_{mm'}, \tag{5.37}$$

$$\langle \Psi^\alpha_{\ell m}(k) \tilde{\Psi}^{\beta *}_{\ell' m'}(k') \rangle = \tilde{\mathcal{C}}^{(\alpha\beta)}_\ell(k, k') \delta_{\ell\ell'} \delta_{mm'}. \tag{5.38}$$

We can construct a generalised power spectrum by using the common structure between Eq. (5.33) and Eq. (5.34):

$$\tilde{\mathcal{C}}^{(\alpha\beta)}_\ell(k_1, k_2) = \left(\frac{2}{\pi}\right)^2 \int k'^2 dk'\, I^{(\alpha)}_\ell(k_1, k') I^{(\beta)}_\ell(k_2, k') P_{\delta\delta}(k'). \tag{5.39}$$

The total redshifted power spectrum will be given by a sum of the various contributions:

$$\tilde{\mathcal{C}}_\ell(k_1, k_2) = \tilde{\mathcal{C}}^{(00)}_\ell(k_1, k_2) + 2\, \tilde{\mathcal{C}}^{(01)}_\ell(k_1, k_2) + \tilde{\mathcal{C}}^{(11)}_\ell(k_1, k_2). \tag{5.40}$$

If we ignore the effects introduced by the selection function, i.e. set $\phi(r) = 1$, then we recover the

result for the unredshifted contributions [251; 184; 90]:

$$\mathcal{C}_\ell^{(00)}(k,k) = P_{\delta\delta}(k). \tag{5.41}$$

These expressions hold for surveys with all-sky coverage. In the presence of homogeneity and isotropy the 3D power spectrum will be independent of radial wave number ℓ. The introduction of a sky mask breaks isotropy and introduces additional mode-mode couplings, the analysis will be generalised to this case in the next section. In the above equations we neglect a number of additional non-linear terms including General Relativistic corrections, velocity terms and lensing terms. It is also possible to adopt a full non-linear approach to RSD where the non-linear spectrum has significantly more complicated angular structure than in linear theory [521]. The RSD information will be dependent on the relative clustering amplitude of the transverse modes and the radial modes, [27]. Our ability to recover information and the extent to which the information radialises will naturally depend on the geometry of the survey and which modes we are able to include.

5.5.4 RSD in sFB Space: Flat Sky Limit

For surveys that cover large opening angles on the sky, the full sFB expansion detailed above is the most natural and convenient choice. This expansion does, however, break down for small-angle surveys where the signal of interest occurs at high-ℓ modes. In such a situation the accurate computation of high-ℓ spherical harmonics is cumbersome and computationally expensive. Instead it is much more natural to approximate the spherical harmonics as sums of exponentials corresponding to a 2D Fourier expansion. Essentially we are replacing the spherical harmonics solutions with a plane-wave approximation valid at high multipoles.

In the flat sky limit we expand a 3D field Ψ at a 3D position $\mathbf{r} \equiv (r, \vec{\theta})$ on the sky using a basis consisting of 2D Fourier modes and radial Bessel functions:

$$f(r,\vec{\theta}) = \sqrt{\frac{2}{\pi}} \int k dk \int \frac{d^2\vec{\ell}}{(2\pi)^2} f(k,\vec{\ell})\, j_\ell(kr)\, e^{i\vec{\ell}\cdot\vec{\theta}} \tag{5.42}$$

$$f(k,\vec{\ell}) = \sqrt{\frac{2}{\pi}} \int r^2 dr \int d^2\theta\, f(r,\vec{\theta})\, k\, j_\ell(kr)\, e^{-i\vec{\ell}\cdot\vec{\theta}} \tag{5.43}$$

where ℓ is a 2D angular wavenumber and k is a conventional radial wavenumber. We can simplify the analysis by adopting coordinates such that the survey corresponds to small angles around the pole of the spherical coordinates, defined by angles (θ, ϕ) for which, in the limit $\theta \to 0$, we can apply a 2D expansion of the plane waves:

$$e^{i\vec{\ell}\cdot\vec{\theta}} \simeq \sqrt{\frac{2\pi}{\ell}} \sum_m i^m Y_{\ell m}(\theta,\phi) e^{-im\varphi_\ell} \tag{5.44}$$

where $\vec{\ell} = (\ell\cos\varphi_\ell, \ell\sin\varphi_\ell)$ and $\vec{\theta} = (\theta\cos\varphi, \theta\sin\varphi)$. The correspondence between the 3D flat-sky and 3D full-sky coefficients can be obtained by substituting Eq. (5.44) into Eq. (5.42) and noting that $\int d^2\vec{\ell} = \int \ell d\ell \int d\varphi_\ell \to \sum_\ell \ell \int d\varphi_\ell$ in the high-ℓ limit. The correspondence can be shown to

be:

$$f_{\ell m}(k) = \sqrt{\frac{\ell}{2\pi}} i^m \int \frac{d\varphi_\ell}{(2\pi)} e^{-im\varphi_\ell} f(k, \vec{\ell}) \tag{5.45}$$

$$f(k, \vec{\ell}) = \sqrt{\frac{2\pi}{\ell}} \sum_m i^{-m} f_{\ell m}(k) e^{im\varphi_\ell} \tag{5.46}$$

We now extend this analysis to RSD by constructing harmonics of a field $\Psi(\mathbf{r})$ in the flat-sky limit when convolved with a selection function $\phi(s)$. These new flat-sky harmonics take into account the RSD much as before:

$$\tilde{\Psi}(k, \vec{\ell}) = \sqrt{\frac{2}{\pi}} \int s^2 ds \int d^2\theta \, k \, \Psi(r, \vec{\theta}) \, [\phi(s) j_\ell(ks)] \, e^{-i\vec{\ell}\cdot\vec{\theta}}. \tag{5.47}$$

Following the same perturbative procedure results in a series expansion in β where:

$$\tilde{\Psi}_\ell(k, \vec{\ell}) = \tilde{\Psi}_\ell^{(0)}(k, \vec{\ell}) + \tilde{\Psi}_\ell^{(1)}(k, \vec{\ell}) + \dots. \tag{5.48}$$

As before the $\tilde{\Psi}_\ell^{(0)}(k, \vec{\ell})$ term represents the unredshifted contribution:

$$\tilde{\Psi}_\ell^{(0)}(k, \vec{\ell}) = \sqrt{\frac{2}{\pi}} \int r^2 dr \int d^2\theta \, \Psi(r, \vec{\theta}) \, k \, [j_\ell(kr)\phi(r)] \, e^{-i\vec{l}\cdot\vec{\theta}} \tag{5.49}$$

$$\begin{aligned} \tilde{\Psi}_\ell^{(1)}(k, \vec{\ell}) = \sqrt{\frac{2}{\pi}} \int r^2 dr \int d^2\theta \, \Psi(r, \vec{\theta}) \, k \\ \times \left\{ \left[\mathbf{v}(\vec{r}) \cdot \vec{\theta} \right] \frac{d}{dr} \left[j_\ell(kr)\psi(r) \right] \right\} e^{-i\vec{\ell}\cdot\vec{\theta}} \end{aligned} \tag{5.50}$$

5.5.5 BAO Wiggles Only

The BAOs can be isolated by constructing a ratio between the observed matter power spectrum $P_{\delta\delta}^{\mathrm{B}}(k)$ and a theoretical matter power spectrum $P_{\delta\delta}^{\mathrm{nB}}(k)$ constructed from a zero-baryon (or no-wiggle) transfer function in which the oscillations do not show up [175]. Using these two power spectra, the ratio $R^P(k)$ will reduce the dynamic range and isolates the oscillatory features of the BAOs:

$$R^P(k) = \frac{P^B(k)}{P^{nB}(k)}. \tag{5.51}$$

This ratio is clearly defined for the Fourier space power spectrum but an appropriate generalisation to the sFB formalism may be constructed by calculating the ratio of the angular power spectra defined in Eq. (5.13), with the matter power spectrum $C_\ell^B(k)$ to the angular power spectrum with the zero-Baryon power spectrum $C_\ell^{nB}(k)$ [452]:

$$R_\ell^C(k) = \frac{C_\ell^B(k)}{C_\ell^{nB}(k)}. \tag{5.52}$$

It is important to note that the characterisation method (i.e. how we choose to construct our ratio) can affect the characteristic scale of the BAOs when we take into account non-linear effects. This means that care has to be taken when comparing results that implement different methods [451]. As an example we could construct our ratio by using the no-wiggles transfer function of [175] or adopt an interpolation scheme to construct a smooth parametric curve [62; 430; 504]. A different choice of smoothed matter power spectra, cosmological parameters, growth history or similar can impact the phenomenological behaviour of the underlying physics (e.g. location of BAO peaks). Finally, we very briefly note that other methods for characterising the acoustic oscillation scales are possible, for example[429; 407], but we do not provide significant details here.

5.5.6 Results: RSD

In Fig. 5.2 we compare $\tilde{C}_l(k)$ against a linear redshift space power spectrum, $P_s(k)$, spectra for $\ell = 5, 50$ at two given surveys corresponding to $r = 100, 1400h^{-1}$Mpc. In this plot the ratios are constructed by considering the differences between the appropriate spectra. The following ratios have been used:

$$R_\ell^{C,\mathrm{RSD}}(k) = \frac{C_\ell^{\mathrm{RSD,Lin,B}}(k)}{C_\ell^{\mathrm{RSD,Lin,nB}}(k)} \tag{5.53}$$

$$R_\ell^{C,\mathrm{nRSD}}(k) = \frac{C_\ell^{\mathrm{nRSD,Lin,B}}(k)}{C_\ell^{\mathrm{nRSD,Lin,nB}}(k)} \tag{5.54}$$

$$R^{P,\mathrm{RSD}}(k) = \frac{P^{\mathrm{RSD,Lin,B}}(k)}{P^{\mathrm{RSD,Lin,nB}}(k)} = R^{P,\mathrm{nRSD}}(k). \tag{5.55}$$

In Fig. 5.2, the blue line corresponds to Eq. (5.53), the purple line to Eq. (5.54) and the red line to Eq. (5.55). Fig. 5.7, Fig. 5.8 and Fig. 5.10] correspond to Eq. (5.53).

The redshift space Fourier power spectrum is simply the result derived in [289] and corresponds to:

$$P^s(k,\mu) = \left[1 + 2\mu^2 f + \mu^4 f^2\right] P(k). \tag{5.56}$$

In this linear limit, the redshift space ratio $R_s(k)$ tends to the real space ratio $R(k)$ as the linear prefactors corresponding to the redshift space corrections cancel. It is apparent that in Fig. 5.2 the sFB spectra are damped relative to the power spectra. This arises due to mode-mixing contributions inherent when working with the sFB formalism. The unredshifted contributions are constructed from products of Bessel functions that form an orthogonal basis and there is no radial mode-mixing. When introducing RSD the higher-order terms are decomposed with respect to products involving derivatives of the spherical Bessel functions which does not form a perfectly orthogonal set of basis functions. As a result of RSD, off-diagonal elements will be generated and there is now coupling between modes. This radial mode-mixing is an intrinsic geometrical artefact of RSD on large scales and carries a distinctive damping signature [251; 606; 519]. Such a mode-mixing term is not present in the Kaiser analysis where the basis functions are plane waves which have well behaved derivatives that maintain the orthogonality of the basis. In the deep survey limit it is seen that the redshift space sFB spectra do tend towards their Fourier spectra

counterparts in terms of the shape, amplitude and phase albeit with the presence of the distinctive damping generated by mode-mixing which is predominantly seen at small scales and hence large k.

The effects of RSD can be seen in Fig. 5.7-Fig. 5.8 in comparison to the equivalent configurations without the presence of RSD in Fig. 5.5-Fig. 5.6. A lower dynamical range comparison is presented in Fig. 5.9-Fig. 5.10 to enhance the impact that RSD have on the BAO. Note the enhanced power at low ℓ and k as well as some level of fuzziness introduced by the mode mixing. The peak amplitudes are damped at low ℓ and all the features can be seen in the corresponding slice plots of Fig. 5.2. In a future paper we will consider the hierarchy of multipole moments in Fourier space RSD and how measures constructed from the multipole moments can be related to RSD in the sFB formalism.

5.6 Realistic Surveys

The results that have been discussed above are somewhat idealised in the sense that we assume all-sky coverage with no noise. In realistic surveys we will often need to take into account the presence of a mask (relating to partial sky-coverage) and noise. If the noise is inhomogeneous we will be presented with a further complication. For partial sky coverage we find mode-mode couplings in the harmonic domain that result in the individual masked harmonics being described by a linear combination of our idealised all-sky harmonics. We do not discuss the role of partial sky-coverage in much detail but do present results generalising our formalism to include a survey mask.

5.6.1 Photometric Error Estimates

The radial coordinates from a survey are typically provided as a photometric redshift with some given error, we denote this estimated radial coordinate by $\tilde{r}$ and let r represent the true coordinate. Following [248], we relate the two coordinates by a conditional probability, which we assume to be Gaussian

$$p\left(\tilde{r}|r\right)d\tilde{r} = \frac{1}{\sqrt{2\pi}\sigma_z}\exp\left[-\frac{\left(z_{\tilde{r}}-z_r\right)^2}{2\sigma_z^2}\right]dz_{\tilde{r}}, \tag{5.57}$$

where the $z_{\tilde{r},r}$ are the redshifts associated with the given coordinate and σ_z is the error. We assume that the error has values, $\sigma_z \sim 0.02 - 0.1$ or more and it is important to note that σ_z may vary with redshift. We can now construct harmonics that represent the average value of the expansion coefficients by using the relation between the estimated distance from photometric redshifts, $\tilde{r}$, and the true distance r in terms of the conditional probability:

$$\Psi_{lm}(k) = \sqrt{\frac{2}{\pi}}\int d^3\tilde{\mathbf{r}}\int d^3\mathbf{r}\, p(\tilde{r}|r)\,\Psi(\mathbf{r})\,k\,j_l(k\tilde{r})\,Y^*_{lm}(\hat{\Omega}). \tag{5.58}$$

Such a Gaussian error leads to photometric redshift smoothing.

5.6.2 Error Estimate

The signal to noise for individual modes for a given power-spectrum can be expressed as:

$$\frac{\delta\mathcal{C}_\ell(k,k)}{\mathcal{C}_\ell(k,k)} = \sqrt{\frac{2}{2\ell+1}}\left(1+\frac{1}{\bar{n}\mathcal{C}_\ell(k,k)}\right) \tag{5.59}$$

Where $\bar{n}$ is the average number density of galaxies and the second term represents the leading order shot-noise contribution. For our results we take $\bar{n} = 10^{-3}h^3\mathrm{Mpc}^{-3}$.

5.6.3 Finite Surveys: Discrete Spherical Fourier-Bessel Transform

Different types of boundary conditions have been employed in the literature for finite surveys [60; 184; 251]. One of the most natural choices for the boundary condition is to assume that the field vanishes at the boundary of the survey $r = R$. This leads to following condition on the radial modes, determined by the zeros of the spherical Bessel functions $j_\ell(x)$:

$$j_\ell(q_{\ell n}) = j_\ell(k_{\ell n}R) = 0; \qquad q_{\ell n} = k_{\ell n}R. \tag{5.60}$$

The closure relation for spherical harmonics will now take the following form:

$$\int_0^1 dz\; z^2 j_\ell(k_{\ell n}z) j_\ell(k_{\ell n}z) = \frac{1}{2}\left[j_{\ell+1}(q_{n\ell})\right]^2 \delta_{\ell\ell'}\delta_{nn'}. \tag{5.61}$$

In terms of the radial wavenumber, the closure relation can be re-expressed as follows:

$$\int_0^R dr\; r^2 k_{n\ell}k_{\ell' n'} j_l(k_{\ell n}r) j_{\ell'}(k_{\ell' n'}r) = \frac{\left[k_{\ell n}\, j_{\ell+1}(q_{\ell n})\right]^2}{2R^{-3}}\delta_{\ell\ell'}\delta_{nn'}. \tag{5.62}$$

The discrete spectrum will be determined by the zeros of the spherical Bessel function. The normalisation coefficients are likewise determined by the closure relation and are given by

$$\frac{1}{\tau_{n\ell}} = \frac{R^3}{2}[k_{n\ell}\, j_{\ell+1}(k_{\ell n}R)]^2. \tag{5.63}$$

The inverse and forward discrete sFB transforms can now be written in terms of the normalisation coefficients and the discrete wavenumbers $k_{\ell n}$:

$$\Psi_{\ell m}(k_{\ell n}) = \tau_{\ell n}\int d^3\mathbf{r}\; \Psi(\mathbf{r})\, k_{\ell n}\, j_\ell(kr)\, Y_{\ell m}(\hat{\Omega}); \tag{5.64}$$

$$\Psi(\mathbf{r}) = \sum_{\ell mn}\tau_{\ell n}\Psi_{\ell m}(k) j_\ell(kr) Y_{\ell m}(\hat{\Omega}). \tag{5.65}$$

As we did in the continuous case, we can seek to relate the discrete sFB coefficients to their Fourier counterparts:

$$\Psi_{\ell m}(k_{\ell n}) = \frac{i^{\ell} k_{\ell n}}{(2\pi)^{3/2}} \int d\hat{\Omega}_k \Psi(k_{\ell n}, \hat{\Omega}_k) Y_{\ell m}(\hat{\Omega}_k) \tag{5.66}$$

In the situation where we have a finite survey, the 3D power-spectrum will therefore only sample discrete radial wave-numbers k_{ln} which is set by the radius of the survey R:

$$\langle \Psi_{\ell m}(k_{\ell n}) \Psi^*_{\ell' m'}(k_{\ell' n'} \rangle = P_{\Psi\Psi}(k_{\ell n}) \delta_{\ell\ell'} \delta_{mm'} \delta_{nn'}. \tag{5.67}$$

5.6.4 Finite Surveys: Masked Surveys and Pseudo-$\mathcal{C}_l$s

In addition to just a finite survey, we can also consider surveys with some angular mask $\chi(\hat{\Omega})$. This corresponds to a situation where, perhaps due to systematics or known glitches, certain parts of a survey are excluded from the analysis. The sFB transform of a masked field will introduce convolved or *pseudo* harmonics $\tilde{\Psi}_{lm}(k_{ln})$:

$$\tilde{\Psi}_{\ell m}(k_{\ell n}) = \tau_{\ell n} \int_0^R r^2 dr \int_\Omega d\hat{\Omega} \left[\phi(r)\chi(\hat{\Omega})\right] \left[k_{\ell n}\, j_\ell(k_{\ell n} r)\right] \Psi(\mathbf{r})\, Y_{\ell m}(\hat{\Omega}).$$

These convolved, *pseudo*-harmonics can be expressed in terms of the all-sky harmonics $\Psi_{lm}(k_{ln})$ by expanding the mask and the field $\Psi()$ into harmonics:

$$\begin{aligned}\tilde{\Psi}_{\ell m}(k_{\ell n}) = \sum_{n'} \sum_{\ell' m'} \sum_{\ell'' m''} \tau_{\ell n} \tau_{\ell' n'} \int_0^R r^2 dr \;\; & \left[k_{\ell n}\, j_\ell(k_{\ell n} r)\right] \left[k_{\ell' n'}\, j_{\ell'}(k_{\ell' n'} r)\right] \\ \times \; & \left[\phi(r)\, \chi_{\ell'' m''}\right] \int_\Omega d\hat{\Omega}\, Y_{\ell m}(\hat{\Omega})\, Y_{\ell' m'}(\hat{\Omega})\, Y_{\ell'' m''}(\hat{\Omega})\end{aligned} \tag{5.68}$$

This can be simplified by evaluating the angular derivative and collapsing terms into a kernel $W(k_{\ell n}, k_{\ell' n'})$. The expression reduces to

$$\begin{aligned}\tilde{\Psi}_{\ell m}(k_{\ell n}) = \sum_{n'} \sum_{\ell' m'} \sum_{\ell'' m''} & \left[\tau_{\ell n} \tau_{\ell' n'}\right] W(k_{\ell n}, k_{\ell' n'})\, \Psi_{\ell m}(k_{\ell' n'}) \\ & \times \chi_{\ell'' m''}\, I_{\ell\ell'\ell''} \begin{pmatrix} \ell & \ell' & \ell'' \\ m & m' & m'' \end{pmatrix} \begin{pmatrix} \ell & \ell' & \ell'' \\ 0 & 0 & 0 \end{pmatrix},\end{aligned} \tag{5.69}$$

where we have defined the selection function $\phi(r)$ dependent kernel $W(k_{\ell n}, k_{\ell' n'})$ by

$$W(k_{\ell n}, k_{\ell' n'}) = \int_0^R r^2\, dr\; \phi(r)\; \left[k_{\ell n}\, j_\ell(k_{\ell n} r)\right] \left[k_{\ell' n'}\, j_\ell(k'_{\ell' n'} r)\right]. \tag{5.70}$$

The pseudo-$\mathcal{C}_\ell$s (PCLs) constructed from these convolved harmonics will be a function of the power spectrum of the angular mask $\mathcal{C}^{\chi}_{\ell''}$, the normalisation coefficients $\tau_{\ell n}$ and $\tau_{\ell' n'}$, and the selection function ϕ. The PCLs are explicitly given by:

$$\tilde{\mathcal{C}}_\ell(k_{\ell n}) = \langle \tilde{\Psi}_{\ell m}(k_{\ell n})\, \tilde{\Psi}^*_{\ell m}(k_{\ell n}) \rangle$$

$$= \sum_{n'} \sum_{\ell'} \sum_{\ell''} \left[\tau_{\ell n} \tau_{\ell' n'}\right]^2 \frac{I^2_{\ell\ell'\ell''}}{2\ell+1} \begin{pmatrix} \ell & \ell' & \ell'' \\ 0 & 0 & 0 \end{pmatrix}^2 \times W^2(k_{\ell n}, k_{\ell' n'})\, \mathcal{C}_{\ell'}(k_{\ell' n'})\, \mathcal{C}^{\chi}_{\ell''}. \tag{5.71}$$

As we can see, the PCLs $\tilde{\mathcal{C}}_\ell(k_{\ell n})$ will be constructed from a linear superposition of the power spectrum of our underlying field $\mathcal{C}_\ell(k_{\ell n})$. This can be re-written in terms of a mixing matrix $M_{\ell n,\ell' n'}$ that encapsulates the mode mixing induced by the mask on the underlying power spectrum. In this form the PCLs are written as

$$\tilde{\mathcal{C}}_\ell(k_{\ell n}) = \sum_{\ell' n'} M_{\ell n,\ell' n'}\, \mathcal{C}_{\ell'}(k_{\ell' n'}); \tag{5.72}$$

where the mixing matrix is explicitly given by

$$M_{\ell n,\ell' n'} = \sum_{\ell''} \left[\tau_{\ell n}\, \tau_{\ell' n'}\right]^2 \frac{I^2_{\ell\ell'\ell''}}{2\ell+1} \begin{pmatrix} \ell & \ell' & \ell'' \\ 0 & 0 & 0 \end{pmatrix}^2 W^2(k_{\ell n}, k_{\ell' n'})\, \mathcal{C}^{\chi}_{\ell''}. \tag{5.73}$$

The angular power spectrum of the mask is defined to be

$$\mathcal{C}^{\chi}_\ell = \langle \chi_{\ell m}\, \chi^*_{\ell m} \rangle. \tag{5.74}$$

Following [585; 267], we construct an unbiased estimator for the 3D power spectra

$$\mathcal{C}_\ell(k_{\ell n}) = \sum_{\ell' n'} M^{-1}_{\ell n,\ell' n'} \tilde{\mathcal{C}}_\ell(k_{\ell' n'}). \tag{5.75}$$

This is just an extension of the well known result for a projected survey [585; 267] to the sFB formalism. For low sky-coverage and small survey volumes, the matrix $M_{\ell n,\ell' n'}$ is expected to be singular and binning of modes may be required.

An alternative choice for the boundary condition may be employed [184]:

$$j_{\ell-1}(k'_{\ell n} R) = 0; \tag{5.76}$$

In this instance, the normalisation constants will be given by:

$$\frac{1}{\tau_{\ell n}} = \frac{R^3}{2} [k_{\ell n} j_\ell(k_{\ell n} R)]^2. \tag{5.77}$$

The expressions derived for the mixing matrix can still be used by simply replacing the normalisation coefficients $\tau_{\ell n}$ with their new values.

Finally, for discrete fields such as the galaxy distribution we can use the PCL approach if we replace the continuous function $\Psi(\mathbf{r})$ with a sum of delta functions that peak at galaxy positions r_s:

$$\Psi(\mathbf{r}) = \sum_{s=1}^{\mathrm{N}} \delta^{3\mathrm{D}}(\mathbf{r} - \mathbf{r}_s); \tag{5.78}$$

here N is the number of galaxies. The sFB transform for a discrete field is given by

$$\Psi_{\ell m}(k) = \sum_{s=1}^{N} \tau_{\ell m}\, j_\ell(r_s k_{\ell n})\, Y_{\ell m}(\hat{\Omega}_s), \tag{5.79}$$

Where the radial and angular position of galaxies are denoted by $\mathbf{r}_s = (r_s, \hat{\Omega}_s) = (r_s, \theta_s, \phi_s)$.

5.6.5 Partial-Sky Coverage and Mode Mixing

Large scale surveys do not, in general, have full-sky coverage. Instead, the information regarding sky-coverage is encapsulated in an angular masking function $\chi(\hat{\Omega})$. In the simplest cases this masking function is simply unity for areas covered in the survey and zero for regions outside the survey. Extending the results presented above to the continuous case, the field harmonics in the presence of a mask are modulated with the new *pseudo* harmonics being given by

$$\tilde{\Psi}_{\ell m}(k) = \sqrt{\frac{2}{\pi}} \int s^2 ds \int d\hat{\Omega}\, \left[\phi(s)\chi(\hat{\Omega})\right] \Psi(\mathbf{r})\, \left[k j_\ell(ks)\right] Y^*_{\ell m}(\hat{\Omega}). \tag{5.80}$$

Expanding the mask and the field into harmonics we find that the pseudo harmonics can be written as

$$\tilde{\Psi}_{\ell m}(k) = \left[\frac{2}{\pi}\right] \int dk_a \sum_{\{\ell_a m_a\}} \chi_{\ell_b m_b}\, \Psi_{\ell_a m_a}(k_a)\, \phi(s)\, \left[k_a j_{\ell_a}(k_a s)\right]\, \left[k j_\ell(ks)\right] \tag{5.81}$$

$$\times \int_\Omega d\hat{\Omega}\, \left[Y^*_{\ell m}(\hat{\Omega})\, Y_{\ell_a m_a}(\hat{\Omega})\, Y_{\ell_b m_b}(\hat{\Omega})\right] \tag{5.82}$$

We can analytically perform the integration over the spherical harmonics, via the Gaunt integral, and we can introduce a window function $W_{\ell\ell_a}(k, k_a)$ to encapsulate the mode mixing terms. The pseudo harmonics therefore reduce down to

$$\tilde{\Psi}_{\ell m}(k) = \left[\frac{2}{\pi}\right] \int dk_a \sum_{\ell_a m_a} \chi_{\ell_b m_b}\, \Psi_{\ell_a m_a}(k_a)\, I_{\ell\ell_a\ell_b} \begin{pmatrix} \ell & \ell_a & \ell_b \\ m & m_a & m_b \end{pmatrix} \tag{5.83}$$

$$\times \begin{pmatrix} \ell & \ell_a & \ell_b \\ 0 & 0 & 0 \end{pmatrix} W_{\ell\ell_a}(k, k_a), \tag{5.84}$$

where we have defined the window function to be

$$W_{\ell\ell_a}(k, k_a) = \int s^2\, ds\, \left[k\, j_\ell(ks)\right]\, \left[k_a\, j_{\ell_a}(k_a s)\right]\, \phi(s). \tag{5.85}$$

The convolved power-spectra in the presence of the mask can now be calculated in the normal manner

$$\tilde{\mathcal{C}}_\ell^{(\alpha\beta)}(k_1, k_2) = \left(\frac{2}{\pi}\right)^2 \sum_{\ell_a} \sum_{\ell_b} \int dk_a \int dk_b$$

$$\times \left[W^{(\alpha)}_{\ell\ell_a}(k_1, k_a) W^{(\beta)}_{\ell\ell_b}(k_2, k_b)\right]\, \frac{I_{\ell\ell_a\ell_b}}{(2\ell_b + 1)}\, \mathcal{C}_{\ell_a}(k_a, k_b)\, \mathcal{C}^\chi_{\ell_b}; \tag{5.86}$$

$$\mathcal{C}_\ell^\chi = \langle \chi_{\ell m} \chi^*_{\ell m} \rangle. \tag{5.87}$$

As written previously, $I_{\ell_1\ell_2\ell_3}$ is related to the Gaunt integral and we have made use of Eq. (2.79). From Eq. (5.86), we see that the convolved power spectrum is a linear combination of the all-sky spectra and is dependent upon the adopted mask and its power spectra.

As a final comment, the PCL estimators are known to be sub-optimal [585; 267; 158; 66; 317] with the estimator induced variance increasing as the sky cut is increased. In the 2D case, such as that applied to CMB studies, the variance of the PCLs scales as

$$\mathrm{Var}(\tilde{\mathcal{C}}_\ell) \approx \frac{1}{f_{\mathrm{sky}}} \mathrm{Var}(\mathcal{C}_\ell). \tag{5.88}$$

An alternative approach is through the quadratic maximum likelihood (QML) formalism, which has been shown to be the minimum variance estimator in a Gaussian framework [554]. If the random field is Gaussian and isotropic, the QML estimator will be a lossless estimator that recovers all information all the relevant information contained within the data. As such the QML estimators are superior to their PCL counterparts. A drawback however, is that there exist technical subtleties and possible constraints due to pixilisation schemes or limited computational resources that could give rise to large biases if not treated with care [158; 449; 182]. Although both approaches depend on the survey mask, the QML estimators also require an accurate model of the pixel-pixel covariance matrix. It also requires priors on the fiducial model $\{\mathcal{C}_\ell\}$ and any other correlations that may be present in the data, such as those induced by noise or systematics. The PCL approach does not use such prior information but turns out to be equivalent to the maximum likelihood analysis when a flat spectrum is assumed for the pixel-pixel correlation [158; 449].

It would be interesting to generalise the sFB results to the QML estimator and compare the results to those derived via the PCL approach, especially in terms of the complexity associated to the different pipelines. Upcoming LSS surveys will provide an unprecedented view of the sky and it suspected that, given the size of these data sets, the QML approach may be limited to low resolution 3D maps. A detailed understanding as to how we can construct accurate and robust estimators that are applied to large data sets is of great importance. The results presented in this Chapter should be viewed as a step towards this goal.

5.7 Non-Linear Power Spectrum

The role of nonlinear gravitational clustering can investigated in the sFB formalism by incorporating higher-order corrections to the power spectrum as described in perturbation theory. The approach we adopt here is standard perturbation theory (SPT), also known as Eulerian perturbation theory, which provides a rigorous framework from which we can investigate the the structure of the sFB spectra in a fully analytic manner [577; 189; 211; 546; 342; 276; 496]. Standard perturbation theory is one of the most straightforward approaches to studies beyond linear theory and is based on a series solution to the hydrodynamical fluid equations in powers of an initial density or velocity field. The nonlinear clustering of matter arises from mode-mode couplings of density fluctuations and velocity divergence as seen from the Fourier space equations. The role of perturbation theory in the nonlinear evolution of the BAO in the power spectrum has been previously in-

vestigated (for an incomplete selection of references please see: [279; 407; 412; 413; 550; 551]). In this paper we generalise these investigations to the sFB approach. The redshift of the Fourier space power spectra was taken to be $z \sim 0.2$ and the effects of growth have not been analysed in detail. For small surveys the growth does not seem to have significant effects.

5.7.1 Standard Perturbation Theory

Consider the hydrodynamic equations of motion for density perturbations δ such that our coming coordinates are denoted by $\mathbf{x}$ and the conformal time by η:

$$\delta'(\mathbf{x},\eta) + \nabla \cdot [(1+\delta(\mathbf{x},\eta))\mathbf{v}(\mathbf{x},\eta)] = 0, \tag{5.89}$$

$$\mathbf{v}'(\mathbf{x},\eta) + [\mathbf{v}(\mathbf{x},\eta)\cdot\nabla]\,\mathbf{v}(\mathbf{x},\eta) + \mathcal{H}(\eta)\mathbf{v}(\mathbf{x},\eta) = -\nabla\phi(\mathbf{x},\eta), \tag{5.90}$$

$$\nabla^2\phi(\mathbf{x},\eta) = \frac{3}{2}\mathcal{H}^2(\eta)\delta(\mathbf{x},\eta), \tag{5.91}$$

where a prime denotes the derivative with respect to the conformal time and $\mathcal{H} = a'/a$. The rotational mode of the peculiar velocity $\mathbf{v}$ is a decaying solution in an expanding universe and can be neglected in this approach. We introduce a scalar field describing the velocity divergence:

$$\Theta(\mathbf{x},\eta) = \nabla\cdot\mathbf{v}(\mathbf{x},\eta). \tag{5.92}$$

In our discussion we will focus on a description of the density perturbations and Fourier decompose the above equations to set up and solve a system of integro-differential equations. The Fourier decomposition of the perturbations are defined by:

$$\delta(\mathbf{x},\eta) = \int \frac{d^3k}{(2\pi)^3}\delta(\mathbf{k},\eta)e^{-i\mathbf{k}\cdot\mathbf{x}}, \tag{5.93}$$

$$\Theta(\mathbf{x},\eta) = \int \frac{d^3k}{(2\pi)^3}\Theta(\mathbf{k},\eta)e^{-i\mathbf{k}\cdot\mathbf{x}} \tag{5.94}$$

The equations of motion can be decomposed as follows:

$$\delta'(\mathbf{x},\eta) + \Theta(\mathbf{k},\eta) = -\int d^3k_1 \int d^3k_2\delta^{(3)}(\mathbf{k}_1+\mathbf{k}_2-\mathbf{k}) \frac{\mathbf{k}\cdot\mathbf{k}_1}{k_1^2}\Theta(\mathbf{k}_1,\eta)\delta(\mathbf{k}_2,\eta), \tag{5.95}$$

$$\Theta'(\mathbf{k},\eta) + \mathcal{H}(\eta)\Theta(\mathbf{k},\eta) + \frac{3}{2}\mathcal{H}^2(\eta)\delta(\mathbf{k},\eta) = -\int d^3k_1 \int d^3k_2\delta^{(3)}(\mathbf{k}_1+\mathbf{k}_2-\mathbf{k})\frac{k^2(\mathbf{k}_1\cdot\mathbf{k}_2)}{2k_1^2k_2^2}\Theta(\mathbf{k}_1,\eta)\Theta(\mathbf{k}_2,\eta). \tag{5.96}$$

In order to solve these coupled integro-differential equations we introduce a perturbative expansion of our variables:

$$\delta(\mathbf{k},\eta) = \sum_{n=1}^{\infty} a^n(\eta)\delta_n(\mathbf{k}), \tag{5.97}$$

$$\Theta(\mathbf{k},\eta) = \mathcal{H}(\eta)\sum_{n=1}^{\infty} a^n(\eta)\Theta_n(\mathbf{k}). \tag{5.98}$$

The general n-th order solutions are given by:

$$\begin{aligned}\delta_n(\mathbf{k}) = &\int d^3q_1 \ldots \int d^3q_n \delta^{(3)}\left(\sum_{i=1}^{n}\mathbf{q}_i - \mathbf{k}\right)\\ &\times F_n(\mathbf{q}_1,\ldots,\mathbf{q}_n)\Pi_{i=1}^{n}\delta_1(\mathbf{q}_i),\end{aligned} \tag{5.99}$$

$$\begin{aligned}\Theta_n(\mathbf{k}) = &-\int d^3q_1 \ldots \int d^3q_n \delta^{(3)}\left(\sum_{i=1}^{n}\mathbf{q}_i - \mathbf{k}\right)\\ &\times G_n(\mathbf{q}_1,\ldots,\mathbf{q}_n)\Pi_{i=1}^{n}\delta_1(\mathbf{q}_i),\end{aligned} \tag{5.100}$$

where the kernels $F_n(\mathbf{q}_1,\ldots,\mathbf{q}_n)$ and $G_n(\mathbf{q}_1,\ldots,\mathbf{q}_n)$ are given by [276]:

$$\begin{aligned}F_n(\mathbf{q}_1,\ldots,\mathbf{q}_n) = &\sum_{m=1}^{n-1}\frac{G_m(\mathbf{q}_1,\ldots,\mathbf{q}_m)}{(2n+3)(n-1)}\\ &\times\left[(1+2n)\frac{\mathbf{k}\cdot\mathbf{k}_1}{k_1^2}F_{n-m}(\mathbf{q}_{m+1},\ldots,\mathbf{q}_n)\right.\\ &\left.+\frac{k^2(\mathbf{k}_1\cdot\mathbf{k}_2)}{k_1^2k_2^2}G_{n-m}(\mathbf{q}_{m+1},\ldots,\mathbf{q}_n)\right],\end{aligned} \tag{5.101}$$

$$\begin{aligned}G_n(\mathbf{q}_1,\ldots,\mathbf{q}_n) = &\sum_{m=1}^{n-1}\frac{G_m(\mathbf{q}_1,\ldots,\mathbf{q}_m)}{(2n+3)(n-1)}\\ &\times\left[3\frac{\mathbf{k}\cdot\mathbf{k}_1}{k_1^2}F_{n-m}(\mathbf{q}_{m+1},\ldots,\mathbf{q}_n)\right.\\ &\left.+n\frac{k^2(\mathbf{k}_1\cdot\mathbf{k}_2)}{k_1^2k_2^2}G_{n-m}(\mathbf{q}_{m+1},\ldots,\mathbf{q}_n)\right],\end{aligned} \tag{5.102}$$

The kernel $F_n(\mathbf{q}_1,\ldots,\mathbf{q}_n)$ is not symmetric under permutations of the argument $\mathbf{q}_1\ldots\mathbf{q}_n$ and must be symmetrised:

$$F_n^{(s)} = \frac{1}{n!}\sum_{\text{Permutations}} F_n(\mathbf{q}_1,\ldots,\mathbf{q}_n). \tag{5.103}$$

As an example, the second order symmetrised solution is given by:

$$F_2^{(s)}(k_1,k_2) = \frac{5}{7} + \frac{2}{7}\frac{(\mathbf{k}_1\cdot\mathbf{k}_2)^2}{k_1^2k_2^2} + \frac{(\mathbf{k}_1\cdot\mathbf{k}_2)}{2}\left(\frac{1}{k_1^2}+\frac{1}{k_2^2}\right). \tag{5.104}$$

The corresponding second order matter power spectrum represents the linear matter power spectrum plus the additional higher-order corrections. This calculation is made under the assumption that the first order density perturbations $\delta_1(\mathbf{k})$ constitute a Gaussian random field. The power spectrum up to second order is given by:

$$P_{\rm SPT}(k,z) = D^2(z)P_{\rm lin}(k) + D^4(z)P_2(k), \tag{5.105}$$

where $P_{\rm lin}$ is the conventional linear matter power spectrum and the second order correction are given by:

$$P_2(k) = P_{22}(k) + 2P_{13}(k). \tag{5.106}$$

These terms correspond to the contributions to the 4-point correlation function from the (2,2) and (1,3) cross-correlations. The explicit form of these terms are given by:

$$P_{22}(k) = 2\int d^3q P_{\rm lin}(|\mathbf{k}-\mathbf{q}|)\left[F_2^s(\mathbf{q},\mathbf{k}-\mathbf{q})\right]^2, \tag{5.107}$$

$$P_{13}(k) = 3P_{\rm lin}(q)\int d^3q P_{\rm lin}(q)F_3^s(\mathbf{q},-\mathbf{q},\mathbf{k}). \tag{5.108}$$

Although any statistical observable can be computed to arbitrary order, typically we are only interested in the second order corrections to the matter power spectrum. Expressions for higher-order corrections have been derived but one of the key issues regarding the inclusion of these terms is the computational costs required for the higher-order corrections. This is, in part, due to the high dimensionality of the integrals even after symmetry arguments have been taken into account. The analytic expressions for the lowest order corrections can be analytically derived and are given by the following [342]:

$$\begin{aligned} P_{13}(k) = \frac{1}{252}\frac{k^3}{4\pi^2}\int_0^\infty dx P_{\rm lin}(k)P_{\rm lin}(kx)\Bigg[&\frac{12}{x^2} - 158 + 100x^2 \\ &- 42x^4 + \frac{3}{x^2}\left(x^2-1\right)^3\left(7x^2+2\right)\log\left|\frac{1+x}{1-x}\right|\Bigg] \end{aligned} \tag{5.109}$$

$$\begin{aligned} P_{22}(k) = \frac{1}{98}\frac{k^3}{4\pi^2}\int_0^\infty dx P_{\rm lin}(kx)\int_{-1}^1 d\mu P_{\rm lin}(k\sqrt{1+x^2-2x\mu}) \\ \times \frac{\left(3x+7\mu-10x\mu^2\right)^2}{\left(1+x^2-2x\mu\right)^2} \end{aligned} \tag{5.110}$$

It should be noted that the analytical predictions arising from standard perturbation theory will eventually break down as the non-linear terms become dominant over the linear theory predictions. [279] demonstrated that one-loop standard perturbation theory was able to fit N-body simulations to greater than 1% accuracy when the maximum wave number $k_{1\%}$ satisfies [550]:

$$\frac{k_{1\%}^2}{6\pi^2}\int_0^{k_{1\%}} dq\, P_{\rm lin}(q;z) = C \tag{5.111}$$

where $C = 0.18$ in standard perturbation theory. SPT theory relies on a straightforward expansion of the set of cosmological hydrodynamical equations and the approach has been repeatedly noted as being insufficiently accurate to model and describe the BAOs [279; 550; 408; 88; 551]. In particular the amplitude of SPT predicts a monotonical increase with wavenumber that overestimates the amplitude (Fig. 5.3) with respect to N-body simulations [550]. This is also seen in the full (k,ℓ) space spectra in Fig. 5.11-Fig. 5.12.

5.7.2 Results: SPT

In Fig. 5.11-Fig. 5.12 we have divided the nonlinear power spectrum by a linear no-baryon power spectrum when constructing the ratio $R_\ell^C(k)$ highlighting the scale dependence introduced by mode coupling. An alternative possibility would be to divide the nonlinear power spectrum $P^{\rm NL}$ by a power spectrum constructed from smoothing the non-linear spectrum $P^{\rm NL}_{\rm smooth}$ that removes the scale dependence and allows for a more detailed comparison of PT predictions against numerical simulations. We construct the ratios as follows:

$$R_\ell^{C,\text{NL/SPT}}(k) = \frac{C_\ell^{\text{NL/SPT,B}}(k)}{C_\ell^{\text{Lin,nB}}(k)} \tag{5.112}$$

$$R_\ell^{C,\text{Lin}}(k) = \frac{C_\ell^{\text{Lin,B}}(k)}{C_\ell^{\text{Lin,nB}}(k)} \tag{5.113}$$

$$R^{P,\text{NL/SPT}}(k) = \frac{P^{\text{NL/SPT,B}}(k)}{P^{\text{Lin,nB}}(k)} \tag{5.114}$$

In Fig. 5.3 the blue spectra corresponds to Eq. (5.112), the purple spectra to Eq. (5.113) and the red spectra to Eq. (5.114). These spectra do not incorporate RSD. In Fig. 5.11-Fig. 5.12 the ratio Eq. (5.112) is used.

5.7.3 Lagrangian Perturbation Theory

LPT [361] provides a description of the formation of structure by relating the Eulerian coordinates, $\mathbf{x}$, to comoving coordinates, $\mathbf{q}$, through the displacement field $\Psi(\mathbf{q}, t)$:

$$\mathbf{x}(\mathbf{q}, t) = \mathbf{q} + \Psi(\mathbf{q}, t). \tag{5.115}$$

With the assumption that the initial density field is sufficiently uniform, the Eulerian density field $\rho(\mathbf{x})$ will satisfy the continuity relation $\rho(\mathbf{x})\, d^3x = \bar{\rho}\, d^3q$ where we have denoted the mean density in comoving coordinates by $\bar{\rho}$. The fraction densities will then be given by:

$$\delta(\mathbf{x}) = \int d^3\, q\, \delta^3\, \left[\mathbf{x} - \mathbf{q} - \Psi(\mathbf{q})\right] - 1, \tag{5.116}$$

$$\delta(\mathbf{k}) = \int d^3\, q\, e^{-i\mathbf{k}\cdot\mathbf{q}} \left[e^{-i\mathbf{k}\cdot\Psi(\mathbf{q})} - 1\right]. \tag{5.117}$$

Assuming a pressureless self-gravitating Newtonian fluid in an expanding FLRW universe, the equations of motion for the displacement field are given by [361]:

$$\frac{d^2}{dt^2}\Psi + 2H\frac{d}{dt}\Psi = -\nabla_{\mathbf{x}}\phi\left[\mathbf{q} + \Psi(\mathbf{q})\right], \tag{5.118}$$

where ϕ is the gravitation potential as determined by Poisson's equation: $\nabla^2_{\mathbf{x}}\phi(\mathbf{x}) = 4\pi G\bar{\rho}a^2\delta(\mathbf{x})$. LPT proceeds by performing a perturbative series expansion of the displacement field:

$$\Psi = \Psi^{(1)} + \Psi^{(2)} + \cdots \tag{5.119}$$

$$\Psi^{(N)} = \mathcal{O}\left(\left[\Psi^{(1)}\right]^N\right) \tag{5.120}$$

The perturbative terms in the series expansion can be written schematically as:

$$\tilde{\Psi}^{(n)}(p) = \frac{i}{n!} D^n(t) \int \frac{d^3p_1}{(2\pi)^3} \cdot \frac{d^3p_n}{(2\pi)^3} \delta^3\left(\sum_{j=1}^{n} p_j - p\right) \times L^{(n)}(p_1, \cdot, p_n)\delta_0(p_1)\cdots\delta_0(p_n). \tag{5.121}$$

We can perform a similar expansion for both the fractional density and the power spectrum, further details can be found in [361] and we will just introduce the results for the power spectrum and how it relates to the predictions of SPT. The power spectrum can be written as:

$$P(k) = \int d^3\, q\, e^{-i\mathbf{k}\cdot\mathbf{q}} \left(\left\langle e^{-\mathbf{k}\cdot[\Psi(\mathbf{q}_1)-\Psi(\mathbf{q}_2)]}\right\rangle - 1\right). \tag{5.122}$$

The two main types of terms that we find in these equations are those terms that depend only on a single position, which are factored out into the first exponential term, and those terms that depend on some separation between positions, as seen in the second exponential term. Using the cumulant expansion theorem the power spectrum can be written as:

$$P(k) = \exp\left[-2\sum_{n=1}^{\infty} \frac{k_{i_1}\cdot k_{i_{2n}}}{(2n)!} A^{(2n)}_{i_1\cdot i_{2n}}\right] \times \int d^3q e^{-i\mathbf{k}\cdot\mathbf{q}} \left\{exp\left[\sum_{N=2}^{\infty} \frac{k_{i_1}\cdot k_{i_N}}{(N!)} B^{(N)}_{i_1\cdot i_N}(q)\right] - 1\right\} \tag{5.123}$$

where $A^{(2n)}_{i_1\cdot i_{2n}}$ and $B^{(N)}_{i_1\cdot i_N}$ are given in [361]. $A^{(N)}$ relates to the cumulant of a displacement vector at a single position and $B^{(N)}$ relates to the cumulant of two displacement vectors separated by $|\mathbf{q}|$. Expanding both the $A^{(N)}$ and the $B^{(N)}$ terms yields SPT. [361], however, proposes expanding only the $B^{(N)}$ terms and leaving the $A^{(N)}$ terms as an exponential prefactor. The justification for this is that this exponential prefactor will contain infinitely higher-order perturbations in terms of SPT and has effectively given a way to resum the infinite series of perturbations found in SPT. Expanding and solving for the $B^{(N)}$ terms yields the standard LPT results [361]:

$$P(k) = e^{-(k\Sigma)^2/2}\left[P_{\text{lin}}(k) + P_{22}(k) + P^{\text{LPT}}_{13}(k)\right]. \tag{5.124}$$

The term P_{22} is identical to it's SPT counterpart but the term P^{LPT}_{13} is now slightly modified but retains much of the structure found in SPT. The expressions are given by

$$P_{13}^{\rm LPT}(k) = \frac{1}{252}\frac{k^3}{4\pi^2}P_{\rm lin}(k)\int_0^\infty dx P_{\rm lin}(kx)\left[\frac{12}{x^2}+10+100x^2 - 42x^4+\frac{3}{x^3}(x^2-1)^3(7x^2+2)\log\left|\frac{1+x}{1-x}\right|\right] \tag{5.125}$$

$$P_{22}^{\rm LPT}(k) = \frac{1}{98}\frac{k^3}{4\pi^2}\int_0^\infty dx P_{\rm lin}(kx)\int_{-1}^1 d\mu\, P_{\rm lin}(k\sqrt{1+x^2-2x\mu}) \times \frac{\left(3x+7\mu-10x\mu^2\right)^2}{\left(1+x^2-2x\mu\right)^2}. \tag{5.126}$$

5.7.4 Results: LPT

In Fig. 5.13-Fig. 5.14 we again divide the nonlinear power spectrum by a linear no-baryon power spectrum when constructing the ratio $R_\ell^C(k)$. The explicit ratios used are:

$$R_\ell^{C,\rm NL/LPT}(k) = \frac{C_\ell^{\rm NL/LPT,B}(k)}{C_\ell^{\rm Lin,nB}(k)} \tag{5.127}$$

$$R_\ell^{C,\rm Lin}(k) = \frac{C_\ell^{\rm Lin,B}(k)}{C_\ell^{\rm Lin,nB}(k)} \tag{5.128}$$

$$R^{P,\rm NL/LPT}(k) = \frac{P^{\rm NL/LPT,B}(k)}{P^{\rm Lin,nB}(k)} \tag{5.129}$$

In Fig. 5.4 the blue spectra corresponds to Eq. (5.127), the purple spectra to Eq. (5.128) and the red spectra to Eq. (5.129). These spectra do not incorporate RSD. In Fig. 5.13-Fig. 5.14 the ratio Eq. (5.127) is used.

The sFB can be seen to mimic the predictions of LPT in consistently underestimating the power at large k but we also see that the sFB power spectra radialise towards the non-linear LPT spectra in the limit $r \to \infty$. This can be seen in Fig. 5.4 where the non-linear sFB tends towards the Fourier space power spectrum in amplitude and phase. We have included a comparison to the linear sFB spectra, which we know to radialise to the linear Fourier space spectra. This behaviour is completely expected due to the nature of the sFB formalism and the fact that the resulting angular spectra are still constructed via products of Bessel functions which form an orthogonal set of basis functions. As such we do not observe the types of mode-mixing that are inherent when considering RSD in the sFB formalism. The damping and smearing of the BAOs in this instance is purely from gravitational instability and is encapsulated in the power spectrum. We also note that the full (ℓ, k) plane is an interesting arena for visualising some of the differences in behaviour between various models for structure formation. This can be seen in the changes to the widths and amplitudes of the BAO wiggles as seen in the plane in Fig. 5.11-Fig. 5.14.

As future wide field surveys will cover both wide and deep regions of the sky we can use the sFB formalism as a tool to distinguish between different models for non-linear evolution of the matter density field. Interesting questions include, how do different theories affect the distribution of power in the radial and tangential modes? How can the sFB formalism be expanded to compare

the RSD results to those as derived from higher-order perturbation theory? How can we best characterise the sFB spectra and how can we characterise the radialisation of information in these higher-order models?

5.8 Conclusion

The baryon acoustic oscillations give rise to a characteristic signature in the observed matter power spectrum that acts as a standard ruler. Unfortunately, the observed matter power spectrum is contaminated and complicated by the non-linear evolution of density perturbations, galaxy clustering bias, RSD and survey specific systematic errors. Additionally, upcoming future surveys will cover both large and deep areas of the sky demanding a formalism that simultaneously treats the both the spherical sky geometry and the extended radial coverage. The sFB basis was proposed as a natural basis for random fields in this geometry. The recent study by [452] was an initial step into investigating the role of the sFB formalism in the study and analysis of the BAO. This study, however, did not go as far as including higher-order contributions to the power spectrum that may impact the radialisation of information by introducing, for example, mode-mode couplings. The stability of this radialisation of information and the information content of tangential (ℓ) and radial (k) modes for higher-order physics is the key topic of interest.

In this Chapter we have presented a short treatment of the effects of **linear** RSD and non-linear corrections to measurements of baryon acoustic oscillations in the sFB expansion. In order to guide this investigation we have extended the formalism and techniques outlined in [452] and the appropriate machinery for partial-sky coverage was introduced. In particular we have been able to use the procedure outlined in [251] to construct a series expansion solution to model RSD. This solution was used to numerically and analytically investigate the modulation to the angular sFB power spectrum. The qualitative behaviour of these corrections was outlined for surveys with varying levels of radial (k-modes) and tangential (ℓ-modes) information. It was seen that the RSD impact the radialisation of information through mode-mixing that generates a distinct signature in the spectra. These RSD were investigated over a range of survey configurations. The mode-mode coupling was related to the presence of derivatives of spherical Bessel functions and was contrasted to the linear Kaiser result in which the basis functions are constructed from plane waves or derivatives of plane waves which simply return a plane wave of the same frequency and preserve orthogonality. This mode-mode coupling can therefore be thought of as a geometrical artefact in the sFB formalism arising from RSD on large scales [251; 606; 519].

Next, we took the analysis a step further by introducing a discussion of realistic survey effects. Idealised surveys constitute a scenario in which we have all-sky coverage and no noise present. This is clearly an unrealistic scenario and we can start to layer in physical effects to describe deviations from this idealised situation. We focus on a few key aspects: photometric redshift errors, errors estimates, finite survey effects and partial sky coverage. In the case of photometric redshift errors, we assumed a Gaussian conditional probability relating the estimated radial coordinate $\tilde{r}$ to the true radial coordinate r. This lead to an expression for the sFB harmonics as a weighted integral over this Gaussian probability. The impact of such an error is to radially smear the harmonics. Secondly, we introduced an expression for the signal-to-noise ratio for individual ℓ modes for a given power spectrum. The expression derived containts a cosmic variance term and a term

relating to the leading order shot noise contribution given in terms of the average number density of galaxies $\bar{n}$. This expression gives us an intuitive feel for an optimal SNR that may be achieved, a simple question of feasibility of a study in the best possible scenario. Thirdly, we were able to write down the sFB harmonics in the case where we have a finite survey, which induces a quantisation of the wavenumber and leads to a modified normalisation coefficient. Finally, we introduced an expression for partial sky coverage in terms of some angular mask $\chi(\hat{\Omega})$. This expression will be of particular importance in working with real data, and therefore upcoming large scale structure surveys, where systematics or glitches force us to exclude certain regions of the sky from our analyis. In brief, the presence of an angular mask induces mode mixing of all sky harmonics leading to a set of convolved or pseudo harmonics. We can use the PCL formalism to perform an inversion of the pseudo power spectrum $\tilde{C}_\ell$ yielding an unbiased estimator for the 3D power spectra.

Additionally we considered the structure and form of the sFB spectra when non-linearity arising from gravitational clustering was considered. We primarily investigated one-loop corrections to the matter power spectrum arising from two mainstream models for leading order corrections as given by SPT and LPT. A brief outline of perturbation theory methods was given and the basic equations for SPT and LPT introduced. The non-linear corrections, and how we expect them to be independent of the notion of radialisation of information in the BAOs, was numerically investigated. The redshift of the Fourier space power spectrum was taken to be $z \sim 0.2$ and the detailed study of the non-linear corrections with redshift will be presented elsewhere. These are not thought to be important at low redshifts or shallow surveys where the impact of growth seems negligible.

In this Chapter we have neglected other contributions to the power spectrum such as General Relativistic corrections and lensing terms. The role of additional non-linearities, more complex treatments of galaxy biasing and more detailed modelling of the hydrodynamical and radiative processes involved in these processes [228; 287] can be investigated in further, more detailed studies. We also note that we have not performed a serious study of systematic errors associated to realistic galaxy surveys (see, for example, the methods in [296] as applied to dark energy studies with 3D weak lensing). It would be interesting to compare the analytical results to those from SKA-like configurations and N-body simulations but this is left for future work.

5.9 Summary of Key Points and Key Results

- Upcoming large scale structure surveys will be both wide and deep. Necessitates a simultaneous treatment of the spherical sky geometry and the extended radial coverage. The spherical Fourier-Bessel (sFB) formalism is the natural basis for such a survey.
- Previous studies of baryon acoustic oscillations (BAOs) in the sFB formalism have only considered the linear, unredshifted spectra. We have extended these studies to incorporate the linear Kaiser effect, governing redshift space distortions (RSDs), and the effect of a non-linear matter power spectra on the full (ℓ, k) plane.
- The presence of RSDs introduces derivatives of the spherical Bessel functions into the equations. These derivatives do not form a complete orthonormal basis inducing mode-mode coupling that smears out the peaks of the BAOs radially.

- The redshifted BAOs have been seen to approximately radialise, given that we have deep radial coverage.
- We have used results from standard perturbation theory (SPT) and Lagrangian perturbation theory (LPT) to demonstrate how detailed modelling of the matter power spectrum impacts the the ratio spectra $R_\ell^C(k)$ over the full (ℓ, k) space. Upcoming surveys can use such studies to perform model selection and model discrimination.
- We derived a set of equations for the sFB harmonics using a discrete sFB transformation. This allows us to detail the effects of finite surveys on our study.
- A system of equations governing the behaviour of sky masks on the sFB analysis was presented, which will be of most interest to connecting the underlying theory to real-world surveys. In this scenario, an angular mask $\chi(\hat{\Omega})$ is used to exclude regions of a survey from the analysis. The introduction of the mask leads to convolved pseudo harmonics that mix together the effects of the sky mask and the true underlying harmonics. An inversion scheme based on the pseudo C_ℓ (PCL) formalism was introduced in order to construct an unbiased estimator for the underlying 3D power spectra. This formalism will be vital for realistic surveys and, due to the low computational costs, will be useful in exploiting upcoming survey measurements.
- Future prospects include: a comparison of quadratic maximum likelihood (QML) methods against the PCL approach derived here; Fisher information matrix studies detailing the level to which we can recover key parameters, such as the growth index for large scale structure or the galaxy bias parameters, from RSD measurements and how RSDs impact these observations; a Bayesian analysis to perform model selection for non-linear corrections to the matter power spectrum.

5.10 Figures

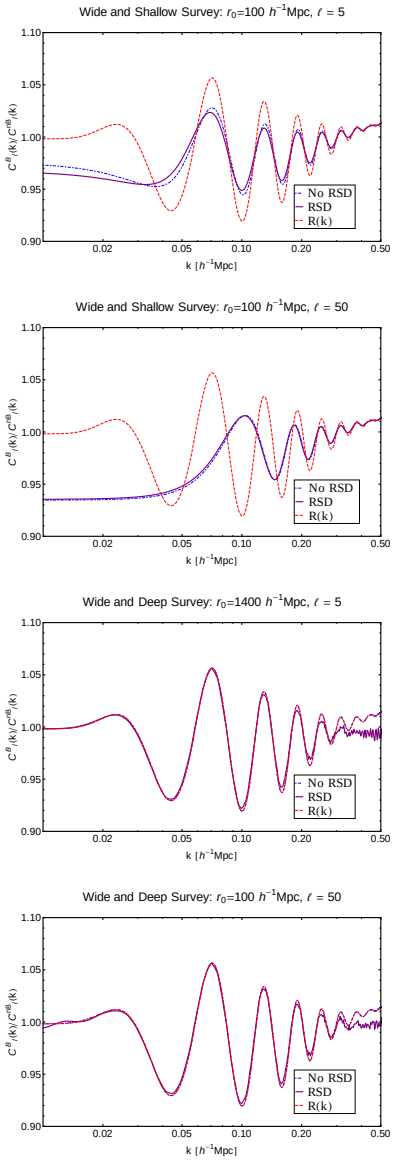

Figure 5.2: Slice in ℓ-space showing $R_l^C(k)$ for a wide and shallow survey of $r_0 = 100h^{-1}Mpc$ at $\ell = 5$ (1st panel) and $\ell = 50$ (2nd panel) and for a wide and deep survey of $r_0 = 1400h^{-1}$Mpc at $\ell = 5$ (3rd panel) and $\ell = 50$ (4th panel). The blue line denotes the $\mathcal{C}^{(00)}$ term, the purple line the sFB spectra incorporating RSD and the red line shows the Fourier space power spectra. In the linear regime the linear prefactors for RSD in the Fourier power spectra cancel and the results correspond to the unredshifted Fourier space power spectra.

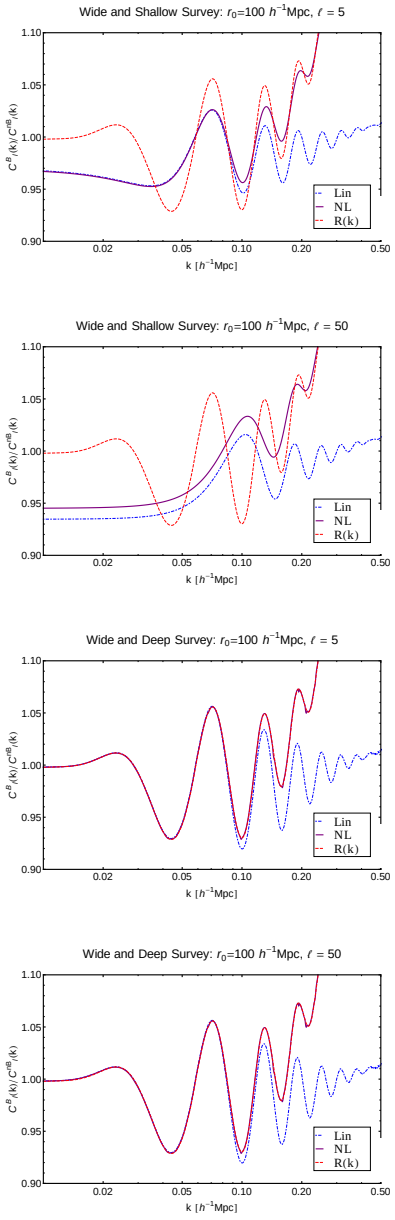

Figure 5.3: Slice in ℓ-space showing $R_\ell^C(k)$ for $\ell = 5$ (top-panels) and $\ell = 50$ (bottom-panels) in a wide and shallow survey of $r_0 = 100h^{-1}$Mpc (left-panels) as well as for a deep survey of $r_0 = 1400h^{-1}$Mpc (right-panels). The solid blue line represents the linear angular spectra, the solid purple line the non-linear 1-loop SPT angular spectra and the dashed line the non-linear 1-loop SPT power spectrum. SPT consistently overestimates the linear power spectrum in the large-k limit and it is well known that SPT works well at high-z and large scales.

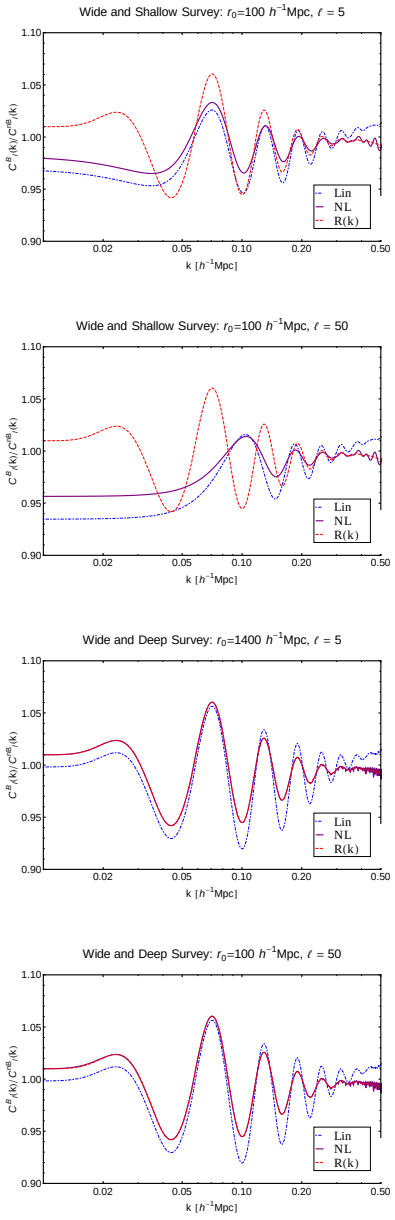

Figure 5.4: Slice in ℓ-space showing $R^C_\ell(k)$ for $\ell = 5$ (top-panels) and $\ell = 50$ (bottom-panels) in a wide and shallow survey of $r_0 = 100h^{-1}$Mpc (left-panels) and a wide and deep survey of $r_0 = 1400h^{-1}$Mpc (right-panels). The solid blue line denotes the linear results, the solid purple line the non-linear 1-loop LPT spectra and the dashed line the non-linear 1-loop LPT spectra. LPT consistently underestimates the power spectrum in the large-k limit contrasting to the divergence at large-k in 1-loop SPT results. This difference occurs due to the effective ressumation of an infinite series of perturbations from SPT that occurs in LPT.

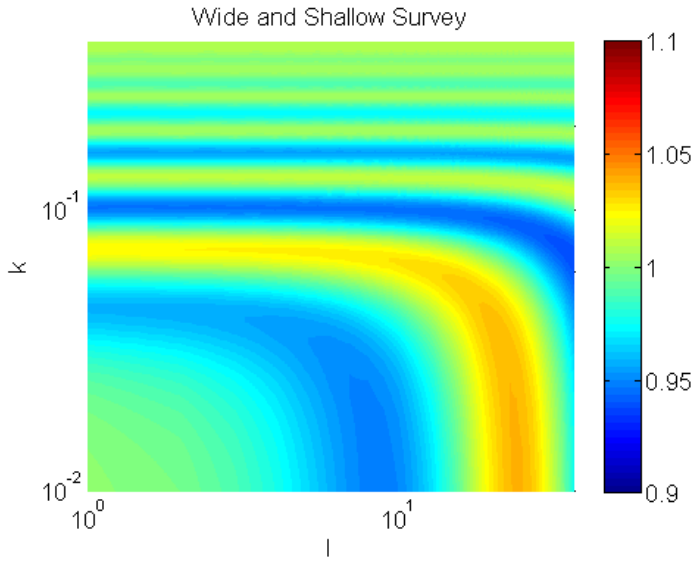

Figure 5.5: Ratio $R_\ell^C(k)$ of sFB spectrum with and without the physical effects of baryons in (ℓ, k) phase space for a wide and shallow survey of $r_0 = 100h^{-1}$Mpc using a Gaussian selection function. The baryonic wiggles are seen in both the radial (k) and tangential (ℓ) directions.

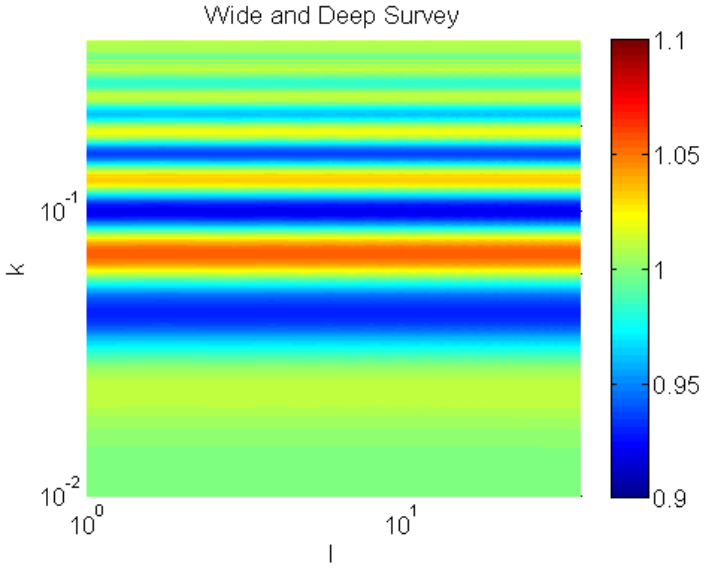

Figure 5.6: Ratio $R_\ell^C(k)$ of sFB spectrum with and without the physical effects of baryons in (ℓ, k) phase space for a wide and deep survey of $r_0 = 1400h^{-1}$Mpc using a Gaussian selection function. The baryonic wiggles are seen in both the radial (k) and tangential (ℓ) directions.

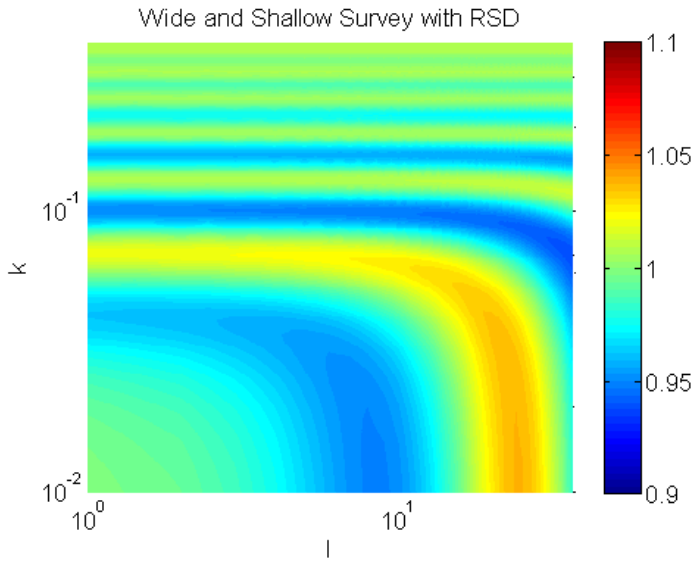

Figure 5.7: Ratio $R_\ell^C(k)$ of sFB spectrum with and without the physical effects of baryons in (ℓ, k) phase space for a wide and shallow survey of $r_0 = 100h^{-1}$Mpc using a Gaussian selection function but with the inclusion of redshift space distortions.

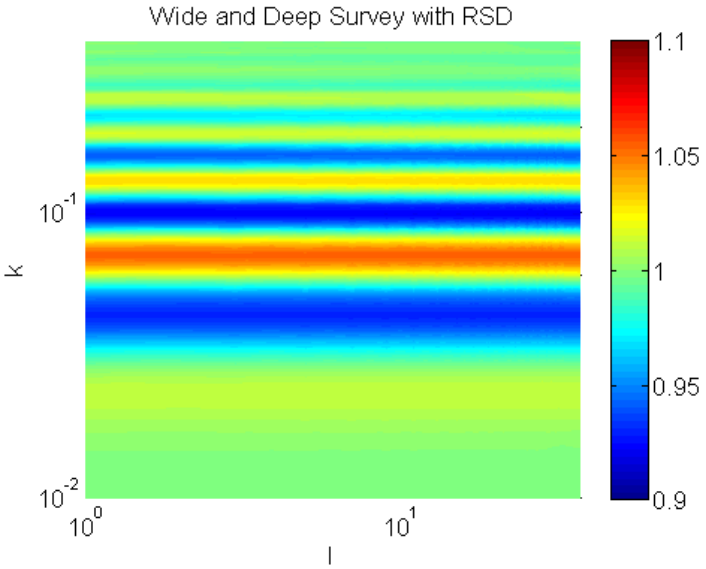

Figure 5.8: Ratio $R_\ell^C(k)$ of sFB spectrum with and without the physical effects of baryons in (ℓ, k) phase space for a wide and deep survey of $r_0 = 1400h^{-1}$Mpc using a Gaussian selection function but with the inclusion of redshift space distortions.

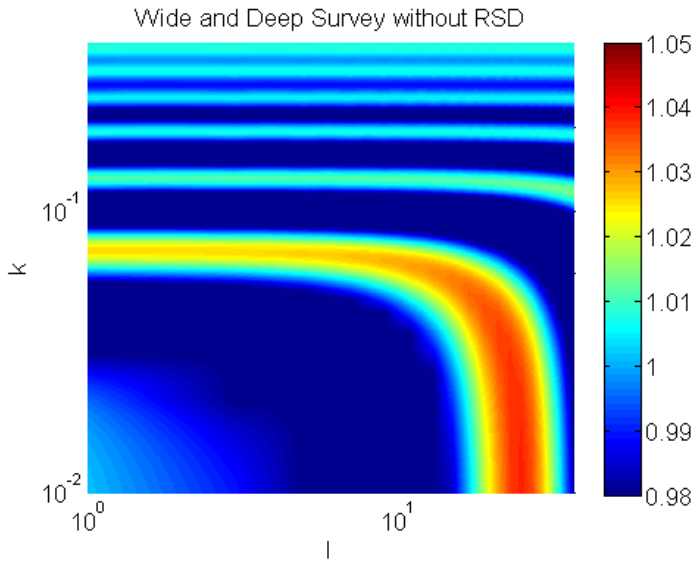

Figure 5.9: Ratio $R_\ell^C(k)$ for a wide and shallow survey of $r_0 = 100h^{-1}$Mpc using a Gaussian selection function without RSD. Here we have reduced the dynamic range to highlight the impact that RSD have on the BAOs. This plot is equivalent to Figure [Fig. 5.5]. Compare to Figure [Fig. 5.10] to see the phenomenological effects of RSD.

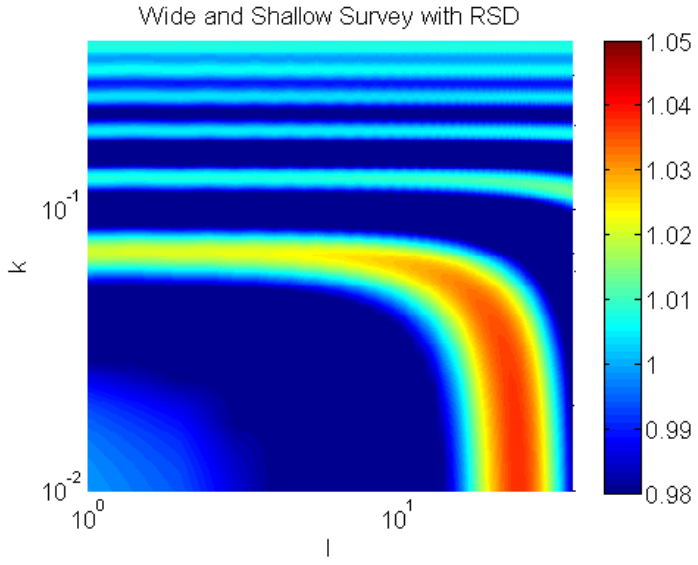

Figure 5.10: Ratio $R_\ell^C(k)$ for a wide and shallow survey of $r_0 = 100h^{-1}$Mpc using a Gaussian selection function with the inclusion of RSDs. We have reduced the dynamic range to highlight the impact that RSD have on the BAOs. This plot is equivalent to Fig. 5.7. Compare to the unredshifted results of Fig. 5.9. RSD suppress the power at lower ℓ and k modes and smear the wiggles in the k direction. Power in the first peak is reduced at low ℓ.

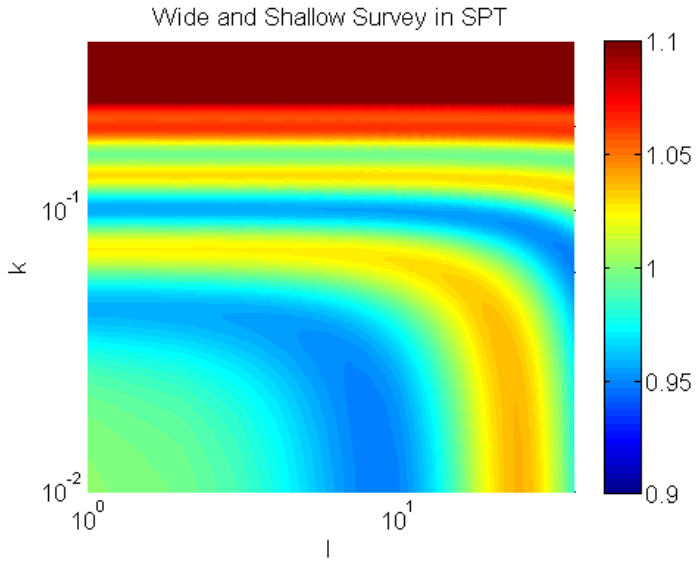

Figure 5.11: Ratio $R_\ell^C(k)$ of sFB spectrum with and without the physical effects of baryons in (ℓ, k) phase space for a wide and shallow survey of $r_0 = 100h^{-1}$Mpc using a Gaussian selection function but with the inclusion of non-linear features as calculated in Standard Perturbation Theory.

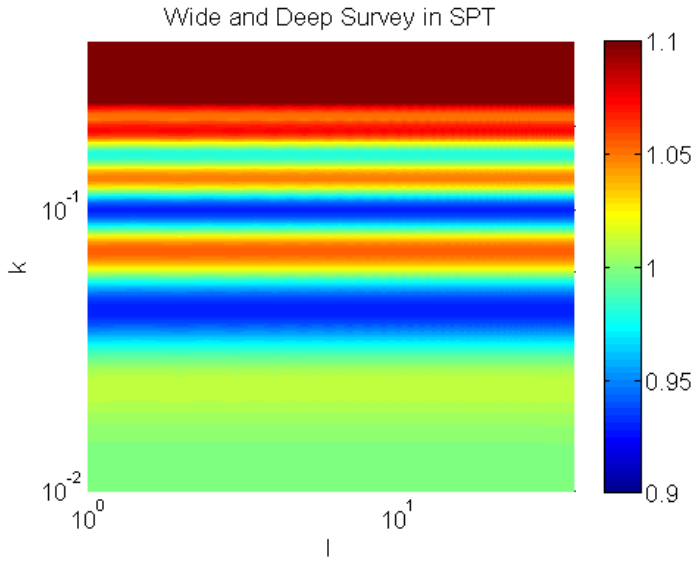

Figure 5.12: Ratio $R_\ell^C(k)$ of sFB spectrum with and without the physical effects of baryons in (ℓ, k) phase space for a wide and deep survey of $r_0 = 1400h^{-1}$Mpc using a Gaussian selection function but with the inclusion of non-linear features as calculated in Standard Perturbation Theory.

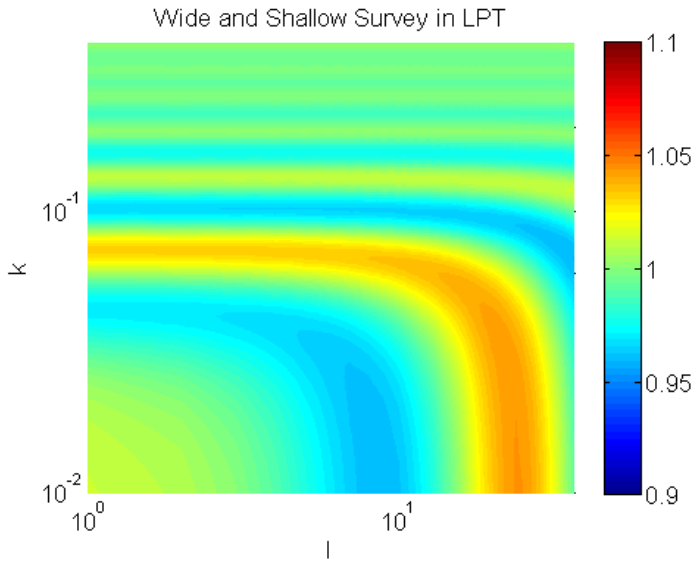

Figure 5.13: Ratio $R_\ell^C(k)$ of sFB spectrum with and without the physical effects of baryons in (ℓ, k) phase space for a wide and shallow survey of $r_0 = 100h^{-1}$Mpc using a Gaussian selection function but with the inclusion of non-linear features as calculated in LPT.

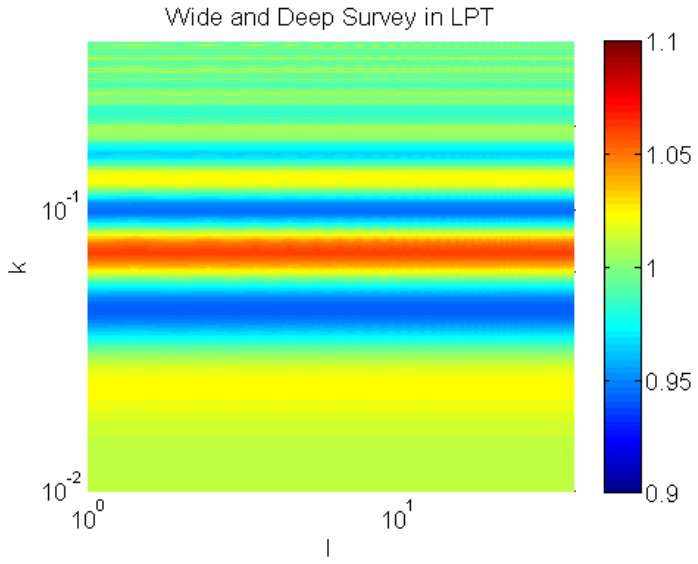

Figure 5.14: Ratio $R_\ell^C(k)$ of sFB spectrum with and without the physical effects of baryons in (ℓ, k) phase space for a wide and deep survey of $r_0 = 1400h^{-1}$Mpc using a Gaussian selection function but with the inclusion of non-linear features as calculated in LPT.

Chapter 6

The Thermal Sunyaev Zel'dovich Effect and Gravitational Weak Lensing

6.1 Introduction

Only 50% of baryons consistent with cosmic microwave background radiation (CMBR) and big bang nucleosynthesis (BBN) observations have been detected observationally [192; 193]. The validation of standard cosmological models relies on our ability to detect the missing baryons observationally [65]. Cosmological simulations suggest that majority of the IGM are in the form of a warm-hot intergalactic medium (WHIM) with temperature $10^5\mathrm{K} < \mathrm{T} < 10^7\mathrm{K}$ [91; 139; 92]. It is also believed that WHIMs reside in moderately overdense structures such as the filaments. WHIMs have a characteristic dark matter mass scale of $M_* \sim 10^{13} M_\odot$. Being collisionally ionized, the baryons residing in these WHIMs do not leave any footprints in the Lyman-α absorption systems. The emission from WHIMs in either UV or X-ray are too weak to be detected given the sensitivity of current instruments and detection in X-ray is also unfeasible given the low level of emission from WHIM. However, the baryons in the cosmic web do have sufficient velocity and column density to produce a detectable CMB secondary effect, known as the kinetic Sunyaev Zeldovich (kSZ) effect [545].

Secondary anisotropies arise at all angular scales; the largest secondary anisotropy at the arcminute scale is the thermal Sunyaev-Zeldovich (tSZ) effect. The tSZ effect is caused by the thermal motion of electrons mainly from hot ionized gas in galaxy clusters where as the *kinetic* Sunyaev Zeldovich (kSZ) effect is attributed to the bulk motion of electrons in an ionized medium [544; 545]. The tSZ can be separated from CMB maps using spectral information. Along with weak lensing of CMB, the kSZ is the most dominant secondary contribution at arcminute scales after the removal of tSZ effect. This is because the primary CMB is sub-dominant on these scales as a result of Silk-damping. Although the tSZ is capable of overwhelming the CMB primaries on cluster scales, the blind detection of the tSZ effect on a random direction in the sky is difficult as the CMB primaries dominate on angular scales larger than that of the clusters. The tSZ and kSZ are both promising probes of the ionized fractions of the baryons with the majority of the tSZ effect being caused by electrons in virialized collapsed objects [596; 254] with overdensities that

can be considerably high $\delta > 100$.

A detailed mapping and understanding of the SZ effect is of particular interest to cosmology and astrophysics [125; 126; 127; 301] as it is thought that the SZ effect will be a powerful method to detect galaxy clusters at high redshifts. One of the key and central features to the tSZ effect is that the efficiency of the free electron distribution in generating the tSZ effect seems to be independent of redshift. Cosmological expansion introduces an energy loss of $1 + z$ to a photon emitted from a source at redshift z but the scattering of these CMB photons off electrons increases the energy of the photons by a factor of $1 + z$. These two effects cancel allowing us to use the tSZ effect as a probe for galaxy clusters at high redshifts. In addition, the tSZ effect will be a powerful probe of the thermal history of our Universe as it is a direct probe of the thermal energy of the intergalactic medium and intracluster medium. Two of the main drawbacks of tSZ studies are that the tSZ has been shown to be sensitive to a wide number of astrophysical processes introducing degeneracies and that the tSZ is a measure of the projected electron thermal energy along the line of sight. This smears all redshift information and the contributions of the various astrophysical processes become badly entangled with the projection effects.

Recent studies have proposed the reconstruction and recovery of redshift information by cross-correlating the tSZ effect with galaxies and their photometric redshift estimates [609; 520]. One of the leading methods proposed in the literature is tomographic reconstruction in which we crudely bin the data into redshift slices and construct the 2D projection for each bin. The auto (single bin) and cross (between bins) correlations can then be used to constrain model parameters and extract information.

This paper is concerned with extending these studies to a full 3D analysis in which we necessarily avoid binning data and therefore avoid the consequential loss of information. In principle, 3D studies would allow a full sky reconstruction that includes the effects of sky curvature and extended radial coverage. As SZ studies are often followed by photometric or spectroscopic galaxy surveys, we expect that photometric redshifts up to $z \sim 1.3 - 2$ will be readily available in due course. We investigate the cross-correlation of the tSZ with an external tracer given by cosmological weak lensing and photometric redshift surveys.

Current ongoing and proposed future ground based surveys, such as SZA[1], ACT[2], APEX[3], SPT[4] and the recently completed all sky Planck survey [4], have published a map of the entire y-sky with a great precision (also see [255]). The high multipole $\ell \sim 3000$ tSZ power spectrum has been observed by the SPT [331; 476; 268; 270; 539; 256] collaboration with the ACT [191; 151; 502; 239; 590] collaboration reporting an analysis on similar scales. It is expected that ongoing surveys will improve these measurements due to the improved sky coverage as well as wider frequency range.

It is important to appreciate why the study of secondaries such as tSZ should be an important aspect of any CMB mission. In addition to the important physics the secondaries probe, accurate modeling of the secondary non-Gaussianities is required to avoid $20\% - 30\%$ constraint degradations in future CMB data-sets such as Planck[5] and COrE[6] [529].

[1] http://astro.uchicago.edu/sza
[2] http://www.physics.princeton.edu/act
[3] http://bolo.berkeley.edu/apexsz
[4] http://pole.uchicago.edu
[5] http://www.rssd.esa.int/index.php?project=planck
[6] http://www.core-mission.org/

While the tSZ surveys described above provide a direct probe of the baryonic Universe, weak lensing observations [387] on the other hand can map the dark matter distribution in an unbiased way. In recent years there has been tremendous progress on the technical front in terms of specification and control of systematics in weak lensing observables. There are many current ongoing weak lensing surveys such as CFHT[7] legacy survey, Pan-STARRS[8] and the Dark Energy survey (DES)[9]. In the future, the Large Synoptic Survey Telescope (LSST)[10], Joint Dark Energy Mission (JDEM)[11] and Euclid [12] will map the dark matter and dark energy distribution of the entire sky in unprecedented detail. Among other things, these surveys hold great promise in shedding light on the nature of dark energy and the origin of neutrino masses [284], where the weak lensing signals dominate the others considered by e.g. the Dark Energy Task Force [11]. However, the optimism that has been associated with weak lensing is predicated on first overcoming the vast systematic uncertainties in both the measurements and the theory [265; 333; 129; 264; 595; 273; 367]. The statistics of the weak lensing convergence have been studied in great detail using an extension of perturbation theory [384; 385; 386] and methods based on the halo model [124; 547; 548]. These studies developed techniques that can be used to predict the lower-order moments (equivalent to the power spectrum and multi-spectra in the harmonic domain) and the entire PDF for a given weak lensing survey. The photometric redshifts of source galaxies are useful for tomographic studies of the dark matter distribution and in establishing a three-dimensional picture of their distribution [393]. Finally, cross correlations with other tracers of large scale structure, such as intensity mapping from future 21cm surveys, could also be considered [98].

This paper is primarily motivated by the recent paper [573] where the CFHTLenS data with Planck tSZ maps was correlated. They measure a non-zero correlation between the two maps out to one degree angular separation on the sky, with an overall significance of six sigma and use the results to conclude a substantial fraction of the *missing* baryons in the universe may reside in a low density warm plasma that traces dark matter. An internal detection of the tSZ effect and CMB lensing cross-correlation in the Planck nominal mission data has also recently been reported at a significance of 6.2 sigma [255]. While these correlations were computed using 2D projections, we develop techniques for cross-correlation studies in 3D that go beyond the tomographic treatment [247; 248; 34; 90; 435].

This Chapter is organised as follows: In Section 6.2 we outline some key notation and cosmological parameters that will be adopted throughout this paper. Section 6.3 introduces the thermal Sunyaev-Zel'dovich effect and defines the key observables. Next, in Section 6.4, we introduce cosmological weak lensing and describe the basic formalism necessary to work with weak lensing on the full sky. There is a brief interlude in Section 6.5 to discuss previous attempts at reconstructing the tSZ-WL cross correlation in 3D via tomography. We then hit the core of the Chapter in Section 6.6 where we define the cross-correlations of the tSZ effect with cosmological WL as an external tracer field. This is described in some detail and a discussion of realistic survey effects is introduced. In order to study the detailed modelling of clustering and pressure fluctuations on large scales we introduce the halo model in Appendix G.1. This allows us to study the cross-

[7] http://www.cfht.hawai.edu/Sciences/CFHLS/
[8] http://pan-starrs.ifa.hawai.edu/
[9] https://www.darkenergysurvey.org/
[10] http://www.lsst.org/llst_home.shtml
[11] http://jdem.gsfc.nasa.gov/
[12] http://sci.esa.int/euclid/

correlations and dependency on mass bins and the halo mass function in a unified manner. In Section 6.9 we study the impact of redshift space distortions on the tSZ-density contrast cross-correlation. Finally, in Section 6.10 we introduce the conclusions to this Chapter.

The work in this Chapter is based on [436].

6.2 Notation

The particular cosmology that we will adopt for numerical studies in this Chapter is specified by the following parameters: $\Omega_\Lambda = 0.741,\ h = 0.72,\ \Omega_b = 0.044,\ \Omega_{\rm CDM} = 0.215,\ \Omega_{\rm M} = \Omega_b + \Omega_{\rm CDM},\ n_s = 0.964,\ w_0 = -1,\ w_a = 0,\ \sigma_8 = 0.803,\ \Omega_\nu = 0$. In such a cosmology, $\Omega_K = 0$ and we can simply assume that $d_A(r) = r$ when performing the numerics. We do, however, keep functions of the curvature in our equations in order to sustain generality. Throughout this Chapter c will denote speed of light and will be set to unity.

6.3 The Thermal Sunyaev Zel'dovitch Effect

The Sunyaev-Zel'dovich effect is generated by inverse Compton scattering of CMB photons by intervening electrons in hot, ionised gas. In short, a low energy CMB photon encounters a high energy electron, the resultant scattering imparts energy onto the photon increasing its frequency. This upsurge in frequency results in a spectral distortion of the CMB in a well understood manner. As energies are relatively low, no more than a few keV in most galaxy clusters, it is often sufficient to restrict ourselves to a non-relativistic treatment. One of the most powerful characteristics of the thermal Sunyaev-Zel'dovich (tSZ) effect is that the main observable, the Compton y-parameter, does not seem to have any significant dependence on the redshift. For this reason it is hoped that large-scale SZ maps can probe the redshift evolution of structures, the intra-cluster medium (ICM) and trace out the thermal history of the Universe. As a side note, it is also important to mention that, in addition to the above, the motion of the hot, ionised gas with respect to the CMB photons produces a spectral distortion arising from Doppler effects, allowing for the estimation of the peculiar velocities of the clusters. As a disclaimer we note that in our analysis we necessarily neglect non-thermal contributions to the tSZ effect.

The tSZ effect generates a contribution to the CMB temperature fluctuation which is typically expressed as

$$\delta_T(\nu, \hat{\Omega}) = \frac{\Delta T(\hat{\Omega})}{\mathrm{T}_0} = g(x) y(\hat{\Omega}). \tag{6.1}$$

In this expression $g(x_\nu)$ corresponds to the spectral dependence and $y(\hat{\Omega})$ encodes the angular dependence; x_ν represents the dimensionless frequency and $\hat{\Omega} = (\theta, \phi)$ corresponds to a unit vector that signifies pixel positions on the sky. A subscript s will be used to denote the smoothed maps e.g. $y_s(\hat{\Omega})$. In the non-relativistic limit $g(x)$ takes the following form:

$$g(x) = x \coth\left(\frac{x}{2}\right) - 4 = \left(x \frac{e^x + 1}{e^x - 1} - 4\right); \qquad x = \frac{h\nu}{k_B \mathrm{T}_0} = \frac{\nu}{56.84\mathrm{GHz}} = \frac{5.28\mathrm{mm}}{\lambda}; \tag{6.2}$$

Here k_B and h are the Boltzmann and Planck constant respectively; ν denotes the frequency of the photon and $\mathrm{T}_0 = 2.726$ K is the mean temperature of the CMB sky. The tSZ effect presents itself as a CMB temperature decrement at $\nu \ll 218\mathrm{GHz}$ and as an temperature increment at $\nu \gg 218\mathrm{GHz}$ with a null point at $\nu = 218\mathrm{GHz}$. In the Rayleigh Jeans limit, characterized by $x \ll 1$, $g(x) \approx -2$ is roughly independent of frequency. The other limiting situation is for $x \gg 1$, for which $g(x) \approx (x - 4)$. Key information on the thermal history of the Universe is encoded in the $y(\hat{\Omega})$ maps that are extracted from the frequency maps obtained through multi frequency CMB observations.

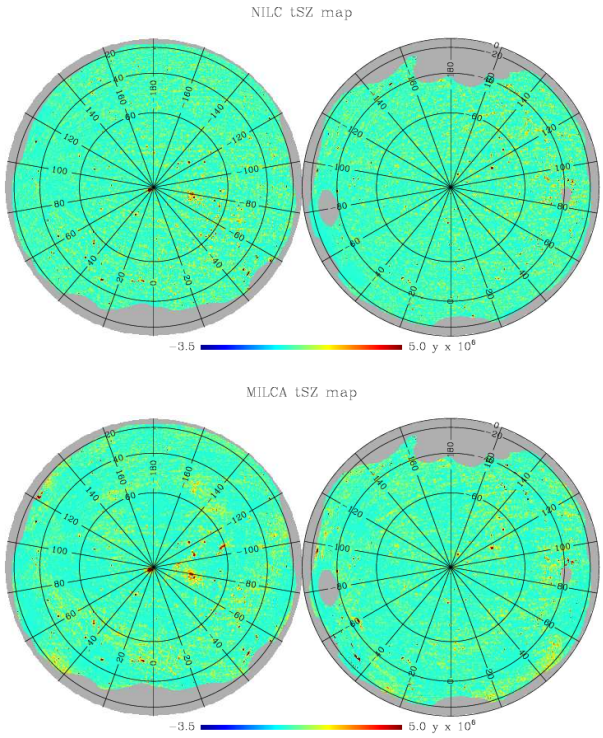

Figure 6.1: Reconstructed Planck all-sky Compton parameter maps for `NILC` (top) and `MILCA` (bottom) in orthographic projections. The difference of contrast observed between the `NILC` and `MILCA` maps comes both from differences in the noise and instrumental systematic contribution and from the differences in the filtering applied for display purpose to the original Compton parameter maps.

The y maps are opacity weighted integrated pressure fluctuations along the line of sight [125] [13]

$$y(\hat{\Omega}) \equiv \int ds\, n_e \sigma_{\mathrm{T}} \frac{k_B T_e}{m_e c^2} \tag{6.3}$$

$$= \frac{\sigma_{\mathrm{T}}}{m_e c^2} \int_0^{r_{\mathrm{H}}} dr\, a(r)\, n_e k_B T_e(\hat{\Omega}, r) \tag{6.4}$$

$$= \frac{\sigma_{\mathrm{T}}}{m_e c^2} \int_0^{\eta_{\mathrm{H}}} d\eta\, a(\eta)\, \Pi_e(\eta, \hat{\Omega}) \tag{6.5}$$

$$= \int_0^{r_{\mathrm{H}}} dr\, w_{\mathrm{SZ}}(r) \pi_e(r). \tag{6.6}$$

[13] Please note that [125] does not separate out the spectral distortions $g(x)$ from y whereas we do, i.e. $y^{\mathrm{Cooray}} = g(x) y(\hat{\Omega})$. This also leads to different definitions for the window function $w_{\mathrm{SZ}}(r)$.

We have introduced various notations that appear in the literature in the context of study of the tSZ effect here $\Pi_e = n_e k_B T_e$. In our notation m_e corresponds to the electron mass, k_B denotes the Boltzmann's constant, $\sigma_{\rm T} = 6.6510^{-25}{\rm cm}^2$ represents the Thompson cross-section, n_e denotes the number density of electrons and T_e to the electron temperature. The conformal time is denoted by $d\eta = dt/a(t)$. The line of sight integral depends on the comoving radial co-ordinate distance r and the corresponding scale factor of the Universe $a(r)$. The weight is defined as[14]

$$w_{\rm SZ}(r) = \dot{\tau}(r) = \sigma_{\rm T} n_e(r) a(r), \tag{6.7}$$

where the dot defines the derivative with respect to comoving radial distance r and the 3D pressure fluctuation is defined as $\pi_e = k_B T_e / m_e c^2$. To our detriment, however, the redshift information is typically lost due to the projection along the line of sight. These projection effects severely compromise the power of the tSZ effect in probing the thermal history of the Universe. Tomographic and 3D methods aim to recover this otherwise discarded information. As such, we aim to cross-correlate the comptonization map $y(\hat{\Omega})$ with tomographic and projected maps from weak lensing surveys to constrain the thermal history of the Universe and its evolution with redshift. Throughout we will consider the Rayleigh-Jeans part of the spectrum $\delta_T = -2y$; for ACT and SPT operating at $\nu = 150{\rm GHz}$ from Eq. (6.2)) we get $g(x) = -0.95$.

Detailed modeling of the bias is required only for the computation of variance. The variance $\langle \delta y^2(\hat{\Omega}) \rangle$ samples the pressure fluctuation power spectrum $P_{\pi\pi}$ and is expressed as:

$$\langle \delta y^2(\hat{\Omega}) \rangle_c = \int_0^{r_s} dr \frac{\omega_{\rm SZ}^2(r)}{d_A^2(r)} \int \frac{d^2\mathbf{l}}{(2\pi)^2} \, {\rm P}_{\pi\pi}\left[\frac{\ell}{d_{\rm A}(r)}, r\right] b_\ell^2(\theta_s). \tag{6.8}$$

The pressure power spectrum ${\rm P}_{\pi\pi}(k,z)$ at a redshift z is expressed in terms of the underlying power spectrum ${\rm P}_{\delta\delta}(k,z)$ using a bias $b_\pi(k,z)$ i.e. ${\rm P}_{\pi\pi}(k,z) = b_\pi^2(k,z){\rm P}_{\delta\delta}(k,z)$. The bias $b_\pi(k,z)$ is assumed to be independent of length scale or equivalently wave number k; i.e. $b_\pi(k,z) = b_\pi(z)$. The redshift dependent bias can be expressed as: $b_\pi(z) = b_\pi(0)/(1+z)$. Here $b_\pi(0)$ can be written as $b_\pi(0) = k_B T_e(0) b_\delta / m_e c^2$. Different values of were reported by various authors; e.g. [454] found $b_\delta \approx 8-9$ and $T_e(0) \approx 0.3-0.4$. On the other hand [515] found $b_\delta \approx 3-4$ and $T_e(0) \approx 0.3-0.4$. Typical value of $b_\pi(0)$ found by [91] is $b_\pi(0) = 0.0039$. This is a factor of two lower than the value used by [207; 208] and [128]. A Gaussian beam $b_\ell(\theta_s)$ with FWHM at θ_s is assumed.

6.4 Weak Gravitational Lensing

6.4.1 Introduction

As a direct probe of the mass distribution of the Universe, cosmological weak lensing is thought to be one of the best tools at our disposal [248; 249]. As the gravitating mass is dominated by dark energy, weak lensing should provide a relatively unbiased observable of the dark Universe. The detection of dark matter on these large, cosmological scales through cosmic shear measurements has been shown to be possible and constraints on cosmological parameters have already been

[14] Note that there exist different conventions for defining the tSZ weight function, e.g. [127]

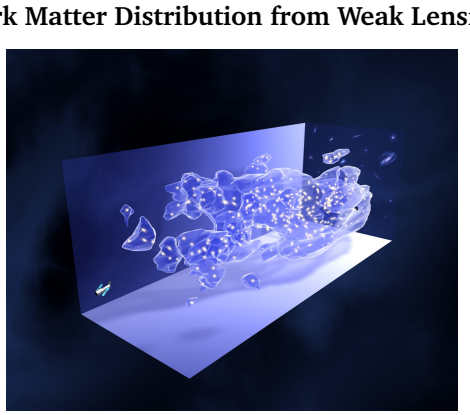

Figure 6.2: This figure is a schematic overview of the reconstruction of the dark matter distribution in the Universe from cosmological weak lensing measurements. This image was created by Lars Lindberg Christensen[15] and the map itself was derived from the COSMOS survey using the Hubble telescope[16].

made, e.g. [31]. The original studies of cosmic shear only used 2-dimensional information from photometric surveys, meaning that the redshifts of the sources are known. This was later extended into tomographic studies by calculating the 2-dimensional power spectrum for various redshift bins, as we have previously discussed. A full 3-dimensional formalism for cosmological weak lensing has recently been proposed as a means to take into account the full redshift information of sources [248; 90]. This is the most exciting possibility as it allows us the opportunity to genuinely reconstruct the full 3-dimensional gravitational potential by an inversion of the weak lensing equations [552; 32; 248].

In addition, large scale galaxy surveys are hindered by the baryonic matter on small scales and necessitates detailed modelling of the bias between dark matter and baryonic matter as well as any baryonic feedback effects. Such effects are avoided in weak lensing studies but, for the full 3-dimensional case, we do require a robust understanding of the systematics that are present in weak lensing surveys. After all, these systematics may eventually dominate the error budget in upcoming large scale structure surveys. One of the most important systematic errors is the redshift distribution of the sources and ignorance of the distribution is a significant source of error. Similarly, the assumption of uncorrelated galaxy ellipticities may need to be refined as tidal effects are suspected to induce correlations throughout the galaxy formation process. Likewise, the effect of source clustering are going to become more important in the near future.

In this section we will predominantly neglect these statistical errors and outline the basiscs of weak lensing theory before introducing the full-sky weak lensing expressions in the tensorial notation of [90]. This is extended to the spin-weighted derivation, as per [90], and an expression for the 3-dimensional power spectra for various weak lensing observables are derived.

6.4.2 Weak Lensing Theory

In General Relativity the presence of mass along the line of sight of a photon travelling from a source to us induces a change in the observed position on the sky of the photon. Gravitational weak lensing distorts the angles, such as the intrinsic source direction $\vec{\theta}_{\rm S}$, into a new image that

can be characterised by a new set of angles $\vec{\theta}_{\rm I}$ describing the image direction on the sky. This introduces a mapping between the two angles that is described by what is known as the *reduced lensing angle* $\delta\vec{\theta} = \vec{\theta}_{\rm I} - \vec{\theta}_{\rm S}$. Here, $\vec{\alpha}$ and $\delta\vec{\theta}$ are 2D vectors in the plane perpendicular to the unperturbed light ray. The deflection angle $\vec{\alpha}$ can be related to the reduced lensing angle the following way

$$\delta\vec{\theta} = \frac{\mathcal{D}(\chi_{\rm LS})}{\mathcal{D}(\chi_{\rm S})}\vec{\alpha} \tag{6.9}$$

where $\mathcal{D}_{\rm i}$ is the comoving angular distance $\mathcal{D}$ to the given object. Here, we have assumed that the deflection angles are sufficiently small such that we may only consider first-order terms. For the most part this wil be a highly accurate approximation to the lensing of null geodesics by the large-scale structure of the Universe. In this framework the source appears to move over the source plan by a comoving distance of

$$\mathcal{D}(\chi_{\rm S})\delta\vec{\theta} = -\mathcal{D}(\chi_{\rm S} - \chi_{\rm L})\vec{\alpha}. \tag{6.10}$$

This can now be integrated over all deflections arising from all potential gradients along the line of sight from the observer to the source

$$\delta\vec{\theta} = \vec{\theta}_{\rm I} - \vec{\theta}_{\rm S} = \frac{2}{c_s^2}\int_0^{\chi_{\rm S}} d\chi \frac{\mathcal{D}(\chi)\mathcal{D}(\chi_{\rm S} - \chi)}{\mathcal{D}(\chi_{\rm S})}\nabla_\perp\Phi(\chi). \tag{6.11}$$

However, in general we will not know the actual position of a source on the sky but only the observed position on the sky. This means that the underlying observable quantities are not the displacements on the sky $\delta\vec{\theta}$ but are rather the distortions that are induced by weak gravitational lensing. The important quantity in this case is the symmetric shear matrix Ψ_{ij} defined by the following (for example, [290])

$$\Psi_{ij} = \frac{\partial\delta\theta_i}{\partial\theta_{sj}} = \frac{2}{c^2}\int_0^{\chi_s} d\chi \frac{\mathcal{D}(\chi)\mathcal{D}(\chi_{\rm S} - \chi)}{\mathcal{D}(\chi_{\rm S})}\nabla_i\nabla_j\Phi(\chi). \tag{6.12}$$

Note that the derivative above implicitly assumes the *weak lensing approximation*, namely that the derivatives $\nabla_i\nabla_j\Phi(\chi)$ of the gravitational potential are computed along the unperturbed trajectory of the photon. This approximation assumes that the components of the shear matrix are small even though the density fluctuations may be large.

6.4.3 Weak Lensing on the Full Sky

6.4.3.1 Introduction

We now wish to extend the earlier discussions to a more complete theory of gravitational weak lensing on the 3D spherical sky. This discussion is based on the formalism as presented in [40; 271; 248; 90]. We now introduce the appropriate tensorial formulation of weak-lensing on the full sky that will form the basis for the 3D spherical Fourier-Bessel expansions later. Let the lens

plane coordinates be denoted by x^i and the source plane coordinates by $\tilde{x}^i$. The displacement vector on the sky is related to the gradient of the lensing potential ϕ:

$$\tilde{x}^i = x^i - \nabla^i \phi. \tag{6.13}$$

The covariant derivative is defined with respect to the lens plane coordinates. There are additional relativistic corrections to this that are non-negligible on large scales but for our work it is sufficient to neglect these [72; 55; 569; 20; 570]. However, in upcoming large scale surveys, such as the SKA, it is thought that such relativistic effects will not only be more pronounced but will also provide a wonderful testing ground for General Relativity and weak lensing theory. Going beyond the deflection, the distortions to the image induced by weak lensing of a source by the intervening matter are described by the changes to the deflection across the lens plane. We therefore introduce the displacement vector to map the changes across from one point on the image to another

$$\delta\tilde{x}^i = \left(g^i{}_j - \nabla^i \nabla_j \phi\right) \delta x^j. \tag{6.14}$$

Often, it will be most convenient to introduce a locally orthonormal frame such that $g_{ij} = \delta_{ij}$ in order to simplify the resulting expressions. In this locally orthonormal frame, the shear and convergence are defined through particular weightings of this displacement vector (for example, [143])

$$\delta\tilde{\mathbf{x}} = \begin{pmatrix} 1-\kappa-\gamma_1 & -\gamma_2 \\ -\gamma_2 & 1-\kappa+\gamma_1 \end{pmatrix} \delta\mathbf{x} \tag{6.15}$$

where the convergence is defined by

$$\kappa = \frac{1}{2}\nabla^2 \phi \tag{6.16}$$

and the two orthogonal components of the shear by

$$\gamma_1 = \frac{1}{2}\left(\nabla_1\nabla_1\phi - \nabla_2\nabla_2\phi\right) \tag{6.17}$$

$$\gamma_2 = \nabla_1\nabla_2\phi. \tag{6.18}$$

Now that we have given a schematic overview of weak lensing in the tensorial approach we will take a step back and introduce an orthogonal but not orthonormal coordinate system and proceed to understand how weak lensing is described by a spin-2 field and how we can relate this to scalar fields via the spin raising and spin lowering operators.

Consider the 2D polar coordinates on the unit sphere (θ, φ) with the metric on the unit sphere given by

$$g_{ij} = \text{diag}\left(1, \sin^2\theta\right). \tag{6.19}$$

This coordinate system is orthogonal but not orthonormal with three non-zero Christoffel symbols, $\Gamma^0_{11} = -\sin\theta\cos\theta$ and $\Gamma^1_{01} = \Gamma^1_{10} = \cot\theta$. First, the shear may be re-expressed in terms of a complex valued variable constructed from the two orthogonal modes of the distortion $\gamma(\mathbf{r}) = \gamma_1(\mathbf{r}) + i\gamma_2(\mathbf{r})$. This shear tensor can be related to the lensing potential via the relation noted above, namely that

$$\left[\nabla_i\nabla_j - \frac{1}{2}g_{ij}\nabla^2\right]\phi(\mathbf{r}) = \left[\gamma_1(\mathbf{r})\sigma_3 + \gamma_2(\mathbf{r})\sigma_1\right]_{ij}. \tag{6.20}$$

Remember, the displacement of a source as a result of lensing is *a priori* not known due to the lack of knowledge of the actual source position. Instead it is the above distortions that constitute our observable quantities. As the shear tensor is a genuine spin-2 field, it is not possible to make comparisons over the entire sky but only locally. This is simply due to the parallel transportation of tensor fields in a curved spacetime and this is necessarily path dependent. It is for this reason that scalar descriptions of the shear field are preferable. The Pauli spin matrices are given by

$$\sigma_1 = \begin{pmatrix} 0 & 1 \\ 1 & 0 \end{pmatrix} \qquad \sigma_3 = \begin{pmatrix} 1 & 0 \\ 0 & -1 \end{pmatrix}. \tag{6.21}$$

We now explicitly evaluate Eq. (6.20) for the given coordinate system [90]

$$\left[\gamma(\mathbf{r})\right]_{ij} = \begin{pmatrix} \gamma_1(\mathbf{r}) & \sin\theta\,\gamma_2(\mathbf{r}) \\ \sin\theta\,\gamma_2(\mathbf{r}) & -\sin^2\theta\,\gamma_1(\mathbf{r}) \end{pmatrix} = \begin{pmatrix} \frac{1}{2}\left[\nabla_\theta\nabla_\theta - \csc^2\theta\nabla_\varphi\nabla_\varphi\right] & \nabla_\varphi\nabla_\theta \\ \nabla_\varphi\nabla_\theta & \frac{1}{2}\left[\nabla_\varphi\nabla_\varphi - \sin^2\theta\nabla_\theta\nabla_\theta\right]\phi(\mathbf{r}) \end{pmatrix} \tag{6.22}$$

From this representation we can immediately read off the two orthogonal modes

$$\gamma_1(\mathbf{r}) = \frac{1}{2}\left[\nabla_\theta\nabla_\theta - \csc^2\theta\nabla_\varphi\nabla_\varphi\right]\phi(\mathbf{r}) \quad \gamma_2(\mathbf{r}) = \csc\theta\nabla_\varphi\nabla_\theta\phi(\mathbf{r}). \tag{6.23}$$

Likewise we can perform an analagous analysis for the scalar convergence κ [90]

$$\left[\kappa(\mathbf{r})\right]_{ij} = \kappa(\mathbf{r})I_{ij} = \frac{1}{2}g_{ij}\nabla^2\phi(\mathbf{r}). \tag{6.24}$$

This scalar field simply corresponds to the magnification of the image and constitutes another means by which we can observe the gravitational lensing potential ϕ. Explicitly evaluating Eq. (6.24) in the given coordinate system, we find that

$$[\kappa(\mathbf{r})]_{ij} = \begin{pmatrix} 1 & 0 \\ 0 & \sin^2\theta \end{pmatrix} \kappa(\mathbf{r}) = \begin{pmatrix} \frac{1}{2}\left[\nabla_\theta\nabla_\theta + \csc^2\theta\nabla_\varphi\nabla_\varphi\right] & 0 \\ 0 & \frac{1}{2}\left[\nabla_\varphi\nabla_\varphi + \csc^2\theta\nabla_\theta\nabla_\theta\right] \end{pmatrix} \phi(\mathbf{r}) \tag{6.25}$$

Reading off the scalar convergence we find that

$$\kappa(\mathbf{r}) = \frac{1}{2}\left[\nabla_\theta\nabla_\theta + \csc^2\theta\nabla_\varphi\nabla_\varphi\right]\phi(\mathbf{r}). \tag{6.26}$$

6.4.3.2 Weak Lensing and Spin-2 Fields

Having introduced the complex valued shear $\gamma(\mathbf{r})$ and the scalar convergence $\kappa(\mathbf{r})$, we now wish to discuss the spin-2 nature of the weak lensing shear in further detail. This section follows the discussion found in [90] with an extended discussion of the spin raising and spin lowering matrices. We poin the readers to [535], Appendix A of [90] and Section C.0.1 for further discussions of the spin raising and spin lowering operators. Parts of this section are based on these references but we also present a full introduction to the topic of spin raising and spin lowering operators in Appendix C.

The shear field transforms under rotations as $\gamma \to \gamma e^{-is\psi}$ where $s = 2$ is the spin weight and ψ is a rotation angle in the anticlockwise direction. The complex shear field is therefore invariant under rotations of π radians, the characteristic property of a spin-2 field. As we discussed in Section 2.4.5, the appropriate basis functions for a spectral decomposition of a spin-s field will be the spin weighted spherical harmonics as the spin-s spherical harmonics constitute a complete orthonormal basis for each s. Using the spin raising and spin lowering operators, we could re-express the spin-2 object as the second edth derivatives of a complex potential

$$\gamma(\mathbf{r}) = \gamma_1(\mathbf{r}) + i\gamma_2(\mathbf{r}) = \frac{1}{2}\eth\,\eth\left[\phi_E(\mathbf{r}) + i\phi_B(\mathbf{r})\right] \tag{6.27}$$

$$\gamma^*(\mathbf{r}) = \gamma_1(\mathbf{r}) - i\gamma_2(\mathbf{r}) = \frac{1}{2}\bar{\eth}\,\bar{\eth}\left[\phi_E(\mathbf{r}) - i\phi_B(\mathbf{r})\right], \tag{6.28}$$

where ϕ_E is a scalar function corresponding to the the even or *electric* part and ϕ_B is a scalar function corresponding to the odd or *magnetic* part. As shown in [90], the spin-2 object $\gamma(\mathbf{r})$ may be expressed in tensorial form as

$$\begin{aligned}[\gamma(\mathbf{r})]_{ij} &= \begin{pmatrix} \gamma_1(\mathbf{r}) & \sin\theta\,\gamma_2(\mathbf{r}) \\ \sin\theta\,\gamma_2(\mathbf{r}) & -\sin^2\theta\,\gamma_1(\mathbf{r})\theta \end{pmatrix}\kappa(\mathbf{r}) \\ &= \begin{pmatrix} \frac{1}{2}\left[\nabla_\theta\nabla_\theta - \csc^2\theta\nabla_\varphi\nabla_\varphi\right] & \nabla_\varphi\nabla_\theta \\ \nabla_\varphi\nabla_\theta & \frac{1}{2}\left[\nabla_\varphi\nabla_\varphi - \sin^2\theta\nabla_\theta\nabla_\theta\right] \end{pmatrix}\phi_E(\mathbf{r}) \\ &\quad + \begin{pmatrix} -\csc\theta\,\nabla_\varphi\nabla_\theta & \frac{1}{2}\left[\sin\theta\,\nabla_\theta\nabla_\theta - \csc\theta\,\nabla_\varphi\nabla_\varphi\right] \\ \frac{1}{2}\left[\sin\theta\,\nabla_\theta\nabla_\theta - \csc\theta\,\nabla_\varphi\nabla_\varphi\right] & \sin\theta\,\nabla_\varphi\nabla_\theta \end{pmatrix}\phi_B(\mathbf{r}). \end{aligned} \tag{6.29}$$

Importantly, if we compare these expressions to those in Eq. (6.22) we see that the only contribution to the shear field induced by gravitational tidal fields is that of the E-modes. This is

related to the fact that density perturbations only produce E-modes, as we would anticipate. The decomposition of weak lensing data into E and B modes holds advantages over the decomposition into γ_1 and γ_2 as on the full sky it allows us to isolate the effect induced by weak lensing and disentangle this from non-linear contributions that generate both E and B modes [90]. Examples of such non-linearities include noise, foregrounds, systematics and, perhaps most imporantly from a fundamental point of view, gravitational waves [487].

6.4.4 Power Spectra

Gravitational lensing is the concomitant deflection of light that arises from fluctuations in the gravitational potential. Lensing of a background source refers to the distortions of the source images generated by the deflection of light, along the line of sight between a source and an observer, caused by the fluctuations in the gravitational potential of the intervening mass distribution. The two most notable effects of gravitational lensing are the shearing and magnification of the images of the sources.

The weak lensing potential $\phi(\mathbf{r})$ can be related to the gravitational potential Φ by the line of sight integral

$$\phi(\mathbf{r}) = \frac{2}{c^2}\int_0^r dr' \frac{f_K(r-r')}{f_K(r)f_K(r')}\Phi(r',\theta,\varphi) \tag{6.30}$$

making using the Born approximation in assuming that the path of the photons is unperturbed by the lens. Here the function $f_K(r)$ is a distance function depending on the curvature of the Universe:

$$f_K(r) = \begin{cases} \sin(r) & \text{if } K<1 \\ r & \text{if} K=1 \\ \sinh(r) & \text{if } K>1 \end{cases} \tag{6.31}$$

Being able to link the 3D lensing potential ϕ to the 3D gravitational potential Φ is one of the most important steps in linking the observables of cosmological weak lensing to theoretical predictions. In a perturbed cosmology, the gravitational potential can be linked to the overdensity field $\delta(\mathbf{r}) = \delta\rho(\mathbf{r})/\rho$ by Poisson's equation in comoving coordinates using the comoving gauge

$$\nabla^2\,\Phi(\mathbf{r}) = \frac{3}{2}\frac{\Omega_m H_0^2}{2a(t)}\,\delta\,(\mathbf{r})\,. \tag{6.32}$$

The aim of 3D weak lensing is to use information of the distance to individual source galaxies to avoid averaging over the redshift distribution of source galaxies. This raises the interesting possibility of being able to determine the full 3D mass density in a non-parametric way by estimating the unprojected tidal shear perpendicular to the line of sight direction from the distortion of a source galaxies' ellipticity. This is fundamentally different to estimations arising from tomographic weak-

lensing or angular line-of-sight approaches which both necessitate the averaging of weak-lensing observables with the line-of-sight galaxy distribution. Distance information is inferred from the corresponding photometric redshift data. The idea of 3D weak lensing was first introduced by [248] and it has been developed further by numerous authors [90; 294; 354; 295; 392; 29]. As we can see, the lensing potential defined in Eq. (6.30) is dependent on the Hubble parameter which is sensitive to the contents of the Universe. This is one of the reasons as to why weak-lensing is a powerful probe of dark energy. In addition, the lensing potential is explicitly related to the gravitational potential which is also dependent on the matter content and non-linear growth of structure through its coupling to $\delta(\mathbf{r})$. Any model that we introduce to describe the non-linear growth of structure will have a direct impact on the behaviour of weak lensing observables.

Performing a spectral decomposition of the lensing potential in the sFB formalism, we find that the lensing harmonics $\phi_{\ell m}$ can be expressed as

$$\phi_{\ell m}(k) = \frac{4k}{\pi c^2}\int_0^\infty dk'\,k'\int_0^\infty dr\,r\,j_\ell(kr)\int_0^r F_K(r,r')j_\ell(k'r')\,\Phi_{\ell m}(k',r'). \tag{6.33}$$

We have introduced a few features in the above. First of all we have the weight $F_K(r,r')$ introduced for convenience,

$$F_K(r,r') = \frac{f_K(r-r')}{[f_K(r)f_K(r')]}. \tag{6.34}$$

Next, the dependence on r appearing after a semi-colon, such as $\Phi_{\ell m}(k;r)$ is just an expression of the time-dependence of the potential. This naturally translates into a dependence on the comoving distance as this intrinsically depends on the look-back time, in a rather circular manner, see [90] for further details. Lastly, we have introduced the harmonic decomposition of the gravitational potential $\Phi_{\ell m}(k;r)$ which an be related to the overdensity via Poisson's equation

$$\Phi_{\ell m}(k;r) = -\frac{3}{2}\frac{\Omega_m H_0^2}{2k^2 a(r)}\delta_{\ell m}(k;r)\,. \tag{6.35}$$

The weak lensing power spectrum will be given by

$$\langle\phi_{\ell m}(k)\phi^*_{\ell' m'}(k')\rangle = \mathcal{C}^{\phi\phi}_{\ell m}(k,k')\delta_{\ell\ell'}\delta_{mm'} \tag{6.36}$$

where we must remember that, due to the nature of look-back time, the 3D lensing potential is not homogeneous and isotropic in 3D space but homogeneous and isotropic on the 2D sky. Expanding the harmonics in the sFB formalism as per Eq. (6.33) we see that the power spectrum can be written as

$$\mathcal{C}^{\phi\phi}_{\ell m}(k_1,k_2) = \frac{16}{\pi^2 c^4}\int dk'k'^2\,\mathcal{I}^\phi_\ell(k_1,k')\,\mathcal{I}^\phi_\ell(k_2,k'), \tag{6.37}$$

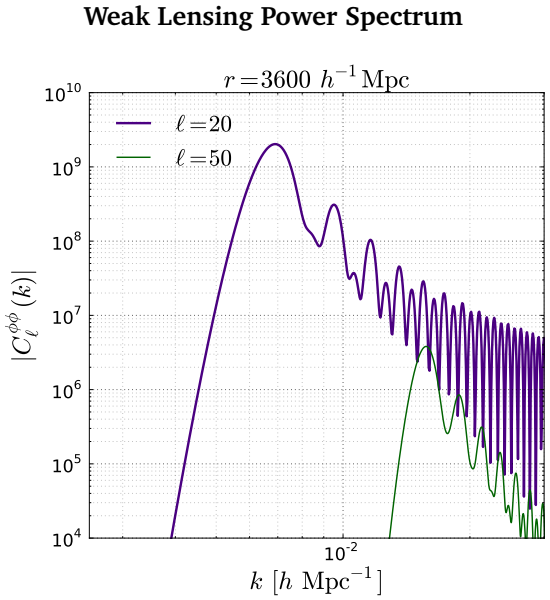

Figure 6.3: Weak lensing potential power spectrum for a survey of depth $r = 3600h^{-1}$Mpc and multipoles $\ell = \{20, 50\}$. The other lensing variables, such as convergence and shear, can be reconstructed from this potential. The lensing spectra are a function of ℓ and two wavenumbers k_1 and k_2. In this plot we only consider the diagonal contribution $k_1 = k_2 = k$. We are interested in the low-k behaviour at scales where linear regime predictions are robust. Scales above $k = 1.5h\mathrm{Mpc}^{-1}$ are entering the highly non-linear regime.

$$\mathcal{I}_\ell^\phi(k_i, k') = k_i \int_0^\infty dr\, r^2\, j_\ell(k_i r) \int_0^r dr'\, F_K(r, r')\, j_\ell(k' r') \sqrt{P^{\Phi\Phi}(k'; r)}. \tag{6.38}$$

Typically, however, we will only look at diagonal cuts in the (k_1, k_2) plane at a given ℓ, though we could certainly consider the full (k_1, k_2, ℓ) space should we need to. In Fig. 6.3 we show typical power spectra for weak-lensing at configurations $\ell = \{20, 50\}$ for $r = 3600h^{-1}\mathrm{Mpc}$. These spectra are in agreement with the results presented in [90] and provide both a useful consistency check as well as a useful guide to the phenomenology of weak lensing cross-correlations.

6.4.5 Shear and Convergence

Weak lensing on the full sky can be aptly described by using spin-weighted spherical harmonics, the weak lensing shear is a spin-2 object after all. The 2D distortion of a source located a given 3D comoving position by intervening matter is given by

$$[\gamma(\mathbf{r})]_{ij} = \begin{bmatrix} \gamma_1(\mathbf{r}) & \sin\theta\,\gamma_2(\mathbf{r}) \\ \sin\theta\,\gamma_2(\mathbf{r}) & -\sin^2\theta\,\gamma_1(\mathbf{r}) \end{bmatrix} = \left[\nabla_i\nabla_j - \frac{1}{2}g_{ij}\nabla^2\right]\phi(\mathbf{r}) \tag{6.39}$$

where γ_1 and γ_2 are components of the weak lensing shear induced by the gravitational tidal field. These can be encapsulated in a complex shear $\gamma(\mathbf{r}) = \gamma_1(\mathbf{r}) + i\gamma_2(\mathbf{r})$ and represent orthogonal modes of the distortion. Additionally we can construct the convergence field tensor that probes the magnification via the isotropic convergence scalar field κ

$$[\kappa(\mathbf{r})]_{ij} = \begin{bmatrix} 1 & 0 \\ 0 & \sin^2\theta \end{bmatrix} \kappa(\mathbf{r}) = \frac{1}{2} g_{ij} \nabla^2 \phi(\mathbf{r}). \tag{6.40}$$

As given in [90], the complex shear may be written in terms of the edth-derivative $\eth$ and its complex conjugate $\overline{\eth}$. These two derivative operators were first introduced by [404] as a generalisation of the covariant derivative to an operator acting on the surface of a sphere. The operator $\eth$ acts as a spin raising operator and $\overline{\eth}$ acts a spin lowering operator on the quantum numbers s of the spin weighted spherical harmonics ${}_sY_{\ell m}$. The power of this approach is that we can relate spin-s objects that are not invariant under rotations of the coordinate frame to scalar quantities that are invariant under rotations of the coordinate frame. The complex shear itself is a spin-2 object but we can now relate it to an $\eth$ derivative of scalar functions. The lensing potential is split into even and odd parts

$$\gamma(\mathbf{r}) = \gamma_1(\mathbf{r}) + i\gamma_2(\mathbf{r}) = \frac{1}{2}\,\eth\,\eth\,[\phi_E(\mathbf{r}) + i\phi_B(\mathbf{r})] \tag{6.41}$$

$$\gamma^*(\mathbf{r}) = \gamma_1(\mathbf{r}) - i\gamma_2(\mathbf{r}) = \frac{1}{2}\,\overline{\eth}\,\overline{\eth}\,[\phi_E(\mathbf{r}) - i\phi_B(\mathbf{r})]\,, \tag{6.42}$$

as we saw previously. In cosmological weak lensing, these equations are simplified as the shear field induced by gravitational tidal fields only has an even parity contribution, i.e. $\phi_B(\mathbf{r}) = 0$. This allows us to recover the orthogonal components of the shear tensor

$$\gamma_1(\mathbf{r}) = \frac{1}{4}\left(\eth\,\eth + \overline{\eth}\,\overline{\eth}\right)\phi(\mathbf{r}) \tag{6.43}$$

$$\gamma_2(\mathbf{r}) = -\frac{i}{4}\left(\eth\,\eth - \overline{\eth}\,\overline{\eth}\right)\phi(\mathbf{r}). \tag{6.44}$$

and convergence scalar

$$\kappa(\mathbf{r}) = \frac{1}{4}\left[\eth\,\overline{\eth} + \overline{\eth}\,\eth\right]\phi(\mathbf{r}). \tag{6.45}$$

Performing a 3D expansion allows us to relate the above equations for the shear and convergence to the lensing potential. This is made possible by knowing the effects of the $\eth$ and $\overline{\eth}$ derivatives on spin weighted spherical harmonics. In particular it can be shown that

$${}_2\gamma_{\ell m}(k) = {}_{-2}\gamma_{\ell m}(k) = \frac{1}{2}\sqrt{\frac{(\ell+2)!}{(\ell-2)!}}\phi_{\ell m}(k) \tag{6.46}$$

$$\kappa_{\ell m}(k) = -\frac{\ell(\ell+1)}{2}\phi_{\ell m}(k). \tag{6.47}$$

Hence we can construct the power spectra of the convergence and shear as follows [90]:

$$\mathcal{C}_\ell^{\kappa\kappa}(k_1, k_2) = \left[\frac{\ell\,(\ell+1)}{2}\right]^2 \mathcal{C}_\ell^{\phi\phi}(k_1, k_2), \tag{6.48}$$

$$\mathcal{C}_\ell^{\gamma\gamma}(k_1,k_2) = \left[\frac{1}{4}\frac{(\ell+2)!}{(\ell-2)!}\right]\mathcal{C}_\ell^{\phi\phi}(k_1,k_2). \tag{6.49}$$

6.5 Tomography

Before we begin our main analysis, we outline the use of tomography, the currently used method in the literature, in the reconstruction and recovery of redshift information in cross-correlation studies. In short, tomography aims to crudely bin data into redshift slices and construct a 2D projection for each bin. From this information one can construct an auto (single bin) or cross (between bins) correlation that is used to constrain model parameters and extract other cosmological information [520; 397]. The key idea at play here is that the dark matter distribution at a given redshift correlates with the tSZ effect generated by the IGM at the same redshift.

In this brief section we will adopt the presentation of [520] in which the tSZ effect is cross-correlated with the matter distribution reconstructed from weak lensing surveys. This closely reflects the situation that we investigate in the remainder of this chapter. A caveat to this approach is that the tomographic reconstruction of [520] uses the Limber approximation to relate the projected power spectrum to an underlying 3D spectrum whereas we will perform our analysis on the full sky.

The angular power spectrum of the tSZ effect in the Rayleigh-Jeans limit can be related to the 3D thermal pressure power spectrum $\Delta^2_\Pi(k,z)$ as follows

$$\frac{\ell^2}{2\pi}\mathcal{C}_\ell^{\rm tSZ} = \int_0^{\chi_{\rm CMB}} \Delta^2_\Pi\left(\frac{\ell}{\chi},z\right) W^2_{\rm tSZ}(z)\,\chi\,d\chi, \tag{6.50}$$

where χ denotes the comoving diameter distance and we implicitly assume a flat cosmology. The tSZ weighting function is given by the following functional form

$$W_{\rm tSZ}(z) = -2\,\sigma_T\,a\,\frac{\langle n_e k_B T_e\rangle}{m_e c^2}. \tag{6.51}$$

The aim of the SZ tomography technique is to reconstruct the time resolved kernel $\mathcal{K}(k,z) = \Delta^2_\Pi(k,z)W^2_{\rm tSZ}(z)$, which tells us about the amplitude of thermal energy and clustering strength at a given redshift [520].

As such we take a matter distribution at redshifts $z=0$ to $z=z_s$. This range of redshifts is divided into a series of bins given by $z_i - \Delta z_i/2 \leq z \leq z_i + \Delta z_i/2$. From this we can associate a comoving distance evaluated at a given redshift $\chi_i = \chi(z_i)$ to derive a series of distance bins with width $\Delta\chi_i = \chi(z_i+\Delta z_i/2) - \chi(z_i - \Delta z_i/2)$. In practice, weak lensing tomography promises to provide maps capable of reconstructing bins of with $\Delta z_i \sim 0.1$ over which $W_{\rm WL}$, the weak lensing weighting function, should be approximately constant. This allows us to construct the cross-correlation of tSZ maps with an overlapping WL region as follows

$$\frac{\ell^2}{2\pi}\mathcal{C}_\ell^{\rm tSZ-WL} = \int_{\chi_i-\frac{\Delta\chi_i}{2}}^{\chi_i+\frac{\Delta\chi_i}{2}} \Delta^2_{\Pi\delta}\left(\frac{\ell}{\chi},\chi\right) W_{\rm tSZ}(\chi)\,W_{\rm WL}(\chi)\,\chi\,d\chi. \tag{6.52}$$

In a suficiently redshift narrow bin it is possible to assume that, as the quantities vary slowly across the redshift bin, the quantity can be reasonably approximated by evaluating the Kernel at the fixed median distance χ_i

$$\frac{\ell^2}{2\pi}\mathcal{C}_\ell^{\mathrm{tSZ-WL}} \approx \Delta^2_{\Pi\delta}\left(\frac{\ell}{\chi_i}, \chi_i\right) W_{\mathrm{tSZ}}(\chi_i)\, W_{\mathrm{WL}}(\chi_i)\, \chi_i\, \Delta\chi. \tag{6.53}$$

Using similar arguments the WL power spectrum is approximately given by

$$\frac{\ell^2}{2\pi}\mathcal{C}_\ell^{\mathrm{WL}} \approx \Delta^2_{\delta}\left(\frac{\ell}{\chi_i}, \chi_i\right) W^2_{\mathrm{WL}}(\chi_i)\, \chi_i\, \Delta\chi_i. \tag{6.54}$$

Finally, we introduce the cross-correlation coefficient between the gas pressure and dark matter distribution

$$r(k,z) = \frac{\Delta^2_{\Pi\delta}(k,z)}{\Delta_\Pi(k,z)\,\Delta_\delta(k,z)}. \tag{6.55}$$

We use this quantity to construct a relation for the time resolved kernel $\mathcal{K}(k,z)$ in the given redshift bin

$$\mathcal{K}(k,z_i) \approx \frac{1}{r^2(k,z_i)}\left[\frac{\ell^2}{2\pi}\right]\frac{\left(\mathcal{C}_\ell^{\mathrm{tSZ-WL}}\right)^2}{\mathcal{C}_\ell^{\mathrm{WL}}}\frac{1}{\chi_i\Delta\chi_i}. \tag{6.56}$$

This can be related to the tSZ power spectrum in a rather trivial way as

$$\frac{\ell^2}{2\pi}\mathcal{C}_\ell^{\mathrm{tSZ}} \approx \sum_i\left[\Delta^2_{\Pi}\left(\frac{\ell}{\chi_i}, z_i\right) W^2_{\mathrm{tSZ}}(z_i)\right]\chi_i\,\Delta\chi_i. \tag{6.57}$$

Hence the time resolved kernel in Eq. (6.56) is the contribution to the tSZ power spectrum from the i-th bin. Hence this tomographic approach allows us to reconstruct the the tSZ contribution by the following prescription:

1. Reconstructing the 3D matter distribution from weak lensing surveys.
2. Measuring the cross power spectrum between the tSZ and matter distribution for data that has been binned into redshift slices.
3. Measuing the angular power spectrum of the matter distribution at the given redshift slice.
4. Reconstructing the contributiont to the tSZ power spectrum from the redshif bin.

The key ingredient in this tomographic reconstruction is detailed knowledge of the cross-correlation coefficient r at a range of redshifts which would allow a more robust interpretation of the measured cross-correlation. In the next section we introduce an alternative way to investigate the tSZ-WL cross-correlation. Rather than crudely binning the data, we will instead advocate the use of the sFB formalism to perform a genuine 3D analysis. This approach avoids the loss of information associated to binning data and avoids making assumptions about how weight functions behave across given bins, instead making use of the full radial and tangential information available.

6.6 tSZ-Weak Lensing Cross-Correlation

6.6.1 tSZ-Weak Lensing

We are now in a position where we can start to put together the various ingredients and construct a cross-correlation between the tSZ effect and cosmological weak lensing. Remember, the tSZ effect directly probes the integrated thermal pressure of free electrons along the line of sight giving us valuable information on the thermal history of our Universe whereas cosmological weak lensing provides an unbiased probe of the dark matter distribution in the Universe. The integrated nature of the tSZ effect means that redshift information is lost, diminishing the ability of tSZ observations to distinguish between different thermal histories. By performing a cross-correlation between the tSZ effect and an external tracer, such as WL, we hope to recover some of this information that has been lost. The unprojected nature of 3D WL makes this a very interesting candidate for an external tracer, especially as many of the current and planned tSZ surveys will have sky coverage that overlaps with upcoming weak lensing surveys. A key idea here, much as in tomography, is that the dark matter distribution up to a given redshift will be correlated with the tSZ effect.

The first ingredient we need is an expression for the harmonically decomposed projection of the 2D tSZ field $y(\hat{\Omega})$ that samples the underlying 3D pressure fluctuation field $\pi_e(r)$

$$y(\hat{\Omega}) = \int_0^\infty dr\, w_{SZ}(r)\, \pi_e(r), \tag{6.58}$$

$$y_{\ell m} = \sqrt{\frac{2}{\pi}} \int_0^\infty dr\, w_{SZ}(r) \int dk\, k\, j_\ell(kr)\, [\pi_e]_{\ell m}(k; r). \tag{6.59}$$

We construct the cross-correlation by correlating these harmonics $y_{\ell m}$ with the lensing potential harmonics $\phi_{\ell m}$ giving the following cross-correlation spectra

$$\langle \phi_{\ell m}(k)\, y_{\ell' m'} \rangle = \mathcal{C}^{\phi y}_{\ell m}(k)\, \delta_{\ell \ell'} \delta_{m m'}, \tag{6.60}$$

where the power spectrum $\mathcal{C}^{\phi y}_{\ell m}(k)$ is explicitly given by

$$\mathcal{C}^{\phi y}_{\ell m}(k) = \frac{4}{\pi c^2} \int_0^\infty dk'\, k'^2\, \mathcal{I}^y_\ell(k')\, \mathcal{I}^\phi_\ell(k, k'); \tag{6.61}$$

$$\mathcal{I}^y_\ell(k) = k^2 \sqrt{\frac{2}{\pi}} \int_0^\infty dr\, w_{SZ}(r)\, j_\ell(kr)\, b_\pi(k; r) \sqrt{P^{\Phi\Phi}(k; r)}; \tag{6.62}$$

$$\mathcal{I}^\phi_\ell(k, k') = k \int_0^\infty dr\, r^2\, j_\ell(kr) \int_0^r dr'\, F_K(r, r')\, j_\ell(k'r') \sqrt{P^{\Phi\Phi}(k'; r)}. \tag{6.63}$$

The bias coefficient $b_\pi(k; r)$ encodes the scale dependent biasing scheme that we introduced

earlier. We assume that the power spectrum is well approximated by

$$P^{\Phi\Phi}(k;r,r') = \sqrt{P^{\Phi\Phi}(k;r)}\sqrt{P^{\Phi\Phi}(k;r')}. \tag{6.64}$$

This is tantamount to stating that we are only interested in correlations in the potential field over small distances for which the lookback time is negligible and hence $r \simeq r'$ [90]. We have also used the result $\mathcal{C}_\ell(k,k') = P(k)$, where the 3D power-spectrum is defined in terms of the Cartesian Fourier transform

$$\Psi(\mathbf{k}) = \frac{1}{(2\pi)^{3/2}}\int d^3\mathbf{k}\,\Psi(\mathbf{k})\,e^{i\mathbf{k}\cdot\mathbf{r}}; \tag{6.65}$$

$$\Psi(\mathbf{r}) = \frac{1}{(2\pi)^{3/2}}\int d^3\mathbf{k}\,\Psi(\mathbf{k})\,e^{-i\mathbf{k}\cdot\mathbf{r}}; \tag{6.66}$$

$$\langle\Psi(\mathbf{k})\Psi^*(\mathbf{k}')\rangle \equiv (2\pi)^3\,P_{\Psi\Psi}(k)\,\delta_{3\mathrm{D}}(\mathbf{k}-\mathbf{k}'). \tag{6.67}$$

In Fig. 6.4 we restrict ourselves to a limited set of cases for numerical calculations. We choose four configurations corresponding to $r_{\rm max} \in \{3600, 4600\}\,h^{-1}$ Mpc and $\ell \in \{20, 50\}$. The results are well-sampled at low k but the resolution of the numerical integrals drops above $k \sim 10^{-1}$ as the approximate Bessel function inequality $kr \geq \ell$ dominates resulting in a highly oscillatory tail that we do not consider of prime importance for this work. As noted in [90], the differences between individual spectra are only slight but there are a wider range of useful ℓ modes that a full 3D study has access to. This increases the sensitivity of the tSZ-WL cross-correlation to cosmological models. In addition to the 3D cross-correlation presented here, recent work has focused on higher order correlations of tSZ and WL using tomographic bins [398], analytical schemes to describe the statistical aspects of the projected y-sky using moment-based methods [394] and topological estimators [395].

6.6.2 tSZ-Weak Lensing: Extended Limber Approximation

The computations of higher-order multispectra are often difficult due to the presence of complex multidimensional integrals that make numerical computations expensive if not prohibitive. The Limber approximation [323], and its Fourier space generalisation, are often used to simplify the numerical calculations by reducing the dimensionality of the integrals. The use of the Limber approximation is valid on small angular separations and hence for large multipole moments ℓ in the harmonic domain. It requires smooth variations of the integrand compared to the Bessel functions or relevant ℓ. A framework for calculating higher order corrections to the Limber approximation was presented in [329]. Starting with the expression for the angular spectra in Eq. (6.61) and the corresponding kernels in Eq. (6.62) and Eq. (6.63) we re-write the spectra as follows

$$\begin{aligned}\mathcal{C}_\ell^{\phi y}(k) = \frac{4k}{\pi c^2}\sqrt{\frac{2}{\pi}}\int dr_a w_{\rm SZ}(r_a)\int dr_b r_b^2 j_\ell(kr_b)\int dr_b' F_K(r_b,r_b');\\ \times\int dk'\,k'^4\,j_\ell(k'r_a)\,j_\ell(k_2 r_b')b_\pi(k';r_a)\sqrt{P_{\Phi\Phi}(k';r_a)P_{\Phi\Phi}(k';r_b')}.\end{aligned} \tag{6.68}$$

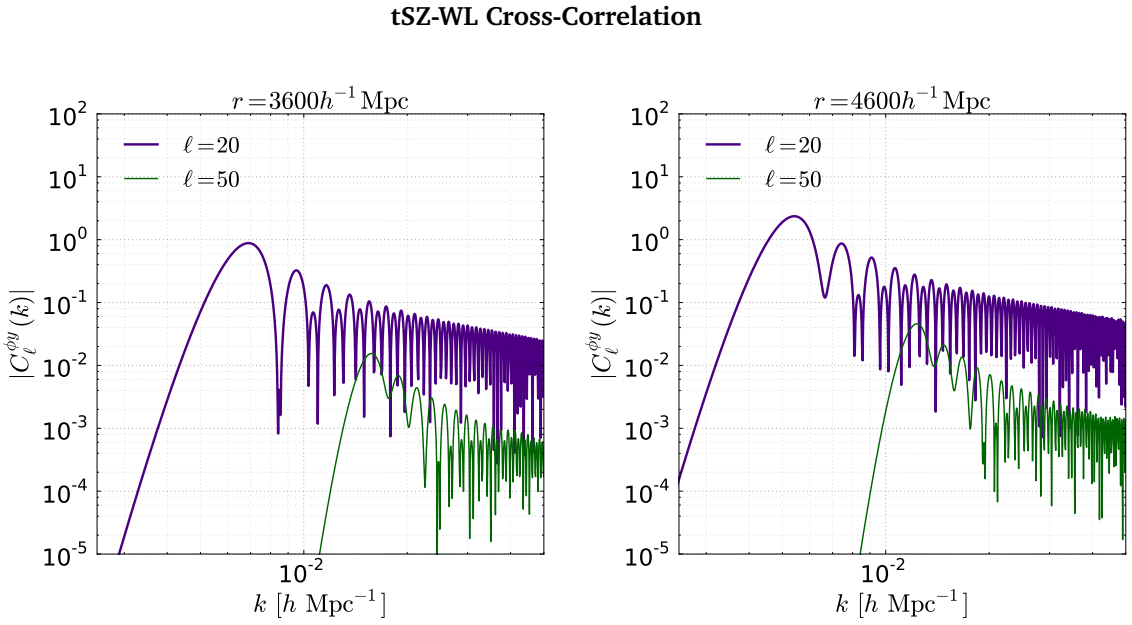

(a) $r = 3600h^{-1}$Mpc. **(b)** $r = 4600h^{-1}$Mpc.

Figure 6.4: The left panel shows the tSZ-WL cross-correlation for a survey of depth $r = 3600h^{-1}\mathrm{Mpc}$ and the right panel for a survey of depth $r = 4600h^{-1}\mathrm{Mpc}$. These plots show the diagonal contribution in the (k_1, k_2) plane for $\ell \in 20, 50\{\}$. Note that the approximate Bessel function inequality comes into play around $kr \geq \ell$ after which we have the decaying oscillatory behaviour. For increasing ℓ the terms become more sharply peaked.

Applying the extended Limber approximation to the k_2 integral, we find the expression collapses to the following:

$$I_\ell(k) = w_{\rm SZ}\left(\frac{\nu}{k}\right) b_\pi\left(k'; \frac{\nu}{k'}\right)\sqrt{P^{\Phi\Phi}\left(k'; \frac{\nu}{k'}\right)}; \tag{6.69}$$

$$I_\ell(k, k') = \frac{\pi}{2}\frac{\nu}{k^2} F_{\rm K}\left(\frac{\nu}{k}, \frac{\nu}{k'}\right)\sqrt{P^{\Phi\Phi}\left(k'; \frac{\nu}{k'}\right)}; \tag{6.70}$$

$$\mathcal{C}_\ell^{\phi y}(k) = \frac{2}{c^2}\frac{\nu}{k^2}\int_0^\infty k'^2 dk' w_{\rm SZ}\left(\frac{\nu}{k'}\right) b_\pi\left(k'; \frac{\nu}{k'}\right) P^{\Phi\Phi}\left(k'; \frac{\nu}{k'}\right); \qquad \nu = \ell + \frac{1}{2}. \tag{6.71}$$

6.6.3 tSZ-Weak Lensing: Shear and Flexions

Alternatively, it is possible to express the power-spectrum of weak lensing observables, such as the convergence, shear, flexions and the Compton y-parameter maps, in terms of $C_\ell^{\phi y}$. As we saw, the components of the 3D shear $\gamma_1(\mathbf{r})$ and $\gamma_2(\mathbf{r})$ and the convergence $\kappa(\mathbf{r})$ can be expressed in terms of the complex 3D lensing potential $\phi(\mathbf{r})$ using the spin-raising $\eth$ and spin-lowering operators $\bar{\eth}$ [90]. We will introduce ${}_{\pm 2}\Gamma(\mathbf{r}) = \gamma_1(\mathbf{r}) \pm i\gamma_2(\mathbf{r})$ to denote the complex shear $\gamma(\mathbf{r})$ and its conjugate $\gamma^*(\mathbf{r})$. The harmonics of Γ can be decomposed in terms of Electric "E" and Magnetic "B" mode polarizations. The Γ's are spin-2 objects and can be decomposed using the spin-2 spherical harmonics [391]

$$ {}_{\pm2}\Gamma_{\ell m} = -[E_{\ell m} \pm iB_{\ell m}]. \tag{6.72} $$

Ignoring the B-mode contribution, as gravitational tidal fields only generate an electric contribution, we have ${}_{\pm2}\Gamma_{\ell m} = -E_{\ell m}$ which is related to the lensing harmonics via

$$ E_{\ell m}(k) = -\frac{1}{2}\sqrt{\frac{(\ell+2)!}{(\ell-2)!}}\phi_{\ell m}(k). \tag{6.73} $$

In addition we have the $\kappa_{\ell m}$ harmonics defined in Eq. (6.47).

Higher order spin objects that can be generated from the lensing potential, known as *flexions*, have often been used to study weak lensing [209; 210; 31]. They are related to the derivatives of the shear or convergence and are sensitive to information about substructures beyond that which can be studied using just the shear or convergence alone. The most commonly used flexions are the spin-1 or *first* flexion $\mathcal{F}$ and the spin-3 or *second* flexion $\mathcal{G}$. Their relationship with the shapelet formalism have been discussed at length in the literature [455; 57; 457]. Both of these flexions have been used extensively in the literature for individual halo profiles and as well as the study of substructures [33]. These flexions can be used to study weak 'arciness' in images of lensed galaxies. The flexions are defined as follows

$$ \mathcal{F}(\mathbf{r}) = \frac{1}{6}\left(\bar{\eth}\,\eth\,\eth + \eth\,\bar{\eth}\,\eth + \eth\,\eth\,\bar{\eth}\right)\phi(\mathbf{r}); \tag{6.74} $$

$$ \mathcal{G}(\mathbf{r}) = \frac{1}{2}\bar{\eth}\,\bar{\eth}\,\bar{\eth}\,\phi(\mathbf{r}). \tag{6.75} $$

The harmonic decomposition of these objects is obtained by expanding in a spin weighted spherical harmonic basis ${}_sY_{\ell m}(\hat{\Omega})$ (see [391] for a detailed derivation and discussion) and evaluating the $\eth$ and $\bar{\eth}$ derivatives on the spin weighted spherical harmonics.

$$ \mathcal{F}_{\ell m} = \frac{1}{6}\left[\ell\,(\ell+1)\right]^{1/2}\left[3\ell^2+3\ell-2\right]\,\phi_{\ell m}; \tag{6.76} $$

$$ \mathcal{G}_{\ell m} = \frac{1}{2}\sqrt{\frac{(\ell+3)!}{(\ell-3)!}}\phi_{\ell m}. \tag{6.77} $$

Using Eq. (6.73), Eq. (6.77), Eq. (6.47) and Eq. (6.61) we arrive at the following expressions for the cross-spectra

$$ \mathcal{C}_\ell^{\Gamma y} = \sqrt{\frac{(\ell+2)!}{(\ell-2)!}}\,\mathcal{C}^{\phi y}; \tag{6.78} $$

$$ \mathcal{C}_\ell^{\kappa y} = \frac{\ell(\ell+1)}{2}\,\mathcal{C}^{\phi y}; \tag{6.79} $$

$$ \mathcal{C}_\ell^{\mathcal{F} y} = \frac{1}{6}\left[\ell\,(\ell+1)\right]^{1/2}\left[3\ell^2+3\ell-2\right]\,\mathcal{C}^{\phi y}; \tag{6.80} $$

$$\mathcal{C}_\ell^{\mathcal{G}y} = \frac{1}{2}\sqrt{\frac{(\ell+3)!}{(\ell-3)!}}\,\mathcal{C}^{\phi y}. \tag{6.81}$$

Note that for both shear components ${}_{\pm 2}\Gamma$ we recover the same power spectrum $\mathcal{C}_\ell^{{}_{\pm 2}\Gamma y} \equiv \mathcal{C}_\ell^{\Gamma y}$.

6.6.4 tSZ-Weak Lensing: Numerical Results

We adopt the fiducial ΛCDM model described in Section 6.2 and restrict our analysis to a survey configuration of $r_{\rm max} = 1800, 3600\,h^{-1}$ Mpc for the multipoles $\ell = \{5, 20, 50, 200\}$. Note that we can see the effect of the approximate Bessel function inequality $kr \geq \ell$ with increasing ℓ as a sharp peak at low k before the oscillatory tail. At high multipoles, the diagonal terms of the cross-spectra do not become important until $\ell \approx kr_{\rm max}$. Similar results are seen in the weak lensing 3D spectra [90].

All of the results obtained so far are simplified in the sense that we have ignored the fact that distance estimates from photometry contain errors and we have ignored the fact that the number density of sources will decrease with redshift. In the sFB formalism, errors in distances are simply radial errors. In the next section we therefore introduce some of the complications that a more realistic survey configuration gives rise to and how this impacts a 3D analysis.

6.7 Survey Effects

6.7.1 Realistic Selection Functions

For the redshift distribution of source galaxies for the surveys we will adopt following analytical fit [272; 520]

$$n(z) = \bar{n}\,\frac{z^2}{2z_0^3}\exp\left(-\frac{z}{z_0}\right); \qquad \int_0^\infty dz\, n(z) = \bar{n}. \tag{6.82}$$

We will consider two different surveys: (1) Dark Energy Survey (DES)[17] and (2) Large Synoptic Survey Telescope (LSST)[18]. We will adopt $z_0 = 0.3$ for the DES and $z_0 = 0.4$ for LSST. The galaxy number density per steradian is denoted above as $\bar{N}_g = 1.2 \times 10^7 \bar{n}_g$, with $\bar{n}$ being the galaxy number density per square arcmin. We will adopt $\bar{n} = 15$ for DES and $\bar{n} = 40$ for LSST.

6.7.2 Photometric Redshift Error

For the depths of surveys proposed in upcoming WL studies, it is often impractical to obtain the spectroscopic redshifts and instead photometric redshifts z_p are obtained form broad band photometry. In order to incorporate photometric redshift errors into our calculations we will need to integrate over the posterior redshift distribution $p(z|\tilde{z})$. In this section we wish to relate the observed convergence $\tilde{\kappa}_{\ell m}(k;r)$ that incorporates photometric redshift errors to the *true* underlying convergence $\kappa_{\ell m}(k;r)$. One of the key advantages to the sFB formalism is that errors in distance,

[17] http://www.darkenergysurvey.org/
[18] http://www.lsst.org/lsst/

such as photometric redshift errors, will simply be radial errors. As such, the angular direction $\hat{\Omega}$ is not affected. The observed convergence harmonics will be given by:

$$\tilde{\kappa}_{\ell m}(k;r) = \sqrt{\frac{2}{\pi}} \int d^3\tilde{\mathbf{r}}\; n(\tilde{r})\; \kappa(\mathbf{r})\; k\; j_\ell(k\tilde{r})\; Y_{lm}(\hat{\Omega})\, w(\tilde{r}) \tag{6.83}$$

where $\tilde{r}$ is the observed radial distance that is inferred from a photometric redshift of $\tilde{z}$. The true convergence naturally depends on the correct distance in the true cosmology r. In the following we neglect uncertainties in the photometric redshift distribution of sources and we ignore the effects of source clustering which will have a sub dominant contribution to the overall error budget. We can therefore relate the observed radial coordinate to a given photometric redshift as follows: $n(\tilde{r})d^3\tilde{r} = \bar{n}_z(\tilde{z})d\tilde{z}\; d\hat{\Omega}/4\pi$. Using the above expression, we can re-write the observed convergence as

$$\tilde{\kappa}_{\ell m}(k;r) = \sqrt{\frac{1}{8\pi^3}} \int dz, d\hat{\Omega}\, \bar{n}_z(\tilde{z})\, \kappa(\mathbf{r})\, k\, j_\ell(k\tilde{r})\, Y_{\ell m}(\hat{\Omega})\, w(\tilde{z}). \tag{6.84}$$

The dominant effect of photometric redshift errors are to smooth the source distribution $\bar{n}(\tilde{z})$ along the line-of-sight. If we introduce $p(z|\tilde{z})$ to denote the conditional probability of the true redshift being z given the photometric redshift $\tilde{z}$, then the above can be re-written as

$$\tilde{\kappa}_{\ell m}(k;r) = \sqrt{\frac{1}{8\pi^3}} \int d\tilde{z} \int dz \int d\hat{\Omega}\; \bar{n}(\tilde{z})\; p(z|\tilde{z})\; \kappa(\mathbf{r})\; k\; j_l(k\tilde{r})\; Y_{lm}(\hat{\Omega})\; w(\tilde{z});\,. \tag{6.85}$$

Now we just need to expand out $\kappa(\mathbf{r})$ with respect to the true radial distance r and use the spherical harmonic relations to perform the angular integration. This eventually reduces to the following expression for the observed convergence harmonics

$$\tilde{\kappa}_{\ell m}(k;r) = \sqrt{\frac{1}{8\pi^3}} \int d\tilde{z} \int dz\; \bar{n}(\tilde{z})\; p(z|\tilde{z})\; k\; j_l(k\tilde{r}) \int dk' k' j_\ell(k'\tilde{r}) w(\tilde{z}) \kappa_{\ell m}(k';r). \tag{6.86}$$

It is now a laborious procedure to construct the cross correlation of $\tilde{\kappa}_{\ell m}(k;r)$ with the tSZ harmonics $y_{\ell m}$ such that $\tilde{\mathcal{C}}_\ell^{\kappa y}(k;r) = \langle \tilde{\kappa}_{\ell m}(k;r) y^*_{\ell m} \rangle$. The power spectrum is given by the following expression (Fig. 6.5)

$$\tilde{\mathcal{C}}_\ell^{\kappa y}(k;r) = \sqrt{\frac{1}{8\pi^3}} \left[\int d\tilde{z} \int dz\; \bar{n}(\tilde{z}) w(\tilde{z}) p(z|\tilde{z}) \right] k j_\ell(k\; \tilde{r}) \int dk' k' j_\ell(k'\tilde{r}) \mathcal{C}_\ell^{\kappa y}(k';\tilde{r}). \tag{6.87}$$

Typically, the conditional probability associated with photometric redshift errors, $p(z|\tilde{z})$, is modelled as a Gaussian for simplicity. This assumption may have catastrophic failures but provides a simple and intuitive starting point for error analysis. The functional form of the conditional probability that we adopt is given by (Fig. 6.6)

$$p(z|\tilde{z}) = \frac{1}{\sqrt{2\pi}\sigma_z(z)} \exp\left[\frac{-(\tilde{z} - z + \beta)^2}{2\; \sigma_z^2(z)} \right]. \tag{6.88}$$

In this expression β is the possible bias in the photometric redshift calibration and $\sigma_z(z)$ is the redshift dependent dispersion in error. For our fiducial model we adopt $\sigma_z(z) = 0.05(1+z)$ and

assume that we can neglect the redshift calibration term, $\beta = 0$. See Fig. 6.6 for the probability kernel defined in Eq. (6.88) for our fiducial model. As we can see, redshift errors simply translate into radial errors and this induces mode-mode couplings, as can be seen by the integral over the true spectra. The result of photometric redshift errors is that the observations are smoothed along our line of sight, this can be seen in Fig. 6.5 where the structure in the oscillatory tail has been smoothed out. See [297] for a more detailed study of photometric redshift errors in 3DWL. In this approach the authors integrate over the posterior redshift distribution for each galaxy $p_g(z|\tilde{z})$ creating a more accurate covariant matrix than the approach taken here of reducing the redshift distributions to a simpler form in which the distributions are assumed to be the same for each galaxy at a given redshift.

κ-y Cross-Correlation: Photometric Redshift Uncertainty

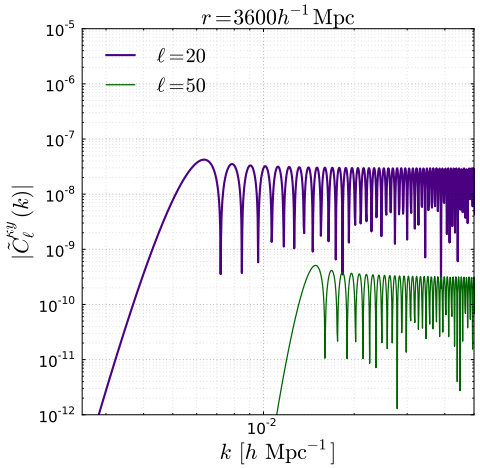

Figure 6.5: In this figure we plot the observable convergence power spectra that have been smoothed due to the effects of photometric redshift uncertainty. Remember, photometric redshift errors are radial errors in the spherical Fourier-Bessel formalism and this means that the observations are smoothed along the line of sight. The adopted fiducial model for redshift error dispersion was $\sigma_z(z) = 0.05(1+z)$. The left panel corresponds to $\ell = 20$ and the right hand panel to $\ell = 50$. Both have been calculated for a survey size of $r = 3600h^{-1}$Mpc.

Conditional Probability Function

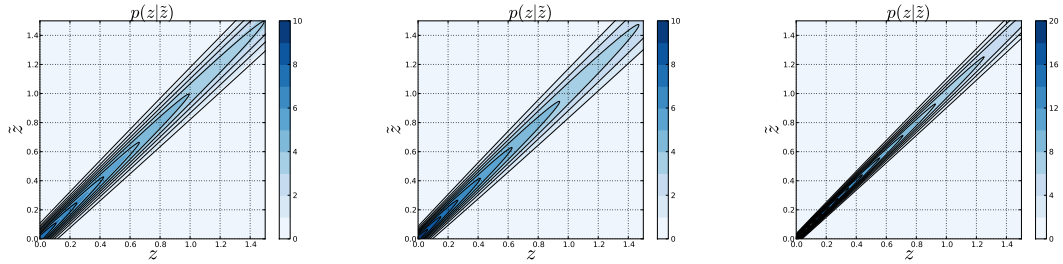

Figure 6.6: The conditional probability function up to a redshift of $z = 1.5$ with a redshift dispersion error given by $\sigma_z(z)$. The fiducial model that we adopt in this Chapter is $\sigma_z(z) = 0.05(1+z)$ on the left most plot. The middle plot is an approximate fitting formula for a 5-band survey and on the far right for a 17-band survey [553]. Note that we have adopted a modified color scale in the final plot for convenience.

6.7.3 Signal To Noise

For two arbitrary data sets X and Y the signal to noise ratio (SNR) of the cross-spectra $\mathcal{C}_\ell^{XY}(k)$ depends on the individual spectra $\mathcal{C}_\ell^{XX}(k)$ and $\mathcal{C}_\ell^{XX}(k)$ as well as the cross-spectra $\mathcal{C}_\ell^{XY}(k)$ itself. The signal to noise for the XY cross-spectra is given as follows

$$[S/N]_\ell(k) = \frac{\mathcal{C}_\ell^{XY}(k)}{\sqrt{\mathcal{C}_\ell^{XX}(k)\mathcal{C}_\ell^{YY}(k) + \left[\mathcal{C}_\ell^{XY}(k)\right]^2}}. \tag{6.89}$$

As an example, we consider the SNR for weak lensing convergence-tSZ cross correlations. From the equation above this simply reduces to (see Fig. 6.7)

$$[S/N]_\ell(k) = \frac{\mathcal{C}_\ell^{\kappa y}(k)}{\sqrt{\mathcal{C}_\ell^{\kappa\kappa}(k)\mathcal{C}_\ell^{yy} + [\mathcal{C}_\ell^{\kappa y}(k)]^2}}. \tag{6.90}$$

We plot a representative signal to noise for our power spectra in Fig. 6.7 for $r = 3600h^{-1}\mathrm{Mpc}$ and $\ell = \{20, 50\}$. At low k the SNR is dominated by the contributions from the tSZ power spectrum via an offset. Remember, both the WL and tSZ-WL power spectra have negligible contributions at very low k as the spectra fall off relatively sharply. As k approaches the peak of the Bessel function at $kr \sim \ell$ the noise induced by the weak lensing power spectra becomes more prominent as does the signal from the tSZ-WL cross-correlation. With regards to worry over low $(S/N)_\ell$, it is important to note that what we have computed is for individual (k, ℓ). We could always include additional ℓ modes in order to increase the overall S/N

$$[S/N](k) = \sum_\ell [S/N]_\ell(k). \tag{6.91}$$

This will preserve all the radial information. In addition, the S/N presented here is purely for cosmic variance limited surveys. More realistically we could include instrumental noise sources and other survey specific errors.

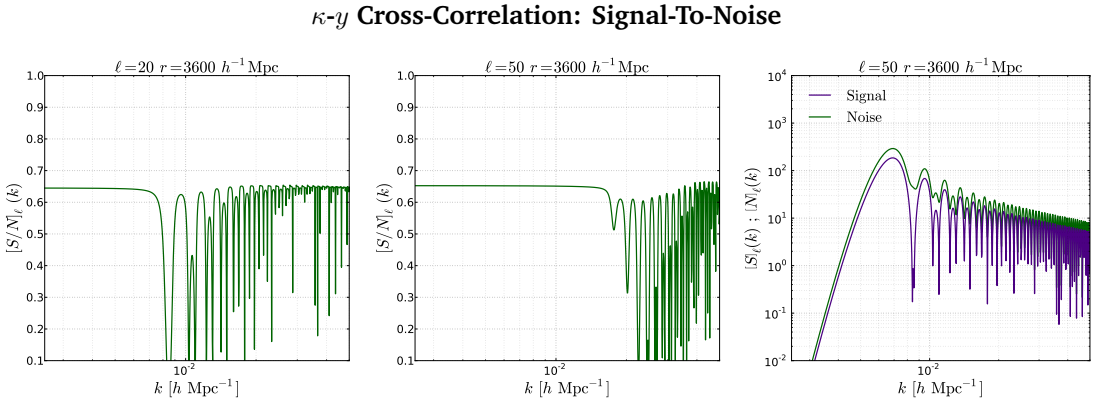

Figure 6.7: We plot the signal-to-noise as defined in Eq. (6.90) for a tSZ-Convergence cross correlation at $\ell = 20, 50$ and $r = 3600h^{-1}\mathrm{Mpc}$. The right most panel is a plot of the signal and noise contributions individually for comparison.

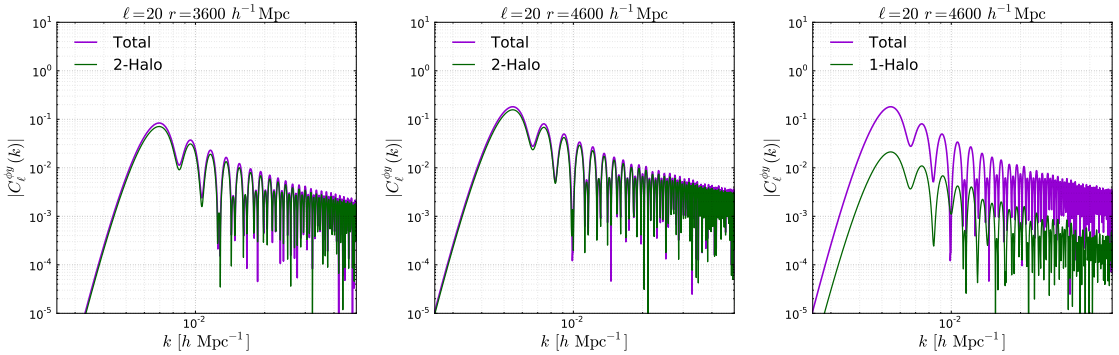

Figure 6.8: The halo model can be used to predict WL-tSZ cross correlation. The figures show the total spectra and the spectra that arises from the 1-halo terms. As expected at these scales, the 2-halo term is dominant and recovers the total spectra to a good degree. The 1-halo terms contribute small but non-negligible corrections to the spectra. This can be seen by inspection of the various power spectra in Fig. G.4, the 1-halo terms fall off too quickly at such low k leaving the 2-halo term dominate.

6.8 The Halo Model: tSZ-Weak Lensing Cross-Correlation

6.8.1 The Halo Model: tSZ-Weak Lensing

Following from the previous results, we can perform an analagous analysis for the tSZ-WL cross-correlation within the halo model framework. The halo model is a tool used in cosmology that provides us with a statistical characterisation of large scale structure and the detailed modelling of its distribution in the Universe. The halo model is based on the proposition that galaxies are clustered in halos distributed throughout space along with a set of basic properties such as the mass or density profile. The halo model is detailed in Appendix G.1 where the framework for calculating various quantities is outlined in detail. In this Chapter we simply use the results to construct the tSZ-WL cross-correlation.

When building the cross correlation in the halo framework, we introduce a number of relatively simple modifications to to Eq. (6.61)-Eq. (6.63) with the changes arising from the halo terms

$$\mathcal{J}^{\phi}_{\ell}(k',k) \equiv k' \int_0^{\infty} dr\, r^2\, j_{\ell}(k'\,r) \int_0^{r} dr' F_{\rm K}(r,r')\, j_{\ell}(kr') \sqrt{P^{\Phi\Phi}(k;r')}\,; \tag{6.92}$$

$$\mathcal{J}^{y}_{\ell}(k) \equiv \bar{T}_e \sqrt{\frac{2}{\pi}} \int_0^{\infty} dr\, w_{\rm SZ}(r)\, j_{\ell}(kr)\, r_{\Pi}(k;r) b_{\Pi}(k;r) \sqrt{P^{\Phi\Phi}(k;r)}\,; \tag{6.93}$$

$$\mathcal{C}^{\phi y}_{\ell}(k) = \frac{4}{\pi c^2} \int_0^{\infty} k'^2 \mathcal{J}^{\phi}_{\ell}(k,k') \mathcal{J}^{y}_{\ell}(k') dk'. \tag{6.94}$$

The bias $b_{\Pi}(k,r)$ in this formalism is not completely ad hoc but is instead an outcome of various inputs and assumptions that go into the halo model. Similar results can be obtained for the 3D cross-correlation of galaxy-surveys against the weak lensing surveys. We adopt the same configurations as for the tSZ-WL cross-correlation defined previously, namely $\ell = \{20, 50\}$ and $r = \{3600, 4600\}\, h^{-1}$Mpc. The results are shown in Fig. 6.8.

6.8.2 The Halo Model: Limber Approximation

As we did previously, we can evaluate the cross-correlation spectra on small angular scales by invoking the Limber approximation. This results in a rather simplified expression for the various terms

$$\mathcal{J}_\ell^\phi(k,k') = \frac{\pi}{2}\,\frac{\nu}{kk'}\,F_{\rm K}\left(\frac{\nu}{k},\frac{\nu}{k'}\right)\sqrt{P^{\Phi\Phi}\left(k';\frac{\nu}{k'}\right)}; \tag{6.95}$$

$$\mathcal{J}_\ell^y(k) = k\sqrt{\nu}\,\bar{T}_e\,w_{\rm SZ}\,\left(\frac{\nu}{k}\right)r_\Pi\left(k;\frac{\nu}{k}\right)b_\Pi\left(k;\frac{\nu}{k}\right); \tag{6.96}$$

$$\mathcal{C}_\ell^{\phi y}(k) = \frac{2\sqrt{\nu}}{c^2}\,\bar{T}_e\int dk' F_K\left(\frac{\nu}{k},\frac{\nu}{k'}\right)w_{\rm SZ}\left(\frac{\nu}{k'}\right)r_\Pi\left(k',\frac{\nu}{k'}\right)b_\Pi\left(k',\frac{\nu}{k'}\right)P^{\Phi\Phi}\left(k',\frac{\nu}{k'}\right); \tag{6.97}$$

$$\nu = \ell + \frac{1}{2}. \tag{6.98}$$

6.8.3 Halo Model: Power Spectra, Cross Spectra and Mass Bins

In addition to the above, we can construct the cross-spectra as a function of mass bins. The halo model, as we saw, is fundamentally dependent on the underlying mass function, see Fig. 6.11 for an example of three different mass bins. This means that at different masses we expect different physics to become more or less dominant. We expect the tSZ to be sensitive to the maximum mass scale and distribution of halos at high masses. This also means that we expect the tSZ to depend on the underlying mass function adopted in the study. Although we have used the Press-Schechter (PS) formalism, there are more modern alternatives that may be used. Examples include the extended Press-Schechter formalism [70], the Sheth-Torman (ST) mass function [523], the Jenkins et al fit [278] and the Tinker et al fit [560]. Each of these has their own pros and cons as well as the underlying assumptions that are fed into the models. For instance the Sheth-Torman mass function is thought to be more accurate at low masses and is a refinement of the Press-Schechter formalism which itself over-estimates the abundance of high mass halos and under-estimates the abundance of low mass halos. In Fig. 6.10 we plot the results obtained from using the ST mass function. These results are preliminary and a more in-depth study of the dependency of the tSZ-WL cross-correlation on the underlying mass function will be presented in a later body of work.

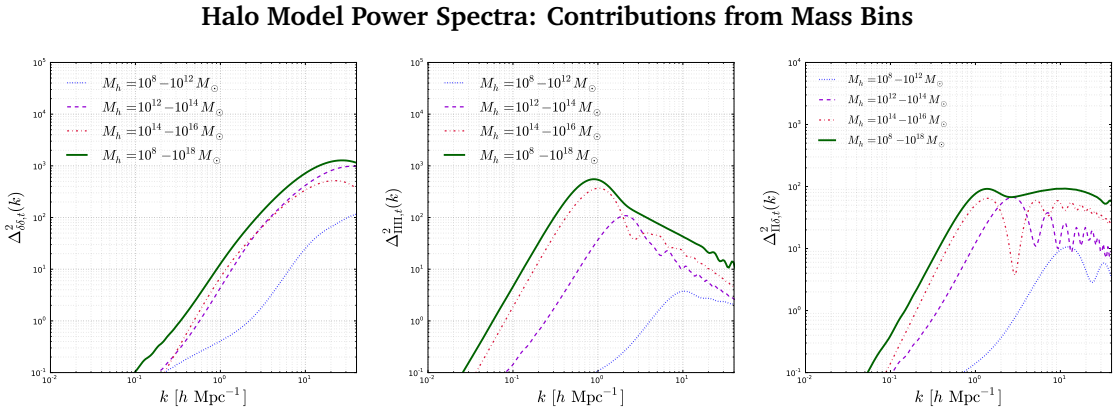

Figure 6.9: The halo model allows us to consider the power spectrum as a function of mass. In this instance we take three different mass scales and look at the contributions to the power spectra in each case. It can clearly be seen that halos at low masses do not contribute significantly to the overall power. Additionally, the low masses are much more sub-dominant in the pressure-pressure spectra and pressure-density spectra than the density-density power alone. The tSZ effect is strongly dependent on the maximum mass. The three mass bins are: $M_h = 10^8 - 10^{12} M_\odot$, $M_h = 10^{12} - 10^{14} M_\odot$ and $M_h = 10^{14} - 10^{18} M_\odot$.

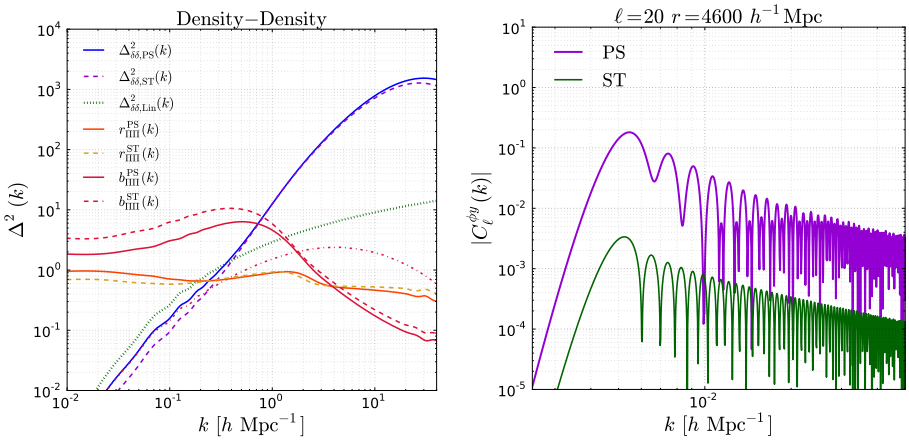

Figure 6.10: The results acquired by using the PS mass function are compared with that from ST mass function. The left panel shows the density-density power spectrum in both PS and ST along with the spectral and bias coefficients. Note that the ST power spectrum is suppressed at very small k but has more power in the pressure-pressure and density-pressure spectra as seen in the cross-spectral coefficient $r_{\Pi\Pi}$. This results in the suppression of the tSZ-WL cross-correlation at the low ℓ modes considered in this Chapter seen in the right panel. Note that for $\ell \sim 20$ the peak of the spectra is on order $10^{-3} - 10^{-2}\ h\mathrm{Mpc}^{-1}$ and this corresponds to the suppressed regime for the ST mass function in the left panel.

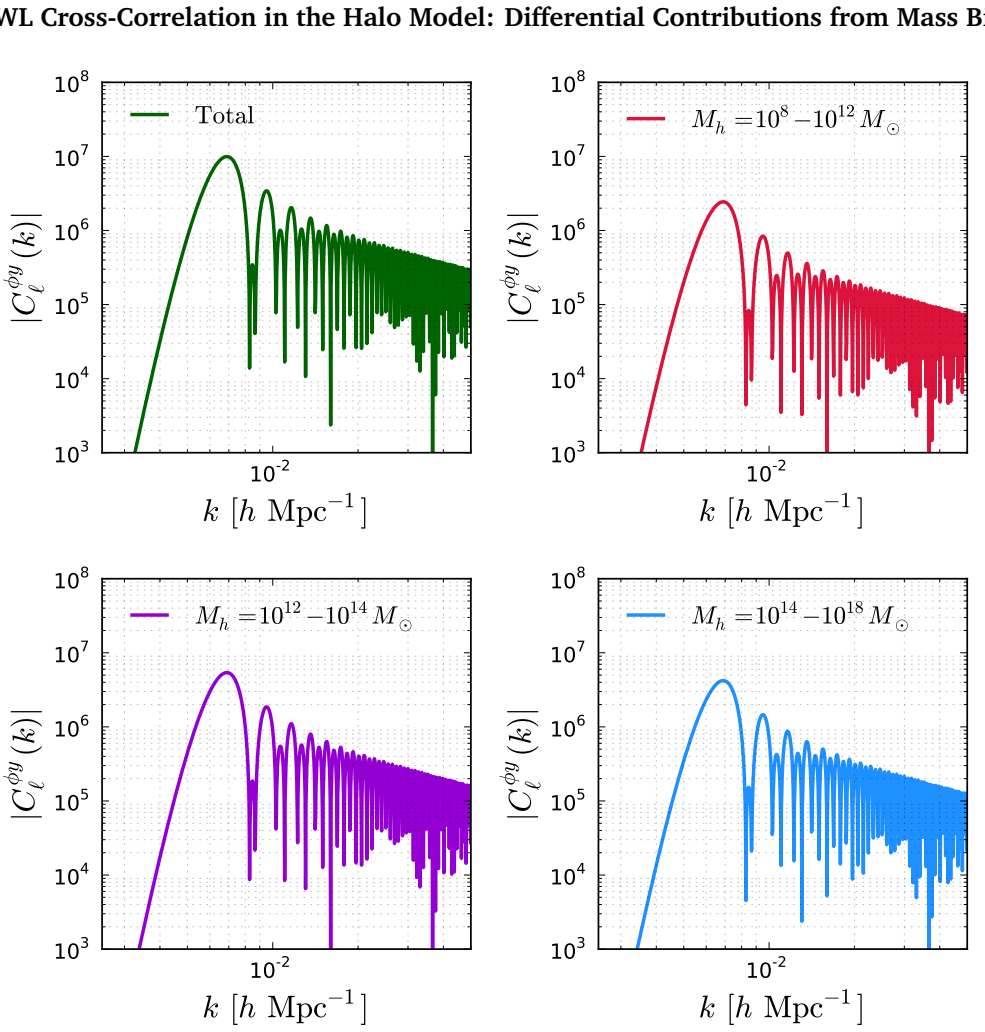

Figure 6.11: In this figure we plot the tSZ-WL cross correlation as a function of mass bin. The upper left panel is the total mass range. The upper right panel is the lowest mass bin $M_h = 10^8 M_\odot - 10^{12} M_\odot$. The lower left panel is an intermediate mass range $M_h = 10^{12} M_\odot - 10^{14} M_\odot$. The lower right panel is the largest mass bin at $M_h = 10^{14} M_\odot - 10^{18} M_\odot$. Note that at high masses the abundance of halos starts to drop off sharply and although the tSZ has strong contributions at high masses, the low abundance suppresses the overall contribution.

6.9 Spectroscopic Redshift Surveys

6.9.1 Introduction

In order to consider the cross-correlation of the tSZ effect with spectroscopic redshift surveys, we need to take into account the partial observation effects that arise from finite survey volumes. In the case of Galaxy surveys, the observed field $\Psi^{\rm obs}(\mathbf{r})$ is convolved with a radial selection function $\phi(r)$ that simply denotes the probability of including a galaxy within a given survey. The observed (*pseudo*) random field can be related to a 3D underlying random field via the survey dependent selection function $\phi(r)$ [452; 435]

$$\Psi^{\rm obs}(\mathbf{r}) = \phi(r)\Psi(\mathbf{r}). \tag{6.99}$$

The observed power-spectrum and the underlying power-spectrum are linked through the following relation [435]:

$$\mathcal{C}_\ell(k_1, k_2) = \int_0^\infty dk'\, k'^2\, \mathcal{I}_\ell^{(0)}(k_1, k')\, \mathcal{I}_\ell^{(0)}(k_2, k')\, P_{\delta\delta}(k') \tag{6.100}$$

$$\mathcal{I}_\ell^{(0)} = \int_0^\infty dr\, r^2\, \phi(r)\, k\, j_\ell(kr) j_\ell(k'r). \tag{6.101}$$

This power spectra will tend to decay rapidly as we move away from the diagonal $k = k'$ and it is often most useful to focus on the diagonal contribution $\mathcal{C}_\ell(k_1, k_1)$. Following the procedure detailed in [435] we can expand these results to include the effect of redshift-space distortions (RSDs). We briefly summarise the key steps but refer the reader to [435] for further details and references. These distortions arise from the effects of a peculiar velocity, or departure from the Hubble flow, $\mathbf{v}(\mathbf{r})$ at $\mathbf{r}$ on the observed galaxy positions in redshift space $\mathbf{s}$

$$\mathbf{s}(\mathbf{r}) = \mathbf{r} + \mathbf{v}(\mathbf{r}) \cdot \hat{\Omega}. \tag{6.102}$$

We then construct the harmonics of the field $\Psi(\mathbf{r})$ convolved with the selection function $\phi(s)$:

$$\tilde{\Psi}_{\ell m}(k) = \sqrt{\frac{2}{\pi}} \int_0^\infty s^2\, ds\, d\hat{\Omega}\, \phi(s) \Psi(\mathbf{r}) j_\ell(ks) Y^*_{\ell m}(\hat{\Omega}). \tag{6.103}$$

The Fourier transform of the velocity field is related to the Fourier transform of the density contrast via the linearised Euler equation:

$$\mathbf{v}(\mathbf{k}) = -i\beta \mathbf{k} \frac{\delta(\mathbf{k})}{k^2}. \tag{6.104}$$

where $\beta = \Omega_m^\gamma / b$ and b is a linear bias parameter. We take $b = 1$ and $\gamma \approx 0.55$ in our numerical calculations. This allows us to establish a series expansion in β where the lowest order coefficient is obtained by neglecting RSD. The series expansion is schematically given by:

$$\tilde{\Psi}_{\ell m}(k) = \tilde{\Psi}^{(0)}_{\ell m}(k) + \tilde{\Psi}^{(1)}_{\ell m}(k) + \ldots \tag{6.105}$$

$$\tilde{\Psi}^{(0)}_{\ell m}(k) = \sqrt{\frac{2}{\pi}} \int_0^\infty dk'\, k'\, \Psi_{\ell m}(k')\, \mathcal{I}^{(0)}_\ell(k', k) \tilde{\Psi}^{(1)}_{\ell m}(k) = \sqrt{\frac{2}{\pi}} \int_0^\infty dk'\, k'\, \Psi_{\ell m}(k')\, \mathcal{I}^{(1)}_\ell(k', k). \tag{6.106}$$

The kernels $\mathcal{I}^{(0)}(k', k)$ and $\mathcal{I}^{(1)}(k', k)$ define the convolution and do depend on the choice of selection function. These kernels are given by:

$$\mathcal{I}^{(0)}_\ell(k, k') = \int_0^\infty dr\, r^2\, \phi(r)\, k\, j_\ell(kr) j_\ell(k'r); \quad \mathcal{I}^{(1)}_\ell(k, k') = \frac{\beta}{k'} \int_0^\infty dr\, r^2 k\, \frac{d}{dr}[\phi(r) j_\ell(kr)] j'_\ell(k'r); \tag{6.107}$$

The power spectra can be calculated from these harmonic coefficients as follows:

$$\left\langle \tilde{\Psi}^{\alpha}_{\ell m}(k) \tilde{\Psi}^{\beta *}_{\ell' m'}(k') \right\rangle = \tilde{\mathcal{C}}^{(\alpha\beta)}_\ell(k, k')\, \delta_{\ell\ell'}\, \delta_{mm'}. \tag{6.108}$$

The total redshifted power spectrum is given as a sum over various contributions:

$$\tilde{\mathcal{C}}_\ell(k_1, k_2) \equiv \sum_{\alpha,\beta} \tilde{\mathcal{C}}^{(\alpha,\beta)}_\ell(k_1, k_2) = \tilde{\mathcal{C}}^{(0,0)}_\ell(k_1, k_2) + 2\tilde{\mathcal{C}}^{(0,1)}_\ell(k_1, k_2) + \tilde{\mathcal{C}}^{(1,1)}_\ell(k_1, k_2) + \cdots; \tag{6.109}$$

$$\tilde{\mathcal{C}}^{(\alpha,\beta)}_\ell(k_1, k_2) \equiv \langle \Psi^{\alpha}_{\ell m} \Psi^{\beta *}_{\ell m} \rangle = \left(\frac{2}{\pi}\right)^2 \int_0^\infty k^2 dk\, \mathcal{I}^{(\alpha)}_\ell(k_1, k)\, \mathcal{I}^{(\beta)}_\ell(k_2, k) P_{\delta\delta}(k). \tag{6.110}$$

Now that we have the machinery in place to construct the spectroscopic redshift survey spectra, we can now construct the cross-correlation between the tSZ pressure fluctuations $y(\Omega)$ and the 3D density contrast δ (Fig. 6.12)

$$\mathcal{C}^{\delta y}_\ell(k) = \frac{4}{\pi^2 c^4} \sum_\alpha \int_0^\infty dk' k'^2 \mathcal{I}^{\alpha}_\ell(k, k') \mathcal{I}^{y}_\ell(k') P_{\delta\delta}(k'); \tag{6.111}$$

In Fig. 6.12 we show features of the 3D tSZ-density power spectrum by taking slices through the full 3D space (k_1, k_2, ℓ). We consider diagonal contributions, $k_1 = k_2$, with a survey up to $r_{\rm max} = 3600 h^{-1}$Mpc, a selection function with radial parameter $r_0 \in \{1400, 3600\}\, h^{-1}$ Mpc and multipoles $\ell = 5, 50$.

6.9.2 Spectroscopic Redshift Surveys: Limber Approximation

Using Limbers' approximation, Eq. (6.101) can be simplified to:

$$\mathcal{C}_\ell(k, k') = \delta_{\rm K}(k - k') \left(\frac{\pi}{2k}\right)^2 \phi^2 \left(\frac{\nu}{k}\right) P_{\delta\delta}(k); \qquad \nu = \ell + \frac{1}{2}. \tag{6.112}$$

and Eq. (6.111) simplifies considerably as the RSD correction terms become negligible in the high ℓ limit. This can be seen from Eq. (2.82) and Eq. (2.82) when substituted into Eq. (6.107). Due to the choice of boundary conditions in the selection function $\phi(r)$ vanishes at $r = 0$ and $r = \infty$, this allows us to reverse the order of integration leading the the above simplifications. This leads to following expressions for the kernels $I^{(0)}_\ell(k, k')$ and $I^{(1)}_\ell(k, k')$

$$I^{(0)}_\ell(k, k') \qquad \equiv \frac{\pi}{2\nu} \frac{1}{k} \phi\left(\frac{\nu}{k}\right) \delta_{1D}(k - k'); \tag{6.113}$$

$$I_\ell^{(1)}(k,k') \equiv \beta\frac{k}{k'}\int_0^\infty r^2 dr \frac{d}{dr}\left[\phi(r) j_\ell(kr)\right] j'_\ell(kr)$$
$$= \beta\frac{k}{k'}\int \phi(r) j_\ell(kr)\left[2r j'_\ell(k'r) + r^2\, k\, j''_\ell(k'r)\right] \quad (6.114)$$
$$= \frac{7}{8}\frac{\pi\beta}{\nu^2}\, k\, \phi\left(\frac{\nu}{k}\right)\delta_{1D}(k-k'). \quad (6.115)$$

Where we have used the following approximate forms for $j'_\ell(x)$ and $j''_\ell(x)$ defined in Eq. (2.82) and Eq. (2.83)

$$j'_\ell(x) \approx -\frac{\pi^{1/2}}{(2\nu)^{3/2}}\delta_{1D}(\nu - x); \quad j''_\ell(x) \approx -\frac{3\pi^{1/2}}{(2\nu)^{5/2}}\delta_{1D}(\nu - x). \quad (6.116)$$

tSZ-Spectroscopic Redshift Survey Cross-Correlation: Total Spectra

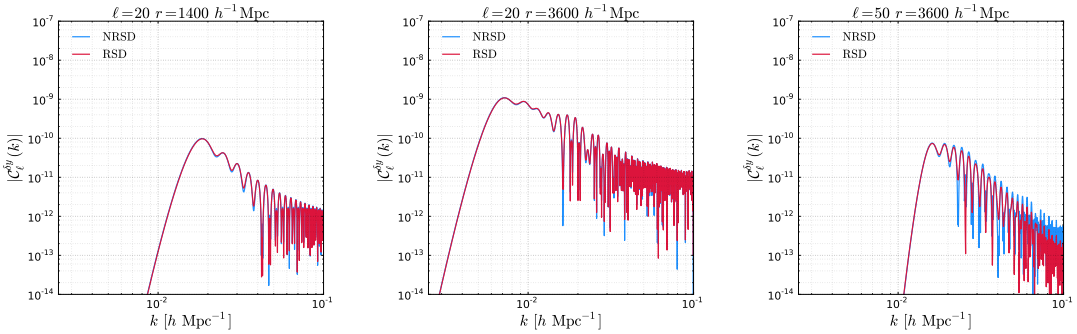

Figure 6.12: Here we plot the effect of redshift space distortions (RSDs) on the galaxy-tSZ cross-correlation. As seen in previous studies [435] the RSDs induce mode-mixing in the power spectra. This occurs due to the redshifted terms being related to derivatives of the spherical Bessel functions which do not form an orthogonal basis. This means that we have off-diagonal elements related to radial mode-mode coupling. As a result the power spectrum is damped. For the spectra shown here, the RSD contributions are rather negligible. For high ℓ we see more prominent contributions, as demonstrated in the right most panel. See Fig. 6.13 for the redshifted spectra divided by the unredshifted spectra isolating the modulations induced by the RSDs.

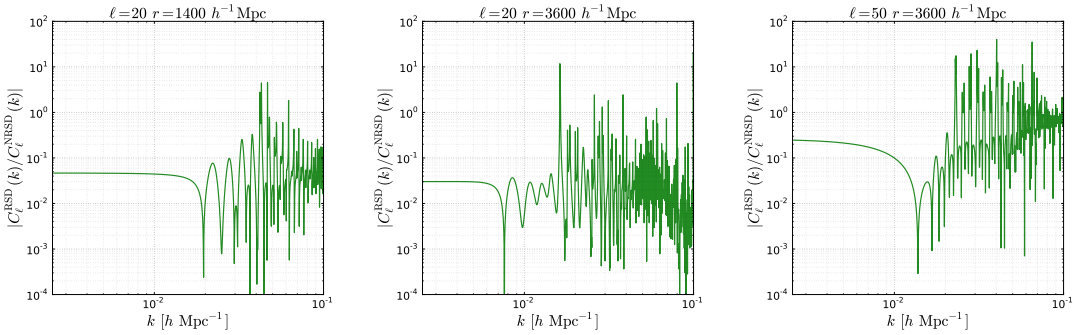

Figure 6.13: Here we plot the effect of redshift space distortions (RSDs) smoothed by the unredshifted power spectra. Each of the panels corresponds to the panels shown in Fig. 6.12. The RSD induce radial mode-mixing meaning that power is smoothed across the modes. This is seen at low k where the spectra including RSD have less power than their unredshifted counterparts. At higher k we hit oscillatory features that differ from those in the pure unredshifted contributions and beyond $k \sim 10^{-1}$ we are in a noise dominated regime where the oscillations of the Bessel functions are prominent and numerics becomes tedious.

6.10 Conclusion

In this Chapter we have extended in detail a study of 3D thermal Sunyaev-Zel'dovich cross correlations with cosmological weak lensing and spectroscopic redshift surveys. Most previous studies to date have focused on either projected studies or tomographic reconstruction. In projection studies, information is lost in the sense that by projecting onto the 2D sky we necessarily disregard information concerning distances to individual sources. An alternative approach is tomography, this is something of a hybrid method between 3D studies and 2D projection. In tomography the sources are divided into redshift slices on which a 2D projection is performed. This means that we foliate our sky with projections in a given redshift bin. This is a rather crude division and does not capture the full 3D information that will be possible in upcoming large scale structure surveys. The method proposed in this Chapter is based on a 3D spherical Fourier-Bessel expansion in which we aim to use distance information from the start. Note that certain parameters will less sensitive to this inclusion of distance information, such as the amplitude of the power spectra, but for others, notably those that depend on the line-of-sight of history of the Universe, 3D methods could be a very promising avenue of research. This Chapter encapsulates a few interesting results as well as summarising some of the key features present in the sFB formalism.

In order to study the tSZ-WL cross correlation, we adopted two different approaches. The first approach used the standard linear power spectrum in the analysis. The second approach used the halo model of large scale clustering to construct a non-linear power spectrum for the analysis. The halo model takes into account a number of interesting physical inputs. These include (amongst other inputs): the dark matter density profile, the gas density profile, the electron temperature as a function of halo mass, the mass function of halos and the overdensity of collapse. This allows us to connect the underlying physics to the predicted spectra in a more explicit manner than before. We know that the tSZ effect is sensitive to the higher mass halos and by combining the WL observations with the tSZ observations we can probe both the underlying baryonic and dark matter distributions as a function of halo mass. We expect the tSZ-WL cross-correlation to be sensitive to the halo mass function and density profiles.

We introduce the conditional probability function of photometric redshifts to bridge survey-dependent observations to the cleaner theoretical predictions. True observations of galaxies have an intrinsic dispersion error on the measured redshifts. In the sFB formalism, redshift errors and errors in distance simply translate into radial errors. This results in a coupling of the modes and the observations become smoothed along our line of sight. We considered survey dependent parameters suitable for the DES and the LSST.

Finally, we constructed the cross-correlation of the tSZ effect with spectroscopic redshift surveys in order to study the effects that redshift space distortions would have on a cross correlation of the tSZ effect with galaxy surveys. The procedure followed the procedure outlined in [435].

In our modelling, we have used different redshift dependent linear biasing schemes at large angular scales for modelling of the diffused tSZ effect in association with the halo-model for collapsed objects as a tool to investigate the tSZ-WL cross-correlations in 3D. We use both the Press-Schechter (PS) as well as the Sheth-Tormen (ST) mass-functions in our calculations, finding that the results are quite sensitive to detailed modelling as most of the contribution to the tSZ effect comes from the extended tail of the mass function (one-halo term). We provide a detailed

analysis of surveys with photometric redshifts. In the case of cross-correlation with spectroscopic redshift surveys we provide detailed estimates of the contributions from redshift-space distortions. The signal-to-noise (S/N) of the resulting cross-spectra $C_\ell(k)$ for individual 3D modes, defined by the radial and tangential wave numbers (k, ℓ), remains comparable to, but below, unity though optimal binning is expected to improve the situation.

In summary, the thermal Sunyaev-Zel'dovich effect acts as a probe of the thermal history of the Universe and the primary observable, the Compton y-parameter, appears to have no significant dependence on the redshift. The integrated nature of the tSZ effect means that redshift information can be lost diminishing our ability to probe the redshift evolution of the baryonic Universe. That is why we also study cosmological weak lensing as a complimentary tracer. Weak lensing is predominantly effected by the gravitational potential along the line of sight and is therefore an external tracer for the underlying dark matter field. By reconstructing the mass distribution of the Universe, we can hopefully recover redshift information and probe the baryonic and dark Universes in a complimentary way. Constraints on the dark sector, such as studies of decaying dark matter or dark matter-dark energy interactions, have recently attracted a lot of attention. Such effects could be probed by the tSZ or kSZ effects (e.g. [599]). Similarly, the halo model for large scale clustering offers strong potential for testing different approaches to the various input ingredients: mass function, dark matter profile, gas density profile, etc. To this extent, we have seen that the tSZ is sensitive to high mass halos and a cross-correlation may be an interesting tool constraining and testing models for large scale clustering physical assumptions that enter the halo model, such as halo density profiles or the halo mass function. In our analysis we neglected General Relativistic corrections which may be both important and interesting in their own right, especially in forthcoming surveys [569; 181; 602; 20; 570]. It would also be interesting to understand how non-Gaussianity and halo bias enters into WL, tSZ and their cross-correlations in a more precise manner [87; 79].

Finally, we would like to point out that it is known that the IGM is most likely have been preheated by non-gravitational sources. The feedback from SN or AGN can play an important role. The analytical modelling of such non-gravitational processes is rather difficult. Numerical simulations [531; 515; 517; 518; 594; 324] have shown that the amplitude of the tSZ signal is sensitive to the non-gravitational processes, e.g. the amount of radiative cooling and energy feedback. It is also not straightforward to disentangle contributions from competing processes. The inputs from simulations are vital for any progress. Our analytical results should be treated as a first step in this direction. We have focused mainly on large angular scales where we expect the gravitational process to dominate and such effects to be minimal. Thus the affect of additional baryonic physics can be separated using the formalism developed here. To understand the effect of baryonic physics we can use the techniques developed in [398] for different components and study them individually.

6.11 Summary of Key Points and Key Results

- Motivated by the missing Baryon problem, we highlighted how the tSZ effect can act as a tracer for the baryonic Universe. Likewise, we highlighted how gravitational weak lensing may be used as a tracer for the dark Universe, which is anticipated to dominate the gravita-

tional potential.

- The tSZ corresponds to a projected, line of sight effect and as such it means that redshift information is smeared out with information becoming entangled with projection effects.

- The redshift information may be recovered by the cross-correlation of the tSZ effect with weak lensing. Previous studies have only used 2D spherical harmonic methods or pseudo-3D tomographic methods.

- We emphasised that upcoming large scale structure surveys, coupled with the Planck all sky y-maps, will provide us with both wide and deep surveys that may be used in the cross correlation. Rather than using pseudo 3D methods, in which information is binned into redshift slices, we advocate the use of the sFB formalism. This approach is both natural, given the survey configurations, and genuinely 3D as it retains the redshift information from the outset.

- We provided explicit formula for the cross-correlation power spectra $\mathcal{C}_\ell^{\phi y}$, with ϕ the weak lensing potential and y the Compton parameter. In addition we provided explicit expressions for writing down the Shear and Flexion cross-correlation spectra. These are related to the potential via spin-raising and spin-lower operations.

- Emphasising the connection to realistic surveys, we introduced a number of survey effects into our approach. We provided explicit expressions for photometric redshift errors, noting that these errors are simply radial errors in the sFB formalism. These expressions were written in terms of the observed convergence harmonics $\tilde{\kappa}_{\ell m}$, which are constructed from a weighted integral over the true underlying convergence harmonics $\kappa_{\ell m}$. The observed harmonics are weighted by the conditional probability relating an observed redshift to the true redshift and an expression for the redshift distribution of source galaxies. We used LSST and DES survey configurations.

- Using these observed convergence harmonics, we constructed the observed sFB power spectra $\tilde{\mathcal{C}}_\ell(k;r)$. This is a more realistic theoretical output that can be compared to observations.

- In addition, we also provided an expression for the signal-to-noise ratio $[S/N]_\ell(k)$ for individual ℓ modes. Here we only take into account cosmic variance contributions and do not extend the expressions as far as instrumental noise contributions.

- Next, we introduced the halo model for large scale galaxy clustering and used this formalism to construct the halo matter power spectrum, written in terms of a bias parameter $b_\Pi(k)$ and a cross-spectral coefficient $r_\Pi(k)$. This lead to a slightly modified expression for the tSZ-WL cross correlation in the halo model. We found that the sFB power spectra was sensitive to the detailed modelling of the astrophysics implicit in the halo model. In addition, we highlighted the dependence of the tSZ-WL cross correlation on the mass range of the mass function that feeds into the halo model. We also used different underlying mass functions, the Press-Schechter and Sheth-Torman functions, in order to highlight how the tSZ-WL effect can be used to probe model dependent effects. An interesting question that can also be asked is with regards to the detailed modelling of the density profile and gas profile.

- In order to compare the sFB results to small angle observations, we used the Limber approximation to derive results for the various sFB power spectra.
- Finally, we derived a set of results for the cross-correlation of the tSZ effect with spectroscopic redshift surveys. Here, the tSZ harmonics are correlated with pseudo harmonics for the observed galaxy clustering field in spectroscopic redshift surveys. We derived the unredshifted results and the results taking into account the linear Kaiser effect. Again, the sFB spectra in the small angle limit were derived using the Limber approximation. We find that RSD do not have a major impact on the tSZ-WL cross correlation.

Chapter 7

Relativistic Cosmology

7.1 Introduction

General Relativity is a theory about differential manifolds with no preferred coordinate charts. It is a theory that is designed to be covariant under general changes of coordinates, there is no reason why coordinates should exist a priori in nature. This is often encapsulated in the statement that General Relativity is a diffeomorphism invariant theory. In essence, this is just a statement to the effect that if we have a spacetime $(\mathcal{M}, g_{ab})$ and a diffeomorphism $\phi : \mathcal{M} \to \mathcal{M}$, then the sets $(\mathcal{M}, g_{ab})$ and $(\mathcal{M}, \phi_* g_{ab})$ will represent the same physics, see [89]. This is just a rather complicated way of stating that General Relativity is coordinate invariant[1] and that diffeomorphisms are the gauge symmetry in general relativity.

This, however, can be a double edged sword as we now have to deal with the *gauge freedom* inherent to General Relativity. This gauge freedom arises in two principal forms: the choice of the coordinates and the freedom to choose a frame basis in the tangent space at each point, we will discuss these points in more detail in due course. First, we outline the problem gauge freedom introduces. Consider the metric tensor which, by definition, is symmetric and hence only has 10 independent components. The vacuum EFEs $G_{ab} = 0$ provides us with 10 independent equations. At first glance this looks nice, but the Bianchi identity $\nabla^b G_{ab} = 0$ reduces the number of independent components by a factor of 4. So in reality we only have 6 independent components, i.e. the metric can be determined up to four arbitrary functions, reflecting the freedom in the choice of coordinate system. In general there will be no natural way to separate the six independent components of g_{ab} in a clear way. In reality, we often impose additional symmetries or restrictions that allows us to achieve such a separation. The 6 degrees of freedom lead to four distinct gravitational phenomena that may be classified as follows: two scalars Ψ and Φ (2 d.o.f), a vector Φ^i (2 d.o.f.) and a tensor E^{ij} (2 d.o.f). These are the true spacetime perturbations as they may not be removed by any change of coordinates.

In many astrophysical and cosmological situations of interest we are not interested in describing an exact spacetime but rather the local features of the model that may be described by introducing small, linear perturbations around the background spacetime. As an example, this

[1] A diffeomorphism can just be viewed as an active coordinate transformation.

is the approach taken when describing the anisotropies of the cosmic microwave background [93; 199; 340; 200; 320; 153] where we introduce linear perturbations around an FLRW spacetime and solve the linearised system of equations. In the next few sections we introduce a number of different ways of tackling perturbation theory in General Relativity, each of which has distinct advantages and disadvantages. The point of view taken in this thesis is that by studying the perturbations to a given spacetime in a number of different approaches, we can start to build up a geometrically and physically meaningful picture that may be related to astrophysical and cosmological observations. Different approaches to a problem often allow us to tackle different aspects of the problem that we are considering.

In Section 7.2 we discuss the notion of gauge invariance and two primary approaches to tackling gauge invariant perturbation theory: the metric approach and the covariant approach. In Section 7.4 we present a detailed and self-contained discussion of the 1+3 [166; 566] covariant and gauge-invariant approach to cosmological perturbation theory. In Section 7.5 we discuss the 1+1+2 formalism [104; 105], a natural extension to the 1+3 formalism adapted to spacetimes with some preferred direction of symmetry. This section also introduces some corrections to the system of equations presented in [105] that become important for a subset of the locally rotationally symmetric (LRS) spacetimes that are vorticity free, the LRS-II spacetimes. In Section 7.6 we introduce an alternative approach based on a covariant 2+2 decomposition of spacetime into spherically symmetric shells and a Lorentzian manifold $\mathcal{M}$ encapsulating the two dynamical coordinates of interest (t, r). The 1+1+2 formalism and the 2+2 formalism will be used in the next two Chapters and lay the foundations for the results presented in this thesis.

7.2 Gauge-Invariant Perturbation Theory

In the following discussion of gauge-invariant perturbation theory, we adopt the framework of [534; 165; 535; 536; 77]. A fundamental problem in General Relativistic perturbation theory is in how we treat perturbations to spacetime itself. Such perturbations give rise to the so-called gauge problem, reflecting the fact that in perturbation theory we are dealing with two spacetime manifolds. The first manifold is the fictional background spacetime $(\bar{\mathcal{M}}, \bar{g}_{ab})$. The second set of manifolds corresponds to a one-parameter family of physical manifolds $\mathcal{M}_\epsilon$ that define smooth deformations from the unperturbed background $\bar{\mathcal{M}}$. Now we must specify a point identification map $\Phi : \bar{\mathcal{M}} \to \mathcal{M}_\epsilon$ that identifies points in the background spacetime $\bar{\mathcal{M}}$ to points in the perturbed spacetime $\mathcal{M}_\epsilon$, such that $\bar{g}_{ab} \to g_{ab} = \bar{g}_{ab} + \delta g_{ab}$. So a *gauge* is simply the one-to-one correspondence $\bar{\mathcal{M}} \to \mathcal{M}_\epsilon$. When we introduce a coordinate system in $\bar{\mathcal{M}}$ the gauge carries it to $\mathcal{M}_\epsilon$. A change in the way we map $\bar{\mathcal{M}} \to \mathcal{M}_\epsilon$ but keeping the background coordinates fixed is known as a gauge transformation. This induces a coordinate transformation in the physical perturbed spacetime but also changes the event in $\mathcal{M}_\epsilon$ that is associated to a particular event in $\bar{\mathcal{M}}$.

This is important as, in our framework, gauge transformations are different from a coordinate transformation, which simply relabels all the events in our spacetime. Consequentially, although we are free to smoothly perturb away from the background spacetime it is by no means a unique process. It will always be possible to choose some alternative background spacetime yielding different values for the perturbed quantity. Intuitively, this tells us that a physical perturbation has been entangled with a spurious artefact generated by the gauge-transformation. This is bad as we

only wish to deal with physically meaningful quantities.

The perturbation of some tensor quantity is the difference between its value at some event in the physical spacetime and its value at the corresponding event in the background spacetime. Following [534; 535; 536] we embed $\mathcal{M}_\epsilon$ as a hypersurface in a 5D manifold $\mathcal{N}$ by introducing the vector field X^A that will be everywhere transverse to $\mathcal{M}_\epsilon$. The points that lie on the integral curve γ of X are then regarded as the same point and are parametrised by $\epsilon\, dx^A/d\epsilon = X^A$. Introducing a geometrical field Q_ϵ defined on $\mathcal{M}_\epsilon$, the perturbation can be defined via a Taylor series along the curve γ

$$\delta Q = Q_\epsilon - \bar{Q} = \epsilon\, \bar{\mathcal{L}}_X Q_\epsilon + \mathcal{O}(\epsilon^2). \tag{7.1}$$

Here, Q_ϵ is the image in $\bar{\mathcal{M}}$ of the perturbed quantity. Frustratingly, quantities that may behave like scalars under general coordinate transformations will not remain invariant under gauge transformations. The perturbation δQ will be completely dependent upon our choice of X and hence our *choice of gauge*. For example, we may opt to fix the gauge by setting surfaces of constant $\bar{Q}$ equal to surfaces of constant Q_ϵ, i.e. $\delta Q = 0$ [165]. The linear perturbation of Q is therefore defined by

$$\delta Q = \epsilon \bar{\mathcal{L}}_X Q_\epsilon \tag{7.2}$$

Computing the difference between two choices of gauge X and Y we find that linear perturbation transforms as

$$\Delta\delta Q = \epsilon \bar{\mathcal{L}}_{X-Y} Q_\epsilon. \tag{7.3}$$

Hence, setting $\xi = \epsilon(X - Y)$ we see that

$$\Delta\delta Q = \bar{\mathcal{L}}_\xi Q_\epsilon \tag{7.4}$$

and that δQ will be gauge-invariant $\Delta\delta Q = 0$ iff $\mathcal{L}_\xi Q_\epsilon = 0$. This holds iff

- $Q_\epsilon = 0$.
- Q_ϵ is a constant scalar.
- Q_ϵ is a linear combination of products of delta functions.

This result is also known as the Stewart-Walker lemma [534] and introduces a well defined set of criteria for gauge-invariant variables. The most useful for us is the first: quantities that vanish in the background spacetime will have well defined perturbations and are natural candidates for gauge-invariant perturbation theory.

7.2.1 Metric Perturbation Theory

One of the most common approaches to describing spacetime is via the metric $g_{ab}(x^k)$, as described in a particular set of local coordinates with the differential properties given by the Christoffel symbols [166]. This is simply called the *metric* approach to General Relativity. Metric based perturb-

ation theory is one of the oldest and most widely used formalisms in the study of perturbations in General Relativity. The approach starts with a metric given in some suitable, often adapted, coordinates and defines perturbations away from this metric. In cosmology, the most widely used application is to study perturbations to the FLRW spacetime. The approach was first introduced to General Relativity in [321] with gauge-invariant completions arising later on [201; 202; 35]. The modern approach is of a more geometric nature and many good reviews exist in the literature [346; 347; 400; 101]. We do not discuss metric based perturbation theory in any significant detail here but simply outline some key details about the approach and how it contrasts with the covariant and gauge invariant approaches. Some of the concepts discussed here will be seen in more detail in our treatment of perturbations in the 2+2 formalism.

The schematic approach to perturbations in this formalism is to introduce linear perturbations to the metric by performing an expansion around the background spacetime

$$g_{ab} = \bar{g}_{ab} + \delta^{(1)} g_{ab} + \delta^{(2)} g_{ab} + \dots, \tag{7.5}$$

where $\delta^{(n)} g_{ab}$ represents the n-th order perturbations. At linear order we construct the linearised curvature tensors and Christoffel symbols and proceed to solve the linearised EFEs. The philosophical point of view in the metric approach is that g_{ab} defines the real, physical spacetime S and $\bar{g}_{ab}$ corresponds to some fictitious background $\bar{S}$, with the linear order perturbations being denoted by $\delta^{(1)} g_{ab}$. This approach is known as a *bottom-top* formalism as we tackle the real spacetime by starting from the fictitious background metric.

The metric approach, being built on a specific choice of coordinates, is plagued by gauge issues. The simplest approach, at linear order, is to systematically find cunning combinations of variables that happen to be gauge invariant under the transformation induced by an infinitesimal change of coordinates [201; 202; 35]. This is due to the fact that the perturbations are dependent on how the map $\Phi : \bar{\mathcal{M}} \to \mathcal{M}$ from $\bar{S}$ to S is chosen. For instance, if we consider a background Universe $\bar{S}$ and we introduce linear perturbations to generate a lumpy Universe S, then the perturbations to each quantity at a given spacetime point can be calculated as the difference between the quantities evaluated in S and $\bar{S}$. As an example, the energy density becomes

$$\delta\mu = \mu - \bar{\mu}. \tag{7.6}$$

However, this approach obscures the reality of the situation as it implies that there exists something special about the way in which the background is related to the bumpy Universe [165]. This is *not* the case and the inverse procedure is *not* unique. Given S can we uniquely reconstruct $\bar{S}$? Without imposing additional restrictions, no. After all, there are infinitely many ways in which we can perturb a family of background spacetimes $\bar{S}$ to recover S. This gives us freedom in the choice of both $\bar{S}$ and Φ called the *gauge freedom*. Similarly, changes to this mapping are known as *gauge transformations*. The result is that the metric approach is non-local, coordinate-dependent but gauge-invariant.

7.2.2 Covariant Perturbation Theory

The gauge-invariant and covariant (GIC) approach of [165; 76; 166; 566] and others holds three distinct advantages over the more standard metric based approaches

1. It allows us to provide a unified treatment of both the exact and linearised theory.
2. The same GI variables are used in perturbing different cosmological models.
3. Gauge invariance of variables is naturally defined due to the Stewart-Walker lemma [534]. If a variable vanishes in the background spacetime it will be gauge-invariant, even under large gauge-transformations.

The first point is principally due to the nature of the GIC approach as a *top-bottom* approach. This means that we start with the full system of equations that govern the real spacetime and linearise about a suitable background spacetime. In this approach we avoid explicit reference to the background and only use it to determine which of our covariant variables are non-zero in the background and hence zeroth order. The linearisation procedure therefore splits the variables into background (zeroth order) plus perturbations (first order). Extending this principle, it is possible to go beyond first order in perturbation theory in a relatively transparent way, though the definition of gauge-invariant variables necessarily becomes more involved. The second point is just another statement with regards to this linearisation procedure. Given the full system of equations, in terms of geometrically well defined variables, then the linearisation procedure is defined with respect to a chosen background spacetime. This means that the geometrical objects will be defined in exactly the same way for perturbations around and FLRW spacetime as they would for a Bianchi spacetime, for example. The final point is a statement regarding the fact that all first order objects are naturally gauge-invariant due to [534]. All variables in the 1+3 and 1+1+2 formalism are geometrically meaningful, by construction, and physically meaningful, due to the natural definition of gauge-invariance in this formalism.

7.3 Locally Rotationally Symmetric Spacetimes

7.3.1 Killing Vector Fields and Isometry Groups

In this section we aim to briefly summarise some of the main key results regarding the symmetry classification of spacetimes and the connection to killing vectors and isometry groups. These ideas will be central to our definition of locally rotationally symmetric (LRS) spacetimes. The concepts in this section closely reflect the discussions in [244; 581; 572; 166; 566; 172].

An isometry of a spacetime $(\mathcal{M}, g)$ is simply a mapping of the manifold $\mathcal{M}$ into itself that leaves the metric tensor g invariant. This operation is encapsulated by the Lie derivative with respect to a vector field ξ, see Appendix E.1.2. The vector field is said to be a generator of a one parameter group of transformations and, likewise, a one parameter group of transformations generates a vector field. The integral curves of the vector field ξ are known as the *orbits* of the group. Invariance of the metric under this operation simply amounts to the requirement that the Lie derivative of the metric with respect to the vector field vanishes, the transformation is then

said to be an isometry

$$\mathcal{L}_\xi g_{ab} = 0. \tag{7.7}$$

This definition is equivalent to the Killing equation

$$\nabla_b \xi_a + \nabla_a \xi_b = 0, \tag{7.8}$$

hence a vector field generating some isometry is also a Killing vector field (KVF), i.e. an isometry of a spacetime is intrinsically linked to the underlying symmetries of the spacetime. We can extend this notion further by nothing that KVFs obey a number of useful relationships, namely

- A linear combination of KVFs will also be a KVF.
- The commutation $[\xi_1, \xi_2]$ of any two KVFs, ξ_1 and ξ_2, will also be a KVF.
- A manifold will admit, at most, a finite number of linearly independent KVFs.

These relations individually are rather unremarkable. However, these relations taken together form what is known as an r-dimensional Lie algebra such that the basis of the algebra is given by ξ_α for $\alpha = 1, 2, \ldots, r$. This is a standard result in group theory, e.g. [493; 315]. The commutation relations, or Lie bracket, of the elements of the Lie algebra $[\xi_\alpha, \xi_\beta]$ are defined by the *structure constants* $C^\mu{}_{\alpha\beta}$ associated to the Lie algebra,

$$[\xi_\alpha, \xi_\beta] = C^\mu{}_{\alpha\beta} \xi_\mu. \tag{7.9}$$

The structure constants are therefore central in determining the group structure of the Lie group. Another standard results that the set of all isometries of a spacetime $(\mathcal{M}, g)$ form a Lie group G_r of dimension r, known as the *isometry group* of the spacetime. The one-dimensional subgroups of G_r define families of curves whose tangent field is associated to a KVF. The Lie group G_r therefore generates the Lie algebra of KVFs or, alternatively, the KVF each define a one-parameter group of isometries and therefore the Lie algebra generate the Lie group. Either way, the concepts of a Lie group, isometries and a KVF are all deeply interconnected. The action of the group on the manifold $\mathcal{M}$ is specified by the orbits of the points in the manifold.

The *orbit* $\mathcal{O}_p$ of the group G_r through a fixed point $p \in \mathcal{M}$ is the set of all points to which elements of G map p. This forms a submanifold of $\mathcal{M}$. The KVFs at the point p are defined to be tangential to the orbit of p. If the dimension of an orbit is equivalent to the dimension of the group, then the group is said to act *simply transitively* on the orbit, otherwise the group acts *multiply transitively*. In the multiply transitive case, the dimension of the orbit s is less than the group dimension r. In the multiply transitive case, the KVFs at a point p are linearly dependent allowing us to form a subspace of the Lie algebra of dimension $d = r - s$ consisting of KVFs that vanish at p. The KVFs on this subspace generate a subgroup of isometries that leave p invariant, called the *isotropy subgroup* $H(p)$ of p. This subgroup generates a group of linear transformations in the tangent space at the point p. As an example, a one-dimensional isotropy group that leaves the timelike vector fixed corresponds to a rotational symmetry at the point p. For an n-dimensional

space both the isometry group G_r and the isotropy subgroup are bounded as follows

$$r \leq \frac{1}{2} n\,(n+1) \tag{7.10}$$

$$d \leq \frac{1}{2} n\,(n-1)\,. \tag{7.11}$$

7.3.2 Classification of Spacetimes

Now that we have introduced KVFs, isometry groups, orbits and the Lie group G_r, we can proceed to classify a cosmological spacetime $(\mathcal{M}, g, \mathbf{u})$, where $\mathbf{u}$ denotes a preferred timelike vector field, s the dimension of the orbits and d the dimension of the isotropy subgroup [2]. As such, d will determine the isotropy of the spacetime and s the homogeneity. The dimension s is sometimes referred to as the dimension of the orbits of the maximal group of motions, e.g. [172].

A spacetime is *spatially homogeneous* is there are spatial hypersurfaces $\{t = \text{const}\}$ for which any point can be moved to any other point by an isometry. This is possible if and only if there are at least three independent KVFs at all points on these hypersurfaces. Similarly, a spacetime is said to be *spherically symmetric* if we can foliate the spacetime by spacelike 2-spheres S^2 everywhere in which the rotation group $O(3)$ acts as an isometry group.

7.3.2.1 Isotropy

In a cosmological spacetime, the isotropy group acts on a three-dimensional tangent space orthogonal to $\mathbf{u}$ that leaves $\mathbf{u}$ invariant. This means that the isotropy group can have dimension d of at most 3. It is not possible for the isotropy subgroup to have a dimension of $d = 2$ as there do not exist any subgroups of dimension 2 of the full 3-dimensional rotation group.

For the isotropy subgroup we have four principle possibilities:

- ***Isotropic and Constant Curvature*** K $(d = 6)$. These spacetimes have isotropic spatial sections with constant Gaussian curvature K. A good example of such a spacetime is the de Sitter spacetime, though it can be argued that this is not a cosmologically relevant spacetime as other matter fields will always be present.

- ***Isotropic*** $(d = 3)$. The isometry group will have a dimension of at least $r = 6$, corresponding the spacetime homogeneous $(s = 4)$ and spatially homogeneous $(s = 3)$ models. This group is the case for the FLRW models for which all spatial directions are equivalent, the Weyl tensor vanishes and all kinematical quantities, except for Θ, vanish.

- ***Local Rotational Symmetry (LRS)*** $(d = 1)$. In these models, there exists one preferred spatial direction $\mathbf{n}$ for which all kinematical and observable quantities are rotationally symmetric about. The Weyl tensor is of Type-D [3]. These LRS models can be split into three classes, I-III [161]. In an LRS-I spacetime, $\mathbf{u}$ is rotating and the metric admits a G_4 group on the timelike hyperplanes. In an LRS-II spacetime, the planes defined by $\mathbf{u}$ and $\mathbf{n}$ are integrable, vorticity free, and there is a G_3 group acting on the 2-surfaces orthogonal to these

[2] Note that we have adopted the notation of [581]. Other conventions, e.g. [172], adopt d as the dimension of the orbits and s as the dimension of the isotropy subgroup.

[3] In the Petrov classification, a Type-D spacetime possesses two double principal null directions, defining radially ingoing and outgoing null congruences. In the Newman-Penrose formalism we demand that $\Psi_0 = \Psi_1 = \Psi_3 = \Psi_4 = 0$.

planes. Finally, in an LRS-III spacetime, the planes are non-integrable and the spacetimes are spatially homogeneous. A spacetime is therefore said to be locally rotationally symmetric if there exists a continuous isotropy group at each point and is hence characterised by the existence of a multi-transitive isometry group acting on the spacetime manifold.

- ***No Isotropy*** $(d = 0)$. In these models, all spacetime directions are inequivalent, though discrete isotropies may be permitted.

7.3.2.2 Homogeneity

- ***Spacetime Homogeneous*** $(s = 4)$. These models are unchanging in both time and space. These models do not constitute useful, realistic cosmological models. In the isotropic case, $d = 3 \Rightarrow r = 7$, we have the Einstein static Universe. This is corresponds to a non-expanding FLRW spacetime and was the first relativistic cosmological model. For the LRS case, $d = 1 \Rightarrow r = 5$, we have the Gödel spacetime [205], a stationary rotating model. Finally, we can have anisotropic models, $d = 0 \Rightarrow r = 4$, which have been completely characterised [419; 420].

- ***Spatially Homogeneous*** $(s = 3)$. These models are homogeneous on 3-dimensional orbits. The case of prime interest in cosmology is for spacelike orbits, hence spatially homogeneous. The field equations reduce to a system of ordinary differential equations. As before, we can subdivide this group based on various isotropy subcases. For $d = 3$, we have the family of FLRW spacetimes. For $d = 1$ we have spatially homogeneous LRS spacetimes and Kantowski-Sachs models. For $d = 0$ we obtain the anisotropic Bianchi models, which posses a transitive group G_3 of isometries acting on the spacelike hypersurfaces. These are subdivided into nine types (Bianchi I to IX) and two classes: *tilted* or *orthogonal*.

- ***Spatially Inhomogeneous*** $s \leq 2$. For $s = 2$ we have a spacetime that is homogeneous on 2-dimensional orbits. As before, the case of interest is for 2-dimensional spacelike orbits. These models will be time-dependent and can be characterised as spatially inhomogeneous with one spatial degree of freedom, e.g. a radial profile. The field equations reduce to a system of partial differential equations in terms of two dynamical coordinates: time and the one spatial degree of freedom. The isotropy subcases are $d = 1$, the inhomogeneous LRS models, and $d = 0$, such as the Abelian G_2 spacetime. The inhomogeneous LRS cases $(d = 1 \rightarrow s = 2, r = 3)$ have a metric of the form

$$ds^2 = -C^2(t, r)dt^2 + A^2(t, r)dr^2 + B^2(t, r)d\Omega^2. \tag{7.12}$$

The LTB spacetime is an important subgroup of this class of spacetimes and will be extensively discussed in Chapter 9. Few models with $s \leq 1$ are known and even fewer have been seriously used as cosmological models. Finally, we note the existence of solutions with no symmetries $(r = 0 \Rightarrow s = 0, d = 0)$. The real Universe is an example of this class of model.

7.4 1+3 Formalism

7.4.0.3 Introduction

The covariant approaches to General Relativity and cosmology were originally introduced in pioneering work by Heckmann, Schücking and Raychaudhuri in the 1950s [246; 453] and has undergone many developments by many authors [159; 160; 307; 565; 161; 242; 533; 162; 243; 163; 120; 121; 244]. More recent reviews may be found in [166; 566; 172]. In this section we outline the basic features of the 1+3 covariant formalism and discuss key results. These equations will form the basis for all of the work we do in the 1+1+2 formalism and many of the concepts will carry through. This section is designed to be relatively self contained and should serve as a useful reference for the work throughout the next two Chapters.

7.4.0.4 Locally Splitting Spacetime

Consider a spacetime $(\mathcal{M}, \mathbf{g})$ and introduce a preferred timelike congruence[4] generated by a set of observers with 4-velocity

$$u^a = \frac{dx^a}{d\tau}, \qquad u_a u^a = -1, \tag{7.13}$$

such that τ is the proper time measured by the observers. Given u^a at each point p, the tangent spaces to spacetime are split in the form $R \otimes H$ in which we identify a subspace H_p of the tangent space T_p at p which is orthogonal to u^a. The collection of these subspaces is called a *smooth specification*. In more physical terms, the velocity field introduces a local threading of spacetime into time and space. The existence of a preferred timelike congruence implies the existence of a preferred rest frame that defines the surfaces of simultaneity for the observers. Given u^a, we can define two unique projection tensors that decompose tensors into parts orthogonal to the timelike congruence and parts parallel to the timelike congruence. The *orthogonal projection tensor* is defined by

$$h_{ab} = g_{ab} + u_a u_b \tag{7.14}$$

and corresponds to the induced effective metric tensor of the 3-surfaces orthogonal to u^a in the vorticity-free case. This will project tensor objects into the instantaneous rest space of the congruence. The projection tensor h_{ab} has the following properties:

$$h^a{}_b\, h^b{}_c = h^a_c \tag{7.15}$$

$$h^a{}_a = 3 \tag{7.16}$$

$$h^a{}_b u^b = 0. \tag{7.17}$$

[4] A congruence is just a set of curves in some open region of spacetime such that every point in the region lies precisely on one curve. If the geodesics cross, the congruence comes to an end at that point.

1+3 Spitting of Spacetime

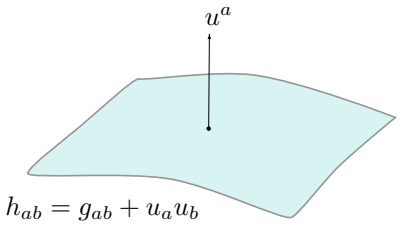

Figure 7.1: Here we show the schematic decomposition of spacetime into a preferred timelike congruence and the concomitant orthogonal surfaces. In the vorticity free case these are just spatial 3-surfaces and u^a is genuinely hypersurface orthogonal.

Secondly, we define the *parallel projection tensor* that projects tensors parallel to the timelike congruence:

$$U^a{}_b = -u^a u_b. \tag{7.18}$$

This *parallel projection tensor* obeys the following relationships:

$$U^a{}_c\, U^c{}_b = U^a{}_b \tag{7.19}$$

$$U^a{}_a = -1 \tag{7.20}$$

$$U_{ab}\, u^b = u_a. \tag{7.21}$$

The tensors U_{ab} and h_{ab} allow us to project any tensor object into parts parallel and orthogonal to u^a. A fundamental example is of the metric tensor itself

$$g_{ab} = h_{ab} + U_{ab}, \tag{7.22}$$

where $g_{\perp ab} = h_{ab}$ and $g_{\parallel ab} = U_{ab}$. The interval in an arbitrary spacetime can therefore be decomposed as follows

$$ds^2 = g_{\mu\nu}\, dx^\mu\, dx^\nu = -\left(u_\mu\, dx^\mu\right)^2 + h_{\mu\nu}\, \left(dx^\mu\, dx^\nu\right). \tag{7.23}$$

7.4.0.5 Volume Element

In the instantaneous rest spaces, there exists a naturally defined *volume element*:

$$\epsilon_{abc} = u^d\, \eta_{dabc}, \tag{7.24}$$

where η_{abcd} is the standard 4-dimensional volume element:

$$\eta_{0123} = \sqrt{|\det g_{ab}|} \tag{7.25}$$

$$\eta_{abcd} = \eta_{[abcd]}. \tag{7.26}$$

The volume element of the spacetime may be re-written in terms of the volume element of the 3-surfaces

$$\eta_{abcd} = 2\epsilon_{ab[c}u_{d]} - 2u_{[a}\epsilon_{b]cd} \tag{7.27}$$

and the volume element of the 3-surfaces obeys the following identities:

$$\epsilon^{abc}\,\epsilon_{def} = 3!\,h^{[a}{}_{d}\,h^{b}{}_{e}\,h^{c]}{}_{f} \tag{7.28}$$

$$\epsilon^{abc}\,\epsilon_{cef} = 2!\,h^{[a}{}_{e}\,h^{b]}{}_{f} \tag{7.29}$$

$$\epsilon^{abc}\,\epsilon_{bcf} = 2!h^{a}{}_{f} \tag{7.30}$$

$$\epsilon^{abc}\,\epsilon_{abc} = 3!. \tag{7.31}$$

7.4.0.6 Derivatives

Having defined the fundamental observer and the corresponding instantaneous rest space, we are now in a position to define two preferred derivatives. The first derivative is a time derivative constructed by taking a convective derivative of a tensor along the worldline of the observer:

$$\dot{T}^{a\ldots b}{}_{c\ldots d} = u^{e}\,\nabla_{e}T^{a\ldots b}{}_{c\ldots d}. \tag{7.32}$$

The second derivative corresponds to a a totally projected derivative in the rest space of the observer:

$$D_{e}T^{a\ldots b}{}_{c\ldots d} = h^{a}{}_{f}\ldots h^{b}{}_{g}\,h^{p}{}_{c}\ldots h^{q}{}_{d}\,h^{r}{}_{e}\nabla_{r}T^{f\ldots g}{}_{p\ldots q}. \tag{7.33}$$

Using these definitions, we can calculate the derivatives of the orthogonal projection tensor and volume element of 3-surfaces:

$$D_{a}h_{bc} = 0 \tag{7.34}$$

$$D_{a}\epsilon_{bcd} = 0 \tag{7.35}$$

$$\dot{h}_{ab} = 2u_{(a}\dot{u}_{b)} \tag{7.36}$$

$$\dot{\epsilon}_{abc} = 3\,\epsilon_{d[ab}u_{c]}\,\dot{u}^{d}. \tag{7.37}$$

7.4.0.7 Decomposition of Tensors

We denote the orthogonal projections of vectors and the orthogonally projected symmetric trace-free (PSTF) part of tensors with angle brackets:

$$v^{\langle a\rangle} = h^{a}{}_{b}v^{b} \tag{7.38}$$

$$T^{\langle ab\rangle} = \left[h^{(a}{}_{c}\,h^{b)}{}_{d} - \frac{1}{3}h^{ab}h_{cd}\right]T^{cd}. \tag{7.39}$$

Angle brackets also denote the orthogonal projections of the convective time-derivatives along u^a (Fermi Derivatives):

$$\dot{v}^{\langle a\rangle} = h^a{}_b \dot{v}^b \tag{7.40}$$

$$\dot{T}^{\langle ab\rangle} = \left[h^{(a}{}_c h^{b)}{}_d - \frac{1}{3}h^{ab}h_{cd}\right]\dot{T}^{cd}. \tag{7.41}$$

Any rank-2 tensor has an irreducible covariant decomposition

$$S_{ab} = \frac{1}{3}\,S\,h_{ab} + S_{[ab]} + S_{\langle ab\rangle}. \tag{7.42}$$

where $S = S_{cd}h^{cd}$. The antisymmetric part may be written in terms of a spatial dual vector, $S^a = \frac{1}{2}\epsilon^{abc}S_{bc}$.

7.4.1 Kinematical Variables

The motion of our set of observers can be covariantly characterised by the irreducible kinematical quantities of the timelike congruence. These variables can be defined by splitting the covariant derivative of u^a into its irreducible parts:

$$\nabla_a u_b = -u_a\dot{u}_b + D_a u_b \tag{7.43}$$

$$= -u_a\dot{u}_b + \frac{1}{3}h_{ab}\Theta + \sigma_{ab} + \omega_{ab}. \tag{7.44}$$

The fundamental kinematical quantities are:

- Expansion

$$\Theta = \nabla_a u^a = D_a u^a, \tag{7.45}$$

  which is defined to be the 3-divergence of the timelike congruence. Physically, the expansion is the volume rate of expansion of the fluid elements. A characteristic length scale can be defined by the volume change of the fluid.

- Acceleration

$$\dot{u}^a = u^b\nabla_b u^a, \tag{7.46}$$

  which describes the motion of the congruence under forces other than gravity. This means that for a freely falling, geodesic observer the acceleration of the congruence will vanish.

- Shear

$$\sigma_{ab} = D_{\langle a}u_{b\rangle}, \tag{7.47}$$

  defines a form of anisotropic expansion of the congruence. For pure shear of the spacetime, we have a distortion without rotation or change of volume. For instance, if there is expansion

in a given direction then there must be a contraction in at least one other orthonormal direction.

- Vorticity

$$\omega_{ab} = D_{[a}u_{b]}, \tag{7.48}$$

is the rate of rotation of the timelike congruence. In the case of pure vorticity, the timelike congruence will only have rotation and no distortion or change of volume.

7.4.2 Matter Fields

In this thesis we are primarily concerned with an energy-momentum tensor that is sourced by an imperfect fluid. Other typical energy-momentum sources include multi-component fluids, gas of particles, electromagnetic fields, gauge-fields (e.g. scalar fields, Yang-Mills fields, (non-)abelian vector fields, spinning particles and so on. The energy-momentum tensor of a general imperfect fluid can be decomposed into its irreducible parts with respect to the fundamental observers as follows:

$$T_{ab} = \mu u_a u_b + p h_{ab} + 2q_{(a}u_{b)} + \pi_{ab}. \tag{7.49}$$

Each of these components has a well defined physical interpretation:

- Relativistic energy density

$$\mu = T_{ab}\, u^a u^b. \tag{7.50}$$

- Isotropic pressure

$$p = \frac{1}{3} T_{ab} h^{ab}. \tag{7.51}$$

- Relativistic momentum density

$$q_a = T_{\langle a\rangle b} u^b. \tag{7.52}$$

- Anisotropic pressure

$$\pi_{ab} = T_{\langle ab\rangle}. \tag{7.53}$$

The relativistic momentum density can be interpreted as the heat flow (or energy flux) relative to the timelike congruence, $q_a u^a = 0$. The anisotropic pressure is both trace-free, $\pi^a{}_a = 0$, and orthogonal to the timelike congruence, $\pi_{ab}u^b = 0$. The trace of the energy-momentum tensor is given by

$$T = T^a{}_a = 3p - \mu. \tag{7.54}$$

In order to model a physical imperfect fluid, we have to define an equation of state that determines the type of matter that we are considering. The equation of state is $p = p(\mu, s)$, where s is the entropy density. One of the most common choices of matter is that of pressureless dust (Cold Dark Matter, CDM) for which $p = 0$, this will be important for the Lemâitre-Tolman-Bondi spacetimes. Alternatively, we may choose to study the EFEs without reference to a specific energy-momentum source. In this situation it is often very useful to impose an energy condition to limit the arbitrariness of the energy-momentum tensor for a wide range of sources. The energy conditions represent covariant restrictions on the energy-momentum tensor [89] that can typically be expressed in terms of scalars constructed from the projection of T_{ab} with respect to timelike t^a, spacelike s^a or null l^a vectors. Some of the most common energy conditions are as follows:

- Weak Energy Condition (Type I)

$$T_{ab}t^a t^b = 0 \qquad \forall t^a \qquad \Rightarrow \qquad \mu \geq 0 \quad \mu + p \geq 0. \tag{7.55}$$

- Null Energy Condition

$$T_{ab}l^a l^b = 0 \qquad \forall l^a \qquad \Rightarrow \quad \mu + p \geq 0. \tag{7.56}$$

  The energy density can now be negative so long as there is a compensatory positive pressure.

- Dominant Energy Condition

$$T^{00} \geq |T^{ab}| \qquad \mu \geq |p|. \tag{7.57}$$

  The dominant energy condition is simply the weak energy condition plus the statement that the pressure should not exceed the energy density. This condition holds for all known forms of matter, though inflationary cosmology requires that the strong energy condition be violated in the standard field theoretic models.

- Null Dominant Energy Condition

$$T_{ab}l^a l^b \geq 0 \qquad T_{ab}T^b{}_c l^a l^c \leq 0 \qquad \Rightarrow \qquad T^{00} \geq |T^{ab}|, \tag{7.58}$$

  where $\mu = -p$ is now allowed. The NDEC excludes all sources excluded by the DEC but allows for negative vacuum energy [89].

- Strong Energy Condition

$$\left(T_{ab} - \frac{1}{2}T g_{ab}\right) t^a t^b > 0 \qquad \Rightarrow \qquad \mu + 3p > 0 \qquad \mu + p > 0. \tag{7.59}$$

  It is the SEC that implies that gravitation is an attractive force, e.g. any non-zero energy-momentum content induces a negative expansion of the timelike congruences. This is just Raychaudhuri's equation.

Most classical states of matter obey the DEC which means that they also obey the less restrictive WEC, NED and NDEC. The SEC can be violated by certain forms of matter, notably a massive scalar

field. This violation of the SEC is exactly what we see and demand in inflationary cosmology, where a scalar field exists in some initially excited state such that its potential energy dominates over its kinetic energy.

7.4.3 The Gravitational Field

The curvature of spacetime is encoded in the Riemann curvature tensor $R_{abc}{}^{d}$ and can be related to the commutation of derivatives acting on a vector field V^d:

$$2\nabla_{[a}\nabla_{b]}V_c = R_{abcd}V^d. \tag{7.60}$$

This is known as the Ricci identity and describes the breakdown of commutativity of derivatives when parallel transporting a vector on a generic manifold. When parallel transported in a small closed curve, a vector will fail to return to it's initial value in a general curved spacetime. The Riemann tensor has the following important symmetries

$$R_{abcd} = R_{[ab][cd]} = R_{cdab} \tag{7.61}$$

$$R_{[abc]}{}^{d} = 0. \tag{7.62}$$

The Riemann tensor also obeys the following differential identity known as the Bianchi identity

$$\nabla_{[a}R_{bc]d}{}^{e} = 0. \tag{7.63}$$

The Ricci tensor is defined by a contraction $R_{ab} = R_{acb}{}^{c}$ and the Ricci scalar is defined by a further contraction $R = R^{a}{}_{a}$. When twice contracted, the Bianchi identity implies $\nabla^b G_{ab} = 0$ such that $\nabla^b T_{ab} = 0$,

$$\nabla_a R^{a}{}_{b} + \nabla_e R^{e}{}_{b} - \nabla_b R = 0 \longleftrightarrow \nabla^a G_{ab} = 0. \tag{7.64}$$

In General Relativity, the Ricci tensor describes the local gravitational field at each point arising due to the local matter content. The gravitational field also has a non-local contribution that is mediated by tidal forces and gravitational waves. This non-local long-range field is encoded in the Weyl tensor C_{abcd}. The decomposition of the Riemann tensor into local and non-local terms is given as follows:

$$R_{abcd} = C_{abcd} + \frac{1}{2}\left(g_{ac}\,R_{bd} + g_{bd}\,R_{ac} - g_{bc}\,R_{ad} - g_{ad}R_{bc}\right) - \frac{1}{6}R\left(g_{ac}\,g_{bd} - g_{ad}\,g_{bc}\right). \tag{7.65}$$

Given a timelike congruence u^a, we can decompose the Weyl tensor into its irreducible parts. This simplifies somewhat as the Weyl tensor is trace-free, $C^{c}{}_{acb} = 0$. The two dynamical components of the Weyl tensor are called the Electric and magnetic Weyl curvature components:

$$E_{ab} = C_{acbd}\,u^c\,u^d \tag{7.66}$$

$$H_{ab} = \frac{1}{2}\epsilon_{acd}C^{cd}{}_{be}\,u^e. \tag{7.67}$$

We can now re-write the Weyl tensor in terms of these two dynamical objects:

$$C_{ab}{}^{cd} = 4\left(u_{[a}\,u^{[c} + h_{[a}{}^{[c}\right)E_{b]}{}^{d]} + 2\epsilon_{abe}u^{[c}H^{d]e} + 2u_{[a}H_{b]e}\epsilon^{cde}. \tag{7.68}$$

The electric and magnetic parts of the Weyl tensor encapsulate the free gravitational field that permits the existence of tidal forces and gravitational waves as well as influencing the motion of matter, as can be seen in the geodesic equation for timelike and null vectors [336; 337; 339; 166; 566]. These tensors are spatial, symmetric and trace-free.

With the above decomposition of the Weyl tensor in place, we now need two more variables in 1+3 notation before we can perform a 1+3 decomposition of the full Riemann tensor. The first of these is the Ricci scalar, the twice contracted Riemann tensor. This can be expressed in a 1+3 form by taking the trace of the EFEs assuming an imperfect fluid source as our energy-momentum tensor. The Ricci scalar reduces to an expression in terms of the matter variables and cosmological constant

$$R = \mu - 3p + 4\Lambda. \tag{7.69}$$

Now we substitute the Ricci scalar into the EFEs to isolate the Ricci tensor:

$$R_{ab} = \frac{1}{2}\left(\mu + 3p - 2\Lambda\right)u_a u_b + \frac{1}{2}\left(\mu - p + 2\Lambda\right)h_{ab} + 2u_{(a}q_{b)} + \pi_{ab}. \tag{7.70}$$

All that is left to do is to substitute these expressions, and those for the Weyl tensor, into the decomposition of the Riemann tensor. Consequentially we see that the curvature tensor can be written in terms of a perfect fluid contribution, an imperfect fluid contribution and contributions form the Electric and Magnetic Weyl sectors:

$$R^{ab}{}_{cd} = R^{ab}_{P\ cd} + R^{ab}_{I\ cd} + R^{ab}_{E\ cd} + R^{ab}_{H\ cd} \tag{7.71}$$

$$R^{ab}_{P\ cd} = \frac{2}{3}\left(\mu + 3p - 2\Lambda\right)u^{[a}\,u_{[c}\,h^{b]}{}_{d]} + \frac{2}{3}\left(\mu + \Lambda\right)h^{[a}{}_{[c}\,h^{b]}{}_{d]}, \tag{7.72}$$

$$R^{ab}_{I\ cd} = -2\,u^{[a}\,h^{b]}{}_{[c}\,q_{d]} - 2\,u_{[c}\,h^{[a}{}_{d]}\,q^{b]} - 2\,u^{[a}\,u_{[c}\,\pi^{b]}{}_{d]} + 2\,h^{[a}{}_{[c}\,\pi^{b]}{}_{d]}, \tag{7.73}$$

$$R^{ab}_{E\ cd} = 4\,u^{[a}\,u_{[c}\,E^{b]}{}_{d]} + 4\,h^{[a}{}_{[c}\,E^{b]}{}_{d]}, \tag{7.74}$$

$$R^{ab}_{H\ cd} = 2\,\epsilon^{abe}\,u_{[c}\,H_{d]e} + 2\,\epsilon_{cde}\,u^{[a}\,H^{b]e}. \tag{7.75}$$

7.4.4 Evolution and Constraint Equations

The fundamental equations describing spacetime in the 1+3 formalism can be derived using the Einstein Field Equations and their associated integrability conditions. As we have previously seen the fundamental gravitational variables that covariantly characterise our spacetime in the 1+3 formalism are given by:

$$\mathbf{X}_{\text{grav}} = \{\Theta, \dot{u}_a, \sigma_{ab}, \omega_{ab}, E_{ab}, H_{ab}\} \tag{7.76}$$

and the fundamental matter variables are given by:

$$\mathbf{X}_{\text{matter}} = \{\mu, p, \Lambda, q_a, \pi_{ab}\}\,. \tag{7.77}$$

Together these 11 variables provide a complete covariant description for spacetimes sourced by an imperfect fluid. Naturally, for additional energy-momentum sources we need to introduce additional variables. Such examples include scalar fields, electromagnetism, gauge-fields, etc.

The first set of equations arise from the Ricci identities. In this instance we take our fundamental observers as the vector field and separate the identity into a part parallel to the timelike congruence and an orthogonally projected part decomposed into the trace, skew symmetric and symmetric trace-free terms. The equations separate into propagation equations (involving convective time derivatives) and constraint equations (involves purely spatial derivatives). The propagation equations are:

- Raychaudhuri Equation

$$\dot{\Theta} = D_a \dot{u}^a - \frac{1}{3}\Theta^2 + (\dot{u}_a \dot{u}^a) - 2\sigma^2 + 2\omega^2 - \frac{1}{2}(\mu + 3p) + \Lambda, \tag{7.78}$$

  this equation encapsulates the attractive nature of the gravitational field. Terms arising from energy-momentum sources give rise to a negative expansion of our timelike congruence corresponding to gravitational collapse.

- Vorticity Equation

$$\dot{\omega}^{\langle a\rangle} = \frac{1}{2}\eta^{abc} D_b \dot{u}_c - \frac{2}{3}\Theta\omega^a + \omega^b \sigma^a{}_b, \tag{7.79}$$

  describing the evolution of vorticity.

- Shear Equation

$$\dot{\sigma}^{\langle ab\rangle} = D^{\langle a}\dot{u}^{b\rangle} - \frac{2}{3}\Theta\sigma^{ab} + \dot{u}^{\langle a}\dot{u}^{b\rangle} - \sigma^{\langle a}{}_b\sigma^{b\rangle c} - \omega^{\langle a}\omega^{b\rangle} - E^{ab} + \frac{1}{2}\pi^{ab}, \tag{7.80}$$

  where we notice how the tidal gravitational field, given by the Electric Weyl tensor E_{ab}, acts as a source for shear and will be fed into the Raychaudhuri equation and vorticity evolution equations. Non-zero tidal gravitational fields therefore change the nature of the timelike congruence.

The constraint equations are given by:

- (0α)-equation

$$(C_1)^a = D_b\sigma^{ab} - \frac{2}{3}D^a\Theta + \eta^{abc}\left[D_b\omega_c + 2\dot{u}_b\omega_c\right] + q^a = 0. \tag{7.81}$$

  Alternatively, this constraint shows how spatial inhomogeneity present in the shear and expansion gives rise to a momentum flux which is otherwise not present for a perfect fluid.

- Vorticity Divergence

$$(C_2) = D_a\omega^a - \dot{u}_a\omega^a = 0 \tag{7.82}$$

- Magnetic Weyl Equation

$$(C_3)^{ab} = H^{ab} + 2\dot{u}^{\langle a}\omega^{b\rangle} + D^{\langle a}\omega^{b\rangle} - (\mathrm{curl}\,\sigma)^{ab}\,, \tag{7.83}$$

this constraint allows us to reconstruct the magnetic Weyl tensor from the distortions of the vorticity and shear of the timelike congruence.

The second set of equations arise from the twice-contracted Bianchi identities which give rise to a set of conservation equations. Following a similar procedure to that above, we project parallel (energy equation) and orthogonally (momentum flux equation) to the timelike congruence and end up with the following:

- Energy Conservation Equation

$$\dot{\mu} = -D_a a^a - \Theta\,(\mu + p) - 2\dot{u}_a q^a - \sigma_{ab}\pi^{ab} \tag{7.84}$$

- Momentum Flux Conservation Equation

$$\dot{q}^{\langle a\rangle} = -D^a p - D_b\pi^{ab} - \frac{4}{3}\Theta q^a - q^b\sigma^a{}_b - (\mu + p)\,\dot{u}^a - \dot{u}_b\pi^{ab} - \eta^{abc}\omega_b q_c \tag{7.85}$$

The final set of equations are derived from the once-contracted Bianchi identities:

$$\nabla_{[a}R_{bc]de} = 0, \tag{7.86}$$

were we to contract the equations again we would simply recover the twice-contracted Bianchi identities considered above. The once-contracted identities Bianchi identities give rise to two propagation and two constraint equations. This can be seen by decomposing the Riemann tensor into the Ricci tensor and Weyl Curvature tensor above. The propagation equations are:

- Electric Weyl Equation

$$\begin{aligned}\dot{E}^{\langle ab\rangle} - (\mathrm{curl}\,H)^{ab} = &-\frac{1}{2}D^{\langle a}q^{b\rangle} - \frac{1}{2}\dot{\pi}^{\langle ab\rangle} - \frac{1}{2}\,(\mu + p)\,\sigma^{ab} - \Theta\left(E^{ab} + \frac{1}{6}\pi^{ab}\right) + \\ &3\sigma^{\langle a}{}_c\left(E^{b\rangle c} - \frac{1}{6}\pi^{b\rangle c}\right) - \dot{u}^{\langle a}q^{b\rangle} + \eta^{cd\langle a}\left[2\dot{u}_c H_d{}^{b\rangle} + \omega_c\left(E_d{}^{b\rangle} + \frac{1}{2}\pi_d{}^{b\rangle}\right)\right]\end{aligned} \tag{7.87}$$

- Magnetic Weyl Equation

$$\begin{aligned}\dot{H}^{\langle ab\rangle} + (\mathrm{curl}\,E)^{ab} = &+\tfrac{1}{2}(\mathrm{curl}\,\pi)^{ab} - \Theta\,H^{ab} + 3\,\sigma^{\langle a}{}_c\,H^{b\rangle c} + \tfrac{3}{2}\,\omega^{\langle a}\,q^{b\rangle} \\ &- \eta^{cd\langle a}\left[\,2\,\dot{u}_c\,E_d{}^{b\rangle} - \tfrac{1}{2}\,\sigma^{b\rangle}{}_c\,q_d - \omega_c\,H_d{}^{b\rangle}\,\right],\end{aligned} \tag{7.88}$$

These two coupled equations are of particular importance and interest as they demonstrate how gravitational radiation manifests itself. It is possible to take a time derivative of the $\dot{E}$ equation and eliminate the remaining H terms to give a wave equation for E. Likewise we can derive a wave equation for H.

The constraint equations obtained from the Bianchi identities are:

- Electric Weyl Constraint

$$\begin{aligned}(C_4)^a \;=\; & \tilde{\nabla}_b(E^{ab} + \tfrac{1}{2}\,\pi^{ab}) - \tfrac{1}{3}\,\tilde{\nabla}^a\mu + \tfrac{1}{3}\,\Theta\,q^a - \tfrac{1}{2}\,\sigma^a{}_b\,q^b - 3\,\omega_b\,H^{ab} \\ & -\; \eta^{abc}\,[\,\sigma_{bd}\,H_c{}^d - \tfrac{3}{2}\,\omega_b\,q_c\,] \;=0\;, \end{aligned} \tag{7.89}$$

- Magnetic Weyl Constraint

$$\begin{aligned}0 = (C_5)^a \;=\; & \tilde{\nabla}_b H^{ab} + (\mu + p)\,\omega^a + 3\,\omega_b\,(E^{ab} - \tfrac{1}{6}\,\pi^{ab}) \\ & +\; \eta^{abc}\,[\,\tfrac{1}{2}\,\tilde{\nabla}_b q_c + \sigma_{bd}\,(E_c{}^d + \tfrac{1}{2}\,\pi_c{}^d)\,] \;=0\;. \end{aligned} \tag{7.90}$$

The above equations bear something of a resemblance to Maxwell's equations which, in addition to the parity of the components, alludes to the Electric and Magnetic nomenclature used in the decomposition of the Weyl tensor.

7.4.5 Geometry of Hypersurfaces

If the fluid flow is irrotational (vorticity free), the tangent planes formed from the rest-spaces of fundamental observers mesh together to form spacelike hypersurfaces orthogonal to the world-lines. These spacelike hypersurfaces are the surfaces of simultaneity for all comoving observers. When the vorticity is non-zero, it is no longer possible to find an integrable submanifold as the subspace planes are allowed to twist around. More formally, at each point p of the spacetime we have a subspace H_p of the tangent space T_p at p which is orthogonal to the timelike congruence u_a. The projection operator h_{ab} is simply the metric in H_p. As mentioned in the introduction, the collection of these subspaces is called a *smooth specification*. When the vorticity is non-zero we can calculate the commutation relation for two vectors A^a and B^a in the smooth specification:

$$[A\,,\,B]^a - h^a{}_b\,[A\,,\,B]^b = -2u^a\,\omega_{bc}\,A^b B^c, \tag{7.91}$$

where the quantity $D^a{}_{bc} = u^a\,\omega_{bc}$ is called the *defect tensor*. This tensor encapsulates the degree to which the commutation of the two vectors does not lie within our smooth specification. When the defect tensor is non-zero, Frobenius' theorem tells us that the smooth specification does not possess integrable submanifolds. For vanishing vorticity, the defect tensor is zero and the collection of our surfaces mesh together to form an integrable submanifold. Consequentially, the intrinsic curvature and metric are induced from the embedding spacetime.
In the dual formulation of Frobenius' Theorem, a vector field χ^a will be hypersurface orthogonal if:

$$\chi_{[a}\nabla_b\chi_{c]} = 0. \tag{7.92}$$

Taking the vector field to be our timelike congruence we observe that:

$$u_{[a}\nabla_b u_{c]} = u_{[a}D_b u_{c]} = u_{[a}\omega_{bc]} \tag{7.93}$$

meaning that for u^a to be hypersurface orthogonal we demand that the vorticity vanish. As the vorticity is involutive, if it vanishes at some initial time then the evolution equation is trivial and the vorticity will vanish at all times:

$$\omega^a\big|_{t=0} = 0 \;\rightarrow\; \dot{\omega}^{\langle a\rangle} = 0 \;\rightarrow\; \omega^a\big|_t = 0\;\forall t. \tag{7.94}$$

7.4.6 u^a is Hypersurface Orthogonal

In the case of vanishing vorticity, the 3-spaces form an integrable submanifold Σ which has an induced metric given by h_{ab} and a derivative into the 3-space D_a. The intrinsic curvature of the 3-spaces may be calculated using the Ricci identity applied to the spatial derivatives:

$$2D_{[a}D_{b]}V_c =^{(3)} R_{abcd}V^d, \tag{7.95}$$

for any 3-vector V^a that lies in the submanifold Σ. The 3-Riemann tensor is related to the 4-dimensional Riemann tensor of our whole spacetime by the Gauss equation:

$${}^{(3)}R_{abcd} = (R_{abcd})_\perp - K_{ac}\,K_{bc} + K_{bc}\,K_{ad}. \tag{7.96}$$

The extrinsic curvature or *second fundamental form*, K_{ab}, is simply related to the covariant derivative of the timelike congruence:

$$K_{ab} = D_a u_b = \frac{1}{3}\Theta h_{ab} + \sigma_{ab}. \tag{7.97}$$

The totally projected Riemann tensor can be shown to reduce to:

$$(R_{abcd})_\perp = \frac{2}{3}\,(\mu+\Lambda)\,h^{[a}{}_{[c}\,h^{b]}{}_{d]} + 2\,h^{[a}{}_{[c}\,\pi^{b]}{}_{d]} + 4\,h^{[a}{}_{[c}\,E^{b]}{}_{d]}. \tag{7.98}$$

Now we want to substitute this expression into the Gauss equation along with our expression for second fundamental form and contract once to recover the 3-Ricci tensor:

$$ {}^{(3)}R_{ab} = \left[\frac{2}{3}(\mu+\Lambda) - \frac{2}{9}\Theta^2\right] h_{ab} - \frac{1}{3}\Theta\sigma_{ab} + E_{ab} + \frac{1}{2}\pi_{ab} + \sigma_{ac}\sigma^{c}{}_{b}. \tag{7.99} $$

Contracting this expression again yields the 3-Ricci scalar:

$$ {}^{(3)}R = 2(\mu+\Lambda) - \frac{2}{3}\Theta^2 + 2\sigma^2. \tag{7.100} $$

7.4.7 u^a is not Hypersurface Orthogonal

In such an instance the 3-spaces orthogonal to the timelike congruence fail to mesh together to form an integrable submanifold. We can, however, still define a 3-curvature tensor by taking the Gauss equation but with an extrinsic curvature given by:

$$ K_{ab} = \frac{1}{3}\Theta h_{ab} + \sigma_{ab} + \omega_{ab}. \tag{7.101} $$

Consequentially, the 3-Ricci tensor is now defined by:

$$ \begin{aligned} {}^{(3)}R_{ab} = \left[\frac{2}{3}(\mu+\Lambda) - \frac{2}{9}\Theta^2\right] h_{ab} - \frac{1}{3}\Theta\,\sigma_{ab} + E_{ab} + \frac{1}{2}\pi_{ab} + \sigma_{ac}\,\sigma^{c}{}_{b} \\ - \frac{1}{3}\Theta\,\omega_{ab} + \sigma_{ac}\omega^{c}{}_{b} + \omega_{ac}\,\sigma^{c}{}_{b} + \omega_{ac}\,\omega^{c}{}_{b}. \end{aligned} \tag{7.102} $$

Lastly, the 3-Ricci scalar is given by:

$$ {}^{(3)}R = 2\,(\mu+\Lambda) - \frac{2}{3}\Theta^2 + 2\left(\sigma^2 - \omega^2\right). \tag{7.103} $$

7.4.8 Commutation Relations

The commutation relations play a vital role in many different formulations of General Relativity. In the 1+3 formalism the commutation relations are between spatial and convective derivatives along the timelike congruence. The commutation relations for scalar, vector and tensor objects can be derived by starting from the Bianchi identity acting on the relevant object and performing a 1+3 decomposition of the variables. By performing the appropriate projections on the derivatives we can derive the concomitant commutation relations. The Bianchi identities used are:

- Scalars

$$ 2\nabla_{[a}\nabla_{b]}T = 0 \tag{7.104} $$

- Vectors

$$ 2\nabla_{[a}\nabla_{b]}T^{c} = R_{ab}{}^{c}{}_{d}Tf^{d} \tag{7.105} $$

- Tensors

$$2\nabla_{[a}\nabla_{b]}T^{cd} = -R_{ab}{}^{ec}\,T_{e}{}^{d} - R_{ab}{}^{ed}\,T^{c}{}_{e}. \tag{7.106}$$

The commutation relations, once decomposed and projected, split into two sets: spatial derivatives acting on spatial derivatives and spatial derivatives acting on convective derivatives along the timelike congruence.
For scalars we see the following relations:

$$D_{[a}D_{b]} = \omega_{ab}\dot{T} \tag{7.107}$$

$$D_a\dot{T} - h_a{}^b\,(D_bT)^{\cdot} = -\dot{T}\,\dot{u}_a + \frac{1}{3}\Theta D_aT + D_bT\,\left(\sigma^b{}_a + \omega^b{}_a\right). \tag{7.108}$$

For 3-vectors T^a living in the 3-spaces, meaning that $T_a\,u^a = 0$, the commutation relations reduce to:

$$2\,D_{[a}\,D_{b]}\,T^c = 2\,\omega_{ab}\,\dot{T}^{\langle c\rangle} - {}^{(3)}R_{abs}{}^{c}\,T^s\,, \tag{7.109}$$

$$\begin{aligned} D_a\,\dot{V}_b - h_a{}^c h_b{}^d\,(D_aT_b)^{\cdot} = &-\dot{u}_a\,\dot{T}_{\langle b\rangle} + \left(\frac{1}{3}\Theta\,h_a{}^c + \sigma_a{}^c + \omega_a{}^c\right)\,[T_c\,\dot{u}_b + D_c\,T_b] \\ &- \epsilon_{dbc}\,T^c\,H_a{}^d - \frac{1}{2}\,h_{ab}\,q_c\,T^c + \frac{1}{2}\,T_a\,q_b. \end{aligned} \tag{7.110}$$

Likewise for a 3-tensor living in the 3-spaces, $T_{ab}\,u^b = 0$, the concomitant commutation relations are:

$$2\,D_{[a}\,D_{b]}\,T^{cd} = 2\,\omega_{ab}\,h_c{}^f\,h_d{}^g\,\left(\dot{T}^{cd}\right) - {}^{(3)}R_{abe}{}^{c}\,T^{ed} - {}^{(3)}R_{abe}{}^{d}\,T^{ce}\,, \tag{7.111}$$

$$\begin{aligned} D_a\dot{T}_{bc} - h_a{}^e\,h_b{}^f\,h_c{}^g\,(D_e\,T_{fg})^{\cdot} = &\left(\frac{1}{3}\Theta\,h_a{}^d + \sigma_a{}^d + \omega_a{}^d\right)\,[\dot{u}_b\,T_{dc} + \dot{u}_c\,T_{bd} + D_d\,T_{bc}] \\ &+ \left[h_{a[e}\,q_{b]} - \epsilon_{ebd}\,H_a{}^d\right]\,T^e{}_c + \left[h_{a[e}\,q_{c]} - \epsilon_{ecd}\,H_a{}^d\right]\,T_b{}^e \\ &- \dot{u}_a\,h_b{}^f\,h_c{}^g\,\left(\dot{T}_{fg}\right). \end{aligned} \tag{7.112}$$

7.5 1+1+2 Formalism

The 1+3 formalism excels in many facets of relativistic cosmology. In particular, it has proven extremely useful in treating non-linear General Relativistic effects such as gauge-invariant, covariant perturbation theory or the cosmic microwave background. The strength of the 1+3 formalism is that for cosmological spacetimes with 3-surfaces of homogeneity that are also isotropic, formally spacetimes admitting a 3-dimensional surface of transitivity and 3-dimensional isotropy group, the only essential coordinate is time. By introducing an appropriately chosen timelike congruence, the full spacetime can be described in terms of ordinary differential equations involving 1+3 scalar variables. The assumption of homogeneity implies that spatial derivatives, spatial projections of vectors and the PSTF parts of tensors must vanish due to the restrictive symmetry. When the spacetime is inhomogeneous or anisotropic the concomitant 1+3 equations are not ordinary differential equations and in many cases they become intractable. Notably, the existence of non-zero vectors and tensors in the background spacetime and the resulting vector-tensor and tensor-tensor couplings that render the equations intractable.

The 1+1+2 formalism represents something of a logical extension the 1+3 formalism. In spacetimes that admit both a preferred timelike and a preferred spacelike congruence we can recover much of the advantages of the 1+3 formalism by introducing an additional frame vector and performing a further splitting of spacetime. This is particularly suited to the studies of spacetimes exhibiting a preferred spatial direction such as the class of *locally rotationally symmetric* (LRS) spacetimes [161; 533; 162; 572] or the inhomogeneous G_2 spacetimes. A 1+1+2 decomposition was originally discussed in the context of deriving a general theory for spacelike congruences and the study of vorticity in relativistic hydrodynamics [223] and has mostly been used in studying symmetries of the Einstein Field Equations (EFEs) [567; 353; 568]. A systematic derivation of the 1+1+2 decomposition, based on a 1+3 covariant split of EFEs, was presented in [104] and further developed in [58; 81; 82; 83; 105; 540]. The 1+1+2 formalism presented in [104] has since been used to study a number of astrophysically interesting examples. Some recent examples in the literature include: perturbations of black holes cite Clarkson03, Betschart04,Clarkson07, almost-Birkhoff theorems [217; 218; 416] and modified gravity [415].

In this section we provide a rather detailed but self-contained introduction to the 1+1+2 formalism. This section contains results beyond that presented in the literature and also corrects errors and typos throughout the literature. See also [437] for some corrections and additions to the existing literature.

7.5.1 Splitting Spacetime Again

The aim of this section is to perform a further split of the 1+3 equations using a preferred spacelike congruence with unit vector n^a normalised such that $n^a\, n_a = 1$ and $n^a\, u_a = 0$. The induced metric of the 2-surfaces, denoted a *sheet*, following the split is given by (see Fig. 7.2):

$$N_{ab} = h_{ab} - n_a\, n_b = g_{ab} + u_a\, u_b - n_a\, n_b \tag{7.113}$$

In analogy to the 1+3 formalism, this tensor projects our tensor objects orthogonally to both u^a and n^a onto the sheet. In the same way that the 3-surfaces before carried a natural volume

element, the sheet will also carry a volume element that is defined by a further projection of the Levi-Civita object:

$$\epsilon_{ab} = \epsilon_{abc}\, n^c = \eta_{dabc}\, u^d\, n^c. \tag{7.114}$$

There exist a number of important and useful relationships for the 2-volume element that will be used in the subsequent derivations:

$$\epsilon_{abc} = \epsilon_{bc}\, n_a + \epsilon_{ca}\, n_b + \epsilon_{ab}\, n_c \tag{7.115}$$

$$\epsilon_{ab}\, \epsilon^{cd} = N_a{}^c\, N_b{}^d - N_a{}^d\, N_b{}^c. \tag{7.116}$$

With these projection operators in place, we can systematically decompose scalars, 3-vectors and 3-tensors into 1+1+2 geometrical objects. For scalars, this is trivial and they remain invariant. Any 3-vector ψ^a may be irreducibly split into a scalar $\mathbf{\Psi}$, the part of the 3-vector parallel to n^a, and a 2-vector $\mathbf{\Psi}^a$, which lies in the 2-surface orthogonal to n^a;

$$\psi^a = \mathbf{\Psi} n^a + \mathbf{\Psi}^a \tag{7.117}$$

$$\mathbf{\Psi} = \psi_a n^a \qquad \mathbf{\Psi}^a = N^{ab}\psi_b = \psi^{\bar{a}}, \tag{7.118}$$

where a bar denotes projection with respect to N_{ab}. Using the same reasoning as above, any PSTF 3-tensor ψ_{ab} may be decomposed into a scalar, 2-vector and 2-tensor;

$$\psi_{ab} = \psi_{\langle ab\rangle} = \mathbf{\Psi}\left(n_a n_b - \frac{1}{2}N_{ab}\right) + 2\mathbf{\Psi}_{(a}n_{b)} + \mathbf{\Psi}_{ab}, \tag{7.119}$$

where the components are defined as follows

$$\mathbf{\Psi} = n^a n^b \psi_{ab} = -N^{ab}\psi_{ab} \tag{7.120}$$

$$\mathbf{\Psi} = N_a{}^b n^c \psi_{bc} = \mathbf{\Psi}_{\bar{a}} \tag{7.121}$$

$$\mathbf{\Psi}_{ab} = \psi_{\{ab\}} = \left(N_{(a}{}^c N_{b)}{}^d - \frac{1}{2}N_{ab}N^{cd}\right)\psi_{cd}. \tag{7.122}$$

We have used curly brackets $\{\dots\}$ to denote the projected, symmetric and trace-free with respect to n^a part of ψ_{ab}. For a rank-2 tensor, PSTF is equivalent to transverse-traceless [105]. This leads to some useful results

$$h_{\{ab\}} = 0 \tag{7.123}$$

$$N_{\langle ab\rangle} = -n_{\langle a}n_{b\rangle} = N_{ab} - \frac{2}{3}h_{ab}. \tag{7.124}$$

As we saw in the 1+3 formalism, the introduction of the preferred timelike congruence led naturally to two new derivative operators. We see that something similar happens in the 1+1+2 formalism in the sense that the introduction of the preferred spacelike congruence leads naturally to two new derivative operators. The first will be called a hat derivative $\hat{\psi}$ and corresponds to a convective derivative along spacelike vector n^a in the surfaces orthogonal to u^a. The second will be a totally projected spatial derivative δ_a that lies in the 2-surface. In spherical symmetry this is

just an angular derivative on the 2-sphere. These two operators are defined as follows [104; 105]

$$\hat{\psi}_{a\ldots b}{}^{c\ldots d} = n^e\, D_e\, \psi_{a\ldots b}{}^{c\ldots d} \tag{7.125}$$

$$\delta_e \psi_{a\ldots b}{}^{c\ldots d} = N_e{}^j N_a{}^f \ldots N_b{}^g N_h{}^c \ldots N_i{}^d\, D_j\, \psi_{f\ldots g}{}^{h\ldots i} \tag{7.126}$$

It is important to note that the definition we have provided here represents a conceptual divergence from that of the 1+3 approach. Namely, we have not treated n^a on an equal footing as u^a due to the appearance of a D_a instead of a ∇_a. This is important as it means that we have retained the primary importance of u^a from the 1+3 formalism. In cosmological applications, where the existence of a preferred congruence of observers is perhaps more natural, this will lead to a very natural splitting of the 1+3 system of equations.

As with the 1+3 formalism, the projection tensor N_{ab} and the Levi-Civitá tensor will be affected by the derivatives in the following way [105]

$$\dot{N}_{ab} = 2u_{(a}\dot{u}_{b)} - 2n_{(a}\dot{n}_{b)} \tag{7.127}$$

$$\hat{N}_{ab} = -2n_{(a}\hat{n}_{b)} \tag{7.128}$$

$$\delta_c N_{ab} = 0 \tag{7.129}$$

$$\dot{\epsilon}_{ab} = -2u_{[a}\epsilon_{b]c}\, N^{cf}\dot{u}_f + 2n_{[a}\epsilon_{b]c}\dot{n}^c \tag{7.130}$$

$$\hat{\epsilon}_{ab} = 2n_{[a}\epsilon_{b]c}\hat{n}^c \tag{7.131}$$

$$\delta_c \epsilon_{ab} = 0. \tag{7.132}$$

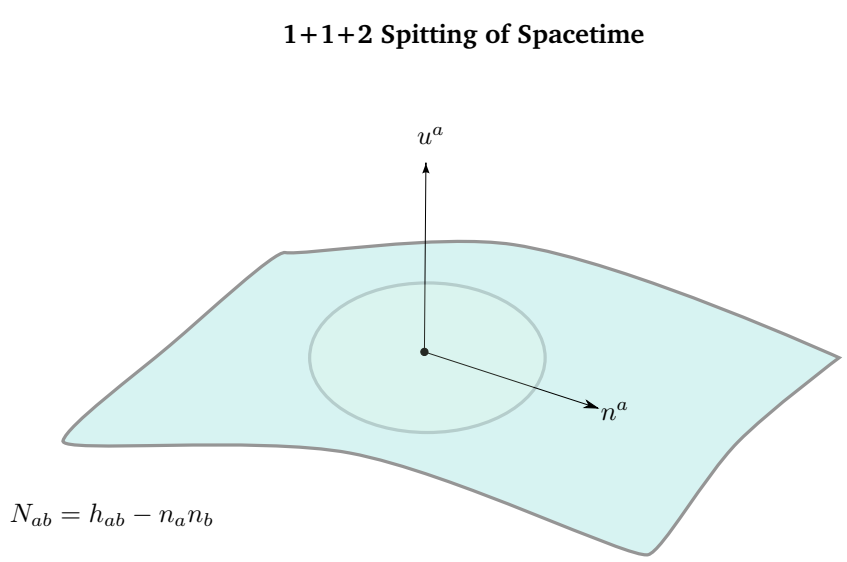

Figure 7.2: Here we show the schematic decomposition of spacetime into a preferred timelike congruence and a preferred spacelike congruence. In the vorticity free case the 2-sheets mesh together to from a genuine surface orthogonal to both u^a and n^a.

7.5.2 Kinematical Variables

As we have done for the 1+3 formalism, the kinematical variables that covariantly characterise the spacetime in the 1+1+2 formalism may be derived by splitting the covariant spatial derivative of the spacelike vector n^a into its irreducible parts:

$$D_a n_b = n_a a_b + \frac{1}{2}\phi N_{ab} + \xi \epsilon_{ab} + \zeta_{ab}. \tag{7.133}$$

The fundamental kinematical variables in the 1+1+2 formalism are:

- Sheet Acceleration

$$a_a = n^c D_c n_a, \tag{7.134}$$

  which denotes the acceleration of the sheet, i.e. how fast the spacelike vector is changing in the radial direction.

- Sheet Expansion

$$\phi = \delta_a n^a, \tag{7.135}$$

  defines the expansion of the sheet and corresponds to the trace of totally projected sheet derivative measuring a volume rate of expansion of the sheet.

- Sheet Distortion

$$\zeta_{ab} = \delta_{\{a} n_{b\}}, \tag{7.136}$$

  this is simply the shear of n^a and measures the anisotropic expansion of the sheets.

- Sheet Rotation

$$\xi = \frac{1}{2}\epsilon^{ab}\delta_a n_b, \tag{7.137}$$

  measures the rotation of the spacelike congruence and amounts to a measure of how much the sheets have twisted. This will vanish if the spacelike congruence is everywhere orthogonal to the spatial 2-surfaces in some foliation of the spacetime. This means that, in a suitable coordinate chart, each 2-surface can be viewed as a surface of constant time and radial parameter. As an example, in a spherically symmetric spacetime, the 2-spheres that foliate the spacetime will be well defined at a given time t and for a given radius r.

These variables constitute the fundamental building blocks of our spacetime and their dynamics encodes all the information regarding the spacetime geometry. In the 1+1+2 formalism these variables are treated on an equal footing to the kinematical variables of u^a that arise in the 1+3 formalism. Performing a 1+1+2 decomposition of the kinematical variables of u^a leads to the following set of variables:

$$\dot{u}^a = \mathcal{A}n^a + \mathcal{A}^a \tag{7.138}$$

$$\omega^a = \Omega n^a + \Omega^a \tag{7.139}$$

$$\sigma_{ab} = \Sigma\left(n_a n_b - \frac{1}{2}N_{ab}\right) + 2\Sigma_{(a}n_{b)} + \Sigma_{ab} \tag{7.140}$$

$$\Theta = \Theta. \tag{7.141}$$

The irreducible set of kinematical variables in the 1+1+2 formalism is therefore given by:

$$\mathbf{X}_{\text{kinematical}} = \{\mathcal{A}, \Sigma, \Theta, \phi, \xi, \Omega, \Omega_a, \Sigma_a, \mathcal{A}_a, a_a, \Sigma_{ab}, \zeta_{ab}\}\,. \tag{7.142}$$

7.5.3 Matter Fields

Adopting the 1+3 energy-momentum tensor for an imperfect fluid as our starting point, the corresponding 1+1+2 variables are derived by performing a decomposition:

$$\mu = \mu \tag{7.143}$$

$$p = p \tag{7.144}$$

$$\Lambda = \Lambda \tag{7.145}$$

$$q_a = Qn_a + Q_a \tag{7.146}$$

$$\pi_{ab} = \Pi\left(n_a n_b - \frac{1}{2}N_{ab}\right) + \Pi_{(a}n_{b)} + \Pi_{ab}. \tag{7.147}$$

The corresponding energy-momentum tensor can now be written explicitly as:

$$T_{ab} = \mu u_a u_b + p h_{ab} + 2u_{(a}\left[Qn_{b)} + Q_{b)}\right] + \Pi\left(n_a n_b - \frac{1}{2}N_{ab}\right) + \Pi_{(a}n_{b)} + \Pi_{ab}. \tag{7.148}$$

The set of irreducible 1+1+2 matter variables are:

$$\mathbf{X}_{\text{matter}} = \{\mu, p, \Lambda, Q, Q_a, \Pi_a, \Pi_{ab}\} \tag{7.149}$$

7.5.4 Gravitational Field

The final sector that we must consider in order to complete our collection of fundamental 1+1+2 variables is that of the gravitational field. As we discussed in relation to the 1+3 formalism, the 1+1+2 variables can be obtained by performing a decomposition of the Electric and Magnetic Weyl tensors:

$$E_{ab} = \mathcal{E}\left(n_a n_b - \frac{1}{2}N_{ab}\right) + \mathcal{E}_{(a}n_{b)} + \mathcal{E}_{ab} \tag{7.150}$$

$$H_{ab} = \mathcal{H}\left(n_a n_b - \frac{1}{2}N_{ab}\right) + \mathcal{H}_{(a}n_{b)} + \mathcal{H}_{ab}. \tag{7.151}$$

The Riemann tensor can now be in terms of the 1+1+2 geometrical objects as follows

$$\begin{aligned}
R^{ab}{}_{cd} &= R^{ab}_{P\ cd} + R^{ab}_{I\ cd} + R^{ab}_{E\ cd} + R^{ab}_{H\ cd} \\
R^{ab}_{P\ cd} &= \frac{2}{3}\left(\mu + 3p - 2\Lambda\right) u^{[a}u_{[c}\left[N^{b]}{}_{d]} + n^{b]}\, n_{d]}\right] + \frac{2}{3}\left(\mu + \Lambda\right)\left[N^{[a}{}_{[c} + n^{[a}\, n_{[c}\right]\left[N^{b]}{}_{d]} + n^{b]}\, n_{d]}\right] \\
R^{ab}_{I\ cd} &= -2u^{[a}\left[N^{b]}{}_{[c} + n^{b]}\, n_{[c}\right]\left[Qn_{d]} + Q_{d]}\right] - 2u_{[c}\left[N^{[a}{}_{d]} + n^{[a}\, n_{d]}\right]\left[Qn^{b]} + Q^{b]}\right] \\
&\quad - 2u^{[a}u_{[c}\left[\Pi\left(n^{b]}n_{d]} - \frac{1}{2}N^{b]}{}_{d]}\right) + \Pi^{b]}n_{d]} + n^{b]}\Pi_{b]} + \Pi^{b]}{}_{d]}\right] \\
&\quad + 2\left[N^{[a}{}_{[c} + n^{[a}\, n_{[c}\right]\left[\Pi\left(n^{b]}n_{d]} - \frac{1}{2}N^{b]}{}_{d]}\right) + \Pi^{b]}n_{d]} + n^{b]}\Pi_{b]} + \Pi^{b]}{}_{d]}\right] \\
R^{ab}_{E\ cd} &= 4u^{[a}u_{[c}\left[\mathcal{E}\left(n^{b]}n_{d]} - \frac{1}{2}N^{b]}{}_{d]}\right) + \mathcal{E}^{b]}n_{d]} + n^{b]}\mathcal{E}_{d]} + \mathcal{E}^{b]}{}_{d]}\right] \\
&\quad + 4\left[N^{[a}{}_{[c} + n^{[a}\, n_{[c}\right]\left[\mathcal{E}\left(n^{b]}n_{d]} - \frac{1}{2}N^{b]}{}_{d]}\right) + \mathcal{E}^{b]}n_{d]} + n^{b]}\mathcal{E}_{d]} + \mathcal{E}^{b]}{}_{d]}\right] \\
R^{ab}_{H\ cd} &= 2\left[n^a\epsilon^{be} - n^b\epsilon^{ae} + n^e\epsilon^{ab}\right]u_{[c}\left[\mathcal{H}\left(n_{d]}n_e - \frac{1}{2}N_{d]e}\right) + \mathcal{H}_{d]}n_e + n_{d]}\mathcal{H}_e + \mathcal{H}_{d]e}\right] \\
&\quad + 2\left[n_c\epsilon_{de} - n_d\epsilon_{ce} + n_e\epsilon_{cd}\right]u^{[a}\left[\mathcal{H}\left(n^{b]}n^e - \frac{1}{2}N^{b]e}\right) + \mathcal{H}^{b]}n^e + n^{b]}\mathcal{H}^e + \mathcal{H}^{b]e}\right].
\end{aligned}$$

The irreducible 1+1+2 gravitational variables are given by

$$\mathbf{X}_{\text{gravitational}} = \{\mathcal{E}, \mathcal{E}_a, \mathcal{E}_{ab}, \mathcal{H}, \mathcal{H}_a, \mathcal{H}_{ab}\}. \tag{7.152}$$

7.5.5 Irreducible 1+1+2 Variables

The full set of irreducible 1+1+2 variables can therefore be given by the combination of the kinematical, matter and gravitational sectors.

$$\mathbf{X}_{\text{full}} = \mathbf{X}_{\text{kinematical}} + \mathbf{X}_{\text{matter}} + \mathbf{X}_{\text{gravitational}}. \tag{7.153}$$

7.5.6 Decomposing the Spatial Derivatives

Some of the most vital identities in the 1+1+2 formalism are given by the spatial derivatives of our scalars, 2-vectors and 2-tensors.

Scalar

$$D_a\mathbf{\Psi} = \hat{\mathbf{\Psi}}n_a + \delta_a\mathbf{\Psi} \tag{7.154}$$

2-Vector

$$D_a \mathbf{\Psi}_b = -n_a n_b \mathbf{\Psi}_c \, a^c + n_a \hat{\mathbf{\Psi}}_{\bar{b}} - n_b \left[\frac{1}{2} \phi \mathbf{\Psi}_a + (\xi \epsilon_{ac} + \zeta_{ac}) \, \mathbf{\Psi}^c \right] + \delta_a \mathbf{\Psi}_b. \tag{7.155}$$

2-Tensor

$$D_a \mathbf{\Psi}_{bc} = -2 n_a n_{(b} \mathbf{\Psi}_{c)d} \, a^d + n_a \hat{\mathbf{\Psi}}_{bc} - 2 n_{(b} \left[\frac{1}{2} \phi \mathbf{\Psi}_{c)a} + \mathbf{\Psi}_{c)}{}^d \, (\xi \epsilon_{ad} + \zeta_{ad}) \right] + \delta_a \mathbf{\Psi}_{bc}. \tag{7.156}$$

See also Appendix E.1.1 for further results on relating various 1+3 quantities to the 1+1+2 formalism taken from Appendix A of [105]. Using these results, along with the definitions above, we can explicitly write out the covariant derivatives of both the timelike and spacelike vectors

$$\begin{aligned} \nabla_a n_b = &-\mathcal{A} \, u_a u_b - u_a \alpha_b + \left(\Sigma + \frac{1}{3} \Theta \right) n_a u_b + (\Sigma_a - \epsilon_{ac} \Omega^c) \, u_b + n_a a_b \\ &+ \frac{1}{2} \phi N_{ab} + \xi \epsilon_{ab} + \zeta_{ab} \\ \nabla_a u_b = &-u_a \left(\mathcal{A} n_b + \mathcal{A}_b \right) + n_a n_b \left(\Sigma + \frac{1}{3} \Theta \right) + n_a \left(\Sigma_b + \epsilon_{bc} \Omega^c \right) \\ &+ (\Sigma_a - \epsilon_{ac} \Omega^c) \, n_b - \frac{1}{2} N_{ab} \left(\Sigma - \frac{2}{3} \Theta \right) + \Omega \epsilon_{ab} + \Sigma_{ab}. \end{aligned}$$

Projecting $\nabla_a u_b$ with respect to n^a yields the following propagation equation

$$\hat{u}_a = \left(\Sigma + \frac{1}{3} \Theta \right) n_a + \Sigma_a + \epsilon_{ab} \Omega^b. \tag{7.157}$$

7.5.7 The Ricci Identities

After we introduce the second congruence, n^a, it is necessary to augment the 1+3 equations with the Ricci identities for n^a. This is important as without this extra expression we do not have enough equations to fully determine the 1+1+2 variables. Following [104; 105] we introduce the following rank-3 tensor

$$R_{abc} = 2 \nabla_{[a} \nabla_{b]} n_c - R_{abcd} n^d = 0. \tag{7.158}$$

This complements the previously introduced Ricci identities for the timelike congruence u^a:

$$B_{abc} = 2 \nabla_{[a} \nabla_{b]} u_c - R_{abcd} u^d = 0. \tag{7.159}$$

These third rank tensors provide the building blocks for the 1+1+2 formalism and they may be covariantly split using n^a and u^a. The dynamical equations split into *evolution* equations, involving dot-derivatives, and *propagation* equations, involving hat derivatives.

7.5.8 Evolution, Propagation and Constraint Equations

In this section we present the system of 1+1+2 equations valid for linear perturbations about LRS-II spacetimes. The LRS-II spacetimes exhibit a local rotational symmetry about some unique preferred spatial direction, i.e. a local axis of symmetry for which the geometry is invariant under rotations about this axis. The spatial vector n^a is chosen to lie along this preferred spatial direction, i.e. n^a is a 'radial' vector. As LRS spacetimes are isotropic, all 2-vectors and 2-tensors will vanish in the background spacetime as there can be no preferred directions on the 2-surface. The restriction to Class-II spacetimes was defined by the integrability and vorticity free nature of the 2-surfaces. This translates into demanding that $\mathcal{H}, \xi$ and Ω vanish in the background. The LRS-II background spacetimes are therefore covariantly characterised by the following non-zero 1+1+2 scalars: $\{\mathcal{A}, \mathcal{E}, \Theta, \phi, \Sigma, \mu, Q, \Pi\}$. Fundamentally, we end up with evolution and propagation equations as we have 2-surfaces of homogeneity leaving us with 2 dynamical coordinates: time and the radial direction. Hence the decomposition of the equations into evolution (time) and propagation (radial) equations. Similarly, the constraint equations are defined over the 2-surface.

Schematically the various evolution, propagation and constraint equations can be extracted from R_{abc} and B_{abc} by appropriate projections with respect to u^a and n^a as well as various symmetry operations. Further details, along with the full system of 1+1+2 equations, can be found in [105]. The equations presented here are derived by taking the full system of 1+1+2 equations and linearising the equations with respect to the non-zero background scalars, 2-vectors and 2-tensors. By imposing the LRS constraint, all vectors and tensors vanish in the background spacetime becoming well defined first order gauge invariant variables. The zeroth order variables are simply the non-vanishing background scalars. In the linearisation procedure, any object of second order or higher is dropped from the system of equations, leaving us with a system of 1st order equations.

The system of evolution equations take the form

$$\dot{\mathbf{X}}_{\rm ev} = \mathcal{E}_{\mathbf{X}}, \tag{7.160}$$

the propagation equations can be written as

$$\hat{\mathbf{X}}_{\rm pr} = \mathcal{P}_{\mathbf{X}}, \tag{7.161}$$

and the constraint equations can be written as

$$\mathcal{C}_{\mathbf{X}} = 0. \tag{7.162}$$

Please note that not all variables in $\mathbf{X}_{\rm irr}$ posses evolution or propagation equations due to the inherent gauge and frame freedom in general relativity, this will be discussed later. Lastly, we note that the equations presented here fix a few errors in [105], these will be detailed shortly.

7.5.8.1 Evolution Equations

$$\dot{\phi} = \left(\Sigma - \frac{2}{3}\Theta\right)\left(\frac{1}{2}\phi - \mathcal{A}\right) + \delta_a \alpha^a + Q \tag{7.163}$$

$$\dot{\xi} = \frac{1}{2}\xi\left(\Sigma - \frac{2}{3}\Theta\right) + \left(\mathcal{A} - \frac{1}{2}\phi\right)\Omega + \frac{1}{2}\epsilon_{ab}\delta^a\alpha^b + \frac{1}{2}\mathcal{H} \tag{7.164}$$

$$\dot{\Omega} = \frac{1}{2}\epsilon_{ab}\delta^a\mathcal{A}^b + \mathcal{A}\xi + \Omega\left(\Sigma - \frac{2}{3}\Theta\right) \tag{7.165}$$

$$\dot{\zeta}_{ab} = \frac{1}{2}\zeta_{ab}\left(\Sigma - \frac{2}{3}\Theta\right) + \left(\mathcal{A} - \frac{1}{2}\phi\right)\Sigma_{ab} + \delta_{\{a}\alpha_{b\}} - \epsilon_{c\{a}\mathcal{H}_{b\}}{}^{c} \tag{7.166}$$

$$\dot{\Sigma}_{ab} = \delta_{\{a}\mathcal{A}_{b\}} + \mathcal{A}\zeta_{ab} + \left(\Sigma - \frac{2}{3}\Theta\right)\Sigma_{ab} - \mathcal{E}_{ab} \tag{7.167}$$

7.5.8.2 Mixed Propagation and Evolution Equations

$$\begin{aligned}\dot{\mathcal{E}} + \frac{1}{2}\dot{\Pi} + \frac{1}{3}\hat{Q} = \epsilon_{ab}\delta^a\mathcal{H}^b + \frac{1}{6}\delta_a Q^a + \frac{3}{2}\mathcal{E}\left(\Sigma - \frac{2}{3}\Theta\right) - \frac{1}{4}\Pi\left(\Sigma + \frac{2}{3}\Theta\right) \\ + \frac{1}{3}Q\left(\frac{1}{2}\phi - 2\mathcal{A}\right) - \frac{1}{2}\left(\mu + p\right)\Sigma.\end{aligned} \tag{7.168}$$

$$\hat{\mathcal{A}} - \left(\dot{\Sigma} + \frac{1}{3}\dot{\Theta}\right) = -\mathcal{A}^2 + \left(\Sigma + \frac{1}{3}\Theta\right)^2 + \mathcal{E} - \frac{1}{2}\Pi + \frac{1}{6}\left(\mu + 3p - 2\Lambda\right) \tag{7.169}$$

$$\hat{\mathcal{A}} - \dot{\Theta} = -\delta_a\mathcal{A}^a - \left(\mathcal{A} + \phi\right)\mathcal{A} + \frac{1}{3}\Theta^2 + \frac{3}{2}\Sigma^2 + \frac{1}{2}\left(\mu + 3p\right) - \Lambda \tag{7.170}$$

$$\dot{\mu} + \hat{Q} = -\delta_a Q^a - \Theta\left(\mu + p\right) - \left(\phi + 2\mathcal{A}\right)Q - \frac{3}{2}\Sigma\Pi \tag{7.171}$$

$$\dot{\Omega}_a + \frac{1}{2}\epsilon_{ab}\hat{\mathcal{A}}^b = -\frac{1}{2}\left(\Sigma + \frac{4}{3}\Theta\right)\Omega_a - \frac{1}{2}\epsilon_{ab}\mathcal{A}a^b + \frac{1}{2}\epsilon_{ab}\delta^b\mathcal{A} - \frac{1}{4}\phi\epsilon_{ab}\mathcal{A}^b \tag{7.172}$$

$$\hat{\alpha}_a - \dot{a}_a = -\left(\frac{1}{2}\phi + \mathcal{A}\right)\alpha_a + \left(\Sigma + \frac{1}{3}\Theta\right)\left(\mathcal{A}_a + a_a\right) + \left(\frac{1}{2}\phi - \mathcal{A}\right)\left(\Sigma_a + \epsilon_{ab}\Omega^b\right) + \frac{1}{2}Q_a - \epsilon_{ab}\mathcal{H}^b \tag{7.173}$$

$$\dot{\Sigma} - \frac{2}{3}\hat{\mathcal{A}} = \frac{2}{3}\left(\mathcal{A} - \frac{1}{2}\phi\right)\mathcal{A} - \frac{1}{2}\left(\Sigma + \frac{4}{3}\Theta\right)\Sigma - \frac{1}{3}\delta_a\mathcal{A}^a - \mathcal{E} + \frac{1}{2}\Pi \tag{7.174}$$

$$\dot{\Sigma}_a - \frac{1}{2}\hat{\mathcal{A}}_a = \frac{1}{2}\delta_a\mathcal{A} + \left(\mathcal{A} - \frac{1}{4}\phi\right)\mathcal{A}_a - \frac{1}{2}\left(\Sigma + \frac{4}{3}\Theta\right)\Sigma_a + \frac{1}{2}\mathcal{A}a_a - \frac{3}{2}\Sigma\alpha_a - \mathcal{E}_a + \frac{1}{2}\Pi_a \tag{7.175}$$

$$\dot{Q}_a + \hat{\Pi}_a = -\delta_a p + \frac{1}{2}\delta_a \Pi - \delta^b \Pi_{ab} - Q\left(\alpha_a + \Sigma_a + \epsilon_{ab}\Omega^b\right) - \frac{3}{2}\Pi a_a + \frac{1}{2}\left(\Sigma - \frac{8}{3}\Theta\right) Q_a - \left(\frac{3}{2}\phi + \mathcal{A}\right)\Pi_a - \left(\mu + p - \frac{1}{2}\Pi\right)\mathcal{A}_a \tag{7.176}$$

$$\dot{\mathcal{E}}_a + \frac{1}{2}\epsilon_{ab}\hat{\mathcal{H}}^b + \frac{1}{2}\dot{\Pi}_a + \frac{1}{4}\hat{Q}_a = \frac{3}{4}\epsilon_{ab}\delta^b \mathcal{H} + \frac{1}{2}\epsilon_{bc}\delta^b \mathcal{H}^c{}_a - \frac{1}{4}\delta_a Q - \frac{1}{2}\left(\mu + p - \frac{3}{2} + \frac{1}{4}\Pi\right)\Sigma_a + \frac{3}{4}\left(\mathcal{E} + \frac{1}{2}\Pi\right)\epsilon_{ab}\Omega^b - \frac{1}{2}Q\mathcal{A}_a - \frac{3}{2}\left(\mathcal{E} + \frac{1}{2}\Pi\right)\alpha_a - \frac{1}{4}Q a_a + \left(\frac{3}{4}\Sigma - \Theta\right)\mathcal{E}_a. \tag{7.177}$$

$$\dot{\mathcal{E}}_{\{ab\}} - \epsilon_{c\{a}\hat{\mathcal{H}}^c{}_{b\}} = -\epsilon_{c\{a}\delta^c \mathcal{H}_{b\}} - \frac{1}{2}\left(\mu + 3\mathcal{E}\right)\Sigma_{ab} - \left(\Theta + \frac{3}{2}\Sigma\right)\mathcal{E}_{ab} + \frac{1}{2}\phi\epsilon_{c\{a}\mathcal{H}_{b\}}{}^c \tag{7.178}$$

$$\dot{\mathcal{H}}_a - \frac{1}{2}\epsilon_{ab}\hat{\mathcal{E}}^b + \frac{1}{4}\epsilon_{ab}\hat{\Pi}^b = -\frac{3}{4}\epsilon_{ab}\delta^b + \frac{3}{8}\epsilon_{ab}\delta^b \Pi - \frac{1}{2}\epsilon_{bc}\delta^b \mathcal{E}^c{}_a + \frac{1}{4}\epsilon_{bc}\delta^b \Pi^c{}_a + \frac{1}{4}\epsilon_{ab}\Sigma^b + \frac{3}{4}Q\Omega_a - \frac{3}{2}\mathcal{E}\epsilon_{ab}\mathcal{A}^b + \frac{3}{4}\left(\mathcal{E} - \frac{1}{2}\Pi\right)\epsilon_{ab}a^b + \left(\frac{1}{4}\phi + \mathcal{A}\right)\epsilon_{ab}\mathcal{E}^b + \left(\frac{3}{4}\Sigma - \Theta\right)\mathcal{H}_a - \frac{3}{8}\Sigma\epsilon_{ab}Q^b - \frac{1}{8}\phi\epsilon_{ab}\Pi^b \tag{7.179}$$

$$\dot{\mathcal{H}}_{\{ab\}} + \epsilon_{c\{a}\hat{\mathcal{E}}_{b\}}{}^c = \epsilon_{c\{a}\delta^c \mathcal{E}_{b\}} + \frac{3}{2}\mathcal{E}\epsilon_{c\{a}\zeta_{b\}}{}^c - \frac{1}{2}\phi\epsilon_{c\{a}\mathcal{E}_{b\}}{}^c - \left(\Theta + \frac{3}{2}\Sigma\right)\mathcal{H}_{ab} \tag{7.180}$$

7.5.8.3 Propagation Equations

$$\hat{\phi} = -\frac{1}{2}\phi^2 - \left(\Sigma - \frac{2}{3}\Theta\right)\left(\Sigma + \frac{1}{3}\Theta\right) + \delta_a a^a - \frac{2}{3}\left(\mu + \Lambda\right) - \frac{1}{2}\Pi - \mathcal{E} \tag{7.181}$$

$$\hat{\xi} = -\phi\xi + \left(\Sigma + \frac{1}{3}\Theta\right)\Omega + \frac{1}{2}\epsilon_{ab}\delta^a a^b \tag{7.182}$$

$$\hat{\Omega} = -\delta_a \Omega^a + \left(\mathcal{A} - \phi\right)\Omega \tag{7.183}$$

$$\hat{\Sigma} - \frac{2}{3}\hat{\Theta} = -\frac{3}{2}\phi\Sigma - \delta_a \Sigma^a - \epsilon_{ab}\delta^a \Omega^b - Q \tag{7.184}$$

$$\hat{\Sigma}_a - \epsilon_{ab}\hat{\Omega}^b = \frac{1}{2}\delta_a \Sigma + \frac{2}{3}\delta_a \Theta - \epsilon_{ab}\delta^b \Omega - \frac{3}{2}\phi\Sigma_a + \left(\frac{1}{2}\phi + 2\mathcal{A}\right)\epsilon_{ab}\Omega^b - \frac{3}{2}\Sigma a_a - \delta^b \Sigma_{ab} - Q_a \tag{7.185}$$

$$\hat{\Sigma}_{\{ab\}} = \delta_{\{a}\Sigma_{b\}} - \epsilon_{c\{a}\delta^{c}\Omega_{b\}} - \frac{1}{2}\phi\Sigma_{ab} + \frac{3}{2}\Sigma\zeta_{ab} - \epsilon_{c\{a}\mathcal{H}_{b\}}{}^{c} \tag{7.186}$$

$$\hat{\zeta}_{\{ab\}} = -\phi\zeta_{ab} + \delta_{\{a}a_{b\}} + \left(\Sigma + \frac{1}{3}\Theta\right)\Sigma_{ab} - \frac{1}{2}\Pi_{ab} - \mathcal{E}_{ab} \tag{7.187}$$

$$\hat{\mathcal{E}} - \frac{1}{3}\hat{\mu} + \frac{1}{2}\hat{\Pi} = -\delta_{a}\mathcal{E}^{a} - \frac{1}{2}\delta_{a}\Pi^{a} - \frac{3}{2}\phi\left(\mathcal{E} + \frac{1}{2}\Pi\right) + \frac{1}{2}\left(\Sigma - \frac{2}{3}\Theta\right)Q \tag{7.188}$$

$$\begin{aligned}\hat{\mathcal{E}}_{a} + \frac{1}{2}\hat{\Pi}_{a} = {}& \frac{1}{2}\delta_{a}\mathcal{E} + \frac{1}{3}\delta_{a}\mu + \frac{1}{4}\delta_{a}\Pi - \delta^{b}\mathcal{E}_{ab} - \frac{1}{2}\delta^{b}\Pi_{ab} + \frac{1}{2}Q\Sigma_{a} - \frac{3}{2}Q\epsilon_{ab}\Omega^{b} - \\ & \frac{3}{2}\left(\mathcal{E} + \frac{1}{2}\Pi\right)a_{a} - \frac{3}{2}\phi\left(\mathcal{E}_{a} + \frac{1}{2}\Pi_{a}\right) - \frac{3}{2}\Sigma\epsilon_{ab}\mathcal{H}^{b} - \frac{1}{4}\left(\Sigma + \frac{4}{3}\Theta\right)Q_{a}\end{aligned} \tag{7.189}$$

$$\hat{\mathcal{H}} = -\delta_{a}\mathcal{H}^{a} - \frac{1}{2}\epsilon_{ab}\delta^{a}Q^{b} - \frac{3}{2}\phi\mathcal{H} - \left(3\mathcal{E} + \mu + p - \frac{1}{2}\Pi\right)\Omega \tag{7.190}$$

$$\begin{aligned}\hat{\mathcal{H}}_{a} - \frac{1}{2}\epsilon_{ab}\hat{Q}^{b} = {}& \frac{1}{2}\delta_{a}\mathcal{H} - \delta^{b}\mathcal{H}_{ab} - \frac{1}{2}\epsilon_{ab}\delta^{b}Q - \frac{3}{2}\left(\mathcal{E} + \frac{1}{2}\Pi\right)\epsilon_{ab}\Sigma^{b} \\ & - \Omega_{a}\left(-\frac{3}{2} + \mu + p + \frac{1}{4}\Pi\right) + Q\epsilon_{ab}a^{b} + \frac{3}{2}\Sigma\epsilon_{ab}\mathcal{E}^{b} - \frac{3}{2}\phi\mathcal{H}_{a} + \frac{1}{4}\phi\epsilon_{ab}Q^{b} + \frac{3}{4}\Sigma\epsilon_{ab}\Pi^{b}.\end{aligned} \tag{7.191}$$

7.5.8.4 Constraint Equations

$$\mathcal{H} = \delta_{a}\Omega^{a} + \epsilon_{ab}\delta^{a}\Sigma^{b} - (2\mathcal{A} - \phi)\Omega + 3\xi\Sigma \tag{7.192}$$

$$\frac{1}{2}\delta_{a}\phi - \epsilon_{ab}\delta^{b}\xi - \delta^{b}\zeta_{ab} = -\frac{1}{2}\left(\Sigma - \frac{2}{3}\Theta\right)\left(\Sigma_{a} - \epsilon_{ab}\Omega^{b}\right) - \frac{1}{2}\Pi_{a} - \mathcal{E}_{a} \tag{7.193}$$

$$\delta_{a}\Sigma - \frac{2}{3}\delta_{a}\Theta = -2\epsilon_{ab}\delta^{b}\Omega - 2\delta^{b}\Sigma_{ab} - \phi\left(\Sigma_{a} - \epsilon_{ab}\Omega^{b}\right) - 2\epsilon_{ab}\mathcal{H}^{b} - Q_{a} \tag{7.194}$$

7.5.8.5 Comments

First, note that there exists no evolution equations for $\mathcal{A}, \mathcal{A}_{a}$ and α_{a} and there is not a propagation equation for a_{a}. This will be true in *any* spacetime, we have the freedom to choose the frame vectors at any point. The motion of these is put into the equations by hand and is not an intrinsic prediction in GR. Additionally, note that not all these equations and it is possible to combine multiple equations in order to reduce the total number of equations, for example Eq. (7.169), Eq. (7.170) and Eq. (7.174) are related.

Finally, we detail the modifications to the system of equations presented in [105]:

Equation 52 of [105] is modified as follows: $-\Sigma_{ab}\left(\frac{1}{2}\Sigma+\frac{2}{3}\Theta\right)\Rightarrow\Sigma_{ab}\left(\Sigma-\frac{2}{3}\Theta\right)$.

Equation 53 of [105] is modified as follows: $\left(\Sigma+\frac{1}{3}\Theta\right)\left(\mathcal{A}_a-a_a\right)\Rightarrow\left(\Sigma+\frac{1}{3}\Theta\right)\left(\mathcal{A}_a+a_a\right)$.

Equation 72 of [105] is modified as follows: $\left(\phi+2\mathcal{A}\right)\epsilon_{ab}\Omega^b\Rightarrow\left(\frac{1}{2}\phi+2\mathcal{A}\right)\epsilon_{ab}\Omega^b$.

Equation 76 of [105] is modified as follows: $-\Sigma\epsilon_{ab}\mathcal{H}^b\Rightarrow-\frac{3}{2}\Sigma\epsilon_{ab}\mathcal{H}^b$.

Equation 80 of [105] is modified as follows: $-\left(\frac{1}{3}\Theta-\frac{1}{2}\Sigma\right)\left(\Sigma_a-\epsilon_{ab}\Omega^b\right)\Rightarrow+\left(\frac{1}{3}\Theta-\frac{1}{2}\Sigma\right)\left(\Sigma_a-\epsilon_{ab}\Omega^b\right)$.

7.5.9 Commutation Relations

In general the various derivatives that we have defined do not commute. As seen in other formulations of General Relativity, the commutation relations play an important role in the 1+1+2 formalism and are vital in terms of the integrability of our system of equations. This is essentially a statement to the effect that the equations must be consistent with one another: the constraints must evolve and propagate consistently. These equations can be derived via a very lengthy expansion and projection of the 1+3 commutation relations [104; 58; 105; 437]. We restrict our commutation relations to linear perturbations of LRS-II spacetimes.

7.5.9.1 Zeroth Order Variables

In a generic LRS-II spacetime, the non-zero background scalars are given by the set

$$\mathbf{X}_{\mathrm{BG}}=\{\mathcal{A},\mathcal{E},\Theta,\phi,\Sigma,\mu,p,Q,\Pi\} \tag{7.195}$$

plus their derivatives. These variables are deemed to be of zeroth order and obey the following commutation relations

Scalar Commutation Relations:

$$\dot{\hat{\psi}}-\hat{\dot{\psi}}=-\mathcal{A}\dot{\psi}+\left(\Sigma+\frac{1}{3}\Theta\right)\hat{\psi}+\left(\Sigma_a+\epsilon_{ab}\Omega^b-\alpha_a\right)\delta^a\psi \tag{7.196}$$

$$\delta_a\dot{\psi}-N_a{}^b\left(\delta_b\psi\right)^{\cdot}=-\mathcal{A}_a\dot{\psi}+\left(\alpha_a+\Sigma_a-\epsilon_{ab}\Omega^b\right)\hat{\psi}-\frac{1}{2}\delta_a\psi\left(\Sigma-\frac{2}{3}\Theta\right)+\left(\Sigma_{ab}+\epsilon_{ab}\Omega\right)\delta^b\psi, \tag{7.197}$$

$$\delta_a\hat{\psi}-N_a{}^b\widehat{\left(\delta_b\psi\right)}=\left(\Sigma_a-\epsilon_{ab}\Omega^b\right)\dot{\psi}+a_a\hat{\psi}+\frac{1}{2}\phi\delta_a\psi+\left(\zeta_{ab}+\epsilon_{ab}\xi\right)\delta^b\psi, \tag{7.198}$$

$$\delta_a\delta_b\psi-\delta_b\delta_a\psi=2\epsilon_{ab}\left(\Omega\dot{\psi}-\xi\hat{\psi}\right)+2a_{[a}\delta_{b]}\psi. \tag{7.199}$$

7.5.9.2 First Order Variables

For all first-order variables in LRS-II spacetimes, the commutation relations for scalars, 2-vectors and 2-tensors will obey the following:

Scalar Commutation Relations:

$$\hat{\dot{\psi}} - \dot{\hat{\psi}} = -\dot{\psi}\mathcal{A} + \left(\Sigma + \frac{1}{3}\Theta\right)\hat{\psi}, \tag{7.200}$$

$$\delta_a\dot{\psi} - N_a{}^b\left(\delta_b\psi\right)^{\cdot} = -\frac{1}{2}\left(\Sigma - \frac{2}{3}\Theta\right)\delta_a\psi, \tag{7.201}$$

$$\delta_a\hat{\psi} - N_a{}^b\widehat{(\delta_a\psi)} = \frac{1}{2}\phi\,\delta_a\psi, \tag{7.202}$$

$$\delta_{[a}\delta_{b]}\psi \quad = 0. \tag{7.203}$$

2-Vector Commutation Relations:

$$\hat{\dot{\psi}}_a - \dot{\hat{\psi}}_a = \left(\Sigma + \frac{1}{3}\Theta\right)\hat{\psi}_a \tag{7.204}$$

$$\delta_a\dot{\psi}_b - N_a{}^c N_b{}^d\left(\delta_c\psi_d\right)^{\cdot} = -\frac{1}{2}\left(\Sigma - \frac{2}{3}\Theta\right)\delta_a\psi_b \tag{7.205}$$

$$\delta_a\hat{\psi}_b - N_a{}^c N_b{}^d\widehat{(\delta_c\psi_d)} = \frac{1}{2}\phi\,\delta_a\psi_b \tag{7.206}$$

$$\delta_{[a}\delta_{b]}\psi_c = -K\psi_{[a}N_{b]c}. \tag{7.207}$$

2-Tensor Commutation Relations:

$$\hat{\dot{\psi}}_{ab} - \dot{\hat{\psi}}_{ab} = -\mathcal{A}\dot{\psi}_{ab} + \left(\Sigma + \frac{1}{3}\Theta\right)\hat{\psi}_{ab} \tag{7.208}$$

$$\delta_a\dot{\psi}_{bc} - \left(\delta_a\psi_{bc}\right)^{\cdot} = -\frac{1}{2}\left(\Sigma - \frac{2}{3}\Theta\right)\delta_a\psi_{bc} \tag{7.209}$$

$$\delta_a\hat{\psi}_{bc} - \widehat{(\delta_a\psi_{bc})} = \frac{1}{2}\phi\,\delta_a\psi_{bc} \tag{7.210}$$

$$\delta_{[a}\delta_{b]}\psi_{cd} = -K\left[N_{c[b}\psi_{a]d} + N_{d[b}\psi_{a]c}\right]. \tag{7.211}$$

7.5.10 Geometry of Sheets

7.5.10.1 Second Fundamental Form

As we did with the decomposition of spacetime into a timelike congruence and the orthogonal 3-surfaces Σ, we can introduce the extrinsic curvature associated to the spacelike 2-surfaces Ω

$$\chi_{ab} = D_a n_b = n_a a_b + \frac{1}{2}\phi N_{ab} + \zeta_{ab}, \tag{7.212}$$

where we have assumed that the 2-surface is vorticity free $\xi = 0$. The mean curvature of these surfaces can be defined as the trace of the extrinsic curvature

$$H = \chi^a{}_a = \phi. \tag{7.213}$$

7.5.10.2 Genuine 2-Surfaces

By inspection of 7.199, we see that the 2-sheet will be a genuine surface in spacetime, implying that δ_a is a genuine covariant derivative, if and only if $\Omega = \xi = a^a = 0$ [105]. If this criterion is not met, the 2-sheet will just be a collection of tangent planes. Alternatively, the two vectors u^a and n^a are 2-surface forming if and only if the commutator $[u, n]$, i.e. 7.196, does not contain any component that lies in the sheet. This is equivalent to demanding that Greenberg's vector

$$\Sigma^a + \epsilon^{ab}\Omega_b - \alpha^a \tag{7.214}$$

vanishes [223; 603; 105].

7.5.10.3 The Geometry of Vorticity Free 2-Surfaces

Following the discussion above, if we restrict ourselves to the set of LRS class II spacetimes, for which $\{\Omega, \xi, \mathcal{H}\}$ along with all 2-vectors and 2-tensors are set to zero, then u^a will be genuinely hypersurface orthogonal to the spatial 3-surfaces. We can use the Gauss equation for u^a to calculate the intrinsic curvature [58]

$$\begin{aligned} {}^3R_{ab} = &\left[\frac{2}{3}(\mu + \Lambda) + \mathcal{E} + \frac{1}{2}\Pi + \Sigma^2 - \frac{1}{3}\Theta\Sigma - \frac{2}{9}\Theta^2\right] n_a n_b \\ &+ \left[\frac{2}{3}(\mu + \Lambda) - \frac{1}{2}\mathcal{E} - \frac{1}{4}\Pi + \frac{1}{4}\Sigma^2 + \frac{1}{6}\Theta\Sigma - \frac{2}{9}\Theta^2\right] N_{ab}. \end{aligned} \tag{7.215}$$

A contraction of the indices yields the Ricci scalar of the 3-surfaces in terms of our 1+1+2 scalars [58]

$${}^3R = 2\left[\mu + \Lambda - \frac{1}{3}\Theta^2 + \frac{3}{4}\Sigma^2\right]. \tag{7.216}$$

Likewise, the vanishing of the sheet distortion ξ implies that the sheet is a genuine 2-surface. The Gauß equation for n^a and the 3-Ricci identities means that we can re-express the 3-Ricci curvature tensor of the spatial 3-surfaces as [58]

$${}^3R_{ab} = -\left[\hat{\phi} + \frac{1}{2}\phi^2\right] n_a n_b - \left[\frac{1}{2}\hat{\phi} + \frac{1}{2}\phi^2 - K\right] N_{ab} \tag{7.217}$$

hence

$${}^3R = -2\left[\hat{\phi} + \frac{3}{4}\phi^2 - K\right]. \tag{7.218}$$

Here, K is the Gaussian curvature of the 2-surfaces defined by ${}^2R_{ab} = KN_{ab}$. Combining 7.163, 7.216 and 7.218 it is possible to derive an identity for the Gaussian curvature K

$$K = \frac{1}{3}(\mu + \Lambda) - \mathcal{E} - \frac{1}{2}\Pi + \frac{1}{4}\phi^2 - \left(\frac{1}{3} - \frac{1}{2}\Sigma\right)^2. \tag{7.219}$$

Using the system of propagation and evolution equations we see that

$$\dot{K} = \left(\Sigma - \frac{2}{3}\Theta\right) K \tag{7.220}$$

$$\hat{K} = -\phi K. \tag{7.221}$$

The expression in 7.220 tells us that if the Gaussian curvature of the 2-surfaces is constant in time but non-zero, then the shear Σ is proportional to the expansion Θ [58]

$$\left\{K \neq 0 \text{ and } \dot{K} = 0\right\} \mapsto \Sigma = \frac{2}{3}\Theta \tag{7.222}$$

A non-vanishing K simply means that the 2-surfaces will posses either spherical or hyperbolic geometries. As discussed in [58], it is always possible to pick static observers, as allowed the frame freedom, for which $\dot{K} = 0$. Choosing such an observer, a spherically symmetric spacetime admits a covariant definition of the radial parameter r via the following relationship

$$r^{-2} = K = \frac{1}{3}(\mu + \Lambda) - \mathcal{E} - \frac{1}{2}\Pi + \frac{1}{4}\phi^2; \qquad \dot{r} = \delta_a r = 0. \tag{7.223}$$

Alternatively, we are free to choose a non-static observer for which $\dot{r} \neq 0$. The choice of observer often depends on the physical quantities of interest as well as the fundamental properties of the spacetime under investigation. In the most general case we find that

$$r^{-2} = K; \quad \dot{r} = -\frac{1}{2}r\left(\Sigma - \frac{2}{3}\Theta\right) \quad \hat{r} = \frac{1}{2}\phi r \quad \delta_a r = 0. \tag{7.224}$$

These relationships will allow us to simply various terms in the 1+1+2 expressions.

7.5.11 Mass and Energy

A useful definition for us to have is a spacetime dependent mass. In general, energy and momentum in General Relativity is a loaded subject and often tantamount to navigating a minefield for the uninitiated. In part, this is due to the fact that there is currently no unique general definition for the total mass or energy of a system, indeed the first definition was by Einstein in 1916 [173]. One of the crowning achievements in classical General Relativity has been the proof of the positivity of the total gravitational energy at both spatial and null infinity [489; 490; 592]. These theorems spurred the search for a more ambitious definition of energy and mass that could be applied to extended but finite spacetime domains, the so called quasi-local definitions. Unluckily, a unique and general definition of quasi-local mass has been extremely difficult to find.

There are a number of reasons why it would be desirable to have such a well defined definition of energy in General Relativity. The first is that a generic gravitating system will emit gravitational waves constituting a loss of energy to the system. The detection of such gravitational waves necessitates a transfer of energy between the gravitational field and the detector itself. It would therefore be useful to have a device that can measure the amount of energy carried away from the system by the gravitational field. Secondly, whilst we have well defined notions of global energy and momentum for isolated gravitating systems, nature is never so kind in reality. We need a more

general definition of energy and momentum that is applicable to systems with reduced symmetry and generic asymptotic behaviour out to null or spacelike infinity. In addition we often want to consider localised domains of spacetime for which a quasi-local prescription would be necessary. As an example, in numerical relativity the computations typically occur on finite spatial domains for which a robust quasi-local prescription of mass and energy can aid in understanding the behaviour of black holes as well as the emitted gravitational radiation. Compactification schemes may be introduced in order to efficiently calculate and extract the emitted gravitational waves at future null infinity $\mathscr{I}^+$, however a robust implementation of such schemes has been difficult to formulate.

A covariant approach to defining mass in spherical symmetry follows the Misner-Sharp prescription [376]. Here we consider spherically symmetric spacetimes where the rotation group SO(3) acts transitively as an isometry. The orbits of this rotation group will be round spheres. Remember, the orbit of a point x in the set X was the set of elements of X to which x can be moved to by the elements of the group G. Intuitively, the rotation group SO(3) takes any point at a given radial parameter r and maps it to another point on the sphere of area $A = 4\pi r_A^2$. This area radius r_A has an invariant meaning, as does it's gradient

$$|\nabla r|^2 = g^{ab}\,\nabla_a r\,\nabla_b r. \tag{7.225}$$

This was then used to construct an expression for the mass of the spacetimes where the gradient of the radius acts as something of an estimate for the bending of ingoing and outgoing null rays from the 2-sphere $\mathcal{S}$. This is formulated in a more rigorous manner by the Hawking mass which, in spherical symmetry, reduces to the Misner-Sharp prescription [243]. The Misner-Sharp mass is defined by

$$m_{\rm MS} = \frac{r}{2}\left(1 - |\nabla r|^2\right). \tag{7.226}$$

In the 1+1+2 prescription the covariant derivative of the radial parameter decomposes as follows

$$\begin{aligned}\nabla_a r &= -u_a\dot{r} + D_a r \\ &= -u_a\dot{r} + n_a\hat{r} + \delta_a r.\end{aligned} \tag{7.227}$$

However, due to spherical symmetry, the angular derivative $\delta_a r$ is necessarily zero. This is true in any LRS background spacetime. Inserting the expressions for the decomposed covariant derivative and metric of the spacetime we find

$$\begin{aligned}g^{ab}\nabla_a r\nabla_b r &= \left(N^{ab} - u^a u^b + n^a n^b\right)\left(-u_a\dot{r} + n_a\hat{r}\right)\left(-u_b\dot{r} + n_b\hat{r}\right) \\ &= -\dot{r}^2 + \hat{r}^2.\end{aligned} \tag{7.228}$$

Inserting into the Misner-Sharp mass, we find

$$m_{\rm MS} = \frac{r}{2}\left[1 + r^2\left\{\left(\frac{\dot{r}}{r}\right)^2 - \left(\frac{\hat{r}}{r}\right)^2\right\}\right]. \tag{7.229}$$

We can now express the Misner-Sharp mass in terms of the kinematical and covariant objects that characterise our spacetimes

$$m_{\rm MS} = \frac{r}{2}\left[1 + r^2\left\{\frac{1}{9}\Theta^2 - \frac{1}{3}\Theta\Sigma + \frac{1}{4}\Sigma^2 - \frac{1}{4}\phi^2\right\}\right]. \tag{7.230}$$

A natural outcome is that for $r = 2m$ we require

$$\frac{1}{9}\Theta^2 - \frac{1}{3}\Theta\Sigma + \frac{1}{4}\Sigma^2 - \frac{1}{4}\phi^2 = 0 \tag{7.231}$$

or, alternatively,

$$\left(\Sigma - \frac{2}{3}\Theta - \phi\right)\left(\Sigma - \frac{2}{3}\Theta + \phi\right) = 0. \tag{7.232}$$

This criteria is necessary for the presence of an apparent horizon, given by the first solution, or a cosmological horizon, given by the second solution [236]. This also corresponds to the well known result that when we have an apparent horizon the mass is simply $m_{\rm MS} = r/2$. We are also free to re-express this mass in terms of the Gaussian curvature of the spacetime

$$m_{\rm MS} = \frac{r}{2}\left[1 + r^2\left(\frac{1}{3}(\mu + \Lambda) - \mathcal{E} - \frac{1}{2}\Pi - K\right)\right] \tag{7.233}$$

From this definition we can evaluate some interesting quantities such as

$$\hat{m}_{\rm MS} = \frac{1}{4}r^3\left[\phi\mu - Q\left(\Sigma - \frac{2}{3}\Theta\right)\right] \tag{7.234}$$

$$\dot{m}_{\rm MS} = \frac{1}{4}r^3\left[(p + \Pi - \Lambda)\left(\Sigma - \frac{2}{3}\Theta\right) - \phi Q\right] \tag{7.235}$$

where we have used the fact that the Gaussian curvature is covariantly defined by $K = r^{-2}$ to eliminate the other terms. This approach to the Misner-Sharp mass allows us to understand the definition of mass in the set of LRS-II spacetimes. In particular, it provides an understanding of how mass is dependent on the radial part of the shear of the timelike congruence Σ, the expansion of the timelike congruence Θ and the expansion of the spacelike congruence ϕ. As always, it is not clear that the definitions given here are well behaved and constitute a well defined measure of mass. In the spherically symmetric case, we simply recover the results of [376] and [243].

7.5.12 Covariant Tensor Harmonic Decomposition

The equations as we have presented them cannot be solved due to the appearance of angular derivatives. As is common in many other areas of physics, it is possible to replace angular derivatives by an appropriate harmonic coefficient. The locally rotationally symmetric nature of the back-

ground spacetime allows us to introduce a set of generalised harmonic functions that are adapted to the symmetry. The convention that we use is that of [103; 104; 58].

We introduce a dimensionless sheet harmonic function $Q = Q^{(k)}$ defined on the background spacetime as an eigenfunction of the two-dimensional Laplace-Beltrami operator. For positive, negative of vanishing Gaussian curvature K we find

$$\delta^2 Q = -\frac{k^2}{r^2} Q, \qquad \hat{Q} = \dot{Q} = 0. \tag{7.236}$$

It is important to note that these harmonics are defined on a sphere of radius r unlike the spherical harmonics which, for comparison, are defined on the unit sphere. As noted before, the function r is covariantly defined by its relation to the Gaussian curvature $K = r^{-2}$ resulting in the following

$$\frac{\hat{r}}{r} = \frac{1}{2}\phi \qquad \frac{\dot{r}}{r} = -\frac{1}{2}\left(\Sigma - \frac{2}{3}\Theta\right) \qquad \delta_a r = 0. \tag{7.237}$$

Using the covariant harmonics, we can expand any first-order scalar ψ as

$$\psi = \sum_k \psi_S^{(k)}\, Q^{(k)} = \psi_S\, Q \tag{7.238}$$

where ψ_S denotes the scalar coefficient associated with the basis function $Q^{(k)}$. These harmonics can be generalised to vector and tensor harmonics by following the conventional procedure. e.g. [13]. The even parity vector harmonics are given by

$$Q_a^{(k)} = r\,\delta_a Q^{(k)} \Rightarrow \hat{Q}_{\bar{a}} = \dot{Q}_{\bar{a}} = 0, \qquad \delta^2 Q_a = (1 - k^2)\, r^{-2}\, Q_a \tag{7.239}$$

and the odd parity vector harmonics are defined by

$$\bar{Q}_a^{(k)} = r\,\epsilon_{ab}\,\delta^b\, Q^{(k)} \Rightarrow \hat{\bar{Q}}_{\bar{a}} = \dot{\bar{Q}}_{\bar{a}} = 0, \qquad \delta^2 \bar{Q}_a = (1 - k^2)\, r^{-2}\, \bar{Q}_a. \tag{7.240}$$

In this formalism $\bar{Q}_a$ will be solenoidal,

$$\delta^a\, \bar{Q}_a = 0 \tag{7.241}$$

while

$$\delta^a\, Q_a = -k^2\, r^{-1}\, Q. \tag{7.242}$$

Also note that

$$\epsilon_{ab}\delta^a Q^b = 0, \qquad \epsilon_{ab}\delta^a \bar{Q}^b = k^2 r^{-1} Q. \tag{7.243}$$

These vector harmonics are orthogonal: $Q^a\,\bar{Q}_a = 0$ for each k. This implies that any first order vector ψ_a may be decomposed into this vector harmonic basis

$$\psi_a = \sum_k \psi_V^{(k)}\, Q_a^{(k)} + \bar{\psi}_V^{(k)}\, \bar{Q}_a^{(k)} = \psi_V Q_a + \bar{\psi}_V \bar{Q}_a. \tag{7.244}$$

Finally, we can define a set of tensor harmonics in a completely analogous manner. The even parity tensor harmonics are defined by [104; 105; 437]

$$Q_{ab} = r^2\,\delta_{\{a}\delta_{b\}} Q \Rightarrow \hat{Q}_{ab} = \dot{Q}_{ab} = 0 \tag{7.245}$$

$$\delta^2 Q_{ab} = (4-k^2) r^{-2}\, Q_{ab} \tag{7.246}$$

and the odd parity tensor harmonic are defined by [104; 105; 437]

$$\bar{Q}_{ab} = r^2\,\epsilon_{c\{a}\delta^c\delta_{b\}} Q \Rightarrow \hat{\bar{Q}}_{ab} = \dot{\bar{Q}}_{ab} = 0 \tag{7.247}$$

$$\delta^2 \bar{Q}_{ab} = (4-k^2) r^{-2}\, \bar{Q}_{ab}. \tag{7.248}$$

Any first order tensor ψ_{ab} can now be decomposed into this tensor harmonic basis as follows

$$\psi_{ab} = \sum_k \psi_T^{(k)} Q_{ab}^{(k)} + \bar{\psi}_T^{(k)} \bar{Q}_{ab}^{(k)} = \psi_T Q_{ab} + \bar{\psi}_T \bar{Q}_{ab}. \tag{7.249}$$

With these relations in place we can systematically calculate all the necessary relationships that are required in order to harmonically decompose the full system of evolution, propagation and constraint equations:

SCALAR			VECTOR			TENSOR		
Ψ	$=$	$\Psi_{\mathsf{S}} Q$	Ψ_a	$=$	$+\Psi_{\mathsf{V}} Q_a + \bar{\Psi}_{\mathsf{V}} \bar{Q}_a$	Ψ_{ab}	$=$	$+\Psi_{\mathsf{T}} Q_{ab} + \bar{\Psi}_{\mathsf{T}} \bar{Q}_{ab}$
$\delta_a \Psi$	$=$	$r^{-1}\Psi_{\mathsf{S}} Q_a$	$\varepsilon_{ab}\Psi^b$	$=$	$-\bar{\Psi}_{\mathsf{V}} Q_a + \Psi_{\mathsf{V}} \bar{Q}_a$	$\varepsilon_{c\{a}\Psi_{b\}}^{\quad c}$	$=$	$-\bar{\Psi}_{\mathsf{T}} Q_{ab} + \Psi_{\mathsf{T}} \bar{Q}_{ab}$
$\varepsilon_{ab}\delta^b\Psi$	$=$	$r^{-1}\Psi_{\mathsf{S}} \bar{Q}_a$	$\delta^a \Psi_a$	$=$	$-k^2 r^{-1} \Psi_{\mathsf{V}} Q$	$\delta^b \Psi_{ab}$	$=$	$\frac{1}{2}(k^2-2) r^{-1} \left(-\Psi_{\mathsf{T}} Q_a + \bar{\Psi}_{\mathsf{T}} \bar{Q}_a\right)$
			$\varepsilon_{ab}\delta^a\Psi^b$	$=$	$+k^2 r^{-1} \bar{\Psi}_{\mathsf{V}} Q$	$\varepsilon_{c\{d}\delta^d\Psi_{a\}}^{\quad c}$	$=$	$\frac{1}{2}(k^2-2) r^{-1} \left(+\bar{\Psi}_{\mathsf{T}} Q_a + \Psi_{\mathsf{T}} \bar{Q}_a\right)$
			$\delta_{\{a}\Psi_{b\}}$	$=$	$r^{-1}\left(\Psi_{\mathsf{V}} Q_{ab} - \bar{\Psi}_{\mathsf{V}} \bar{Q}_{ab}\right)$			
			$\varepsilon_{c\{a}\delta^c\Psi_{b\}}$	$=$	$r^{-1}\left(\bar{\Psi}_{\mathsf{V}} Q_{ab} + \Psi_{\mathsf{V}} \bar{Q}_{ab}\right)$			

(7.250)

7.5.13 Gauge and Frame Invariance

We finally make some comments regarding the choice of frame and gauge invariance in the 1+1+2 framework following the discussion detailed in [104]. The 1+1+2 formalism is known as a

partial-frame of partial-tetrad approach as it introduces two preferred basis vectors corresponding to the existence of a preferred timelike and a preferred spacelike congruence. In General Relativity we actually have two types of gauge freedom: the freedom in the choice of coordinates but also the freedom to choose a frame basis in the tangent space at each point.

Gauge freedom is a tricky subject and contains many subtleties. The choice of coordinate system often amounts to a fixing of the mapping between the background and perturbed spacetimes. This allows us to directly compare scalar, vector and tensor objects in the two spacetimes [165; 77; 78; 104]. In the metric approach we find a nice coordinate system in the perturbed spacetime, corresponding to that in the background, and writing down a system of equations for the derivatives of the perturbations to our scalar, vector and tensor objects.

In the partial-frame formalism, we *do no* make any explicit reference to the background spacetime and only use a background spacetime to determine which quantities will be of zeroth order, i.e. those that are non-vanishing in the background. In this sense covariant simply means coordinate-invariant. If we are given a set of frame vectors, we can write down a system of covariant equations that describe the true spacetime. It is here that we invoke the Stewart-Walker lemma [534] stating that if all of our variables vanish in the background spacetime then they will naturally be gauge-invariant. The covariant variables, however, are defined as projections of tensors with respect to our frame vectors u^a and n^a. The projected parts will depend on the choice of frame vectors. This is where a problem kicks in, the true spacetime typically lacks any symmetries and we cannot define any unique frame vectors as it is always permissible to perform a first order rotation of these [104]. This is a reflection of the fact that in any spacetime we can choose the frame vectors at any point freely. Consequentially, there are no evolution equations for $\mathcal{A}, \mathcal{A}_a$ and α_a and there is no propagation equation for a_a. Instead we would have to supply the equations of motion for these by hand.

So, the 1+1+2 formalism is covariant, can define natural gauge-invariant objects but is not frame invariant. This is no different to other similar approaches such as the Newman-Penrose approach [403].

7.6 2+2 Formalism

7.6.1 Historical Introduction

Perturbations of a spherically symmetric spacetime are one of the first non-trivial exercises that we can analytically perform in General Relativistic perturbation theory. As such this situation has been considered many times in the literature, often in the context of modelling perturbations to static and stationary stars or black holes. Different formalisms exist in the literature for the construction of both the system of perturbations and the gauge-invariant variables. Gerlach and Sengupta (GS) [201; 202] introduced a covariant 2+2 split of the metric and energy-momentum tensor as a means to reduce the problem into a 2-dimensional problem for the two coordinates of primary importance: time and a radial parameter. This 2+2 approach is based on metric perturbation theory and casts the field equations as a system of second order PDEs. Gundlach and Martin-Garcia (GMG) [229] provided something of a completion to the work of GS by introducing a systematic derivation of the gauge- invariant variables as well as performing a decomposition of

the reduced 2-dimensional tensors and tensor equations into frame-components using a natural frame provided by the fluid. This is, in some ways, analogous to the introduction of a preferred fundamental observer that we made in our 1+3 and 1+1+2 decompositions earlier. The resulting system of equations is linearly gauge-invariant and independent of the background coordinates. In addition, GMG were able to write down a system of master equations that describe all perturbations.

7.6.2 Splitting Spacetime Even More

The 2+2 formalism is built around the decomposition of the background manifold into a warped product $M^4 = M^2 \times S^2$ of a two-dimensional Lorentzian manifold M^2 and the 2-sphere S^2. We will use upper case Latin indices $A, B, C, \ldots$ to denote coordinates in M^2 and lower case Latin indices $a, b, c, \ldots$ to denote coordinates in S^2. Greek indices $\mu, \nu, \chi, \ldots$ to denote coordinates in the full 4-dimensional spacetime. This section follows the formalism as presented by [201; 202; 350; 229; 351]. The metric of our spacetime can be written as the semidirect product of the metric on M^2 denoted g_{AB} and the metric on the unit curvature sphere S^2 denoted γ_{ab}:

$$g_{\mu\nu} = \text{diag}\left(g_{AB}\,,\, r^2\,\gamma_{ab}\right). \tag{7.251}$$

The scalar $r = r(X^A)$ is defined on M^2 and can be identified as the invariantly defined radial coordinate of spherically-symmetric spacetimes such that $r = 0$ defines the boundary of M^2. Following this decomposition we can define three different covariant derivatives. In addition to the usual covariant derivative on the full 4-dimensional spacetime,

$$g_{\alpha\beta;\gamma} = 0, \tag{7.252}$$

we also define covariant derivatives in the two submanifolds:

$$g_{AB|C} = 0 \tag{7.253}$$

$$\gamma_{ab:c} = 0. \tag{7.254}$$

A comma denotes the 4-dimensional covariant derivative, the vertical bar a covariant derivative on M^2 and a comma a covariant derivative on S^2. It is possible to define completely antisymmetric covariant unit tensors on the submanifolds such that:

$$\epsilon_{AB|C} = \epsilon_{ab:c} = 0 \tag{7.255}$$

$$\epsilon_{AC}\,\epsilon^{BC} = -g_A{}^B \tag{7.256}$$

$$\epsilon_{ac}\,\epsilon^{bc} = -\gamma_a{}^b. \tag{7.257}$$

We can decompose the energy-momentum tensor in a spherically symmetric spacetime in an analogous way to the metric:

$$T_{\mu\nu} = \text{diag}\left(t_{AB}\,,\, Q(x^C)\,r^2\,\gamma_{ab}\right). \tag{7.258}$$

For convenience we also define the following variable:

$$v_A = \frac{r_{|A}}{r}. \tag{7.259}$$

Einstein's field equations $G_{\mu\nu} = 8\pi t_{\mu\nu}$ in spherical symmetry can now be re-written in the following 2+2 decomposed form

$$-2\left(v_{A|B} + v_A\, v_B\right) + 2\left({v_C}^{|C} + 3v_C\, v^C - \frac{1}{r^2}\right) g_{AB} = 8\pi t_{AB} \tag{7.260}$$

$${v_C}^{|C} + v_C\, v^C - \mathcal{R} = 8\pi Q, \tag{7.261}$$

where $\mathcal{R} = \frac{1}{2}R^A{}_A$ is the Gaussian curvature of g_{AB}. The energy-momentum conservation equation in spherical symmetry becomes:

$${t_{AB}}^{|B} + 2t_{AB}\, v^B - 2v^A Q = 0. \tag{7.262}$$

7.6.3 Nonspherical Perturbations and Gauge-Invariant Variables

In conventional FLRW cosmology, perturbations can be split into scalar, vector and tensor (SVT) modes that decouple from each other and evolve independently at linear order. This classification scheme is a generalisation of Helmholtz's theorem and is based on the transformation properties of the perturbations on the homogeneous and isotropic spatial hypersurfaces [535].

The SVT decomposition scheme does not work in spatially inhomogeneous backgrounds as the modes written in such a way would couple together. Instead, linear perturbations around a spherically symmetric background may be decomposed into scalar, vector or tensor spherical harmonics whereby the classification of perturbations is based on their transformation properties on the surfaces of spherical symmetry. The perturbative variables then decouple into a scalar, vector or tensor field on M^2 times a spherical harmonics scalar, vector or tensor field on S^2. This is particularly useful as the perturbation problem is reduced to a 2-dimensional problem, typically involving a spatial and time coordinate. The tensor harmonics are decomposed into two independent modes called *polar* (or even) and *axial* (or odd). These two sectors transform differently under parity transformations: $(-1)^\ell$ for polar modes and $(-1)^{\ell+1}$ for axial modes. This split is analogous but not equivalent to the SVT modes in FLRW cosmology.

The appropriate set of basis functions for S^2 are tensor spherical harmonics. These functions can be derived from the standard spherical harmonics $Y^{(\ell m)}(x^a)$ which are eigenfunctions of the covariant Laplacian on the unit sphere:

$$\bar{\nabla}^2 Y^{(\ell m)} = -\ell\left(\ell + 1\right), \tag{7.263}$$

where ℓ is the multipole giving the angular scale of the perturbation. The covariant Laplacian on the unit sphere $\bar{\nabla}^2$ is defined by: $\bar{\nabla}^2 Y = \gamma^{ab} Y_{:ab}$. Scalar perturbations on S^2 are now expanded as:

$$\phi\left(x^A, x^a\right) = \sum_{\ell=0}^{\infty} \sum_{m=-\ell}^{m=\ell} \phi^{(\ell m)}(x^A)\, Y^{(\ell m)}(x^a). \tag{7.264}$$

Harmonic vector and tensor fields on S^2 can be constructed from covariant derivatives of the scalar harmonics and contractions of those tensors with the fundamental antisymmetric tensor, ϵ_{ab}. Perturbations containing and even power of ϵ_{ab} are polar and models containing an odd power of ϵ_{ab} are axial. A basis of harmonic vector fields on S^2 is formed for $\ell \geq 1$ by:

$$Y_a^{(\ell m)} = Y_{:a}^{(\ell m)} \tag{7.265}$$

$$\bar{Y}_a^{(\ell m)} = \epsilon_a{}^b\, Y_{:b}^{(\ell m)}. \tag{7.266}$$

For both parities the vector harmonics obey the Laplacian equation:

$$\bar{\nabla}^2\, Y_a^{(\ell m)} = \left[1 - \ell\left(\ell + 1\right)\right]\, Y_a^{(\ell m)} \tag{7.267}$$

$$\bar{\nabla}^2\, \bar{Y}_a^{(\ell m)} = \left[1 - \ell\left(\ell + 1\right)\right]\, \bar{Y}_a^{(\ell m)}. \tag{7.268}$$

As the vector harmonics are orthogonal for each ℓ, any rank-1 tensor can be expanded in terms of these vector harmonics:

$$\phi_a\left(x^A, x^a\right) = \sum_{\ell=0}^{\infty} \sum_{m=-\ell}^{m=\ell} \phi^{(\ell m)}(x^A)\, Y_a^{(\ell m)}(x^a) \;+\; \bar{\phi}^{(\ell m)}(x^A)\, \bar{Y}_a^{(\ell m)}(x^a), \tag{7.269}$$

where $\phi^{(\ell m)}$ and $\bar{\phi}^{(\ell m)}$ decouple for different (ℓm) and are defined to be:

$$\phi^{(\ell m)} = -\frac{1}{\ell\left(\ell + 1\right)} \int d\Omega\, \left[\phi^a{}_{:a}\right]\, Y^*_{(\ell m)} \tag{7.270}$$

$$\phi^{(\ell m)} = -\frac{1}{\ell\left(\ell + 1\right)} \int d\Omega\, \left[\epsilon^{ab}\, \phi_{b:a}\right]\, Y^*_{(\ell m)}. \tag{7.271}$$

Note that there are no $\ell = 0$ vector degrees of freedom as $\ell = 0$ describes spherical modes.

A basis of tensor harmonics on S^2 can be formed for $\ell \geq 2$ as follows:

$$Y_{ab}^{(\ell m)} = Y_{:ab}^{(\ell m)} + \frac{\ell\left(\ell + 1\right)}{2}\, Y^{(\ell m)} \gamma_{ab} \tag{7.272}$$

$$\bar{Y}_{ab}^{(\ell m)} = 2\bar{Y}_{(a:b)}^{(\ell m)} = -2\epsilon^d{}_{(a} Y_{:b)d}^{(\ell m)}, \tag{7.273}$$

where the tensor harmonics obey the Laplacian equation:

$$\bar{\nabla}^2\, Y_{ab}^{(\ell m)} = \left[1 - \ell\left(\ell + 1\right)\right]\, Y_{ab}^{(\ell m)} \tag{7.274}$$

$$\bar{\nabla}^2 \bar{Y}_{ab}^{(\ell m)} = \left[1 - \ell\left(\ell+1\right)\right] \bar{Y}_{ab}^{(\ell m)}. \tag{7.275}$$

Any rank-2 tensor perturbation can be expanded as:

$$\phi_{ab}\left(x^A, x^a\right) = \sum_{\ell=0}^{\infty} \sum_{m=-\ell}^{m=\ell} \phi^{(\ell m)}(x^A)\, Y_{ab}^{(\ell m)}(x^a) \;+\; \bar{\phi}^{(\ell m)}(x^A)\, \bar{Y}_{ab}^{(\ell m)}(x^a), \tag{7.276}$$

where the coefficients are reconstructed as follows:

$$\phi^{(\ell m)} = 2\frac{(\ell-2)!}{(\ell+2)!} \int d\Omega \, \left[\phi^{ab}{}_{:ba}\right] \, Y^*_{(\ell m)} \tag{7.277}$$

$$\phi^{(\ell m)} = 2\frac{(\ell-2)!}{(\ell+2)!} \int d\Omega \, \left[\epsilon_a{}^c \, \phi^{ab}{}_{:bc}\right] \, Y^*_{(\ell m)} \tag{7.278}$$

All perturbations with different (ℓm) decouple due to spherical symmetry. Perturbations with differing m for the same value of ℓ will have the same dynamics in spherical symmetry. As a result we see that m never appears in the field equations.

7.6.4 Gauge Invariant Perturbations

Following our discussion about the importance of gauge-invariant variables, we now consider linear perturbations around a fixed background and how to systematically construct gauge-invariant variables (e.g. Fig. 7.3)

$$g_{\mu\nu} = g^{(0)}_{\mu\nu} + h_{\mu\nu} = g^{(0)}_{\mu\nu} + h^{\text{Polar}}_{\mu\nu} + h^{\text{Axial}}_{\mu\nu} \tag{7.279}$$

$$T_{\mu\nu} = T^{(0)}_{\mu\nu} + \Delta T_{\mu\nu} = g^{(0)}_{\mu\nu} + \Delta T^{\text{Polar}}_{\mu\nu} + \Delta T^{\text{Axial}}_{\mu\nu} \tag{7.280}$$

The general axial metric and matter perturbations are parametrised as follows:

$$h^{\text{Axial}}_{\mu\nu} = \begin{pmatrix} 0 & h^{\text{Axial}}_A \bar{Y}_a \\ h^{\text{Axial}}_A \bar{Y}_a & h\bar{Y}_{ab} \end{pmatrix}. \tag{7.281}$$

$$\Delta T^{\text{Axial}}_{\mu\nu} = \begin{pmatrix} 0 & \Delta t^{\text{Axial}}_A \bar{Y}_a \\ \Delta t^{\text{Axial}}_A \bar{Y}_a & \Delta t^{(1)} \bar{Y}_{ab} \end{pmatrix}, \tag{7.282}$$

and the polar metric and matter perturbations are parametrised as:

$$h^{\text{Polar}}_{\mu\nu} = \begin{pmatrix} h_{AB}\, Y & h^{\text{Polar}}_A Y_a \\ h^{\text{Polar}}_A Y_a & r^2\left(K\, Y\, \gamma_{ab} + G Y_{:ab}\right) \end{pmatrix}. \tag{7.283}$$

$$\Delta T^{\text{Polar}}_{\mu\nu} = \begin{pmatrix} \Delta t_{AB} & \Delta t^{\text{Polar}}_A Y_a \\ \Delta t^{\text{Polar}}_A Y_a & \Delta t^{(2)} Y_{ab} + r^2 \Delta t^{(3)}\, Y\, \gamma_{ab} \end{pmatrix}. \tag{7.284}$$

The coefficients $\left\{h, h^{\text{Polar}}_A, h^{\text{Axial}}_A, h_{AB}, K, G, \Delta t_{AB}, \Delta t^{\text{Axial}}_A, \Delta^{\text{Polar}}_A, \Delta t^{(1)}, \Delta t^{(2)}, \Delta t^{(3)}\right\}$ are in general functions of x^A.

If X is an arbitrary tensor field on the background spacetime with linear perturbation ΔX,

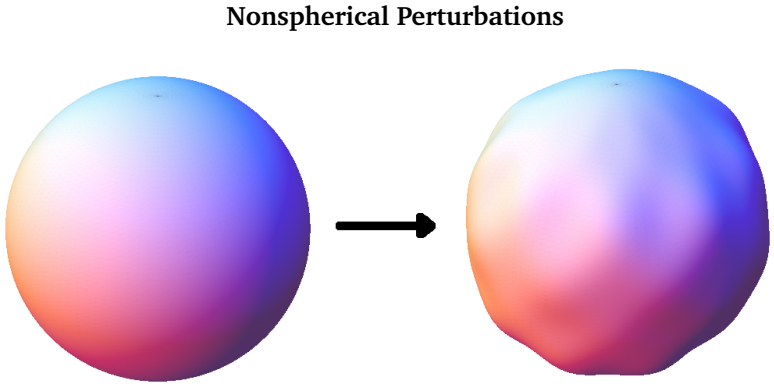

Figure 7.3: A schematic picture of non-spherical perturbations. We introduce linear perturbations around a spherically symmetric background spacetime via $g_{\mu\nu} = g^{(0)}_{\mu\nu} + h_{\mu\nu}$.

then under an infinitesimal coordinate transformation $x^\mu \to x^\mu + \xi^\mu$ the linear perturbation will be mixed with the background:

$$\Delta X \to \Delta X + \mathcal{L}_\xi X, \tag{7.285}$$

where $\mathcal{L}_\xi$ is the Lie derivative with respect to the vector field ξ. Importantly, this tells us that the perturbation variable ΔX is gauge invariant to linear order if and only if $\mathcal{L}_\xi X = 0$. This means that gauge-invariance of a perturbation variable is intrinsically linked to the existence of symmetries in the background spacetime. If $\mathcal{L}_\xi X$ vanishes, the perturbation variable X will be invariant under the Lie dragging of the variable along the congruence generated by ξ^μ.

It was shown by [229] that in order to obtain the bare perturbations in an arbitrary gauge, one just needs to fix $\{h, h^{\rm Polar}_A, G\}$ arbitrarily and all other bare perturbations can be obtained algebraically. This leads us to introduce a preferred gauge known as the *Regge-Wheeler gauge* (RW) [458; 229] for which $h = h^{\rm Polar}_A = G = 0$. In this gauge, the gauge invariant variables are defined to correspond one-to-one with the remaining bare perturbations. Importantly, the framework of [201; 202; 229] tells us that even if we adopt the RW gauge we can still transform to any other gauge using the known algebraic relations. Adopting the RW gauge greatly simplified our perturbations. For the axial sector, they reduce to

$$h^{\rm Axial}_{\mu\nu} = \begin{pmatrix} 0 & k_A \bar{Y}_a \\ k_A \bar{Y}_a & 0 \end{pmatrix}. \tag{7.286}$$

$$\Delta T^{\rm Axial}_{\mu\nu} = \begin{pmatrix} 0 & \Delta L_A \bar{Y}_a \\ L_A \bar{Y}_a & L\bar{Y}_{ab} \end{pmatrix}, \tag{7.287}$$

and for the polar sector they reduce to

$$h^{\rm Polar}_{\mu\nu} = \begin{pmatrix} k_{AB} Y & 0 \\ 0 & kr^2 Y \gamma_{ab} \end{pmatrix}. \tag{7.288}$$

$$\Delta T^{\text{Polar}}_{\mu\nu} = \begin{pmatrix} \Delta T_{AB} & T_A\, Y_a \\ T_A\, Y_a & T^2 Y_{ab} + r^2 T^3\, Y\, \gamma_{ab} \end{pmatrix}. \tag{7.289}$$

7.6.5 Perfect Fluid

We mostly consider spherically symmetric perfect fluids coupled to gravity. This means that the pressure is isotropic, entropy is conserved along each particle trajectory and we neglect heat fluxes, viscosity, chemical reactions and make the assumption that the fluid only has one component. If we assume that the entropy is constant in time and space then the equation of state reduces to $p = p(\rho)$, a barotropic fluid. In the GMG formalism this is equivalent to setting the specific entropy s to a constant and keeping perturbations to the specific entropy σ equal to zero.

The energy-momentum tensor for a perfect fluid is simply given by:

$$T_{\mu\nu} = (p + \rho)\, u_\mu u_\nu + p g_{\mu\nu}, \tag{7.290}$$

where p is the pressure, ρ is the density and u_μ is the fluid 4-velocity. This is much the same as we saw earlier in the 1+3 and 1+1+2 approaches. In spherical symmetry to fluid 4-velocity will only depend on terms in M^2 and the angular terms will go to zero, $u_\mu = (u_A, 0)$. This allows us to introduce a rather natural orthonormal basis $\{u_A, n_B\}$ on M^2 defined by the timelike unit vector u_A:

$$n_A = -\epsilon_{AB}\, u^B \Rightarrow n_A\, u^a = 0, \tag{7.291}$$

where n_A is a spacelike vector. The introduction of this fluid-frame allows us to decompose all tensor fields and tensor equations on M^2 into scalar fields and scalar equations. For instance, the metric and antisymmetric tensor on M^2 may be decomposed with respect to the fluid frame as follows:

$$g_{AB} = -u_A\, u_B + n_A\, n_B \tag{7.292}$$

$$\epsilon_{AB} = n_A\, u_B - u_A\, n_B. \tag{7.293}$$

Following the parametrisation of the energy momentum tensor in the 2+2 formalism 7.258, we immediately see that the energy-momentum tensor for a spherically symmetric background described by a perfect fluid 7.290 becomes:

$$t_{AB} = \rho\, u_A\, u_B + p\, n_A\, n_B \tag{7.294}$$

$$Q = p. \tag{7.295}$$

Convective frame derivatives can be introduced in analogy to the procedure adopted in the 1+3 formalism by projection along our timelike and spacelike basis vectors:

$$\dot{f} = u^A f_{|A} \tag{7.296}$$
$$f' = n^A f_{|A}. \tag{7.297}$$

GMG introduce a series of fundamental scalars that allow us to rewrite the EFEs in terms of pure scalar quantities:[5]

$$\begin{aligned}\Omega &= \ln \rho \\ U &= u^A v_A \\ W &= n^a v_A \\ \tau &= u^A{}_{|A} \\ \nu &= n^A{}_{|A}.\end{aligned}$$

It can sometimes be useful to reparametrise U and W in terms of the vector we defined earlier

$$|v|^2 = v^A v_A = W^2 - U^2 \tag{7.298}$$

as well as a velocity of the fluid V with respect to constant r observers

$$V = \frac{U}{W}. \tag{7.299}$$

Much as in the other approaches discussed, commutation relations play a central role in the 2+2 formalism. The commutation between frame derivatives obeys the following relation:

$$\left(\dot{f}\right)' - \left(f'\right)^{\cdot} = \tau f' - \nu \dot{f}. \tag{7.300}$$

The fluid equation of motion are derived from the conservation of energy-momentum and constitute a relativistic generalisation of the Euler-equations:

$$\dot{\Omega} + \left(1 + \frac{p}{\rho}\right)(\tau + 2U) = 0 \tag{7.301}$$
$$c_s^2\, \Omega' + \left(1 + \frac{p}{\rho}\right)\nu = 0. \tag{7.302}$$

The first equation is simply the energy conservation equation and the second equation is the Euler equation. The quantity c_s^2 is the speed of sound in the isentropic fluid trajectories. Einstein's field equations can be decomposed in the fluid frame to yield a set of scalar evolution and constraint equations:

$$U' = W(\tau - U) \tag{7.303}$$
$$\dot{W} = U(\nu - W) \tag{7.304}$$

[5] Please note that we have replaced μ in [229] with τ to avoid confusion with the energy-density in the 1+3 and 1+1+2 approaches defined previously.

$$W' = -4\pi\rho - W^2 + U\,\tau + \frac{m}{r^3} \tag{7.305}$$

$$\dot{U} = -4\pi\rho - U^2 + W\,\nu - \frac{m}{r^3}. \tag{7.306}$$

It can also be shown that:

$$\dot{\tau} - \nu' + \tau^2 - \nu^2 = \mathcal{R} = -4\pi\,(p+\rho) + \frac{2m}{r^3}. \tag{7.307}$$

We have also introduced the spacetime-dependent Hawking mass m in spherical symmetry:

$$m = \frac{r}{2}\left[1 - r_{|A}\,r^{|A}\right] = \frac{r}{2}\left[1 + r^2\left(U^2 - W^2\right)\right], \tag{7.308}$$

where the limit of m at spacelike infinity reproduces the ADM mass and the limit of m in future null infinity is the Bondi mass. For $m = r/2$ we note the presence of an apparent horizon. These results are in agreement with the covariant results derived in the 1+1+2 formalism presented earlier.

7.6.6 Nonspherical Perfect Fluid Perturbations

There are 4 independent fluid perturbations: a density perturbation and a 3-velocity perturbation. We follow the ansatz of GMG for parametrising the perturbations to the fluid 4-velocity:

$$\Delta u_\mu = \left[\left(w\,n_A + \frac{1}{2}h_{AB}\,u^B\right)\,Y\,,\; v\,Y_a\right] \tag{7.309}$$

for polar perturbations, and

$$\Delta u_\mu = \left(0, \bar{v}\,\bar{Y}_a\right) \tag{7.310}$$

for axial perturbations. The variables $\{v, \bar{v}, w\}$ are all functions of x^A. We also introduce the following parametrisation for the spacelike radial vector to allow for a frame degree of freedom associated with the 1+1+2 formalism:

$$\Delta n_\mu = \left[\left(w u_A + \frac{1}{2}h_{AB}n^B\right)Y, gY_a\right]. \tag{7.311}$$

The density and pressure perturbations are given by:

$$\rho \to \rho + \Delta\rho Y$$
$$p \to p + c_s^2\,\Delta\rho Y.$$

Note that in the above Δ corresponds to a gauge-invariant perturbation variable and does not denote a perturbed variable. The gauge-invariant tensors for energy-momentum perturbations

can be written in terms of the perfect fluid gauge-invariant perturbations:

$$\begin{aligned} T_{AB} &= (\rho + p)\left[w\left(u_A n_B + n_A u_B\right) + \frac{1}{2}\left(k_{AC} u_B + u_A k_{BC}\right) u^C\right] \\ &\quad + \Delta\rho\left(u_A u_B + c_s^2 n_A n_B\right) + p k_{AB}. \\ T_A &= v\left(\rho + p\right) u_A \\ T^3 &= p\,\varphi + c_s^2 \rho \Delta \\ T^2 &= 0 \end{aligned}$$

for the polar sector, and

$$L_A = \bar{v}\ (\rho + p)\ u_A \tag{7.312}$$

$$L = 0 \tag{7.313}$$

for the axial sector.

7.6.7 Initial Value Problem: Polar and Axial Perturbations

7.6.7.1 Axial Perturbations

Building a well-posed initial value problem in the GMG formalism turns out to be reasonably straightforward using the results of Gerlach and Sengupta. The only non-trivial matter conservation equation, for a perfect fluid, is given by:

$$\left(r^2\, L^A\right)_{|A} = 0. \tag{7.314}$$

This means that the hydrodynamical equations reduce to a relatively simple form:

$$\dot{\bar{v}} - c_s^2\left(2U + \tau\right)\bar{v} = 0. \tag{7.315}$$

Gerlach and Sengupta demonstrated that we can introduce a scalar master variable Π that allows the EFEs for k_A to be reduced to a single scalar wave equation. The master variable is defined by:

$$\Pi = \epsilon^{AB}\left(\frac{k_A}{r^2}\right)_{|B} \tag{7.316}$$

and the corresponding master equation is:

$$\left[\frac{1}{r^2}\left(r^4\,\Pi\right)_{|A}\right]^{|A} - \left(\ell - 1\right)\ \left(\ell + 2\right)\ \Pi = -16\pi\epsilon^{AB}\, L_{A|B}. \tag{7.317}$$

The master variable Π can be shown to obey a wave equation of characteristic speed unity with $\bar{v}$ as a source and encodes all the information about the evolution of the axial gravitational waves in the spacetime. Intuitively, a non-vanishing $\bar{v}$ can couple to the non-linear oscillations of the background inducing axial gravitational waves. It was also shown by Gerlach and Sengupta that knowledge of Π allows us to reconstruct the metric perturbation k_A via:

$$(\ell-1)\ (\ell+2)\ k_A = 16\pi r^2 L_A - \epsilon_{AB}\ \left(r^4\Pi\right)^{|B}\,. \tag{7.318}$$

Solutions to this equation are determined by specifying initial data on a Cauchy surface, $\left\{\bar{v}, \Pi, \dot{\Pi}\right\}$, constituting a system with three first order degrees of freedom. In a vacuum spacetime, these system of equations are greatly simplified. The hydrodynamical equations of motion only depend on the axial fluid velocity perturbation $\bar{v}$ with the solutions providing a constant value of $\bar{v}$ along integral curves of u^A.

7.6.7.2 Polar Perturbations

The polar sector is in many ways richer in dynamical content and more entangled than the axial sector. The starting point is to decomposed the symmetric tensor k_{AB} in a coordinate-independent way by making use of the naturally induced fluid frame in M^2. This provides us a way of splitting k_{AB} into three gauge-invariant variables $\{\eta, \phi, \varsigma\}$:

$$k_{AB} = \eta\ (n_A\, n_B - u_A\, u_B) + \phi\ (n_A\, n_B + u_A\, u_B) + \varsigma\ (u_A\, n_B + n_A\, u_B)\,. \tag{7.319}$$

We then define a new variable χ to replace ϕ as an independent variable:

$$\chi = \phi - \varphi + \eta. \tag{7.320}$$

It is now possible to combine the EFEs with the energy-momentum equations to obtain the perturbation equations: for $\ell \geq 2$,

$$\eta = 0 \tag{7.321}$$

for $\ell \geq 1$,

$$-\ddot{\chi} + \chi'' + 2\ (\tau - U)\,\varsigma' = \mathcal{S}_\chi \tag{7.322}$$

$$-\ddot{\varphi} + c_s^2\,\varphi'' - 2c_s^2\,U\,\varphi' = \mathcal{S}_\varphi \tag{7.323}$$

$$-\dot{\varsigma} = \mathcal{S}_\varsigma \tag{7.324}$$

$$16\pi\,(\rho + p)\ v = \varsigma' + \mathcal{C}_v \tag{7.325}$$

$$-\dot{v} = \mathcal{S}_v \tag{7.326}$$

$$-\dot{\Delta} - \left(1 + \frac{p}{\rho}\right) w' = \bar{\mathcal{S}}_\Delta \tag{7.327}$$

$$\left(1 + \frac{p}{\rho}\right) \dot{w} + c_s^2 \, \Delta' = \bar{\mathcal{S}}_w \tag{7.328}$$

for $\ell \geq 0$,

$$8\pi \ (\rho + p) \ w = (\dot{\varphi})' + \mathcal{C}_w \tag{7.329}$$

$$8\pi\rho \, \Delta = -\varphi'' + 2U \, \varphi' + \mathcal{C}_\Delta . \tag{7.330}$$

We have relegated the detailed source terms $\mathcal{S}_X$ and constraint terms $\mathcal{C}_X$ to an Appendix. The three source terms $\mathcal{S}_\Delta, \mathcal{S}_w$ and $\mathcal{S}_v$ are linear in the matter perturbations $\{v, w, \Delta\}$ as well as the metric perturbations plus their first derivatives $\{\chi, \varphi, \varsigma, \chi', \varphi', \dot{\chi}, \dot{\varphi}\}$. The metric perturbation source terms $\mathcal{S}_\chi, \mathcal{S}_\varphi$ and $\mathcal{S}_\varsigma$ are also homogeneously linear in the metric perturbations and their first derivatives.

The polar sector is governed by a set of 10 variables:

$$u_{\text{pert}} = \{\chi, \varphi, \varsigma, v, w, \Delta, \dot{\chi}, \dot{\varphi}, \chi', \varphi'\} . \tag{7.331}$$

The structure of the polar sector equations is given by 10 evolution equations to 5 constraint equations. This means that we have 5 true degrees of freedom that can be specified freely on a Cauchy surface. An evolution equation is an equation containing a convective time-derivative $\dot{u}$ whereas a constraint equation contains only u or u' and can be solved within a single timelike hypersurface. Following Seidel and GMG, the 5 true degrees of freedom are associated with the initial data for the metric perturbations:

$$u_{\text{free}} = \{\chi, \varphi, \varsigma, \dot{\chi}, \dot{\varphi}\} . \tag{7.332}$$

The variable χ is associated with polar gravitational waves as the highest derivatives of χ form a wave equation with characteristic speed of unity with initial data that may be set independently from the matter perturbations. This led GMG to associate χ to gravitational waves inside the matter. Similarly, φ obeys a wave equation but with a characteristic speed set by c_s^2 and can be said to parametrise longitudinal gravitational waves. The final variable ς is advected with the fluid and we see that it is related to v via spatial derivatives.

7.7 Relating the Harmonic Decompositions

As a brief final point, we can relate the harmonics in the 1+1+2 formalism to the harmonics in the 2+2 formalism. The difference being that the 2+2 harmonics are defined over a unit sphere whereas the 1+1+2 harmonics are defined on a sphere of radius r. Additionally, the 2+2

harmonics are explicitly spherical harmonics whereas the 1+1+2 harmonics are dimensionless harmonic functions that are defined on any LRS background as functions of the 2-dimensional Laplace-Beltrami operator.

The relation for scalar harmonics is trivial:

$$Q = Y. \tag{7.333}$$

For vector harmonics we find:

$$Q_a = rY_a \tag{7.334}$$

$$\bar{Q}_a = r\bar{Y}_a. \tag{7.335}$$

Finally, for tensor harmonics:

$$Q_{ab} = r^2 Y_{ab} \tag{7.336}$$

$$\bar{Q}_{ab} = -\frac{r^2}{2}\bar{Y}_{ab}. \tag{7.337}$$

This covariant rescaling in terms of the radial parameter r will be important when we seek the relate the two formalism, especially so for the tensor harmonics. Remember, the 2+2 formalism performs a spectral decomposition in the spherical harmonic basis and the 1+1+2 equations are given in the covariant harmonic basis.

Chapter 8

Covariant Perturbations of the Schwarzschild Spacetime

8.1 The Spherically Symmetric Vacuum Solution

8.1.1 Introduction

One of the first systems that we are naturally led to consider in General Relativity is that of a spherically symmetric spacetime. Such a spacetime can be used to model the external gravitational field created by a black hole or other stellar object to a reasonable approximation. Formally, the Schwarzschild solution describes a one-parameter family of spherically symmetric, static and vacuum spacetimes, where the one-parameter is taken to be the mass of the spacetime M. The Schwarzschild spacetime also imposes the restriction that the external spacetime is vacuum, meaning that there is no matter content $T_{ab} = 0$. In General Relativity, the spherically symmetric vacuum solution is a unique solution given by the Schwarzschild spacetime [494]. This theorem is known as *Birkhoff's theorem* or the *Jebsen-Birkhoff theorem* [277; 61] and has been extended to the notion of *almost* Birkhoff theorems involving deviations from spherical symmetry and matter perturbations [217; 218; 171]. This is one of the most important spacetimes in General Relativity and has provided some fantastic insights into the physical and mathematical aspects of General Relativity. Before we begin our covariant analysis, we introduce some of the basic properties of this spacetime and its characteristics.

In spherical coordinates $\{t, r, \theta, \phi\}$, typically referred to as Schwarzschild coordinates, the spacetime metric takes the following form

$$ds^2 = -\left(1 - \frac{2M}{r}\right) dt^2 + \left(1 - \frac{2M}{r}\right)^{-1} dr^2 + r^2 d\Omega^2 \tag{8.1}$$

where $d\Omega^2$ is the metric on the unit sphere

$$d\Omega^2 = d\theta^2 + \sin^2\theta\, d\phi^2. \tag{8.2}$$

In the Schwarzschild spacetime, the constant M can be associated to the mass of the gravitating object. The Schwarzschild metric is valid in the exterior region of the spacetime as it only models the gravitational field outside a spherical mass. As such the metric is defined, in Schwarzschild coordinates, for $r > 2M > 0$. These Schwarzschild coordinates are not good over the entire manifold and break down at $r = 2M$. Should we wish to consider the entire manifold of the Schwarzschild spacetime we can invoke adapted coordinate systems, notably the maximally extended Schwarzschild solution given in Kruskal coordinates.

In a solution outside the body, we will only be interested in the vacuum Einstein Field Equations and will not consider matter content external to our gravitating body. In vacuum, Einstein's field equations simplify considerably

$$R_{\mu\nu} - \frac{1}{2}g_{\mu\nu}R = 0 \qquad \rightarrow \qquad R_{\mu\nu} = 0. \tag{8.3}$$

In addition, by employing the Schwarzschild metric, we are implicitly assuming that our gravitating source is both static and spherically symmetric. A static spacetime is a particular restrictive property related to the existence and behaviour of a timelike Killing vector. In particular a spacetime will be *static* if it possesses a timelike Killing vector that is orthogonal to a family of hypersurfaces

$$t_{[a}\nabla_b t_{c]} = 0 \tag{8.4}$$

where t^a is our timelike Killing vector. This can be seen from the metric defined above as, if the components of g_{ab} are independent of t, the surfaces of which the Killing vector t_a will be orthogonal will be defined by $t = \text{constant}$. A *spherically symmetric* spacetime possesses three spacelike Killing vector fields which form the Lie-Algebra of $SO(3)$. By this we simply mean that the structure of our symmetry transformations is given by the commutation relations for the transformations which are, in turn, characterised by the structure constants of the Lie algebra. The general relation is

$$[V_a, V_b] = f_{abc}V^c, \tag{8.5}$$

where f_{abc} is the structure constant of the Lie algebra. As is expected from the name, spherical symmetry simply means possessing the same symmetries as the sphere, i.e. invariant under rotations on the surfaces of constant radius. In 3-dimensions these are set by the special orthogonal group $SO(3)$. The commutation relation defined above closes as we can write the commutation of any two fields as a linear combination of other fields within the set. This statement can be related to Frobenius' theorem as the set of Killing vector fields $V^\mu_{(a)}$ will fit together to form an integral submanifold iff all of the commutators are in the space spanned by the Killing vector fields

[582; 89]

$$\left[V_{(a)}, V_{(b)}\right]^{\mu} = \alpha^{c}\, V^{\mu}_{(c)}. \tag{8.6}$$

By imposing spherical symmetry we are therefore stating that we can foliate our spacetime with integrable 2-dimensional submanifolds S^2 that mesh together to form a surface.

We can also discuss these concepts in a more physically intuitive way. A static spacetime will just be a spacetime that is not doing anything at all at any point in time. For the Schwarzschild spacetime we simply have a spherically symmetric gravitating source, such as a black hole, that sits there for all eternity with no changes to its intrinsic properties. In the Schwarzschild spacetime the entire Universe consists of *just* this gravitating body and nothing else. Clearly this is not a good approximation to the real Universe, where objects do not exist in such extreme isolation, but it does enable us to perform powerful analytical studies of the rich phenomenology present in General Relativity. Similarly, spherical symmetry is related to the invariance of the solution under arbitrary rotations about the 2-sphere.

8.1.2 Perturbations

Black hole perturbation theory has been vital for understanding the stability and oscillatory properties of black hole spacetimes as well as understanding the process of black hole formation from gravitational collapse [578; 579; 441; 97; 444; 445; 561; 562; 446; 512; 447; 513]. The application of perturbation theory to the Schwarzschild black hole led to the discovery that perturbations to this spherically symmetric black hole solution are characterised by decaying modes of oscillation that only depend on the mass-parameter of the black hole. These are the black hole quasi-normal modes (QNMs) that describe how a perturbed Schwarzschild black hole settles down to a stationary and static configuration by the emission of gravitational radiation [578; 579; 441; 97]. See [304; 411] for fairly recent reviews of the subject.

The foundations of non-spherical perturbations to the Schwarzschild black hole are built on linear perturbation theory where we introduce a small linear perturbation around the background spacetime

$$g_{\mu\nu} = \bar{g}_{\mu\nu} + h_{\mu\nu}, \tag{8.7}$$

leading to a variation of EFEs of the form

$$\delta G_{\mu\nu} = 8\pi G\, \delta T_{\mu\nu}. \tag{8.8}$$

It was shown that we can construct combinations of various components of $h_{\mu\nu}$ that obey closed wave equations that completely govern the gravitational perturbations to the Schwarzschild spacetime. The odd parity case was first demonstrated by [458], who derived a master variable $\chi^{O}_{\ell m}$ governing odd parity gravitational perturbations. The radial component for a perturbation outside the event horizon was shown to obey the following wave equation [458]

$$\left[-\frac{\partial^2}{\partial t^2} + \frac{\partial^2}{\partial r_*^2}\right] \chi_{\ell m} = V_{\ell}(r)\, \chi_{\ell m}, \tag{8.9}$$

where we have introduced the tortoise coordinates defined by

$$r_* = r + 2M \ln\left(\frac{r}{2M} - 1\right). \tag{8.10}$$

The potential for these axial perturbations was shown to be [458]

$$V_\ell(r) = V_\ell^{\mathrm{RW}}(r) = \left(1 - \frac{2M}{r}\right)\left[\frac{\ell(\ell+1)}{r^2} + 2(1-s^2)\frac{M}{r^3}\right], \tag{8.11}$$

where the form of this potential is defined for spin-s perturbations such that s is 0 for scalars, 1 for electromagnetic perturbations and 2 for gravitational perturbations. The even parity perturbations proved to be a more involved problem. It took over a decade before a master variable $\chi_{\ell m}^{\mathrm{E}}$ was found. Amazingly, it was shown that this even parity master variable obeys the same wave equation Eq. (8.9) as the odd parity master variable but with a modified effective potential [607; 608]

$$V_\ell(r) = V_\ell^{\mathrm{Z}}(r) = \left(1 - \frac{2M}{r}\right)\frac{2n^2(n+1)r^3 + 6n^2Mr^2 + 18nM^2r + 18M^3}{r^3(nr+3M)^2}, \tag{8.12}$$

where $n = (\ell+2)(\ell-1)/2$. As a caveat, these equations were explicitly derived in the Regge-Wheeler gauge. A unified, gauge-invariant treatment was provided in [381]. These perturbations are well defined for $\ell \geq 2$, corresponding to the *radiative* degrees of freedom, i.e. gravitational waves. The $\ell = 0$ mode is only of even parity and can be shown to be a pure gauge mode. This is because $\ell = 0$ is purely a spherical perturbation and may just be re-absorbed by a variation of the mass parameter. The dipole perturbation $\ell = 1$ in the even parity sector is of pure gauge type and cannot be removed by a suitable gauge-transformation [608]. In the odd parity sector $\ell = 1$ can be shown to be related to the introduction of angular momentum into the background metric [608; 399; 349].

A further breakthrough was made when [96] noted that the axial and polar perturbations may be related by a transformation involving differential operators. See also [17] for further discussion of the duality relationship between the axial and polar perturbations. The Regge-Wheeler equation Eq. (8.9) with potentials Eq. (8.11) and Eq. (8.12) may be solved as an eigenvalue problem given the following boundary conditions: at spatial infinity we have pure *outgoing* waves

$$\chi_{\ell m}^O, \chi_{\ell m}^E \sim \exp(-i\omega_n r_*) \qquad \text{for } r_* \to +\infty \tag{8.13}$$

and at the event horizon we have pure *ingoing* waves

$$\chi_{\ell m}^O, \chi_{\ell m}^E \sim \exp(i\omega_n r_*) \qquad \text{for } r_* \to -\infty. \tag{8.14}$$

In the vacuum case, i.e. source-free, the mode solutions of the RW equation are the quasi-normal modes (QNMs) mentioned previously. The real part of ω_n represents the oscillation frequency and the imaginary part of ω_n represents the damping time. These solutions have some very important properties [399]:

- All QNMs have positive imaginary parts, meaning that the perturbations are damped modes and thus Schwarzschild will be *linearly stable* against perturbations.

- The damping time of the QNMs is linearly dependent on the mass of the black hole. For higher order modes, the damping time decreases and hence high order perturbations die off quicker.

- The *ringdown* of a perturbed black hole can be modelled as a superposition of QNMs and the late time dynamics or *tail* of the ringdown is very well described by a power-law representing the envelope of the decaying QNMs. Extensions of this work have included mode-mode couplings [424], second order QNMs [274] as well as other phenomenological features such as mirror modes [313; 314].

- The QNMs are *isospectral*. This means that the even and odd parity perturbations will posses the same complex eigenfrequencies. The reason this arises is that black holes are relatively simple objects and can be, in the most general case, completely characterised by three parameters: the mass M, the charge Q and the angular momentum J. For a Schwarzschild black hole we just have the mass M and this means that there is a uniqueness in the way in which a black hole may dynamically react to a perturbation. This is not true for more complex black holes, perhaps coupled to matter, or for stellar perturbations.

8.2 Background Spacetime

8.2.1 The 2+2 Formalism

We re-express the Schwarzschild metric in the following form

$$ds^2 = -e^{-2\Lambda(r)}dt^2 + e^{2\Lambda(r)}dr^2 + r^2\left(d\theta^2 + \sin^2(\theta)\,d\phi^2\right) \tag{8.15}$$

where the function $\Lambda(r)$ is an unknown function that must be determined by the EFE and we have adopted the conventional Schwarzschild coordinates. Solving the vacuum field equations $R_{\mu\nu} = 0$, the variable $\Lambda(r)$ is related to a new function M, the gravitational mass, as follows:

$$\Lambda(r) = -\frac{1}{2}\ln\left(1 - \frac{2M}{r}\right). \tag{8.16}$$

The GSGM formalism can now be applied to this metric with great simplifications arising due to the fact that we are dealing with a vacuum spacetime and hence all matter perturbations are set to zero. However, we do restrict ourselves to purely metric perturbations neglecting any first order energy-momentum perturbations. For a static background we choose the background frame basis vectors $\left\{\hat{u}^A, \hat{n}^A\right\}$ as follows:

$$\hat{u}^A = \left(e^{\Lambda(r)}, 0\right) \tag{8.17}$$

$$\hat{n}^A = \left(0, e^{-\Lambda(r)}\right). \tag{8.18}$$

We now systematically evaluate all the GSGM scalars:

$$U = 0 \tag{8.19}$$
$$\tau = 0 \tag{8.20}$$
$$\nu = \frac{m}{r^2}\left(1 - \frac{2M}{r}\right)^{-1/2} \tag{8.21}$$
$$W = \frac{1}{r}\left(1 - \frac{2M}{r}\right)^{1/2}. \tag{8.22}$$

The frame derivatives for a generic scalar function $f(x^A)$ are given by:

$$\dot{f} = e^{\Lambda(r)}\partial_t f \tag{8.23}$$
$$f' = e^{-\Lambda(r)}\,\partial_r f, \tag{8.24}$$

which, in the Schwarzschild coordinates, explicitly evaluates to

$$\dot{f} = \left(1 - \frac{2M}{r}\right)^{-1/2}\partial_t f \tag{8.25}$$
$$f' = \left(1 - \frac{2M}{r}\right)^{1/2}\partial_r f. \tag{8.26}$$

The gravitational mass of the spacetime can be calculated by evaluating the Hawking mass in the Schwarzschild spacetime and reduces to 7.226

$$M(r) = \frac{r}{2}\left[1 - e^{-2\Lambda(r)}\right] = M. \tag{8.27}$$

8.2.2 The 1+1+2 Formalism

The Schwarzschild spacetime is covariantly characterised by three non-zero scalars. Due to the high symmetry of the Schwarzschild solution, being a subset of the LRS-II spacetimes, all vectors and tensors will be zero in the background along with all time derivatives, due to the static nature of the metric. The only non-zero 1+1+2 scalars are $\mathbf{X}_{\rm BG} = \{\mathcal{E}, \mathcal{A}, \phi\}$ and their derivatives $\left\{\hat{\mathcal{E}}, \hat{\mathcal{A}}, \hat{\phi}\right\}$. The background equations governing the Schwarzschild spacetime are [104]:

$$\hat{\phi} = -\frac{1}{2}\phi^2 - \mathcal{E} \tag{8.28}$$
$$\hat{\mathcal{E}} = -\frac{3}{2}\phi\,\mathcal{E} \tag{8.29}$$
$$\mathcal{E} + \mathcal{A}\,\phi = 0. \tag{8.30}$$

This system of equations can be parametrically solved to give the following solutions in terms of the usual Schwarzschild coordinates [104] (Fig. 8.1):

$$\mathcal{E} = -\frac{2M}{r^3} \tag{8.31}$$

$$\mathcal{A} = \frac{M}{r^2}\left(1 - \frac{2M}{r}\right)^{-1/2} \tag{8.32}$$

$$\phi = \frac{2}{r}\left(1 - \frac{2M}{r}\right)^{1/2}. \tag{8.33}$$

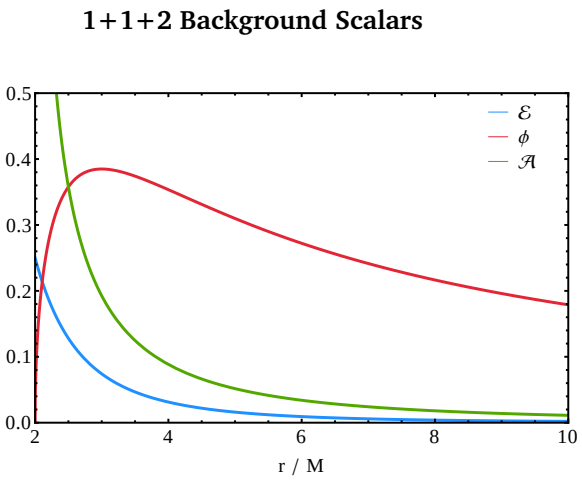

Figure 8.1: Here we plot the radial evolution of the 1+1+2 background scalars $\{\mathcal{A}, \mathcal{E}, \phi\}$. The variable ϕ is zero on the horizon, no sheet expansion, with the maxima occurring at the photon sphere $r = 3m$. The acceleration component $\mathcal{A}$ tends towards infinity for $r \to 2M$ and decays as $r \to \infty$. This is a reproduction of Figure 1 from [104].

It is clear that we can associate the 2+2 background scalars to our 1+1+2 objects. Explicitly we have the following:

$$\nu = \mathcal{A} \tag{8.34}$$

$$W = \frac{1}{2}\phi \tag{8.35}$$

$$\frac{M}{r^3} = -\frac{1}{2}\mathcal{E}. \tag{8.36}$$

As discussed, background variables are not intrinsically gauge-invariant and we need to construct first-order variables in order for the equations have a clear physical and geometrical meaning. To do this we exploit the spherical symmetry of the background and construct a set of gauge-invariant variables by taking angular derivatives of our background scalars

$$\mathbf{X}_{\rm GI} = \delta_a \mathbf{X}_{\rm BG}. \tag{8.37}$$

yielding the following set of gauge-invariant variables

$$\mathbf{X}_{\rm GI} = \{X_a = \delta_a \mathcal{E}, Y_a = \delta_a \phi, Z_a = \delta_a \mathcal{A}\}. \tag{8.38}$$

These variables replace the background scalars in our propagation and evolution equations such that we do not have any zeroth order terms appearing in our equations. Note that these equations are for a static coordinate system in which $\{\mathcal{A}, \mathcal{E}, \phi\} \neq 0$ and all other 1+1+2 scalars are zero. Should we choose a different coordinate system, such as isotropic or freely falling charts, then the LRS-II scalars will differ for each case as will the coordinate relations.

8.3 Linear Perturbations: Axial Sector

8.3.1 Introduction

The general form of axial perturbations to the Schwarzschild metric in the RW gauge are given by:

$$ds^2 = -\left(1 - \frac{2M}{r}\right) d\,t^2 + \left(1 - \frac{2M}{r}\right)^{-1} d\,r^2 + r^2 d\Omega^2 + 2k_A\, \bar{Y}_b\, dx^A\, dx^b, \tag{8.39}$$

with $k_A = (k_t, k_r)$ being the metric perturbation of the GSGM formalism. As we are dealing with a vacuum spacetime and we restrict ourselves such that no first-order energy-momentum perturbations are present, the fundamental 4-velocity takes on a rather straightforward form:

$$u_\mu = (\hat{u}_A\,,\, 0) \tag{8.40}$$

$$\hat{u}_A = \left[-\left(1 - \frac{2M}{r}\right)^{1/2}\,,\, 0\right]. \tag{8.41}$$

When constructing the spacelike basis vector on M^2 we still retain the variable $\bar{g}$ to track the frame degree of freedom:

$$n_\mu = \left(\hat{n}_A\,,\, \bar{g}\bar{Y}_a\right) \tag{8.42}$$

$$\hat{n}_A = \left[0, \left(1 - \frac{2M}{r}\right)^{-1/2}\right]. \tag{8.43}$$

Note that the basis vectors on M^2 obey the appropriate normalisations along with the restriction that $\Delta\left(g_{\mu\nu}u^\mu u^\nu\right) = 0$ and $\Delta\left(g_{\mu\nu}n^\mu n^\nu\right) = 0$ to linear order. We can now perform a 1+1+2 decomposition of this metric using the defined basis vectors on M^2 to project out all variables appropriately.

8.3.2 Correspondence

8.3.2.1 Axial Perturbations: Scalars

For scalars we only expect the 1+1+2 variables $\mathcal{H}, \Omega$ to have non-zero first order perturbations as these are axial with the other scalars $\mathcal{E}, \Theta, \phi, \mathcal{A}$ being even parity. We will use 1+1+2 index notation unless explicitly referenced and we adopt the notation that $X^{(0)}$ denotes the variable evaluated in the background spacetime and ΔX denotes the linear order perturbation to the variable. Remember, $\{\mathcal{E}, \Theta, \phi, \Sigma, \mathcal{A}\}$ are intrinsically even parity scalars and we do not expect them to appear in the axial sector beyond the background scalars. The odd parity scalars $\{\mathcal{H}, \Omega, \xi\}$ will be non-vanishing in the axial sector and we do anticipate a non-zero value.

$$\mathcal{E} = \mathcal{E}^{(0)} + \Delta\mathcal{E} \tag{8.44}$$
$$\mathcal{E}^{(0)} = -\frac{2M}{r^3} \tag{8.45}$$
$$\Delta\mathcal{E} = 0. \tag{8.46}$$

$$\Theta = \Theta^{(0)} + \Delta\Theta \tag{8.47}$$
$$\Theta^{(0)} = 0 \tag{8.48}$$
$$\Delta\Theta = 0. \tag{8.49}$$

$$\Sigma = \Sigma^{(0)} + \Delta\Sigma \tag{8.50}$$
$$\Sigma^{(0)} = 0 \tag{8.51}$$
$$\Delta\Sigma = 0. \tag{8.52}$$

$$\phi = \phi^{(0)} + \Delta\phi \tag{8.53}$$
$$\phi^{(0)} = \frac{2}{r}\left(1 - \frac{2M}{r}\right)^{1/2} \tag{8.54}$$
$$\Delta\phi = 0. \tag{8.55}$$

$$\mathcal{A} = \mathcal{A}^{(0)} + \Delta\mathcal{A} \tag{8.56}$$
$$\mathcal{A}^{(0)} = \frac{M}{r^2}\left(1 - \frac{2M}{r^2}\right)^{-1/2} \tag{8.57}$$
$$\Delta\mathcal{A} = 0. \tag{8.58}$$

$$\mathcal{H} = \mathcal{H}^{(0)} + \Delta\mathcal{H} \tag{8.59}$$
$$\mathcal{H}^{(0)} = 0 \tag{8.60}$$
$$\Delta\mathcal{H} = Y \left[\frac{1}{2}\frac{\ell\left(\ell+1\right)}{r^2}\left\{-\left(1-\frac{2M}{r}\right)^{-1/2} k_t' + \frac{2}{r}\,k_t + \left(1-\frac{2M}{r}\right)^{1/2}\dot{k}_r\right\}\right]. \tag{8.61}$$

$$\Omega = \Omega^{(0)} + \Delta\Omega \tag{8.62}$$
$$\Omega^{(0)} = 0 \tag{8.63}$$
$$\Delta\Omega = 0. \tag{8.64}$$

$$\xi = \xi^{(0)} + \Delta\xi \tag{8.65}$$
$$\xi^{(0)} = 0 \tag{8.66}$$
$$\Delta\xi = Y \left[-\frac{1}{2}\frac{\ell\left(\ell+1\right)}{r^2}\,\bar{g}\right] \tag{8.67}$$

8.3.2.2 Axial Perturbations: 2-Vectors

For 2-vectors, all quantities are explicitly first order as these are necessarily zero in the background spacetime:

$$\mathcal{E}_a = \mathcal{E}_a^{(0)} + \Delta\mathcal{E}_a \tag{8.68}$$
$$\mathcal{E}_a^{(0)} = 0 \tag{8.69}$$
$$\Delta\mathcal{E}_a = \bar{Y}_a \left[+\frac{1}{4}\frac{\ell\left(\ell-2\right)}{r^2}\left(1-\frac{2M}{r}\right)^{1/2} + \ldots\right]. \tag{8.70}$$

$$\alpha_a = \alpha_a^{(0)} + \Delta\alpha_a \tag{8.71}$$
$$\alpha_a^{(0)} = 0 \tag{8.72}$$
$$\Delta\alpha_a = \bar{Y}_a \left[\bar{g}\left(1-\frac{2M}{r}\right)^{-1/2} - \frac{k_t}{r}\right]. \tag{8.73}$$

$$\Omega_a = \Omega_a^{(0)} + \Delta\Omega_a \tag{8.74}$$
$$\Omega_a^{(0)} = 0 \tag{8.75}$$
$$\Delta\Omega_a = 0. \tag{8.76}$$

$$a_a = a_a^{(0)} + \Delta a_a \tag{8.77}$$
$$a_a^{(0)} = 0 \tag{8.78}$$
$$\Delta a_a = \bar{Y}_a \left[-\partial_r \bar{g} \left(1 - \frac{2M}{r}\right)^{1/2} + \left(1 - \frac{2M}{r}\right) \frac{k_r}{r} \right] \tag{8.79}$$

$$\Sigma_a = \Sigma_a^{(0)} + \Delta\Sigma_a \tag{8.80}$$
$$\Sigma_a^{(0)} = 0 \tag{8.81}$$
$$\Delta\Sigma_a = 0. \tag{8.82}$$

8.3.2.3 Axial Sector: 2-Tensors

For 2-tensors we find:

$$\mathcal{E}_{ab} = \mathcal{E}_{ab}^{(0)} + \Delta\mathcal{E}_{ab} \tag{8.83}$$
$$\mathcal{E}_{ab}^{(0)} = 0 \tag{8.84}$$
$$\Delta\mathcal{E}_{ab} = \frac{1}{4} \bar{Y}_{ab} \left[\left(1 - \frac{2M}{r}\right)^{1/2} k_r' + \left(1 - \frac{2M}{r}\right)^{-1/2} \dot{k}_t \right] \tag{8.85}$$

$$\zeta_{ab} = \zeta_{ab}^{(0)} + \Delta\zeta_{ab} \tag{8.86}$$
$$\zeta_{ab}^{(0)} = 0 \tag{8.87}$$
$$\Delta\zeta_{ab} = \bar{Y}_{ab} \left[\frac{1}{2} \bar{g} - \frac{1}{2} \left(1 - \frac{2M}{r}\right)^{1/2} k_r \right]. \tag{8.88}$$

$$\Sigma_{ab} = \Sigma_{ab}^{(0)} + \Delta\Sigma_{ab} \tag{8.89}$$
$$\Sigma_{ab}^{(0)} = 0 \tag{8.90}$$
$$\Sigma_{ab} = \bar{Y}_{ab} \left[\frac{1}{2} \bar{v} - \frac{1}{2} \left(1 - \frac{2M}{r}\right)^{-1/2} k_t \right]. \tag{8.91}$$

$$\mathcal{H}_{ab} = \mathcal{H}_{ab}^{(0)} + \Delta\mathcal{H}_{ab} \tag{8.92}$$
$$\mathcal{H}_{ab}^{(0)} = 0 \tag{8.93}$$
$$\mathcal{H}_{ab} = Y_{ab} \left[\left(1 - \frac{2M}{r}\right)^{-1} \frac{M}{r^2} k_t - \left(1 - \frac{2M}{r}\right)^{-1/2} k_t' - \left(1 - \frac{2M}{r}\right)^{1/2} \dot{k}_r \right] \tag{8.94}$$

In addition to these basic 1+1+2 variables we also need the gauge-invariant variables: $\{X_a, Y_a, Z_a\}$.

8.3.3 Ricci Tensor

The Ricci tensor in Schwarzschild spacetime vanishes in the background. As per the Stewart-Walker lemma [534], this tensor will be a natural gauge-invariant variable as it vanishes in the background spacetime. The perturbations to the Ricci tensor will therefore correspond to physically meaningful perturbations. In the 2+2 formalism, the full perturbed Ricci tensor can be decomposed in the same way that the metric perturbations are decomposed: into scalar, vector and tensor harmonics [349]:

$$R_{AB} = 0 \tag{8.95}$$
$$R_{Ab} = S_A \bar{Y}_b \tag{8.96}$$
$$R_{ab} = S \bar{Y}_{ab}, \tag{8.97}$$

where the following variables have been introduced for convenience:

$$S = \nabla_A k^A = \frac{2M}{r^2} k_r - \left(1 - \frac{2M}{r}\right)^{-1} \partial_t k_t + \left(1 - \frac{2M}{r}\right) \partial_r k_r \tag{8.98}$$
$$S_t = \frac{1}{2} k_t \left[\frac{\ell(\ell+1)}{r^2} - \frac{4M}{r^3}\right] + \frac{1}{r}\left(1 - \frac{2M}{r}\right) \partial_t k_r + \frac{1}{2}\left(1 - \frac{2M}{r}\right) \partial_{rt} k_r - \frac{1}{2}\left(1 - \frac{2M}{r}\right) \partial_r^2 k_t \tag{8.99}$$
$$S_r = \frac{1}{2} k_r \left[\frac{(\ell+2)(\ell-1)}{r^2}\right] + \frac{1}{r}\left(1 - \frac{2M}{r}\right)^{-1} \partial_t k_t - \frac{1}{2}\left(1 - \frac{2M}{r}\right)^{-1} \partial_{rt} k_t + \frac{1}{2}\left(1 - \frac{2M}{r}\right)^{-1} \partial_t^2 k_r. \tag{8.100}$$

However, from the EFE we know that the source terms should vanish and hence $S = 0$ provides a constraint on the metric functions whereby

$$\partial_t k_t = \left(1 - \frac{2M}{r}\right)^2 \partial_r k_r + \left(1 - \frac{2M}{r}\right)\left[\frac{2M}{r^2}\right] k_r \tag{8.101}$$
$$\dot{k}_t = \left(1 - \frac{2M}{r}\right) k_r' + \left(1 - \frac{2M}{r}\right)^{1/2} \frac{2M}{r^2} k_r. \tag{8.102}$$

This relationship can be used to simplify other equations such as 8.85. These equations are a specialisation of the full Ricci perturbations in a spherically symmetric spacetime. The expression for the full perturbations can be found in [349].

8.3.4 Master Variable and Master Equations

8.3.4.1 Cunningham-Price-Moncrief Master Variable

The definition of a master variable is by no means a unique process. Some of the most commonly cited definitions include the Cunningham-Price-Moncrief (CPM) function and the Regge-Wheeler (RW) function. The Cunningham-Price-Moncrief function can be reformulated in a covariant

manner, albeit with a different normalisation, as was demonstrated by Gerlach and Sengupta [201; 202]. The covariant CPM-GS function is given by:

$$\Psi^{\ell m}_{\text{odd}} = \frac{2r}{(\ell-1)\,(\ell+2)}\,\epsilon^{AB}\left(\nabla_A\,\tilde{h}^{\ell m}_B - \frac{2}{r}\,r_A\tilde{h}^{\ell m}_B\right). \tag{8.103}$$

This definition and normalisation is in agreement with [283]. The normalisation is chosen for convenience when studying gravitational radiation at future null infinity and on the horizon. Inserting this variable into the perturbation equations recovers a wave equation for the master variable whose result is the well known Regge-Wheeler equation [458]:

$$(\Box - V_{\text{odd}})\;\Psi_{\text{odd}} = \mathcal{S}_{\text{odd}}. \tag{8.104}$$

In the vacuum limit, neglecting first order energy-momentum perturbations, the source term vanishes. The odd-parity potential is:

$$V_{\text{odd}} = \frac{\ell\,(\ell+1)}{r^2} - \frac{6M}{r^3}. \tag{8.105}$$

It is interesting to note that the CPM function is closely related to the originally defined RW function:

$$\Psi^{\ell m}_{\text{RW}} = \frac{1}{r}v^A\,\tilde{h}^{\ell m}_A \tag{8.106}$$

$$\Psi^{\ell m}_{\text{RW}} = \frac{1}{2}t^A\nabla_A\Psi^{\ell m}_{\text{odd}} + \frac{r}{(\ell-1)\,(\ell+2)}\,v_A\,S^A \tag{8.107}$$

In our vacuum limit, the RW function is simply a weighted time-derivative of the CPM function. Explicitly evaluating the RW function for the Schwarzschild spacetime in the Schwarzschild coordinates we find:

$$\Psi_{\text{RW}} = \frac{k_r}{r}\left(1 - \frac{2M}{r}\right). \tag{8.108}$$

It is now our task to find which combination of 1+1+2 variables is equivalent to the above. Using the correspondence defined above we see that the definition given in Clarkson and Barrett is equivalent to the Regge-Wheeler function:

$$W^Y_{ab} = Y_{ab}\left[\frac{1}{2}\phi r^2\bar{\zeta}_T + \frac{1}{3}\frac{r}{\mathcal{E}}\bar{X}_V\right] \tag{8.109}$$

$$W^Q_{ab} = -\frac{2}{r^2}W^Y_{ab} = Q_{ab}\left[\frac{1}{2}\phi r^2\bar{\zeta}_T + \frac{1}{3}\frac{r}{\mathcal{E}}\bar{X}_V\right] \tag{8.110}$$

$$= \left[1 - \frac{2M}{r}\right]\frac{k_r}{r}, \tag{8.111}$$

where we have used W^Y to denote the RW tensor in the tensorial harmonic basis and W^Q to denote the RW tensor in the covariant harmonic basis. The covariant Regge-Wheeler tensor can be reconstructed from these expressions

$$W_{ab} = \frac{1}{2}\phi r^2 \zeta_{ab} - \frac{1}{3}\frac{r}{\mathcal{E}}\delta_{\{a}X_{b\}}, \tag{8.112}$$

with the accompanying covariant wave equation [104; 437]:

$$\ddot{W}_{\{ab\}} - \hat{\hat{W}}_{\{ab\}} - \mathcal{A}\hat{W}_{\{ab\}} + \left(\phi^2 - \mathcal{E}\right) W_{\{ab\}} - \delta^2 W_{\{ab\}} = 0. \tag{8.113}$$

This can be harmonically decomposed to the following

$$\ddot{W} - \hat{\hat{W}} - \mathcal{A}\hat{W} + \left\{\frac{\ell(\ell+1)}{r^2} + 3\mathcal{E}\right\} W = 0, \tag{8.114}$$

where $W = \{W_T, \bar{W}_T\}$. Importantly [104] was able to show that both the even *and* odd parity parts of W_{ab}, denoted by just W, obey the same covariant wave equation Eq. (8.219) or, alternatively, the harmonic representation given in Eq. (8.114). Though we derived this equation by using the correspondence between the 2+2 and 1+1+2 approaches, the Regge-Wheeler tensor may be completely determined using the 1+1+2 formalism alone [104; 437]. In the pure 1+1+2 approach, the question asked is if we can find a combination of basic tensors that obey a *closed*, covariant wave equation. It was previously shown that, yes, this is certainly possible [104]. In addition to the 1+1+2 transverse-traceless set of 2-tensors $\{\mathcal{E}_{ab}, \mathcal{H}_{ab}, \Sigma_{ab}, \zeta_{ab}\}$, remember these are just the PSTF with respect to n^a terms in our formalism, we can also construct TT tensors from the δ derivative applied to scalars and vectors. For example, $\delta_{\{a}X_{b\}}$ or $\delta_{\{a}\delta_{b\}}\mathcal{H}$ are legitimate TT tensors. We construct wave equations by the appropriate evolution and propagation equations by calculating the wave operator $\ddot{\Psi}_{\{ab\}} - \hat{\hat{\Psi}}_{\{ab\}}$ for the 2-tensor Ψ_{ab}. The fact that these two approaches coincide and give a sane result is a good and useful consistency check. More importantly, it allows us to imbue the master variable with a geometrically and physically meaningful interpretation. Remember, the gauge-invariant variable X_a corresponds the angular gradient of the electric Weyl tensor $X_a = \delta_a\mathcal{E}$. The term on the RHS of equation 8.112 is therefore related to the angular projection of the spatial fluctuations to the radial tidal force. The term $X_a/\mathcal{E}$ is simply a measure of the fractional gradient of the radial tidal forces over the 2-surface telling us how these forces are changing from point to point on the vibrating 2-surface [104]. The Regge-Wheeler tensor as defined in equation 8.112 is therefore encapsulating the shearing distortion of the radial tidal force gradient across the 2-surfaces. Likewise the first term in equation 8.112 is also of a shearing nature. This time it tells us about the TT part of the shear to the spacelike congruence, how the 2-surfaces are distorted. This plays nicely into the analogy of the vibrating 2-surfaces and how the surfaces are being distorted and how this feeds into the changes to the tidal forces and the concomitant distortion of gravitational waves arising from the presence of the black hole [446; 562; 541; 104]. In reality, we are free to re-write ζ_{ab} in terms of purely Weyl contributions [104]. This is particularly apparent in 7.180 if we linearise the equations around the Schwarzschild spacetime.

We can take this one step further in order to connect our results with the literature at large. In particular we can demonstrate that Eq. (8.219) is the Regge-Wheeler equation by making the appropriate transformations and substitutions [104]. First, we introduce the time harmonics, as defined in Section 7.5.12. Next, we introduce appropriate coordinates by letting the affine parameter $\rho \to r$, as per Section 8.2.2, and then transform to the tortoise coordinates of [458]

$$r_* = r + 2M \ln\left(\frac{r}{2M} - 1\right). \tag{8.115}$$

We then introduce a variable ψ defined such that

$$\psi = \psi_{\rm RW} = \bar{W}_T. \tag{8.116}$$

Reducing everything down we find that Eq. (8.219) reduces to

$$\left(\frac{d^2}{dr_*^2} + \sigma^2\right) \psi = V\,\psi, \tag{8.117}$$

where

$$V = V_{\rm RW} = \frac{(r-2m)}{r^4}\left[\ell(\ell+1)r - 6m\right], \tag{8.118}$$

which is just the standard Regge-Wheeler potential [458; 104].

8.3.4.2 Gerlach-Sengupta Master Variable

Alternatively, we can construct another decoupled perturbation variable from the magnetic Weyl scalar, $\mathcal{H}$. Adopting the GS master variable from equation 7.316, we find that

$$\Pi = \frac{1}{r^2}\left[-\left(1-\frac{2M}{r}\right)^{-1/2} k_t' + \frac{2}{r}k_t + \left(1-\frac{2M}{r}\right)^{1/2} \dot{k}_r\right] \tag{8.119}$$

By inspection with the correspondence defined above, we see that the GS-GMG master variable is simply the magnetic Weyl scalar with a given multipole weighting

$$\Pi = \frac{2}{\ell\,(\ell+1)}\mathcal{H}. \tag{8.120}$$

As the pre-factor is composed of purely angular terms, having no time and radial dependence, we can simply rescale this variable to form

$$\mathcal{V} = \mathcal{H}. \tag{8.121}$$

The harmonic wave equation that this rescaled variable obeys is determined by evaluating the GS master equation in the axial sector for the Schwarzschild background

$$\ddot{\mathcal{V}} - \hat{\hat{\mathcal{V}}} - (\mathcal{A} + 3\phi)\,\hat{\mathcal{V}} + \left[\frac{\ell\,(\ell+1)}{r^2} - \frac{3}{2}\phi^2 + 6\mathcal{E}\right]\mathcal{V} = 0. \tag{8.122}$$

Covariantly reconstructing the variable we simply find that

$$\mathcal{V}_{\{ab\}} = r^2 \delta_{\{a}\delta_{b\}}\mathcal{H}. \tag{8.123}$$

Likewise, the corresponding covariant wave equation is

$$\ddot{\mathcal{V}}_{\{ab\}} - \hat{\hat{\mathcal{V}}}_{\{ab\}} - (\mathcal{A} + 3\phi)\,\hat{\mathcal{V}}_{\{ab\}} - \left[\delta^2 + 2K\right]\mathcal{V}_{\{ab\}} = 0. \tag{8.124}$$

Where K is the Gaussian curvature of the 2-surfaces as introduced earlier and δ^2 is our angular Laplacian on the 2-surfaces. This structure will be remarkably similar to a result in the LTB spacetime, as one may hope in the limit that $\mu \to 0$ of a spherically symmetric dust spacetime. The physical interpretation of $\mathcal{H}$ is somewhat trickier as this variable does not have a well defined Newtonian counterpart. Instead, this variable constitutes a genuinely relativistic degree of freedom that can be associated to relativistic effects in the spacetime such as frame dragging and gravitational waves. The variable itself vanishes in the background spacetime and therefore constitutes a well defined gauge-invariant variable to linear order.

An important observation can be made by introducing a simple rescaling of the variable $\mathcal{V}$ such that $\mathcal{J} = r^3\mathcal{V}$. Substituting this into Eq. (8.122) we find that the equation reduces to

$$\frac{1}{r^3}\left[\ddot{\mathcal{J}} - \hat{\hat{\mathcal{J}}} - \mathcal{A}\hat{\mathcal{J}} + \left\{\frac{\ell(\ell+1)}{r^2} + 3\mathcal{E}\right\}\mathcal{J}\right] = 0 \tag{8.125}$$

$$\ddot{\mathcal{J}} - \hat{\hat{\mathcal{J}}} - \mathcal{A}\hat{\mathcal{J}} + \left\{\frac{\ell(\ell+1)}{r^2} + 3\mathcal{E}\right\}\mathcal{J} = 0 \tag{8.126}$$

This is nothing more than the Regge-Wheeler equation that we saw in 8.114. This leads us to the conclusion that $\mathcal{H}$ is just a Regge-Wheeler variable. This was also noted in the analysis of [83] who introduced complex gravito-electromagnetic variables to study decoupled perturbations. This variable can also be shown to correspond to the imaginary part of a scaled Newman-Penrose scalar Ψ_0, namely $r^3\mathrm{Im}[\Psi_0]$. This was first noted in [445] and related to the 1+1+2 formalism in [83]. Though, in many ways, this should not be too surprising given that the magnetic Weyl tensor is a natural odd parity variable that implicitly is related to the free gravitational field and thereby to gravitational perturbations. We also point the reader to [410] for an investigation into the relation between the 2+2 gauge invariant variables an the Newman-Penrose scalars $\{\Psi_0, \Psi_1, \Psi_2, \Psi_3, \Psi_4\}$.

Using these results, we can numerically evaluate the Regge-Wheeler equation for reasonable initial data. One of the most intuitive examples that we can consider is a Gaussian wave packet scattering off our Schwarzschild black hole, this is a classic test and has been well documented in the literature [578; 579; 18; 424]. At the linear order considered here, modes with different angular structure will decouple from each other due to spherical symmetry. Additionally, as we mentioned earlier, the even and odd parity sectors are dynamically independent. The complete

spectrum of QNMs could be obtained by the numerical evaluation of the RW eqn 8.126 but more sophisticated methods, such as those in the classic paper by [313], are more reliable and powerful. In our simple numerical scattering example we adopt the so called time-derivative (TD) initial data prescribed by (e.g. [424])

$$\mathcal{J}(t=0,r)=0, \tag{8.127}$$

$$\partial_t\mathcal{J}(t=0,r)=e^{-(r-r_0)^2/\sigma^2}. \tag{8.128}$$

We only consider a pulse positioned initially at $r_0=20M$, for a Gaussian packet of width $\sigma=4M$ and for the multipole $(\ell,m)=(2,2)$. The observer for this example is positioned at a radius of $40M$. The RW variable $\mathcal{J}$ is shown in Fig. 8.2 and the logarithm of its absolute value in Fig. 8.3. In these plots we demonstrate the response of a Schwarzschild black hole to an incident Gaussian wavepacket of width $\sigma=4M$ and an initial position set by $r_0=20M$. We see an initial bump around $t\approx 20M$ which corresponds to the initial Gaussian pulse on the way to the black hole followed by the quasinormal mode ringing that dominates the signal from around $t\approx 80M$. At late times we start to approach a power-law fall-off known as the *tail*. The late time tail corresponds to backscattering off the weak potential in the far wave zone. Similar investigations can be constructed for more complex scenarios, such as the radial infall of point particles [377] or the tidal distortions and response of the black hole to orbiting particles [348], in order to garner insight into the physical origin of black hole quasinormal modes. Fundamental questions of this nature will become increasingly important as we edge closer and closer to the first gravitational wave detection. It is thought that observations of the ringdown regime of a perturbed black hole will provide strong insights and constraints into binary black hole systems [291; 292; 216]. It should be noted that it would be extraordinarily useful to extend the covariant and gauge-invariant approach to study perturbations to a Kerr black hole. After all, astrophysical black holes are highly likely to be spinning and hence perturbations to the Kerr black hole are astrophysically more interesting to study [557; 558; 442; 559]. A further complication is that the initial conditions become intractably complex due to the extremely non- linear nature of binary black hole inspirals meaning that studies of the physical origin of the ringdown mode structure are often limited to more simplistic cases, such as the radial infall of a particle described above. It is hoped that covariant methods may be able to shed some light on the physical characteristics, such as tidal shears and the electric Weyl tensor, that influence the mode structure in a black hole ringdown and how this may contain some memory of the perturbing mechanism.

In this sub-section we have related this variable to the work of [229], derived the covariant wave equation 8.124 for a covariant tensor 8.123 and made explicit the relation between the 1+1+2 variables and the literature at large in Section 8.3.4.1. All these approaches constitute different ways to study the same basic problem: vacuum gravitational perturbations to the Schwarzschild spacetime.

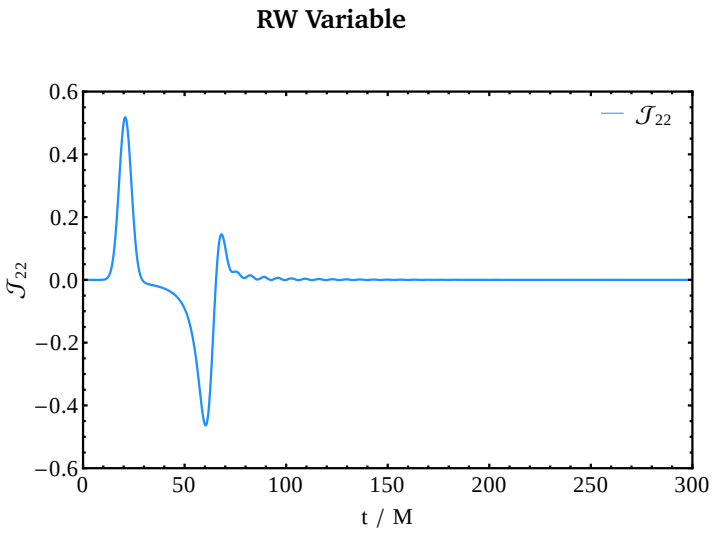

Figure 8.2: Here we plot the response of a Schwarzschild black hole to a Gaussian wavepacket of width $\sigma = 4M$ and an initial position set by $r_0 = 20M$. We see an initial bump around $t \approx 20M$ which corresponds to the initial Gaussian pulse on the way to the black hole followed by the quasinormal mode ringing that dominates the signal from around $t \approx 80M$. At late times we start to approach a power-law fall-off known as the *tail*. The late time tail corresponds to backscattering off the weak potential in the far wave zone. Finally, we note that the Regge-Wheeler variable $\mathcal{J}$ here is simply related to a re-scaling of the scalar part of the magnetic Weyl tensor via $\mathcal{J} = r^3\mathcal{H}$.

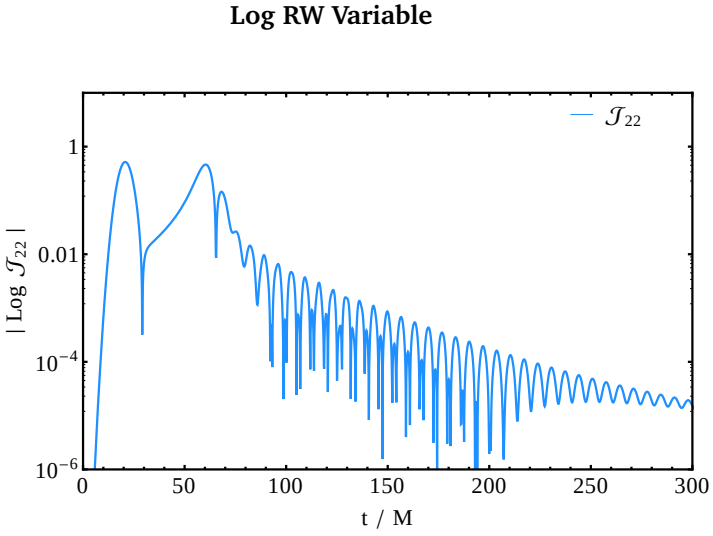

Figure 8.3: Here we plot the evolution of the logarithm of the absolute value of the RW variable in response to a Gaussian pulse scattering off the Schwarzschild black hole. Description of the phenomenology is the same as in Fig. 8.2.

8.4 Linear Perturbations: Polar Sector

8.4.1 Introduction

The most general form of polar perturbations to the metric in the RW gauge can be written as:

$$\begin{aligned} ds^2 = &-\left[1+(2\eta-\chi-\varphi)\,Y\right]\left(1-\frac{2M}{r}\right)dt^2 - 2\varsigma Y dt dr \\ &+\left[1+(\chi+\varphi)\,Y\right]\left(1-\frac{2M}{r}\right)^{-1}dr^2 + r^2\left(1+\varphi Y\right)d\Omega^2 \end{aligned} \tag{8.129}$$

As we saw in the axial case, the fundamental 4-velocity simplifies considerably as the matter perturbations vanish for pure vacuum gravitational perturbations. The perturbed 4-velocity can therefore be written as

$$u_a = \left[\hat{u}_A + \frac{1}{2}h_{AB}\,\hat{u}^B Y, 0\right], \tag{8.130}$$

where $\hat{u}^A$ is the background fluid 4-velocity given by Equation 8.41. Note that the ansatz adopted for Δu_A ensures that to linear order $\Delta\left(g_{\mu\nu}u^\mu u^\nu\right) = 0$ and hence our vector remains normalised. The spacelike basis vector is constructed by orthogonalising on M^2

$$n_a = \left[\hat{n}_A + \frac{1}{2}h_{AB}\,\hat{u}^B Y, gY_a\right], \tag{8.131}$$

where the background spacelike vector is given by Equation 8.43. Here we have included a frame degree of freedom g encapsulating the gauge freedom in the choice of frame vectors at each point. The ansatz adopted for Δn_A ensures that the spacelike vector remains appropriately normalised to linear order. Note that on a static background the fluid basis will coincide with the radial basis defined by

$$n^A = \frac{v_A}{v} \tag{8.132}$$

where v^A is defined by 7.259 and v is defined by 7.298.

We are now ready to perform a 1+1+2 decomposition of the polar sector perturbations and, as before, we adopt the 1+1+2 index notation.

8.4.2 Correspondence

8.4.2.1 Polar Perturbations: Scalars

In the polar sector, the odd parity variables $\{\mathcal{H}, \Omega, \xi\}$ will vanish at all orders and we will be left with only the even parity scalars $\{\mathcal{A}, \Theta, \phi, \mathcal{E}, \Sigma\}$. We will use 1+1+2 index notation unless explicitly referenced and we adopt the notation that $X^{(0)}$ denotes the variable evaluated in the background spacetime and ΔX denotes the linear order perturbation to the variable.

$$\mathcal{E} = \mathcal{E}^{(0)} + \Delta\mathcal{E} \tag{8.133}$$

$$\mathcal{E}^{(0)} = -\frac{2M}{r^3} \tag{8.134}$$

$$\Delta\mathcal{E} \neq 0. \tag{8.135}$$

$$\Theta = \Theta^{(0)} + \Delta\Theta \tag{8.136}$$

$$\Theta^{(0)} = 0 \tag{8.137}$$

$$\Delta\Theta = Y\left[\frac{1}{2}\varsigma\left(\mathcal{A}+\phi\right) + \frac{3}{2}\dot{\varphi} + \frac{1}{2}\dot{\chi} + \frac{1}{2}\varsigma'\right]. \tag{8.138}$$

$$\Sigma = \Sigma^{(0)} + \Delta\Sigma \tag{8.139}$$

$$\Sigma^{(0)} = 0 \tag{8.140}$$

$$\Delta\Sigma = Y\left[\frac{\varsigma}{3}\left(\mathcal{A} - \frac{1}{2}\phi\right) + \frac{1}{3}\dot{\chi} + \frac{1}{3}\varsigma'\right]. \tag{8.141}$$

$$\phi = \phi^{(0)} + \Delta\phi \tag{8.142}$$

$$\phi^{(0)} = \frac{2}{r}\left(1 - \frac{2M}{r}\right)^{1/2} \tag{8.143}$$

$$\Delta\phi \neq 0. \tag{8.144}$$

$$\mathcal{A} = \mathcal{A}^{(0)} + \Delta\mathcal{A} \tag{8.145}$$

$$\mathcal{A}^{(0)} = \frac{M}{r^2}\left(1 - \frac{2M}{r^2}\right)^{-1/2} \tag{8.146}$$

$$\Delta\mathcal{A} \neq 0. \tag{8.147}$$

$$\mathcal{H} = \mathcal{H}^{(0)} + \Delta\mathcal{H} \tag{8.148}$$

$$\mathcal{H}^{(0)} = 0 \tag{8.149}$$

$$\Delta\mathcal{H} = 0. \tag{8.150}$$

$$\Omega = \Omega^{(0)} + \Delta\Omega \tag{8.151}$$

$$\Omega^{(0)} = 0 \tag{8.152}$$
$$\Delta\Omega = 0. \tag{8.153}$$

$$\xi = \xi^{(0)} + \Delta\xi \tag{8.154}$$
$$\xi^{(0)} = 0 \tag{8.155}$$
$$\Delta\xi = 0. \tag{8.156}$$

8.4.2.2 Polar Perturbations: 2-Vectors

For 2-vectors, all quantities are explicitly first order as these are necessarily zero in the background spacetime:

$$\mathcal{E}_a = \mathcal{E}_a^{(0)} + \Delta\mathcal{E}_a \tag{8.157}$$
$$\mathcal{E}_a^{(0)} = 0 \tag{8.158}$$
$$\Delta\mathcal{E}_a = Y_a \left[-\frac{1}{2}(\chi+\varphi)\left(\mathcal{A} - \frac{1}{2}\phi\right) - \frac{3}{2}\mathcal{E}g - \frac{1}{4}\chi' - \frac{1}{2}\varphi' - \frac{1}{4}\dot{\varsigma} \right]. \tag{8.159}$$

$$\mathcal{H}_a = \mathcal{H}_a^{(0)} + \Delta\mathcal{H}_a \tag{8.160}$$
$$\mathcal{H}_a^{(0)} = 0 \tag{8.161}$$
$$\Delta\mathcal{H}_a = \bar{Y}_a \left[\frac{1}{4}\varsigma' \left(1 - \frac{2M}{r}\right) - \frac{1}{4}\varsigma \left(\frac{2}{r} - \frac{6M}{r^2}\right)\left(1 - \frac{2M}{r}\right)^{-1/2} + \frac{1}{4}\dot{\chi}\left(1 - \frac{2M}{r}\right)^{-1/2} \right]. \tag{8.162}$$

$$\alpha_a = \alpha_a^{(0)} + \Delta\alpha_a \tag{8.163}$$
$$\alpha_a^{(0)} = 0 \tag{8.164}$$
$$\Delta\alpha_a = Y_a \left[\frac{1}{2}\varsigma + \dot{g} \right]. \tag{8.165}$$

$$\mathcal{A}_a = \mathcal{A}_a^{(0)} + \Delta\mathcal{A}_a \tag{8.166}$$
$$\mathcal{A}_a^{(0)} = 0 \tag{8.167}$$
$$\Delta\mathcal{A}_a = Y_a \left[-g\mathcal{A} - \frac{1}{2}(\chi+\varphi) \right]. \tag{8.168}$$

$$\Omega_a = \Omega_a^{(0)} + \Delta\Omega_a \tag{8.169}$$
$$\Omega_a^{(0)} = 0 \tag{8.170}$$

$$\Delta\Omega_a = \bar{Y}_a \left[\frac{1}{4}\varsigma\right]. \tag{8.171}$$

$$a_a = a_a^{(0)} + \Delta a_a \tag{8.172}$$
$$a_a^{(0)} = 0 \tag{8.173}$$
$$\Delta a_a = Y_a \left[-\frac{1}{2}(\chi+\varphi) + g'\right] \tag{8.174}$$

$$\Sigma_a = \Sigma_a^{(0)} + \Delta\Sigma_a \tag{8.175}$$
$$\Sigma_a^{(0)} = 0 \tag{8.176}$$
$$\Delta\Sigma_a = Y_a \left[\frac{1}{4}\varsigma\right]. \tag{8.177}$$

8.4.2.3 Polar Perturbations: 2-Tensors

For 2-tensors we find:

$$\mathcal{E}_{ab} = \mathcal{E}_{ab}^{(0)} + \Delta\mathcal{E}_{ab} \tag{8.178}$$
$$\mathcal{E}_{ab}^{(0)} = 0 \tag{8.179}$$
$$\Delta\mathcal{E}_{ab} = Y_{ab} \left[-\frac{1}{2}(\chi+\varphi)\right]. \tag{8.180}$$

$$\zeta_{ab} = \zeta_{ab}^{(0)} + \Delta\zeta_{ab} \tag{8.181}$$
$$\zeta_{ab}^{(0)} = 0 \tag{8.182}$$
$$\Delta\zeta_{ab} = Y_{ab}\,[g]. \tag{8.183}$$

$$\Sigma_{ab} = \Sigma_{ab}^{(0)} + \Delta\Sigma_{ab} \tag{8.184}$$
$$\Sigma_{ab}^{(0)} = 0 \tag{8.185}$$
$$\Sigma_{ab} = 0. \tag{8.186}$$

$$\mathcal{H}_{ab} = \mathcal{H}_{ab}^{(0)} + \Delta\mathcal{H}_{ab} \tag{8.187}$$
$$\mathcal{H}_{ab}^{(0)} = 0 \tag{8.188}$$
$$\mathcal{H}_{ab} = \bar{Y}_{ab} \left[\frac{1}{4}\varsigma\right] \tag{8.189}$$

8.4.3 Master Variables and Master Equations

8.4.3.1 The Equations

For exterior, vacuum, gravitational perturbations in the Schwarzschild spacetime, the system of equations simplifies considerably. As we consider vacuum perturbations, there can be no fluid perturbations

$$(v, w, \Delta) \mapsto 0. \tag{8.190}$$

This means that the evolution equations for the fluid perturbations now become constraints for the metric perturbations (specialising GMG93, GMG94 and GMG95 from [229] to the Schwarzschild spacetime [351])

$$0 = \dot{\varphi}' - W\dot{\chi} + \frac{1}{2}\frac{\ell(\ell+1)}{r^2}\varsigma \tag{8.191}$$

$$0 = -\varphi'' + \frac{\ell(\ell+1)}{r^2}(\chi+\varphi) - \frac{(\ell+2)(\ell-1)}{2r^2}\chi + W\chi' - 2W\varphi' \tag{8.192}$$

$$0 = \varsigma' + 2\nu\varsigma + \dot{\chi} + 2\dot{\varphi} \tag{8.193}$$

$$0 = \eta. \tag{8.194}$$

These can be re-written in terms of the 1+1+2 scalars as follows

$$0 = \dot{\varphi}' - \frac{1}{2}\phi\dot{\chi} + \frac{1}{2}\frac{\ell(\ell+1)}{r^2}\varsigma \tag{8.195}$$

$$0 = -\varphi'' + \frac{\ell(\ell+1)}{r^2}(\chi+\varphi) - \frac{(\ell+2)(\ell-1)}{2r^2}\chi + \frac{1}{2}\phi\chi' - \phi\varphi' \tag{8.196}$$

$$0 = \varsigma' + 2\mathcal{A}\varsigma + \dot{\chi} + 2\dot{\varphi} \tag{8.197}$$

$$\eta = 0. \tag{8.198}$$

The concomitant master equations for χ, φ, ς reduce to (specialising GMG98, GMG99 and GMG100 from [229] to the Schwarzschild spacetime)

$$-\ddot{\chi} + \chi'' = -2\left[2\nu^2 - 6\frac{M}{r^3}\right](\chi+\varphi) + \frac{(\ell+2)(\ell-1)}{r^2}\chi - (5\nu - 2W)\chi' \tag{8.199}$$

$$-\ddot{\varphi} = -W\chi' - \nu\varphi' - 4\frac{M}{r^3}(\chi+\varphi) - \frac{(\ell+2)(\ell-1)}{2r^2}\chi \tag{8.200}$$

$$-\dot{\varsigma} = 2\nu(\chi+\varphi) + \chi'. \tag{8.201}$$

Again, these can be re-written in terms of the 1+1+2 variables as follows

$$-\ddot{\chi} + \chi'' = -4\left[\mathcal{A}^2 + \frac{3}{2}\mathcal{E}\right](\chi+\varphi) + \frac{(\ell+2)(\ell-1)}{r^2}\chi - [5\mathcal{A} - \phi]\chi' \tag{8.202}$$

$$-\ddot{\varphi} = -\frac{1}{2}\phi\chi' - \mathcal{A}\varphi' - 2\mathcal{E}(\chi+\varphi) - \frac{(\ell+2)(\ell-1)}{2r^2}\chi \tag{8.203}$$

$$-\dot{\varsigma} = 2\mathcal{A}(\chi+\varphi) + \chi'. \tag{8.204}$$

8.4.3.2 The Covariant Regge-Wheeler and Zerilli Equations

The work of [104] was able to demonstrate that Eq. (8.112) obeys a closed covariant wave equation for both the polar and axial terms. In the polar case the harmonic components of Eq. (8.112) are given by

$$W_T = \frac{1}{2}\phi r^2 \zeta_T - \frac{r}{3}\frac{X_V}{\mathcal{E}}. \tag{8.205}$$

In the same body of work [104] they also demonstrated that we can construct a Zerilli like tensor from the following object

$$\mathcal{Z}_T = \frac{2}{3}c_3^{-1}\left[3r\phi\Sigma_T - 2\frac{\bar{\mathcal{H}}_V}{\mathcal{A}}\right] \tag{8.206}$$

where the coefficient c_j is defined by

$$c_j = 4\left[\ell\left(\ell+1\right)+1\right] - jr^2\phi^2 \tag{8.207}$$

and the Zerilli equation is given by

$$\ddot{\mathcal{Z}} - \hat{\hat{\mathcal{Z}}} - \mathcal{A}\,\hat{\mathcal{Z}} + \frac{1}{3}r^{-2}\left[\frac{1}{4}c_3 + 32c_3^{-2}\,\ell(\ell+1)\left\{(\ell-1)(\ell+2)\right\}^2\right]\mathcal{Z} = 0. \tag{8.208}$$

Again, we can take this one step further in order to connect with the literature at large. First, we introduce time coordinates. Next, we introduce tortoise coordinates and, following [104], we make the association that

$$\psi = \psi_{\mathcal{Z}} = \mathcal{Z}. \tag{8.209}$$

This will then obey Eq. (8.117) but the potential will now be given by

$$V = V_{\mathcal{Z}} = \frac{(r-2m)}{r^4\left\{(L-1)r+6M\right\}^2}\left[(L-1)^2[r^3(L+7)+24Mr^2]+36M^2r(L-1)+72M^3\right], \tag{8.210}$$

where [104] defined $L = \ell(\ell+1)$ for brevity. Though it is anticipated that the analysis of [437] will lead to modifications in the covariant reconstruction of the Zerilli wave equation.

8.5 Weyl Curvature Tensor

8.5.1 Introduction

In this section we highlight an additional result that arises from considering the wave equations that are generated by the electric and magnetic Weyl 2-tensors. As can seen in the correspondence presented in this Chapter, these tensors are intricately linked to the 2+2 master variables $\{\chi, \varphi, \varsigma\}$. It is therefore reasonable to suspect that they may indeed play a fundamental role in the description of gravitational perturbations of the Schwarzschild spacetime, especially given the

role of the Weyl tensor in General Relativity. What we seek is a covariant tensor that unifies the even and odd parity perturbations and the corresponding master equation to go with this variable. Schematically, we will need to isolate a closed equation in the harmonic domain before performing a covariant reconstruction. This is due to the way in which we use the harmonic decomposition to factor out the δ-derivatives. As such we find a master variable that obeys a closed wave equation in the odd parity sector and check the consistency of this variable in the even parity sector. Once we have a variable that is consistent in both the even and odd parity sectors we can write down a covariant wave equation for this covariant tensor.

8.5.2 Odd Parity

Our starting point in this investigation is to construct the wave operator $\ddot{\Psi}_T - \hat{\hat{\Psi}}_T$ applied to the electric Weyl 2-tensor $\bar{\mathcal{E}}_T$ and the magnetic Weyl 2-tensor $\mathcal{H}_T$. This generates a pair of wave equations in the harmonic domain

$$\ddot{\mathcal{H}}_T - \hat{\hat{\mathcal{H}}}_T - (\phi + 3\mathcal{A})\,\hat{\mathcal{H}}_T + \left[\frac{\ell(\ell+1)}{r^2} - \mathcal{E} - \frac{1}{2}\phi^2\right]\mathcal{H}_T = 3\mathcal{E}\,(\phi - \mathcal{A})\,\bar{\Sigma}_T + 2\frac{\mathcal{H}_V}{r}\,(\phi - \mathcal{A}) \quad (8.211)$$

and

$$\ddot{\bar{\mathcal{E}}}_T - \hat{\hat{\bar{\mathcal{E}}}}_T - (\phi + 3\mathcal{A})\,\hat{\bar{\mathcal{E}}}_T + \left[\frac{\ell(\ell+1)}{r^2} - \mathcal{E} - \frac{1}{2}\phi^2\right]\bar{\mathcal{E}}_T = 3\mathcal{E}\,(\phi - \mathcal{A})\,\bar{\zeta}_T - 2\frac{\bar{\mathcal{E}}_V}{r}\,(\phi - \mathcal{A})\,. \quad (8.212)$$

These equations are not closed as they contain forcing terms from other 1+1+2 variables. The magnetic Weyl tensor is principally forced by the shear of the timelike congruence u^a while the electric Weyl tensor is principally forced by the shear of the spacelike congruence n^a. A reconstruction of the covariant form of these equations from their harmonic expressions provides the following pair of equations

$$\ddot{\mathcal{H}}_{\{ab\}} - \hat{\hat{\mathcal{H}}}_{\{ab\}} - (\phi + 3\mathcal{A})\,\hat{\mathcal{H}}_{\{ab\}} - \delta^2\mathcal{H}_{\{ab\}} + \left[\frac{1}{2}\phi^2 - 5\mathcal{E}\right]\mathcal{H}_{\{ab\}} = \left[3\mathcal{E}\Sigma_{\{ab\}} + 2\delta_{\{a}\mathcal{H}_{b\}}\right](\phi - \mathcal{A}) \quad (8.213)$$

and

$$\ddot{\bar{\mathcal{E}}}_{\{ab\}} - \hat{\hat{\bar{\mathcal{E}}}}_{\{ab\}} - (\phi + 3\mathcal{A})\,\hat{\bar{\mathcal{E}}}_{\{ab\}} - \delta^2\bar{\mathcal{E}}_{\{ab\}} + \left[\frac{1}{2}\phi^2 - 5\mathcal{E}\right]\bar{\mathcal{E}}_{\{ab\}} = \left[3\mathcal{E}\zeta_{\{ab\}} + 2\delta_{\{a}\mathcal{E}_{b\}}\right](\phi - \mathcal{A})\,. \quad (8.214)$$

Although these appear somewhat ungainly, by looking closely at the equations we can identify a very common structure between the two suggesting a rather natural perturbation variable that may decouple

$$\mathcal{W}_{\{ab\}} = \mathcal{E}_{\{ab\}} + \epsilon_{a\{c}\mathcal{H}_{b\}}{}^{c}. \tag{8.215}$$

This variable can be harmonically decomposed into its even (polar) and odd (axial) parity components

$$\mathcal{W}_{\{ab\}} = \left[\mathcal{E}_T - \bar{\mathcal{H}}_T\right] Q_{ab} + \left[\bar{\mathcal{E}}_T + \mathcal{H}_T\right] \bar{Q}_{ab} \tag{8.216}$$

$$= \mathcal{W}_T\, Q_{ab} + \bar{\mathcal{W}}_T\, \bar{Q}_{ab}. \tag{8.217}$$

In order to see if this is a legitimate candidate for a covariant tensor that unifies the axial and polar gravitational perturbations we will need to ensure that both parities obey the same wave equation. We first consider the even parity equation and then ensure that the odd parity equation is consistent.

We construct a wave equation for the variable $\bar{\mathcal{W}}_T$ by making use of 8.211 and 8.212. In particular, we see that, after combining these equations, the remaining terms may be cancelled by the timelike and radial derivatives of our master variable $\bar{\mathcal{W}}_T$ along with a potential term multiplied by $\bar{\mathcal{W}}_T$. This can be seen by looking at the terms on the RHS of equations 7.178 and 7.180. The concomitant closed wave equation reduces down to

$$\ddot{\bar{\mathcal{W}}}_T - \hat{\hat{\bar{\mathcal{W}}}}_T - (\mathcal{A} + 3\phi)\,\hat{\bar{\mathcal{W}}}_T - (2\mathcal{A} - 2\phi)\,\dot{\bar{\mathcal{W}}}_T + \left[\frac{\ell\,(\ell+1)}{r^2} - \frac{3}{2}\phi^2 + 2\mathcal{E} + 4\mathcal{A}^2\right]\bar{\mathcal{W}}_T = 0. \tag{8.218}$$

The covariant wave equation that this master variable would obey is given by

$$\ddot{\mathcal{W}}_{\{ab\}} - \hat{\hat{\mathcal{W}}}_{\{ab\}} - (\mathcal{A} + 3\phi)\,\hat{\mathcal{W}}_{\{ab\}} - (2\mathcal{A} - 2\phi)\,\dot{\mathcal{W}}_{\{ab\}} - \left(\delta^2 + 2K\right)\mathcal{W}_{\{ab\}} + \left(4\mathcal{A}^2 - 4\mathcal{E}\right)\mathcal{W}_{\{ab\}} = 0. \tag{8.219}$$

Now that we have this identity we must switch to the even parity sector and make sure that this wave equation is consistent and valid.

8.5.2.1 Even Parity

We perform the same procedure as we did for the odd parity variable $\bar{\mathcal{W}}_T$, this time with the even parity terms. We construct the wave equation for the electric and magnetic Weyl 2-tensors resulting in the following pair of harmonic wave equations

$$\ddot{\bar{\mathcal{H}}}_T - \hat{\hat{\bar{\mathcal{H}}}}_T - (\phi + 3\mathcal{A})\,\hat{\bar{\mathcal{H}}}_T + \left[\frac{\ell(\ell+1)}{r^2} - \mathcal{E} - \frac{1}{2}\phi^2\right]\bar{\mathcal{H}}_T = 3\mathcal{E}\,(\phi - \mathcal{A})\,\Sigma_T - 2\frac{\bar{\mathcal{H}}_V}{r}\,(\phi - \mathcal{A}) \tag{8.220}$$

and

$$\ddot{\mathcal{E}}_T - \hat{\hat{\mathcal{E}}}_T - (\phi + 3\mathcal{A})\,\hat{\mathcal{E}}_T + \left[\frac{\ell(\ell+1)}{r^2} - \mathcal{E} - \frac{1}{2}\phi^2\right]\mathcal{E}_T = 3\mathcal{E}\,(\phi - \mathcal{A})\,\zeta_T + 2\frac{\mathcal{E}_V}{r}\,(\phi - \mathcal{A})\,. \tag{8.221}$$

As hoped, these equations correspond to the even parity harmonic decomposition of 8.211 and 8.212. Applying the wave operator to the even parity variable $\mathcal{W}_T$ and killing off any remaining terms with timelike and spacelike derivatives of $\mathcal{W}_T$ or a potential term multiplied by $\mathcal{W}_T$ yields

$$\ddot{\mathcal{W}}_T - \hat{\hat{\mathcal{W}}}_T - (\mathcal{A} + 3\phi)\,\hat{\mathcal{W}}_T - (2\mathcal{A} - 2\phi)\,\dot{\mathcal{W}}_T + \left[\frac{\ell\,(\ell+1)}{r^2} - \frac{3}{2}\phi^2 + 2\mathcal{E} + 4\mathcal{A}^2\right]\mathcal{W}_T = 0. \tag{8.222}$$

Finally, the covariant reconstruction of this even parity wave equation leads us to exactly the same covariant wave equation 8.219 that the odd parity variable $\bar{\mathcal{W}}_T$ obeys thus demonstrating the consistency of the master variable we defined previously.

8.5.3 Unified Master Equation and Master Variable

Piecing this all back together, we have derived a covariant, gauge- and frame-invariant, transverse-traceless tensor

$$\mathcal{W}_{\{ab\}} = \mathcal{E}_{\{ab\}} + \epsilon_{a\{c}\mathcal{H}_{b\}}{}^{c} \tag{8.223}$$

along with its concomitant closed covariant wave equation

$$\begin{aligned}\ddot{\mathcal{W}}_{\{ab\}} - \hat{\hat{\mathcal{W}}}_{\{ab\}} - (\mathcal{A} + 3\phi)\,\hat{\mathcal{W}}_{\{ab\}} - (2\mathcal{A} - 2\phi)\,\dot{\mathcal{W}}_{\{ab\}} \\ - \left(\delta^2 + 2K\right)\mathcal{W}_{\{ab\}} + \left(4\mathcal{A}^2 - 4\mathcal{E}\right)\mathcal{W}_{\{ab\}} = 0.\end{aligned} \tag{8.224}$$

This tensor will describe gravitational waves in the Schwarzschild spacetime and the even and odd parity components of this wave equation will be analogous to the more commonly used Regge-Wheeler and Zerilli equations. A similar decoupling was seen in [82] who used elegant complex methods to decoupled the equations. In many ways this master equation is a rather cute result as it explicitly expresses a wave equation in terms of the Weyl curvature tensors which correspond to the free part of the gravitational field responsible for action at a distance. In the case of a Schwarzschild black hole, this corresponds to the propagation of the Weyl curvature variables with distortion terms arising from the black hole itself. In addition, as $\mathcal{E}_{ab}$ and $\mathcal{H}_{ab}$ themselves are frame invariant, the frame-invariance of W_{ab} is natural.

In principle, this tensor is related to a linear combination of the 2+2 gauge-invariant variables. As an example, in the polar sector we would find

$$\mathcal{W}_T = \mathcal{E}_T - \bar{\mathcal{H}}_T = \frac{1}{2r^2}\left[-(\chi + \varphi) + \varsigma\right]. \tag{8.225}$$

8.6 Conclusions

Metric perturbations of the Schwarzschild spacetime are amongst the oldest and most interesting applications of General Relativity. The work was initiated by [458; 578; 579; 607; 608; 381; 201; 202] but has since been expanded and extended with applications to many physically interesting situations. Not only does this spacetime provide useful physical insight and intuition into General Relativity but it is also the prototypical starting point for the exterior solution of a single isolated black hole or stellar object. The spacetime has also been highly influential in understanding the gravitational wave emission from point particles in orbit around a black hole [348; 473; 399; 349].

The initial studies made use of gauge-invariant objects constructed by finding linear combinations of metric perturbations that are invariant under infinitesimal coordinate transformations [381]. Historically, some of the most useful coordinates have been the normal Schwarzschild coordinates (t, r, θ, ϕ) along with the *Regge-Wheeler gauge* which have proved to be useful for many purposes of interest, though not all. For example, the Schwarzschild coordinates are often poorly behaved at the event horizon complicating any such analysis. To study the behaviour of the perturbations at the horizon it is more useful to adopt the *incoming radiation gauge* which expresses the perturbations in terms of advanced coordinates (v, r, θ, ϕ) [349]. Similarly, the behaviour of the perturbations at future null infinity is well described by adopting the *outgoing radiation gauge* and expressing the perturbations in terms of retarded coordinates (u, r, θ, ϕ) [349].

The work of [201; 202] reformulated the problem in terms of an arbitrary coordinate system and derived sets of gauge-invariant objects. A further completion was made by [229] who made the system of equations explicit by systematically deriving a set of closed master equations describing all the perturbations for a set of well defined gauge invariant variables. The work of [350; 229; 351] was amongst the first of a recent flurry in papers aimed at constructing well defined covariant and gauge-invariant frameworks for the study of perturbations to the Schwarzschild spacetime [470; 104; 348; 399; 349; 105; 437].

In this Chapter we have extended the study of [104; 437] introducing new relationships for decoupled perturbations that constitute new master equations. It was explicitly shown that the GMG [229] master variable Π corresponds to the magnetic Weyl scalar $\mathcal{H}$ and a concomitant wave equation derived. Likewise we were able to show that the axial components of the covariant Regge-Wheeler tensor W_{ab} correspond to the Regge-Wheeler variable defined in terms of an axial metric perturbation k_r. We then proceeded to show that the linear combination of Weyl curvature tensors $\mathcal{W}_{ab} = \mathcal{E}_{ab} + \epsilon_{a\{c}\mathcal{H}_{b\}}{}^{c}$ obey their own closed wave equation with both the axial and polar sectors satisfying the same harmonic equation. This is a wonderful connection to gravitational perturbations as the Weyl tensor is known to govern the free gravitational field, i.e. gravitational radiation. This is made explicit in the 1+1+2 formalism.

In parallel to these investigations in the 1+1+2 formalism we were able to set up and demonstrate a correspondence between the 2+2 gauge invariant variables and the covariant, gauge-invariant 1+1+2 geometrical objects. The power and advantage of the 1+1+2 formalism is that it provides clear, physically and geometrically meaningful insight into the system of equations. The major complication in the 1+1+2 approach is in setting up and finding a reduced set of master variables. In fact, this is often the bottle neck in such studies.

8.7 Summary of Key Points and Key Results

- We have been able to express the 2+2 background scalars in terms of geometrical 1+1+2 scalars.
- Writing down a general form for the axial perturbations to the Schwarzschild metric, we were able to construct a dictionary that maps us from the 1+1+2 variables to the 2+2 variables and vice versa. Key identifications include the identification of the Regge-Wheeler tensor W_{ab}, derived in [104], to the metric perturbation k_r. Accordingly, we demonstrated that various definitions for the Regge-Wheeler variable in different formalisms are identical obeying a covariant wave equation, as detailed in [104; 437].
- Secondly, we were able to demonstrate that the GMG axial master variable Π is simply the radial part of the Magnetic Weyl tensor $\mathcal{H}$. This variable characterises axial gravitational waves and can also be related to the imaginary part of the Newman-Penrose scalar Ψ_0. We gave an explicit expression for the covariant wave equation that this variable obeys.
- A similar analysis was conducted for the polar sector, allowing us to relate the 2+2 perturbations to the 1+1+2 variables.
- An interesting outcome of a unified analysis of the perturbations to the polar and axial sector was that we were able to identify a linear combination of the electric and magnetic Weyl 2-tensors $\mathcal{W}_{ab}$ that decouples, obeying a closed covariant wave equation for gravitational perturbations to the Schwarzschild spacetime.
- This can be related to the 2+2 formalism by noting that $\mathcal{E}_{ab} \propto (\chi + \varphi)$ and $\mathcal{H}_{ab} \propto \varsigma$. Here, the 2+2 master variable χ characterises polar gravitational waves, obeying a wave equation with a wave speed of unity. The variable ς is a genuinely relativistic degree of freedom that can be related to purely physical effects, such as frame dragging.
- Whilst these results are of no great surprise,perturbations to the Schwarzschild spacetime are well detailed, it does provide a suitable testing ground for the covariant and gauge invariant 1+1+2 formalism. By recovering these results, we are able to demonstrate the power of the Weyl variables in covariantly characterising gravitational waves as well as detailing some of the geometrically interesting properties of these variables that are otherwise heavily obscured in metric and spinor based approaches.
- As a final note, the results in this Chapter should be viewed as a testing bed for the 1+1+2 formalism. The real power of the results in this Chapter are that the covariant wave equation for the Weyl master variable $\mathcal{W}_{ab}$ is a limiting case of a master variable that covariantly characterises gravitational perturbations to LRS-II spacetimes. Likewise, the Weyl master variable for axial gravitational waves $\mathcal{V}_{ab}$ is a limiting case of a master variable governing axial gravitational waves in LRS-II spacetimes. This will be discussed in further detail in the next Chapter. Such an analysis allows us to compare the space of cosmological spacetimes in a physically meaningful way.

Chapter 9

Covariant Perturbations of the The Lemaître-Tolman-Bondi Spacetime

9.1 Introduction

The Lemaître-Tolman-Bondi (LTB) spacetime corresponds to spherically symmetric but radially inhomogeneous solution to Einstein's Field Equations [319; 563; 71] and are one of the first steps we can take to a genuinely inhomogeneous spacetime. These models correspond to a spherically symmetric but radially inhomogeneous spacetime with only dust as an energy-momentum contribution. Spherical symmetry is enforced as isotropic observations, which are heavily constrained by the CMB, in the presence of dust imply spherical symmetry. These models can be used as an attempt to replace dark energy, we cannot disentangle temporal and spatial evolutions, given the appropriate density profile, or they can be used with a cosmological constant as a means to constrain and understand radial inhomogeneities. In this thesis I will adopt something of the second standpoint, LTB models can tell us a lot about structure formation in the presence of genuine global inhomogeneity and can help us to understand the physical consequences implied by assuming spatial homogeneity in the standard model. In addition the LTB solution can be embedded in the FLRW models, or other cosmological spacetimes, as an attempt to model structure in the Universe allowing us to understand how structure interacts with rest of the Universe.

We can test both the background LTB model as well as the perturbed LTB models. In the perturbed scenario we allow for small-scale inhomogeneities to dynamically grow in the background. This allows us to develop robust predictions for structure in the LTB spacetime and to confront the LTB models with all observables at our disposal. The equations for perturbations of the LTB models have been presented in their full generality by [106] and the application of these general equations to the structure formation problem is incomplete. In part this is due to the additional complications that an inhomogeneous background introduces. A numerical study was recently presented in [181] for a range of different initial conditions. In addition, there have been studies on the self-similar LTB spacetime [588; 150] in a more mathematically elegant way. All of these studies were completed within the 2+2 covariant framework.

An alternative approach, the one pursued here, is based on the 1+1+2 formalism of [104;

105]. A preliminary application of this approach to LTB models was given in [610; 611] where the evolution of the perturbations was given in terms of linear transfer functions. This approach assumed both that decaying modes may be ignored and that the silent approximation, where the magnetic part of the Weyl tensor is neglected, holds. There is, however, no strong motivation for enforcing the silent approximation and it is very likely that dynamical features are erased by doing so [338]. Another study was undertaken in [152] to understand how an inhomogeneous Universe can mimic the standard ΛCDM cosmology. We present the LTB system of equations in their full generality and derive a master equation for the axial perturbations and a preliminary master equation that is valid for both polar and axial perturbations [438]. This final result is incomplete as the equation couples to other $1+1+2$ variables and it is likely that we would need to supplement the equation with auxiliary equations in order to derive a complete, closed system of equations. This equation does close correctly when we take a vacuum limit and allow $\mu \to 0$. This leads us to an auxiliary result that for LRS-II spacetimes, namely that the electric and magnetic Weyl 2-tensors can form a master variable that obeys a closed covariant wave equation for $\{\mathcal{A}, \mathcal{E}, \Sigma, \Theta, \phi\} \neq 0$ in the background.

9.2 Motivation

9.2.1 The Standard Model of Cosmology

The standard model of cosmology is a highly simplistic construction based on linear perturbations about a spatially homogeneous and isotropic background. This approach explicitly assumes that the Universe can be approximated by a cosmological spacetime with high degrees of symmetry. This is clearly not true in a realistic Universe filled with structure on both large and small scales. Surprisingly, and rather impressively, this standard picture can easily account for nearly all cosmological observations which probe a vast range of scales, both spatial and in time, with only a small number of parameters. Unfortunately for us, the picture that we are slowly building up is one in which the early Universe is dominated by a period of exponential expansion driven by inflation and the late Universe is dominated by a dark energy component that drives us towards late time de Sitter expansion. We happen to be anthropically selected to live in an era between these two extremes in which structure formation can occur and the expansion seems to be well approximated by a perfect fluid FLRW spacetime. Frustratingly, we also have very little theoretical understanding of inflation, dark energy and dark matter. Whilst paradigms and mechanisms do exist that are in agreement with observations, such as the field theoretic overview of inflation given in Chapter 3, there is no fundamental description of these three components.

This lack of a connection to fundamental physics means that we should be very careful as to the statements we make and we should take every effort to ensure that cosmological observables are interpreted in a rigorous manner. For instance, many cosmological observations demand that we fix a cosmology and its parameters in order to extract the physically meaningful information. However, spatial homogeneity of the Universe, when smoothed over sufficiently large scales, is introduced as an assumption and is not yet an observationally proven fact. To what degree does observational data *uniquely* indicate that the FLRW background geometry is a valid approximation? This is important as tests of homogeneity on cosmological scales become rather involved, as

we shall see shortly [538; 107; 170; 341; 252; 110].

To this end, we want to briefly outline the founding principles of the standard model cosmology and how we can develop our understanding of relativistic cosmology. One approach is to explore the space of cosmological spacetimes starting from the maximally symmetric FLRW Universes and systematically stripping away the symmetries to understand the phenomenological behaviour and dynamics of cosmological models in General Relativity [167; 168]. This is the philosophy emphasised in this Chapter. The LTB models can be tightly constrained via observations and, realistically, we certainly do not expect them to be a more robust or valid description of the Universe. Instead, we see the LTB models as being the first stepping stone towards a genuinely inhomogeneous spacetime for which the relaxed assumptions on homogeneity open up rich, new phenomenological features that may not be present in the homogeneous FLRW models. Such rich structure has also been observed in the anisotropic case. For completeness, a handful of key results relating to anisotropic cosmologies may be found in [161; 533; 162; 163; 121; 206] with detailed overviews provided by [581; 169] and more recent applications of these models given by, for example, [85; 542; 448].

9.2.2 Founding Principles in Cosmology

The philosophical point of view adopted in this thesis is that the FLRW spacetime is an approximation to the real Universe and that it is important to demonstrate that the FLRW approximation holds from a purely observational point of view without *a priori* assuming FLRW. This means finding tests independent of, for example, the field equations from which we can distinguish models. Two of the main issues that arise when considering such are problem are the *Copernican* and *Cosmological* principles [110]

- **The Copernican Principle:** We do not occupy a special location in the Universe.
- **The Cosmological Principle:** Smoothed on sufficiently large scales, the Universe is spatially homogeneous and isotropic.

The standard formulation of the FLRW spacetime arises by imposing the Copernican principle and using the high isotropy of the CMB coupled with the approximate isotropy of local observables to arrive at the Cosmological principle. This can be shown to be true in an exact sense. Namely that if all observers measure a distance-redshift relation that is exactly isotropic, then the spacetime will be exactly FLRW [160]. This is *not* realistic. A more appropriate statement would read [110]: If most observers measure observables that are consistent with small levels of anisotropy, then the metric of the Universe will be roughly FLRW when smoothed on sufficiently large scales. This has introduced a number of subtleties that may or may not be realistic. For instance, what do we mean by smoothing? Smoothing observables is not the same thing as spatial smoothing and, even worse, smoothing geometry is an ill defined procedure for which we do not recover the same geometry as that from a smoothed energy-momentum tensor [109; 73; 19; 110]. These all add additional complications to the correct interpretation or cosmological observables on large scales.

Ignoring such subtleties we can see that mapping ourselves from the Copernican principle to an almost FLRW procedure seems very reasonable under a large range of circumstances [334; 335; 538; 102; 39; 406]. This necessitates that we can observationally test the Copernican principle

[110]. This is where a problem kicks in. On large scales (on the order of Gpc), we *effectively* have a view of the Universe from a single spacetime event and observations amount to looking down our past lightcone Fig. 9.1. This is important as homogeneity is defined over spatial surfaces but observations down the past null cone amount to observations that intersect with the spatial hypersurfaces *not* across the spatial hypersurfaces. Heuristically, this corresponds to the well known phenomena that looking at objects that are further away, i.e. higher redshifts, means that we are looking at objects that are in the distant past. This is just the causal nature of General Relativity. However, on large scales we see that temporal and spatial evolution can become entangled, more so for the cosmological models with reduced symmetry, making interpretations of observables more complicated. We can test the Copernican principle *locally* but to do so in a more *global* sense requires more sophisticated analysis methods [110].

One particular avenue of research is to reconstruct the metric of the Universe from observational data [164; 22; 23; 253; 584; 24; 67]. In this approach, cosmological observations are used to re-construct initial data on the past null cone which can then be integrated into the interior [110]. The important observation here is if this procedure reconstructs something that is highly FLRW and if it will necessarily result in something that is highly FLRW. In some ways this is perhaps the most fundamental approach of those available..

9.2.3 Constraints on LTB

We do not wish to discuss this point in any significant detail, it would take up too much space, but we note that a number of tests of the LTB models have been devised. Examples include

- Distance-redshift relations, volume element and number counts.
- CMB and Hubble Parameter.
- Scattering of the CMB: The Compton-y parameter along with the kSZ and tSZ effects.
- BAOs.
- Growth of large scale structure and density perturbations.

The basic point here is that different scales will be probed by different astrophysical observations. A compendium of tests and cross-correlations between cosmological observables is likely to provide the most stringent constraints on these models. For detailed, in-depth reviews see [107; 170; 341; 110] and the references within. From here on we will focus on the study of gravitational perturbations in the LTB spacetime. We leave a detailed study of the astrophysical and cosmological implications to future work.

9.3 Background Spacetime

Assuming a pure dust spacetime, the isotropy of the CMB implies spherical symmetry which leads to the Lemaître-Tolman-Bondi (LTB) spacetime [318; 563; 71] or the ΛLTB spacetime, should we allow for Λ. After all, there is no reason *a priori* why we should rule out a dark energy contribution even if we are using a cosmological spacetime with relaxed symmetries. It is perfectly acceptable

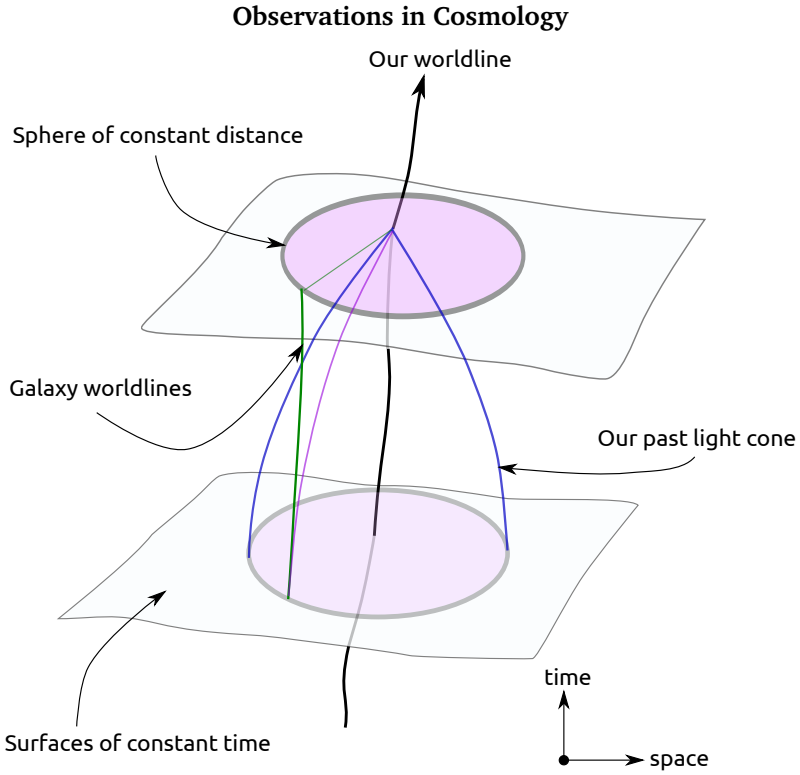

Figure 9.1: This figure is essentially a reproduction of Figure 2 in [110]. Observations in cosmology amount to looking down our past null cone. This is the well known phenomena that looking at more distant objects amounts to looking at objects that are in our past. This is the causal nature of General Relativity. The problem for cosmologists is that observations on the null light cone correspond to observations that intersect spatial surfaces and are not made *across* the spatial surfaces themselves. We can therefore test the Copernican principle *locally* but this becomes more complicated on large scales where spatial and temporal evolution become entangled.

to have both. As we impose spherical symmetry, we are implicitly stating that the vorticity must vanish and, as we are dealing with a dust energy-momentum source, the fundamental observers will be geodesic. This means that we can write the LTB metric in a comoving form

$$ds^2 = -dt^2 + X^2(t,r)dr^2 + A^2(t,r)d\Omega^2. \tag{9.1}$$

From this metric we can calculate the Christoffel symbols and the EFEs Appendix D.1.1. Typically the metric functions $X(t,r)$ and $A(t,r)$ can be defined in terms of a curvature function $\kappa(r)$ as follows

$$X(t,r) = \frac{a_{\parallel}(t,r)}{\sqrt{1-\kappa(r)\,r^2}} \tag{9.2}$$

$$A(t,r) = a_{\perp}(t,r)\,r. \tag{9.3}$$

where we have introduced two new scale factors: a scale factor parallel to the radial direction $a_{\parallel} = \partial_r(a_{\perp}r)$ and a scale factor perpendicular to the radial direction, i.e. angular, $a_{\perp}(t,r)$. The curvature function $\kappa(r)$ is a free function of r. Hence the unperturbed LTB metric may be written

in the following form

$$ds^2 = -dt^2 + \frac{a_\parallel^2(t,r)}{(1-\kappa r^2)}dr^2 + a_\perp^2(t,r)\, r^2\, d\Omega^2, \tag{9.4}$$

Using these two scale factors we can introduce two Hubble parameters

$$H_\parallel = \frac{\dot{a}_\parallel}{a_\parallel} \quad \text{and} \quad H_\perp = \frac{\dot{a}_\perp}{a_\perp} \tag{9.5}$$

where the dot operator is just ∂_t. As may be expected, we can construct analogues to the Friedmann equation

$$H_\perp^2 = \frac{M}{a_\perp^3 r^3} - \frac{\kappa}{a_\perp^2 r^2} \tag{9.6}$$

with $M = M(r)$ being a free function of r. The locally measured energy density is

$$8\pi\mu = \frac{(Mr^3)_{,r}}{a_\parallel a_\perp^2 r^2} \tag{9.7}$$

where μ obeys the conservation equation that arises from the Bianchi identity

$$\dot{\mu} + (2H_\perp + H_\parallel)\mu = 0. \tag{9.8}$$

Rather unsurprisingly we can also define two acceleration equations, one for the parallel scale factor and one for the perpendicular scale factor

$$\frac{\ddot{a}_\perp}{a_\perp} = -\frac{M}{2a_\perp^3 r^3} \quad \text{and} \quad \frac{\ddot{a}_\parallel}{a_\parallel} = -4\pi\rho + \frac{M}{a_\perp^3 r^3}. \tag{9.9}$$

Much as we did in the FLRW spacetimes, we can also introduce dimensionless density parameters for CDM and the curvature function κ

$$\Omega_\kappa(r) = -\frac{\kappa}{H_{\perp_0}^2} \qquad \Omega_m(r) = \frac{M}{H_{\perp_0}^2} \tag{9.10}$$

such that $\Omega_m(r) + \Omega_\kappa(r) = 1$ and the Friedmann equation reduces to the rather familiar form from Chapter 1

$$\frac{H_\perp^2}{H_{\perp_0}^2} = \Omega_m\, a_\perp^{-3} + \Omega_\kappa\, a_\perp^{-2}. \tag{9.11}$$

We can analytically integrate this Friedmann equation from an initial time corresponding to the big bang, the *bang time* $t_B(r)$, to some later time t

$$\tau(r,r) = t - t_B = \frac{1}{H_{\perp_0}(r)} \int_0^{a_\perp(t,r)} \frac{d\chi}{\sqrt{\Omega_m(r)\chi^{-1} + \Omega_\kappa(r)}}. \tag{9.12}$$

This yields two free functional degrees of freedom: the matter density profile $\Omega_m(r)$ and the bang time $t_B(r)$ [110]. Typically we can obtain a solution by fixing the choice of coordinates, much as we did in FLRW, such that $a_\perp(t_0, r) = 1$ and $H_{\perp_0}(r = 0) = H_0$. The distance-redshift relations in the LTB spacetime can be written down once we have specified our observers. For instance, on the past null cone, an observer at the center of the LTB metric may write down the pair of coordinates t, r as a function of the redshift z

$$\frac{dt}{dz} = -\frac{1}{(1+z)H_\parallel}, \qquad \frac{dr}{dz} = \frac{\sqrt{1-\kappa r^2}}{(1+z)a_\parallel H_\parallel}. \tag{9.13}$$

The angular area distance is just related to the angular part of the metric and the luminosity distance as a redshifted area distance

$$d_A(z) = a_\perp(t(z), r(z))\, r(z), \qquad d_L(z) = (1+z)^2 d_A(z). \tag{9.14}$$

Finally, we note that the volume element can also be written as a function of redshift [110]

$$\frac{dV}{dz} = \frac{4\pi d_A(z)^2}{(1+z)H_\parallel(z)}. \tag{9.15}$$

9.3.1 2+2 Formalism

The background timelike and spacelike unit vectors $\tilde{u}^A$ and $\tilde{n}^A$ in the LTB spacetime Eq. (9.4) are given by

$$\tilde{u}^A = (1, 0) \quad \text{and} \quad \tilde{n}^A = \left(0, \frac{\sqrt{1-\kappa r^2}}{a_\parallel}\right). \tag{9.16}$$

These variables obey the appropriate normalisations $u_\mu u^\mu = -1$ and $n_\mu n^\mu = +1$. Following [229] we can calculate the scalar background variables and the frame derivatives for the LTB metric Eq. (9.4). The scalars are given by

$$\Omega = \ln \rho \tag{9.17}$$
$$U = H_\perp \tag{9.18}$$
$$V = \frac{U}{W} \tag{9.19}$$
$$\tau = H_\parallel \tag{9.20}$$
$$\nu = 0, \tag{9.21}$$

where we have introduced a curvature function W defined by

$$W = \frac{\sqrt{1-\kappa r^2}}{a_\perp r}. \tag{9.22}$$

Following [106], we will seek to eliminate κ in favour of W. This will be particularly useful when relating the 2+2 formalism to the 1+1+2 formalism, as we will see shortly. The frame derivatives

are given by

$$\dot{X} = \partial_t X \tag{9.23}$$

$$X' = \frac{\sqrt{1-\kappa r^2}}{a_\parallel}\,\partial_r X, \tag{9.24}$$

and obey the commutation relation

$$\left(\dot{f}\right)' - \left(f'\right)^{\cdot} = H_\parallel f'. \tag{9.25}$$

The background relations from GMG reduce to the following expressions

$$H_\perp' = W(H_\parallel - H_\perp) \tag{9.26}$$

$$\dot{H}_\perp = -H_\perp^2 - \frac{M}{2a_\perp^3 r^3}, \tag{9.27}$$

$$\dot{W} = -H_\perp W, \tag{9.28}$$

$$W' = -W^2 - 4\pi\rho + H_\perp H_\parallel + \frac{M}{2a_\perp^3 r^3}. \tag{9.29}$$

The quasilocal Misner-Sharp mass reduces to

$$M = \frac{r}{2}\left[1 + r^2\left(H_\perp^2 - W^2\right)\right] \tag{9.30}$$

which is related to the integral over the energy density μ via

$$M' = 4\pi r^2\,(rW)\;\rho. \tag{9.31}$$

As we will see in the next subsection, these background equations can be re-expressed in the covariant and gauge-invariant framework of the 1+1+2 formalism.

9.3.2 1+1+2 Formalism

We now want to specialise to the class of inhomogeneous, spherically symmetric dust spacetimes known as the Lemâitre-Tolman-Bondi spacetime. Introducing a set of comoving fundamental observers $u^a = \delta^a_0$, the energy-momentum tensor for this pure dust spacetime reduces to

$$T_{ab} = \mu\, u_a u_b. \tag{9.32}$$

In a pure dust spacetime, corresponding to $p = 0$, the comoving worldlines will be geodesic and the radial component of the acceleration of u^a, $\mathcal{A}$, will vanish. Remember, $\mathcal{A}$ is simply a measure of non-gravitational forces acting on our timelike congruence and geodesic motion has a vanishing acceleration. The LTB spacetime can therefore be covariantly characterised by the following 1+1+2 scalars that are non-zero in the background spacetime

$$\mathbf{X}_{\rm LTB} = \{\phi, \Theta, \Sigma, \mathcal{E}, \mu\}, \tag{9.33}$$

along with the radial $\hat{\mathbf{X}}$ and timelike derivatives $\dot{\mathbf{X}}$ as these do not vanish in the background. The background propagation and evolution equations are obtained by taking the full system of equations and retaining only the terms that are non-zero in the background. The resulting system of equations that covariantly describe the background LTB spacetime are given by

Background Propagation Equations:

$$\hat{\phi} = -\frac{1}{2}\phi^2 - \left(\Sigma - \frac{2}{3}\Theta\right)\left(\Sigma + \frac{1}{3}\Theta\right) - \frac{2}{3}\mu - \mathcal{E} \tag{9.34}$$

$$\hat{\Sigma} = -\frac{3}{2}\phi\Sigma + \frac{2}{3}\hat{\Theta} \tag{9.35}$$

$$\hat{\mathcal{E}} = -\frac{3}{2}\phi\mathcal{E} + \frac{1}{3}\hat{\mu}. \tag{9.36}$$

Background Evolution Equations:

$$\dot{\phi} = \frac{1}{2}\phi\left(\Sigma - \frac{2}{3}\Theta\right) \tag{9.37}$$

$$\dot{\Sigma} = -\frac{1}{2}\Sigma\left(\Sigma + \frac{4}{3}\Theta\right) - \mathcal{E} \tag{9.38}$$

$$\dot{\mathcal{E}} = \frac{3}{2}\mathcal{E}\left(\Sigma - \frac{2}{3}\Theta\right) - \frac{1}{2}\mu\Sigma \tag{9.39}$$

$$\dot{\mu} = -\Theta\mu \tag{9.40}$$

$$\dot{\Theta} = -\frac{1}{3}\Theta^2 - \frac{3}{2}\Sigma^2 - \frac{1}{2}\mu. \tag{9.41}$$

As we saw in the Schwarzschild spacetime, these 1+1+2 covariant objects may be mapped onto the set of 2+2 variables that describe the background spacetime. Using the metric 9.4, we can equate the 1+1+2 variables to metric functions by taking the appropriate projections and covariant derivatives [58]

$$\phi = 2\frac{\sqrt{1-\kappa r^2}}{a_\perp r}, \tag{9.42}$$

$$\Theta = H_\parallel + 2H_\perp, \tag{9.43}$$

$$\Sigma = \frac{2}{3}\left(H_\parallel - H_\perp\right), \tag{9.44}$$

$$\mathcal{E} = \frac{\mu}{3} - \frac{M}{2a_\perp^3 r^3}, \tag{9.45}$$

$$\mu = \frac{(Mr^3)_{,r}}{a_\parallel a_\perp^2 r^2}. \tag{9.46}$$

9.4 Linearised Equations

9.4.1 1+1+2 Formalism

Next we construct the set of linearised equations by dropping all terms at second order and higher. These equations constitute a specialisation for the system of equations given in Section 7.5.8 and

are reproduced here for clarity and reference.

Linearised Propagation Equations:

$$\hat{\xi} = -\phi\xi + \frac{1}{2}\epsilon_{ab}\delta^a a^b + \left(\Sigma + \frac{1}{3}\Theta\right)\Omega \tag{9.47}$$

$$\hat{\Omega} = -\delta_a\Omega^a - \phi\Omega \tag{9.48}$$

$$\hat{\mathcal{H}} = -\delta_a\mathcal{H}^a - \frac{3}{2}\phi\mathcal{H} - \Omega\left(3\mathcal{E} + \mu\right) \tag{9.49}$$

$$\hat{\Sigma}_{\bar{a}} - \epsilon_{ab}\hat{\Omega}^b = \frac{1}{2}\delta_a\Sigma + \frac{2}{3}\delta_a\Theta - \epsilon_{ab}\delta^b\Omega - \frac{3}{2}\phi\Sigma_a + \frac{1}{2}\phi\epsilon_{ab}\Omega^b - \frac{3}{2}\Sigma a_a - \delta^b\Sigma_{ab} \tag{9.50}$$

$$\hat{\mathcal{E}}_a = \frac{1}{2}\delta_a\mathcal{E} + \frac{1}{3}\delta_a\mu - \frac{3}{2}\mathcal{E}a_a - \frac{3}{2}\phi\mathcal{E}_a - \frac{3}{2}\Sigma\epsilon_{ab}\mathcal{H}^b - \delta^b\mathcal{E}_{ab} \tag{9.51}$$

$$\hat{\mathcal{H}}_a = \frac{1}{2}\delta_a\mathcal{H} - \delta^b\mathcal{H}_{ab} - \frac{3}{2}\mathcal{E}\epsilon_{ab}\Sigma^b + \Omega_a\left(\frac{3}{2}\mathcal{E} - \mu\right) + \frac{3}{2}\Sigma\epsilon_{ab}\mathcal{E}^b - \frac{3}{2}\phi\mathcal{H}_a \tag{9.52}$$

$$\hat{\zeta}_{\{ab\}} = -\phi\zeta_{ab} + \delta_{\{a}a_{b\}} + \left(\Sigma + \frac{1}{3}\Theta\right)\Sigma_{ab} - \mathcal{E}_{ab} \tag{9.53}$$

$$\hat{\Sigma}_{\{ab\}} = \delta_{\{a}\Sigma_{b\}} - \epsilon_{c\{a}\delta^c\Omega_{b\}} - \frac{1}{2}\phi\Sigma_{ab} + \frac{3}{2}\Sigma\zeta_{ab} - \epsilon_{c\{a}\mathcal{H}_{b\}}{}^c. \tag{9.54}$$

Linearised Evolution Equations:

$$\dot{\xi} = \frac{1}{2}\xi\left(\Sigma - \frac{2}{3}\Theta\right) - \frac{1}{2}\phi\Omega + \frac{1}{2}\epsilon_{ab}\delta^a\alpha^b + \frac{1}{2}\mathcal{H} \tag{9.55}$$

$$\dot{\Omega} = \Omega\left(\Sigma - \frac{2}{3}\Theta\right) \tag{9.56}$$

$$\dot{\mathcal{H}} = -\epsilon_{ab}\delta^a\mathcal{E}^b - 3\xi\mathcal{E} + \frac{3}{2}\mathcal{H}\left(\Sigma - \frac{2}{3}\Theta\right) \tag{9.57}$$

$$\dot{\Omega}_a = -\Omega_a\left(\frac{1}{2}\Sigma + \frac{2}{3}\Theta\right) \tag{9.58}$$

$$\dot{\Sigma}_a = -\left(\frac{1}{2}\Sigma + \frac{2}{3}\Theta\right)\Sigma_a - \frac{3}{2}\Sigma\alpha_a - \mathcal{E}_a \tag{9.59}$$

$$\dot{\mathcal{E}}_a = \frac{1}{2}\epsilon_{ab}\delta^b\mathcal{H} - \frac{1}{2}\mu\Sigma_a - \frac{3}{2}\mathcal{E}\alpha_a + \frac{1}{2}\phi\epsilon_{ab}\mathcal{H}^b + \frac{3}{2}\left(\Sigma - \frac{2}{3}\Theta\right)\mathcal{E}_a + \frac{1}{2}\mu\epsilon_{ab}\Omega^b - \epsilon_{c\{d}\delta^d\mathcal{H}_{a\}}{}^c$$

$$\dot{\mathcal{H}} = -\epsilon_{ab}\delta^a\mathcal{E}^b - 3\xi\mathcal{E} + \frac{3}{2}\mathcal{H}\left(\Sigma - \frac{2}{3}\Theta\right) \tag{9.60}$$

$$\dot{\mathcal{H}}_a = -\frac{1}{2}\epsilon_{ab}\delta^b\mathcal{E} + \frac{1}{6}\epsilon\delta^b\mu - \frac{1}{2}\phi\epsilon_{ab}\mathcal{E}^b + \frac{3}{2}\left(\Sigma - \frac{2}{3}\Theta\right)\mathcal{H}_a + \epsilon_{c\{d}\delta^d\mathcal{E}_{a\}}{}^c \tag{9.61}$$

$$\dot{\zeta}_{\{ab\}} = \frac{1}{2}\zeta_{ab}\left(\Sigma - \frac{2}{3}\Theta\right) - \frac{1}{2}\phi\Sigma_{ab} + \delta_{\{a}\alpha_{b\}} - \epsilon_{c\{a}\mathcal{H}_{b\}}{}^c \tag{9.62}$$

$$\dot{\Sigma}_{\{ab\}} = \left(\Sigma - \frac{2}{3}\Theta\right)\Sigma_{ab} - \mathcal{E}_{ab}. \tag{9.63}$$

Linearised Mixed Evolution and Propagation Equations:

$$\hat{\alpha}_{\bar{a}} - \dot{a}_{\bar{a}} = -\frac{1}{2}\phi\alpha_a + a_a\left(\Sigma + \frac{1}{3}\Theta\right) + \frac{1}{2}\phi\left(\Sigma_a + \epsilon_{ab}\Omega^b\right) - \epsilon_{ab}\mathcal{H}^b \tag{9.64}$$

$$\dot{\mathcal{E}}_{\{ab\}} - \epsilon_{c\{a}\hat{\mathcal{H}}^{c}{}_{b\}} = -\epsilon_{c\{a}\delta^{c}\mathcal{H}_{b\}} - \frac{1}{2}\left(\mu + 3\mathcal{E}\right)\Sigma_{ab} + \frac{1}{2}\phi\epsilon_{c\{a}\mathcal{H}_{b\}}{}^{c} - \frac{3}{2}\left(\Sigma + \frac{2}{3}\Theta\right)\mathcal{E}_{ab} \tag{9.65}$$

$$\dot{\mathcal{H}}_{\{ab\}} + \epsilon_{c\{a}\hat{\mathcal{E}}_{b\}}{}^{c} = \epsilon_{c\{a}\delta^{c}\mathcal{E}_{b\}} + \frac{3}{2}\mathcal{E}\epsilon_{c\{a}\zeta_{b\}}{}^{c} - \frac{1}{2}\phi\epsilon_{c\{a}\mathcal{E}_{b\}}{}^{c} - \frac{3}{2}\left(\Sigma + \frac{2}{3}\Theta\right)\mathcal{H}_{ab} \tag{9.66}$$

9.4.2 Gauge Invariant Variables

We can introduce a set of gauge-invariant (GI) variables by taking $\delta-$derivatives of the background variables as these should, thanks to spherical symmetry, vanish in the background spacetime: $\mathbf{X}_{\rm GI} = \delta_a \mathbf{X}_{\rm LTB}$. We therefore introduce the following set of gauge-invariant variables

$$\delta_a\left\{\mathcal{E}, \phi, \Theta, \Sigma, \mu, \hat{\mu}, \hat{\Theta}\right\} \rightarrow \left\{X_a, Y_a, K_a, L_a, M_a, N_a, P_a\right\}. \tag{9.67}$$

A set of propagation, evolution and constraint equations for these variables can be obtained by making use of the commutation relations defined in Section 7.5.9.

Gauge Invariant Linearised Evolution Equations:

$$\dot{X}_a = 2X_a\left(\Sigma - \frac{2}{3}\Theta\right) + \mathcal{E}\left(\frac{3}{2}L_a - K_a\right) - \frac{1}{2}\left(\Sigma M_a + \mu L_a\right) + \epsilon_{bc}\delta_a\delta^b\mathcal{H}^c - \left(\alpha_a + \Sigma_a - \epsilon_{ab}\Omega^b\right)\left[\frac{1}{3}\hat{\mu} - \frac{3}{2}\phi\mathcal{E}\right] \tag{9.68}$$

$$\begin{aligned}\dot{Y}_a = {} & Y_a\left(\Sigma - \frac{2}{3}\Theta\right) + \frac{1}{2}\phi\left(L_a - \frac{2}{3}K_a\right) + \delta_a\delta_b\alpha^b \\ & - \left(\alpha_a + \Sigma_a - \epsilon_{ab}\Omega^b\right)\left[-\frac{1}{2}\phi^2 - \left(\Sigma + \frac{1}{3}\Theta\right)\left(\Sigma - \frac{2}{3}\Theta\right) - \frac{2}{3}\mu - \mathcal{E}\right]\end{aligned} \tag{9.69}$$

$$\dot{M}_a = -\mu K_a - \Theta M_a + \frac{1}{2}M_a\left(\Sigma - \frac{2}{3}\Theta\right) - \left(\alpha_a + \Sigma_a - \epsilon_{ab}\Omega^b\right)\hat{\mu} \tag{9.70}$$

$$\dot{N}_a = \delta_a\left[\dot{\hat{\mu}}\right] + \frac{1}{2}\left(\Sigma - \frac{2}{3}\Theta\right)N_a \tag{9.71}$$

$$\dot{K}_a = -\frac{2}{3}\Theta K_a - 3\Sigma L_a - \frac{1}{2}M_a - \left(\alpha_a + \Sigma_a - \epsilon_{ab}\Omega^b\right)\gamma + \frac{1}{2}K_a\left(\Sigma - \frac{2}{3}\Theta\right) \tag{9.72}$$

$$\dot{L}_a = -L_a\Theta - \Sigma\left(\frac{1}{2}L_a + \frac{2}{3}K_a\right) - X_a - \left(\alpha_a + \Sigma_a - \epsilon_{ab}\Omega^b\right)\left[-\frac{3}{2}\phi\Sigma + \frac{2}{3}\gamma\right]. \tag{9.73}$$

Gauge Invariant Linearised Propagation Equations:

$$\hat{X}_a = \frac{1}{3}N_a - \delta_a\delta_b\mathcal{E}^b - 2\phi X_a - \frac{3}{2}Y_a\mathcal{E} + 2\epsilon_{ab}\Omega^b\left[\mathcal{E}\left(\frac{3}{2}\Sigma - \Theta\right) - \frac{1}{2}\mu\Sigma\right] - a_a\left[\frac{1}{3}\hat{\mu} - \frac{3}{2}\phi\mathcal{E}\right] \tag{9.74}$$

$$\begin{aligned}\hat{Y}_a = {} & -\frac{3}{2}\phi Y_a + \frac{1}{3}\Theta\left(L_a + \frac{1}{3}K_a\right) + \Sigma\left(\frac{1}{3}K_a - 2L_a\right) + \delta_a\delta_b a^b - \frac{2}{3}M_a - X_a + \phi\epsilon_{ab}\Omega^b\left(\Sigma - \frac{2}{3}\Theta\right) \\ & - a_a\left[-\frac{1}{2}\phi^2 - \left(\Sigma + \frac{1}{3}\Theta\right)\left(\Sigma - \frac{2}{3}\Theta\right) - \frac{2}{3}\mu - \mathcal{E}\right]\end{aligned} \tag{9.75}$$

$$\hat{M}_a = N_a - 2\epsilon_{ab}\Omega^b\Theta\mu - a_a\hat{\mu} - \frac{1}{2}\phi M_a \tag{9.76}$$

$$\hat{N}_a = \delta_a\left[\hat{\dot{\mu}}\right] - \frac{1}{2}\phi N_a \tag{9.77}$$

$$\hat{K}_a = P_a + 2\epsilon_{ab}\Omega^b\left[-\frac{1}{3}\Theta^2 - \frac{3}{2}\Sigma^2 - \frac{1}{2}\mu\right] - a_a\hat{\Theta} - \frac{1}{2}\phi K_a \tag{9.78}$$

$$\hat{L}_a = \frac{2}{3}\delta_a\hat{\Theta} - \frac{3}{2}Y_a\Sigma - \frac{3}{2}\phi L_a - \delta_a\delta_b\Sigma^b - \epsilon_{bc}\delta_a\delta^b\Omega^c + 2\epsilon_{ab}\Omega^b\left[-\Sigma\left(\frac{1}{2}\Sigma + \frac{2}{3}\Theta\right) - \mathcal{E}\right] - a_a\left[\frac{2}{3}\hat{\Theta} - \frac{3}{2}\phi\Sigma\right] - \frac{1}{2}\phi L_a. \tag{9.79}$$

Gauge Invariant Linearised Constraint Equations:

$$Y_a = 2\epsilon_{ab}\delta^b\xi + 2\delta^2\zeta_{ab} + \left(\Sigma - \frac{2}{3}\Theta\right)\left(\Sigma_a - \epsilon_{ab}\Omega^b\right) - 2\mathcal{E}_a \tag{9.80}$$

$$L_a - \frac{2}{3}K_a = -2\epsilon_{ab}\delta^b\Omega - 2\delta^b\Sigma_{ab} - \phi\left(\Sigma_a - \epsilon_{ab}\Omega^b\right) - 2\epsilon_{ab}\mathcal{H}^b \tag{9.81}$$

$$\epsilon_{ab}\delta^a X^b = 3\Omega\mathcal{E}\left(\Sigma - \frac{2}{3}\Theta\right) - \mu\Sigma\Omega - \frac{2}{3}\xi\hat{\mu} + 3\phi\mathcal{E}\xi \tag{9.82}$$

$$\epsilon_{ab}\delta^a Y^b = \phi\Omega\left(\Sigma - \frac{2}{3}\Theta\right) + \xi\phi^2 + 2\xi\left(\Sigma + \frac{1}{3}\Theta\right)\left(\Sigma - \frac{2}{3}\Theta\right) + \frac{4}{3}\xi\mu + 2\xi\mathcal{E} \tag{9.83}$$

$$\epsilon_{ab}\delta^a K^b = -\frac{2}{3}\Omega\Theta^2 - 3\Omega\Sigma^2 - \Omega\mu - 2\xi\hat{\Theta} \tag{9.84}$$

$$\epsilon_{ab}\delta^a L^b = -\Omega\Sigma\left(\Sigma + \frac{4}{3}\Theta\right) - 2\Omega\mathcal{E} - \frac{4}{3}\xi\hat{\Theta} + 3\xi\Sigma\phi \tag{9.85}$$

$$\epsilon_{ab}\delta^a M^b = -2\Omega\Theta\mu - 2\xi\hat{\mu} \tag{9.86}$$

9.5 Linear Perturbations: Polar Sector

9.5.1 Introduction

The general form of the polar metric perturbations in the RW gauge is given by [106]

$$ds^2 = -\left[1 + (2\eta - \chi - \varphi)Y\right]dt^2 - \frac{2a_\parallel\varsigma Y}{\sqrt{1-\kappa r^2}}dtdr + \left[1 + (\chi + \varphi)\,Y\right]\frac{a_\parallel^2 dr^2}{(1-\kappa r^2)} + a_\perp^2 r^2\left(1 + \varphi Y\right)d\Omega^2, \tag{9.87}$$

with $\eta(t,r), \chi(t,r), \varphi(t,r)$ and $\varsigma(t,r)$ the gauge invariant metric variables introduced by GS and GMG. The perturbations to the matter variables in the polar sector is parametrised as follows

$$u_\alpha = \left[\tilde{u}_A + \left(w\,\tilde{n}_A + \frac{1}{2}h_{AB}\tilde{u}^B\right)Y, vY_a\right] \tag{9.88}$$

$$\rho = \rho^{\mathrm{LTB}}\left(1 + \Delta Y\right) \tag{9.89}$$

with v, w and Δ the gauge invariant matter variables of GS and GMG. Note that the adopted ansatz for the matter sector perturbations ensures that the normalisation of the vectors obeys $u_\mu u^\mu = -1$ to linear order, i.e. $\Delta(u_\mu u^\mu) = 0$. The gauge invariant w parametrises radial fluid perturbations and v parametrises polar tangential fluid perturbations.

9.5.2 Correspondence

9.5.2.1 Polar Perturbations: Scalars

$$\phi = \phi^{(0)} + \Delta\phi$$
$$\phi^{(0)} = 2W \tag{9.90}$$
$$\Delta\phi = Y\Bigg[- W\varphi - W\chi - \left(H_\perp + \frac{1}{2}H_\parallel\right)\varsigma + \left(2H_\perp + H_\parallel\right)w - \left(\frac{\ell\left(\ell+1\right)}{a_\perp^2 r^2}\right)g + \frac{1}{2}\varphi' - \frac{1}{2}\chi' - \frac{1}{2}\partial_t\varsigma + \partial_t w\Bigg] \tag{9.91}$$

$$\Theta = \Theta^{(0)} + \Delta\Theta$$
$$\Theta^{(0)} = H_\parallel + 2H_\perp \tag{9.92}$$
$$\Delta\Theta = Y\Bigg[\left(H_\perp + \frac{1}{2}H_\parallel\right)\varphi + \left(H_\perp + \frac{1}{2}H_\parallel\right)\chi + W\varsigma + 2Ww - \frac{\ell\left(\ell+1\right)}{a^2 r^2}v + \frac{1}{2}\varsigma' + w' + \frac{3}{2}\partial_t\varphi + \frac{1}{2}\partial_t\chi\Bigg] \tag{9.93}$$

$$\Sigma = \Sigma^{(0)} + \Delta\Sigma$$
$$\Sigma^{(0)} = \frac{2}{3}\Bigg[H_\parallel - H_\perp\Bigg] \tag{9.94}$$
$$\Delta\Sigma = Y\Bigg[\left(\frac{1}{3}H_\parallel - \frac{1}{3}H_\perp\right)\varphi + \left(\frac{1}{3}H_\parallel - \frac{1}{3}H_\perp\right)\chi - \frac{1}{3}W\varsigma - \frac{2}{3}Ww + \frac{1}{3}\frac{\ell\left(\ell+1\right)}{a_\perp^2 r^2}v + \frac{1}{3}\varsigma' + \frac{2}{3}w' + \frac{1}{3}\partial_t\chi\Bigg] \tag{9.95}$$

$$\mathcal{E} = \mathcal{E}^{(0)} + \Delta\mathcal{E}$$
$$\mathcal{E}^{(0)} = \frac{8\pi\mu}{3} - \frac{M}{a_\perp^3 r^3} \tag{9.96}$$
$$\Delta\mathcal{E} = Y\Bigg[\frac{1}{3}\left\{2H_\perp H_\parallel - 2H_\perp^2 - \frac{1}{a_\perp^2 r^2}\right\}\chi + \frac{1}{3}\left\{2H_\perp H_\parallel - 2H_\perp^2 - \frac{1}{2}\frac{\ell(\ell+1)}{a_\perp^2 r^2}\right\}\varphi + \frac{1}{3}\left[2W\left(H_\parallel - H_\perp\right) - H_\parallel'\right]\varsigma + \frac{1}{3}W\chi' - \frac{1}{6}\chi'' + \frac{1}{3}\left[H_\perp - \frac{3}{2}H_\parallel\right]\dot{\chi} - \frac{1}{6}\ddot{\chi} + \frac{1}{3}\left[H_\perp - 2H_\parallel\right]\varsigma' - \frac{1}{3}\dot{\varsigma'} + \frac{1}{3}W\varphi' - \frac{1}{3}\varphi'' + \frac{1}{3}W\dot{\varsigma} + \frac{1}{3}\left(H_\perp - H_\parallel\right)\dot{\varphi}\Bigg] \tag{9.97}$$

$$\mu = \mu^{(0)} + \Delta\mu$$
$$\mu^{(0)} = \rho + \rho_\Lambda \tag{9.98}$$
$$\Delta\mu = Y\left[\rho\Delta\right] \tag{9.99}$$

$$\hat{\Theta} = \hat{\Theta}^{(0)} + \Delta\hat{\Theta}$$
$$\hat{\Theta}^{(0)} = H'_\parallel + 2W\left(H_\parallel - H_\perp\right) \tag{9.100}$$
$$\Delta\hat{\Theta} = Y\left[\ldots\right] \tag{9.101}$$

$$\hat{\mu} = \hat{\mu}^{(0)} + \Delta\hat{\mu}$$
$$\hat{\mu}^{(0)} = \rho' \tag{9.102}$$
$$\Delta\hat{\mu} = Y\left[\left\{-\frac{1}{2}\left(\chi+\varphi\right)+\Delta\right\}\rho' + \Delta'\rho + \left(w - \frac{1}{2}\varsigma\right)\partial_t\rho\right] \tag{9.103}$$

The final 3 scalars $\{\Omega, \xi, \mathcal{H}\}$ are axial in nature and do not have a polar analogy. These are necessarily zero and the fact that they vanish in the 1+1+2 to 2+2 correspondence is somewhat reassuring.

$$\Omega = \Omega^{(0)} + \Delta\Omega$$
$$\Omega^{(0)} = 0 \tag{9.104}$$
$$\Delta\Omega = 0 \tag{9.105}$$

$$\xi = \xi^{(0)} + \Delta\xi$$
$$\xi^{(0)} = 0 \tag{9.106}$$
$$\Delta\xi = 0 \tag{9.107}$$

$$\mathcal{H} = \mathcal{H}^{(0)} + \Delta\mathcal{H}$$
$$\mathcal{H}^{(0)} = 0 \tag{9.108}$$
$$\Delta\mathcal{H} = 0 \tag{9.109}$$

9.5.2.2 Polar Perturbations: 2-Vectors

$$\alpha_a = \alpha_a^{(0} + \Delta\alpha_a$$

$$\alpha_a^{(0)} = 0$$

$$\Delta\alpha_a = Y_a\left[\frac{1}{2}\varsigma + Wv - H_\perp g + \partial_t g\right] \tag{9.110}$$

$$= Q_a\left[\frac{1}{2}\frac{\varsigma}{r} + W\frac{v}{r} - H_\perp\frac{g}{r} + \partial_t\frac{g}{r}\right] \tag{9.111}$$

$$a_a = a_a^{(0)} + \Delta a_a$$

$$a_a^{(0)} = 0$$

$$\delta a_a = Y_a\left[-\frac{1}{2}\varphi - \frac{1}{2}\chi - H_\parallel v + g'\right] \tag{9.112}$$

$$= Q_a\left[-\frac{1}{2}\frac{\varphi}{r} - \frac{1}{2}\frac{\chi}{r} - H_\parallel\frac{v}{r} + \frac{g'}{r}\right] \tag{9.113}$$

$$\Sigma_a = \Sigma_a^{(0)} + \Delta\Sigma_a$$

$$\Sigma_a^{(0)} = 0$$

$$\delta\Sigma_a = Y_a\left[\frac{1}{4}\varsigma + \frac{1}{2}w - Wv + \left(H_\perp - H_\parallel\right)g + \frac{1}{2}v'\right] \tag{9.114}$$

$$= Q_a\left[\frac{1}{4}\frac{\varsigma}{r} + \frac{1}{2}\frac{w}{r} - W\frac{v}{r} + \left(H_\perp - H_\parallel\right)\frac{g}{r} + \frac{1}{2}\frac{v'}{r}\right] \tag{9.115}$$

$$\mathcal{E} = \mathcal{E}_a^{(0)} + \Delta\mathcal{E}_a$$

$$\mathcal{E}_a^{(0)} = 0$$

$$\delta\mathcal{E}_a = Y_a\left[-\frac{1}{4}\partial_t\varsigma - \frac{1}{2}\varphi' - \frac{1}{4}\chi' + \frac{1}{2}\left(\chi+\varphi\right)W + \frac{1}{2}\left(H_\perp - H_\parallel\right)\varsigma + g\left(-4\pi\mu + \frac{3}{2}\frac{M}{a_\perp^3 r^3}\right)\right] \tag{9.116}$$

$$= \frac{Q_a}{r}\left[-\frac{1}{4}\partial_t\varsigma - \frac{1}{2}\varphi' - \frac{1}{4}\chi' + \frac{1}{2}\left(\chi+\varphi\right)W + \frac{1}{2}\left(H_\perp - H_\parallel\right)\varsigma + g\left(-4\pi\mu + \frac{3}{2}\frac{M}{a_\perp^3 r^3}\right)\right] \tag{9.117}$$

$$\Omega_a = \Omega^{(0)} + \Delta\Omega_a$$

$$\Omega_a^{(0)} = 0$$

$$\delta\Omega_a = \bar{Y}_a\left[-\frac{1}{2}w + \frac{1}{4}\varsigma + \frac{1}{2}v'\right] \tag{9.118}$$

$$= \bar{Q}_a\left[-\frac{1}{2}\frac{w}{r} + \frac{1}{4}\frac{\varsigma}{r} + \frac{1}{2}\frac{v'}{r}\right] \tag{9.119}$$

$$
\begin{aligned}
\mathcal{H}_a &= \mathcal{H}_a^{(0)} + \Delta\mathcal{H}_a \\
\bar{\mathcal{H}}_a^{(0)} &= 0 \\
\delta\bar{\mathcal{H}}_a &= \bar{Y}_a\left[-\frac{1}{2}\left(\chi+\varphi\right)\left(H_\perp - H_\parallel\right) - \frac{1}{2}\varsigma W + \frac{1}{4}\varsigma' + \frac{1}{4}\partial_t\chi - \frac{3}{2}v\left(\frac{8\pi\mu}{3} - \frac{M}{a_\perp^3 r^3}\right)\right] && (9.120)\\
&= \frac{\bar{Q}_a}{r}\left[-\frac{1}{2}\left(\chi+\varphi\right)\left(H_\perp - H_\parallel\right) - \frac{1}{2}\varsigma W + \frac{1}{4}\varsigma' + \frac{1}{4}\partial_t\chi - \frac{3}{2}v\left(\frac{8\pi\mu}{3} - \frac{M}{a_\perp^3 r^3}\right)\right] && (9.121)
\end{aligned}
$$

9.5.2.3 Polar Perturbations: 2-Tensors

$$
\begin{aligned}
\Sigma_{ab} &= \Sigma_{ab}^{(0)} + \Delta\Sigma_{ab} \\
\Sigma_{ab}^{(0)} &= 0 \\
\delta\Sigma_{ab} &= Y_{ab}\left[v\right] && (9.122)\\
&= Q_{ab}\left[\frac{v}{r^2}\right] && (9.123)
\end{aligned}
$$

$$
\begin{aligned}
\zeta_{ab} &= \zeta_{ab}^{(0)} + \Delta\zeta_{ab} \\
\zeta_{ab}^{(0)} &= 0 \\
\delta\zeta_{ab} &= Y_{ab}\left[g\right] && (9.124)\\
&= Q_{ab}\left[\frac{g}{r^2}\right] && (9.125)
\end{aligned}
$$

$$
\begin{aligned}
\mathcal{E}_{ab} &= \mathcal{E}_{ab}^{(0)} + \Delta\mathcal{E}_{ab} \\
\mathcal{E}_{ab}^{(0)} &= 0 \\
\delta\mathcal{E}_{ab} &= Y_{ab}\left[-\frac{1}{2}\left(\varphi+\chi\right)\right] && (9.126)\\
&= Q_{ab}\left[-\frac{1}{2r^2}\left(\varphi+\chi\right)\right] && (9.127)
\end{aligned}
$$

$$
\begin{aligned}
\mathcal{H}_{ab} &= \mathcal{H}_{ab}^{(0)} + \Delta\mathcal{H}_{ab} \\
\bar{\mathcal{H}}_{ab}^{(0)} &= 0 \\
\delta\bar{\mathcal{H}}_{ab} &= \bar{Y}_{ab}\left[+\frac{1}{4}\varsigma\right] && (9.128)\\
&= \bar{Q}_{ab}\left[-\frac{1}{2}\frac{\varsigma}{r^2}\right] && (9.129)
\end{aligned}
$$

9.5.3 Master Variables and Master Equations

9.5.3.1 The GMG Master Equations

The three primary evolution equations for the variables $\{\chi, \varphi, \varsigma\}$ are given by [106]

$$-\ddot{\chi} + \chi'' - 3H_{\parallel}\dot{\chi} - 2W\chi' + 2\left[16\pi\mu - \frac{6M}{a_{\perp}^3 r^3} - 4H_{\perp}\left(H_{\parallel} - H_{\perp}\right)\right](\chi + \varphi) - \frac{(\ell+2)(\ell-1)}{a_{\perp}^2 r^2}\chi$$
$$= -2\left(H_{\parallel} - H_{\perp}\right)\varsigma' - 2\left[H_{\parallel}' - 2(H_{\parallel} - H_{\perp})W\right]\varsigma + 4(H_{\parallel} - H_{\perp})\dot{\varphi} \tag{9.130}$$

$$\ddot{\varphi} + 4H_{\perp}\dot{\varphi} - (\chi + \varphi)\left[\frac{2}{a_{\perp}^2 r^2} - 2W^2\right] = -H_{\perp}\dot{\chi} + W\chi' + \chi\left[\frac{(\ell+1)(\ell-2)}{2a_{\perp}^2 r^2}\right] + 2W\varsigma\left(H_{\parallel} - H_{\perp}\right) \tag{9.131}$$

$$\dot{\varsigma} + 2H_{\parallel}\varsigma = -\chi'. \tag{9.132}$$

The left hand side of the the $\ddot{\varphi}$ equation, if we move the χ term back to the RHS, has exactly the same equation as for a curved FLRW model [106]. An important difference is that in the inhomogeneous LTB spacetime, the scale factors and Hubble parameters are all additionally dependent on the radius r. The RHS of this equation couples us to the gravitational wave degree of freedom χ and the generalised vector modes ς [106]. In turn these two modes are sourced by φ, the *generalised gravitational potential*. The important insight here is that large scale structure will evolve differently to a dust FLRW model due to the dissipation of potential energy into gravitational radiation and rotational degrees of freedom [106; 110]. The relation of φ, χ and ς to standard perturbation variables in an FLRW limit was derived and discussed in [106]. Here they note the complicated nature of these variables and how they excite and couple scalar, vector and tensor modes.

9.5.3.2 The 1+1+2 Correspondence

The correspondence introduced above gives rise to a number of important and interesting observations. The first observation is that the variable χ is clearly related to the Electric Weyl tensor. This is useful as χ is expected to describe polar gravitational waves and therefore behave as a propagating degree of freedom. In [229] χ was shown to obey a wave equation with characteristics set by the metric and free Cauchy data $\{\chi, \dot{\chi}\}$ that may be set independently of the matter perturbations. This relationship is upheld by identification of χ to the transverse traceless part of the electric Weyl tensor as this governs the evolution of the free gravitational field

$$(\chi + \varphi) = -2\, r^2\, \mathcal{E}_T. \tag{9.133}$$

Similarly, we see that φ is coupled to χ and the electric Weyl tensor. It is not possible to trivially decouple these quantities in as clean a manner as we may have hoped. Instead we could make use of the gauge-invariant variable X_a and substitute out higher derivative terms. This will eventually lead to a decoupled expression for χ and φ in terms of 1+1+2 variables. For example, χ can be

expressed as follows

$$\chi_T\left[\frac{\ell(\ell+1)}{r^2}-2K\right]=-2\,\mathcal{E}_T\left[\frac{\ell(\ell+1)}{r^2}-2K\right]+\frac{3}{2}\phi\Sigma\bar{\mathcal{H}}_T+2\frac{\bar{\mathcal{H}}_V}{r}\left[\Sigma-\frac{2}{3}\Theta\right]-\frac{2}{3}\frac{M_V}{r}+2\frac{X_V}{r}+2\frac{\mathcal{E}_V}{r}, \tag{9.134}$$

where we have introduced the following notation

$$\chi_T=\frac{\chi}{r^2}\quad\underset{\text{Polar}}{\longrightarrow}\quad\chi_{ab}=\chi_T\,Q_{ab}\;=\frac{\chi}{r^2}\,Q_{ab}=\chi\,Y_{ab}. \tag{9.135}$$

Following from this results, we can perform a covariant reconstruction of Eq. (9.134) by using the covariant harmonic relationships

$$-2\delta_{\{a}\delta^c\chi_{b\}c}=4\delta_{\{a}\delta^c\mathcal{E}_{b\}c}+\frac{3}{2}\phi\Sigma\mathcal{H}_{ab}+2\delta_{\{a}\mathcal{H}_{b\}}\left[\Sigma-\frac{2}{3}\Theta\right]- \tag{9.136}$$

$$\frac{2}{3}\delta_{\{a}M_{b\}}+2\delta_{\{a}X_{b\}}+2\delta_{\{a}\mathcal{E}_{b\}}. \tag{9.137}$$

Finally, ς is associated to the transverse traceless part of the magnetic Weyl tensor. The interpretation we give to this variable is that it encapsulates genuinely relativistic degrees of freedom that is sourced by relativistic effects such as frame dragging and gravitational waves [181].

$$\varsigma=-2r^2\bar{\mathcal{H}}_T. \tag{9.138}$$

We can also isolate other gauge invariant perturbations of interest, such as v. We know from [229] that the free Cauchy data $\mathscr{C}$ for the polar sector perturbations is given by

$$\mathscr{C}_{\text{Free}}=\{\chi,\varphi,\varsigma,\dot{\chi},\dot{\varphi}\}, \tag{9.139}$$

meaning that all matter perturbations can be reconstructed from the metric perturbations plus their first derivatives. From the correspondence outlined above, we immediately see that the polar tangential fluid perturbation is given by

$$v=r^2\Sigma_T. \tag{9.140}$$

i.e. the polar tangential fluid perturbations simply correspond to the shear of the timelike congruence u^a. We also know that v is related to the spatial derivative of φ via the 2+2 formalism. In the 1+1+2 formalism this translates into Σ_T being related to the mixed evolution and propagation equation of the Weyl curvature 2-tensors in 9.65. In addition, the evolution equation for v becomes trivial and we find that

$$\begin{aligned}\dot{v}&=2\frac{\dot{r}}{r}\,r^2\,\Sigma_T+r^2\dot{\Sigma}_T\\&=-\left(\Sigma-\frac{2}{3}\Theta\right)\,\left[r^2\Sigma_T\right]+r^2\left[\Sigma_T\,\left(\Sigma-\frac{2}{3}\Theta\right)-\mathcal{E}_T\right]\\&=-r^2\mathcal{E}_T\end{aligned}$$

$$= \frac{1}{2}\left(\chi + \varphi\right). \tag{9.141}$$

This completely agrees with the 2+2 evolution equation for v. The frame-dependent term that we introduced in our ansatz for the spacelike vector n^A can be seen to be related the shear of the spacelike congruence

$$g = r^2 \zeta_T. \tag{9.142}$$

The polar tangential fluid perturbation is more intricate and involves a number of dependencies

$$w = -4r^2\bar{\mathcal{H}}_T - r^2\phi\Sigma_T - 2r\Sigma_V + \frac{3}{2}r^2\Sigma\zeta_T, \tag{9.143}$$

though this is not particularly unexpected given the complexity of the constraint equation in the 2+2 formalism.

9.6 Linear Perturbations: Axial Sector

9.6.1 Introduction

The general form of axial metric perturbations in the RW gauge can be written as [106]

$$ds^2 = -dt^2 + \frac{a_\parallel^2}{(1-\kappa r^2)}dr^2 + a_\perp^2 r^2 d\Omega^2 + 2k_A \bar{Y}_b dx^A dx^b, \tag{9.144}$$

with $k_A = (k_t, k_r)$ the gauge invariant metric perturbation of GS. In the axial case, however, the structure of the perturbations to the matter sector is significantly simplified and collapses down to

$$u_\mu = (\tilde{u}_A, \bar{v}\bar{Y}_a), \tag{9.145}$$

with $\bar{v}$ being the gauge invariant matter variable of GMG that parametrises axial tangential fluid perturbations. We also introduce the notation $\tilde{k}_r = k_r/X$ for convenience, where $X = \sqrt{g_{rr}}$.

9.6.2 Correspondence

9.6.2.1 Axial Perturbations: Scalars

$$\phi^{(0)} = 2W \tag{9.146}$$

$$\delta\phi = 0. \tag{9.147}$$

$$\Theta^{(0)} = H_\parallel + 2H_\perp \tag{9.148}$$

$$\delta\Theta = 0. \tag{9.149}$$

$$\Sigma^{(0)} = \frac{2}{3}\left[H_{\parallel} - H_{\perp}\right] \tag{9.150}$$

$$\delta\Sigma = 0. \tag{9.151}$$

$$\mathcal{E}^{(0)} = \frac{8\pi\mu}{3} - \frac{M}{a_{\perp}^{3} r^{3}} \tag{9.152}$$

$$\delta\mathcal{E} = 0. \tag{9.153}$$

$$\mu^{(0)} = \rho + \rho_{\Lambda} \tag{9.154}$$

$$\delta\mu = 0. \tag{9.155}$$

$$\Omega^{(0)} = 0 \tag{9.156}$$

$$\delta\Omega = \epsilon Y \left[\frac{1}{2}\frac{\ell\left(\ell+1\right)}{r^{2}}\bar{v}\right] \tag{9.157}$$

$$\xi^{(0)} = 0 \tag{9.158}$$

$$\delta\xi = \epsilon Y \left[-\frac{1}{2}\frac{\ell\left(\ell+1\right)}{r^{2}}\bar{g}\right] \tag{9.159}$$

$$\mathcal{H}^{(0)} = 0 \tag{9.160}$$

$$\delta\mathcal{H} = \epsilon Y \left[\frac{1}{2}\frac{\ell\left(\ell+1\right)}{r^{2}}\left(-k_{t}' + \partial_{t}\left(\tilde{k}_{r}\right) + \tilde{k}_{r}H_{\parallel} - 2\tilde{k}_{r}H_{\perp} + 2k_{t}W\right)\right] \tag{9.161}$$

9.6.2.2 Axial Perturbations: 2-Vectors

$$\alpha_{a}^{(0)} = 0 \tag{9.162}$$

$$\delta\alpha_{a} = \epsilon\,\bar{Y}_{a}\left[\bar{v}W + \frac{1}{2}k_{t}' + \tilde{k_{r}}H_{\perp} - k_{t}W - \bar{g}H_{\perp} - \bar{g}H_{\perp} + \partial_{t}\bar{g} - \frac{1}{2}\partial_{t}\tilde{k_{r}} + \frac{1}{2}k_{r}H_{\parallel}\right] \tag{9.163}$$

$$= \epsilon\,\frac{\bar{Q}_{a}}{r}\left[\bar{v}W + \frac{1}{2}k_{t}' + \tilde{k_{r}}H_{\perp} - k_{t}W - \bar{g}H_{\perp} - \bar{g}H_{\perp} + \partial_{t}\bar{g} - \frac{1}{2}\partial_{t}\tilde{k_{r}} + \frac{1}{2}k_{r}H_{\parallel}\right] \tag{9.164}$$

$$a_{a} = a_{a}^{(0)} + \Delta a_{a}$$

$$
\begin{aligned}
a_a^{(0)} &= 0 \\
\Delta a_a &= \epsilon \bar{Y}_a \left[-\bar{v} H_\parallel + \bar{g}' \right] && (9.165) \\
&= \epsilon \bar{Y}_a \left[-\frac{\bar{v}}{r} H_\parallel + \frac{\bar{g}'}{r} \right] && (9.166)
\end{aligned}
$$

$$
\begin{aligned}
\Sigma_a &= \Sigma_a^{(0)} + \Delta\Sigma_a \\
\Sigma_a^{(0)} &= 0 \\
\Delta\Sigma_a &= \epsilon \bar{Y}_a \left[\frac{1}{2}\bar{v}' + \frac{1}{2}\partial_t \tilde{k_r} + \frac{1}{2}\tilde{k_r} H_\parallel - \frac{1}{2}k_t' + k_t W - \bar{v} W - \bar{g} H_\parallel + \bar{g} H_\perp - \tilde{k_r} H_\perp \right] && (9.167) \\
&= \epsilon \frac{\bar{Q}_a}{r} \left[\frac{1}{2}\bar{v}' + \frac{1}{2}\partial_t \tilde{k_r} + \frac{1}{2}\tilde{k_r} H_\parallel - \frac{1}{2}k_t' + k_t W - \bar{v} W - \bar{g} H_\parallel + \bar{g} H_\perp - \tilde{k_r} H_\perp \right] && (9.168)
\end{aligned}
$$

$$
\begin{aligned}
\mathcal{E}_a &= \mathcal{E}_a^{(0)} + \Delta\mathcal{E}_a \\
\mathcal{E}_a^{(0)} &= 0 \\
\delta\mathcal{E}_a &= \epsilon \bar{Y}_a \, \frac{1}{2} \left[\frac{1}{4}\frac{\partial_{rt} k_r}{X} - \frac{1}{4}\frac{\partial_{tt} k_r}{X} - \frac{1}{4} H_\parallel \frac{\partial_r k_t}{X} - \frac{1}{2}\partial_t k_t W + \frac{\partial_t k_r}{X} \left(\frac{1}{2} H_\perp + \frac{1}{4} H_\parallel \right) \right. && (9.169) \\
&\quad \left. + \frac{1}{2} H_\perp W k_t + \frac{1}{4}\bar{k}_r \left(\frac{\ell(\ell+1)}{A^2} - \frac{1}{2A^2} - \frac{1}{2} H_\perp H_\parallel \right) + \frac{1}{2}\bar{g} \left(W' + \dot{H}_\parallel - \dot{H}_\perp + H_\parallel^2 - H_\perp H_\parallel + \frac{1}{2A^2} \right) \right] \\
&= \epsilon \frac{\bar{Q}_a}{r} \, \frac{1}{2} \left[\frac{1}{4}\frac{\partial_{rt} k_r}{X} - \frac{1}{4}\frac{\partial_{tt} k_r}{X} - \frac{1}{4} H_\parallel \frac{\partial_r k_t}{X} - \frac{1}{2}\partial_t k_t W + \frac{\partial_t k_r}{X} \left(\frac{1}{2} H_\perp + \frac{1}{4} H_\parallel \right) \right. && (9.170) \\
&\quad \left. + \frac{1}{2} H_\perp W k_t + \frac{1}{4}\bar{k}_r \left(\frac{\ell(\ell+1)}{A^2} - \frac{1}{2A^2} - \frac{1}{2} H_\perp H_\parallel \right) + \frac{1}{2}\bar{g} \left(W' + \dot{H}_\parallel - \dot{H}_\perp + H_\parallel^2 - H_\perp H_\parallel + \frac{1}{2A^2} \right) \right] && (9.171)
\end{aligned}
$$

$$
\begin{aligned}
\Omega_a &= \Omega_a^{(0)} + \Delta\Omega_a \\
\Omega_a^{(0)} &= 0 && (9.172) \\
\Delta\Omega_a &= \epsilon Y_a \left[-\frac{1}{2}\bar{v}' \right] && (9.173) \\
&= \epsilon Q_a \left[-\frac{1}{2}\frac{\bar{v}'}{r} \right] && (9.174)
\end{aligned}
$$

$$
\begin{aligned}
\mathcal{H}_a &= \mathcal{H}_a^{(0)} + \Delta\mathcal{H}_a \\
\mathcal{H}_a^{(0)} &= 0
\end{aligned}
$$

$$\Delta\mathcal{H}_a = \epsilon\, Y_a\, \frac{1}{2}\left[\tilde{k_r}\left(-H_\parallel W + H_\perp W + H_\perp Q\right) + \dots\right] \tag{9.175}$$

$$= \epsilon\, Q_a\, \frac{1}{2}\left[\frac{\tilde{k_r}}{r^2}\left(-H_\parallel W + H_\perp W + H_\perp Q\right) + \dots\right] \tag{9.176}$$

9.6.2.3 Axial Perturbations: 2-Tensors

$$\begin{aligned}
\Sigma_{ab} &= \Sigma^{(0)}_{ab} + \Delta\Sigma_{ab} \\
\Sigma^{(0)}_{ab} &= 0 \\
\Delta\Sigma_{ab} &= \epsilon\bar{Y}_{ab}\left[-\frac{1}{2}\left(k_t - \bar{v}\right)\right] && (9.177)\\
&= \epsilon\bar{Q}_{ab}\left[\frac{k_t}{r^2} - \frac{\bar{v}}{r^2}\right] && (9.178)
\end{aligned}$$

$$\begin{aligned}
\zeta_{ab} &= \zeta^{(0)}_{ab} + \Delta\zeta_{ab} \\
\zeta^{(0)}_{ab} &= 0 \\
\Delta\zeta_{ab} &= \epsilon\bar{Y}_{ab}\left[-\frac{1}{2}\left(\tilde{k_r} - \bar{g}\right)\right] && (9.179)\\
&= \epsilon\bar{Q}_{ab}\left[\frac{\tilde{k_r}}{r^2} - \frac{\bar{g}}{r^2}\right] && (9.180)
\end{aligned}$$

$$\begin{aligned}
\mathcal{E}_{ab} &= \mathcal{E}^{(0)}_{ab} + \Delta\mathcal{E}_{ab} \\
\mathcal{E}^{(0)}_{ab} &= 0 \\
\Delta\mathcal{E}_{ab} &= \epsilon\bar{Y}_{ab}\left[\frac{1}{4}\partial_t k_t + \frac{1}{4}\tilde{k_r}' - \frac{1}{4}H_\parallel k_t\right] && (9.181)\\
&= \epsilon\bar{Q}_{ab}\left[-\frac{1}{2}\frac{\partial_t k_t}{r^2} - \frac{1}{2}\frac{\tilde{k_r}'}{r^2} + \frac{1}{2}H_\parallel\frac{k_t}{r^2}\right] && (9.182)
\end{aligned}$$

$$\begin{aligned}
\mathcal{H}_{ab} &= \mathcal{H}^{(0)}_{ab} + \Delta\mathcal{H}_{ab} \\
\mathcal{H}^{(0)}_{ab} &= 0 \\
\Delta\mathcal{H}_{ab} &= \epsilon Y_{ab}\left[-\frac{1}{2}k_t' + \frac{1}{2}\tilde{k_r}H_\parallel - \frac{1}{2}\partial_t\tilde{k_r}\right] && (9.183)\\
&= \epsilon Q_{ab}\left[-\frac{1}{2}\frac{k_t'}{r^2} + \frac{1}{2}\frac{\tilde{k_r}}{r^2}H_\parallel - \frac{1}{2}\frac{\partial_t\tilde{k_r}}{r^2}\right] && (9.184)
\end{aligned}$$

9.6.3 Master Variables and Master Equations

Following [202], we first introduce the following scalar master variable

$$\Pi = \epsilon^{AB}\left(\frac{k_A}{r^2}\right)_{|B} \tag{9.185}$$

such that the EFEs for k_A can be reduced to the following odd parity master equation:

$$\left[\frac{1}{r^2}\left(r^4\Pi\right)_{|A}\right]^{|A} - (\ell-1)(\ell+2)\,\Pi = -16\pi\epsilon^{AB}L_{A|B}. \tag{9.186}$$

In the LTB spacetime this explicitly reduces down to

$$(\ell-1)(\ell+2)\,k_A = 16\pi\rho\, a_\perp^2 r^2\,\bar{v}\,u_A - \epsilon_{AB}\left(a_\perp^4 r^4\Pi\right)^{|B}. \tag{9.187}$$

Likewise, we can explicitly evaluate the scalar master variable for the perturbed LTB spacetime giving us an axial master variable defined in terms of the gauge-invariant perturbations from GMG

$$\Pi = \frac{1}{A^2}\left[-k_0' + 2Wk_0 + \partial_t\tilde{k_1} + H_\parallel\tilde{k_1} - 2H_\perp\tilde{k_1}\right]. \tag{9.188}$$

Using the 2+2 to 1+1+2 correspondence defined above, we immediately see that the master variable Π can be re-expressed in terms of the radial part of the magnetic Weyl tensor

$$\Pi = \frac{2}{\ell(\ell+1)}\,\mathcal{H}_S. \tag{9.189}$$

Clearly, the pre-factor does not propagate or evolve and is just a re-scaling of the scalar. As such, we drop this pre-factor and see a covariant wave equation for a transverse-traceless tensor constructed from the magnetic Weyl scalar

$$\mathcal{M}_{ab} = r^2\delta_{\{a}\delta_{b\}}\mathcal{H} = \mathcal{H}\,Q_{ab}. \tag{9.190}$$

This equation can be shown to obey the following covariant wave equation

$$\ddot{\mathcal{M}}_{\{ab\}} - \hat{\hat{\mathcal{M}}}_{\{ab\}} - \left(2\Sigma - \frac{7}{3}\Theta\right)\dot{\mathcal{M}}_{\{ab\}} - 3\phi\hat{\mathcal{M}}_{\{ab\}} - \delta^2\mathcal{M}_{\{ab\}} + [2\mu - 2K]\,\mathcal{M}_{\{ab\}} = 2K\,\hat{\Gamma}_{\{ab\}}. \tag{9.191}$$

where the source term is defined to be

$$\Gamma_{\{ab\}} = r^4\,\mu\,\delta_{\{a}\delta_{b\}}\Omega = \left[r^2\mu\,\Omega\right]Q_{ab}. \tag{9.192}$$

We can expand equation 9.191 into covariant harmonics, simplifying the expression to

$$\ddot{\mathcal{M}}_T - \hat{\hat{\mathcal{M}}}_T - \left(2\Sigma - \frac{7}{3}\Theta\right)\dot{\mathcal{M}}_T - 3\phi\hat{\mathcal{M}}_T + \left[2\mu - 6K + \frac{\ell\,(\ell+1)}{r^2}\right]\mathcal{M}_T = 2K\,\widehat{(\mu\Omega r^2)}. \quad (9.193)$$

As we can see from this equation, axial gravitational perturbations are sourced by density and vorticity gradients. This covariant equation is a rather neat way of studying axial gravitational perturbations and constitutes something of a generalisation of the Regge-Wheeler tensor to the LTB spacetime [458]. Unluckily for us, this tensor is *not* a candidate for a tensor that unifies the axial and polar perturbations as this tensor is purely axial in nature, the magnetic Weyl scalar $\mathcal{H}$ vanishes in the even parity sector. It is interesting to note that this tensor will characterise axial perturbations of vacuum (geodesic) LRS-II spacetimes with $\{\Sigma, \Theta, \phi, \mathcal{E}\}$ non-zero in the background. This will also extend to the case where $\mathcal{A}$ is non-zero but, naturally, this will give rise to additional pre-factors in the wave equation that depend on $\mathcal{A}$.

An ancillary observation that we can make is that the axial tangential perturbation $\bar{v}$ is simply related to the radial part of the vorticity Ω as follows

$$\bar{v} = 2\frac{r^2}{\ell\,(\ell+1)}\Omega. \quad (9.194)$$

The evolution equation for this variable is trivial and we see that

$$\dot{\bar{v}} = \frac{4}{\ell(\ell+1)}\frac{\dot{r}}{r}r^2\Omega + \frac{2}{\ell(\ell+1)}r^2\dot{\Omega} \quad (9.195)$$

$$= -\frac{2}{\ell(\ell+1)}\left(\Sigma - \frac{2}{3}\Theta\right)r^2\Omega + \frac{2}{\ell(\ell+1)}\left(\Sigma - \frac{2}{3}\Theta\right)r^2\Omega \quad (9.196)$$

$$= 0, \quad (9.197)$$

as we require from the 2+2 equations.

9.7 Weyl Curvature Perturbations

We now take a look at the Weyl curvature tensor and try to understand its dynamics. As we have seen in previous sections χ and φ are explicitly related to the electric Weyl curvature 2-tensor $\mathcal{E}_{ab}$ whereas ς is related to $\mathcal{H}_{ab}$. In addition, the axial master variable Π is explicitly related to the radial part of the magnetic Weyl tensor $\mathcal{H}$. These relations suggest that the Weyl curvature tensor plays a dominant role in describing gravitational perturbations of locally rotationally symmetric spacetimes. Naturally, in the non-vacuum case, we expect coupling terms to the energy-momentum content of the spacetime. This motivates us to introduce the following variable

$$\mathscr{I}_{\{ab\}} = \mathcal{E}_{\{ab\}} + \epsilon_{c\{a}\mathcal{H}_{b\}}{}^{c}. \quad (9.198)$$

We can construct a wave equation for $\mathcal{E}_{ab}$ by taking a time derivative of 9.65 and substituting

for the radial derivative of 9.66, making use of the 2-tensor commutation relation defined in 7.208. Likewise we can construct a wave equation for $\mathcal{H}_{ab}$ by taking a time derivative of 9.66 and substituting for the radial derivative of 9.65, again using the 2-tensor commutation relation defined in 7.208. Combining these ancillary equations allows us to construct the concomitant wave equation for $\mathscr{I}_{ab}$. We can then calculate the wave operator $\ddot{\mathscr{I}}_{\{ab\}} - \hat{\hat{\mathscr{I}}}_{\{ab\}}$ and use the evolution and propagation of $\mathscr{I}_{\{ab\}}$ to simplify the remaining terms. The resulting covariant wave equation is given by

$$\ddot{\mathscr{I}}_{\{ab\}} - \hat{\hat{\mathscr{I}}}_{\{ab\}} + \left(2\phi - 2\Sigma + \frac{7}{3}\Theta\right)\dot{\mathscr{I}}_{\{ab\}} - (3\phi - 6\Sigma)\,\hat{\mathscr{I}}_{\{ab\}} - \mathcal{F}_{\rm BG}\,\mathscr{I}_{\{ab\}} = \Gamma_{\{ab\}}. \tag{9.199}$$

Where the source term is given by

$$\Gamma_{\{ab\}} = -\frac{1}{2}\hat{\mu}\zeta_{\{ab\}} - \frac{1}{2}\delta_{\{a}\delta_{b\}}\mu + 2\mu\,\epsilon_{c\{a}\delta^{c}\Omega_{b\}} + \Sigma_{\{ab\}}\left(2\mu\Sigma + \frac{1}{6}\Theta\mu - \hat{\mu} - \phi\mu\right) \tag{9.200}$$

and the zeroth-order background term $\mathcal{F}_{\rm BG}$ by the messy looking

$$\mathcal{F}_{\rm BG} = -3\phi\Sigma + \frac{8}{3}\Sigma\Theta - 2\phi\Theta + \phi^2 + 7\Sigma^2 - 2\hat{\Theta} + 2K + 4\mathcal{E} + \frac{2}{3}\mu - \frac{\ell(\ell+1)}{r^2} - \frac{8}{9}\Theta^2, \tag{9.201}$$

though this expression may be simplified by explicitly evaluating for the Gaussian curvature. Although this expression is valid for both even and odd parities, it contains a forcing term arising from the coupling of the energy density to the shear of the timelike congruence $\Sigma_{\{ab\}}$ and the shear of the spacelike congruence $\zeta_{\{ab\}}$. In the limit that $\mu \to 0$, this quantity cleanly decouples and defines a tensor that governs the gravitational perturbations for LRS-II spacetimes covariantly characterised by $\{\phi, \Sigma, \Theta, \mathcal{E}\}$ non-zero in the background. In the vacuum limit we have therefore found a covariant tensor that unifies the even and odd parity perturbations.

9.8 Conclusions

In this Chapter we have extended the framework of Chapter 7 and analysis of Chapter 8 to the spherically symmetric but radially inhomogeneous LTB spacetime. We started out by providing a brief overview and motivation for studying the LTB solutions in Section 9.2, emphasising the philosophical point of view that the LTB solutions, whilst constrained observationally, are still important as a first step towards an understanding of the dynamics and phenomenology of globally inhomogeneous spacetimes. Understanding the growth of perturbations will be important in developing robust test and constraints on various cosmological spacetimes. In Section 9.3, we introduced the LTB spacetime and discussed some of the key features. Section 9.3.2 provides an explicit correspondence between the 1+1+2 and 2+2 approaches for the background spacetime. In Section 9.4 then detailed the system of linearised equations in the LTB spacetime and provided a complete set of gauge invariant variables along with the concomitant propagation and evolution equations. These equations are used when constructing the covariant, gauge-invariant and frame-invariant wave equations.

We then proceed to systematically analyse the correspondence between the 2+2 formalism

and the 1+1+2 formalism for the polar perturbations in Section 9.5 and axial perturbations in Section 9.6. We identified a mapping from the 2+2 gauge invariants to combinations of 1+1+2 variables and started to construct a system of master variables and master equations in the 1+1+2 formalism.

Key identifications include the association of $\mathcal{H}$ to the axial gauge-invariant variable Π of [229] and the polar relation $\mathcal{E}_T \propto (\chi + \varphi)$. We provide a covariant master equation for axial perturbations in Eq. (9.191), nothing that $\mathcal{H}$ is intrinsically an axial variable and hence vanishes in the polar sector. The second tentative equation that we present is for the variable proposed in Eq. (9.198). This leads to the wave equation given in Eq. (9.199) with the source term Eq. (9.200). Unfortunately, as can be seen in Eq. (9.200), the variable couples to Σ_{ab} and ζ_{ab} and therefore does not close. However, as the wave equation is obeyed for both the polar and axial sectors, it is highly suggestive that this equation may close once supplied with auxiliary variables. As can be seen, when taking the vacuum limit $\mu \to 0$, this equation closes and becomes a well defined master variable and master equation for the set of vacuum LRS-II spacetimes. This leads to the association of Eq. (9.198) and Eq. (9.190) to master variables for gravitational perturbations of LRS-II spacetimes. The covariant wave equation presented in Eq. (9.199) is valid for vacuum LRS-II spacetimes covariantly characterised by the set of non-vanishing background scalars $\{\Sigma, \Theta, \phi, \mathcal{E}\}$. The generalisation of this equation to vacuum LRS-II spacetimes governed by $\{\Sigma, \Theta, \phi, \mathcal{E}, \mathcal{A}\}$ will be presented in a supplementary publication [439] along with a discussion of specific spacetimes, e.g. Schwarzschild $\{\mathcal{A}, \mathcal{E}, \phi\}$, as limiting subgroups of the full solution. This should provide some insights into the space of cosmological spacetimes and the structure of gravitational perturbations in these vacuum LRS-II spacetimes and extend the studies of LRS spacetimes presented in [572; 58; 105; 82; 83].

9.9 Summary of Key Points and Key Results

- In the introduction we outlined the motivation for considering spatially inhomogeneous cosmologies as a means to relax the assumption of homogeneity. This allows us to slow move towards genuinely inhomogeneous spacetimes, such as the real Universe. The approach taken is to detail and understand the structure of the master equations governing gravitational perturbations of cosmological spacetimes. This is done by relating the master equations for a specific class of cosmological models to the equations for specific sub-classes. As an example, the Schwarzschild spacetime is the vacuum limit of the LTB spacetime. This leads to many similarities in the structure of the equations in the covariant and geometrically meaningful approach adopted here.

- We reviewed the 2+2 and 1+1+2 approaches to the unperturbed LTB spacetime, setting up a correspondence between the variables. The LTB spacetime was shown to be covariantly characterised by the following non-zero 1+1+2 scalars $\{\Sigma, \mathcal{E}, \phi, \Theta, \mu\}$.

- The full system of 1+1+2 equations was explicitly written down along with expressions for the evolution and propagation equations for the gauge-invariant variables $\delta_a \mathbf{X}$.

- First, we studied the general form of polar perturbations to the LTB spacetime and identi-

fied a mapping between the 2+2 master variables and the corresponding 1+1+2 variables. Important identifications include: $\mathcal{E}_T \propto (\chi + \varphi)$ and $\mathcal{H}_T \propto \varsigma$. This leads to the association of the 2+2 master variable ς to a truly relativistic degree of freedom, as H_{ab} has no Newtonian analogue, characterising gravitational waves and frame dragging effects. The master variable χ was known to characterise polar gravitational waves, in complete agreement with the role of the electric Weyl tensor in relativistic cosmology.

- First we considered the general form of axial perturbations to the LTB spacetime. We introduced a correspondence between the 2+2 perturbation variables and the 1+1+2 variables. This allows us to outline the physical meaning of gauge invariant variables in the 2+2 formalism. The key results here are the association of the axial master variable Π to the radial part of the magnetic Weyl scalar $\mathcal{H}$. This is intuitive as the magnetic Weyl tensor corresponds to the axial part of the free gravitational field and encapsulates genuinely relativistic effects, as discussed before. The fluid master variable $\bar{v}$ was shown to be proportional to vorticity of the timelike congruence Ω.

- A covariant master equation for axial gravitational waves, of the form $\ddot{\mathcal{M}}_{ab} - \hat{\mathcal{M}}_{ab}$ was explicitly written down. Similarities to the structure of the master equation for axial gravitational waves in the Schwarzschild spacetime can be seen.

- Finally, we discussed the role of the Weyl 2-tensors in describing a master equation for gravitational perturbations. We introduced a master variable $\mathscr{I}_{\{ab\}} = \mathcal{E}_{\{ab\}} + \epsilon_{c\{a}\mathcal{H}_{b\}}{}^{c}$ that was shown to obey a wave equation coupled to a source term. Unfortunately, this source term includes the 2-tensors Σ_{ab} and ζ_{ab} and therefore does not close as hoped. It is expected that an auxiliary equation can be written for these 2-tensors allowing the equation to be closed. It was noted that in the vacuum limit the equation closes, as anticipated. The structure of this equation was related to the Weyl perturbations of the Schwarzschild spacetime and a brief discussion was outlined as to how $\mathscr{I}_{ab}$ can be generalised to vacuum LRS-II spacetimes covariantly characterised by $\{\mathcal{A}, \mathcal{E}, \Sigma, \Theta, \phi\}$. In other words, $\mathscr{I}_{ab}$ is the master variable governing gravitational perturbations for LRS-II spacetimes and obeys a closed covariant wave equation valid for both even and odd parities. This will be detailed in [438] and [439].

- These results allows us to understand the connections between individual subgroups, such as the Schwarzschild spacetime and the LTB spacetime, and the behaviour of gravitational perturbations in the larger group of spacetimes as a whole. In this case, we seek to understand the dynamics and the behaviour of perturbations to perfect fluid LRS-II spacetimes. In brief, we want to understand the space of cosmological spacetimes.

- This formalism can be used to study the propagation of gravitational waves in cosmological spacetimes, such as a void model represented by the LTB spacetime, or to study the interaction of gravitational waves with cosmological structure, e.g. modelling a dark matter halo with the LTB spacetime. The aim here is to understand the effects of cosmological structure, even if at the percent level, on a standard siren in gravitational wave physics [475; 571]. Does weak lensing of gravitational waves lead to non-trivial amplitude and phase modulations that may introduce parameter biases? Does the presence of structure affect distance

estimates leading to biases? It has been suggested that this will be the case for SN observations and we expect that similar effects may arise in upcoming gravitational wave physics [108]. These questions could be treated in a more exact and fully relativistic approach using the formalism outlined here.

- The 1+1+2 formalism can also be used to study the behaviour of tensor perturbations in non-standard cosmological backgrounds. This can then be used to analytically and numerically predict temperature and polarisation anisotropies in the CMB, thus extending the FLRW results in the 1+3 formalism [335; 93; 199; 94; 95; 200; 320].

Appendices

Appendix A

Appendix A

A.1 Topology Primer

A.1.1 Topological Space

The following is extensively based on [315] where we summarise the key subjects of immediate interest.

A topology on a set X consists of a collection U of subsets of X called open sets that obey:

- X and $\emptyset$ are open.
- The union of a open sets is open.
- Intersection of finite family of open sets is itself open.

The pair (X, U) describes a set X and the topology U on X and is refered to as a topological space. Consider a point $p \in X$ and a subset $S \subset X$.

- The interior of S is the union of all open subsets of X contained in the subset S.
- The exterior of S is the union of all open subsets of X contained in the coset $X \setminus S$
- The boundary of S is denoted ∂S and is all the points that are neither in the interior or exterior of S.
- A neighbourhood of p is an open set containing p.

Given two topological spaces X and Y we can define relationships between the spaces. In particular the notion of continuity will be important.

- A map $F : X \to Y$ is continuous is for every open set $U \subset Y$ the inverse image $F^{-1}(U)$ is open in X.
- A homeomorphism is a continuous $1-1$ (bijective) map $F : X \to Y$ such that the inverse mapping exists and is continuous.
- If $\exists$ a homeomorphism from X to Y then the two topological spaces are homeomorphic.

Two important topological spaces are metric and Hausdorff spaces:

A.1.2 Metric Space

A metric space is a set X equipped with a metric $d : X \times X \to \mathbb{R}$ such that $\forall x, y, z \in X$ the metric obeys:

- Positivity: $d(x, y) > 0\,;\; x \neq y\,;\; d(x, x) = 0$.
- Symmetry: $d(x, y) = d(y, x)$.

Consider a point $x \in X$ and a radius r. We can introduce the concept of an open ball of radius r as the set:

$$B_r(x) = y \in X : d(x, y) < r.$$

Similiarly the closed ball of radius r is defined to be:

$$B^*_r(x) = y \in X : d(x, y) \leq r.$$

An open subset $S \subset X$ is defined by requiring that for every point $x \in S$ there exists some radius $r > 0$ such that the open ball $B_r(x)$ is contained in the subset S. A topology can then be induced on the set X by the collection of all open subsets of X. A sequence of points x_i in X is Cauchy if for every $\epsilon > 0$ we have an integer n such that for $a, b \in n$ we have $d(x_a, x_b) < \epsilon$. A metric space X is then said to be complete if every Cauchy sequence in X converges to some point in X.

A.1.3 Hausdorff Space

A topological space is said to be Hausdorff if for very pair of distinct points $a, b \in X$ there exist disjoint open subsets $U \subset X$ containing a and $V \subset X$ containing b.

A.1.4 Covers

An open cover of a topological space X is a collection U of open subsets of X such that X is a subset of the union of sets in the collection. A subcover is a subcollection of U that is still an open cover.

A.1.5 Connectivity

If X is a topological space then the separation of X is the pair of non-empty open subsets $U, V \subset X$ whose union is X. If a separation of X exists then the toplogical space is said to be disconnected. If no separation exists then the topological space is connected. Alternatively X is connected iff the only subsets of X that are both open and closed are the set X and the null set $\emptyset$.

A.1.6 Compactness

A topological space X is compact if all open covers of X have a finite subcover. Naively this just means that our topological space can be covered by a finite number of r-balls for all r, i.e. it is a generalisation of a space being closed and bounded.

Appendix B

Appendix B

B.1 GMG Source Terms

$$\begin{aligned}\mathcal{S}_\chi = &-2\left[2\nu^2+8\pi\rho-\frac{6m}{r^3}-2U(\tau-U)\right](\chi+\varphi)+\frac{(l-1)(l+2)}{r^2}\chi\\ &+3\tau\dot{\chi}+4(\tau-U)\dot{\varphi}-(5\nu-2W)\chi'-2[2\tau\nu-2(\tau-U)W+\tau'-\dot{\nu}]\zeta\\ &+2\eta''-2(\tau-U)\dot{\eta}+(8\nu-6W)\eta'\\ &-\left[-4\nu^2+\frac{l(l+1)+8}{r^2}+8\nu W+4(2\tau U+U^2-4W^2-8\pi\rho)\right]\eta, \end{aligned} \tag{B.1}$$

$$\begin{aligned}\mathcal{S}_\varphi = &(1+c_s^2)U\dot{\chi}+[4U+c_s^2(\tau+2U)]\dot{\varphi}-W(1-c_s^2)\chi'-(\nu+2Wc_s^2)\varphi'\\ &-\left[2\left(\frac{1}{r^2}-W^2\right)+8\pi p-c_s^2\left(\frac{l(l+1)}{r^2}+2U(2\tau+U)-8\pi\rho\right)\right](\chi+\varphi)\\ &-\frac{(l-1)(l+2)}{2r^2}(1+c_s^2)\chi+2[-\tau W(1-c_s^2)+(\nu+W)U(1+c_s^2)]\zeta+8\pi C\rho\sigma\\ &-2U\dot{\eta}+2W\eta'+\left[\frac{l(l+1)+2}{r^2}-6W^2+16\pi p-2U(2\tau+U)c_s^2\right]\eta, \end{aligned} \tag{B.2}$$

$$\mathcal{S}_\zeta = 2\nu(\chi+\varphi)+2\tau\zeta+\chi'-2\eta(\nu-W)-2\eta', \tag{B.3}$$

$$\begin{aligned}\mathcal{C}_w = &-W\dot{\chi}+U\chi'-(\tau-2U)\varphi'+\frac{1}{2}\left[\frac{l(l+1)+2}{r^2}+2U(2\tau+U)\right.\\ &\left.-2W(2\nu+W)+8\pi(p-\rho)\right]\zeta-2U\eta', \end{aligned} \tag{B.4}$$

$$\mathcal{C}_\Delta = \left[\frac{l(l+1)}{r^2}+2U(2\tau+U)-8\pi\rho\right](\chi+\varphi)-\frac{(l-1)(l+2)}{2r^2}\chi+2[\nu U+(\tau+U)W]\zeta \tag{B.5}$$

$$\mathcal{C}_\alpha = 2\tau(\chi+\varphi)+2\nu\zeta+\dot{\chi}+2\dot{\varphi}-2\eta(\tau+U), \tag{B.6}$$

$$\begin{aligned}\bar{\mathcal{S}}_\Delta = &\left(1+\frac{p}{\rho}\right)\left[\left(-\frac{l(l+1)}{r^2}+8\pi(\rho+p)\right)\alpha+\frac{\dot{\varphi}}{2}+(\tau+U)\eta-\tau(\chi+\varphi)\right]+(\tau+2U)\left(c_s^2-\frac{p}{\rho}\right)\Delta\\ &+C(\tau+2U)\sigma-\frac{1}{c_s^2}\left[s'C+\left(1+\frac{p}{\rho}\right)(\nu-2Wc_s^2)\right]\left(w+\frac{\zeta}{2}\right)\end{aligned}$$

$$+\nu\left(1+\frac{p}{\rho}\right)\left(w-\frac{\zeta}{2}\right), \tag{B.7}$$

$$\begin{aligned}\bar{\mathcal{S}}_w = \left(1+\frac{p}{\rho}\right)\left[\frac{\varphi'}{2}+\left(c_s^2(\tau+2U)-\tau\right)\left(w-\frac{\zeta}{2}\right)-\tau\zeta-\nu(\chi+\varphi)+(\nu-W)\eta\right]\\ -C\sigma'-\sigma C\left[\nu+\frac{s'}{C}\frac{\partial C}{\partial s}-\left(\frac{\nu}{C}\left(1+\frac{p}{\rho}\right)+s'\right)\frac{1}{c_s^2}\frac{\partial c_s^2}{\partial s}\right]\\ +\Delta\left[\nu\left(\frac{p}{\rho}-c_s^2\right)+s'\left(C-\frac{\partial c_s^2}{\partial s}\right)+\left[\nu(\rho+p)+\rho C s'\right]\frac{1}{c_s^2}\frac{\partial c_s^2}{\partial \rho}\right].\end{aligned} \tag{B.8}$$

Appendix C

Appendix C

C.0.1 Spin Raising $\eth$ and Spin Lowering $\overline{\eth}$ Operators

Given the 2D Riemannian manifold S^2, we can define a null tetrad $\{m, \bar{m}\}$ constructed from the orthonormal basis vectors $\{\hat{e}_1, \hat{e}_2\}$ spanning S^2

$$m^a = \frac{1}{\sqrt{2}}\left(\hat{e}_1^a + i\hat{e}_2^a\right) \tag{C.1}$$

$$\bar{m}^a = \frac{1}{\sqrt{2}}\left(\hat{e}_1^a - i\hat{e}_2^a\right) \tag{C.2}$$

where $m^a\bar{m}_a = +1$ and $m^a m_a = \bar{m}^a\bar{m}_a = 0$. Using these results we can formally define the $\eth$ and $\overline{\eth}$ operators as totally projected convective covariant derivatives with respect to the null tetrad. First, let $\eta_{a\ldots by\ldots z}$ be a tensor on S^2, meaning that it has been projected into S^2 on every index such that there are p indices in the first index and q indices in the second. This means that we can define spin s quantities as follows:

$${}_s\eta = \eta_{a_1\ldots a_s}\, m^{a_1}\ldots m^{a_s} \tag{C.3}$$

$${}_{-s}\eta = \eta_{a_1\ldots a_s}\, \bar{m}^{a_1}\ldots \bar{m}^{a_s} \tag{C.4}$$

$$\eta_{a\ldots by\ldots z} = [{}_s\eta]\, m^a\ldots m^b + [{}_{-s}\eta]\, \bar{m}^y\ldots\bar{m}^z. \tag{C.5}$$

These objects transform under rotations as ${}_s\eta \to_s \eta\, e^{is\psi}$, where $s = p - q$ denotes the spin weight of η. Now we are in a position to define *edth* $\eth$ and *edth bar* $\overline{\eth}$ by

$$\eth\,[{}_s\eta] = m^a\ldots m^b\bar{m}^y\ldots\bar{m}^z\, m^c\nabla_c\,\eta_{a\ldots by\ldots z} \tag{C.6}$$

$$\overline{\eth}\,[{}_s\eta] = m^a\ldots m^b\bar{m}^y\ldots\bar{m}^z\,\bar{m}^c\nabla_c\,\eta_{a\ldots by\ldots z}, \tag{C.7}$$

where ∇_c is the covariant derivative defined with respect to S^2. If η has a spin weight of $+1$ then $\eth\,\eta$ has a spin weight of $s+1$ and $\overline{\eth}\,\eta$ a spin weight of $s-1$. This is why $\eth$ is known as a spin

raising operator and $\overline{\eth}$ a spin lowering operator.

It is often most convenient to jump straight into a coordinate dependent definition for a general spin-s field ${}_s\eta$. We assume that we are dealing with the standard unit sphere in spherical polar coordinates with a metric given by:

$$g_{ab} = \mathrm{diag}\left(1, \sin^2\theta\right) \tag{C.8}$$

for which we have the following non-zero Christoffel symbols:

$$\Gamma^0_{11} = -\sin\theta\,\cos\theta \tag{C.9}$$
$$\Gamma^1_{01} = \Gamma^1_{10} = \cot\theta. \tag{C.10}$$

In these coordinates, the natural null tetrad vectors are given by

$$m^a = \frac{1}{\sqrt{2}}\,(1, i\csc\theta) \tag{C.11}$$
$$m_a = \frac{1}{\sqrt{2}}\,(1, i\sin\theta) \tag{C.12}$$

where the conjugate vectors are trivially defined. Using these definitions, we simply substitute these into Eqn. (C.6) and Eqn. (C.7). This results in the following general formula for $\eth$ and $\overline{\eth}$ on the 2D sky

$$\eth\,{}_s\eta = -\sin^s\theta\,\left(\partial_\theta + i\csc\theta\,\partial_\phi\right)\,\left(\sin^{-s}\theta\right)\,{}_s\eta \tag{C.13}$$
$$\overline{\eth}\,{}_s\eta = -\sin^{-s}\theta\,\left(\partial_\theta - i\csc\theta\,\partial_\phi\right)\,\left(\sin^{s}\theta\right)\,{}_s\eta. \tag{C.14}$$

Appendix D

Appendix D

D.1 Lemaître-Tolman-Bondi Spacetime

D.1.1 Metric Formalism

The non-vanishing Christoffel symbols in the LTB spacetime are given by:

$$\Gamma^t_{rr} = X\,\partial_t X \tag{D.1}$$
$$\Gamma^t_{aa} = A\,\partial_t A\,\gamma_{aa} \tag{D.2}$$
$$\Gamma^r_{rt} = \Gamma^r_{tr} = \frac{\partial_t X}{X} \tag{D.3}$$
$$\Gamma^r_{rr} = \frac{\partial_r X}{X} \tag{D.4}$$
$$\Gamma^r_{aa} = -\frac{A\partial_r A}{X^2}\gamma_{aa} \tag{D.5}$$
$$\Gamma^\theta_{t\theta} = \Gamma^\theta_{\theta t} = \Gamma^\phi_{t\phi} = \Gamma^\phi_{\phi t} = \frac{\partial_t A}{A} \tag{D.6}$$
$$\Gamma^\theta_{r\theta} = \Gamma^\theta_{r\theta} = \Gamma^\phi_{r\phi} = \Gamma^\phi_{\phi r} = \frac{\partial_r A}{A} \tag{D.7}$$
$$\Gamma^\phi_{\theta\theta} = -\sin\theta\,\cos\theta \tag{D.8}$$
$$\Gamma^\phi_{\theta\phi} = \Gamma^\phi_{\phi\theta} = \cot\theta. \tag{D.9}$$

where $\gamma_{ab} = \mathrm{diag}(1, \sin^2\theta)$ is the metric on the unit sphere.

The EFEs in terms of the metric components $X(t,r)$ and $A(t,r)$ reduces to the following non-vanishing components:

$$G_{tt} = -\frac{(\partial_r A)^2}{A^2X^2} - \frac{1}{A^2}\left[(\partial_t A)^2 + 1\right] - 2\frac{\partial_t X\,\partial_t A}{AX} - 2\frac{\partial_r X\partial_r A}{AX} + 2\frac{\partial_r^2 A}{AX^2} \tag{D.10}$$
$$G_{tr} = -2\frac{\partial_t X\,\partial_r A}{AX} + 2\frac{\partial_{tr} A}{A} \tag{D.11}$$
$$G_{rr} = -2\frac{\partial_t^2 A}{A} - \frac{1}{A^2}\left[(\partial_t A)^2 + 1\right] \tag{D.12}$$

$$G_{\theta\theta} = G_{\phi\phi} = -\frac{\partial_t X\, \partial_t A}{AX} - \frac{\partial_t^2 A}{A} - \frac{\partial_t^2 X}{X} + \frac{\partial_r^2 A}{X^2 A} - \frac{\partial_r X\, \partial_r A}{X^3 A}. \tag{D.13}$$

Appendix E

Appendix E

E.1 Additional Relativistic Cosmology Results

E.1.1 Useful Relations for Decomposing the 1+3 System of Equations

This section is identical to Appendix A in [105] and is a very useful reference to have on hand when relating the 1+3 system of equations to the 1+1+2 equations. It is included in the Appendix for completeness and reference.

Given any 1+3 vectors and tensors, we may decompose them as

$$\begin{aligned}
x^a &= Xn^a + X^a, \\
y^a &= Yn^a + Y^a, \\
\psi_{ab} &= \psi_{\langle ab\rangle} = \Psi\left(n_a n_b - \tfrac{1}{2}N_{ab}\right) + 2\Psi_{(a}n_{b)} + \Psi_{ab}, \\
\phi_{ab} &= \phi_{\langle ab\rangle} = \Phi\left(n_a n_b - \tfrac{1}{2}N_{ab}\right) + 2\Phi_{(a}n_{b)} + \Phi_{ab}.
\end{aligned}$$

Then we have the following expansions from 1+3 quantities $\longrightarrow$ 1+1+2 variables:

$$\begin{aligned}
x_a x^a &= X^2 + X_a X^a, \\
\eta_{abc}x^b y^c &= \left(\varepsilon_{bc}X^b Y^c\right)n_a + \varepsilon_{ab}\left(YX^b - XY^b\right), \\
x_{\langle a}y_{b\rangle} &= \tfrac{1}{3}\left(2XY - X_cY^c\right)\left(n_a n_b - \tfrac{1}{2}N_{ab}\right) + \left[XY_{(a} + YX_{(a}\right]n_{b)} + X_{\{a}Y_{b\}}, \\
\psi_{ab}x^b &= \left(X\Psi + X_b\Psi^b\right)n_a - \tfrac{1}{2}\Psi X_a + X\Psi_a + \Psi_{ab}X^b, \\
\eta_{cd\langle a}x^c\psi_{b\rangle}{}^d &= \varepsilon_{cd}X^c\Psi^d\left(n_a n_b - \tfrac{1}{2}N_{ab}\right) + \left[\left(X\Psi^c - \tfrac{3}{2}\Psi X^c\right)\varepsilon_{c(a} + \varepsilon_{cd}X^c\Psi^d{}_{(a}\right]n_{b)} \\
&\quad + X\varepsilon_{c\{a}\Psi_{b\}}{}^c - X^c\varepsilon_{c\{a}\Psi_{b\}}, \\
\psi_{ab}\psi^{ab} &= \tfrac{3}{2}\Psi^2 + 2\Psi_a\Psi^a + \Psi_{ab}\Psi^{ab}, \\
\psi_{c\langle a}\phi_{b\rangle}{}^c &= \left(\tfrac{1}{2}\Psi\Phi + \tfrac{1}{3}\Psi_c\Phi^c - \tfrac{1}{3}\Psi_{cd}\Phi^{cd}\right)\left(n_a n_b - \tfrac{1}{2}N_{ab}\right) + \left[\tfrac{1}{2}\Psi\Phi_{(a} + \tfrac{1}{2}\Phi\Psi_{(a} + \Psi^c\Phi_{c(a} + \Phi^c\Psi_{c(a}\right]n_{b)} \\
&\quad - \tfrac{1}{2}\Psi\Phi_{ab} - \tfrac{1}{2}\Phi\Psi_{ab} + \Psi_{\{a}\Phi_{b\}} + \Psi_{c\{a}\Phi_{b\}}{}^c, \\
\eta_{abc}\psi^b{}_d\phi^{dc} &= n_a\varepsilon_{bc}\Psi^b{}_d\Phi^{dc} + \tfrac{3}{2}\varepsilon_{ab}\left(\Phi\Psi^b - \Psi\Phi^b\right).
\end{aligned}$$

For 1+3 derivatives we find:

$$
\begin{aligned}
\dot{x}_{\langle a\rangle} &= \left(\dot{X} - X_b\alpha^b\right) n_a + X\alpha_a + \dot{X}_{\bar{a}},\\
\dot{\psi}_{\langle ab\rangle} &= \left(\dot{\Psi} - 2\Psi_c\alpha^c\right) n_a n_b - \tfrac{1}{2}\dot{\Psi}N_{ab} + \left[3\Psi\alpha_{(a} + 2\dot{\Psi}_{(\bar{a}} - 2\alpha^c\Psi_{c(a}\right] n_{b)}\\
&\quad +2\Psi_{(a}\alpha_{b)} + \dot{\Psi}_{\{ab\}},\\
\mathrm{D}_a x^a &= \hat{X} + X\phi - X_a a^a + \delta_a X^a,\\
\eta_{abc}\mathrm{D}^b x^c &= \left(2X\xi + \varepsilon_{bc}\delta^b X^c\right) n_a + \xi X_a + \varepsilon_{ab}\left[-Xa^b + \delta^b X - \hat{X}^b - \tfrac{1}{2}\phi X^b - \zeta^{bc}X_c\right],\\
\mathrm{D}_{\langle a}x_{b\rangle} &= \tfrac{1}{3}\left[2\hat{X} - \phi X - 2X_c a^c - \delta_c X^c\right]\left(n_a n_b - \tfrac{1}{2}N_{ab}\right)\\
&\quad + \left[Xa_{(a} + \delta_{(a}X + \hat{X}_{(\bar{a}} - \tfrac{1}{2}\phi X_{(a} + X^c\left(\xi\varepsilon_{c(a} - \zeta_{c(a)}\right)\right] n_{b)} + X\zeta_{ab} + \delta_{\{a}X_{b\}},\\
\mathrm{D}^b\psi_{ab} &= \left(\hat{\Psi} + \tfrac{3}{2}\phi\Psi - 2\Psi_b a^b + \delta_b\Psi^b - \Psi_{bc}\zeta^{bc}\right) n_a + \hat{\Psi}_{\bar{a}} + \tfrac{3}{2}\phi\Psi_a + \tfrac{3}{2}\Psi a_a - \tfrac{1}{2}\delta_a\Psi\\
&\quad -\Psi_{ab}a^b + \left[-\xi\varepsilon_{ab} + \zeta_{ab}\right]\Psi^b + \delta^b\Psi_{ab},\\
\eta_{cd\langle a}\mathrm{D}^c\psi_{b\rangle}{}^d &= \left(3\xi\Psi + \varepsilon_{cd}\delta^c\Psi^d - \varepsilon_{cd}\Psi^{de}\zeta^c{}_e\right)\left(n_a n_b - \tfrac{1}{2}N_{ab}\right)\\
&\quad + \left\{\left[-\tfrac{3}{2}\delta^c\Psi + \tfrac{3}{2}\Psi a^c + \hat{\Psi}^c + \tfrac{1}{2}\phi\Psi^c + 2\Psi_d\zeta^{cd}\right]\varepsilon_{c(a} + 5\xi\Psi_{(a} + \varepsilon^{cd}\left[\Psi_d\zeta_{c(a} + \delta_c\Psi_{d(a}\right]\right\} n_{b)}\\
&\quad -\varepsilon_{c\{a}\delta^c\Psi_{b\}} + 2\varepsilon_{c\{a}a^c\Psi_{b\}} + \varepsilon_{c\{a}\hat{\Psi}^c{}_{b\}} + \tfrac{1}{2}\phi\varepsilon_{c\{a}\Psi^c{}_{b\}} -\\
&\quad \tfrac{3}{2}\Psi\varepsilon_{c\{a}\zeta^c{}_{b\}} + \xi\Psi_{ab} + \varepsilon_{c\{a}\Psi_{b\}d}\zeta^{cd}.
\end{aligned}
$$

E.1.2 The Lie Derivative

In addition to defining the covariant derivative, a more natural derivative operator may be introduced by characterising the rate of change of a tensor field under the flow of a diffeomorphism. To this extent we introduce a one-parameter family of diffeomorphisms ϕ_t that may be thought of as some smooth map $\mathbf{R}\times M\to M$ for which each $t\in\mathbf{R}$ the diffeomorphism satisfies $\phi_s\circ\phi_t = \phi_{s+t}$. This last condition insures that ϕ_0 will be the identity map.

As a brief side note we state that diffeomorphisms can be viewed as active coordinate transformations whereas coordinate transformations are considered to be passive. As an example, given an n-dimensional manifold M we can introduce coordinates $x^\mu : M\to\mathbf{R}^n$. To change these coordinates we could introduce a new set of coordinate functions $y^\mu : M\to\mathbf{R}^n$ or we could introduce a diffeomorphism $\phi : M\to M$ after which the coordinate functions are given by $(\phi^* x)^\mu : M\to\mathbf{R}^n$. The first operation is akin to keeping the manifold fixed but changing the coordinate map. The second operation, the active approach, is akin to moving the points on the manifold and re-evaluating the coordinates of the new points. Both lead us to the same goal but in different ways.

The diffeomorphism can be viewed as being generated by a vector field. If we associate to ϕ_t a vector field v, then for fixed $p\in M, \phi_t(p) : \mathbf{R}\to M$ defines a curve called an *orbit* of ϕ_t passing through p at $t=0$. Let $v|_p$ denote the tangent to this curve at $t=0$. Associated to a one-parameter group of diffeomorphisms of M will be a vector field v, the infinitesimal generator of these transformations. In essence, we define a vector field $v^\mu(x)$ as the set of tangent vectors to each of the curves at every point evaluated at $t=0$. Given a vector field v^μ, the *integral curves* of

the vector field are the set of curves $x^\mu(t)$ that solve

$$\frac{dx^\mu}{dt} = v^\mu. \tag{E.1}$$

The diffeomorphisms therefore represent the *flow* down the integral curves, as for each point $p \in M$ we define $\phi_t(p)$ to be the point lying at a parameter t along the integral curve of v starting at p.

Given a vector field v^μ, we can introduce a family of diffeomorphisms parameterised by t and calculate how the tensor changes as we flow down the integral curves. This amounts to calculating the difference between the tensor at a point p and the value of the tensor at $\phi(p)$ pulled back to p is denoted by Δ_t,

$$\Delta_t T^{a\ldots c}{}_{d\ldots g}(p) = \phi_t^* \left[T^{a\ldots c}{}_{d\ldots g}(\phi(p))\right] - T^{a\ldots c}{}_{d\ldots g}(p). \tag{E.2}$$

The Lie derivative is then simply the defined with respect to this infinitesimal change

$$\mathcal{L}_v T^{a\ldots c}{}_{d\ldots g} = \lim_{t\to 0}\left(\frac{\Delta_t T^{a\ldots c}{}_{d\ldots g}}{t}\right). \tag{E.3}$$

In practice we will simply use the following functional form

$$\begin{aligned}
\mathcal{L}_v T^{a\ldots c}{}_{d\ldots g} &= v^r \nabla_r T^{a\ldots c}{}_{d\ldots g} && \text{(E.4)}\\
&- (\nabla_r v^a)\, T^{rb\ldots c}{}_{d\ldots g} && \text{(E.5)}\\
&- (\nabla_r v^v)\, T^{ar\ldots c}{}_{d\ldots g} - \ldots && \text{(E.6)}\\
&+ (\nabla_d v^r)\, T^{a\ldots c}{}_{re\ldots g} && \text{(E.7)}\\
&+ (\nabla_e v^r)\, T^{a\ldots c}{}_{dr\ldots g} + \ldots. && \text{(E.8)}
\end{aligned}$$

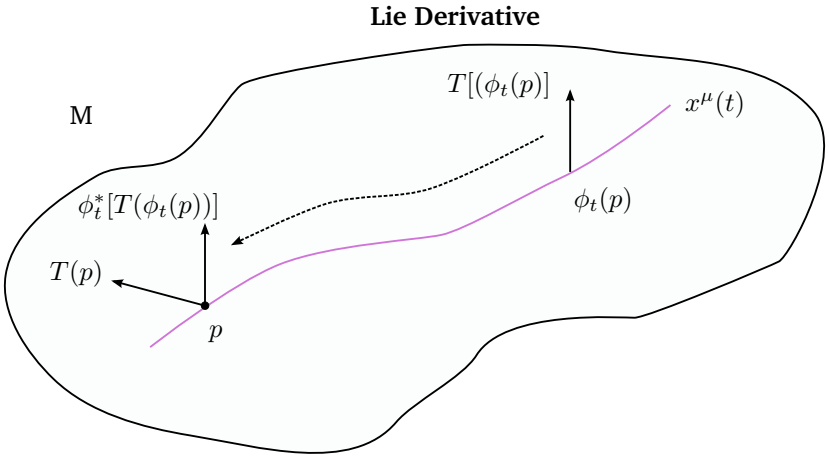

Figure E.1: Schematically, a Lie derivative is defined as the rate of change of a tensor along the integral curves associated to a one-parameter diffeomorphism ϕ_t. We compare the original tensor $T(p)$ at a point p to the value of T at a point $\phi_t(p)$ by pulling back $T(\phi_t(p))$ to the point p. This is a recreation of Figure B.3 in [89].

Appendix F

Appendix G

F.1 Cosmological Random Fields

In this appendix we collect a number of useful and important definitions in the description of cosmological random fields. Elements of this appendix should be considered standard reference material.

F.1.1 Random Fields

We begin by first making an explicit definition of what we mean when we talk about a random field. This will be used to define several ancillary terms and will lay the foundations for our discussion of random fields in both Fourier space as well as the spherical Fourier-Bessel space.

Definition F.1. A *random variable* $f(\mathbf{x})$ is the assignment of a real value to an element $\mathbf{x} \in \mathbb{R}$ according to a probability density function $P[f(\mathbf{x})]$. Consequentially, the probability that the random variable lies in the infinitesimal cube with boundaries set by $f(\mathbf{x})$ and $f(\mathbf{x}) + df(\mathbf{x})$ is denoted by $P[f(\mathbf{x})]\ df(\mathbf{x})$.

Definition F.2. A *random field* f is formed from a set of N random variables $f(\mathbf{x}_i)$ for which $\mathbf{x}_i \in \mathbb{R}^n$ according to a joint probability distribution.

Definition F.3. A *joint probability distribution* generalises the probability density function to a random field:

$$P[f(\mathbf{x}_1)\ ,\ \ldots\ ,\ f(\mathbf{x}_N)]\ \forall N \in \mathbb{N}. \tag{F.1}$$

Definition F.4. A *realisation* of the random field f is simply one assignment of the values of the random variables $f(x_i)$, which we denote by f_i.

Definition F.5. The random variables f_i are *independent* if the joint probability distribution factorises into a product of individual probability density functions for each random variable. Intuitively,

this means that a realisation of one random variable will not affect the other random variables.

$$P\left[f_1\,,\,\ldots\,,\,f_N\right] = P\left[f_1\right]\ldots P\left[f_N\right] \tag{F.2}$$

In addition, a random field can be further constrained by imposing symmetries on the field. Invariance under spatial translations and invariance under spatial rotations are the two most commonly imposed symmetries.

Definition F.6. A random field is *homogeneous* if all the joint probability density functions are invariant under spatial translations

$$P\left[f\left(\mathbf{x}_1+\mathbf{r}\right), f\left(\mathbf{x}_2+\mathbf{r}\right), \ldots, f\left(\mathbf{x}_N+\mathbf{r}\right)\right] = P\left[f\left(\mathbf{x}_1\right), f\left(\mathbf{x}_2\right), \ldots, f\left(\mathbf{x}_N\right)\right]\ \forall\,\mathbf{r}\in\mathbb{R}^n, \tag{F.3}$$

meaning that the probability depends only on the relative positions.

Definition F.7. The random field will be *isotropic* if all the joint probability density functions are invariant under spatial rotations

$$P\left[f\left(\mathcal{R}\mathbf{x}_1\right), f\left(\mathcal{R}\mathbf{x}_2\right), \ldots, f\left(\mathcal{R}\mathbf{x}_N\right)\right] = P\left[f\left(\mathbf{x}_1\right), f\left(\mathbf{x}_2\right), \ldots, f\left(\mathbf{x}_N\right)\right]\ \forall\,\mathcal{R}. \tag{F.4}$$

For the most part we will assume that cosmological random fields are statistically homogeneous and isotropic, though this is not always the case. For example, redshift space distortions introduce non-trivial deviations from statistical homogeneity and isotropy in the redshift-space density field.

Definition F.8. The *moment* of a random field is given by the expectation value about a value c:

$$\mu_n = \left\langle f\left(\mathbf{x}\right) - c\right\rangle = \int df\left(\mathbf{x}\right)\,\left[f\left(\mathbf{x}\right)-c\right]^n\,P\left[f\left(\mathbf{x}\right)\right]. \tag{F.5}$$

The two most common implementations of the moment are for $c=0$, known as a *raw moment*, or for $c=\mu\left(\mathbf{x}\right)$, known as a *central moment*.

Definition F.9. The *raw moment*, also known as a moment about zero, of a random field g with probability density function P is defined by the ensemble average $\langle\ldots\rangle$ over products of evaluations of the random field. Implicitly assuming a continuous field, we have:

$$\left\langle f_1\,f_2\,\ldots\,f_N\right\rangle = \int df_1\,df_2\,\ldots\,df_N\,f_1\,f_2\,\ldots\,f_N\,P\left[f_1\,,\,f_2\,,\,\ldots\,,\,f_N\,\right]. \tag{F.6}$$

The order of the raw moment is simply given by the sum of the powers: $m=\sum n_i$. This is a crucial concept as the statistical properties of the random field are completely described if we have knowledge of all m-order moments for all $m\in\mathbb{N}$. This does not, however, uniquely specify the distribution. The hierarchy of moments can be thought of as something of a quantitative measure of the shape of the distribution.

Definition F.10. The *expectation* of a random field f is defined to be the zeroth order moment. From the definition above we see that

$$\mu\left(\mathbf{x}\right) = \left\langle f\left(\mathbf{x}\right)\right\rangle = \int df\left(\mathbf{x}\right)\,f\left(\mathbf{x}\right)\,P\left[f\left(\mathbf{x}\right)\right]. \tag{F.7}$$

Definition F.11. The second type of moment that is commonly used is the *central moment*, defined as the n-th order raw moment about the mean μ:

$$\langle \left[f\left(\mathbf{x}\right) - \langle f\left(\mathbf{x}\right)\rangle\right]^n\rangle = \langle \left(f\left(\mathbf{x}\right) - \mu\left(\mathbf{x}\right)\right)^n\rangle = \int df\left(\mathbf{x}\right)\ \left[f\left(\mathbf{x}\right) - \mu\left(\mathbf{x}\right)\right]^n\ P\left[f\left(\mathbf{x}\right)\right]. \tag{F.8}$$

Definition F.12. The *variance* is defined to be the second-order central moment and is equal to the square of the standard deviation. This is given by:

$$\sigma^2\left(\mathbf{x}\right) = \left\langle \left[f\left(\mathbf{x}\right) - \mu\left(\mathbf{x}\right)\right]^2 \right\rangle = \int df\left(\mathbf{x}\right)\ \left[f\left(\mathbf{x}\right) - \mu\left(\mathbf{x}\right)\right]^2\ P\left[f\left(\mathbf{x}\right)\right]. \tag{F.9}$$

Definition F.13. The *covariance* is defined by calculating the second-order central moment of a random field at two different locations $\mathbf{x}, \mathbf{y} \in \mathbb{R}$

$$\sigma\left(\mathbf{x}, \mathbf{y}\right) = \langle \left[f\left(\mathbf{x}\right) - \langle f\left(\mathbf{x}\right)\rangle\right]\ \left[f\left(\mathbf{y}\right) - \langle f\left(\mathbf{y}\right)\rangle\right] \rangle. \tag{F.10}$$

We can see that the variance is a subset of the covariance for which $\sigma\left(\mathbf{x}, \mathbf{x}\right) = \sigma^2\left(\mathbf{x}\right)$. Intuitively, the covariance provides a measure of how correlated the the random field is at the two locations $\mathbf{x}, \mathbf{y} \in \mathbb{R}$. In addition to correlating a single random field we will often construct a cross-correlation between two different random fields. This will be discussed in more detail later.

Definition F.14. The *reduced n-point correlation function* can be defined in terms of cumulants (or connected moments) and expresses the part of the n-point correlation function that may not be obtained from lower order reduced correlation functions. The n-th order reduced correlation functions are defined as follows, where we have explicitly written out the first three n-point correlation functions,

$$\langle f_1\rangle_c = \langle f_1\rangle \tag{F.11}$$

$$\langle f_1 f_2\rangle_c = \langle f_1 f_2\rangle - \langle f_1\rangle_c \langle f_2\rangle_c \tag{F.12}$$

$$\begin{aligned}\langle f_1 f_2 f_3\rangle_c = {} & \langle f_1 f_2 f_3\rangle - \langle f_1\rangle_c \langle f_2\rangle_c \langle f_3\rangle_c - \langle f_1\rangle_c \langle f_2 f_3\rangle_c - \langle f_2\rangle_c \langle f_1 f_3\rangle \\ & - \langle f_3\rangle_c \langle f_1 f_2\rangle_c\end{aligned} \tag{F.13}$$

$$\begin{aligned}\langle f_1 f_2 \dots f_N\rangle_c = {} & \langle f_1 f_2 \dots\rangle \\ & - \langle f_1\rangle_c \langle f_2\rangle_c \dots \langle f_N\rangle_c - \langle f_1\rangle_c \langle f_2 \dots f_N\rangle_c + \text{permutations} \\ & - \langle f_1 f_2\rangle_c \langle f_3 \dots f_N\rangle_c + \text{permutations} \\ & - \dots \\ & - \langle f_1 \dots f_{N-1}\rangle_c \langle f_N\rangle_c + \text{permutations}.\end{aligned}$$

In the case of a Gaussian random field with zero mean, the above relations signify considerably. The 3-point correlation function vanishes identically and the 4-point correlation function factorises into products of the 2-point correlator. Generalising to higher order moments, all even correlators are described by the 2-point correlation function and all odd correlators vanish identically. This is why the power spectrum completely defines the statistical properties of a Gaussian random field, all higher order correlators are related to products of the power spectrum. The definitions above

can be defined in either real space or Fourier space, as we will introduce shortly. In this thesis we will focus on the Fourier space definition. Any time we refer to an n-point correlation function, it should be assumed that we are referring to an n-point correlation function defined in the Fourier domain in terms of the Fourier coefficients $f(\mathbf{k}_i)$.

F.1.2 Random Fields in Fourier Space

The vast majority of our work will be completed in the Fourier domain. It is therefore important to outline the conventions adopted.

Definition F.15. The *Fourier transform* $\mathcal{F}$ of the random field $g : \mathbb{R}^n \to \mathbb{R}$ is defined by

$$\mathcal{F}\left[f\left(\mathbf{x}\right)\right] = \tilde{f}\left(\mathbf{k}\right) = \int d^n x \, f\left(\mathbf{x}\right) \, e^{-i\,\mathbf{k}\cdot\mathbf{x}} \tag{F.14}$$

The *inverse Fourier transform* $\mathcal{F}^{-1}$ of the function $\tilde{f} : \mathbb{R}^n \to \mathcal{C}$ is defined by

$$\mathcal{F}^{-1}\left[\tilde{f}\left(\mathbf{k}\right)\right] = f\left(\mathbf{x}\right) = \int \frac{d^n k}{(2\pi)^n} \, \tilde{f}\left(\mathbf{k}\right) \, e^{i\mathbf{k}\cdot\mathbf{x}}. \tag{F.15}$$

The Fourier transform is a very powerful tool due to the properties of its transformations. The Fourier transform is linear in its arguments:

$$\mathcal{F}\left[a\, f\left(\mathbf{x}\right) + b\, f\left(\mathbf{x}\right)\right] = a\mathcal{F}\left[f\left(\mathbf{x}\right)\right] + b\mathcal{F}\left[f\left(\mathbf{x}\right)\right]. \tag{F.16}$$

The Fourier transform of the n-th order derivative of a function f simply becomes

$$\mathcal{F}\left[f^{(n)}\left(\mathbf{x}\right)\right]\ \left(\mathbf{k}\right) = -\left(i\mathbf{k}\right)^n \ f\left(\mathbf{k}\right). \tag{F.17}$$

This leads to the following useful identity

$$\mathcal{F}\left[\nabla^2 f(\mathbf{x})\right] = -k^2 f(\mathbf{k}). \tag{F.18}$$

Finally, the Fourier transform of a convolution between two functions reduces to a product

$$\mathcal{F}\left[f\left(\mathbf{x}\right) \star f\left(\mathbf{x}\right)\right] = \mathcal{F}\left[f\left(\mathbf{x}\right)\right] \cdot \mathcal{F}\left[f\left(\mathbf{x}\right)\right]. \tag{F.19}$$

Analogous to earlier, we can define a hierarchy of statistical moments in Fourier space. The lowest order moment of significant interest is the 2-point correlation function or *power spectrum* $P(k)$. The power spectrum for an n-dimensional homogeneous random field can be defined as:

$$\left\langle \tilde{f}\left(\mathbf{k}\right) \ \tilde{f}\left(\mathbf{k}'\right) \right\rangle = (2\pi)^n \ \delta_D\left(\mathbf{k} - \mathbf{k}'\right) \ P\left(\mathbf{k}\right). \tag{F.20}$$

The power spectrum quantifies the correlation of structure on a given scale. Enforcing homogeneity gives rise to the Dirac delta function and translates into the statement that different Fourier modes are not correlated. An important result in Fourier analysis is the Wiener-Khienchin the-

orem stating that the two-point correlation function of a random field can be directly related to the power spectrum as follows:

$$P(\mathbf{k}) = \int d^3x\, \xi(\mathbf{x})\; e^{i\mathbf{k}\cdot\mathbf{x}}, \tag{F.21}$$

where we are implicitly assuming a 3-dimensional random field. Polyspectra for higher order correlators can be defined in an analogous manner.

Definition F.16. Assuming homogeneity of the random field, the 3-point correlation function or *bispectrum* is defined in 3 spatial dimensions by

$$\left\langle \tilde{f}(\mathbf{k}_1)\, \tilde{f}(\mathbf{k}_2)\, \tilde{f}(\mathbf{k}_3) \right\rangle_c = (2\pi)^3\; \delta_D(\mathbf{k}_1 + \mathbf{k}_2 + \mathbf{k}_3)\; B(\mathbf{k}_1, \mathbf{k}_2, \mathbf{k}_3)\,. \tag{F.22}$$

Definition F.17. The 4-point correlation function or the *trispectrum* is defined by

$$\left\langle \tilde{f}(\mathbf{k}_1)\, \tilde{f}(\mathbf{k}_2)\, \tilde{f}(\mathbf{k}_3)\, \tilde{f}(\mathbf{k}_4) \right\rangle_c = (2\pi)^3\; \delta_D(\mathbf{k}_1 + \mathbf{k}_2 + \mathbf{k}_3 + \mathbf{k}_4)\; T(\mathbf{k}_1, \mathbf{k}_2, \mathbf{k}_3, \mathbf{k}_4)\,. \tag{F.23}$$

We could proceed to construct real space counterparts to the polyspectra but these will not be needed in this thesis and are therefore not included.

F.1.3 Gaussian Random Field

One of the most important types of random field in cosmology and statistics is that of a Gaussian random field (GRF).

Definition F.18. The *multivariate joint probability distribution function* of a Gaussian random field has the form:

$$P[f_1, \ldots, f_N]\; df_1\; \ldots\; df_N = \frac{1}{\sqrt{(2\pi)^N\, \det\sigma}}\, \exp\left[-\frac{1}{2}\sum_{ab} f_a\, \sigma^{-1}_{ab}\, f_b\right]\; df_1\; \ldots\; df_N, \tag{F.24}$$

where σ_{ab} is the covariance matrix constructed from $\langle f_a f_b \rangle$.

If the random variables are independent then the covariance matrix diagonalises, as there should be no cross-correlations between the variables, and the multivariate probability distribution function simplifies significantly:

$$P[f_1] \ldots P[f_N]\; df_1\; \ldots\; df_N = \prod_{i=1}^{N} \frac{df_1 \ldots df_N}{\sqrt{2\pi\, \sigma^2}}\, \exp\left[\frac{-g_i^2}{2\sigma_i^2}\right]. \tag{F.25}$$

Definition F.19. One of the most important results relevant to Gaussian random fields is the *Wick theorem*. This states that the moments of a Gaussian random field may be factorised into products of the two-point correlation function with odd moments being equal to zero:

$$\langle f_1 \ldots f_{2n} \rangle = \sum_{\text{permutations}} \langle f_1 f_2 \rangle_c \ldots \langle f_{2n-1} f_{2n} \rangle_c \tag{F.26}$$

$$\langle f_1 \ldots f_{2n-1} \rangle = 0. \tag{F.27}$$

As a consequence, we can see that the bispectrum is the lowest order correlator for which a non-zero measurement signifies a deviation from Gaussianity. This is important as non-Gaussianity is an ill-defined concept beyond the fact that somehow the statistical distribution fails to be Gaussian, as an infinite hierarchy of moments would allude to. In a cosmological context the higher order moments are significantly suppressed and the bispectrum and trispectrum are natural candidates for tests for non-Gaussianity.

F.1.4 Characteristic Function

The characteristic function of a real-valued random variable will completely define the probability distribution, it is a very powerful tool in statistics. If a random field has an associated probability density function, the characteristic function is its Fourier dual. Even if a distribution does not have a probability density function or moment generating function, the characteristic function will always exist. The function is defined to be equal to the expectation value of the exponential random field:

$$\begin{aligned} \phi\left(t\right) = \left\langle\, e^{itg} \,\right\rangle &= \mathcal{F}\Big[P\left[g\right]\Big]\left(t\right) \\ &= \int dg\, P\left[g\right]\, e^{itg} \\ &= \sum_{k=0}^{\infty} \frac{\left(it\right)^k}{k!}\, \mu'_k \end{aligned} \tag{F.28}$$

where $t \in \mathbb{R}$ is just the argument of the characteristic function, μ'_n is the n-th moment about zero and we reserve μ_n for the n-th central moment. Using the Fourier transform we obtain the Inversion theorem:

Theorem F.20. *Given a characteristic function ϕ of a random field f, it will uniquely determine the probability density function and vice versa.*

The characteristic function can be used to generate the n-th moments about zero by taking the n-th order derivative of $\phi(t)$ around the point $t = 0$:

$$\phi^{(n)}\left(0\right) = \left[\frac{d^n\phi}{dt^n}\right]_{t=0} = i^n \mu'_n. \tag{F.29}$$

Alternatively, we can use the series expansion of the natural logarithm of the characteristic function to generate the cumulants of the random field:

$$\ln \phi\left(t\right) = \sum_{n=0}^{\infty} \kappa_n \frac{\left(it\right)^n}{n!}. \tag{F.30}$$

Appendix G

Appendix E

G.1 The Halo Model for Large Scale Clustering

G.1.1 Introduction

An important and challenging area of modern cosmology is the statistical characterisation of large scale structure and the detailed modelling of its distribution throughout the Universe. There are many different approaches to this problem ranging from analytical perturbation theory through to the numerical N-body simulations. The aim of these studies is to provide accurate descriptions of cosmological models that allow us to test comsological models with observational evidence. A detailed modelling of these observables will be all the more important given the accuracy and survey size of the next Generation of telescopes. In this Section we want to introduce a particular analytical technique, known as the halo model, that is reasonably straightforward but has proven itself to be robust, powerful and flexible.

The halo model is based on the proposition that galaxies are clustered in halos distributed throughout space with a set of basic properties such as their size, their mass, internal density profile and spatial position with respect to other halos. Such clustering arises from the gravitational collapse of primordial perturbations to the highly Gaussian dark matter distribution. The halos grow and evolve through hierarchical formation [593] such that the galaxies that form inside a halo have characteristics that are related to those of the parent dark matter halo.

Recent simulations have suggested that most of the baryons are at low overdensity regions $\delta < 10$ at high redshifts z but are within collapsed halos at low redshifts $z \lesssim 1$. This implies that baryons with overdensities $\lesssim 10$ track the underlying dark matter distribution. These baryons have temperatures on order that of the photoionisation temperature of hydrogen and helium. In this section we will follow [125; 126; 127; 456] and calculate the SZ effect due to the baryons within collapsed virialised halos at low redshifts using the halo model for large scale clustering. This is expected to be valid beyond the range of validity of the linear biasing scheme that we implemented in the previous sections. We will compute the 3D cross-spectra in this formalism and compare the results to those form the linear biasing scheme above. First, however, we wish to provide a detailed introduction to the halo model and its ingredients.

G.1.2 Spherical Collapse

G.1.2.1 Closed Universe

The growth and formation of non-linear structure is one of the leading areas of reasearch in modern cosmology. Understanding the structure of non-linearities induced by gravitational collapse is vital for our understanding of how large scale structure forms and evolves. As the statistics of dark matter halos necessarily deals with non-linear objects, it can be very tough to find robust analytic models. For more complex scenarios it is not atypical to use numerical simulations to generate phenomenological fits to halo statistics. However, if we assume a high degree of symmetry then there are special configurations that can be solved explicitly to yield the non-linear evolution of the density contrast. This analytically tractable model is based on the evolution of a spherical matter overdensity embedded in a homogeneous and isotropic Universe. This was the case studied by [230] who considered the collapse of an initially top-hat density perturbation, i.e. with sharp boundary. This is known in the literature as the *spherical collapse model*.

Assuming a flat, matter dominated Universe, such that $K = 0$ and $\Omega_{\rm M} = 1$, we wish to consider the evolution of a spherical overdensity. A consequence of Birkhoff's theorem is that the exterior and interior of the spherical shell of matter will evolve independently. At an initial time, the spherical perturbation will have a radius of a_i and an average density of $\rho(a_i, t_i) = \bar{\rho}\,[1 + \delta]$. Our spherical shell of matter will therefore evolve as if it were a closed Universe of density $\Omega_m = 1 + \delta$. In such a closed Universe the Friedmann equation reduces to

$$\frac{\dot{a}}{a} = H_0 \left(\frac{\Omega_m}{a^3} + \frac{(1 - \Omega_m)}{a^2} \right)^{1/2}. \tag{G.1}$$

This permits a rather neat paramteric solution to the Friedmann equations (see [117], or other Cosmology textbooks, for an introduction) defined over the interval $\theta \in (0, 2\pi]$

$$a(\theta) = \frac{a_m}{2} (1 - \cos\theta) \tag{G.2}$$

$$t(\theta) = \frac{t_m}{\pi} (\theta - \sin\theta)\,. \tag{G.3}$$

where we have introduced

$$a_m = a_0 \frac{\Omega_m}{\Omega_{\rm M} - 1} \tag{G.4}$$

$$t_m = \frac{\pi}{2H_0} \frac{\Omega_m}{(\Omega_m - 1)^{3/2}}. \tag{G.5}$$

This solution describes an initial growth of the expansion parameter, in accordance with an expansion velocity equal to that of the background, which slowly decelerates until it reaches a maximum radius a_m at a time t_m for which $\theta = \theta_m = \pi$. After this point, the structure begins to collapse reaching a singularity $a \to 0$ at a maximum time of $t = 2t_m$ for $\theta = 2\pi$ (see Fig. G.1).
We can perform a series expansion of the trigonometric functions in order to study their behaviour in a given limit. Expanding to second order we see that

$$\lim_{\theta \to 0} a(\theta) = \frac{a_m}{2} \left(\frac{1}{2}\theta^2 - \frac{1}{24}\theta^4 + \mathcal{O}(\theta^6) \right) \tag{G.6}$$

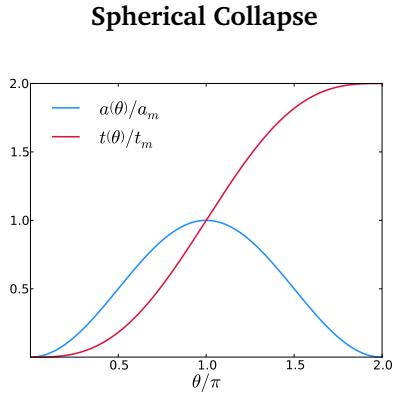

Figure G.1: This is a plot showing the evolution of the radius and time in the simple spherical collapse model using the given parametric solution.

$$\lim_{\theta\to 0} t(\theta) = \frac{t_m}{\pi}\left(\frac{1}{6}\theta^3 - \frac{1}{210}\theta^5 + \mathcal{O}(\theta^7)\right). \tag{G.7}$$

At leading order, we recover $a \propto t^{2/3}$ as anticipated in an Einstein-de Sitter Universe. At next-to-leading order we can substitute $t(\theta)$ into the expression for $a(\theta)$ to recover

$$\frac{a(\theta)}{a_m} = \frac{1}{2}\left(6\pi\frac{t}{t_m}\right)^{2/3}\left[1 - \frac{1}{20}\left(6\pi\frac{t}{t_m}\right)^{2/3}\right] + \mathcal{O}\left[\left(\frac{t}{t_m}\right)^{6/3}\right]. \tag{G.8}$$

From our expression for the density, $\rho = 3M/4\pi a^3$, and the definition of the overdensity we can acquire an expression for the linear theory overdensity

$$\delta = \frac{\rho - \bar{\rho}}{\bar{\rho}} \approx \frac{3}{20}\left(6\pi\frac{t}{t_m}\right)^{2/3}. \tag{G.9}$$

As per the discussion earlier, this overdensity becomes *collapsed* at $t = 2t_m$ leading to a prediction for the threshold overdensity of spherical collapse

$$\delta_c = \delta(2t_m) \simeq 1.686. \tag{G.10}$$

We can also re-introduce the redshift dependence of the density contrast by evolving the contrast using the growth factor

$$\delta_c(z) = G(z)\,\delta_c(z_c = 0) = \frac{1.686}{1+z}. \tag{G.11}$$

As we have stressed throughout, this result corresponds to a highly simplified scenario. We do not expect an overdensity to be perfectly spherical nor homogeneous. In practice, the simplicity of this result is powerful and allows us to quickly analyse a number of interesting relationships that are of immediate use. As an example, we can derive the overdensity of collapse which is defined to be the overdensity at the time of virialisation. Spherical collapse does not proceed to a point but rather it reaches a virial equilibrium with the kinetic energy being approximately half the potential energy. For our EdS Universe, the time scale on which this occurs can be approximated by the free

fall time of a uniform sphere with a density defined at $t = t_m$. The density of virialisation will be given by scaling this quantity by a factor of 2^3, as the radius has simply halved,

$$\rho(t_{\rm coll}) = 8\rho(t_m) \tag{G.12}$$

$$= \frac{3\pi}{Gt_{\rm coll}^2}. \tag{G.13}$$

We then compare this quantity to the background density $\bar{\rho} = 1/(16\pi G t^2)$ which tells us the overdensity of collapse at the time of virialisation

$$\Delta_{\rm vir} = \frac{\rho(t_{\rm coll})}{\bar{\rho}(t_{\rm coll})} \tag{G.14}$$

$$= 18\pi^2 \approx 178.$$

More realistic and more recent treatments have gone beyond this result, extending the calculations to non-spherical and elliptical mass distributions [380; 522] as well as cosmologies beyond EdS [250].

G.1.3 Halo Mass Function

G.1.3.1 Press-Schechter Formalism

The next key ingredient that we require to implement the halo model is a description of the mass distribution of the dark matter halos. Remember, the halo model assumes that all dark matter is distributed in spherical halos. The total number of halos of mass M per unit comoving volume and per unit mass at a redshift z is given by a halo mass function, written schematically as

$$\frac{dn}{dM} = \frac{\bar{\rho}}{M}\frac{d\nu}{dM} f(\nu). \tag{G.15}$$

The parameter ν is defined by

$$\nu(M, z) = \frac{\delta_c}{\sigma(M, z)}, \tag{G.16}$$

with $\sigma(M, z)$ the linear rms mass fluctuation in a sphere of radius R given by $M = 4\pi\bar{\rho}R^3/3$ at a redshift z. This quantity may be evaluated from the linear power spectrum $P_{\rm lin}(k, z)$. The approach we take to define our mass function is that of Press and Schecter (PS) [443] who derived a simple model based on the spherical collapse formalism presented earlier. In the PS approach, we consider the density field at some initial time t_i or redshift z_i such that the density field $\delta(\mathbf{x}, t_i)$ may be described as a Gaussian random field. This field is assumed to be smoothed $\delta_R(\mathbf{x}, t_i)$ with the smoothing kernel given by a top-hat window function. The probability distribution for the smoothed density field is given by

$$P(\delta_R, R, z) = \frac{1}{\sqrt{2\pi}\sigma(R, z)} \exp\left(-\frac{\delta_R^2}{2\sigma^2(R, z)}\right). \tag{G.17}$$

where $\sigma^2(R,z) = \langle\delta_R^2\rangle$ is the variance of the density field smoothed with a window function $W_R(k)$. We can associate a mass to the smoothing scale by equating it to the mass enclosed in a volume of radius R, for a top hat filter this simplifies to $M = (4\pi/3)\bar{\rho}R^3$. Given these relationships, we can conveniently characterise the halos by the smoothing scale R, the variance σ^2 or the mass M. According to the PS prescription, an object of mass M will be collapsed if the density contrast exceeds the threshold, i.e. $\delta > \delta_c$. The cumulative probability function for regions of scale R to have a density contrast δ_R above the threshold is given by [443]

$$\begin{aligned} F(R,z) &= \int_{\delta_c}^{\infty} d\delta\, P(\delta_R; R, z) \\ &= \frac{1}{2}\text{erfc}\left(\frac{\delta_c}{\sqrt{2\sigma^2(R,z)}}\right). \end{aligned} \tag{G.18}$$

From this cumulative probability we can calculate the number of newly collapsed regions dF when the enclosed mass is increased by dM. This quantity can be converted to a number density by weighting with $\bar{\rho}/M$. Enforcing that all mass should be contained within the halos motivates us to incorporate a factor of 2 in the analysis. Press and Schechter [443] argue that this correction corresponds to the fact that half of the total mass that was originally unaccounted for, corresponding to initially underdense regions, and will accrete onto the collapsed objects and result in an approximate doubling of the mass [443]. The number of newly collapsed regions is typically re-written in terms of a shape function $f(\nu)$ such that

$$2\frac{dF(M)}{dM} = \frac{d\nu}{dM} f(\nu). \tag{G.19}$$

By inspection with the original probability distribution function Eq. (G.17) we see that the shape function $f(\nu)$ is now taken to be

$$f(\nu) = \sqrt{\frac{2}{\pi}}\, e^{-\nu^2/2}. \tag{G.20}$$

Finally, for halos of mass M, the mass function according to PS is given by

$$\frac{dn}{dM} = \sqrt{\frac{2}{\pi}}\frac{\bar{\rho}}{M}\frac{\delta_c}{\sigma^2}\frac{d\sigma}{dM}\exp\left[-\frac{\delta_c^2}{2\sigma^2}\right]. \tag{G.21}$$

Fig. G.2 shows the PS mass function as a function of redshift, where the dependency on redshift is primarily due to the redshift dependence of the variance $\sigma^2(R,z)$.

G.1.3.2 Sheth-Tormen Formalism

The Press-Schechter function is known to overestimate the abundance of high mass halos whilst underestimating the low mass halos. It was this observation that led to the introduction of the Sheth-Tormen mass function [522] as an improved and upgraded approach to the Press-Schechter formalism. The Sheth-Tormen mass function is derived via a fitting to numerical simulations. Note that Sheth and Tormen [522] use a different definition of ν, namely $\nu = (\delta_c/\sigma_R)^2$.

As before, we start with the total number of halos of mass M per unit comoving volume per

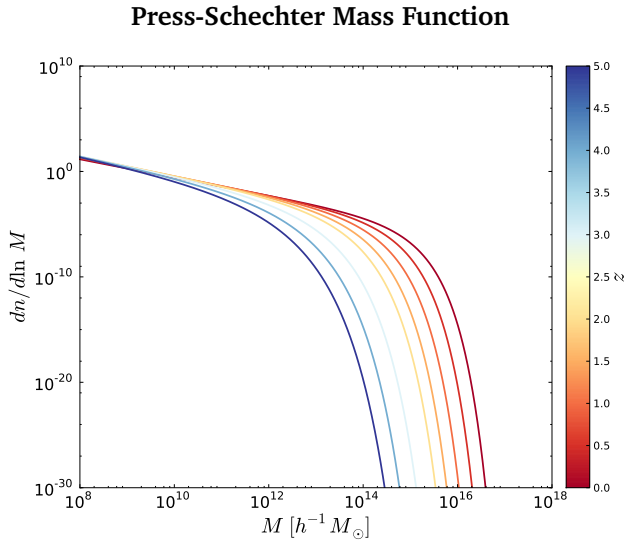

Figure G.2: This is a plot showing the evolution with redshift of the Press-Schechter halo mass function.

unit mass at a redshift z

$$\frac{dn}{dM} = \frac{\bar{\rho}}{M}\frac{d\nu}{dM} f(\nu), \tag{G.22}$$

however, unlike Press-Schechter, the functional form for the shape function is given by

$$f(\nu) = A\sqrt{\frac{a\nu^2}{2\pi}}\left[1 + \frac{1}{(a\nu^2)^p}\right]\exp\left(-\frac{a\nu^2}{2}\right) \tag{G.23}$$

The normalisation is defined such that $\int n_{\rm ST}(m) m\, dm = \bar{\rho}$ and the coefficients a and p are fit to the numerical data. Typical values of these coefficients are $A \sim 0.322$, $a = 0.7 \sim 0.75$ and $p = 0.3$. The original Press-Schechter formalism is recovered for $a = 1$, $p = 0$ and $A = 1/2$.

This can be extended again to completely empirical fitting functions, such as the study by [278]. A more detailed and careful treatment of the dependency of the tSZ-WL cross correlation on the underlying mass function and halo biasing prescription would be a good future project.

G.1.4 Halo Bias

Another crucial component is that the dark matter halos themselves are taken to be locally biased tracers of linear density perturbations. Cosmological biasing can occur in several different forms. For example, the non-linear dark matter density field will be biased with respect to the linear dark matter density field due to the non-linear nature of gravitational collapse. If halos form without regard to the underlying density field and undergo normal gravitational collapse, then halos would be an unbiased tracer of the dark matter density field. The spherical collapse toy model, however, states that the formation of halos is necessarily dependent on the initial density field. This means that the large scale dark matter density, acting as a background, can lead to an enhanced probability of a halo forming. This leads to the peak-background split pciture of [379]. In essence, this tells us that baryonic clustering that sits around dark matter overdensities

are more likely to collapse to form halos due to the lowered effective threshold. The halos will therefore be a biased tracer of the underlying dark matter distribution.

Following [379], we can introduce a Taylor series expansion that allows us to relate the over-density of halos to the linear density fluctuations

$$\delta_h\left(\mathbf{x}, M; z\right) = b_0 + b_1(M; z)\delta_{\rm lin}(\mathbf{x}; z) + \frac{1}{2}b_2(M; z)\delta^2_{\rm lin}(\mathbf{x}; z) + \dots \tag{G.24}$$

where $b_\beta(M; z)$ denote the set of halo bias parameters that will be dependent on model specific details, such as the mass function. As the halos are biased tracers of the density perturbations, the number density of halos will fluctuate according to

$$\frac{dn}{dM}(\mathbf{x}; z) = \frac{d\bar{n}}{dM}(M; z)\,\delta_h(\mathbf{x}, M; z) \tag{G.25}$$

$$= \frac{d\bar{n}}{dM}(M; z)\left[b_0 + b_1(M; z)\,\delta_{\rm lin}(\mathbf{x}; z) + \frac{1}{2}b_2(M; z)\delta^2_{\rm lin}(\mathbf{x}; z) + \dots\right]. \tag{G.26}$$

The bias parameters are defined as follows [379]

$$b_0(M; z) = 1 \tag{G.27}$$

$$b_1(M; z) = 1 + \frac{\nu^2(M; z) - 1}{\delta_c} \tag{G.28}$$

$$b_2(M; z) = \frac{8}{21}\left[b_1(M; z) - 1\right] + \frac{\nu^2(M; z) - 3}{\sigma^2(M; z)}, \tag{G.29}$$

with ν defined in Eq. (G.16). We neglect bias terms of cubic order or higher as these will make contributons at a level less than 1% [127].

Following a similar argument as above, the bias parameters in the Sheth-Tormen approach are given by [522; 499]

$$b_0(M; z) = 1 \tag{G.30}$$

$$b_1(M; z) = 1 + \frac{a\nu^2 - 1}{\delta_c} + \frac{2p}{\delta_c}\left[1 + \left(a\nu^2\right)^p\right]^{-1} \tag{G.31}$$

$$b_2(M; z) = \frac{8}{21}\left[\frac{a\nu^2 - 1}{\delta_c} + \frac{2p}{\delta_c\left[1 + (a\nu^2)^p\right]}\right] + \frac{a\nu^2}{\delta_f^2}\left(a\nu^2 - 3\right) \tag{G.32}$$

$$+ \frac{2p}{\delta_f\left[1 + (a\nu^2)^p\right]}\left[\frac{1 + 2p}{\delta_f} + \frac{2\left(a\nu^2 - 1\right)}{\delta_f}\right],$$

where $\delta_f = \delta_c D(z_0)/D(z_1)$. If the observing redshift z_0 is the same as the formation redshift z_1 then $\delta_f = \delta_c$. These can be shown to reduce to the expressions derived in [379] in the Press-Schechter limit, i.e. $a \to 1$, $p \to 0$ and $\delta_f \to \delta_c$.

G.1.5 Dark Matter Density Profile

The spherically averaged dark matter profiles $\rho_\delta(x)$ for collapsed halos are given by the Navarro-Frenk-White (NFW) [402] density distribution. The NFW profile assumes that the profile shape of

halos is universal and can be characterised by a scaling radius x_s and scaling density ρ_s

$$\rho_\delta(x) = \frac{\rho_s}{(x/x_s)(1+x/x_s)^2}. \tag{G.33}$$

The mass of the profile within the virial radius x_v can be calculated integrating the NFW profile to yield

$$M_{\rm vir} = 4\pi\rho_s\, x_s^3 \left[\log(1+c_s) - \frac{c_s}{1+c_s}\right]. \tag{G.34}$$

Here we have introduced the concentration parameter $c_s = x_v/x_s$, telling us how centrally peaked the profile is. Assuming the spherical collapse model, the virial mass $M_{\rm vir}$ within the virial radius x_v can be expressed as

$$M_{\rm vir} = \frac{4\pi}{3} x_v^3\, \Delta_c(z)\, \bar\rho(z); \qquad \bar\rho(z) = \bar\rho\, E^2(z) \tag{G.35}$$

$$\Delta_c(z) = 18\pi^2 + 82[\Omega_{\rm M}(z) - 1] - 39[\Omega_{\rm M}(z) - 1]^2; \qquad \Omega_{\rm M}(z) = \Omega_{\rm M}\frac{(1+z)^3}{E^2(z)}. \tag{G.36}$$

Where $\Delta_c(z)$ is the overdensity of collapse defined earlier and $E^2(z)$ is the function introduced in Eq. (3.116). By evaluating the overdensity of collapse for our given cosmology we can obtain the virial radius x_v for a given mass $M_{\rm vir}$. The concentration parameter c_s for a halo of mass M can then be re-expressed in terms of a characteristic mass scale M_* defined by $\sigma(M_*; z) = \delta_c$ or, equivalently, $\nu = 1$. Using fitting formula calibrated to ΛCDM simulations, the concentration-mass relationship is taken to be given by

$$c_s(M,z) = a(z)\left[\frac{M}{M_*(z)}\right]^{-b(z)}; \qquad a(z) = 10.3(1+z)^{-0.3}; \qquad b(z) = 0.24(1+z)^{-0.3}. \tag{G.37}$$

This correspondence between the two mass definitions allows us to eliminate the scaling density ρ_s by equating the virial mass $M_{\rm vir}$ computed in Eq. (G.35) with the virial mass computed using the NFW density profile in Eq. (G.34).

$$\rho_s = \frac{c_s^3}{x_v^3}\frac{M_{\rm vir}}{4\pi}\left[\log(1+{\rm c_s}) - \frac{\rm c_s}{1+{\rm c_s}}\right]^{-1} \tag{G.38}$$

Once we have determined the concentration parameter for a given virial mass, we can explicitly evaluate ρ_s and hence explicitly determine the NFW halo profile. The halos in a given cosmological background can therefore be characterised with just two parameters: the halo mass M and the concentration parameter c_s. Remember, the virial radius is determined by the halo mass and the background cosmology dependent overdensity of collapse and is therefore not an independent parameter.

G.1.6 Gas Density Profile

In order to describe large scale pressure fluctuations, and hence the SZ effect, we will assume a hydrostatic equilibrium between the gas distribution and the dark matter distribution in halos

[343]. This enables us to relate the gas density profile to an underlying dark matter halo profile in a reasonable and physical manner [514; 126; 299]. The equation of state is assumed to be well modelled by a polytropic fluid with polytropic index γ. Hydrostatic equilibrium implies that we have

$$\frac{k_B T_e}{\mu\, m_p} \frac{d\log\rho_g(x)}{dx} = -\frac{GM(<x)}{x^2}. \tag{G.39}$$

where $M(<x)$ is the mass inside a radius x. The above relationship implicitly assumes that the gas distribution obeys an isothermal temperature distribution. As the dark matter profile is assumed to obey a scaling relationship, the gas density profile will also obey a scaling relationship in terms of a physical parameter b and scale radius x_s:

$$\rho_g(x) = \rho_{g0}\; e^{-b}\left(1+\frac{x}{x_s}\right)^{bx_s/x}; \qquad b = \frac{4\pi G\mu m_p \rho_s x_s^2}{k_B T_e}. \tag{G.40}$$

The physical parameter is intrinsically related to the virial temperature of the gas T_e

$$k_B T_e = \frac{1}{3r_v}\gamma G\mu m_p M_\delta(x_v). \tag{G.41}$$

In this work we adopt a polytropic index of $\gamma = 3/2$ and a mean molecular weight of $\mu = 0.59$ to accompany the proton mass m_p. The total mass of the gas in a dark matter halo within a virial radius x_v will be given by:

$$M_g(x_v) = 4\pi\rho_{g0}\; e^{-b}\; x_s^3 \int_0^c dq\; q^2(1+q)^{b/q}. \tag{G.42}$$

The final ingredient we need is a prescription for the calculation of the galaxy-pressure power spectrum. In order to do this we need to specify an average occupancy of galaxies in halos. This is simply assumed to have a general form given by

$$\begin{aligned}\langle N_g\rangle &= \left(\frac{M}{M_{\rm min}}\right)^{0.6} \quad \text{for} \;\; M \geq M_{\rm min};\\ &= 0 \qquad\qquad\quad \text{for}\; M < M_{\rm min}.\end{aligned} \tag{G.43}$$

The minimum dark matter halo mass is taken to be $M_{\rm min} = 10^9 h^{-1} M_\odot$. Consequentially, the mean number density of galaxies $\bar{n}_g$ and the average density weighted temperature $\bar{T}_e$ can be expressed as

$$\bar{n}_g = \int dM \langle N_g\rangle \frac{dn}{dM}(M,z); \quad \bar{T}_e = \int dM \frac{M}{\rho_p}\frac{dn}{dM}(M,z) T_e(M,z). \tag{G.44}$$

When studying the correlations between power spectra and cross-spectra it will be useful to introduce the bias $b_\Pi(k,r)$ and cross-spectral coefficient $r_{\Pi\Pi}(k,r)$

$$b_\Pi(k) = \frac{1}{\bar{T}_e}\sqrt{\frac{P_{\Pi\Pi}(k)}{P_{\delta\delta}(k)}}; \quad r_{\Pi\Pi}(k) = \frac{P_{\Pi\delta}(k)}{\sqrt{P_{\delta\delta}(k)P_{\Pi\Pi}(k)}}. \tag{G.45}$$

These coefficients will encapsulate the dependencies between the dark matter, pressure and dark matter-pressure power spectra. Finally, it is important to note that halo model, as presented here, does not incorporate non-thermal pressures, such as that caused by turbulence, gas cooling or star formation. This is a topical area and has been the focus of recent studies (e.g. [525]). Detailed modelling of such non-thermal pressures could be of interest for future studies of the tSZ effect and its cross correlations with other external tracers.

G.1.7 Halo Model: Power Spectra

We are now in a position to put all of our various ingredients together in order to construct physically interesting quantities such as the power spectra of our various components. Following the literature [128; 126; 127], we introduce a general integral over the halo mass function that contains terms related to the dark matter, gas pressure and baryon density fields

$$I^{\beta,\eta,\gamma}_{\mu,i_1,i_2\dots i_\mu}(k_1,\dots,k_\mu;z) \equiv \int d\ln M \left(\frac{M}{\bar{\rho}}\right)^{\mu} \frac{dn}{d\ln M}(M,z)\, b_\beta(M) \left(\frac{\bar{\rho}}{M}\frac{\langle N_g\rangle}{\bar{n}_g}\right)^{\gamma} \times [T_e(M,z)]^{\eta}\, y_{i_1}(k_1,M)\dots y_{i_\mu}(k_\mu,M). \tag{G.46}$$

The above integral contains the bias parameters $b_\beta(M,z)$, telling us how the halos trace the over-density field, the halo mass function $[d\bar{n}/dM](M,z)$ giving the number density of halos at a given virialised mass, the electron temperature $T_e(M;z)$ to account for clustering properties associated with baryons and the 3D Fourier transform of the density profiles $y_{i,\mu}(k_\mu,M)$. The Fourier transform is explicitly given by

$$y_i(k,M) = \frac{1}{M_i}\int_0^{r_v} dx\, x^2\, 4\pi\, \rho_i(x,M)\, j_0(kx). \tag{G.47}$$

where the subscript i represents the density δ or gas g. The Fourier transform has been normalised such that it approaches unity as $k\to 0$, as can be seen in Fig. G.3. The power spectra are decomposed into contributions from the single halos $P^{PP}_{ij}(k)$ and contributions from the halo-halo correlations $P^{hh}_{ij}(k)$. Here we explicitly write out the various definitions for the power spectra and cross-spectra that we consider in this Chapter (Fig. G.4):

$$(i)\quad \delta\delta:\quad P^t_{\delta\delta} = P^{\rm PP}_{\delta\delta} + P^{hh}_{\delta\delta} \quad ; P^{\rm PP}_{\delta\delta}(k) = I^{0,0,0}_{2,\delta\delta}(k,k) \quad ; P^{hh}_{\delta\delta}(k) = [I^{0,0,0}_{1,\delta}]^2 P_{\rm lin}(k) \tag{G.48}$$

$$(ii)\quad \Pi\Pi:\quad P^t_{\Pi\Pi} = P^{PP}_{\Pi\Pi} + P^{hh}_{\Pi\Pi} \quad ; P^{\rm PP}_{\delta\delta}(k) = I^{0,2,0}_{2,gg}(k,k) \quad ; P^{hh}_{\delta\delta}(k) = [I^{1,1,0}_{1,g}]^2 P_{\rm lin}(k) \tag{G.49}$$

$$(iii)\quad \delta\Pi:\quad P^t_{\Pi\delta} = P^{PP}_{\Pi\delta} + P^{hh}_{\Pi\delta} \quad ; P^{\rm PP}_{\Pi\delta}(k) = I^{0,1,0}_{2,g\delta}(k,k) \quad ; P^{hh}_{\Pi\delta}(k) = [I^{1,1,0}_{1,g}][I^{1,0,0}_{1,\delta}] P_{\rm lin}(k) \tag{G.50}$$

$$(iv)\quad g\Pi:\quad P^t_{\Pi\delta} = P^{PP}_{\Pi\delta} + P^{hh}_{\Pi\delta} \quad ; P^{\rm PP}_{\Pi\delta}(k) = I^{0,1,1}_{2,g\delta}(k,k) \quad ; P^{hh}_{\Pi\delta}(k) = [I^{1,1,0}_{1,g}][I^{1,0,1}_{1,\delta}] P_{\rm lin}(k) \quad . \tag{G.51}$$

We now gather all the various ingredients to construct the halo model power spectra. We take $M_{\rm max} = 10^{16} h^{-1} M_\odot$ and $M_{\rm min} = 10^9 h^{-1} M_\odot$. In Fig. G.4 we present the numerical results for the

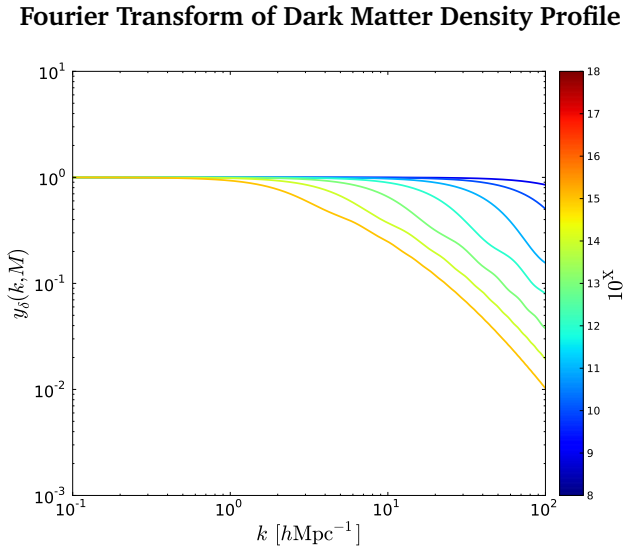

Figure G.3: This is a plot showing the Fourier transform of the NFW profile for a range of halo masses.

density-density, pressure-pressure and density-pressure spectra along with the bias and spectral correlation coefficients.

G.1.8 Uses of the Halo Model

The halo model is a flexible and useful framework from which we can study the statistical properties of a wide variet of astrophysical and cosmological phenomena. In this brief section we discuss and introduce a number of potential applications of the halo model. We focus on three applications: galaxy clustering, weak lensing and the thermal Sunyaev-Zel'dovich effect. We could also consider additional observables such as the non-linear integrated Sachs-Wolfe effect and a detailed review is given in [130].

- **Galaxy Clustering** It was early work by [593] that introduced to concept of galaxies existing in a parent halo whose properties are intrinsically linked to the formation and evolution of galaxies. The halo model is particularly suited to the study of the distribution of galaxies and the study of large scale clustering of galaxies. On large scales, it is thought that gravitational collapse is the dominant mechanism but at smaller scales significant non-linear behaviour kicks in along with a plethora of baryonic processes that introduce feedback mechanisms. One of the key inputs into the halo model was the mass function describing the abundance of halos with a given mass. Using these functions we can infer the distribution of galaxies within a halo hence allowing us to calculate the cross-correlation of the galaxy distribution with a parent halo as well as the auto-correlation. The physical inputs into the halo model allow us to investigate how the distribution of dark matter within a halo relates to the distribution of baryonic material. It is hoped that by investigating such clustering properties, we can study the detailed nature of the formation and evolution of galaxies and the concomitant feedback mechanisms.

- **Weak Gravitational Lensing** Once we have a model that allows us to construct a power spec-

trum in the halo model, there are immediately a number of interesting observables that may be constructed. As we discussed earlier, weak gravitational lensing traces the underlying dark matter distribution as the gravitational mass induces small perturbations to the path of a photon along the line of sight. The halo model allows us to construct both a matter and pressure power spectrum based on reasonable physical assumptions, such as the dark matter and gas density profiles. Such detailed modelling is then fed back into the spectra themselves as well as the cross-spectral coefficients that measure the correlations between the baryonic and dark matter sectors. This means that weak lensing observables are likely to be dependent on this detailed modelling and procedures such as a cross correlation between weak-lensing and the tSZ effect may be a very interesting probe of the baryonic and dark Universe. Alternatively, we could choose to cross correlate the weak lensing observables with the galaxy distribution. In this case, the galaxy distribution acts as a biased tracer of the dark matter distribution. Such correlations may help to shed light on biasing and any scale dependence of biasing [379]. Finally, we could go further than the halo model presented here and introduce sub-structure effects, such as clumping, into our calculations [524].

- **The Sunyaev-Zel'dovich Effect** As we discussed in the introduction, the tSZ effect traces baryons within virialised halos at low redshifts with temperatures on order the photoionisation temperature of hydrogen and helium. The procedure for extending the halo model to incorporate the tSZ effect is sometimes a little cumbersome but in practice is reasonably straightforward. To describe pressure fluctuations on large scales, we assume that hydrostatic equilibrium between the gas and dark matter distriubtions holds such that we may relate the dark matter density profile to the gas density profile in a physically plausible and reasonable manner. This necessarily involves some calibration via the polytropic index, mean molecular weight and an accurate measure of the virial temperature of the gas. Once we have these we can reconstruct the the gas pressure power spectrum as well as the cross-correlated spectra. This extension forms the core of the resulting WL-tSZ cross- correlation analysis in the halo model. As expected, this effect is dependent on the detailed modelling that enters our calculations. This includes the halo mass function, gas and matter density profiles and biasing scheme.

Halo Model Power Spectra: Contributions from Halo Terms

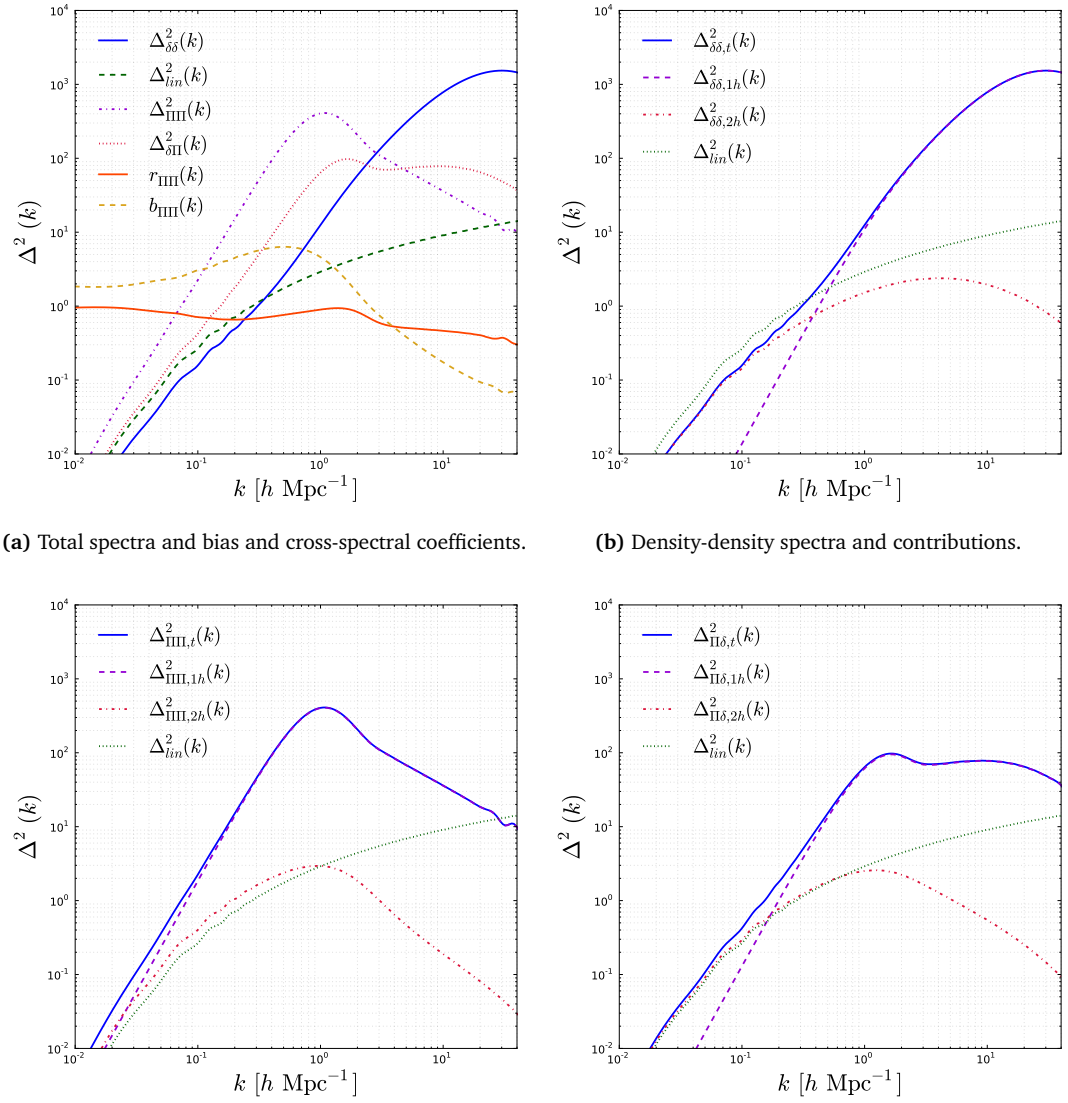

(a) Total spectra and bias and cross-spectral coefficients.

(b) Density-density spectra and contributions.

(c) Pressure-pressure spectra and contributions.

(d) Density-Pressure Spectra and Contributions.

Figure G.4: We show the various power spectra with single halo (1h), double halo (2h) and total (t) contributions. As can be seen, the 1-halo contribution dominates the various spectra. The virial temperature describes the electrons allowing us to construct the pressure bias $b_\Pi(k)$ and the correlation coefficient $r_\Pi(k)$ between the dark matter and baryonic distributions. Most of the contribution to the SZ effect arises from massive clusters of galaxies whereas the smaller mass halos and structures at low electron temperature do not contribute as significantly.

Bibliography

[1] R. J. Adler, The Geometry of Random Fields (1981) Chichester: Wiley

[2] L. R. Abramo, P. H. Reimberg and H. S. Xavier, "CMB in a box: causal structure and the Fourier-Bessel expansion," PRD **82** (2010) 043510 arXiv:1005.0563.

[3] P. A. R. Ade *et al.* [BICEP2 Collaboration], "BICEP2 I: Detection Of B-mode Polarization at Degree Angular Scales," arXiv:1403.3985.

[4] P. A. R. Ade *et al.* [Planck Collaboration], "Planck 2013 results. XXI. Cosmology with the all-sky Planck Compton parameter y-map," arXiv:1303.5081.

[5] J. K. Adelman-McCarthy *et al.* [SDSS Collaboration], "The Sixth Data Release of the Sloan Digital Sky Survey," ApJSuppl. **175** (2008) 297 [arXiv:0707.3413 [astro-ph]].

[6] P. Adshead and E. A. Lim, "3-pt Statistics of Cosmological Stochastic Gravitational Waves," PRD **82** (2010) 024023 arXiv:0912.1615.

[7] P. Adshead, R. Easther and E. A. Lim, "Cosmology With Many Light Scalar Fields: Stochastic Inflation and Loop Corrections," Phys. Rev. D **79** (2009) 063504 arXiv:0809.4008.

[8] P. Adshead, C. Dvorkin, W. Hu and E. A. Lim, "Non-Gaussianity from Step Features in the Inflationary Potential," PRD **85** (2012) 023531 arXiv:1110.3050.

[9] U. Alam and V. Sahni, "Confronting braneworld cosmology with supernova data and baryon oscillations," PRD **73** (2006) 084024 arXiv:astro-ph/0511473.

[10] A. Albrecht, G. Bernstein, R. Cahn, W. L. Freedman, J. Hewitt, W. Hu, J. Huth and M. Kamionkowski *et al.*, "Report of the Dark Energy Task Force," arXiv:astro-ph/0609591.

[11] A. Albrecht, L. Amendola, G. Bernstein, D. Clowe, D. Eisenstein, L. Guzzo, C. Hirata and D. Huterer *et al.*, "Findings of the Joint Dark Energy Mission Figure of Merit Science Working Group," arXiv:0901.0721.

[12] C. Alcock and B. Paczynski, "An evolution free test for non-zero cosmological constant," Nature **281** (1979) 358.

[13] M. Alcubierre, Introduction to 3+1 Numerical Relativity, ISBN 978-0-19-920567-7 (HB), Published by Oxford University Press, Oxford, UK (2008)

[14] M. Alishahiha, E. Silverstein and D. Tong, "DBI in the sky," PRD **70** (2004) 123505 arXiv:hep-th/0404084.

[15] B. Allen, "Vacuum States in de Sitter Space," Phys. Rev. D **32** (1985) 3136.

[16] L. Amendola, C. Quercellini and E. Giallongo, "Constraints on perfect fluid and scalar field dark energy models from future redshift surveys," MNRAS **357** (2005) 429 arXiv:astro-ph/0404599.

[17] A. Anderson and R. H. Price, "Intertwining of the equations of black hole perturbations," Phys. Rev. D **43** (1991) 3147.

[18] N. Andersson and B. P. Jensen, "Scattering by black holes. Chapter 0.1," In *Pike, R. (ed.) et al.: Scattering, vol. 2* 1607-1626 arXiv:gr-qc/0011025.

[19] L. Andersson and A. Coley, "Inhomogeneous cosmological models and averaging in cosmology: overview," Class. Quant. Grav. **28** (2011) 160301.

[20] S. Andrianomena, C. Clarkson, P. Patel, O. Umeh and J. -P. Uzan, "Non-linear relativistic contributions to the cosmological weak-lensing convergence," arXiv:1402.4350

[21] R. L. Arnowitt, S. Deser and C. W. Misner, "The Dynamics of general relativity," Gen. Rel. Grav. **40** (2008) 1997 arXiv:gr-qc/0405109.

[22] M. E. Araujo, W. R. Stoeger, R. C. Arcuri and M. L. Bedran, "Solving Einstein Field Equations in Observational Coordinates with Cosmological Data Functions: Spherically Symmetric Universes with Cosmological Constant," Phys. Rev. D **78** (2008) 063513 arXiv:0807.4193.

[23] M. E. Araujo and W. R. Stoeger, "Obtaining the time evolution for spherically symmetric Lemaitre-Tolman-Bondi models given data on our past light cone," Phys. Rev. D **80** (2009) 123517 [Erratum-ibid. D **81** (2010) 049903] arXiv:0904.0730.

[24] M. E. Araujo and W. R. Stoeger, "Finding a Spherically Symmetric Cosmology from Observations in Observational Coordinates – Advantages and Challenges," JCAP **1107** (2011) 029 arXiv:1011.6110.

[25] F. Arroja, S. Mizuno and K. Koyama, "Non-gaussianity from the bispectrum in general multiple field inflation," JCAP **0808** (2008) 015 arXiv:0806.0619.

[26] F. Arroja, S. Mizuno, K. Koyama and T. Tanaka, "On the full trispectrum in single field DBI-inflation," PRD **80** (2009) 043527 arXiv:0905.3641.

[27] J. Asorey, M. Crocce, E. Gaztanaga and A. Lewis, "Recovering 3D clustering information with angular correlations," arXiv:1207.6487.

[28] J. Asorey, M. Crocce and E. Gaztanaga, "Redshift-space distortions from the cross-correlation of photometric populations," arXiv:1305.0934.

[29] Y. Ayaita, B. M. Schaefer and M. Weber, "Investigating clustering dark energy with 3d weak cosmic shear," MNRAS **422** (2012) 3056 arXiv:arXiv:1110.1985.

[30] D. Babich, "Optimal estimation of non-Gaussianity," PRD **72** (2005) 043003 arXiv:astro-ph/0503375.

[31] D. J. Bacon, A. R. Refregier and R. S. Ellis, "Detection of weak gravitational lensing by large-scale structure," MNRAS **318** (2000) 625 arXiv:astro-ph/0003008.

[32] D. J. Bacon and A. N. Taylor, "Mapping the 3-d dark matter potential with weak shear," Mon. Not. Roy. Astron. Soc. **344** (2003) 1307 arXiv:astro-ph/0212266.

[33] D. J. Bacon, D. M. Goldberg, B. T. P. Rowe and A. N. Taylor, "Weak gravitational flexion," MNRAS **365** (2006) 414 arXiv:astro-ph/0504478.

[34] W. Ballinger, A. F. Heavens and A. N. Taylor, "The real-space power spectrum of IRAS galaxies on large scales and the redshift distortion," MNRAS **276** (1995) 59

[35] J. M. Bardeen, "Gauge Invariant Cosmological Perturbations," Phys. Rev. D **22** (1980) 1882.

[36] J. M. Bardeen, J. R. Bond, N. Kaiser and A. S. Szalay, "The Statistics of Peaks of Gaussian Random Fields," ApJ **304** (1986) 15.

[37] N. Barnaby and M. Peloso, "Large Nongaussianity in Axion Inflation," Phys. Rev. Lett. **106** (2011) 181301 arXiv:1011.1500.

[38] N. Barnaby, E. Pajer and M. Peloso, "Gauge Field Production in Axion Inflation: Consequences for Monodromy, non-Gaussianity in the CMB, and Gravitational Waves at Interferometers," PRD **85** (2012) 023525 arXiv:1110.3327.

[39] R. K. Barrett and C. A. Clarkson, "Undermining the cosmological principle: almost isotropic observations in inhomogeneous cosmologies," Class. Quantum Grav. **17** (2000) 5047, arXiv:astro-ph/9911235.

[40] M. Bartelmann and P. Schneider, "Weak gravitational lensing," Phys. Rept. **340** (2001) 291 arXiv:astro-ph/9912508

[41] N. Bartolo, E. Dimastrogiovanni, S. Matarrese and A. Riotto, "Anisotropic bispectrum of curvature perturbations from primordial non-Abelian vector fields," JCAP **0910** (2009) 015 arXiv:0906.4944.

[42] N. Bartolo, M. Fasiello, S. Matarrese and A. Riotto, "Large non-Gaussianities in the Effective Field Theory Approach to Single-Field Inflation: the Trispectrum," JCAP **1009** (2010) 035 arXiv:1006.5411.

[43] T. Battefeld and R. Easther, "Non-Gaussianities in Multi-field Inflation," JCAP **0703** (2007) 020 arXiv:astro-ph/0610296.

[44] D. Baumann *et al.* [CMBPol Study Team Collaboration], "CMBPol Mission Concept Study: Probing Inflation with CMB Polarization," AIP Conf. Proc. **1141** (2009) 10 arXiv:0811.3919.

[46] D. Baumann, "TASI Lectures on Inflation," arXiv:0907.5424.

[46] D. Baumann and L. McAllister, "Advances in Inflation in String Theory," Ann. Rev. Nucl. Part. Sci. **59** (2009) 67 arXiv:0901.0265.

[47] D. Baumann and D. Green, "Equilateral Non-Gaussianity and New Physics on the Horizon," JCAP **1109** (2011) 014 arXiv:arXiv:1102.5343.

[48] R. Bean, X. Chen, H. Peiris and J. Xu, "Comparing Infrared Dirac-Born-Infeld Brane Inflation to Observations," PRD **77** (2008) 023527 arXiv:0710.1812.

[49] C. Beisbart, T. Buchert and H. Wagner, "Morphometry of spatial patterns," Physica A **293** (2001) 592 arXiv:astro-ph/0007459.

[50] C. Beisbart, R. Dahlke, K. Mecke and H. Wagner "Characterizing cluster morphology using vector-valued Minkowski functionals," physics/0203072.

[51] N. Benitez, E. Gaztanaga, R. Miquel, F. Castander, M. Moles, M. Crocce, A. Fernandez-Soto and P. Fosalba *et al.*, "Measuring Baryon Acoustic Oscillations along the line of sight with photometric redshifs: the PAU survey," ApJ **691** (2009) 241 arXiv:0807.0535.

[52] F. Bernardeau, "The Effects of smoothing on the statistical properties of large scale cosmic fields," Astron. Astrophys. **291** (1994) 697 arXiv:astro-ph/9403020.

[53] F. Bernardeau, "Skewness and Kurtosis in large scale cosmic fields," Astrophys. J. **433** (1994) 1 arXiv:astro-ph/9312026.

[54] F. Bernardeau, S. Colombi, E. Gaztanaga and R. Scoccimarro, "Large scale structure of the universe and cosmological perturbation theory," Phys. Rept. **367** (2002) 1 arXiv:astro-ph/0112551.

[55] F. Bernardeau, C. Bonvin and F. Vernizzi, "Full-sky lensing shear at second order," PRD **81**, 083002 (2010) arXiv:0911.2244

[56] F. Bernardeau, C. Bonvin, N. Van de Rijt and F. Vernizzi, "Cosmic shear bispectrum from second-order perturbations in General Relativity," PRD **86** (2012) 023001 arXiv:1112.4430.

[57] G. M. Bernstein and M. Jarvis, "Shapes and shears, stars and smears: optimal measurements for weak lensing," Astron. J. **123** (2002) 583 arXiv:astro-ph/0107431.

[58] G. Betschart and C. A. Clarkson, "Scalar and electromagnetic perturbations on LRS class II space-times," CQG **21** (2004) 5587 arXiv:gr-qc/0404116.

[59] D. Bianchi, L. Guzzo, E. Branchini, E. Majerotto, S. de la Torre, F. Marulli, L. Moscardini and R. E. Angulo, "Statistical and systematic errors in redshift-space distortion measurements from large surveys," MNRAS **427** (2012) 2420 arXiv:1203.1545.

[60] J. Binney and T. Quinn, MNRAS **249** (1991) 678-683 "Gaussian random fields in spherical coordinates,"

[61] G. D. Birkhoff, "Relativity and Modern Physics," Cambridge, MA: Harvard University Press (1923).

[62] C. Blake, D. Parkinson, B. Bassett, K. Glazebrook, M. Kunz and R. C. Nichol, "Universal fitting formulae for baryon oscillation surveys," MNRAS **365** (2006) 255 arXiv:astro-ph/0510239.

[63] C. Blake, T. Davis, G. Poole, D. Parkinson, S. Brough, M. Colless, C. Contreras and W. Couch *et al.*, "The WiggleZ Dark Energy Survey: testing the cosmological model with baryon acoustic oscillations at z=0.6," Mon. Not. Roy. Astron. Soc. **415** (2011) 2892 arXiv:1105.2862.

[64] W. Blaschke, *Integralgeometrie*. Erstes Heft, (1936), Bernd G. Teubner, Leipzig, Berlin.

[65] J. N. Bregman, "The Search for the Missing Baryons at Low Redshift," Ann. Rev. Astron. Astrophys. **45** (2007) 221 arXiv:0706.1787.

[66] M. L. Brown, P. G. Castro and A. N. Taylor, "CMB temperature and polarisation pseudo-C(l) estimators and covariances," MNRAS **360** (2005) 1262 arXiv:astro-ph/0410394.

[67] K. Bolejko, C. Hellaby and A. H. A. Alfedeel, "The Metric of the Cosmos from Luminosity and Age Data," JCAP **1109** (2011) 011 arXiv:1102.3370.

[68] J. R. Bond and A. S. Szalay, "The Collisionless Damping of Density Fluctuations in an Expanding Universe," Astrophys. J. **274** (1983) 443.

[69] J. R. Bond and G. Efstathiou, "Cosmic background radiation anisotropies in universes dominated by nonbaryonic dark matter," ApJ **285** (1984) L45.

[70] J. R. Bond, S. Cole, G. Efstathiou and N. Kaiser, "Excursion set mass functions for hierarchical Gaussian fluctuations," ApJ **379** (1991) 440.

[71] H. Bondi, "Spherically symmetric models in general relativity," MNRAS **107** (1947) 410.

[72] C. Bonvin, "Effect of Peculiar Motion in Weak Lensing," PRD **78** (2008) 123530 arXiv:0810.0180

[73] T. Buchert and S. Räsänen, "Backreaction in late-time cosmology," Ann. Rev. Nucl. Part. Sci. **62** (2012) 57 arXiv:1112.5335.

[74] F. R. Bouchet *et al.* [COrE Collaboration], "COrE (Cosmic Origins Explorer) A White Paper," arXiv:1102.2181.

[75] R. Brunetti, K. Fredenhagen and S. Hollands, "A Remark on alpha vacua for quantum field theories on de Sitter space," JHEP **0505** (2005) 063 arXiv:hep-th/0503022.

[76] M. Bruni, P. K. S. Dunsby and G. F. R. Ellis, "Cosmological perturbations and the physical meaning of gauge invariant variables," Astrophys. J. **395** (1992) 34.

[77] M. Bruni, S. Matarrese, S. Mollerach and S. Sonego, "Perturbations of space-time: Gauge transformations and gauge invariance at second order and beyond," Class. Quant. Grav. **14** (1997) 2585 arXiv:gr-qc/9609040.

[78] M. Bruni and S. Sonego, "Observables and gauge invariance in the theory of nonlinear space-time perturbations: Letter to the editor," Class. Quant. Grav. **16** (1999) L29 arXiv:gr-qc/9906017.

[79] M. Bruni, R. Crittenden, K. Koyama, R. Maartens, C. Pitrou and D. Wands, "Disentangling non-Gaussianity, bias and GR effects in the galaxy distribution," PRD **85** (2012) 041301 arXiv:1106.3999

[80] C. Burrage, R. H. Ribeiro and D. Seery, "Large slow-roll corrections to the bispectrum of noncanonical inflation," JCAP **1107** (2011) 032 arXiv:1103.4126.

[81] R. B. Burston and A. W. C. Lun, "Covariant Schwarzschild perturbations. I: Initial value formulation for scalars of spin-weight +- 2," arXiv:gr-qc/0611052.

[82] R. B. Burston, "1+1+2 gravitational perturbations on LRS class II space-times: Decoupling GEM tensor harmonic amplitudes," Class. Quant. Grav. **25** (2008) 075004 arXiv:0708.1812.

[83] R. B. Burston, "1+1+2 gravitational perturbations on LRS class II space-times: GEM scalar harmonic amplitudes," Class. Quantum Grav. **25** (2008) 235004 arXiv:0708.2558, arXiv:0708.2559

[84] P. Cabella, F. K. Hansen, M. Liguori, D. Marinucci, S. Matarrese, L. Moscardini and N. Vittorio, "The integrated bispectrum as a test of cmb non-gaussianity: detection power and limits on f(nl) with wmap data," MNRAS **369** (2006) 819 arXiv:astro-ph/0512112.

[85] S. Calogero and J. M. Heinzle, "Bianchi Cosmologies with Anisotropic Matter: Locally Rotationally Symmetric Models," Physica D **240** (2011) 636 arXiv:0911.0667.

[86] A. Canavezes, V. Springel, S. J. Oliver, M. Rowan-Robinson, O. Keeble, S. D. M. White, W. Saunders and G. Efstathiou *et al.*, "The Topology of the IRAS Point Source Catalogue Redshift Survey," MNRAS **297** (1998) 777 arXiv:astro-ph/9712228.

[87] C. Carbone, L. Verde and S. Matarrese, "Non-Gaussian halo bias and future galaxy surveys," ApJ **684** (2008) L1 arXiv:0806.1950.

[88] J. Carlson, M. White and N. Padmanabhan, "A critical look at cosmological perturbation theory techniques," PRD **80** (2009) 043531 arXiv:0905.0479.

[89] S. Carroll, "Spacetime and Geometry: An Introduction to General Relativity," Addinson-Wesley (2003)

[90] P. G. Castro, A. F. Heavens and T. D. Kitching, "Weak lensing analysis in three dimensions," PRD **72** (2005) 023516 arXiv:astro-ph/0503479

[91] R. Cen and J. P. Ostriker, "Where are the baryons?," ApJ **514** (1999) 1 arXiv:astro-ph/9806281.

[92] R. Cen and J. P. Ostriker, "Where are the baryons? 2. feedback effects," ApJ **650** (2006) 560 arXiv:astro-ph/0601008.

[93] A. Challinor and A. Lasenby, "A Covariant and gauge invariant analysis of CMB anisotropies from scalar perturbations," PRD **58** (1998) 023001 arXiv:astro-ph/9804150

[94] A. Challinor and A. Lasenby, "Cosmic microwave background anisotropies in the CDM model: A Covariant and gauge invariant approach," Astrophys. J. **513** (1999) 1 arXiv:astro-ph/9804301.

[95] A. Challinor, "Microwave background anisotropies from gravitational waves: The (1+3) covariant approach," Class. Quant. Grav. **17** (2000) 871 arXiv:astro-ph/9906474.

[96] S. Chandrasekhar, "On the equations governing the perturbations of the Schwarzschild black hole,âĂİ Proc. R. Soc. London, Ser. A **343** (1975) 289âĂŞ298.

[97] S. Chandrasekhar and S. L. Detweiler, "The quasi-normal modes of the Schwarzschild black hole," Proc. Roy. Soc. Lond. A **344** (1975) 441.

[98] T. -C. Chang, U. -L. Pen, J. B. Peterson and P. McDonald, "Baryon Acoustic Oscillation Intensity Mapping as a Test of Dark Energy," Phys. Rev. Lett. **100** (2008) 091303 arXiv:0709.3672.

[99] X. Chen, M. x. Huang, S. Kachru and G. Shiu, "Observational signatures and non-Gaussianities of general single field inflation," JCAP **0701** (2007) 002 arXiv:hep-th/0605045.

[100] X. Chen, "Primordial Non-Gaussianities from Inflation Models," Adv. Astron. **2010** (2010) 638979 arXiv:1002.1416

[101] A. J. Christopherson, K. A. Malik, D. R. Matravers and K. Nakamura, "Comparing different formulations of non-linear cosmological perturbation theory," Class. Quant. Grav. **28** (2011) 225024 arXiv:1101.3525.

[102] C. A. Clarkson and R. Barrett, "Does the isotropy of the CMB imply a homogeneous universe? Some generalized EGS theorems," Class. Quant. Grav. **16** (1999) 3781 arXiv:gr-qc/9906097.

[103] C. A. Clarkson and R. K. Barrett, "Covariant perturbations of Schwarzschild black holes," CQG **20** (2003) 3855 arXiv:gr-qc/0209051

[104] C. A. Clarkson, M. Marklund, G. Betschart and P. K. S. Dunsby, "The electromagnetic signature of black hole ringdown," ApJ **613** (2004) 492 arXiv:astro-ph/0310323

[105] C. Clarkson, "A Covariant approach for perturbations of rotationally symmetric spacetimes," PRD **76** (2007) 104034 arXiv:0708.1398

[106] C. Clarkson, T. Clifton and S. February, "Perturbation Theory in Lemaitre-Tolman-Bondi Cosmology," JCAP **0906** (2009) 025 arXiv:0903.5040

[107] C. Clarkson and R. Maartens, "Inhomogeneity and the foundations of concordance cosmology," CQG **27** (2010) 124008 arXiv:1005.2165

[108] C. Clarkson, G. F. R. Ellis, A. Faltenbacher, R. Maartens, O. Umeh and J. -P. Uzan, "(Mis-)Interpreting supernovae observations in a lumpy universe," MNRAS **426** (2012) 1121 arXiv:1109.2484

[109] C. Clarkson, G. Ellis, J. Larena and O. Umeh, "Does the growth of structure affect our dynamical models of the universe? The averaging, backreaction and fitting problems in cosmology," Rept. Prog. Phys. **74** (2011) 112901 arXiv:1109.2314.

[110] C. Clarkson, "Establishing homogeneity of the universe in the shadow of dark energy," Comptes Rendus Physique **13** (2012) 682 arXiv:1204.5505

[111] T. Clifton, P. G. Ferreira, A. Padilla and C. Skordis, "Modified Gravity and Cosmology," Phys. Rept. **513** (2012) 1 arXiv:1106.2476

[112] S. Cole, K. B. Fisher and D. H. Weinberg, "Fourier analysis of redshift space distortions and the determination of Omega," Mon. Not. Roy. Astron. Soc. **267** (1994) 785 arXiv:astro-ph/9308003.

[113] P. Coles, "Statistical geometry and the microwave background," MNRAS **234** (1988) 509

[114] P. Coles and M. Plionis, "Topology in two dimensions. I - The Lick Galaxy Catalogue," MNRAS **250** (1991) 75.

[115] P. Coles, A. G. Davies and R. C. Pearson, "Quantifying the topology of large scale structure," arXiv:astro-ph/9603139.

[116] P. Coles and P. Erdogdu, "Scale-dependent Galaxy Bias," JCAP **0710** (2007) 007 arXiv:0706.0412.

[117] P. Coles and F. Lucchin, "Cosmology: The Origin and evolution of cosmic structure," Chichester, UK: Wiley (2002) 492 p

[118] W. N. Colley, J. R. Gott and C.Park, MNRAS **281** (1996) 4 L82-L84 arXiv:astro-ph/9601084v1.

[119] M. Colless, B. A. Peterson, C. Jackson, J. A. Peacock, S. Cole, P. Norberg, I. K. Baldry and C. M. Baugh *et al.*, "The 2dF Galaxy Redshift Survey: Final data release," arXiv:astro-ph/0306581.

[120] C. B. Collins and S. W. Hawking, "Why is the Universe isotropic?," Astrophys. J. **180** (1973) 317.

[121] C. B. Collins and S. W. Hawking, "The rotation and distortion of the Universe," Mon. Not. Roy. Astron. Soc. **162** (1973) 307.

[122] H. Collins, R. Holman and M. R. Martin, "The Fate of the alpha vacuum," PRD **68** (2003) 124012 arXiv:hep-th/0306028.

[123] H. Collins, "Primordial non-Gaussianities from inflation," arXiv:1101.1308.

[124] A. Cooray, W. Hu and J. Miralda-Escude, "Weak lensing by large scale structure: A Dark matter halo approach," Astrophys. J. **535** (2000) L9 arXiv:astro-ph/0003205.

[125] A. Cooray, W. Hu and M. Tegmark, "Large scale Sunyaev-Zel'dovich effect: Measuring statistical properties with multifrequency maps," ApJ **540** (2000) 1 arXiv:astro-ph/0002238.

[126] A. Cooray, "Large scale pressure fluctuations and the Sunyaev-Zel'dovich effect," PRD **62** (2000) 103506 arXiv:astro-ph/0005287.

[127] A. Cooray, "Non/gussian aspects of thermal and kinetic Sunyaev-Zel'dovich effects," PRD **64** (2001) 063514 arXiv:astro-ph/0105063.

[128] A. Cooray and W. Hu, "Weak gravitational lensing bispectrum," ApJ **548** (2001) 7 arXiv:astro-ph/0004151.

[129] A. Cooray and W. Hu, "Second order corrections to weak lensing by large scale structure," Astrophys. J. **574** (2002) 19 arXiv:astro-ph/0202411.

[130] A. Cooray and R. K. Sheth, "Halo models of large scale structure," Phys. Rept. **372** (2002) 1 arXiv:astro-ph/0206508.

[131] P. Creminelli, "On non-Gaussianities in single-field inflation," JCAP **0310** (2003) 003 arXiv:astro-ph/0306122.

[132] P. Creminelli, A. Nicolis, L. Senatore, M. Tegmark and M. Zaldarriaga, "Limits on non-gaussianities from wmap data," JCAP **0605** (2006) 004 arXiv:astro-ph/0509029.

[133] M. Crocce and R. Scoccimarro, "Nonlinear Evolution of Baryon Acoustic Oscillations," PRD **77** (2008) 023533 arXiv:0704.2783.

[134] M. Crocce, P. Fosalba, F. J. Castander and E. Gaztanaga, "Simulating the Universe with MICE: The abundance of massive clusters," MNRAS **403** (2010) 1353 arXiv:0907.0019.

[135] M. W. Crofton, "On the theory of local probability, applied to straight lines drawn at random in a plane; the methods used being also extended to the proof of certain new theorems in the integral calculus," Phil. Trans. Roy. Soc. London **158** (1868) 181-199.

[136] N. Dalal, O. Dore, D. Huterer and A. Shirokov, "The imprints of primordial non-gaussianities on large-scale structure: scale dependent bias and abundance of virialized objects," PRD **77** (2008) 123514 arXiv:0710.4560.

[137] U. H. Danielsson, "A Note on inflation and transPlanckian physics," PRD **66** (2002) 023511 arXiv:hep-th/0203198.

[138] U. H. Danielsson, "Transplanckian energy production and slow roll inflation," PRD **71** (2005) 023516 arXiv:hep-th/0411172.

[139] R. Dave, R. Cen, J. P. Ostriker, G. L. Bryan, L. Hernquist, N. Katz, D. H. Weinberg and M. L. Norman *et al.*, "Baryons in the warm-hot intergalactic medium," ApJ **552** (2001) 473 arXiv:astro-ph/0007217.

[140] J. de Boer, V. Jejjala and D. Minic, "Alpha-states in de Sitter space," PRD **71** (2005) 044013 arXiv:hep-th/0406217.

[141] A. De Felice and S. Tsujikawa, "f(R) theories," Living Rev. Rel. **13**, 3 (2010) arXiv:1002.4928

[142] S. de la Torre and L. Guzzo, "Modelling non-linear redshift-space distortions in the galaxy clustering pattern: systematic errors on the growth rate parameter," arXiv:1202.5559.

[143] R. de Putter and M. Takada, "Halo-Galaxy Lensing: A Full Sky Approach," PRD **82** (2010) 103522 arXiv:1007.4809

[144] V. Desjacques and U. Seljak, "Primordial non-Gaussianity in the large scale structure of the Universe," (2010) arXiv:1006.4763

[145] G. De Troia, P. A. R. Ade, J. J. Bock, J. R. Bond, J. Borrill, A. Boscaleri, P. Cabella and C. R. Contaldi *et al.*, "Searching for non-Gaussian signals in the BOOMERanG 2003 CMB maps," ApJ **670** (2007) L36 arXiv:0705.1615.

[146] M. Dias, "Cosmology at the boundary of de Sitter using the dS/QFT correspondence," PRD **84** (2011) 023512 arXiv:1104.0625.

[147] E. Dimastrogiovanni and N. Bartolo, "One-loop graviton corrections to the curvature perturbation from inflation," JCAP **0811** (2008) 016 arXiv:0807.2790.

[148] E. Dimastrogiovanni, N. Bartolo, S. Matarrese and A. Riotto, "Non-Gaussianity and Statistical Anisotropy from Vector Field Populated Inflationary Models," Adv. Astron. **2010** (2010) 752670 arXiv:1001.4049.

[149] D. Dolney, B. Jain and M. Takada, "Baryon oscillations and dark-energy constraints from imaging surveys," MNRAS **366** (2006) 884 arXiv:astro-ph/0409445.

[150] E. M. Duffy and B. C. Nolan, "Odd Parity Perturbations of the Self-Similar LTB Spacetime," CQG **28** (2011) 105020 arXiv:1012.2766

[151] J. Dunkley, R. Hlozek, J. Sievers, V. Acquaviva, P. A. R. Ade, P. Aguirre, M. Amiri and J. W. Appel *et al.*, "The Atacama Cosmology Telescope: Cosmological Parameters from the 2008 Power Spectra," ApJ **739** (2011) 52 arXiv:1009.0866.

[152] P. Dunsby, N. Goheer, B. Osano and J. -P. Uzan, "How close can an Inhomogeneous Universe mimic the Concordance Model?," JCAP **1006**, 017 (2010) arXiv:1002.2397

[153] R. Durrer, "The theory of CMB anisotropies," J. Phys. Stud. **5** (2001) 177 [astro-ph/0109522].

[154] R. Durrer, "The Cosmic Microwave Background," (2008), Cambridge University Press, Cambridge, UK.

[155] R. Easther, B. R. Greene, W. H. Kinney and G. Shiu, "Inflation as a probe of short distance physics," PRD **64** (2001) 103502 arXiv:hep-th/0104102.

[156] R. Easther, B. R. Greene, W. H. Kinney and G. Shiu, "A Generic estimate of transPlanckian modifications to the primordial power spectrum in inflation," PRD **66** (2002) 023518 arXiv:hep-th/0204129.

[157] G. Efstathiou, M. Davis, C. S. Frenk and S. D. M. White, "Numerical Techniques for Large Cosmological N-Body Simulations," Astrophys. J. Suppl. **57** (1985) 241.

[158] G. Efstathiou, "A Maximum likelihood analysis of the low CMB multipoles from WMAP," Mon. Not. Roy. Astron. Soc. **348** (2004) 885 arXiv:astro-ph/0310207.

[159] J. Ehlers, "Contributions to the relativistic mechanics of continuous media," Gen. Rel. Grav. **25** (1993) 1225 [Abh. Akad. Wiss. Lit. Mainz. Nat. Kl. **11** (1961) 793].

[160] J. Ehlers, P. Geren and R. K. Sachs, "Isotropic solutions of the Einstein-Liouville equations," J. Math. Phys. **9** (1968) 1344.

[161] G. F. R. Ellis, "Dynamics of pressure free matter in general relativity," J. Math. Phys. **8** (1967) 1171.

[162] G. F. R. Ellis and M. A. H. MacCallum, "A Class of homogeneous cosmological models," Commun. Math. Phys. **12** (1969) 108.

[163] G. F. R. Ellis, Proceedings of the International School of Physics "Enrico Fermi", Course 47: General relativity and cosmology, Ed. R.K. Sachs, Academic Press, 1971, pp. 104-182.

[164] G. F. R. Ellis, S. D. Nel, R. Maartens, W. R. Stoeger and A. P. Whitman, "Ideal Observational Cosmology," Phys. Rept. **124** (1985) 315.

[165] G. F. R. Ellis and M. Bruni, "Covariant and Gauge Invariant Approach to Cosmological Density Fluctuations," PRD **40** (1989) 1804.

[166] G. F. R. Ellis and H. van Elst, "Cosmological models: Cargese lectures 1998," NATO Adv. Study Inst. Ser. C. Math. Phys. Sci. **541** (1999) 1 arXiv:gr-qc/9812046

[167] G. F. R. Ellis, "The Space of cosmological space-times," J. Hyperbol. Diff. Equat. **2** (2005) 331. Miami Waves 2004, Lecture Notes I.

[168] G. F. R. Ellis, "Issues in the philosophy of cosmology," arXiv:astro-ph/0602280.

[169] G. F. R. Ellis, "The Bianchi models: Then and now," Gen. Rel. Grav. **38** (2006) 1003.

[170] G. F. R. Ellis, "Inhomogeneity effects in Cosmology," Class. Quant. Grav. **28** (2011) 164001 arXiv:1103.2335.

[171] G. F. R. Ellis and R. Goswami, "Variations on Birkhoff's theorem," Gen. Rel. Grav. **45** (2013) 2123 [arXiv:1304.3253 [gr-qc]]. arXiv:1304.3253

[172] G. F. R. Ellis, R. Maartens and M. A. H. MacCallum, "Relativistic Cosmology," Cambridge University Press, Cambridge, 2012.

[173] A. Einstein, "The Foundation of the General Theory of Relativity," Annalen Phys. **49** (1916) 769 [Annalen Phys. **14** (2005) 517].

[174] D. J. Eisenstein and W. Hu, "Power spectra for cold dark matter and its variants," ApJ **511** (1997) 5 arXiv:astro-ph/9710252.

[175] D. J. Eisenstein and W. Hu, "Baryonic features in the matter transfer function," ApJ **496** (1998) 605 arXiv:astro-ph/9709112.

[176] D. J. Eisenstein *et al.* [SDSS Collaboration], "Detection of the baryon acoustic peak in the large-scale correlation function of SDSS luminous red galaxies," ApJ **633** (2005) 560 arXiv:astro-ph/0501171.

[177] P. Erdogdu, O. Lahav, J. P. Huchra, M. Colless, R. M. Cutri, E. Falco, T. George and T. Jarrett *et al.*, "Reconstructed Density and Velocity Fields from the 2MASS Redshift Survey," MNRAS **373** (2006) 45 arXiv:astro-ph/0610005.

[178] H. K. Eriksen, D. I. Novikov, P. B. Lilje, A. J. Banday and K. M. Gorski, "Testing for non-Gaussianity in the WMAP data: Minkowski functionals and the length of the skeleton," ApJ **612** (2004) 64 arXiv:astro-ph/0401276.

[179] N. A. Fava and L. A. Santalo, "Random processes of manifolds in Rn," Z. Wahrscheinlichkeitstheorie verw. Gebiete **50** (1979) 85âĂŞ96.

[180] S. February, C. Clarkson and R. Maartens, "Galaxy correlations and the BAO in a void universe: structure formation as a test of the Copernican Principle," JCAP **1303** (2013) 023 arXiv:1206.1602

[181] S. February, J. Larena, C. Clarkson and D. Pollney, "Evolution of linear perturbations in spherically symmetric dust models," arXiv:1311.5241 [astro-ph.CO].

[182] S. M. Feeney, H. V. Peiris and A. Pontzen, "Avoiding bias in reconstructing the largest observable scales from partial-sky data," PRD **84** (2011) 103002 arXiv:1107.5466.

[183] K. B. Fisher, C. A. Scharf and O. Lahav, "A Spherical Harmonic Approach to Redshift Distortion and a Measurement of Omega from the 1.2 Jy IRAS Redshift Survey," Mon. Not. Roy. Astron. Soc. **266** (1994) 219 arXiv:astro-ph/9309027.

[184] K. B. Fisher, O. Lahav, Y. Hoffman, D. Lynden-Bell and S. Zaroubi, "Wiener reconstruction of density, velocity, and potential fields from all sky galaxy redshift surveys," MNRAS **272** (1995) 885.

[185] R. Flauger and E. Pajer, "Resonant Non-Gaussianity," JCAP **1101** (2011) 017 arXiv:1002.0833.

[186] P. Franche, R. Gwyn, B. Underwood and A. Wissanji, "Attractive Lagrangians for Non-Canonical Inflation," Phys. Rev. D **81** (2010) 123526 arXiv:0912.1857.

[187] A. Friedman, Zeitschrift für Physik **10** (1922) 377-386.

[188] A. Friedmann, Zeitschrift für Physik **21** (1924) 326-332.

[189] J. N. Fry, "The Galaxy correlation hierarchy in perturbation theory," ApJ **279** (1984) 499.

[190] J. N. Fry and E. Gaztanaga, "Biasing and hierarchical statistics in large scale structure," ApJ **413** (1993) 447 arXiv:astro-ph/9302009.

[191] J. W. Fowler *et al.* [ACT Collaboration], "The Atacama Cosmology Telescope: A Measurement of the 600< ell <8000 Cosmic Microwave Background Power Spectrum at 148 GHz," ApJ **722** (2010) 1148 arXiv:1001.2934.

[192] M. Fukugita and P. J. E. Peebles, "The Cosmic energy inventory," ApJ **616** (2004) 643 arXiv:astro-ph/0406095.

[193] M. Fukugita and P. J. E. Peebles, "Massive coronae of galaxies," ApJ **639** (2006) 590 arXiv:astro-ph/0508040.

[194] J. Garcia-Bellido and T. Haugboelle, "Confronting Lemaitre-Tolman-Bondi models with Observational Cosmology," JCAP **0804** (2008) 003 arXiv:0802.1523.

[195] J. Garcia-Bellido and T. Haugboelle, "The radial BAO scale and Cosmic Shear, a new observable for Inhomogeneous Cosmologies," JCAP **0909** (2009) 028 arXiv:0810.4939.

[196] A. Gangui, F. Lucchin, S. Matarrese and S. Mollerach, "The Three point correlation function of the cosmic microwave background in inflationary models," ApJ **430** (1994) 447 arXiv:astro-ph/9312033.

[197] E. Gaztanaga, R. Miquel and E. Sanchez, "First Cosmological Constraints on Dark Energy from the Radial Baryon Acoustic Scale," Phys. Rev. Lett. **103** (2009) 091302 arXiv:arXiv:0808.1921.

[198] E. Gaztanaga, M. Eriksen, M. Crocce, F. Castander, P. Fosalba, P. Marti, R. Miquel and A. Cabre, "Cross-Correlation of spectroscopic and photometric galaxy surveys: cosmology from lensing and redshift distortions," arXiv:1109.4852.

[199] T. Gebbie and G. F. R. Ellis, "GIC approach to cosmic background radiation anisotropies. Part 1.," Annals Phys. **282** (2006) 285 arXiv:astro-ph/9804316.

[200] T. Gebbie, P. Dunsby and G. F. R. Ellis, "(1+3) covariant cosmic microwave background anisotropies. 2. The Almost Friedmann Lemaitre model," Annals Phys. **282** (2000) 321 arXiv:astro-ph/9904408.

[201] U. H. Gerlach and U. K. Sengupta, "Gauge Invariant Perturbations On Most General Spherically Symmetric Space-times," PRD **19** (1979) 2268.

[202] U. H. Gerlach and U. K. Sengupta, "Gauge Invariant Coupled Gravitational, Acoustical, And Electromagnetic Modes On Most General Spherical Space-times," PRD **22** (1980) 1300.

[203] L. Gleser, A. Nusser, B. Ciardi and V. Desjacques, "The morphology of cosmological reionization by means of Minkowski functionals," MNRAS **370** (2006) 1329 arXiv:astro-ph/0602616.

[223] F. J. Greenberg, J. Math. Anal. and Applic. **30** (1970) 128.

[205] K. Godel, "An Example of a new type of cosmological solutions of Einstein's field equations of graviation," Rev. Mod. Phys. **21** (1949) 447.

[206] M. Goliath and G. F. R. Ellis, "Homogeneous cosmologies with cosmological constant," Phys. Rev. D **60** (1999) 023502 arXiv:gr-qc/9811068.

[207] D. M. Goldberg and D. N. Spergel, "Microwave background bispectrum. 2. A probe of the low redshift universe," PRD **59** (1999) 103001 arXiv:astro-ph/9811252.

[208] D. M. Goldberg and D. N. Spergel, "Microwave background bispectrum. 2. A probe of the low redshift universe," PRD **59** (1999) 103002 arXiv:astro-ph/9811251.

[209] D. M. Goldberg and P. Natarajan, "The galaxy octopole moment as a probe of weak lensing shear fields," ApJ **564** (2002) 65 arXiv:astro-ph/0107187.

[210] D. M. Goldberg and D. J. Bacon, "Galaxy-galaxy flexion: Weak lensing to second order," ApJ **619** (2005) 741 arXiv:astro-ph/0406376.

[211] M. H. Goroff, B. Grinstein, S. J. Rey and M. B. Wise, "Coupling of Modes of Cosmological Mass Density Fluctuations," ApJ **311** (1986) 6.

[212] J. R. Gott, III, M. Dickinson and A. L. Melott, "The Sponge - like topology of large - scale structure in the Universe," ApJ **306** (1986) 341.

[213] J. R. Gott, et al., ApJ **340** (1989) 625

[214] J. R. Gott, et al., ApJ **352** (1990) 1-14

[215] J. R. Gott, S. Mao, C. Park, O. Lahav, ApJ **385** (1992) 26

[216] S. Gossan, J. Veitch and B. S. Sathyaprakash, "Bayesian model selection for testing the no-hair theorem with black hole ringdowns," Phys. Rev. D **85** (2012) 124056 arXiv:1111.5819.

[217] R. Goswami and G. F. R. Ellis, "Almost Birkhoff Theorem in General Relativity," Gen. Rel. Grav. **43** (2011) 2157 arXiv:1101.4520

[218] R. Goswami and G. F. R. Ellis, "Birkhoff Theorem and Matter," Gen. Rel. Grav. **44** (2012) 2037 arXiv:1202.0240

[219] A. Goobar, S. Hannestad, E. Mortsell and H. Tu, "A new bound on the neutrino mass from the sdss baryon acoustic peak," JCAP **0606** (2006) 019 arXiv:astro-ph/0602155.

[220] E. Gourgoulhon, "3+1 formalism and bases of numerical relativity," arXiv:gr-qc/0703035.

[221] A. Grassi and B. M. Schaefer, "Detecting baryon acoustic oscillations by 3d weak lensing," arXiv:1303.1024.

[222] J. Green, P. Schechter, C. Baltay, R. Bean, D. Bennett, R. Brown, C. Conselice and M. Donahue *et al.*, "Wide-Field InfraRed Survey Telescope (WFIRST) Interim Report," arXiv:1108.1374.

[223] P. J. Greenberg, J. Math. Anal. Applic. **30** 128 (1970)

[224] B. Greene, M. Parikh and J. P. van der Schaar, "Universal correction to the inflationary vacuum," JHEP **0604** (2006) 057 arXiv:hep-th/0512243.

[225] L. P. Grishchuk, "Amplification of gravitational waves in an istropic universe," Sov. Phys. JETP **40** (1975) 409 [Zh. Eksp. Teor. Fiz. **67** (1974) 825].

[226] L. P. Grishchuk, "Graviton Creation in the Early Universe," Annals N. Y. Acad. Sci. **302** (1977) 439.

[227] L. P. Grishchuk and Y. .V. Sidorov, "Squeezed quantum states of relic gravitons and primordial density fluctuations," Phys. Rev. D **42** (1990) 3413.

[228] T. Guillet, R. Teyssier and S. Colombi, "The effect of baryons on the variance and the skewness of the mass distribution in the universe at small scales," MNRAS **405** (2010) 525 arXiv:0905.2615.

[229] C. Gundlach and J. M. Martin-Garcia, "Gauge invariant and coordinate independent perturbations of stellar collapse. 1. The Interior," PRD **61** (2000) 084024 arXiv:gr-qc/9906068

[230] J. E. Gunn and J. R. Gott, III, "On the Infall of Matter into Clusters of Galaxies and Some Effects on Their Evolution," ApJ **176** (1972) 1.

[231] A. H. Guth and S. Y. Pi, "Fluctuations in the New Inflationary Universe," Phys. Rev. Lett. **49** (1982) 1110.

[232] L. Guzzo, M. Pierleoni, B. Meneux, E. Branchini, O. L. Fevre, C. Marinoni, B. Garilli and J. Blaizot *et al.*, "A test of the nature of cosmic acceleration using galaxy redshift distortions," Nature **451** (2008) 541 arXiv:0802.1944.

[233] H. Hadwiger, *Altes und Neus über Konvexe Körper*, (1955), Birkhäuser, Basel.

[234] H. Hadwiger, *Vorlesungen über Inhalt, Oberfläche und Isoperimetrie*, (1957), Springer Verlag, Berlin.

[235] H. Hadwiger, *Das Wills'sche Funktional*. (1959)

[236] A. I. M. Hamid, R. Goswami and S. D. Maharaj, "Cosmic Censorship Conjecture revisited: Covariantly," arXiv:1402.4355

[237] A. J. S. Hamilton, "Measuring Omega and the real correlation function from the redshift correlation function," ApJ **385** (1992) L5.

[238] A. J. S. Hamilton, "Linear redshift distortions: A Review," arXiv:astro-ph/9708102.

[239] N. Hand, J. W. Appel, N. Battaglia, J R. Bond, S. Das, M. J. Devlin, J. Dunkley and R. Dunner *et al.*, "The Atacama Cosmology Telescope: Detection of Sunyaev-Zel'dovich Decrement in Groups and Clusters Associated with Luminous Red Galaxies," ApJ **736** (2011) 39 arXiv:arXiv:1101.1951.

[240] S. Hannestad, T. Haugbolle, P. R. Jarnhus and M. S. Sloth, "Non-Gaussianity from Axion Monodromy Inflation," JCAP **1006** (2010) 001 arXiv:0912.3527.

[241] D. Harlow and D. Stanford, "Operator Dictionaries and Wave Functions in AdS/CFT and dS/CFT," arXiv:1104.2621.

[242] S. W. Hawking, "Perturbations of an expanding universe," Astrophys. J. **145** (1966) 544.

[243] S. Hawking, "Gravitational radiation in an expanding universe," J. Math. Phys. **9** (1968) 598.

[244] S. W. Hawking and G. F. R. Ellis, "The Large scale structure of space-time," Cambridge University Press, Cambridge, 1973

[245] S. W. Hawking, "The Development of Irregularities in a Single Bubble Inflationary Universe," Phys. Lett. B **115** (1982) 295.

[246] O. Heckmann and E. Schücking, Zeits. f. Astroph.**38** (1955) 95 .

[247] A. F. Heavens and A. N. Taylor, "A Spherical Harmonic Analysis of Redshift Space," MNRAS **275** (1995) 483 arXiv:astro-ph/9409027.

[248] A. Heavens, "3d weak lensing," MNRAS **343** (2003) 1327 arXiv:astro-ph/0304151

[249] A. F. Heavens, T. D. Kitching and A. N. Taylor, "Measuring dark energy properties with 3D cosmic shear," MNRAS **373** (2006) 105 arXiv:astro-ph/0606568.

[250] J. P. Henry, "Measuring cosmological parameters from the evolution of cluster X-ray temperatures," ApJ **534** (2000) 565 arXiv:astro-ph/0002365.

[251] A. F. Heavens and A. N. Taylor, "A Spherical Harmonic Analysis of Redshift Space," MNRAS **275** (1995) 483 arXiv:astro-ph/9409027.

[252] A. F. Heavens, R. Jimenez and R. Maartens, "Testing homogeneity with the fossil record of galaxies," JCAP **1109** (2011) 035 arXiv:1107.5910

[253] C. Hellaby and A. H. A. Alfedeel, "Solving the Observer Metric," Phys. Rev. D **79** (2009) 043501 arXiv:0811.1676.

[254] C. Hernandez-Monteagudo, H. Trac, R. Jimenez and L. Verde, "The thermal Sunyaev-Zel'dovich Signature of Baryons in the Local Universe," ApJ **652** (2006) L1 arXiv:astro-ph/0606172.

[255] J. C. Hill and D. N. Spergel, "Detection of thermal SZ-CMB lensing cross-correlation in Planck nominal mission data," JCAP **1402** (2014) 030 arXiv:1312.4525.

[256] F. W. High, H. Hoekstra, N. Leethochawalit, T. de Haan, L. Abramson, K. A. Aird, R. Armstrong and M. L. N. Ashby *et al.*, "Weak-Lensing Mass Measurements of Five Galaxy Clusters in the South Pole Telescope Survey Using Magellan/Megacam," ApJ **758** (2012) 68 arXiv:1205.3103.

[257] C. Hikage *et al.* [SDSS Collaboration], "Three-dimensional genus statistics of galaxies in the SDSS early data release," Publ. Astron. Soc. Jap. **54** (2002) 707 arXiv:astro-ph/0207377.

[258] C. Hikage, A. Taruya and Y. Suto, "Biasing and genus statistics of dark matter halos in the Hubble volume simulation," Publ. Astron. Soc. Jap. **55** (2003) 335 [astro-ph/0302444].

[259] C. Hikage *et al.* [SDSS Collaboration], "Minkowski Functionals of SDSS galaxies. 1. Analysis of excursion sets," Publ. Astron. Soc. Jap. **55** (2003) 911 arXiv:astro-ph/0304455.

[260] C. Hikage, E. Komatsu and T. Matsubara, "Primordial Non-Gaussianity and Analytical Formula for Minkowski Functionals of the Cosmic Microwave Background and Large-scale Structure," ApJ **653** (2006) 11 arXiv:astro-ph/0607284.

[261] C. Hikage, T. Matsubara, P. Coles, M. Liguori, F. K. Hansen and S. Matarrese, "Limits on Primordial Non-Gaussianity from Minkowski Functionals of the WMAP Temperature Anisotropies," MNRAS **389** (2008) 1439 arXiv:0802.3677.

[262] C. Hikage, P. Coles, M. Grossi, L. Moscardini, K. Dolag, E. Branchini and S. Matarrese, "The Effect of Primordial Non–Gaussianity on the Topology of Large-Scale Structure," MNRAS **385** (2008) 1513 arXiv:0711.3603.

[263] C. Hikage, M. Takada and D. N. Spergel, "Using galaxy-galaxy weak lensing measurements to correct the Finger-of-God," MNRAS **419** (2012) 3457 arXiv:1106.1640.

[264] C. M. Hirata and U. Seljak, "Reconstruction of lensing from the cosmic microwave background polarization," Phys. Rev. D **68** (2003) 083002 arXiv:astro-ph/0306354.

[265] C. M. Hirata and U. Seljak, "Intrinsic alignment-lensing interference as a contaminant of cosmic shear," Phys. Rev. D **70** (2004) 063526 [Erratum-ibid. D **82** (2010) 049901] arXiv:astro-ph/0406275.

[266] E. Hivon, F. R. Bouchet, S. Colombi and R. Juszkiewicz, "Redshift distortions of clustering: A Lagrangian approach," A&A **298** (1995) 643 arXiv:astro-ph/9407049.

[267] E. Hivon, K. M. Gorski, C. B. Netterfield, B. P. Crill, S. Prunet and F. Hansen, "Master of the cosmic microwave background anisotropy power spectrum: a fast method for statistical analysis of large and complex cosmic microwave background data sets," ApJ **567** (2002) 2 arXiv:astro-ph/0105302.

[268] G. P. Holder, M. P. Viero, O. Zahn, K. A. Aird, B. A. Benson, S. Bhattacharya, L. E. Bleem and M. Brodwin *et al.*, "A Cosmic Microwave Background Lensing Mass Map and Its Correlation with the Cosmic Infrared Background," Astrophys. J. **771** (2013) L16 arXiv:1303.5048.

[269] S. Hotchkiss and S. Sarkar, "Non-Gaussianity from violation of slow-roll in multiple inflation," JCAP **1005** (2010) 024 arXiv:0910.3373.

[270] Z. Hou, C. L. Reichardt, K. T. Story, B. Follin, R. Keisler, K. A. Aird, B. A. Benson and L. E. Bleem *et al.*, "Constraints on Cosmology from the Cosmic Microwave Background Power Spectrum of the 2500-square degree SPT-SZ Survey," ApJ **782** (2014) 74 arXiv:1212.6267.

[271] W. Hu, "Weak lensing of the CMB: A harmonic approach," PRD **62** (2000) 043007 arXiv:astro-ph/0001303

[272] D. Huterer, "Weak lensing and dark energy," PRD **65** (2002) 063001 arXiv:astro-ph/0106399.

[273] D. Huterer, M. Takada, G. Bernstein and B. Jain, "Systematic errors in future weak lensing surveys: Requirements and prospects for self-calibration," MNRAS **366** (2006) 101 arXiv:astro-ph/0506030.

[274] K. Ioka and H. Nakano, "Second and higher-order quasi-normal modes in binary black hole mergers," Phys. Rev. D **76** (2007) 061503 arXiv:0704.3467.

[275] J. C. Jackson, "Fingers of God," MNRAS **156** (1972) 1 arXiv:arXiv:0810.3908.

[276] B. Jain and E. Bertschinger, "Second order power spectrum and nonlinear evolution at high redshift," ApJ **431** (1994) 495 arXiv:astro-ph/9311070.

[277] J.T. Jebsen, "ÃIJber die allgemeinen kugelsymmetrischen LÃűsungen der Einsteinschen Gravitationsgleichungen im Vakuum," Reprinted as a Golden Oldie: Ark.Mat.Astron.Fys. **15** (1921) 18

[278] A. Jenkins, C. S. Frenk, S. D. M. White, J. M. Colberg, S. Cole, A. E. Evrard, H. M. P. Couchman and N. Yoshida, "The Mass function of dark matter halos," MNRAS **321** (2001) 372 arXiv:astro-ph/0005260.

[279] D. Jeong and E. Komatsu, "Perturbation theory reloaded: analytical calculation of non-linearity in baryonic oscillations in the real space matter power spectrum," ApJ **651** (2006) 619 arXiv:astro-ph/0604075.

[280] D. Jeong and E. Komatsu, "Perturbation Theory Reloaded II: Non-linear Bias, Baryon Acoustic Oscillations and Millennium Simulation In Real Space," ApJ **691** (2009) 569 arXiv:0805.2632.

[281] D. Jeong and E. Komatsu, "Primordial non-Gaussianity, scale-dependent bias, and the bispectrum of galaxies," ApJ **703** (2009) 1230 arXiv:0904.0497.

[282] D. Jeong and E. Komatsu, "Perturbation Theory Reloaded II: Non-linear Bias, Baryon Acoustic Oscillations and Millennium Simulation In Real Space," ApJ **691** (2009) 569 arXiv:arXiv:0805.2632.

[283] S. Jhingan and T. Tanaka, "Improvement on the metric reconstruction scheme in Regge-Wheeler-Zerilli formalism," Phys. Rev. D **67** (2003) 104018 arXiv:gr-qc/0211060.

[284] S. Joudaki and M. Kaplinghat, "Dark Energy and Neutrino Masses from Future Measurements of the Expansion History and Growth of Structure," PRD **86** (2012) 023526 arXiv:1106.0299.

[285] R. Juszkiewicz, F. R. Bouchet and S. Colombi, "Skewness induced by gravity," Astrophys. J. **412** (1993) L9 arXiv:astro-ph/9306003.

[286] R. Juszkiewicz, D. H. Weinberg, P. Amsterdamski, M. Chodorowski and F. Bouchet, "Weakly nonlinear Gaussian fluctuations and the Edgeworth expansion," Astrophys. J. **442** (1995) 39.

[287] R. Juszkiewicz, W. A. Hellwing and R. van de Weygaert, "Skewness as a probe of Baryon Acoustic Oscillations," arXiv:1205.6163.

[288] S. Kachru, R. Kallosh, A. D. Linde and S. P. Trivedi, "De Sitter vacua in string theory," PRD **68** (2003) 046005 arXiv:hep-th/0301240.

[289] N. Kaiser, "Clustering in real space and in redshift space," MNRAS **227** (1987) 1.

[290] N. Kaiser, "Weak gravitational lensing of distant galaxies," ApJ **388** (1992) 272.

[291] I. Kamaretsos, M. Hannam, S. Husa and B. S. Sathyaprakash, "Black-hole hair loss: learning about binary progenitors from ringdown signals," Phys. Rev. D **85** (2012) 024018 arXiv:1107.0854.

[292] I. Kamaretsos, M. Hannam and B. Sathyaprakash, "Is black-hole ringdown a memory of its progenitor?," Phys. Rev. Lett. **109** (2012) 141102 arXiv:1207.0399.

[293] M. Kerscher, K. Mecke, J. Schmalzing, C. Beisbart, T. Buchert and H. Wagner, "Morphological fluctuations of large scale structure: The PSCz survey," A&A **373** (2001) 1 arXiv:astro-ph/0101238.

[294] T. D. Kitching, A. F. Heavens, A. N. Taylor, M. L. Brown, K. Meisenheimer, C. Wolf, M. E. Gray and D. J. Bacon, "Cosmological constraints from COMBO-17 using 3D weak lensing," MNRAS **376** (2007) 771 arXiv:astro-ph/0610284.

[295] T. D. Kitching, A. F. Heavens, L. Verde, P. Serra and A. Melchiorri, "Finding Evidence for Massive Neutrinos using 3D Weak Lensing," PRD **77** (2008) 103008 arXiv:0801.4565.

[296] T. D. Kitching, A. N. Taylor and A. F. Heavens, "Systematic effects on dark energy from 3D weak shear," MNRAS **389** (2008) 173 arXiv:0801.3270.

[297] T. D. Kitching, A. F. Heavens and L. Miller "3D Photometric Cosmic Shear," MNRAS **413** (2011) 4, 2923 arXiv:arXiv:1007.2953.

[298] J. J. Koenderink, "The Structure of Images," Biol. Cybern. **50** (1984) 363-370

[299] E. Komatsu and U. Seljak, "Universal gas density and temperature profile," MNRAS **327** (2001) 1353 arXiv:astro-ph/0106151.

[300] E. Komatsu and D. N. Spergel, "Acoustic signatures in the primary microwave background bispectrum," PRD **63** (2001) 063002 [astro-ph/0005036].

[301] E. Komatsu and U. Seljak, "The Sunyaev-Zel'dovich angular power spectrum as a probe of cosmological parameters," MNRAS **336** (2002) 1256 arXiv:astro-ph/0205468.

[302] E. Komatsu, D. N. Spergel and B. D. Wandelt, "Measuring primordial non-Gaussianity in the cosmic microwave background," ApJ **634** (2005) 14 arXiv:astro-ph/0305189.

[303] E. Komatsu *et al.* [WMAP Collaboration], "First year Wilkinson Microwave Anisotropy Probe (WMAP) observations: tests of gaussianity," ApJSuppl. **148** (2003) 119 arXiv:astro-ph/0302223.

[304] K. D. Kokkotas and B. G. Schmidt, "Quasinormal modes of stars and black holes," Living Rev. Rel. **2** (1999) 2 arXiv:gr-qc/9909058

[305] E. Komatsu *et al.* [WMAP Collaboration], "Seven-Year Wilkinson Microwave Anisotropy Probe (WMAP) Observations: Cosmological Interpretation," ApJSuppl. **192** (2011) 18 arXiv:1001.4538.

[306] K. Koyama, "Non-Gaussianity of quantum fields during inflation," CQG **27**, 124001 (2010) arXiv:1002.0600

[307] W. Kundt and M. Trümper, "Contributions to the theory of gravitational radiation fields," BeitrÃđge zur Theorie der Gravitations-Strahlungsfelder, Akad. Wiss. Mainz Nr. **12** (1962) 967-1000.

[308] D. Langlois, S. Renaux-Petel, D. A. Steer and T. Tanaka, "Primordial perturbations and non-Gaussianities in DBI and general multi-field inflation," PRD **78** (2008) 063523 arXiv:0806.0336.

[309] F. Lanusse, A. Rassat and J. L. Starck, "Spherical 3D Isotropic Wavelets," arXiv:1112.0561.

[310] A. Cimatti, R. Laureijs, B. Leibundgut, S. Lilly, R. Nichol, A. Refregier, P. Rosati and M. Steinmetz *et al.*, "Euclid Assessment Study Report for the ESA Cosmic Visions," arXiv:0912.0914.

[311] R. Laureijs *et al.* [EUCLID Collaboration], "Euclid Definition Study Report," arXiv:1110.3193.

[312] R. Lazkoz, R. Maartens and E. Majerotto, "Observational constraints on phantom-like braneworld cosmologies," PRD **74** (2006) 083510 arXiv:astro-ph/0605701.

[313] E. W. Leaver, "An Analytic representation for the quasi normal modes of Kerr black holes," Proc. Roy. Soc. Lond. A **402** (1985) 285.

[314] E. W. Leaver, "Spectral decomposition of the perturbation response of the Schwarzschild geometry," Phys. Rev. D **34** (1986) 384.

[315] J. M. Lee, "Topological Manifolds," Graduate Texts in Mathematics, Springer, 2nd Edition, 2010.

[316] B. Leistedt, A. Rassat, A. Refregier and J. L. Starck, "3DEX: a code for Fast Fourier-Bessel Decomposition of Spherical 3D Surveys," arXiv:1111.3591.

[317] B. Leistedt, H. V. Peiris, D. J. Mortlock, A. Ãľl. Benoit-LÃľvy and A. Pontzen, "Estimating the large-scale angular power spectrum in the presence of systematics: a case study of Sloan Digital Sky Survey quasars," arXiv:1306.0005.

[318] A. G. Lemaître, Annales de la Société Scientifique de Bruxelles **A53** (1933) 51.

[319] G. Lemaitre, "The expanding universe," Gen. Rel. Grav. **29**, 641 (1997) [Annales Soc. Sci. Brux. Ser. I Sci. Math. Astron. Phys. A **53**, 51 (1933)].

[320] A. Lewis, A. Challinor and A. Lasenby, "Efficient computation of CMB anisotropies in closed FRW models," Astrophys. J. **538** (2000) 473 arXiv:astro-ph/9911177.

[321] E. M. Lifshitz, J. Phys. (USSR) **10** (1946) 116.

[322] M. Liguori, E. Sefusatti, J. R. Fergusson and E. P. S. Shellard, "Primordial non-Gaussianity and Bispectrum Measurements in the Cosmic Microwave Background and Large-Scale Structure," (2010) arXiv:1001.4707

[323] D. N. Limber, "The Analysis of Counts of the Extragalactic Nebulae in Terms of a Fluctuating Density Field. II," ApJ **119** (1954) 655.

[324] K. -Y. Lin, L. Lin, T. -P. Woo, Y. -H. Tseng and T. Chiueh, "Effects of preheated clusters on the CMB spectrum," ApJ **608** (2004) L1 arXiv:astro-ph/0210323.

[325] A. D. Linde, "A New Inflationary Universe Scenario: A Possible Solution of the Horizon, Flatness, Homogeneity, Isotropy and Primordial Monopole Problems," Phys. Lett. B **108** (1982) 389.

[326] A. D. Linde, "Chaotic Inflation," Phys. Lett. B **129** (1983) 177.

[327] E. V. Linder, "Cosmic growth history and expansion history," PRD **72** (2005) 043529 arXiv:astro-ph/0507263.

[328] E. L. Lokas, R. Juszkiewicz, D. H. Weinberg and F. R. Bouchet, "Kurtosis of large scale cosmic fields," MNRAS **274** (1995) 730 arXiv:astro-ph/9407095.

[329] M. LoVerde and N. Afshordi, "Extended Limber Approximation," PRD **78** (2008) 123506 arXiv:0809.5112.

[330] D. Lovelock, "The Einstein tensor and its generalizations," J. Math. Phys. **12** (1971) 498.

[331] M. Lueker, C. L. Reichardt, K. K. Schaffer, O. Zahn, P. A. R. Ade, K. A. Aird, B. A. Benson and L. E. Bleem *et al.*, "Measurements of Secondary Cosmic Microwave Background Anisotropies with the South Pole Telescope," Astrophys. J. **719** (2010) 1045 arXiv:0912.4317.

[332] C. -P. Ma, R. R. Caldwell, P. Bode and L. -M. Wang, "The mass power spectrum in quintessence cosmological models," ApJ **521** (1999) L1 arXiv:astro-ph/9906174.

[333] Z. -M. Ma, W. Hu and D. Huterer, "Effect of photometric redshift uncertainties on weak lensing tomography," Astrophys. J. **636** (2005) 21 arXiv:astro-ph/0506614.

[334] R. Maartens, G. F. R. Ellis and W. R. Stoeger, S.J., "Limits on anisotropy and inhomogeneity from the cosmic background radiation," PRD **51** (1995) 1525 arXiv:astro-ph/9501016

[335] R. Maartens, G. F. R. Ellis and W. R. Stoeger, S.J., "Anisotropy and inhomogeneity of the universe from Delta(T) / T," Astron. Astrophys. **309** (1996) L7 arXiv:astro-ph/9510126.

[336] R. Maartens, "Linearization instability of gravity waves?," PRD **55** (1997) 463 arXiv:astro-ph/9609198

[337] R. Maartens, G. F. R. Ellis and S. T. C. Siklos, "Local freedom in the gravitational field," CQG **14** (1997) 1927 arXiv:gr-qc/9611003

[338] R. Maartens, W. M. Lesame and G. F. R. Ellis, "Consistency of dust solutions with div H = 0," PRD **55** (1997) 5219 arXiv:gr-qc/9703080

[339] R. Maartens and B. A. Bassett, "Gravitoelectromagnetism," CQG **15** (1998) 705 arXiv:gr-qc/9704059

[340] R. Maartens, T. Gebbie and G. F. R. Ellis, "Covariant cosmic microwave background anisotropies. 2. Nonlinear dynamics," PRD **59** (1999) 083506 arXiv:astro-ph/9808163

[341] R. Maartens, "Is the Universe homogeneous?," Phil. Trans. Roy. Soc. Lond. A **369** (2011) 5115 arXiv:1104.1300

[342] N. Makino, M. Sasaki and Y. Suto, "Analytic approach to the perturbative expansion of nonlinear gravitational fluctuations in cosmological density and velocity fields," PRD **46** (1992) 585.

[343] N. Makino, S. Sasaki and Y. Suto, APJ **497** (1997) 555 "X-ray gas density profile of clusters of galaxies from the universal dark matter halo," arXiv:astro-ph/9710344.

[344] J. M. Maldacena, "The Large N limit of superconformal field theories and supergravity," Adv. Theor. Math. Phys. **2** (1998) 231 arXiv:hep-th/9711200.

[345] J. M. Maldacena, "Non-Gaussian features of primordial fluctuations in single field inflationary models," JHEP **0305** (2003) 013 arXiv:astro-ph/0210603

[346] K. A. Malik and D. R. Matravers, "A Concise Introduction to Perturbation Theory in Cosmology," Class. Quant. Grav. **25** (2008) 193001 arXiv:0804.3276.

[347] K. A. Malik and D. Wands, "Cosmological perturbations," Phys. Rept. **475** (2009) 1 arXiv:0809.4944.

[348] K. Martel, "Gravitational wave forms from a point particle orbiting a Schwarzschild black hole," Phys. Rev. D **69** (2004) 044025 arXiv:gr-qc/0311017.

[349] K. Martel and E. Poisson, "Gravitational perturbations of the Schwarzschild spacetime: A Practical covariant and gauge-invariant formalism," PRD **71** (2005) 104003 arXiv:gr-qc/0502028

[350] J. M. Martin-Garcia and C. Gundlach, "All nonspherical perturbations of the Choptuik space-time decay," Phys. Rev. D **59** (1999) 064031 arXiv:gr-qc/9809059.

[351] J. M. Martin-Garcia and C. Gundlach, "Gauge invariant and coordinate independent perturbations of stellar collapse. 2. Matching to the exterior," PRD **64** (2001) 024012 [gr-qc/0012056]. arXiv:gr-qc/0012056

[352] J. Martin, "Inflationary perturbations: The Cosmological Schwinger effect," Lect. Notes Phys. **738** (2008) 193 arXiv:0704.3540.

[353] D. P. Mason and M. Tsamparlis, "Spacelike conformal Killing vectors and spacelike congruences," J. Math. Phys. **26** (1985) 2881.

[354] R. Massey, J. Rhodes, A. Leauthaud, P. Capak, R. Ellis, A. Koekemoer, A. Refregier and N. Scoville *et al.*, "COSMOS: 3D weak lensing and the growth of structure," ApJSuppl. **172** (2007) 239 arXiv:astro-ph/0701480.

[355] S. Matarrese and L. Verde, "The effect of primordial non-Gaussianity on halo bias," ApJ **677** (2008) L77 arXiv:0801.4826.

[356] T. Matsubara, Astrophys. J. Lett. **434** (1994) L43 arXiv:astro-ph/9405037

[357] T. Matsubara, ApJ **535** (2000) 1-23. "The Correlation function in redshift space: General formula with wide angle effects and cosmological distortions," arXiv:astro-ph/9908056.

[358] T. Matsubara and B. Jain, "The topology of weak lensing fields," ApJ **552** (2001) Issue 2 L89-L92, arXiv:astro-ph/0009402.

[359] T. Matsubara, "Statistics of isodensity contours in redshift space," Astrophys. J. **457** (1996) 13 arXiv:astro-ph/9501055.

[360] T. Matsubara, "Statistics of Smoothed Cosmic Fields in Perturbation Theory. 1. Formulation and Useful Formulae in Second Order Perturbation Theory," ApJ **584** (2003) 1 arXiv:astro-ph/0006269.

[361] T. Matsubara, "Resumming Cosmological Perturbations via the Lagrangian Picture: One-loop Results in Real Space and in Redshift Space," PRD **77** (2008) 063530 arXiv:0711.2521.

[362] T. Matsubara, "Nonlinear perturbation theory with halo bias and redshift-space distortions via the Lagrangian picture," PRD **78** (2008) 083519 [Erratum-ibid. D **78** (2008) 109901] arXiv:0807.1733.

[363] T. Matsubara, "Analytic Minkowski Functionals of the Cosmic Microwave Background: Second-order Non-Gaussianity with Bispectrum and Trispectrum," PRD **81** (2010) 083505 arXiv:1001.2321.

[364] T. Matsubara, "Nonlinear Perturbation Theory Integrated with Nonlocal Bias, Redshift-space Distortions, and Primordial Non-Gaussianity," PRD **83** (2011) 083518 arXiv:1102.4619.

[365] L. McAllister, E. Silverstein and A. Westphal, "Gravity Waves and Linear Inflation from Axion Monodromy," PRD **82** (2010) 046003 arXiv:0808.0706.

[367] P. McDonald, H. Trac and C. Contaldi, "Dependence of the non-linear mass power spectrum on the equation of state of dark energy," Mon. Not. Roy. Astron. Soc. **366** (2006) 547 arXiv:astro-ph/0505565.

[367] P. McDonald, "Clustering of dark matter tracers: Renormalizing the bias parameters," PRD **74** (2006) 103512 [Erratum-ibid. D **74** (2006) 129901] arXiv:astro-ph/0609413.

[368] P. McDonald, "Primordial non-Gaussianity: large-scale structure signature in the perturbative bias model," PRD **78** (2008) 123519 arXiv:0806.1061

[369] E. McDonough and R. H. Brandenberger, "Searching for Signatures of Cosmic String Wakes in 21cm Redshift Surveys using Minkowski Functionals," JCAP **1302** (2013) 045 1109.2627.

[370] K. R. Mecke, T. Buchert and H. Wagner, "Robust morphological measures for large scale structure in the universe," A&A **288** (1994) 697 arXiv:astro-ph/9312028.

[371] J. Medeiros and C. R. Contaldi, "Non-gaussian foreground residuals of the wmap first year maps," MNRAS **367** (2006) 39 arXiv:astro-ph/0510816.

[372] P. D. Meerburg, J. P. van der Schaar and P. S. Corasaniti, "Signatures of Initial State Modifications on Bispectrum Statistics," JCAP **0905** (2009) 018 arXiv:0901.4044.

[373] A. L. Melott Phys. Rep. **193** (1990) 1.

[374] K. Michielsen and H. De Raedt, "Integral-Geometry Morphological Image Analysi," Physics Reports **347** (2001) 461-538.

[375] H. Minkowski, *Volumen und Oberfläche* (1903), Mathematische Annalen **57**, 447-495.

[376] C. W. Misner and D. H. Sharp, "Relativistic equations for adiabatic, spherically symmetric gravitational collapse," Phys. Rev. **136** (1964) B571.

[377] E. Mitsou, "Gravitational radiation from radial infall of a particle into a Schwarzschild black hole. A numerical study of the spectra, quasi-normal modes and power-law tails," Phys. Rev. D **83** (2011) 044039 arXiv:1012.2028.

[378] S. Mizuno, F. Arroja and K. Koyama, "On the full trispectrum in multi-field DBI inflation," PRD **80** (2009) 083517 arXiv:0907.2439.

[379] H. J. Mo, Y. P. Jing and S. D. M. White, "High-order correlations of peaks and halos: A Step toward understanding galaxy biasing," MNRAS **284** (1997) 189-201, arXiv:astro-ph/9603039.

[380] P. Monaco, "The Mass function of cosmic structures with nonspherical collapse," ApJ **447** (1995) 23 arXiv:astro-ph/9406029.

[381] V. Moncrief, "Gravitational perturbations of spherically symmetric systems. I. The exterior problem.," Annals Phys. **88** (1974) 323.

[382] B. Moore, et al., MNRAS **256** (1992) 477

[383] V. F. Mukhanov and G. V. Chibisov, "Quantum Fluctuation and Nonsingular Universe. (In Russian)," JETP Lett. **33** (1981) 532 [Pisma Zh. Eksp. Teor. Fiz. **33** (1981) 549].

[384] D. Munshi and B. Jain, "The statistics of weak lensing at small angular scales: probability distribution function," Mon. Not. Roy. Astron. Soc. **318** (2000) 109 arXiv:astro-ph/9911502.

[385] D. Munshi and B. Jain, "Statistics of weak lensing at small angular scales: analytical predictions for lower order moments," Mon. Not. Roy. Astron. Soc. **322** (2001) 107 arXiv:astro-ph/9912330.

[386] D. Munshi, P. Valageas and A. J. Barber, "Weak lensing shear and aperture - mass from linear to non-linear scales," Mon. Not. Roy. Astron. Soc. **350** (2004) 77 arXiv:astro-ph/0309698.

[387] D. Munshi, P. Valageas, L. Van Waerbeke and A. Heavens, "Cosmology with Weak Lensing Surveys," Phys. Rept. **462** (2008) 67 arXiv:astro-ph/0612667.

[388] D. Munshi and A. Heavens, "A New Approach to Probing Primordial Non-Gaussianity," MNRAS **401** (2010) 2406 arXiv:0904.4478.

[389] D. Munshi, P. Coles, A. Cooray, A. Heavens and J. Smidt, "Primordial Non-Gaussianity from a Joint Analysis of Cosmic Microwave Background Temperature and Polarization," MNRAS **410** (2011) 1295 arXiv:1002.4998.

[390] D. Munshi, J. Smidt and A. Cooray, "A New Approach to Probing Minkowski Functionals," MNRAS, 434, **2830** (2013) arXiv:1011.5224.

[391] D. Munshi, J. Smidt, A. Heavens, P. Coles and A. Cooray, "Higher-order Statistics of Weak Lensing Shear and Flexion," MNRAS **411** (2011) 2241 arXiv:1003.5003.

[392] D. Munshi, A. Heavens and P. Coles, "Higher-order Convergence Statistics for Three-dimensional Weak Gravitational Lensing," MNRAS **411** (2011) 2161 arXiv:1002.2089.

[393] D. Munshi, T. Kitching, A. Heavens and P. Coles, "Higher Order Statistics for Three-dimensional Shear and Flexion," MNRAS **416** (2011) 629 arXiv:1012.3658.

[394] D. Munshi, S. Joudaki, J. Smidt and P. Coles, "Statistical Properties of Thermal Sunyaev-Zel'dovich Maps," MNRAS **429** (2013) 1564 arXiv:1106.0766

[395] D. Munshi, J. Smidt, S. Joudaki and P. Coles, "The Morphology of the Thermal Sunyaev-Zel'dovich Sky," MNRAS **419** (2012) 138 arXiv:1105.5139.

[396] D. Munshi, L. van Waerbeke, J. Smidt and P. Coles, "From Weak Lensing to non-Gaussianity via Minkowski Functionals," MNRAS **419** (2012) 536 arXiv:1103.1876.

[397] D. Munshi, P. Coles and M. Kilbinger, "Tomography and Weak lensing Statistics," JCAP **1404** (2014) 004 arXiv:1112.0495.

[398] D. Munshi, S. Joudaki, P. Coles and J. Smidt, "Cross-correlating Sunyaev-Zel'dovich and Weak Lensing Maps," arXiv:1111.5010.

[399] A. Nagar and L. Rezzolla, "Gauge-invariant non-spherical metric perturbations of Schwarzschild black-hole spacetimes," CQG **22** (2005) R167 [Erratum-ibid. **23** (2006) 4297] arXiv:gr-qc/0502064

[400] K. Nakamura, "Second-order Gauge-Invariant Cosmological Perturbation Theory: Current Status," Adv. Astron. **2010** (2010) 576273 arXiv:1001.2621.

[401] P. Natoli, G. De Troia, C. Hikage, E. Komatsu, M. Migliaccio, P. A. R. Ade, J. J. Bock and J. R. Bond *et al.*, "BOOMERanG Constraints on Primordial Non-Gaussianity from Analytical Minkowski Functionals," arXiv:0905.4301.

[402] J. F. Navarro, C. S. Frenk and S. D. M. White, "A Universal density profile from hierarchical clustering," ApJ **490** (1997) 493 arXiv:astro-ph/9611107.

[403] E. Newman and R. Penrose, "An Approach to gravitational radiation by a method of spin coefficients," J. Math. Phys. **3** (1962) 566.

[404] E. T. Newman and R. Penrose, "Note on the Bondi-Metzner-Sachs group," J. Math. Phys. **7** (1966) 863.

[405] A. Nicola, A. Refregier, A. Amara and A. Paranjape, "3-dimensional spherical analyses of cosmological spectroscopic surveys," arXiv:1405.3660.

[406] U. S. Nilsson, C. Uggla, J. Wainwright and W. C. Lim, "An Almost isotropic cosmic microwave temperature does not imply an almost isotropic universe," Astrophys. J. **522** (1999) L1 arXiv:astro-ph/9904252.

[407] T. Nishimichi, H. Ohmuro, M. Nakamichi, A. Taruya, K. Yahata, A. Shirata, S. Saito and H. Nomura *et al.*, "Characteristic Scales of Baryon Acoustic Oscillations from Perturbation Theory: Non-linearity and Redshift-Space Distortion Effects," PASJ **59** (2007) 1049 arXiv:0705.1589.

[408] T. Nishimichi, A. Shirata, A. Taruya, K. Yahata, S. Saito, Y. Suto, R. Takahashi and N. Yoshida *et al.*, "Modeling Nonlinear Evolution of Baryon Acoustic Oscillations: Convergence Regime of N-body Simulations and Analytic Models," PASJ **61** (2009) 321 arXiv:0810.0813.

[409] K. Nock, W. J. Percival and A. J. Ross, "The effect of redshift-space distortions on projected 2-pt clustering measurements," MNRAS **407** (2010) 520 arXiv:1003.0896.

[410] B. C. Nolan, "Physical interpretation of gauge invariant perturbations of spherically symmetric space-times," PRD **70** (2004) 044004 arXiv:gr-qc/0406048

[411] H. -P. Nollert, "TOPICAL REVIEW: Quasinormal modes: the characteristic 'sound' of black holes and neutron stars," CQG **16** (1999) R159.

[412] H. Nomura, K. Yamamoto and T. Nishimichi, "Damping of the baryon acoustic oscillations in the matter power spectrum as a probe of the growth factor," JCAP **0810** (2008) 031 arXiv:0809.4538.

[413] H. Nomura, K. Yamamoto, G. Hutsi and T. Nishimichi, "Confronting the damping of the baryon acoustic oscillations with observation," PRD **79** (2009) 063512 arXiv:0903.1883.

[414] D. Novikov, J. Schmalzing and V. F. Mukhanov, "On nongaussianity in the cosmic microwave background," A&A **364** (2000) 17 arXiv:astro-ph/0006097.

[415] A. M. Nzioki, S. Carloni, R. Goswami and P. K. S. Dunsby, "A New framework for studying spherically symmetric static solutions in f(R) gravity," PRD **81** (2010) 084028 arXiv:0908.3333

[416] A. M. Nzioki, R. Goswami and P. K. S. Dunsby, "Jebsen-Birkhoff theorem and its stability in f(R) gravity," arXiv:1312.6790

[417] T. Okumura and Y. P. Jing, "Systematic Effects on Determination of the Growth Factor from Redshift-space Distortions," ApJ **726** (2011) 5 arXiv:1004.3548.

[418] T. Okamura, A. Taruya and T. Matsubara, "Next-to-leading resummation of cosmological perturbations via the Lagrangian picture: 2-loop correction in real and redshift spaces," JCAP **1108** (2011) 012 arXiv:1105.1491.

[419] I. Ozsváth, "New homogeneous solutions of Einstein's field equations with incoherent matter obtained by a spinor technique," J. Math. Phys **6** (1965) 590.

[420] I. Ozsváth, "Dust-filled universes of class II and class III," J. Math. Phys **11** (1970) 2871.

[421] N. Padmanabhan *et al.* [SDSS Collaboration], "The Clustering of Luminous Red Galaxies in the Sloan Digital Sky Survey Imaging Data," Mon. Not. Roy. Astron. Soc. **378** (2007) 852 arXiv:astro-ph/0605302.

[422] C. Park and J. R. Gott, BAAS **20** (1988) 987

[423] C. Park *et al.* [SDSS Collaboration], "Topology analysis of the Sloan Digital Sky Survey. 1. Scale and luminosity dependence," ApJ **633** (2005) 11 arXiv:astro-ph/0507059.

[424] E. Pazos, D. Brizuela, J. M. Martin-Garcia and M. Tiglio, "Mode coupling of Schwarzschild perturbations: Ringdown frequencies," Phys. Rev. D **82** (2010) 104028 arXiv:1009.4665.

[425] J. A. Peacock, "Large scale surveys and cosmic structure," arXiv:astro-ph/0309240.

[426] P. J. E. Peebles and J. T. Yu, "Primeval adiabatic perturbation in an expanding universe," ApJ **162** (1970) 815.

[427] P. J. E. Peebles 'The Large Scale Structure of the Universe" (1980) Princeton University Press.

[428] W. J. Percival *et al.* [2dFGRS Collaboration], "The 2dF Galaxy Redshift Survey: Spherical harmonics analysis of fluctuations in the final catalogue," MNRAS **353** (2004) 1201 arXiv:astro-ph/0406513.

[429] W. J. Percival, R. C. Nichol, D. J. Eisenstein, D. H. Weinberg, M. Fukugita, A. C. Pope, D. P. Schneider and A. S. Szalay *et al.*, "Measuring the matter density using baryon oscillations in the SDSS," ApJ **657** (2007) 51 arXiv:astro-ph/0608635.

[430] W. J. Percival, S. Cole, D. J. Eisenstein, R. C. Nichol, J. A. Peacock, A. C. Pope and A. S. Szalay, "Measuring the Baryon Acoustic Oscillation scale using the SDSS and 2dFGRS," MNRAS **381** (2007) 1053 arXiv:0705.3323.

[431] W. J. Percival *et al.* [SDSS Collaboration], "Baryon Acoustic Oscillations in the Sloan Digital Sky Survey Data Release 7 Galaxy Sample," MNRAS **401** (2010) 2148 arXiv:0907.1660.

[432] P. Peter and J-P. Uzan, "Primordial Cosmology," Oxford Graduate Texts, Oxford University Press, 2009.

[433] J. Tauber *et al.* [Planck Collaboration], "The Scientific programme of Planck," arXiv:astro-ph/0604069.

[434] G. Pratten and D. Munshi, "Non-Gaussianity in Large Scale Structure and Minkowski Functionals," MNRAS **423** (2012) 3209 arXiv:1108.1985.

[435] G. Pratten and D. Munshi, "BAOs and Non-linearities: 3D Spherical Analysis," MNRAS **436** (2013) 3792 arXiv:1301.3673.

[436] G. Pratten and D. Munshi, "Reconstructing the Thermal Sunyaev-Zel'dovich Effect in 3D," MNRAS **442** 1 arXiv:1404.2782.

[437] G. Pratten, "Comment on 'Covariant perturbations of Schwarzschild black holes'," CQG **31** (2014) 038001.

[438] G. Pratten and C. Clarkson, "Covariant Perturbations of LTB Spacetimes," *In Preparation*, (2014).

[439] G. Pratten, "Covariant Perturbations of Vacuum LRS-II Spacetimes," *In Preparation*, (2014).

[440] G. Pratten, "Covariant Perturbations of f(R) Black Holes: The Weyl Terms," *In Preparation*, (2014).

[441] W. H. Press, "Long Wave Trains of Gravitational Waves from a Vibrating Black Hole," ApJ **170** (1971) L105.

[442] W. H. Press and S. A. Teukolsky, "Perturbations of a Rotating Black Hole. II. Dynamical Stability of the Kerr Metric," Astrophys. J. **185** (1973) 649.

[443] W. H. Press and P. Schechter, "Formation of galaxies and clusters of galaxies by selfsimilar gravitational condensation," ApJ **187** (1974) 425.

[444] R. H. Price, "Nonspherical perturbations of relativistic gravitational collapse. 1. Scalar and gravitational perturbations," PRD **5** (1972) 2419.

[445] R. H. Price, "Nonspherical Perturbations of Relativistic Gravitational Collapse. II. Integer-Spin, Zero-Rest-Mass Fields," PRD **5** (1972) 2439.

[446] R. H. Price and K. S. Thorne, "Membrane Viewpoint on Black Holes: Properties and Evolution of the Stretched Horizon," PRD **33** (1986) 915.

[447] E. Poisson and W. Israel, "Internal structure of black holes," PRD **41** (1990) 1796.

[448] A. Pontzen and A. Challinor, "Linearization of homogeneous, nearly-isotropic cosmological models," Class. Quant. Grav. **28** (2011) 185007 arXiv:1009.3935.

[449] A. Pontzen and H. V. Peiris, "The cut-sky cosmic microwave background is not anomalous," PRD **81** (2010) 103008 arXiv:1004.2706.

[450] T. Pyne and S. M. Carroll, "Higher order gravitational perturbations of the cosmic microwave background," PRD **53** (1996) 2920 arXiv:astro-ph/9510041

[451] A. Rassat, A. Amara, L. Amendola, F. J. Castander, T. Kitching, M. Kunz, A. Refregier and Y. Wang *et al.*, "Deconstructing Baryon Acoustic Oscillations: A Comparison of Methods," arXiv:0810.0003.

[452] A. Rassat and A. Refregier, "3D Spherical Analysis of Baryon Acoustic Oscillations," arXiv:1112.3100.

[453] A. Raychaudhuri, "Relativistic and Newtonian cosmology," Zeits. f. Astroph. **43** (1957) 161.

[454] A. Refregier, E. Komatsu, D. N. Spergel and U. -L. Pen, "Power spectrum of the Sunyaev-Zel'dovich effect," PRD **61** (2000) 123001 arXiv:astro-ph/9912180.

[455] A. Refregier, "Shapelets: I. a method for image analysis," MNRAS **338** (2003) 35 arXiv:astro-ph/0105178.

[456] A. Refregier and R. Teyssier, "Numerical and analytical predictions for the large scale Sunyaev-Zel'dovich effect," PRD **66** (2002) 043002 arXiv:astro-ph/0012086.

[457] A. Refregier and D. Bacon, "Shapelets. 2. A method for weak lensing measurements," MNRAS **338** (2003) 48 arXiv:astro-ph/0105179.

[458] T. Regge and J. A. Wheeler, "Stability of a Schwarzschild singularity," Phys. Rev. **108** (1957) 1063.

[459] A. Rendall, "Partial Differential Equations in General Relativity," Oxford Graduate Texts in Mathematics, Oxford University Press, 2008.

[460] A. Riotto and M. S. Sloth, "On Resumming Inflationary Perturbations beyond One-loop," JCAP **0804** (2008) 030 arXiv:0801.1845.

[461] J. E. Rhoads, J. R. Gott, M. Postman, ApJ **421** (1994) 1

[462] H. P. Robertson, "Relativistic Cosmology," Rev. Mod. Phys. **5** (1933) 62.

[463] A. JRoss, W. JPercival, M. Crocce, A. Cabre and E. Gaztanaga, "Measuring Redshift-Space Distortions using Photometric Surveys," MNRAS **415** (2011) 2193 arXiv:1102.0968.

[464] B. S. Ryden, A. L. Melott, D. A. Craig, J. R. Gott, D. H. Weinberg, R. Scherrer, S. P. Bhavsar and J. M. Miller, "The area of isodensity contours in cosmological models and galaxy surveys," ApJ **340** (1988) 647-660

[465] V. Sahni, B. S. Sathyaprakash and S. F. Shandarin, "Probing large scale structure using percolation and genus curves," Astrophys. J. **476** (1997) L1 arXiv:astro-ph/9612029.

[466] V. Sahni, B. S. Sathyaprakash and S. F. Shandarin, "Shapefinders: A New shape diagnostic for large scale structure," ApJ **495** (1998) L5 arXiv:astro-ph/9801053.

[467] D. S. Salopek and J. R. Bond, "Nonlinear evolution of long wavelength metric fluctuations in inflationary models," PRD **42** (1990) 3936.

[468] L. Samushia, W. J. Percival, L. Guzzo, Y. Wang, A. Cimatti, C. Baugh, J. E. Geach and C. Lacey *et al.*, "Effects of cosmological model assumptions on galaxy redshift survey measurements," MNRAS **410** (2011) 1993 arXiv:1006.0609.

[469] L. A. Santaló, *Integral Geometry and Geometric Probability* (1976), Addison-Wesley, Reading, MA.

[470] O. Sarbach and M. Tiglio, "Gauge invariant perturbations of Schwarzschild black holes in horizon penetrating coordinates," Phys. Rev. D **64** (2001) 084016 arXiv:gr-qc/0104061.

[471] M. Sasaki, "Gauge Invariant Scalar Perturbations in the New Inflationary Universe," Prog. Theor. Phys. **70** (1983) 394.

[472] M. Sasaki, "Large Scale Quantum Fluctuations in the Inflationary Universe," Prog. Theor. Phys. **76** (1986) 1036.

[473] M. Sasaki and H. Tagoshi, "Analytic black hole perturbation approach to gravitational radiation," Living Rev. Rel. **6** (2003) 6 arXiv:gr-qc/0306120.

[474] B. S. Sathyaprakash, V. Sahni and S. F. Shandarin, "Morphology of clusters and superclusters in N body simulations of cosmological gravitational clustering," Astrophys. J. **508** (1998) 551 arXiv:astro-ph/9805285.

[475] B. S. Sathyaprakash, B. F. Schutz and C. Van Den Broeck, "Cosmography with the Einstein Telescope," Class. Quant. Grav. **27** (2010) 215006 arXiv:0906.4151.

[476] A. Saro *et al.* [SPT Collaboration], "Constraints on the CMB Temperature Evolution using Multi-Band Measurements of the Sunyaev Zel'dovich Effect with the South Pole Telescope," arXiv:1312.2462.

[477] J. 'i. Sato, M. Takada, Y. P. Jing and T. Futamase, "Implication of ω_m through the morphological analysis of weak lensing fields," ApJ **551** Issue 1 L5-L8, arXiv:astro-ph/0104015.

[478] M. Sato and T. Matsubara, "Nonlinear Biasing and Redshift-Space Distortions in Lagrangian Resummation Theory and N-body Simulations," PRD **84** (2011) 043501 arXiv:1105.5007.

[479] K. Schalm, G. Shiu and J. P. van der Schaar, "The Cosmological vacuum ambiguity, effective actions, and transplanckian effects in inflation," AIP Conf. Proc. **743** (2005) 362 arXiv:hep-th/0412288.

[480] D. Schlegel *et al.* [BigBoss Experiment Collaboration], "The BigBOSS Experiment," arXiv:1106.1706.

[481] J. Schmalzing, M. Kerscher and T. Buchert, "Minkowski functionals in cosmology," In *Varenna 1995, Dark matter in the universe* 281-291 arXiv:astro-ph/9508154.

[482] J. Schmalzing, "Koenderink filters and the microwave background," arXiv:astro-ph/9704164.

[483] J. Schmalzing and T. Buchert, "Beyond genus statistics: A Unifying approach to the morphology of cosmic structure," ApJ **482** (1997) L1 arXiv:astro-ph/9702130.

[484] J. Schmalzing and K. M. Gorski, MNRAS **297** (1998) 355.

[485] J. Schmalzing, T. Buchert, A. L. Melott, V. Sahni, B. S. Sathyaprakash and S. F. Shandarin, "Disentangling the cosmic web I: morphology of isodensity contours," ApJ **526** (1999) 568 arXiv:astro-ph/9904384.

[486] J. Schmalzing and A. Diaferio, "Topology and geometry of the CfA2 redshift survey," MNRAS **312** (2000) 638 arXiv:astro-ph/9910228.

[487] F. Schmidt and D. Jeong, "Large-Scale Structure with Gravitational Waves II: Shear," Phys. Rev. D **86** (2012) 083513 arXiv:1205.1514.

[488] R. Schneider, *Curvature Measures of Convex Bodies*, Ann. Math. pura appl. **116** (1978) 101-134

[489] R. Schoen and S. -T. Yau, "On the Proof of the positive mass conjecture in general relativity," Commun. Math. Phys. **65** (1979) 45.

[490] R. Schoen and S. -T. Yau, "Proof of the positive mass theorem. 2.," Commun. Math. Phys. **79** (1981) 231.

[491] G. E. SchrÃűder-Turk, W. Mickel, S. C. Kapfer, F. M. Schaller, B. Breidenbach, D. Hug and K. Mecke, New J. Phys. **15** (2013) 083028

[492] B. F. Schutz, "A First Course In General Relativity," Cambridge University Press, 1985.

[493] B. F. Schutz, "Geometrical Methods of Mathematical Physics," Cambridge University Press, 1980.

[494] K. Schwarzschild, Sitzungsberichte der KÃűniglich Preussischen Akademie der Wissenschaften zu Berlin, Phys.-Math. Klasse (1916) 189-196.

[495] J. S. Schwinger, "On gauge invariance and vacuum polarization," Phys. Rev. **82** (1951) 664.

[496] R. Scoccimarro and J. Frieman, "Loop corrections in nonlinear cosmological perturbation theory 2. Two point statistics and selfsimilarity," ApJ **473** (1996) 620 arXiv:astro-ph/9602070.

[497] R. Scoccimarro, H. M. P. Couchman and J. A. Frieman, "The Bispectrum as a signature of gravitational instability in redshift-space," ApJ **517** (1999) 531 arXiv:astro-ph/9808305.

[498] R. Scoccimarro, ApJ **544** (2000) 597-615 "The bispectrum: from theory to observations," arXiv:astro-ph/0004086.

[499] R. Scoccimarro, R. K. Sheth, L. Hui and B. Jain, "How many galaxies fit in a halo? Constraints on galaxy formation efficiency from spatial clustering," Astrophys. J. **546** (2001) 20 arXiv:astro-ph/0006319.

[500] R. Scoccimarro, E. Sefusatti and M. Zaldarriaga, "Probing primordial non-Gaussianity with large - scale structure," PRD **69** (2004) 103513 arXiv:astro-ph/0312286.

[501] R. Scoccimarro, "Redshift-space distortions, pairwise velocities and nonlinearities," PRD **70** (2004) 083007 arXiv:astro-ph/0407214.

[502] N. Sehgal, H. Trac, V. Acquaviva, P. A. R. Ade, P. Aguirre, M. Amiri, J. W. Appel and L. F. Barrientos *et al.*, "The Atacama Cosmology Telescope: Cosmology from Galaxy Clusters Detected via the Sunyaev-Zel'dovich Effect," Astrophys. J. **732** (2011) 44 arXiv:1010.1025.

[503] H. -J. Seo and D. J. Eisenstein, "Probing dark energy with baryonic acoustic oscillations from future large galaxy redshift surveys," ApJ **598** (2003) 720 arXiv:astro-ph/0307460.

[504] H. -J. Seo and D. J. Eisenstein, "Improved forecasts for the baryon acoustic oscillations and cosmological distance scale," ApJ **665** (2007) 14 arXiv:astro-ph/0701079.

[505] D. Seery and J. E. Lidsey, "Primordial non-Gaussianities in single field inflation," JCAP **0506** (2005) 003 arXiv:astro-ph/0503692

[506] D. Seery and J. E. Lidsey, "Primordial non-Gaussianities from multiple-field inflation," JCAP **0509** (2005) 011 arXiv:astro-ph/0506056

[508] D. Seery and J. E. Lidsey, "Non-Gaussian Inflationary Perturbations from the dS/CFT Correspondence," JCAP **0606** (2006) 001 arXiv:astro-ph/0604209.

[508] D. Seery, J. E. Lidsey and M. S. Sloth, "The inflationary trispectrum," JCAP **0701** (2007) 027 arXiv:astro-ph/0610210.

[509] D. Seery, "One-loop corrections to a scalar field during inflation," JCAP **0711** (2007) 025 arXiv:0707.3377.

[510] D. Seery, "One-loop corrections to the curvature perturbation from inflation," JCAP **0802** (2008) 006 arXiv:0707.3378.

[511] E. Sefusatti and E. Komatsu, "The bispectrum of galaxies from high-redshift galaxy surveys: Primordial non-Gaussianity and non-linear galaxy bias," PRD **76** (2007) 083004 [arXiv:0705.0343 [astro-ph]].

[512] E. Seidel, "Gravitational radiation from even parity perturbations of stellar collapse: Mathematical formalism and numerical methods," PRD **42** (1990) 1884.

[513] E. Seidel, "Normal mode excitation from stellar collapse to a black hole: Odd parity perturbations," PRD **44** (1991) 950.

[514] U. Seljak, "Analytic model for galaxy and dark matter clustering," MNRAS **318** (2000) 203 arXiv:astro-ph/0001493.

[515] U. Seljak, J. Burwell and U. -L. Pen, "Sunyaev-Zeldovich effect from hydrodynamical simulations: Maps and low order statistics," PRD **63** (2001) 063001 arXiv:astro-ph/0001120.

[516] L. Senatore and M. Zaldarriaga, "The Effective Field Theory of Multifield Inflation," JHEP **1204** (2012) 024 arXiv:1009.2093.

[517] A. C. da Silva, D. Barbosa, A. R. Liddle and P. A. Thomas, "Hydrodynamical simulations of the sunyaev-zel'dovich effect," MNRAS **317** (2000) 37 arXiv:astro-ph/9907224.

[518] A. C. da Silva, S. T. Kay, A. R. Liddle and P. A. Thomas, "Hydrodynamical simulations of the sunyaev-zel'dovich effect: cluster scaling relations and x-ray properties," MNRAS **348** (2004) 1401 arXiv:astro-ph/0308074.

[519] C. Shapiro, R. G. Crittenden and W. J. Percival, "The Complementarity of Redshift-space Distortions and the Integrated Sachs-Wolfe Effect: A 3D Spherical Analysis," MNRAS **422** (2012) 2341 arXiv:1109.1981.

[520] J. Shao, P. Zhang, W. Lin and Y. Jing, "The thermal SZ tomography," ApJ **730** (2011) 127 arXiv:0903.5317.

[521] J. R. Shaw and A. Lewis, "Non-linear Redshift-Space Power Spectra," PRD **78** (2008) 103512 arXiv:0808.1724.

[522] R. K. Sheth, H. J. Mo and G. Tormen, "Ellipsoidal collapse and an improved model for the number and spatial distribution of dark matter haloes," MNRAS **323** (2001) 1 arXiv:astro-ph/9907024.

[523] R. K. Sheth and G. Tormen, "Large scale bias and the peak background split," MNRAS **308** (1999) 119 [astro-ph/9901122].

[524] R. K. Sheth and B. Jain, "Substructure and the halo model of large scale structure," Mon. Not. Roy. Astron. Soc. **345** (2003) 529 arXiv:astro-ph/0208353.

[525] X. Shi and E. Komatsu, "Analytical model for non-thermal pressure in galaxy clusters," arXiv:1401.7657

[526] A. Slosar, S. Ho, M. White and T. Louis, "The Acoustic Peak in the Lyman Alpha Forest," JCAP **0910** (2009) 019 arXiv:0906.2414.

[527] M. S. Sloth, "On the one loop corrections to inflation and the CMB anisotropies," Nucl. Phys. B **748** (2006) 149 arXiv:astro-ph/0604488.

[528] M. S. Sloth, "On the one loop corrections to inflation. II. The Consistency relation," Nucl. Phys. B **775** (2007) 78 arXiv:hep-th/0612138.

[529] J. Smidt, S. Joudaki, P. Serra, A. Amblard and A. Cooray, "The Impact of Secondary non-Gaussianities in the CMB on Cosmological Parameter Estimation," Phys. Rev. D **81** (2010) 123528 arXiv:0909.3515.

[530] K. M. Smith, L. Senatore and M. Zaldarriaga, "Optimal limits on $f_{NL}^{\rm local}$ from WMAP 5-year data," JCAP **0909** (2009) 006 arXiv:0901.2572.

[531] V. Springel, M. J. White and L. Hernquist, ApJ **549** (2001) 681 "Hydrodynamic simulations of the Sunyaev-Zel'dovich effect(s)," arXiv:astro-ph/0008133.

[532] A. A. Starobinsky, "Dynamics of Phase Transition in the New Inflationary Universe Scenario and Generation of Perturbations," Phys. Lett. B **117** (1982) 175.

[533] J. M. Stewart and G. F. R. Ellis, "Solutions of Einstein's equations for a fluid which exhibit local rotational symmetry," J. Math. Phys. **9** (1968) 1072.

[534] J. M. Stewart and M. Walker, "Perturbations of spacetimes in general relativity," Proc. Roy. Soc. Lond. A **341** (1974) 49.

[535] J. M. Stewart, "Perturbations of Friedmann-Robertson-Walker cosmological models," CQG **7** (1990) 1169.

[536] J. M. Stewart, "Advanced general relativity," Cambridge University Press, Cambridge, 1990

[537] A. Strominger, "The dS / CFT correspondence," JHEP **0110** (2001) 034 arXiv:hep-th/0106113.

[538] W. R. Stoeger, S.J., R. Maartens and G. F. R. Ellis, "Proving almost homogeneity of the universe: An Almost Ehlers-Geren-Sachs theorem," ApJ **443** (1995) 1.

[539] K. T. Story, C. L. Reichardt, Z. Hou, R. Keisler, K. A. Aird, B. A. Benson, L. E. Bleem and J. E. Carlstrom *et al.*, "A Measurement of the Cosmic Microwave Background Damping Tail from the 2500-square-degree SPT-SZ survey," Astrophys. J. **779** (2013) 86 arXiv:1210.7231.

[540] B. de Swardt, P. K. S. Dunsby and C. Clarkson, "Gravitational Lensing in Spherically Symmetric Spacetimes," arXiv:1002.2041 [gr-qc]. arXiv:1002.2041

[541] W. M. Suen, R. H. Price and I. H. Redmount, "Membrane Viewpoint on Black Holes: Gravitational Perturbations of the Horizon," PRD **37** (1988) 2761.

[542] R. Sung and P. Coles, "Temperature and Polarization Patterns in Anisotropic Cosmologies," JCAP **1106** (2011) 036 arXiv:1004.0957.

[543] R. A. Sunyaev and Y. .B. Zeldovich, "Small scale fluctuations of relic radiation," Astrophys. Space Sci. **7** (1970) 3.

[544] R. A. Sunyaev and Y. .B. Zeldovich, "Formation of clusters of galaxies: Protocluster fragmentation and intergalactic gas heating," Astron. Astrophys. **20** (1972) 189.

[545] R. A. Sunyaev and Y. .B. Zeldovich, "The Velocity of clusters of galaxies relative to the microwave background. The Possibility of its measurement," Mon. Not. Roy. Astron. Soc. **190** (1980) 413.

[546] Y. Suto and M. Sasaki, "Quasi nonlinear theory of cosmological selfgravitating systems," Phys. Rev. Lett. **66** (1991) 264.

[547] M. Takada and B. Jain, "The Kurtosis of the cosmic shear field," Mon. Not. Roy. Astron. Soc. **337** (2002) 875 arXiv:astro-ph/0205055.

[548] M. Takada and B. Jain, "The Three - point correlation function in cosmology," Mon. Not. Roy. Astron. Soc. **340** (2003) 580 arXiv:astro-ph/0209167.

[549] A. Taruya, M. Takada, T. Hamana, I. Kayo and T. Futamase, "Lognormal property of weak-lensing fields," ApJ **571** (2002) 638 arXiv:astro-ph/0202090.

[550] A. Taruya, T. Nishimichi, S. Saito and T. Hiramatsu, "Non-linear Evolution of Baryon Acoustic Oscillations from Improved Perturbation Theory in Real and Redshift Spaces," PRD **80** (2009) 123503 arXiv:0906.0507.

[551] A. Taruya, T. Nishimichi and S. Saito, "Baryon Acoustic Oscillations in 2D: Modeling Redshift-space Power Spectrum from Perturbation Theory," PRD **82** (2010) 063522 arXiv:1006.0699.

[552] A. N. Taylor, "Imaging the 3-d cosmological mass distribution with weak gravitational lensing," arXiv:astro-ph/0111605.

[553] A. N. Taylor, T. D. Kitching, D. J. Bacon and A. F. Heavens, "Probing dark energy with the shear-ratio geometric test," MNRAS **374** (2007) 1377 arXiv:astro-ph/0606416.

[554] M. Tegmark, "How to measure CMB power spectra without losing information," PRD **55** (1997) 5895 arXiv:astro-ph/9611174.

[555] M. Tegmark *et al.* [SDSS Collaboration], "Cosmological parameters from SDSS and WMAP," PRD **69** (2004) 103501 arXiv:astro-ph/0310723.

[556] M. Tegmark *et al.* [SDSS Collaboration], "The 3-D power spectrum of galaxies from the SDSS," ApJ **606** (2004) 702 arXiv:astro-ph/0310725.

[557] S. A. Teukolsky, "Rotating black holes - separable wave equations for gravitational and electromagnetic perturbations," Phys. Rev. Lett. **29** (1972) 1114.

[558] S. A. Teukolsky, "Perturbations of a rotating black hole. 1. Fundamental equations for gravitational electromagnetic and neutrino field perturbations," Astrophys. J. **185** (1973) 635.

[559] S. A. Teukolsky and W. H. Press, "Perturbations of a rotating black hole. III - Interaction of the hole with gravitational and electromagnet ic radiation," Astrophys. J. **193** (1974) 443.

[560] J. L. Tinker, A. V. Kravtsov, A. Klypin, K. Abazajian, M. S. Warren, G. Yepes, S. Gottlober and D. E. Holz, "Toward a halo mass function for precision cosmology: The Limits of universality," ApJ **688** (2008) 709 arXiv:0803.2706.

[561] K. S. Thorne, "Multipole Expansions of Gravitational Radiation," Rev. Mod. Phys. **52** (1980) 299.

[562] K. S. Thorne, R. H. Price and D. A. Macdonald, "Black Holes: The Membrane Paradigm," NEW HAVEN, USA: YALE UNIV. PR. (1986) 367p

[563] R. C. Tolman, Proceedings of the National Academy of Sciences of the USA **20** (1934) 169.

[564] H. Tomita, Progr. Theor. Phys. **76** (1986) 952.

[565] M. Trümper, "Contributions to actual problems in General Relativity," J. Math. Phys. **6** (1965) 584.

[566] C. G. Tsagas, A. Challinor and R. Maartens, "Relativistic cosmology and large-scale structure," Phys. Rept. **465** (2008) 61 arXiv:0705.4397

[567] M. Tsamparlis and D. P. Mason, "On spacelike congruences in general relativity," J. Math. Phys. **24** (1983) 1577.

[568] M. Tsamparlis, "Geometrization of a general collineation," J. Math. Phys. **33** (1992) 1472.

[569] O. Umeh, C. Clarkson and R. Maartens, "Nonlinear general relativistic corrections to redshift space distortions, gravitational lensing magnification and cosmological distances," arXiv:1207.2109

[570] O. Umeh, C. Clarkson and R. Maartens, "Nonlinear relativistic corrections to cosmological distances, redshift and gravitational lensing magnification. II - Derivation," arXiv:1402.1933.

[571] C. Van Den Broeck, M. Trias, B. S. Sathyaprakash and A. M. Sintes, "Weak lensing effects in the measurement of the dark energy equation of state with LISA," PRD **81** (2010) 124031 arXiv:1001.3099.

[572] H. van Elst and G. F. R. Ellis, "The Covariant approach to LRS perfect fluid space-time geometries," CQG **13** (1996) 1099 arXiv:gr-qc/9510044.

[573] L. Van Waerbeke, G. Hinshaw and N. Murray, "Detection of warm and diffuse baryons in large scale structure from the cross-correlation of gravitational lensing and the thermal Sunyaev-Zeldovich effect," Phys. Rev. D **89** (2014) 023508 arXiv:1310.5721.

[574] S. E. Vazquez, "Constraining Modified Gravity with Large non-Gaussianities," PRD **79** (2009) 043520 arXiv:0806.0603.

[575] L. Verde, L. -M. Wang, A. Heavens and M. Kamionkowski, "Large scale structure, the cosmic microwave background, and primordial non-gaussianity," MNRAS **313** (2000) L141 arXiv:astro-ph/9906301.

[576] L. Verde, "Non-Gaussianity from Large-Scale Structure Surveys," (2010) arXiv:1001.5217

[577] E. Vishniac MNRAS **203** (1983) 345.

[578] C. V. Vishveshwara, "Stability of the schwarzschild metric," PRD **1** (1970) 2870.

[579] C. V. Vishveshwara, "Scattering of Gravitational Radiation by a Schwarzschild Black-hole," Nature **227** (1970) 936.

[580] M. S. Vogeley, C. Park, M. J. Geller, J. P. Huchra and J. R. Gott, "Topological analysis of the CFA redshift survey," ApJ **420** (1994) 525.

[581] J. Wainwright and G. F. R. Ellis, "Dynamical Systems in Cosmology," Cambridge University Press, Cambridge, 2005.

[582] R. M. Wald, "General Relativity," University of Chicago Press, Chicago, (1984).

[583] A. G. Walker, "Complete Symmetric Spaces," J. Lond. Math. Soc. **19** (1944) 219.

[584] P. J. van der Walt and N. T. Bishop, "Observational cosmology using characteristic numerical relativity," Phys. Rev. D **82** (2010) 084001 arXiv:1007.3189.

[585] B. D. Wandelt, E. Hivon and K. M. Gorski, "The pseudo-c_ℓ method: cosmic microwave background anisotropy power spectrum statistics for high precision cosmology," PRD **64** (2001) 083003 arXiv:astro-ph/0008111.

[586] Y. Wang, D. N. Spergel and M. A. Strauss, "Cosmology in the next millennium: Combining MAP and SDSS data to constrain inflationary models," ApJ **510** (1999) 20 arXiv:astro-ph/9802231.

[587] Y. Wang and P. Mukherjee, "Robust dark energy constraints from supernovae, galaxy clustering, and three-year wilkinson microwave anisotropy probe observations," ApJ **650** (2006) 1 arXiv:astro-ph/0604051.

[588] T. J. Waters and B. C. Nolan, "Gauge invariant perturbations of self-similar Lemaitre-Tolman-Bondi spacetime: Even parity modes with $\ell \geq 2$," PRD **79** (2009) 084002 arXiv:0903.3243

[589] S. Weinberg, "Quantum contributions to cosmological correlations," PRD **72** (2005) 043514 arXiv:hep-th/0506236

[590] M. J. Wilson, B. D. Sherwin, J. C. Hill, G. Addison, N. Battaglia, J. R. Bond, S. Das and M. J. Devlin *et al.*, "The Atacama Cosmology Telescope: A Measurement of the Thermal Sunyaev-Zel'dovich Effect Using the Skewness of the CMB Temperature Distribution," Phys. Rev. D **86** (2012) 122005 arXiv:1203.6633.

[591] S. Winitzki and A. Kosowsky, "Minkowski functional description of microwave background Gaussianity," New Astron. **3** (1998) 75 arXiv:astro-ph/9710164.

[592] E. Witten, "A Simple Proof of the Positive Energy Theorem," Commun. Math. Phys. **80** (1981) 381.

[593] S. D. M. White and M. J. Rees, "Core condensation in heavy halos: A Two stage theory for galaxy formation and clusters," Mon. Not. Roy. Astron. Soc. **183** (1978) 341.

[594] M. J. White, 1, L. Hernquist and V. Springel, "Simulating the Sunyaev-Zel'dovich effect(s): Including radiative cooling and energy injection by galactic winds," ApJ **579** (2002) 16 arXiv:astro-ph/0205437.

[595] M. J. White, 1, "Baryons and weak lensing power spectra," Astropart. Phys. **22** (2004) 211 arXiv:astro-ph/0405593.

[596] M. White, Y. -S. Song and W. J. Percival, "Forecasting Cosmological Constraints from Redshift Surveys," Mon. Not. Roy. Astron. Soc. **397** (2008) 1348 arXiv:0810.1518.

[597] T. Wrase and M. Zagermann, "On Classical de Sitter Vacua in String Theory," Fortsch. Phys. **58** (2010) 906 arXiv:1003.0029.

[598] X. Xu, M. White, N. Padmanabhan, D. Eisenstein, J. Eckel, K. Mehta, M. Metchnik and P. Pinto *et al.*, "A New Statistic for Analyzing Baryon Acoustic Oscillations," ApJ **718** (2010) 1224 arXiv:1001.2324.

[599] X. -D. Xu, B. Wang, P. Zhang and F. Atrio-Barandela, "The effect of Dark Matter and Dark Energy interactions on the peculiar velocity field and the kinetic Sunyaev-Zel'dovich effect," JCAP **1312** (2013) 001 arXiv:1308.1475.

[600] W. Xue and B. Chen, "alpha-vacuum and inflationary bispectrum," PRD **79** (2009) 043518 arXiv:0806.4109.

[601] D. G. York *et al.* [SDSS Collaboration], "The Sloan Digital Sky Survey: Technical Summary," Astron. J. **120** (2000) 1579 arXiv:astro-ph/0006396.

[602] J. Yoo and V. Desjacques, "All-Sky Analysis of the General Relativistic Galaxy Power Spectrum," PRD **88** (2013) 2, 023502 arXiv:1301.4501.

[603] E. Zafiris, "Incorporation of space-time symmetries in Einstein's field equations," J. Math. Phys. **38** (1997) 5854 arXiv:gr-qc/9710103

[604] M. Zaldarriaga, U. Seljak and E. Bertschinger, "Integral solution for the microwave background anisotropies in nonflat universes," ApJ **494** (1998) 491 arXiv:astro-ph/9704265.

[605] S. Zaroubi, Y. Hoffman, K. B. Fisher and O. Lahav, "Wiener Reconstruction of The Large Scale Structure," Astrophys. J. **449** (1995) 446 arXiv:astro-ph/9410080.

[606] S. Zaroubi, Y. Hoffman, ApJ **462** (1996) 25 arXiv:astro-ph/9311013.

[607] F. J. Zerilli, "Effective potential for even parity Regge-Wheeler gravitational perturbation equations," Phys. Rev. Lett. **24** (1970) 737.

[608] F. J. Zerilli, "Gravitational field of a particle falling in a schwarzschild geometry analyzed in tensor harmonics," Phys. Rev. D **2** (1970) 2141.

[609] P. -J. Zhang and U. -L. Pen, "Deprojecting Sunyaev-Zeldovich statistics," ApJ **549** (2001) 18 arXiv:astro-ph/0007462.

[610] J. P. Zibin, "Scalar Perturbations on Lemaitre-Tolman-Bondi Spacetimes," PRD **78** (2008) 043504 arXiv:0804.1787

[611] J. P. Zibin, "Can decaying modes save void models for acceleration?," PRD **84** (2011) 123508 arXiv:1108.3068